University of Southampton

Faculty of Environmental and Life Sciences

School of Biological Sciences

Targeting tumour necrosis factor alpha during chronic neurodegeneration using enhanced delivery of biologics across the blood-brain barrier

by

Joe Kirit Chouhan MSci

ORCID ID: 0000-0002-8067-5352

Thesis for the degree of Doctor of Philosophy

October 2021

University of Southampton

Abstract

Faculty of Environmental and Life Sciences

Biological Sciences

Doctor of Philosophy

Targeting tumour necrosis factor alpha during chronic neurodegeneration using enhanced delivery of biologics across the blood-brain barrier

by

Joe Kirit Chouhan

Alzheimer's disease (AD) is a progressive neurodegenerative disease that affects memory and higher cognitive functions. Currently available therapies only treat symptoms meaning there is a clinical unmet need for disease-modifying therapies. Systemic inflammation has been shown to exacerbate the progression of neurodegenerative diseases through modulation of neuroinflammation. Evidence shows that increases in serum tumour necrosis factor alpha (TNF-α) is associated with an increased rate of cognitive decline in AD patients and its neutralisation provides a potential novel therapeutic strategy. A clinical complication with treating neurodegenerative diseases is the requirement to reach therapeutic targets in the brain and this requires delivery across the blood-brain barrier (BBB). Evidence suggests that enhanced brain delivery of immunotherapies can be achieved by targeting the transferrin receptor (TfR). Recent developments in antibody engineering allow for binding of multiple targets in the same therapy, using bispecific antibodies or fusion proteins. I hypothesise that enhanced delivery of a bispecific anti-TfR-anti-TNF-α fusion protein across the BBB can slow disease progression in a model of neurodegeneration and limit the effects of systemic inflammation on neurodegeneration.

The ME7 prion model of neurodegeneration (ME7 mice) is a robust model where disease progression can be followed non-invasively using behavioural tests and shows increased brain cytokine expression. Infection with *Salmonella typhimurium* in mice can effectively model systemic inflammation and in ME7 mice results in increased microglial activation and cytokine production, including TNF-α. Furthermore, the neuroinflammatory response is exaggerated when ME7 mice are exposed to a systemic bacterial infection at later stages of disease. To investigate neutralisation of TNF-α in peripheral and central compartments, I generated two novel bispecific fusion proteins that neutralise TNF-α *in vitro*: $8D3_{130}$ hIgG1 TM ΔK-mTNFR2, which binds mouse TfR for enhanced brain delivery and NIP228 hIgG1 TM ΔK-mTNFR2, which acts in the periphery. Treatment of ME7 mice with bispecific anti-TNF-α fusion proteins had no effect on mouse behaviours or neuroinflammation at the cellular and molecular level. In addition, administration of bispecific anti-TNF-α fusion proteins after infection with *Salmonella typhimurium* in ME7 mice had no effect on the increased microglial activation or cytokine expression.

These data suggest that treatment with an anti-TNF-α fusion proteins, that can act in the periphery or in the brain, has no effect on disease progression in a model of neurodegeneration and is unable to attenuate the exacerbatory effects of systemic inflammation on neuroinflammation. Further work is required to establish whether intervention was administered at the optimum time and whether treatment prior to systemic inflammation could be beneficial in neurodegenerative diseases.

Table of Contents

Table of Tables

Table of Tables

Table of Figures

Table of Figures

Table of Figures

Research Thesis: Declaration of Authorship

Print name: Joe Kirit Chouhan

Title of thesis: Targeting tumour necrosis factor alpha during chronic neurodegeneration using enhanced delivery of biologics across the blood-brain barrier

I declare that this thesis and the work presented in it are my own and has been generated by me as the result of my own original research.

I confirm that:

1. This work was done wholly or mainly while in candidature for a research degree at this University;
2. Where any part of this thesis has previously been submitted for a degree or any other qualification at this University or any other institution, this has been clearly stated;
3. Where I have consulted the published work of others, this is always clearly attributed;
4. Where I have quoted from the work of others, the source is always given. With the exception of such quotations, this thesis is entirely my own work;
5. I have acknowledged all main sources of help;
6. Where the thesis is based on work done by myself jointly with others, I have made clear exactly what was done by others and what I have contributed myself;
7. Parts of this work have been published as:-

Chouhan, J.K., Fowler, S.B., Webster, C.I., Teeling, J.L. The ME7 prion model of neurodegeneration as a tool to understand and target neuroinflammation in Alzheimer's disease. *Drug Discov. Today Dis. Model*, 25–26, 45–52. doi: 10.1016/j.ddmod.2018.10.004

Signature: ..... Date: .....

Presentation of the work in this thesis

Oral Presentations

Southampton Neuroscience Group (SoNG) Seminars, University of Southampton, Southampton 2017 – 2019

Wessex Immunology Group Annual Spring Meeting: Immunoregulation, University of Southampton, Southampton 2019

1st Place Oral Presentation Prize

Biological Sciences Annual Postgraduate Symposium, University of Southampton, Southampton 2019

UK & Ireland Early Career Blood-Brain Barrier Symposium, Open University, Milton Keynes 2019

ARUK South Coast Network Annual Scientific Meeting, Liphook, 2021

Poster Presentations

SoNG Annual Conference: Sensing Our World Meeting, University of Southampton, Southampton 2017

Biological Sciences Annual Postgraduate Symposium, University of Southampton, Southampton 2018

Alzheimer's Research UK (ARUK) Conference, Harrogate, 2019

British Society for Immunology Congress, Liverpool, 2019

Acknowledgements

Firstly, I would like to thank my supervisory team at Southampton, Profs. Jessica Teeling and Clive Holmes, and at AstraZeneca, Susan Fowler and Carl Webster, for their support and advice throughout my PhD. Thank you to Jessica for your enthusiasm about my PhD when I occasionally lacked it. Thank you to Susan for your support and care whilst I was in Cambridge.

I'm especially grateful to past and present researchers on Level D for their advice in the lab and for the evenings of food and drink in the pub. A huge thank you to Daniel Cohn, Paul Ibbett and Renzo Mancuso for their time and patience when teaching me the techniques I needed to get this project started, and thank you to Elena Pipi, Juliane Obst, Emilie Simon, Joanna Gould, and Michael Hurley for their advice in and out of the lab. A huge thank you to Ben Coles, Gemma Fryatt and Georgie Dawes, for providing the perfect work environment of good conversation, big laughs, and technical support, even though I may have distracted them from working on occasion (read: everyday!).

A special thank you goes to Sarah Howard - this PhD journey would've been a lot harder and a lot less enjoyable without your help and support throughout. Thanks for listening to the multitude of experimental queries, helping with countless behaviour and perfusion sessions in the BRF and for providing great company whilst doing so. Thank you to Charlotte Hill, Lawrence Singleton, Rachel Owen, Chris Winnard and Monika Kudelska for the numerous fun nights in Southampton and Poland. A huge thank you to Aleksandra Pitera, I'm grateful for your friendship and advice, but more importantly for sharing the highs and lows of being a Liverpool supporter with me! A massive thanks to Tim Muntslag for being one of the kindest and most genuine people I've ever met, for your friendship, conversations and shared love of basketball and Formula 1!

I would also like to thank the staff in the BRF, especially Mike Broome, Russell Soper and Lesley Lawes for the wonderful job of caring for my mice and for the enjoyable conversations along the way. Thank you to master's student Hanna Davies for her hard work and application in analysis of spleen tissues in this thesis. Thank you to everyone I worked with at AstraZeneca for being available for advice and experimental help whenever I needed it – with particular thanks to Liz English and Matt Burrell, and especially to Alan Sandercock, Esther Martin, and Jen Spooner for performing aspects of the characterisation and quality control analyses of my fusion proteins. A big thank you to Sophia Berry, Camilla Trevor, Michael Price, Olivier Lan Chow Wing, Alessia Taccogna and Francesca Zerbini for making my time in Cambridge outside of the lab very enjoyable too!

To my Mum, Dad, and brother: thanks for always supporting me and being there for me when things got too stressful over the past four and a half(!) years - I couldn't have done this without you. Finally, to Pops, you won't get to read this, but I'm forever indebted to you for instilling me with a passionate, caring, and hard-working nature.

Definitions and Abbreviations

AAV	adeno-associated virus
Aβ	amyloid beta
Acetate pH 5.0	25 mM sodium acetate, 175 mM sodium chloride, pH 5.0
AD	Alzheimer's disease
ADA	anti-drug antibodies
ADCC	antibody-dependent cell-mediated cytotoxicity
AMPA	α-amino-3-hydroxy-5-methyl-4-isoxazolepropionic acid
AMPAR	α-amino-3-hydroxy-5-methyl-4-isoxazolepropionic acid receptor
ANOVA	analysis of variance
APP	amyloid precursor protein
ASC	apoptosis-associated speck-like protein containing a CARD
BACE1	beta-site amyloid precursor protein cleaving enzyme 1
BBB	blood-brain barrier
BCR	B-cell receptor
BLI	bio-layer interferometry
BMVEC	brain microvessel endothelial cell
BSA	bovine serum albumin
CA	cornu Ammonis
CCL	chemokine (C-C motif) ligand
CD	cluster of differentiation
CDC	complement-dependent cytotoxicity
cDNA	complementary deoxyribose nucleic acid
cFLIP	cellular FLICE-like inhibitory protein
cfu	colony forming units
CHO	Chinese Hamster ovary

Definitions and Abbreviations

CIA	collagen-induced arthritis
cIAP	cellular inhibitor of apoptosis
CNS	central nervous system
CrD	Crohn's disease
CSF	cerebrospinal fluid
CSF1R	colony stimulating factor 1 receptor
Ct	threshold cycle
CV	column volumes
CVO	circumventricular organ
Da	Daltons
DAB	3, 3'-diaminobenzidine
DAMP	danger-associated molecular pattern
DMEM	Dulbecco's modified Eagle's media
dpi	days post-injection
dnTNF	dominant-negative tumour necrosis factor alpha
D-PBS	Dulbecco's phosphate buffered saline
EAE	experimental autoimmune encephalitis
ECD	extracellular domain
ELISA	enzyme-linked immunosorbent assay
EMH	extramedullary haematopoiesis
E. coli	*Escherichia coli*
FADD	Fas-associated death domain
FBS	fetal bovine serum
Fc	fragment crystallisable region
FcγR	fragment crystallisable, gamma receptor
FPS	frames per second
GABA	γ-aminobutyric acid

Gapdh	glyceraldehyde 3-phosphate dehydrogenase
GOI	gene of interest
hIgG1	human immunoglobulin G, subclass 1
huTNFR:Fc	human tumour necrosis factor receptor-fragment crystallisable fusion protein
HPLC	high performance liquid chromatography
IBA-1	ionized calcium-binding adapter molecule 1
IBD	inflammatory bowel disease
ICAM-1	intercellular adhesion molecule 1
IFN-γ	interferon gamma
Ig	immunoglobulin
IHC	immunohistochemistry
IL	interleukin
IL-1RA	interleukin 1 receptor antagonist
IL-1Rap	interleukin 1 receptor accessory protein
IL-1RI	interleukin 1 receptor, type 1
InsR	insulin receptor
IRAK	interleukin-1 receptor-associated kinase
i.c.v.	intracerebroventricular
i.p.	intraperitoneal
i.v.	intravenous
JNK	c-Jun N-terminal kinase
LAL	Limulus amoebocyte lysate
LPS	lipopolysaccharide
LRP1	low-density lipoprotein receptor-related protein 1
LTP	long-term potentiation
MAPK	mitogen-associated protein kinase

MCI	mild cognitive impairment
MCP-1	monocyte chemoattractant protein 1
ME7	ME7 prion-injected mice
ME7/SL3261	ME7 prion-injected mice infected with *S. typhimurium* SL3261
MHC	major histocompatibility complex
MHCI	major histocompatibility complex, class 1
MHCII	major histocompatibility complex, class 2
mGluR1	metabotropic glutamate receptor, type 1
MMSE	Mini-Metal State Examination
MPS	mucopolysaccharidosis
MPTP	1-methyl-4-phenyl-1,2,3,6-tetrahydropyridine
mRNA	messenger ribonucleic acid
MS	multiple sclerosis
mTfR	mouse transferrin receptor, type 1
mTNF-α	mouse tumour necrosis factor alpha
mTNFR2	mouse tumour necrosis factor receptor type 2
MyD88	myeloid differentiation primary response gene 88
NAS	normal animal serum
NBH	normal brain homogenate
NF-κB	nuclear factor of kappa B
NFT	neurofibrillary tangle
NLRP3	NLR family pyrin domain containing 3
NMDAR	N-methyl-D-aspartate receptor
OCT	optimal cutting temperature embedding medium
PAMP	pathogen-associated molecular patterns
PBS	phosphate buffered saline
PBS-T	phosphate buffered saline containing 0.1% Tween-20

PBS-TX	phosphate buffered saline containing 0.01% Triton X-100
PCR	polymerase chain reaction
PD	Parkinson's disease
pEU1.4	human immunoglobulin G heavy chain expression vector
pEU3.4	human immunoglobulin G kappa light chain expression vector
Pgk1	phosphoglycerate kinase 1
Poly I:C	polyinosinic:polycytidylic acid
PrP^{Sc}	prion protein, scrapie form
PRR	pattern recognition receptor
PS	presenilin
P. gingivalis	*Porphyromonas gingivalis*
qPCR	quantitative polymerase chain reaction
RA	rheumatoid arthritis
RIP	receptor-interacting kinase
RML	Rocky Mountain Lab scrapie
RMT	receptor-mediated transcytosis
RNA	ribonucleic acid
RT	room temperature
RT-PCR	reverse transcription polymerase chain reaction
Salmonella	*Salmonella enterica*
scFv	single chain variable fragment
SD	standard deviation
SDS-PAGE	sodium dodecyl sulphate–polyacrylamide gel electrophoresis
SEC	size exclusion chromatography
SEM	standard error of the mean
SIE	systemic inflammatory events
SOD	superoxide dismutase

Definitions and Abbreviations

SODD	silencer of death domains
S. typhi	*Salmonella enterica* subspecies enterica serovar Typhi
S. typhimurium	*Salmonella enterica* subspecies enterica serovar Typhimurium
sTNF-α	soluble tumour necrosis factor alpha
sTNFR1	soluble tumour necrosis factor receptor type 1
sTNFR2	soluble tumour necrosis factor receptor type 2
TAE	Tris-acetate-ethylenediaminetetraacetic acid
TCR	T-cell receptor
Tf	transferrin
TfR	transferrin receptor, type 1
T_H	helper T cell
TLR	toll-like receptor
TM	triple mutation
tmTNF-α	transmembrane tumour necrosis factor alpha
TNFR	tumour necrosis factor receptor
TNF-α	tumour necrosis factor alpha
TRADD	tumour necrosis factor receptor-associated death domain
TRAF	tumour necrosis factor receptor-associated factor
U/ml	units per millilitre
UV	ultraviolet
VCAM-1	vascular cell adhesion molecule 1
V_H	heavy chain variable region
V_L	light chain variable region
wpi	weeks post-injection
6-OHDA	6-hydroxydopamine
%CV	coefficient of variation (percentage)
%ID	percentage of injected dose

Chapter 1 General Introduction

Here I will give a short introduction into the cellular components of the central nervous system (CNS) before going on to briefly describe the systemic immune system, how these two systems interact and the consequences for brain function in health and disease.

1.1 Structure and immunology of the central nervous system

The brain itself is a heterogenous organ, with the simplest division being between distinct areas of grey and white matter (for additional references in this section see (Kandel et al., 2013; Purves et al., 2018)). Grey matter being made up of cell bodies and the neuropil, and white matter comprised of myelinated axons. The brain is also organised into functional circuits, with neurons receiving and projecting signals between different brain regions, and this transmission and integration is the process by which information processing and human behaviours occur.

1.1.1 Neurons and brain function

Neurons are the basic unit of the brain and consist of four morphologically distinct regions that all contribute to the function of a nerve cell (for additional references in this section see (Kandel et al., 2013; Purves et al., 2018)). The soma, or cell body, contains the components for cell metabolism; the dendrites are short, branched processes that receive incoming signals; the axon which propagates the electrical signal; and the presynaptic terminals which transmits signals to other neurons. The electrical signal relayed along the axon, known as an action potential, is initiated by depolarisation of the neuronal membrane from its resting potential of -70 mV by influx of ions, such as Na^+, through voltage-gated ion channels. Action potentials are propagated along the axon in a single direction by repeated regeneration of the signal along the length of the axon at sites called the Nodes of Ranvier. These action potentials are highly stereotyped and therefore the integration and analysis of information is not dependent on the form of the signal but the pathway along which it is relayed. Synapses transmit the signal from the axon of one

neuron, the presynaptic cell, to the dendrite of another, the postsynaptic cell. However, neurons are not physically connected and are separated by the synaptic cleft. The transmission of the electric signal along an axon results in the release of a chemical quanta, known as a neurotransmitter (e.g., glutamate) into the synaptic cleft where it can bind receptors on the postsynaptic membrane. Binding of neurotransmitter to its receptor (e.g., N-methyl-D-aspartate (NMDA) receptors; NMDARs) results in opening of an ion channel (e.g., Na^+) and depolarisation of the postsynaptic membrane and propagation of an action potential along the dendrite. The structure of a neuron also contributes to its function within the brain – a neuron with a vast dendritic tree can receive inputs from multiple neurons and integrate large amounts of information; whilst a neuron with many axonal terminals can relay information between multiple pathways.

1.1.2 The blood-brain barrier

The brain is considered to be an "immunologically privileged" site, whereby it has a tissue barrier that prevents access of most blood-borne molecules to the CNS (Bechmann et al., 2007; Galea et al., 2007). This blood-brain barrier (BBB) is comprised of a number of highly adapted cells, collectively referred to as the neurovascular unit, to restrict entry of solutes into the brain (Figure 1.1) (Abbott et al., 2010). Tight junctions between brain endothelial cells reduce transport of solutes through extracellular pathways, and thus limits diffusion across the BBB to gases and small (< 400 Daltons, Da), lipophilic molecules (Sweeney et al., 2019). Endothelial cells are surrounded by pericytes, which are associated with the basal lamina, and help to regulate capillary permeability (Bell et al., 2010; Villaseñor et al., 2016). Finally, astrocytic end-feet produces trophic factors that support and maintain the integrity of the neurovascular unit (Zlokovic, 2008).

Like any other organ, the brain still requires nutrients from the blood and for this there are specific methods of transportation across the BBB. Larger nutrients (> 400 Da), such as glucose and amino acids, are actively transported across endothelial cells through specific carriers, whilst proteins, such as transferrin (Tf) and insulin, utilise their respective receptors and undergo a process called receptor-mediated transcytosis (RMT) to enter the brain parenchyma (Abbott, 2013; Pardridge, 2012). There are regions within the CNS where other brain barriers exist, such as the blood-cerebrospinal fluid (CSF) barrier at the

choroid plexus, which are anatomically and functionally distinct from the BBB. The blood-CSF barrier is greater than 100-fold leakier than the BBB and thus more permeable to solutes (Pardridge, 2020a, 2016).

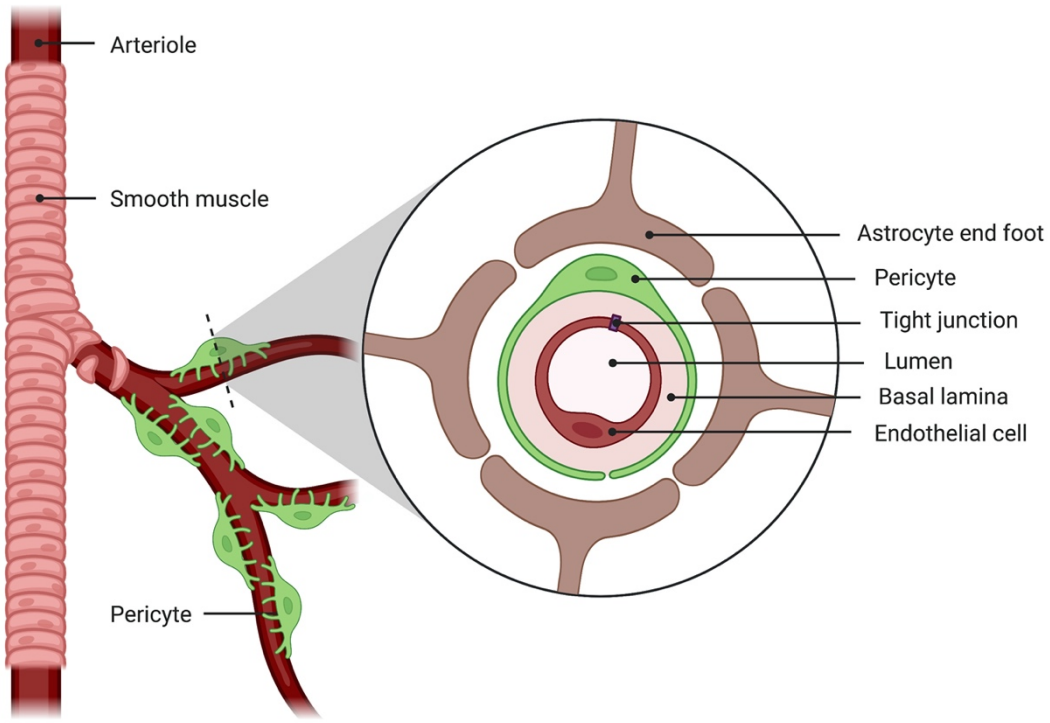

Figure 1.1 The cellular composition of the blood-brain barrier
Several cell types exist in close association to maintain blood-brain barrier integrity. Cerebral endothelial cells are the key cells in the formation of the BBB, as their tight junctions restrict the movement of molecules via paracellular pathways. Pericytes partially envelop endothelial cells meaning they share a basal lamina and contribute to barrier formation. Encapsulating both cell types are astrocyte endfeet which are involved in maintenance of the barrier and can couple blood flow to neural activity.

1.1.3 Glial cells

Neurons are not the only cells within the CNS, with non-neuronal glial cells vastly outnumbering neurons by two to ten times (for additional references in this section see (Kandel et al., 2013; Purves et al., 2018)). Glial cells do not partake in direct signalling or synaptic transmission but can modulate activity and aid in recovery from neural injury. Three types of glial cell are present in the brain: oligodendrocytes, astrocytes, and microglia. Oligodendrocytes are responsible for the production and maintenance of myelin within the CNS, which helps to enhance signal conduction by segregating voltage-gated ion channels. Astrocytes are the major class of glial cells and owe their name to

their star-like ("astral") processes. The main function of astrocytes is to support and maintain the CNS environment. This is achieved through buffering of ions, such as K^+, to facilitate effective neuronal signalling; uptake and metabolism of neurotransmitters to limit excessive activation and trophic support through coupling of brain perfusion with neuronal activity via contacts with arterioles and capillaries.

1.1.3.1 Microglia

Despite being an "immunologically privileged" site, the CNS does contain cells capable of responding to infection and injury within the CNS. Microglia are the main immunocompetent cells in the brain and are derived from erythro-myeloid progenitors in the embryonic yolk-sac (Ginhoux et al., 2010; Ginhoux and Prinz, 2015). Microglia express classical myeloid cell markers (discussed further in Section 1.2.1.1), such as cluster of differentiation (CD) 68 and CD11b, but have lower levels of major histocompatibility complex (MHC) class II (MHCII), fragment crystallisable, gamma receptors (FcγRs) and CD45 which means they can be phenotypically distinguished from other CNS macrophage populations (Kettenmann et al., 2011; Perry and Teeling, 2013). Microglia are thought to account for 5-12% of glial cells in the adult mouse brain, with a high degree of regional variability, especially between the grey and white matter (Askew et al., 2017; Lawson et al., 1990). Recent studies suggest that the microglial population is not replenished by peripheral myeloid cells and are renewed by local proliferation (Ajami et al., 2007; Mildner et al., 2007). Furthermore, microglial numbers in the adult mouse brain are controlled by coupled proliferation and apoptosis, with 0.5% of microglia undergoing division at any one time (Askew et al., 2017).

Microglial function is critical to the maintenance of the CNS during both health and disease. In the healthy brain, microglia exist in a 'surveillant' state, where its phenotype of fine, motile processes allow it to survey the entirety of its local environment every hour (Nimmerjahn et al., 2005). Furthermore, microglia phagocytose dying cells and cell debris to prevent local inflammation and they support neuronal function through direct contact and monitoring of the synapse and control of adult neurogenesis (Gomez-Nicola and Perry, 2015; Perry, 2016). One major role for microglia is the regulation of the immune response and inflammatory status of the brain. Upon activation, following recognition of microbial pathogens, microglia become ameboid in morphology with shorter, thicker

processes and increased expression of CD11b, MHCII and FcγRs (Perry, 2016; Perry and Teeling, 2013). This activation has previously been proposed to fit into M1-like and M2-like macrophage phenotypes; with M1 being 'classical activation' linked to pro-inflammatory responses to injury and infection, and M2 being 'alternative activation' associated with wound healing and immunosuppression (Cunningham, 2013; Lyman et al., 2014). However, given the functional range of microglia within the CNS it is unlikely that such reductive nomenclature fully reflects their potential phenotypic expression (Ransohoff, 2016a).

1.2 The systemic immune system

The mammalian immune system is comprised of two arms: the adaptive and innate immune response. The innate immune response is the molecular and cellular mechanisms involved in preventing infection or quickly eliminating invading pathogens that is initiated within hours of exposure. The adaptive immune response takes days to initiate and is a longer-lived immunity that provides greater specificity against pathogens through the generation of immune memory (for additional references in this section see (Murphy and Weaver, 2017; Punt et al., 2018)). Here I will focus on the innate immune response during systemic infection and the pathways relevant to this thesis.

1.2.1 Immune cells

All leukocytes are derived from sequential differentiation of haematopoietic stem cells (Figure 1.2), and are separated into two lineages: lymphoid cells, involved in the adaptive immune response, and myeloid cells which play a critical role in early innate immune responses. However, this is a rather oversimplification of the two lineages as successful immunity requires communication between myeloid and lymphoid cells (for additional references in this section see (Murphy and Weaver, 2017; Punt et al., 2018)).

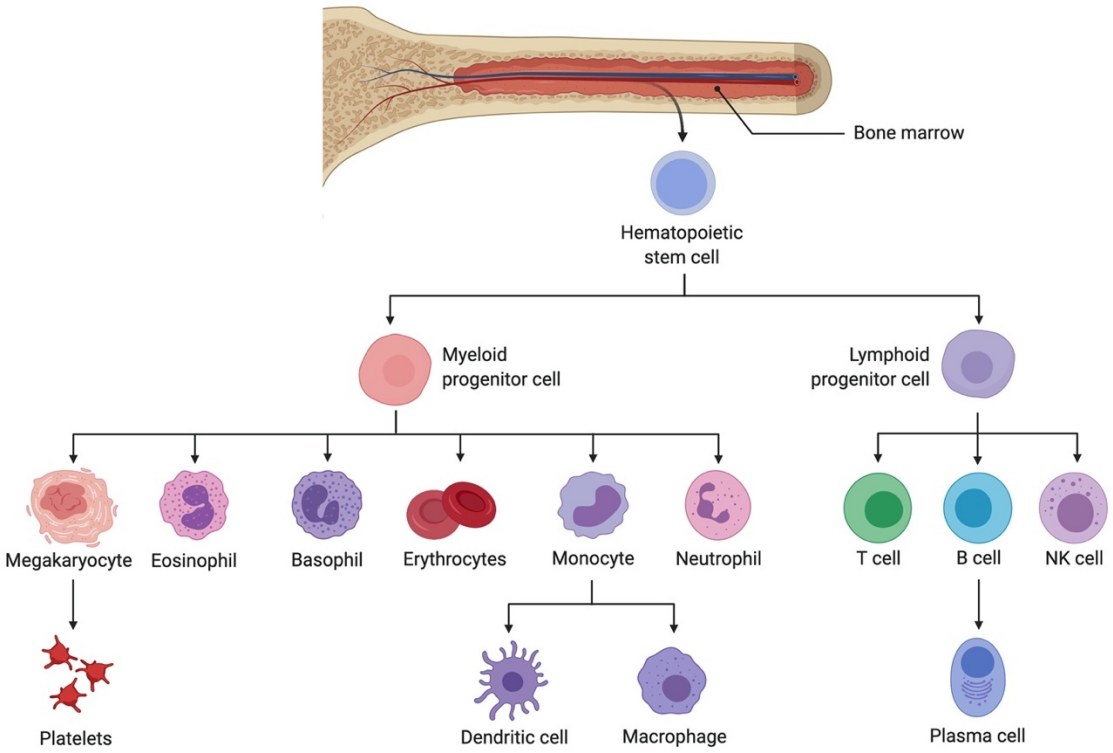

Figure 1.2 Haematopoiesis and differentiation of lymphoid and myeloid cells
Self-renewing haematopoietic stem cells give rise to myeloid or lymphoid progenitors. A common lymphoid progenitor gives rise to natural killer (NK) cells, T and B lymphocytes, and can also produce dendritic cells. A common myeloid progenitor differentiates to give a megakaryocyte/erythrocyte progenitor, which further differentiates to give red blood cells and platelets. Whilst differentiation of a common myeloid progenitor into a granulocyte/monocyte progenitor gives rise to neutrophils, macrophages, dendritic cells, and other myeloid effector cells.

1.2.1.1 Myeloid cells

Myeloid cells are derived from the bone marrow, with proliferation in balance with generation of erythroid progenitors, and can be further differentiated into blood-derived monocytes, granulocytes (e.g., neutrophils and eosinophils) and tissue macrophages (Figure 1.2) (for additional references in this section see (Murphy and Weaver, 2017; Punt et al., 2018)). Monocytes comprise 2-12% of the circulating leukocyte population, remaining in the blood for one to three days, before tissue infiltration and differentiation into tissue-resident macrophages and dendritic cells, which can be identified from monocytes by higher expression of CD11c (Poltorak and Schraml, 2015). Neutrophils can account for 50-70% of all circulating immune cells and are the main recruited cell following tissue inflammation. Myeloid cells can be distinguished from lymphoid cells

through cell-specific markers, including high expression of CD11b, a key protein in the complement cascade, and expression of F4/80, which is rarely expressed on lymphoid cells (Yu et al., 2016).

1.2.1.2 Lymphoid cells

Lymphocytes are involved in the adaptive immune response and comprise T and B cells (for additional references in this section see (Murphy and Weaver, 2017; Punt et al., 2018)). Natural Killer (NK) cells are also lymphocytes, but their main function is associated with the innate immune response and the release of cytotoxic granules (Martinet and Smyth, 2015). Lymphocytes comprise most cells within the lymphatic system and contribute 20-40% of circulating leukocytes; with T and B cells making up to 24% and 10%, respectively. Lymphocytes are morphologically similar and therefore identification relies upon the expression of surface proteins, specifically the antigen receptor. The B cell receptor (BCR) is formed of immunoglobulin (Ig) domains from the same genes that encode antibodies; whilst the T cell receptor (TCR) is related to the Ig family but is formed of two protein chains: α and β (Jiang et al., 2019). In addition, the site of lymphocyte maturation contributes to identification: B cells are matured within the bone marrow, and T cells are matured in the thymus, where exposure to host antigens and subsequent removal from circulation confer immune tolerance. Furthermore, activation of mature B cells via BCR results in proliferation and differentiation into a plasma cell, the effector B cell. Whereas T cells can be subdivided through expression of specific membrane glycoproteins: CD8 on cytotoxic T cells and CD4 on helper T cells.

1.2.2 Innate immunity

The immune system protects its host from a broad range of pathogens, including bacteria, viruses and fungi (for additional references in this section see (Murphy and Weaver, 2017; Punt et al., 2018)). The function of the innate immune system is to be able to detect these pathogens and control pathogen growth whilst activating the adaptive immune system to generate an antigen-specific immune response. Recognition of pathogens involves the detection of pathogen-associated molecular patterns (PAMPs), such as

lipopolysaccharides (LPS) of the bacterial cell wall, by pattern recognition receptors (PRRs). PRRs include transmembrane receptors, such as the mannose receptor and toll-like receptors (TLR) 2 and 4 which can respond to bacterial PAMPS, and intracellular PRRs, including NOD-like receptors that detect intracellular bacteria and those that can bind viral RNA/DNA, such as TLR3/7/9. Initial detection of pathogens is performed by macrophages and dendritic cells via membrane expressed PRRs and resulting activation of intracellular pathways. Macrophages and dendritic cells are more effective following activation through increased phagocytic activity, production of cytokines and chemokines, and activation of T cells by antigen presentation. Phagocytosis of pathogens or infected cells results in lysosomal degradation of phagocytosed material and subsequent presentation of antigens via MHC. Cytokine release and chemokine secretion influence other immune cells. With chemokines attracting circulating cells to the site of inflammation and cytokines enabling extravasation through the activation of endothelial cells. Furthermore, this localised inflammatory response increases lymphatic flow and facilitates antigen presentation to naïve T cells by dendritic cells in secondary immune sites, such as lymph nodes.

1.2.3 Adaptive immunity

Activation of antigen-specific T lymphocytes is mediated through binding of MHC complexes with TCRs (for additional references in this section see (Murphy and Weaver, 2017; Punt et al., 2018)). MHC class I (MHCI) and II (MHCII) are expressed at the cell surface and present antigens, usually in the form of peptide fragments, to T cells, where activation occurs if the TCR is specific for the antigen (Jiang et al., 2019); and the response conferred is dependent on the type of T cell. MHCI molecules are expressed by all nucleated cells; whilst MHCII molecules are only expressed by antigen-presenting cells. Cytotoxic T cells are responsible for the removal of cells that express foreign antigens in complex with MHCI, in the case of viral infections. Helper T cells, however, can have a variety of responses dependent on MHCII antigen presentation and cytokine production. Type 1 helper (T_H1) T cells produce high levels of interferon gamma (IFN-γ) and promote phagocytic activity and stimulate production of opsonizing antibodies for protection against intracellular pathogens, including *Salmonella* (Cosmi et al., 2014; Re and

Strominger, 2001). T_H17 T cells regulate clearance of extracellular pathogens through recruitment of neutrophils via direct interleukin (IL)-8 production or promoting IL-8 production in tissue-resident macrophages (Annunziato et al., 2012). T_H2 lymphocytes are important for the differentiation of B cells and antibody production, as well as the eradication of extracellular parasites. Differentiation of T_H lymphocytes from naïve CD4+ T cells will depend on the presence and activation by different sets of cytokines – T_H1 lymphocytes are induced by IL-12 and IFN-γ, T_H2 lymphocytes by IL-4 and T_H17 lymphocytes require the presence of both IL-1β and IL-23 (Annunziato et al., 2012; Cosmi et al., 2014).

B lymphocytes are responsible for producing antibodies as part of the adaptive immune response and this usually occurs at specialised immune sites, such as the spleen. The activation of B lymphocytes is usually dependent on T cells; however, they can bind soluble antigens, including LPS (Vos et al., 2000). T cell-dependent B cell activation requires binding and internalisation of an antigen by the B cell and presentation to a T cell via MHCII (Parker, 1993). Co-stimulation of the B cell upon binding of TCR with MHCII (e.g., by CD40-CD40 ligand interactions) results in class switching, somatic hypermutation and clonal expansion to produce antigen-specific type G Ig (IgG) antibodies. Memory B cells, which express the antibody produced during clonal expansion, enable rapid antigen-specific immune responses during a second exposure to the pathogenic antigen.

1.2.4 Cytokines and signalling pathways

Cytokines are the molecules that allow communication between cells of the immune system; a summary of relevant cytokines is presented in Table 1.1. In general, the binding of a cytokine to its receptor results in changes in expression of adhesion molecules and chemokine receptors on the target cell membrane that allow it to move to sites of infection (for additional references in this section see (Murphy and Weaver, 2017; Punt et al., 2018)). Furthermore, cytokines can also signal immune cells to alter their intracellular activity that results in changes to its effector functions, such as upregulation of transcription factors (e.g., nuclear factor of kappa B (NF-κB)) and increased release of cytokines (e.g., IL-1 beta (IL-1β), tumour necrosis factor alpha (TNF-α)). Chemokines, such as chemokine (C-C motif) ligand 2 (CCL2), are a subset of cytokines that are specifically

involved in the migration of immune cells and attract cells by influencing cell motility and expression of cell surface adhesion molecules.

Cytokines also act on a variety of different systems to fight infection. IL-6 and TNF-α can act on the liver to induce production of acute phase proteins, such as C-reactive protein, and components of the complement pathway, all of which go on to complete their own specific function in the immune response.

Table 1.1 Selected cytokines involved in the innate and adaptive immune systems

Cytokine	Secreted by	Effects
IL-1β	Macrophages, endothelial and epithelial cells	Fever, T-cell activation, and macrophage activation
IL-6	T-cells (T_H2) macrophages and epithelial cells	T- and B-cell growth and differentiation, acute phase proteins, fever
IL-10	Macrophages, dendritic cells, T- and B-cells	Suppressor of macrophage functions
IL-12	Macrophages and dendritic cells	T_H1 differentiation and NK cell activation
TNF-α	Macrophages, NK cells, activated T-cells	Promotes inflammation, apoptosis, and endothelial cell activation
Interferon gamma	T-cells (T_H1 and CD8+), NK cells, neutrophils	Macrophage activation, suppression of T_H2, T_H17 cells, MHC expression, antigen presentation
CCL2*	Monocytes, macrophages, and dendritic cells	T-cells, monocytes, NK cells and dendritic cell chemoattraction

*CCL2, also known as monocyte chemoattractant protein 1 (MCP-1), is classified as a chemokine. All information from (Murphy and Weaver, 2017; Punt et al., 2018).

1.2.4.1 Tumour Necrosis Factor Receptors (TNFR)

TNF-α is expressed as a 26 kDa type II transmembrane protein and proteolytic cleavage results in the release of a 157 amino acid polypeptide chain that forms homotrimers capable of activating two different receptors, TNFR1 (p55/p60) and TNFR2 (p75/p80) (Canault et al., 2004; Cicha and Urschel, 2015). Expression of TNFR1 is ubiquitous in various cell types, whilst TNFR2 expression is restricted to immune cells (Cabal-Hierro and Lazo, 2012; Dong et al., 2015). TNFR1 has a similar affinity for transmembrane (tmTNF-α) and soluble TNF-α (sTNF-α), whereas TNFR2 has a higher affinity for tmTNF-α (Cicha and Urschel, 2015; Grell et al., 1995). The activation of each receptor leads to differential biological processes, including cell growth and death and immune, stress and inflammatory responses. Activation of both TNFR1 and TNFR2 results in promotion of inflammatory responses, whereas TNFR1 is also able to activate apoptosis through its

various signalling pathways (Montgomery & Bowers, 2012). As both receptors lack intrinsic enzymatic activity, signalling through these receptors is dependent on the recruitment of adapter proteins (Figure 1.3).

TNFR1-induced cellular apoptosis is dependent on the formation of two molecular complexes (Complex I and II), whose formations are temporally and spatially separate, but are limited by the formation and activation of Complex I (Micheau and Tschopp, 2003). Activation of TNFR1 by sTNF-α binding results in the dissociation of the inhibitory molecule SODD (silencer of death domains) from the intracellular domain of the receptor. This allows for the formation of Complex I by the binding of TRADD (TNF receptor-associated death domain) and the recruitment of adapter proteins, including receptor-interacting kinase 1 (RIP1), TNF receptor-associated factor (TRAF) 2, cellular inhibitor of apoptosis (cIAP) 1 and 2 (Dong et al., 2015; Wajant and Scheurich, 2011). This signalling complex activates the catalytic activity of the of IκB kinase (IKK) complex, and results in phosphorylation, and subsequent dissociation, of IκB from NF-κB (Dong et al., 2015; Wajant, 2002; Wajant et al., 2003). NF-κB activation leads to translocation to the nucleus and initiation of transcription of anti-apoptotic proteins, including cFLIP (cellular FLICE-like inhibitory protein), to inhibit the release of caspase 8. If Complex I fails to activate NF-κB, then the recruitment of Complex II enables apoptotic processing to be triggered. This occurs through the recruitment of FADD (Fas-associated death domain) and pre-caspase 8 to TNFR1 after ligand binding, along with TRADD, RIP1 and TRAF2 (Jiang et al., 1999). The formation of Complex II brings pre-caspase 8 molecules into close proximity where autoproteolytic cleavage results in their activation (Cicha and Urschel, 2015; Micheau and Tschopp, 2003). The relative propagation of apoptosis is related to the levels of cFLIP after NF-κB activation, as cFLIP can inhibit caspase 8-mediated apoptosis (Micheau and Tschopp, 2003). The transcription of NF-κB target genes, including IL-1β and IL-6, is responsible for the inflammatory effects of TNFR1 signalling (Decourt et al., 2017).

TNFR2 activation by membrane-bound TNF-α can alter the balance between pro-apoptotic and anti-apoptotic signalling. TNFR2 lacks death domains but does have two binding domains for TRAF2. Therefore, TNFR2 can recruit TRAF2, cIAP1 and cIAP2 and results in downstream activation of NF-κB through its non-canonical pathway, via the proteasomal degradation of NF-κB inducing kinase and activation of both IκBα and IKKα (Dong et al., 2015). As well as non-canonical NF-κB activation, TNFR2 can also activate C-

Jun N-terminal kinase (JNK) and mitogen-activated protein kinase (MAPK) signalling pathways through association of TRAF2 and cIAP1/2 with both TRAF3 and RIP, and helps to mediate cell survival (Cicha and Urschel, 2015; Dong et al., 2015; Wajant, 2002). In addition, activation of JNK and MAPK pathways result in activation of the transcription factor AP-1 and induces expression of target genes such as CCL2 and IL-6 (Weber et al., 2010).

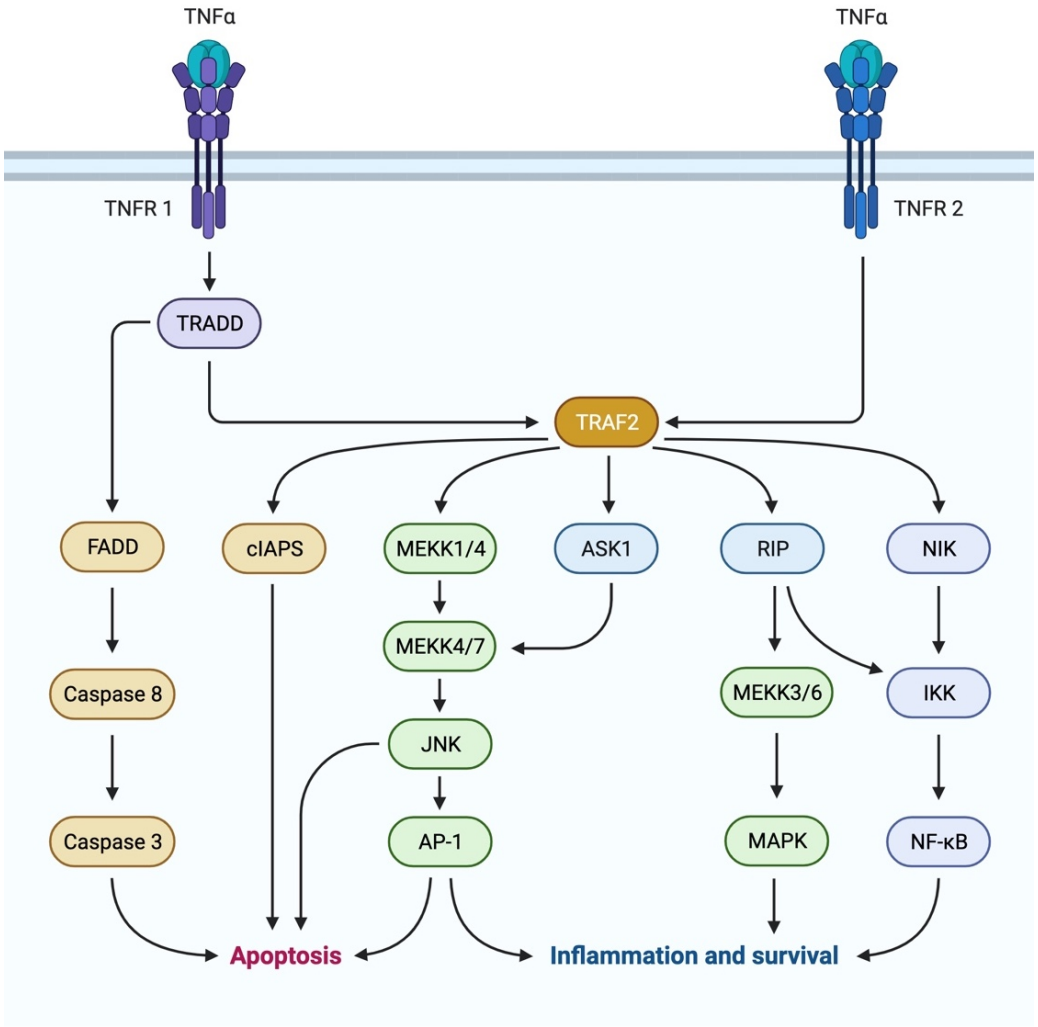

Figure 1.3 Intracellular pathways of TNFRs following binding of TNF-α
Engagement of TNFRs by trimeric TNF-α results in activation of distinct cellular protein complex formation and activation leading to either inflammation and cell survival or apoptosis. Activation via TRAF2 following binding of TNF-α to TNFR1 or TNFR2 leads to promotion of cell survival, via JNK and MAPK pathways, and downstream activation of the IKK complex and subsequent translocation of NF-κB to the nucleus, which results in inflammation. Activation via TRADD after TNFR1 activation leads to recruitment of FADD and downstream processes for cellular apoptosis, including autoproteolytic activation of caspase-8 and caspase-3. Abbreviations: ASK1, apoptosis signal-regulating kinase 1.

1.2.5 Immune-to-brain communication

Immune-to-brain communication is a vital part of a host organism's response to inflammation and infection. A variety of metabolic and behavioural changes are initiated during infection with the overall aim of limiting wider effects of inflammation and mounting an effective immune response, whilst also preventing the spread of infection to other organisms (Dantzer, 2004). These changes are termed sickness behaviours and include fever, anorexia, anhedonia, social withdrawal, reduced locomotion and motivation, as well as cognitive impairments (Dantzer, 2004, 2001).

Systemic inflammatory challenge, including with *Salmonella*, can induce sickness behaviours and neuroinflammation, suggesting immune crosstalk mediated by cytokines (Dantzer et al., 2008; Godinez et al., 2008). The brain monitors innate immune responses within the periphery by collating information from multiple sources (D'Mello and Swain, 2016). One pathway involves afferent nerve activation, such as the vagus nerve during peritoneal inflammation and the trigeminal nerve during oro-lingual infections (Dantzer et al., 2008). A second humoral pathway involves activation of resident immune cells within circumventricular organs (CVOs) and the choroid plexus by circulating PAMPs and translation to the brain via production of pro-inflammatory cytokines (Quan et al., 1998). A third pathway involves saturable transport mechanisms at the BBB initiated by high peripheral levels of cytokines. Whilst activation of endothelial cells, propagates peripheral inflammation across the BBB via production of prostaglandins (Dantzer et al., 2008). It is possible that the combination of vagal afferent signalling and propagation of cytokines at CVOs create a representation of the peripheral response that better informs the brain of how to respond, based on the molecular components of the initial innate immune response (Dantzer et al., 2008).

1.2.5.1 Vagus nerve innervation

The Vagus nerve innervates the viscera and vessels of the thorax and abdomen. Abdominal efferent fibres in the gastrointestinal tract, project to nucleus tractus solitarii and this information is relayed to other regions of the CNS, including the amygdala and area postrema (Berthoud and Neuhuber, 2000). Vagal afferents contain a variety of

receptors including, mechano- and chemoreceptors in the stomach, small intestine and sensory endings in the liver and pancreas (Berthoud and Neuhuber, 2000). Vagal afferents are also capable of detecting inflammation through IL-1 receptors and macrophages (Ek et al., 1998), with evidence of early responses to infection through increased c-fos expression in brain regions innervated by afferent vagal nerve projections (Gaykema et al., 2007; Wan et al., 1993). Furthermore, there is evidence that vagal stimulation can induce anti-inflammatory effects through cholinergic pathways (Borovikova et al., 2000; Van Der Zanden et al., 2009).

The importance of the Vagus nerve in immune-to-brain communication has been observed by experiments involving vagotomy and LPS. Subdiaphragmatic vagotomy prevents sickness behaviours in mice following intraperitoneal (i.p.) administration of LPS, but not after intracerebroventricular (i.c.v.) or intravenous (i.v.) administration (Bluthe et al., 1996; Bret-Dibat et al., 1995). Vagotomy also reduces social interaction behaviours following higher doses of LPS (Konsman et al., 2000). Whilst subpyrogenic doses of LPS (1-100 μg/kg) can induce sickness behaviours, including reduced burrowing (Teeling et al., 2007), subdiaphragmatic vagotomy had no effect on food intake or open field behaviours following peripheral challenge with LPS or IL-1β (Wieczorek et al., 2005). There are contrasting reports as to the effects of vagotomy on brain levels of cytokines: brain IL-1β messenger ribonucleic acid (mRNA) production in mice following systemic LPS (400 μg/kg) is attenuated (Laye et al., 1995); whilst vagotomy had no effect on IL-1β levels in the brain with lower doses of LPS (10-100 μg/kg) (Hansen et al., 2000).

1.2.5.2 Circumventricular Organs

Circumventricular organs (CVOs), such as the area postrema and vascular organ of lamina terminalis, are areas of the brain that are highly vascularised but lack an intact BBB (Ransohoff et al., 2003). CVOs are also sites for leukocyte entry, with CD45+ cells observed in CVOs in mice with experimental autoimmune encephalitis (Schulz and Engelhardt, 2005). Whilst immune cells can traverse CVOs, diffusion of tracers has been shown to be excluded for large molecular weight molecules and limited for small molecular weight molecules by tanycytes (Peruzzo et al., 2000). This suggests that translation of the peripheral effects of cytokines must be required at these sites to induce

fever and sickness behaviours following detection of LPS. Evidence for this was shown when systematic disruption of IL-1β signalling identified fenestrated capillaries within the CVOs as necessary for induction of sickness behaviours following i.c.v. administration of IL-1β (Knoll et al., 2017). Furthermore, systemic administration of IL-1β and TNF-α results in increased expression of CCL2, a potent chemokine, within CVOs (Nadeau and Rivest, 2000; Thibeault et al., 2001). Monitoring of cerebrospinal fluid (CSF) also occurs at the choroid plexus, where fenestrated capillaries form a leaky barrier by which cytokines can diffuse across and cells can migrate (Bechmann et al., 2007). It is possible that these inflammatory mediators can diffuse into the brain from the blood and can also be transported across the BBB (Banks and Erickson, 2010; Quan and Banks, 2007).

1.2.5.3 Brain endothelial cells

Brain endothelial cells express receptors for IL-1β and TNF-α (Nadeau and Rivest, 1999). This means that systemic cytokines can act on endothelial cells to trigger prostaglandin release, which then propagates neuroinflammation across the BBB and can mediate LPS-induced fever (Inoue et al., 2002). The central effects of peripheral low dose LPS can be ameliorated by inhibition of prostaglandin release, specifically through cyclo-oxygenase 1 inhibition (Teeling et al., 2010). In addition, application of LPS on brain endothelial cells results in secretion of IL-6 from its luminal surface (Verma et al., 2006). Furthermore, LPS and cytokines can have direct effects on microglia and perivascular macrophages (Teeling and Perry, 2009). However, penetration of LPS at the level of the BBB has been shown to be minimal *in vivo* (Banks and Robinson, 2010). Moreover, systemic inflammation induces upregulation of adhesion molecules, including intercellular adhesion molecule 1 (ICAM-1) and vascular cell adhesion molecule 1 (VCAM-1), on endothelial cells and this facilitates the transport of leukocytes from the blood (Engelhardt, 2008).

1.3 Bacterial infection as a model of chronic systemic inflammation

Pathogenic infectious bacteria are responsible for a huge range of prevalent diseases, including typhoid fever (*Salmonella typhi*), listeria (*Listeria monocytogenes*) and tuberculosis (*Mycobacterium tuberculosis*). There is also a vastly diverse profile in a host organism's immune response because of differences in method of infection and type of bacteria, such as Gram-positive vs Gram-negative and intracellular vs extracellular. Intracellular bacteria, such as *S. typhi*, are some of the most common serious infections for humans and result from infection of immune cells, such as B lymphocytes, and proliferation of bacteria inside the cell (Fillatreau, 2011).

Salmonella enterica subspecies *enterica* serovar Typhimurium (*S. typhimurium*) is a Gram-negative bacterium capable of infecting both humans and mice (Kurtz et al., 2017; Santos et al., 2001). Ingestion of *S. typhimurium* in humans results in enteritis, as opposed to typhoid as seen with *S. typhi*, but in mice oral pathogenesis can lead to symptoms similar to typhoid fever in humans (Kurtz et al., 2017; Santos et al., 2001). As a result, *S. typhimurium* is commonly used as a murine model of systemic infections, such as gastroenteritis and septicaemia (Broz et al., 2012; Ruby et al., 2012). *S. typhimurium* SL3261 is an attenuated strain of *S. typhimurium* that when inoculated in C57BL/6 mice results in reduced colonisation of liver and spleen compared to its parent strain, SL3144 (Benjamin et al., 1990; Peters et al., 2010). The reasons for this reduction in virulence are attributed to transposon insertion in the *aroA* gene, which prevents synthesis of p-amino-benzoic acid and folate, thus limiting bacterial proliferation by preventing DNA synthesis (Hoiseth and Stocker, 1981). Attenuated strains, often used for vaccination, produce a milder disease course and reduced incidences of death in mice and are essential for chronic infection in susceptible mice (Hoiseth and Stocker, 1981; Ruby et al., 2012). Whilst milder, invasion of phagocytes by attenuated strains still results in persistent infection through activation of the innate immune system and a strong adaptive immune response (Ruby et al., 2012). Furthermore, *Salmonella* can persist within peripheral tissues for greater than 60 days, even when evidence of peripheral response, such as splenomegaly, is no longer observed (Monack et al., 2004a). *Salmonella* infections induce a reproducible and robust increase in peripheral cytokines that can be a model for long-term infection/chronic low-grade systemic inflammation (Petersen and Pedersen, 2005).

1.3.1 Immune response to *Salmonella* infection

Intraperitoneal injection of *S. typhimurium* allows free bacteria to enter the bloodstream, as opposed to invasion of the gut mucosa following oral administration, where bacteria are rapidly cleared from the blood via the complement system. However, both routes result in colonisation of organs with large populations of phagocytic cells, such as the spleen and liver (Dougan et al., 2011; Mastroeni et al., 2009). Macrophages and dendritic cells detect extracellular bacteria through pathogenic antigens via activation of PRRs, including TLR2 and TLR4, and secretion of proinflammatory cytokines downstream of NF-κB (Balaram et al., 2009; Broz and Monack, 2011). Phagocytosis after detection leads to internalisation of *Salmonella* in phagosomes and results in the formation of *Salmonella*-containing vacuoles (Jantsch et al., 2011; Monack et al., 2004a). Control of bacterial growth within *Salmonella*-containing vacuoles is partly dependent on expression of a divalent cation transporter, *Nramp1*, that controls availability of iron and mutations in which can exacerbate infection (Brown et al., 2013; Nairz et al., 2009). *Salmonella* can also be recognised by intracellular PRRs and initiate cytosolic mechanisms of innate immunity, such as NOD-like receptors (Broz et al., 2012; Broz and Monack, 2011). The NLRP3 inflammasome is responsible for the subsequent activation of pro-IL-1β to IL-1β and induces pyroptosis which is thought to benefit the host by removing the intracellular niche for *Salmonella* (Broz et al., 2012; Broz and Monack, 2011). IL-1β and TNF-α which are produced during *Salmonella* infection can induce sickness behaviours, such as apathy and anorexia, through crosstalk with the CNS (Section 1.2.5). These behaviours are most likely an energy conserving response by the host organism to focus on combating the infection (Dantzer, 2004).

Local production of cytokines, including TNF-α, IL-1β, IL-6, IL-12 and IL-18, from M1 polarised macrophages results in recruitment of neutrophils and NK cells to potentiate the innate immune response (Kolaczkowska and Kubes, 2013; Mittrucker and Kaufmann, 2000; Schuetze et al., 2005). Formation of multicellular lesions called granulomas, which consist of both infected and recruited cells, around sites of infection aim to prevent the spread of infection to other cells (Mastroeni et al., 2009, 1992a). In addition, specific cytokines can act on naïve CD4+ T lymphocytes and polarise them towards specific responses, for example IFN-γ and IL-12 towards T_H1 responses (Godinez et al., 2008; Lapaque et al., 2009). T_H1 lymphocytes produce IFN-γ which acts to polarise macrophages

towards an M1 phenotype and this supports further T_H1 differentiation via a feed-forward loop (Esther van de Vosse and Ottenhoff, 2006). This feed-forward loop is thought to contribute to the suppression of bacterial growth and initiation of the adaptive phase of the immune response to *Salmonella* (Figure 1.4) (Mastroeni, 2002).

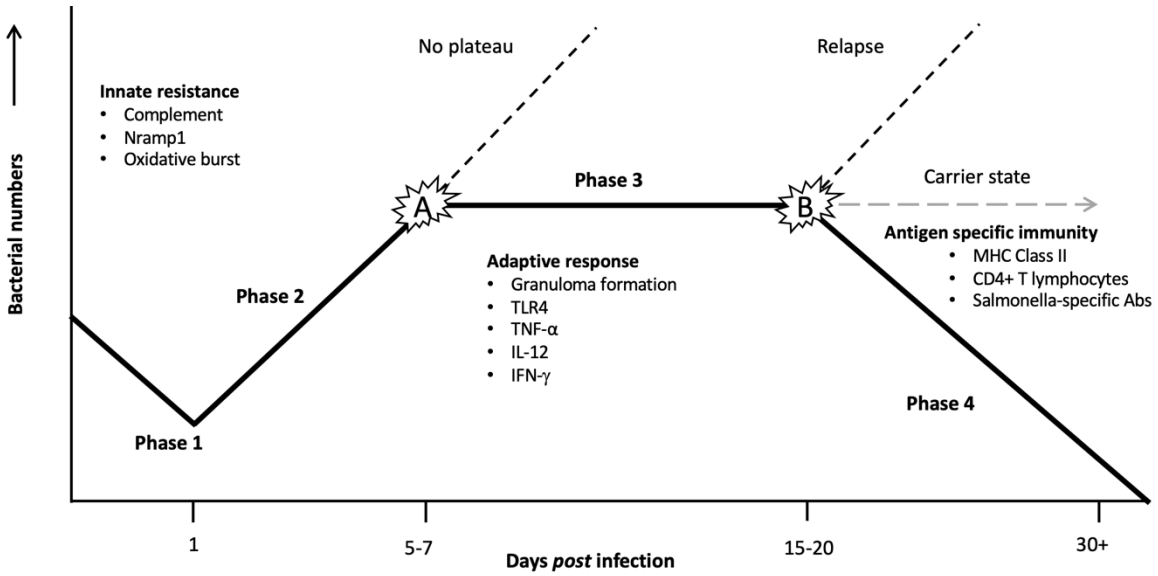

Figure 1.4 The phases of primary *Salmonella* infection
The solid line represents the course of a sub-lethal *Salmonella* infection in wild-type mice. Dotted lines highlight course if checkpoints A and B were not present, e.g., because of interruption to IFN-γ and/or TNF-α signalling. Checkpoint A coincides with the onset of adaptive immune responses and checkpoint B with the intervention of antigen-specific immunity. Modified from Mastroeni, 2002.

Clearance of bacteria is thought to be mediated by CD4+ T lymphocytes without contribution of CD8+ cytotoxic T cells (Hess et al., 1996; McSorley and Jenkins, 2000). Whilst both CD4+ and CD8+ T lymphocytes are required for protection against re-infection following prior vaccination with attenuated bacteria (Mastroeni et al., 1993a, 1992a). In addition, cytokines involved in T_H1 response are thought to confer resistance upon secondary infection as they drive bacterial killing and neutralisation of IFN-γ and TNF-α has been shown to exacerbate re-infection (Hess et al., 1996; Mastroeni et al., 1998, 1992a). Persistence of *Salmonella* during chronic infection is thought to be associated with a balance in T_H cell responses, with IL-10 and IL-4 from T_H2 cells being permissive of infection and high antibody titres following *Salmonella* infection consistent with a T_H2-biased immune response (Kurtz et al., 2017; Monack et al., 2004a).

B lymphocytes appear to have little to no contribution in bacterial clearance, with B cell deficient mice capable of clearing infection with attenuated strains of *S. typhimurium* (Mastroeni et al., 2000; Mittrücker et al., 2000; Nanton et al., 2012). Interestingly, higher bacterial loads were found in the blood of B cell deficient mice suggesting that an antibody response may be involved in preventing systemic spread of bacteria (Cunningham et al., 2007). However, B cells can contribute to both early and late phases of *Salmonella* infection. It has been shown that TLR activation and MyD88-dependent mechanisms of cytokine secretion are required for control of infection through differentiation of T_H1 cells (Barr et al., 2010; Talbot et al., 2009). In addition, B cell deficient mice show reduced T cell responses to *S. typhimurium* that limits acquired resistance in response to secondary infection (Mastroeni et al., 2000; Nanton et al., 2012). Furthermore, BCR recognition and MHCII-antigen presentation is necessary for development of CD4+ memory T cells (Barr et al., 2010).

1.3.2 Live bacteria vs bacterial mimetics as models of chronic inflammation

There are many studies that have investigated the effects of systemic inflammation in mice, however most studies have used LPS, a component of the cell wall, as a bacterial mimetic. The immune response following systemic administration of LPS has been well characterised in both the periphery and the CNS. Systemic challenge with LPS increases serum levels of IL-1β, TNF-α and IL-6 which peak between two and six hours after injection in a dose-dependent fashion (Pardon, 2015). In these studies, a peak in anti-inflammatory cytokines is observed later, before all cytokine levels are back at baseline by 24 hours (Pardon, 2015). Furthermore, brain proinflammatory cytokines are associated with sickness behaviours and show peak expression in the hippocampus and hypothalamus at 1 hour post-injection that is resolved by three hours (Laye et al., 1994; Layé et al., 2000). However, administration of subpyrogenic levels of LPS (< 100 μg/kg) results in a transient induction of cytokines that has a different timeframe, with a peak at two to three hours and resolution after six hours (Teeling et al., 2010, 2007). Moreover, both high and low doses of LPS are able to induce sickness behaviours and transiently reduce burrowing behaviours in mice (Dantzer, 2004; Teeling et al., 2010, 2007). Interestingly, for the majority of detectable cytokines in both the periphery and brain

following systemic LPS there is no distinct temporal pattern between the two compartments (Erickson and Banks, 2011).

In attempts to mimic chronic bacterial inflammation, experimenters have taken to using repeated doses of LPS. Multiple high doses of LPS (3 mg/kg) was able to induce significant upregulation of cytokines in the brain, including TNF-α, CCL2 (MCP-1), and IL-6 but interestingly had no effect on IL-1β expression (Erickson and Banks, 2011). This lack of IL-1β upregulation after multiple doses is likely caused by endotoxin tolerance, or hypo-responsiveness, that means subsequent LPS challenges result in attenuated immune responses to prevent excessive tissue damage and development of sepsis (Biswas and Lopez-Collazo, 2009). Endotoxin tolerance was also observed for brain IL-1β and IFN-γ expression following three doses of 0.5 mg/kg LPS, in conjunction with endotoxin tolerance in the periphery (Püntener et al., 2012). Bacterial infection with *S. typhimurium* results in a delayed and extended immune response in the brain following systemic challenge compared to peripheral responses with LPS. Brain endothelial cells are activated at seven days post-infection with increased expression of VCAM-1, ICAM-1 and MHCII, whilst these changes are not apparent following LPS injection (Püntener et al., 2012). Furthermore, activation of the endothelium is followed by increasing expression of proinflammatory cytokines IL-1β and IL-12, which peak at 21 days in the hippocampus/thalamus. Injection of LPS directly into the hippocampus without prior systemic challenge has also been shown to induce cytokine expression with an increase in IL-1β transcript levels (Cunningham *et al.*, 2005). Whilst intracerebral injection of LPS 28 days after *S. typhimurium* infection induces exaggerated expression of MHCII and CD11c compared to LPS only suggesting that microglia are primed by the initial systemic bacterial challenge (Püntener et al., 2012).

These data combined suggest that immune-to-brain communication is evident after both systemic administration of LPS and *Salmonella*, with increased cytokine production and behavioural consequences. However, systemic challenge with bacterial mimetics, either as single or multiple injections, fails to accurately replicate live bacterial infection. Overall, a delayed central response and a prolonged effect on the vasculature suggest that live bacterial infection is a more desirable systemic inflammatory challenge when modelling chronic inflammation.

1.4 The impact of systemic inflammation on neurodegeneration

1.4.1 Neurodegeneration

Due to the importance of the brain in the undertaking of everyday tasks, any alterations in its functionality usually result in severe impairments. Disorders of the CNS that cause the dysfunction and eventual death of nerve cells are termed neurodegenerative diseases. As individual neuronal circuits control different aspects of brain function, the symptoms related to different neurodegenerative diseases are usually specific to the region affected. Parkinson's disease (PD) affects motor function because of reduced dopaminergic release into the substantia nigra, whilst Alzheimer's disease (AD) manifests as memory impairments, due to synaptic dysfunction and neuronal loss in the hippocampus, and progresses to higher cognitive deficits from neuronal death in the cortex – together these memory and cognitive deficits are termed 'dementia' (Martin, 1999). Neurodegenerative diseases are usually associated with ageing and/or genetic factors, with the majority also linked to deposition of misfolded protein and the resulting neuroinflammatory response. With an ageing population, the number of dementia sufferers is expected to double by 2030 (Prince et al., 2015, 2013). Currently the only treatments available are palliative and thus there is a clear, unmet clinical need for novel disease-modifying treatments (Kumar and Singh, 2015).

1.4.1.1 Alzheimer's disease

Alzheimer's disease (AD) is the most common form of dementia, accounting for over 60% of all dementia cases (Alzheimer's Association, 2015). Two types of AD exist: the sporadic form, also known as late-onset AD, causing over 90% of AD cases; and familial forms, also known as early onset AD, linked to mutations in genes involved in the processing of amyloid precursor protein (APP) (Bertram et al., 2010). AD initially manifests as loss of episodic memory – the ability to recall the what, when and where of a specific memory (Tulving, 2002) – and inabilities in forming new memories, followed by the progressive decline in cognitive function (Arnaiz and Almkvist, 2003). Mild cognitive impairment (MCI) refers to patients with early signs of cognitive impairment, relative to their age group, and

a patient with MCI is five times more likely to develop dementia (Marcos et al., 2016; Petersen, 2016).

AD is histologically defined by the presence of two neuropathological hallmarks, extracellular deposits of aggregated β-amyloid (Aβ) and intraneuronal deposits of hyperphosphorylated tau protein, that are known to spread in a systematic fashion throughout the brain during disease progression (Braak et al., 2011). Plaques, containing Aβ, form when APP is misprocessed and proceeds down the amyloidogenic pathway, whereby cleavage of APP by β-secretase produces small fragments of protein (ranging from 39 to 43 residues in length) that bind to each other to form oligomers, which seed the formation of fibrils and finally extracellular plaques. Misprocessing of APP by β-secretase can be caused by mutations in the genes for presenilin (PS) 1 and 2, *PSEN1* and *PSEN2*, which encode for γ-secretase, and in the *APP* gene itself (Bertram et al., 2010). Interestingly, deposition of Aβ is not indicative of cognitive dysfunction, with healthy elderly patients showing evidence of plaques upon their deaths (Perl, 2010). Tau is a microtubule binding protein that upon hyperphosphorylation dissociates from the microtubule and binds other hyperphosphorylated tau proteins to form intraneuronal neurofibrillary tangles (NFTs). The progression of these NFTs has been closely linked to cognitive decline in patients, with initial deposition in the locus coeruleus and transentorhinal cortex and then spreading to synaptically connected regions such as the hippocampus, and finally into the neocortex at later stages of disease (Braak et al., 2011; Murray et al., 2015). Accumulation of tau in NFTs is not unique to AD, with other neurodegenerative diseases containing tangles, such as Pick's disease, linked to mutations in the *MAPT* gene that cause tau to be more aggregation-prone; however, none of these mutations have been linked with AD (Tolnay and Probst, 1999).

1.4.2 Inflammation as a risk factor for neurodegeneration

There is now growing evidence that one aspect common to many neurodegenerative diseases is microglial activation and a state of chronically induced neuroinflammation due to the presence of protein aggregates. As a result of this neuroinflammation, low levels of proinflammatory cytokines are constantly being released into the extracellular milieu and it is thought that this state may exacerbate ongoing disease and/or contribute to the

onset of disease (Ransohoff, 2016b). It has been shown that AD patients have increased mRNA expression of colony stimulating factor-1 receptor (CSF1R), a key regulator of microglial proliferation, in the temporal cortex compared to age-matched controls (Olmos-Alonso et al., 2016). In addition, AD patients also have increased mRNA expression of the immune marker CD68, whose expression has been linked to poorer cognitive function (Minett et al., 2016; Rakic et al., 2018).

Neuroinflammation was thought to occur with very little involvement from the systemic immune system, however recent evidence suggests that it can be influenced by aspects of the peripheral immune response (Boyko et al., 2017; Hammond et al., 2019; Heppner et al., 2015; Klein and Hunter, 2017; Machado et al., 2011). Further evidence that suggests inflammation, both central and peripheral, could affect disease progression comes from evidence that immune signalling is altered and can be a risk factor in neurodegenerative diseases (Busse et al., 2017; Parachikova et al., 2007; Thome et al., 2018; Torres et al., 2014; Van Der Willik et al., 2019). Moreover, epidemiological studies investigating levels of cytokines in serum and CSF from AD and MCI patients show a variety of changes that associate with disease progression (D'Anna et al., 2017; Llano et al., 2012; Morimoto et al., 2011; Tarkowski et al., 2003).

Acute systemic inflammatory events (SIEs), such as respiratory and gastrointestinal infections, can increase serum levels of proinflammatory cytokines, such as IL-1β and TNF-α, and negatively impact cognitive function in AD patients (Dursun et al., 2015; Gezen-Ak et al., 2013; Holmes et al., 2009, 2003). Evidence from AD patients with periodontitis, a gum infection caused by *Porphyromonas gingivalis* (*P. gingivalis*), has been associated with a six-fold increase in the rate of cognitive decline, but was not correlated to initial baseline cognition (Ide et al., 2016). In addition, virulence factors of *P. gingivalis* have been detected in the brains of AD patients and also correlate with pathological tau load (Dominy et al., 2019). Clinical studies designed to assess the effects of systemic cytokine levels on the progression of AD showed that increased serum levels of TNF-α at initial assessment were associated with an increased rate of cognitive decline during the six-month study (Holmes et al., 2011). Furthermore, patients who suffered a SIE during the study period, that resulted in acutely increased cytokine levels, showed a two-fold increase in the rate of cognitive decline compared to patients that did not record a SIE (Holmes et al., 2011).

Preclinical studies into the effects of ongoing inflammation on the progression of neurodegenerative diseases have shown that systemic inflammation has an exacerbating effect on disease. Systemic inflammation induced by twice-weekly dosing of 100 μg/kg LPS for six weeks in 4-month old 3xTg-AD mice resulted in increased phosphorylation of tau as detected by AT8 and AT180 immunoblotting (Kitazawa et al., 2005). Additionally, 12 weeks of 50 μg/ml LPS in 11-month old APPswe mice increased levels of both $A\beta_{1-42}$ and $A\beta_{1-40}$ and also the association of Aβ with neurons (Sheng et al., 2003). Induction of ulcerative colitis, a chronic systemic inflammatory disease, after LPS-induced neuronal damage in the substantia nigra resulted in increased neurodegeneration (Villarán et al., 2010). Peripheral injection of the TLR3 agonist polyinosinic:polycytidylic acid (poly I:C) increased hippocampal IL-1β and IL-6 expression as well as the ratio of $A\beta_{1-42}$ species compared to $A\beta_{1-40}$ species (Krstic et al., 2012). Furthermore, this same poly I:C treatment significantly impaired cognitive performance in the alternating Y-maze (Krstic et al., 2012). In addition, chronic systemic expression of IL-1β was able to induce neurodegeneration in mice with ongoing neuropathology (Pott Godoy et al., 2008). Microglia are associated with the production of pro-inflammatory cytokines and microglial depletion studies that reduce microglia numbers by inhibiting signalling through the CSF1R have shown improvements in hippocampal-dependent tasks in mouse models of AD (Dagher et al., 2015; Olmos-Alonso et al., 2016). Moreover, the improved cognitive function of microglia-depleted APP/PS1 mice was associated with decreased synaptic degeneration in the hippocampus (Olmos-Alonso et al., 2016).

These studies present compelling evidence for a role of systemic inflammation, and by association, neuroinflammation in the progression of cognitive decline associated with AD. The remaining question from these studies is: would inhibition of both central and peripheral proinflammatory cytokines show clear halting of cognitive decline in patients and improve disease outcomes?

1.4.3 Evidence for targeting TNF-α in AD

Clinical studies suggest that TNF-α can exacerbate disease pathology in neurodegeneration. Detectable levels of TNF-α in mild AD patients are correlated with a reduction in hippocampal functional connectivity in both the left and right hemispheres

compared to mild AD patients that did not have detectable TNF-α levels (Magalhães et al., 2017). In addition, functional pathway analysis of biomarkers in serum and CSF of MCI patients showed that 'TNF signalling' associated with total tau and phosphorylated Tau in CSF and plasma of MCI patients (Pillai et al., 2019). Although TNF-α levels did not correlate with tau levels, increased soluble TNFR2 (sTNFR2) was positively correlated with phosphorylated Tau in both CSF and plasma (Pillai et al., 2019). Furthermore, analysis of MCI patients identified a correlation in CSF levels of soluble TNFR1 (sTNFR1) and sTNFR2 with cognitive decline and conversion from MCI to AD (Diniz et al., 2010; Zhao et al., 2020). sTNFR2 levels were associated with a protective effect, with increased CSF levels resulted in slower conversion from MCI to AD (Zhao et al., 2020). Whilst increases in CSF sTNFR1 levels were predictive of a faster decline in cognition and conversion to AD from MCI (Diniz et al., 2010). A recent small Phase II clinical trial of a single dose of etanercept, a peripherally acting anti-TNF-α fusion protein, provides further evidence for a role of inflammation in progression of neurodegenerative diseases. The rate of cognitive decline, as assessed by Mini-Mental State Examination (MMSE), in patients treated with etanercept trended towards a significant reduction compared to untreated patients (Butchart et al., 2015). A small, single-centre open-label six-month study involving weekly perispinal delivery of etanercept (25-50 mg) to mild-to-severe AD patients resulted in a clinical improvement in cognition, as seen with an increase in MMSE scores (Tobinick et al., 2006). Further investigation for over two years suggests a sustained positive improvement in these patients (Tobinick, 2007). Although these studies were small in sample size, they do suggest a role for TNF-α in the progression of AD.

Whilst in preclinical experiments, the overexpression of TNF-α in the hippocampus from two months of age in the 3xTg-AD mouse model results in neuronal loss in the cornu Ammonis (CA) region 1 (CA1) after ten months of expression (Janelsins et al., 2008). In addition, i.c.v. treatment of 12-month old APP/PS1 mice with the anti-TNF-α antibody, infliximab, on three consecutive days resulted in a significant reduction in amyloid plaque number and the levels of soluble $A\beta_{1-42}$ at three and seven days after the final injection (Shi et al., 2011). Combined, these clinical and preclinical investigations suggest that TNF-α presents as a suitable therapeutic target for AD, and potentially other neurodegenerative diseases.

1.5 Murine ME7 model of chronic neurodegeneration

In this thesis I investigate chronic neurodegeneration using a well characterised prion disease model. Prion diseases, or transmissible spongiform encephalopathies, are rare neurodegenerative diseases that cause distinct pathology: vacuolar brain degeneration, brain deposition of misfolded conformations of prion protein as amyloid fibres (PrP^{Sc}), and transmissibility between brain regions. Due to protein deposition, activation of an inflammatory response and the progressive nature of prion disease, this pathology bears a huge resemblance to other proteinopathies, such as AD and PD, and thus provides a model of chronic neurodegeneration that can be utilised by researchers for testing of potential therapeutics (Chouhan et al., 2017; Stopschinski and Diamond, 2017).

ME7 is a *Prnp*^{a} mouse-adapted ovine prion strain, that was isolated through passage of scrapie infected sheep's spleen in RIII mice and then in C57BL/6 mice (Striebel et al., 2011; Zlotnik and Rennie, 1963). ME7 prion has a predominantly hippocampal and thalamic lesion profile (Cunningham et al. 2005; Hilton et al. 2013; Carroll et al. 2016). Duration of ME7 disease incubation period in mice is experimentally 20-24 weeks before overt clinical signs, such as hunched posture, poor coat condition and reduced mobility are seen. In this incubation period, specific behavioural and histological changes are known to occur in a progressive and well-characterised manner (Betmouni et al., 1999b, 1996). Eight weeks after intracranial injection of ME7 prion brain homogenate (ME7), there is histological evidence of hypertrophic astrocytes, with increased expression of glial fibrillary acidic protein, and microglial activation, which show increased immunoreactivity for CD68 compared to mice injected with normal brain homogenate (NBH) (Betmouni et al., 1999b, 1996). This gliosis increases from 12 weeks post-injection (wpi), with an increase in the number of both astrocytes and microglia in the hippocampus and thalamus compared to NBH controls until clinical onset (Gómez-Nicola et al., 2013). At 13 wpi, there is a reduction in synaptic density in the hippocampus, as assessed by synaptophysin staining (Hilton et al., 2013), that leads to loss of hippocampal CA1 neurons at 18-19 wpi and visible vacuolation of the parenchyma (Cunningham et al., 2003).

A battery of behavioural tests established by Betmouni and colleagues utilises various non-cognitive assessments to identify any links between behaviour and pathological

changes that occur in the preclinical stages of disease (Betmouni et al., 1999b; Deacon et al., 2001; Felton et al., 2005; Guenther et al., 2001). This battery of tests was designed to measure changes in innate behavioural tasks, such as burrowing and nesting; motivation, such as glucose consumption; and motor deficits using the inverted screen and horizontal bar tasks. ME7 prion-injected (ME7) mice also show progressive decline with deficits in burrowing and nesting appearing after 8-10 wpi, hyper-reactivity in the open field becoming evident after 14-16 wpi, and worsening performance in both horizontal bar and inverted screen tasks visible from 16 wpi (Cunningham et al., 2003; Guenther et al., 2001). In addition, cognitive tests have been used to assess various aspects of memory, such as a 'paddling' Y-maze for spatial learning (Cunningham et al., 2009) and spontaneous alternation in a T-maze for working memory (Guenther et al., 2001).

Research characterising behaviour in various strains of murine prion disease have shown that in 22L, 79A and ME7 strains of murine prion disease the same behavioural changes (glucose consumption, burrowing, nesting) that occur at 12 wpi, before the onset of clinical signs, have the same pattern across these three strains (Cunningham et al. 2005). However, the neurobiological deficits that are present after clinical onset of prion disease are distinct between the strains. ME7 and 79A strains show a significant amount of neuronal loss in the hippocampus, yet the 22L strain shows significant neuronal cell loss in the cerebellar Purkinje layer. A potential explanation for the differential effects of prion strains would be that each strain has a varying degree of regional selectivity. To address this a recent study has shown that the concentration of PrP^{Sc}, as assessed by real-time quaking-induced conversion, does not differ between regions, regardless of evident neurodegeneration, and thus suggests a difference in regional susceptibility to individual prion strains (Alibhai et al., 2016). All three strains show a reduction in synaptic density of the thalamus and within the hippocampus; with the reduction in ME7 prion being more pronounced than in the 22L and 79A strains (Cunningham et al. 2005; Hilton et al. 2013). These data suggest that behavioural changes may be because of hippocampal synaptic loss, particularly in the CA1, and that this synaptic loss does not need to be substantial to produce a visible change in normal mouse behaviours. This is supported by experiments in mice that show that burrowing is significantly reduced following cytotoxic lesion of the dorsal hippocampus (Deacon et al., 2002; Deacon and Rawlins, 2005). Furthermore, these changes in behaviour are reflective of impairments observed in "Activities of Daily Living"

in AD patients (Potkin, 2002; Reisberg et al., 2001). Acute effects of dorsal hippocampal lesion on open field locomotion suggests a trend towards increased activity but a clear reduction in rearing behaviours (Deacon et al., 2002; Deacon and Rawlins, 2005). Interestingly, kainic acid-induced CA3 neuronal damage results in increased open field locomotion and rearing behaviours (Chen et al., 2002). This may suggest that the later effects on open field behaviour observed in ME7 mice could be mediated by dysfunction of CA3 neurons.

1.5.1 Chronic neurodegeneration and inflammation

Analysis of hippocampal mRNA using quantitative polymerase chain reaction (qPCR) highlights an increased expression of pro-inflammatory cytokines, including IL-1β and TNF-α, in ME7 mice challenged with LPS at 19 wpi, and this was further confirmed by protein levels (Combrinck et al., 2002; Cunningham et al., 2005c). Furthermore, systemic challenge with LPS (500 μg/kg) between 14-15 wpi in ME7 mice results in the earlier onset of impairments in inverted screen and horizontal bar tasks, as well as a reduction in the hyper-reactivity in open field locomotion exhibited by unchallenged ME7 mice (Cunningham et al., 2009). It was also shown that these deficits were temporally separate from the acute effects of an LPS challenge, and together provide evidence to suggest that systemic inflammation can accelerate the disease process in ME7 mice. Overall, these data suggest that microglia, which show an activated 'primed' phenotype from 12 wpi, do not produce increased levels of proinflammatory cytokines until they undergo a secondary challenge, and this challenge results in hastened disease progression (Perry and Holmes, 2014; Perry and Teeling, 2013). Concomitantly, this secondary insult can also cause *de novo* pathology in other animal models of neurodegeneration, which suggests a potential role for neuroinflammation, and specifically brain cytokines, in progression of neurodegenerative diseases as a whole (Kitazawa et al., 2011, 2005; Krstic et al., 2012; Lee et al., 2008; Pott Godoy et al., 2008; Sheng et al., 2003).

1.5.2 Targeting proinflammatory cytokines in chronic neurodegeneration

Systemic inflammatory events, and increased serum levels of cytokines, have been shown to accelerate cognitive decline in human AD patients (Holmes et al., 2009, 2003). There is evidence to suggest there may be a therapeutic benefit from inhibiting the effects of proinflammatory cytokines, such as TNF-α, in human AD patients (Sections 1.4.2 - 1.4.3). However, it is still unclear if neutralisation of cytokines in both the peripheral and central compartments will lead to further improvements.

1.5.2.1 Modulating the TNF-alpha pathway

It has been shown that in mice lacking parts of the TNF-α signalling pathway, by knocking out both TNFRs or TNF-α itself, that TNF-α has no effect on progression of RML prion disease (Tamgüney et al., 2008). In agreement with this, TNFR1 knock out mice all developed scrapie after either intracerebral inoculation or i.p. administration of RML scrapie in inbred 129Sv mice (Klein et al., 1997). In contrast, in mice given ME7 prion via the i.p. route pharmacological inhibition of TNF-α can delay disease onset. Administration of a fusion protein containing human sTNFR2 fused to fragment crystallisable (Fc) region (huTNFR:Fc) five days before inoculation with ME7 prion results in a significant prolonging of incubation period by 47 days (Mabbott et al., 2002). In addition, time to development of neurological disease occurred 19 days later in mice treated with huTNFR:Fc at 14 days post-injection (dpi) compared to mice treated with control IgG. However, later treatment at 38 dpi had no effect on incubation period (Mabbott et al., 2002). Intracerebral injection of prion and subsequent systemic treatment with huTNFR:Fc, either five days before or 14 dpi, had no effect on scrapie pathogenesis (Mabbott et al., 2002). However, the fusion protein used in this study would have limited BBB penetration and therefore might not be expected to prevent neuroinvasion. As a result, the likelihood of any efficacy in preventing or modulating neuropathogenesis would be limited to passive diffusion of the antibody across the BBB.

Considering the above studies, the evidence suggests that pharmacological neutralisation rather than genetic manipulation of the TNF-α signalling pathway results in a delayed onset of prion disease. As previous studies have only administered peripheral TNF-α

inhibitors it remains to be seen whether you would see improvements with an anti-TNF-α biologic that has enhanced brain penetration. Given that peripheral levels of TNF-α have been associated with hastened progression of cognitive decline, an anti-TNF-α biologic with enhanced brain penetrance that can neutralise both central and peripheral TNF-α could prove beneficial in a model of neurodegeneration in isolation or with additional systemic inflammation.

1.6 Improving delivery of immunotherapies to the CNS

Passive immunotherapy, in the form of monoclonal antibodies, is a valuable approach for therapeutics with high target specificity, reduced off-target side effects and improved pharmacokinetics compared to small molecule drugs for CNS-based disorders (Buss et al., 2012; Carter, 2011; Yu and Watts, 2013). When addressing immunotherapy for CNS disorders, one significant complication with potential efficacy is the ability of the antibody to reach its target. With CNS disorders, such as AD, potential targets are located primarily in the brain parenchyma, and thus potential therapies are required to enter the brain to exert their physiological effect. The BBB (Section 1.1.2) prevents access of large molecules (> 400 Da), including 98% of small molecule drugs, from entering the brain parenchyma (Pardridge, 2006). This results in less than 0.2% of peripherally administered antibody reaching the parenchyma of mice and thus the BBB needs to be crossed for effective antibody delivery (Banks et al., 2002; Levites et al., 2006; St-Amour et al., 2013). The low levels of endocytic activity in brain endothelial cells and degradation of IgG in lysosomes is thought to account for the limited delivery of antibodies across the BBB (Triguero et al., 1989; Villaseñor et al., 2016). However, with over 400 miles of capillaries and short travel distances, less than 40 μm, to reach CNS-based cells, targeting the BBB with various approaches can take advantage of this vast vascular network for enhanced delivery (Banks, 2008; Pardridge, 2002; Yu and Watts, 2013).

1.6.1 Antibody structure and function

IgG antibodies are the most abundant antibody class found in human serum and have a similar basic structure that consist of four polypeptide chains - two heavy chains and two light chains – and they perform two main functions: antigen recognition, through the antigen binding Fab fragment, and engagement of the immune system, through the Fc fragment. The antigen specificity of the Fab fragment is comprised of two variable domains, one from the heavy chain (V_H) and one from the light chain (V_L), as well as a single constant domain from the heavy and light chains (Figure 1.5A). The majority of antigen specificity is conferred by three hypervariable loops within the V_H and V_L regions and enables antibodies to recognise an almost infinite number of antigens (Morea et al., 2000). The Fc fragment contains four constant domains, two from each heavy chain, that can engage FcγRs, to induce antibody-dependent cell-mediated cytotoxicity (ADCC), and complement-dependent cytotoxicity (CDC) through the binding of C1q (Oganesyan et al., 2008). The Fab and Fc fragments are separated by a flexible hinge region that also contains a disulphide bond between the two heavy chains (Figure 1.5A).

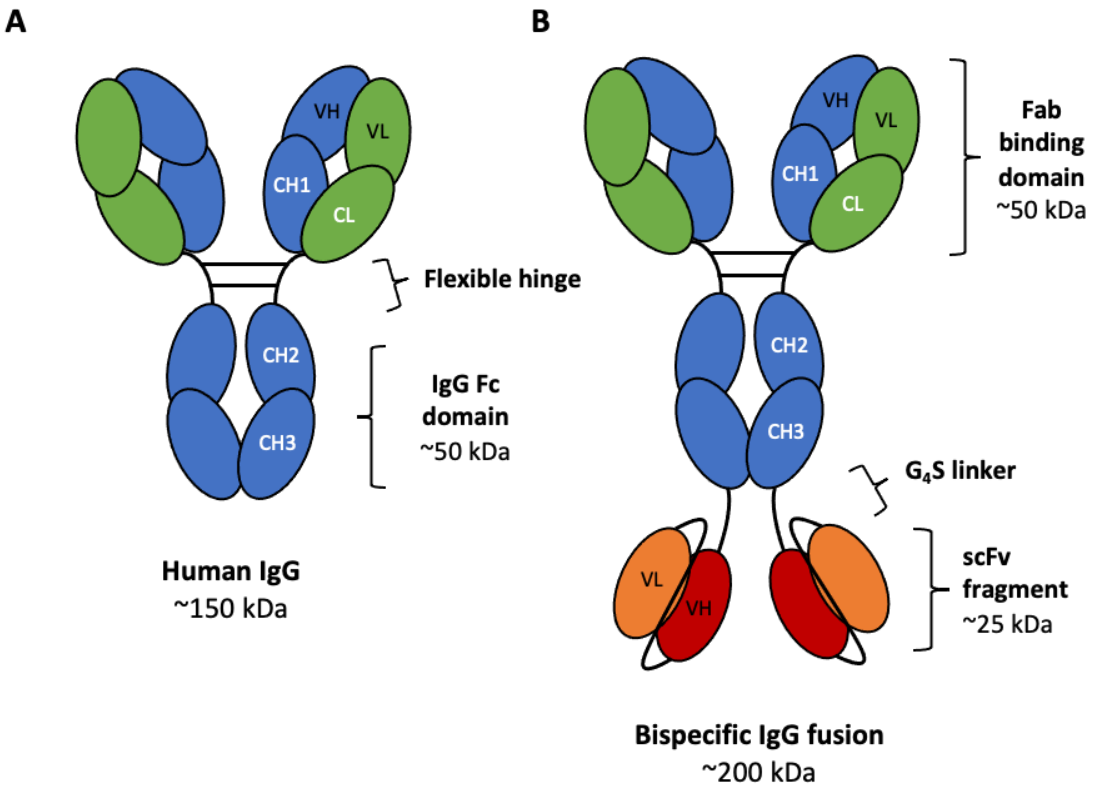

Figure 1.5 Schematic representation of IgG antibody and a bispecific IgG fusion
(A) Immunoglobulin domains from both heavy (blue) and light (green) chains combine to form an IgG with a molecular weight of 150 kDa. (B) Fusion of a single chain variable region (scFv) fragment of a second antibody (red/orange) via a flexible polypeptide linker (G_4S) to the C-terminal end of the IgG heavy chain generates a bispecific fusion antibody approximately 200 kDa in size.

However, the large molecular weight of IgG antibodies, at ~150 kDa, severely restricts their delivery across the BBB, as mentioned in Section 1.1.2. Thus, with this limitation in mind, antibodies that target specific receptors on brain endothelial cells, called "Molecular Trojan-horses", have been developed to increase delivery of therapeutic antibodies to the brain parenchyma (Pardridge, 2017, 2012). Natural antibodies are monospecific, recognising a single antigen, however antibodies which can recognise multiple antigens provide a broader spectrum of applications within both a therapeutic and diagnostic setting. Bispecific, or multivalent, antibodies are artificial molecules created through molecular or genetic approaches and can be found in a variety of formats (Brinkmann and Kontermann, 2017). In this thesis, the most important bispecific format is the Bis3 format (Oganesyan et al., 2008), where a variable binding domain, consisting of a V_H and a V_L, is formatted into a single polypeptide chain (scFv) and fused to the C-terminal end of the heavy chain via a flexible peptide linker (Figure 1.5B).

1.6.2 IgG transport at the brain endothelium

The neonatal Fc receptor, FcRn, is the only Fc receptor expressed on brain endothelial cells and has been shown to regulate transcytosis across the BBB by facilitating active efflux, or recycling, of IgG from the brain to the blood (Schlachetzki et al., 2002; Zhang and Pardridge, 2001a). IgG transcytosis in BMVEC-like cells *in vitro* is Fc-independent and non-saturable suggesting that FcRn does not contribute to this pathway (Ruano-Salguero and Lee, 2020). Recent evidence suggests that pericytes may also be involved in controlling IgG transcytosis, with pericyte knock-out resulting in significant detection of parenchymal IgG following peripheral administration (Villaseñor et al., 2016).

Interactions of IgG with FcRn are directly linked to serum half-life with deletion of the beta-2 microglobulin subunit of FcRn resulting in extremely short half-life (Ghetie et al., 1996; Ward and Ober, 2018). Internalisation, through fluid phase pinocytosis, IgG is trafficked to the early endosome. The acidic environment of the early endosome allows for enhanced binding of FcRn to IgG, sorting away from lysosomal degradation and promotes antibody recycling (Junghans and Anderson, 1996; Roopenian et al., 2014). The circulating half-life of IgG is roughly 10-21 days, and is mediated by binding of an IgG via its Fc domain, and alterations to this Fc domain aimed at promoting FcRn interactions results in enhanced serum persistence compared to an unaltered IgG (Ghetie et al., 1997). Furthermore, the lower the affinity of an IgG for FcRn the shorter the half-life in mice (Medesan et al., 1997). However, there has been recent evidence that suggests that this is not always the case (Datta-Mannan et al., 2007; Gurbaxani et al., 2006). Human FcRn shows very stringent binding compared to mouse FcRn, with human, mouse, rat, guinea pig and rabbit IgG subtypes binding to mouse FcRn, but only human IgG, rabbit and guinea pig IgG binding to human FcRn (Ober et al., 2001). Interestingly, binding of human IgG to mouse FcRn is of greater affinity than with its endogenous human FcRn (Ober et al., 2001). This would suggest that human Fc region-containing antibodies would have a prolonged serum half-life when used in mice and therefore provide valuable preclinical pharmacokinetic data.

1.6.3 Transferrin receptor as a target for CNS delivery

There are two types of macromolecule transport across brain endothelial cells: receptor-mediated transcytosis (RMT) and non-selective adsorptive transcytosis, with clathrin-coated vesicles considered the main form of internalisation (Ayloo and Gu, 2019; Pulgar, 2019). Endocytic activity and the frequency of RMT at the level of the BBB is relatively downregulated compared to other endothelial cells and many factors contribute to successful transcytosis (Preston et al., 2014; Stewart, 2000). Recycling and degradation of receptor-ligand complexes is dependent on endosomal sorting, through the early endosome or recycling endosomes for exocytosis (Thompson et al., 2007), and regulatory cues, such as geometry and pH (Cullen and Steinberg, 2018). However, there are still some receptors capable of transporting large molecules across the BBB through initiation of RMT, including transferrin receptor type 1 (TfR), insulin receptor (InsR) and low density lipoprotein receptor-related protein 1 (LRP1) (Preston et al., 2014). InsR and TfR are two of the most studied receptors for the clinical development of RMT to deliver therapies to the CNS; however, here, I will focus on TfR (Lajoie and Shusta, 2015; Paterson and Webster, 2016).

1.6.3.1 Transferrin receptor-mediated transcytosis at the BBB

The transferrin receptor type 1 (TfR) is a transmembrane glycoprotein that consists of two disulfide linked 85-kDa subunits that is involved in the transport of iron across membranes via RMT. The exact mechanism and kinetics by which iron is transported across brain endothelial cells has yet to be fully elucidated, but it could be through both transferrin (Tf)-dependent and Tf-independent mechanisms (Burdo et al., 2003; Khan et al., 2018). It has been proposed that Tf-bound iron, or holo-Tf, undergoes RMT at the level of brain microvascular endothelial cells (BMVECs) (Descamps et al., 1996; Fishman et al., 1987). However, it is unclear what percentage of TfR itself actually transcytoses across to the abluminal surface or recycles back to the luminal side, with varying reports suggesting a major role of recycling or transcytosis for the transport of iron (Morris et al., 1992; Raub and Newton, 1991). The first experiments to investigate the transport of iron at the BBB were conducted by Fishman and colleagues where they observed initial increases in microvascular radioactivity after perfusion of rat brain with iodinated Tf, and

that after a longer duration this increased radioactivity was observed in the non-vascular compartment (Fishman et al., 1987). Moreover, the addition of cold excesses of Tf resulted in a ~65% decrease in microvascular and ~75% decrease in non-vascular radioactivity, suggesting a receptor-mediated uptake and transcytosis process within brain endothelial cells for Tf (Fishman et al., 1987). Descamps and colleagues report that in co-cultures of bovine brain capillary endothelial cells 10% of Tf was recycled to the luminal side, using pulse-chase experiments, and there was no evidence of degradation suggesting that the majority of Tf is transcytosed to the abluminal membrane (Descamps et al., 1996). In contrast, Raub and Newton showed that accumulation of fluid-phase tracer in primary cultures of bovine brain microvessel endothelial cells identified recycling of Tf-TfR complexes towards the luminal side, 48% of radiolabelled-Tf was present after washing in the luminal side of a transwell compared to 15% in the abluminal side (Raub and Newton, 1991). This suggests that transcytosis of Tf is minimal within brain endothelial cells and might not be the dominant pathway for iron transport. In support of this, Morris and colleagues, showed using autoradiography studies, that there is minimal uptake of iodinated Tf after 24 hours and that there was no real regional distribution (Morris et al., 1992). They suggested that this represents a lack of a transcytotic mechanism for Tf at the level of the brain endothelium, which is at odds with previous reports from Fishman and colleagues.

Furthermore, there is increasing evidence to suggest that iron itself dissociates from Tf early during endocytosis of the TfR-Tf complex and its transport therefore diverges from the fate of TfR within the cell (McCarthy and Kosman, 2013, 2012). Binding of Tf to its receptor induces endocytosis, thus facilitating the movement of iron into the cell and eventually the cytosol (Figure 1.6). The change in pH between lysosomal and endosomal compartments results in dissociation of iron from Tf and from there iron can leave the cell via ferroportin. Once iron has dissociated from Tf, the receptor is believed to be recycled to the cell surface and available to bind another Tf molecule and undergo the process again (McCarthy and Kosman, 2015).

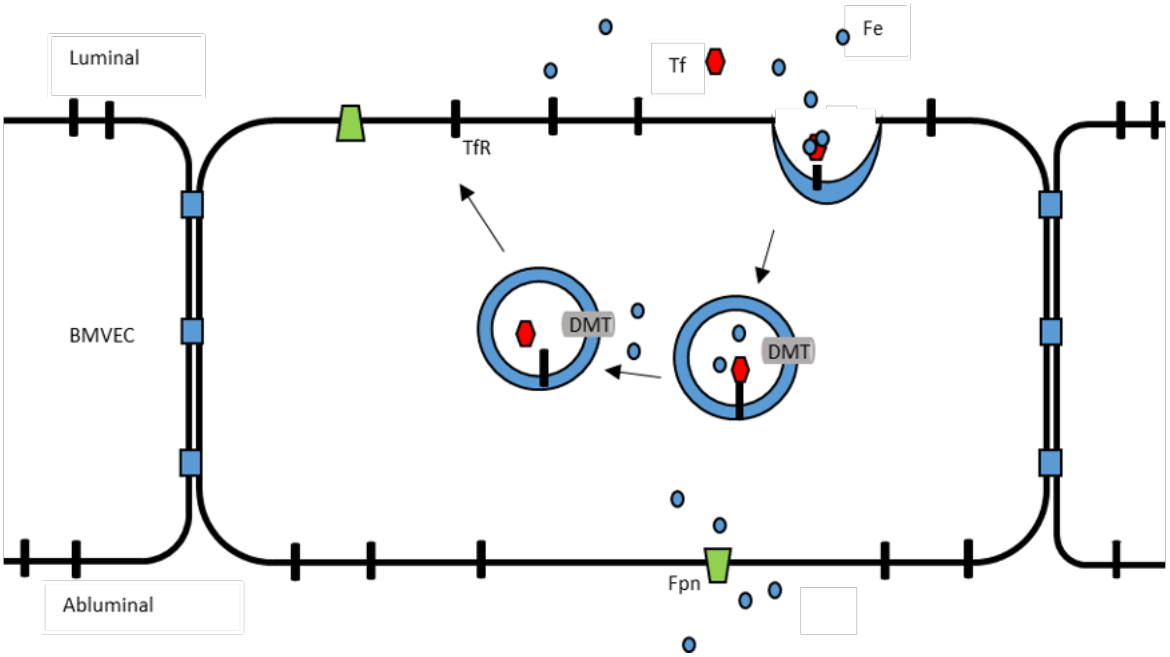

Figure 1.6 Schematic representation of iron transport across brain endothelial cells via TfR-mediated transcytosis

Iron trafficking can occur via binding of Fe^{2+} to transferrin (Tf) and of holo-Tf to the transferrin receptor on the luminal side of brain endothelial cells (BMVECs). Endocytosis of the receptor results in a change in pH and the dissociation of Fe^{2+} from Tf. Fe is transported out the endosome via the divalent metal transporter 1, where it can accumulate in the cytosol. Iron efflux can occur through ferroportin on both the luminal and abluminal membranes of BECs, where it is converted to Fe^{3+} for utilisation. Abbreviations: DMT, divalent metal transporter 1; Fpn, ferroportin.

Regardless of the mechanism by which TfR mediates iron transport across brain endothelial cells, with expression of TfR on both the luminal and abluminal sides of endothelial cells, movement of anti-TfR antibodies is possible from both blood-to-brain and brain-to-blood (Huwyler and Pardridge, 1998; Zhang and Pardridge, 2001b). TfR is thought to be continually internalising and recycling, a process that is rapid and independent of Tf binding, and this leads to a huge pool of available receptors, with BMVECs expressing an estimated 100,000 TfR molecules on their plasma membrane (McCarthy and Kosman, 2015; Raub and Newton, 1991). Thus, levels of available antibody delivered to the parenchyma will be dependent on the relative luminal and abluminal expression of the receptor, as well as the rates of receptor internalisation and transcytosis. Combined these features with the ability to cross BMVECs and deliver iron to the brain, TfR is an attractive target for delivering therapeutics to the CNS to treat neurodegenerative diseases, such as AD and PD.

1.6.4 Antibody engineering for enhanced brain penetration

Previous studies have shown effective delivery of antibodies that target both mouse TfR (mTfR) and a therapeutic target (e.g., beta site APP cleaving enzyme 1; BACE1), each through a single Fab arm, into the brain parenchyma and a dose-dependent reduction in brain and plasma Aβ levels in mice injected with Anti-TfR/Anti-BACE1 antibodies compared to Anti-BACE1 antibodies (Couch et al., 2013; Yu et al., 2011). It has also been shown that there is an inverse relationship between the affinity of an antibody binding domain for mTfR and its ability to effectively penetrate the brain parenchyma (Yu and Watts, 2013). A modified antibody with lower affinity for mTfR, Anti-TfR^{D}, showed increased brain penetration compared to control IgG and an antibody with higher affinity for mTfR, Anti-TfR^{A} (Yu et al., 2011). Brain penetrance can be measured by multiple methods and the two most used methods are: a ratio of brain-to-serum concentration of antibody (brain/serum ratio) or percentage of injected dose per gram of brain (%ID/g brain). There is some potential confusion when making comparisons between reported values of brain penetrance depending on the method used. Anti-TfR^{D} showed a 5.66-fold increase in brain penetration over control IgG, measured using brain/serum ratio, after 24 hours and a 2.24-fold increase over a high affinity anti-TfR antibody, Anti-TfR^{A} (Yu et al., 2011). However, these fold-changes differ when %ID/g brain is used, becoming a four-fold increase and a three-fold increase respectively (Yu et al., 2011). Reports of therapeutic antibodies that show brain penetration have referred to brain/plasma ratios of 0.1-0.2%, however they are actually citing CSF/plasma ratios (Atwal et al., 2011; Bohrmann et al., 2012). Furthermore, reporting of CSF drug penetration comparative to plasma levels following i.v. administration is not reflective of parenchymal drug penetration. The blood-CSF barrier is leakier than the BBB and drugs in the plasma can passively distribute into the CSF, where the resulting CSF/plasma ratio does reflect the reported values at 0.22% (Pardridge, 2020a). Distribution of antibodies following i.v. injection and measurement in the brain, not the CSF, results in a ratio that is approximately 10-fold lower, and has been reported as low as 0.01% (Pardridge, 2020b; Yadav et al., 2017). These discrepancies between plasma/CSF ratios and brain/CSF ratios could confound reports and give a slightly biased view towards the extent of brain penetrance achieved by an antibody. Correcting for volume of distribution, by using %ID/ g brain, avoids misrepresenting parenchymal delivery as may be suggested with plasma/CSF ratio, and better reflects

influx for antibodies with protein targets in the brain, where retention may be expected (Bickel, 2005). However, this approach is technically more difficult as even small amounts of remaining blood following perfusion of the brain can result in vast overestimates of brain concentrations.

Niewoehner and colleagues showed that antibodies bivalent for TfR can reduce cell surface expression of TfR in a time- and concentration-dependent manner (Niewoehner et al., 2014). Extracellular expression was affected within one hour of exposure to the bivalent antibody, and that both extracellular and total TfR expression levels were decreased after 24 hours. These changes in expression levels are partly caused by the bivalent anti-TfR antibodies causing a switch in lysosomal trafficking of TfR which results in degradation of the receptor in lysosomes, and thus prevents the normal recycling of the receptor back to the cell membrane (Niewoehner et al., 2014). An antibody monovalent for TfR showed increased transcytosis and target engagement compared to a bivalent anti-TfR antibody after treatment with equimolar concentrations (Niewoehner et al., 2014). Overall, these data helped to confirm a theory that an antibody targeted against TfR could be used as a potential therapy for diseases that require access to the brain parenchyma, and that relative affinity of such antibodies for their RMT target may influence their penetrance and as a result their therapeutic efficacy.

Research is still ongoing to produce clinically effective antibodies that utilise such mechanisms for entry to the brain with delivery of therapies across the BBB has not just utilised antibodies targeting TfR, but also peptide sequences and coating of liposomes or nanoparticles (Clark and Davis, 2015; Gregori et al., 2016; Wiley et al., 2013). However, recent advances into the clinic have shown safety and efficacy for RMT-mediated therapies in patients with mucopolysaccharidosis (MPS) Type I and II (Giugliani et al., 2018; Okuyama et al., 2020, 2019; Pardridge et al., 2018a; Sonoda et al., 2018). Preclinical studies have used the TfR system in various models of AD with the generation of a fusion protein against both TfR and Aβ (cTfRMAb-scFv) resulting in a 58-fold increase in delivery to the brain compared to an antibody without TfR specificity (Boado et al., 2010). This same fusion protein was also shown to effectively reduce levels of A$\beta_{1\text{-}42}$ in the brains of 14-month-old APP/PS1 mice after 24 injections over three months (Qing-hui Hui Zhou et

al., 2011). Generation of an antibody with monovalent binding to TfR and bivalent target engagement with Aβ, sFab-mAb31, resulted in increased binding to amyloid plaques in the brains of PS2-APP and a reduction in plaque number after chronic 14-week treatment compared to a control anti-Aβ antibody which lacked TfR binding (Niewoehner et al., 2014). In 6-month old APP/PS1 mice, weekly injection of a BBB-penetrant anti-TNF fusion protein resulted in decreased brain protein levels of $A\beta_{1-42}$ compared to a non-BBB penetrant anti-TNF fusion protein (Chang et al., 2017). Furthermore, a bispecific anti-TfR-BACE1 antibody showed a four-fold increase in brain penetration compared to an anti-BACE antibody at 24 hours after intravenous injection, which also produced a significant decrease in brain $A\beta_{1-40}$ levels in naïve C57Bl/6 mice (Yu et al., 2011). In addition to increasing delivery of therapies in models of AD, anti-TfR fusion proteins have been shown to reduce mechanical hyperalgesia in a model of neuropathic pain by increasing brain delivery of an anti-TfR-IL-1RA fusion compared to a non-BBB penetrant control (Webster et al., 2017). This experimental approach of enhancing delivery of antibodies across the BBB through targeting TfR, as well as a therapeutic target, provides us with a method of being able to assess the individual effects of both systemic and central proinflammatory cytokine expression.

1.7 Complications of antibody delivery with BBB breakdown

One aspect of CNS disorders that could potentially complicate delivery of antibodies is the breakdown of the BBB. In relation to RMT-targeted antibodies, BBB breakdown may cause altered expression of the intended target or result in bypass of the system if the breakdown was severe. These potential changes could result in RMT-targeting becoming a limiting factor in target engagement and effective therapy. Systemic inflammation, as well as being implicated in the progression of certain CNS disorders, has also been shown to cause histological and molecular changes in the BBB that result in both disruptive and non-disruptive BBB changes (Table 1.2) (Varatharaj and Galea, 2017). Some of these changes are relevant to disease pathology, such as a decrease in Aβ efflux caused by downregulation of LRP1 and accelerated Aβ deposition, and thus may explain a role for

inflammation in progression of certain diseases, such as AD (Erickson and Banks, 2013; Jaeger et al., 2009; Takeda et al., 2013; Weintraub et al., 2014).

Table 1.2 Distinctions between disruptive and non-disruptive changes that can occur during systemic inflammation

Disruptive BBB change	Non-disruptive BBB change
Usually occurs at a histological level	Usually occurs at a molecular level
Visible change in histological architecture	No visible change in histological architecture
Change in anatomy	Change in function
Detected using inert tracers	Not detected with inert tracers
Generally, not substrate-specific	Substance-specific
Not a prerequisite for cellular traffic; can happen because of intense cellular traffic	Main mechanism underlying changes in cellular traffic
Changes may include alterations in tight- and adherens junctions, denudation of glycocalyx, damage to endothelial cells and astrocytopathy, evidence of re-introduced fenestrae, breakdown of glia limitans, increased vesicular traffic	Changes may include cytokine production by endothelial cells, upregulation of endothelial cell receptors and transporters, enhanced pathogen neuroinvasion, modulation of astrocyte function

1.7.1 BBB breakdown in models of neurodegeneration

As murine prion diseases possess characteristics of dementia and related neurodegenerative diseases, it is interesting to see how the BBB is affected in other models of dementia; for example, in murine models of AD there are disparate reports of BBB breakdown (Ulrich et al., 2015). Bien-Ly and colleagues report that in various models of AD, there is a lack of BBB breakdown to molecules of varying permeability, with sizes ranging from 86 Da and expected permeability up to 150 kDa and no permeability, being vastly spared independent of age and genotype (Bien-Ly et al., 2015). To confirm BBB breakdown, Bien-Ly and colleagues utilise a model of multiple sclerosis (MS), experimental autoimmune encephalitis (EAE), as a positive control of BBB breakdown. Using this model, they establish that antibody penetration, after dosing of a bispecific Anti-TfR^{D}/BACE-1 in the cortex is 10-fold greater than control IgG in naïve mice and between two-to-three-fold greater in EAE. They also studied levels in spinal cord and

contrastingly, there was more control IgG than TfR-targeted antibody in EAE mice, and they use this to suggest greater barrier dysfunction that leads to increases in passive movement of antibodies (Bien-Ly et al., 2015). However, at no point do the authors consider the possibility of bidirectional transport of TfR-targeted antibodies and thus their quantification of brain penetration may underestimate the uptake of antibody in these mice. Concomitantly, respective increases in cortical and decreases in spinal cord TfR levels may account for the disparate findings between the two compartments (Bien-Ly et al., 2015). In the PS2-APP transgenic mouse model of AD, Bien-Ly and colleagues determine BBB permeability using radiolabelled tracers, including 3-kDa and 67-kDa dextran, at two different time-points: at 5-6 months where there is limited plaque deposition and at 15-16 months where there is extensive plaque deposition. There was no detectable difference between levels of radiotracers between young and old PS2-APP mice when compared to their respective wild-type controls, and no effect of ageing either (Bien-Ly et al., 2015). Further investigation in 10-13-month-old PS2-APP mice and WT controls showed a four-fold increase in brain-penetration with a TfR-targeted antibody compared to control IgG, thus providing evidence that TfR-mediated uptake remains unaffected in this disease model (Bien-Ly et al., 2015). These data were replicated in human tau P301L and human tau P301S models of tauopathy, suggesting that many frequently used mouse models of neurodegeneration have a functionally intact BBB (Bien-Ly et al., 2015).

Recent reports from AD patients carrying risk-associated alleles for the *APOE* gene suggest that there is evidence for increased BBB breakdown as a result of pericyte loss (Halliday et al., 2015). In addition, Minogue and colleagues were able to show increased BBB permeability in an APP/PS1 transgenic mouse model of AD using gadolinium-enhanced contrast magnetic resonance imaging (Minogue et al., 2014). Minogue and colleagues report both an increased permeability of a low molecular weight gadolinium salt (545 Da) in transgenic mice compared to wild-type controls, as well as a significant increase in BBB permeability of 24-month old transgenic mice compared to 14-month old transgenic mice, suggesting an age-related component of BBB permeability (Minogue et al., 2014). In accordance with Minogue and colleagues, Montagne and colleagues have shown through analysis in humans that there is an age-dependent breakdown of the BBB in the hippocampus and that this breakdown, especially in the CA1 and dentate gyrus,

worsens with MCI and injury of pericytes (Montagne et al., 2015). These data combined suggest that BBB breakdown that may be present in AD may associated with smaller molecules and therefore would not affect RMT-targeted immunotherapies.

1.7.2 Transferrin receptor and BBB breakdown in disease models

Autoradiography studies have shown, through the binding of Tf, high expression levels of TfR in the hippocampus and cortex of the rodent brain (Hill et al., 1985; Morris et al., 1992). Kalaria and colleagues showed that there is differential binding of iodinated-Tf across various regions of the human brain, with white matter and substantia nigra showing decreased binding compared to the hippocampus (Kalaria et al., 1992). Furthermore, it was shown that there were no significant differences in iodinated-Tf binding on isolated cerebral microvessels between AD subjects and age-matched controls (Kalaria et al., 1992). However, these vessels were isolated from the frontal cortex and thus any regional differences between the frontal cortex and disease-related regions would not have been detected. A more recent study assessed TfR protein levels using western blot in cortical tissue from mouse models of neurodegeneration – including human tau P301L and P301S tauopathy models and the mutant superoxide dismutase 1 ($SOD1^{G93A}$) model of amyotrophic lateral sclerosis – and in all models protein levels of TfR were similar to those observed in wild-type littermates (Bien-Ly et al., 2015). In addition, western blot analysis to assess TfR protein levels in the entorhinal cortex of human AD patients showed there was no difference in TfR protein levels compared to age-matched controls (Bien-Ly et al., 2015). Importantly investigation into the effects of neuropathology on TfR expression, showed that in the 3xTg-AD mice there was no difference in protein expression on brain endothelial cells, nor an effect on internalisation, compared to age-matched controls (Bourassa et al., 2019). As a result, these data suggest that TfR proves to be a useful target for delivery of antibodies into the brain parenchyma, especially if that delivery could be to disease relevant regions such as the hippocampus, and as its expression is not compromised in disease state this would not be a limiting factor in target engagement.

However, analysis of microarray data from Lunnon and colleagues shows that *Tfrc*, the gene encoding for TfR, hippocampal/thalamus transcript levels are significantly decreased

in ME7 mice at 18 wpi compared to NBH controls (Lunnon et al., 2011). This decreased *Tfrc* expression is exacerbated by systemic inflammatory challenge with a greater decrease in expression in ME7 mice 6 hours after LPS injection (Lunnon et al., 2011). BBB breakdown has been shown after systemic LPS challenge in ME7 mice by staining for mouse IgG, where there is clear extravasation of mouse IgG that is not seen in NBH mice treated with LPS (Lunnon et al., 2011). Moreover, magnetic resonance imaging of juvenile rats that received a unilateral injection of IL-1β (1 ng/μl) into the striatum showed a significantly reduced apparent diffusion coefficient of administered contrast agent compared to contralateral controls from 6 hours after injection, that remained reduced up to 5 days after injection (Blamire et al., 2000). Therefore, as BBB breakdown with live infection has not been described in the literature for ME7 mice nor other models of neurodegeneration, there is a need to establish any potential complications with brain penetration of TfR-targeted therapeutic antibodies in a translationally improved model of systemic inflammation. TfR is an attractive target for enhanced brain penetrance, and it is critical to understand whether TfR expression is altered in the context of neurodegeneration as this would limit its application and efficacy within the clinic. Furthermore, downregulation of expression resulting from systemic inflammation would also impact on enhanced brain delivery and the ability for neutralisation in both the periphery and the brain.

1.8 Summary and Objectives

In conclusion, there is evidence to suggest a role for inflammation in the progression of neurodegenerative diseases, such as AD, e.g., systemic inflammation increases rate of cognitive decline. To model this effect, I have selected the ME7 prion model and *S. typhimurium* as models of neurodegeneration and chronic systemic inflammation respectively. These models are suitable for the testing of potential therapeutics, such as neutralisation of TNF-α. When addressing CNS disorders central neutralisation of cytokines may further enhance the potential benefits for patients. Therefore, the development of antibodies engineered to cross the BBB and increase central target engagement provide an interesting tool for the treatment of neurodegenerative diseases. The main aim of this thesis is to identify a suitable cytokine target in inflammation and

neurodegeneration and test the hypothesis that intervention with a brain-penetrant anti-cytokine fusion protein could beneficially alter disease progression in a model of neurodegeneration alone or with additional systemic inflammation.

1.8.1 Hypothesis

Both neuroinflammation and systemic inflammation contribute to progression of neurodegenerative diseases. In addition, central activity of therapeutic antibodies is limited by the BBB. Therefore, I hypothesise that the targeting of TNF-α using a brain-penetrant antibody-fusion protein in a model of neurodegeneration would alter disease progression, and in the presence of systemic bacterial infection.

1.8.2 Aims

1. To investigate the effect of systemic inflammation in the ME7 prion model of neurodegeneration

2. To generate, purify and characterise a BBB-crossing anti-mTfR-anti-TNF-α fusion protein

3. To establish the efficacy of anti-TNF-α therapy in the ME7 prion model of neurodegeneration

4. To investigate whether anti-TNF-α therapy can reduce the impact of systemic inflammation on neuroinflammation and neurodegeneration.

Chapter 2 Methods

2.1 *In vivo* experiments

2.1.1 Experimental animals

Mice were housed in groups of four to six, under a 12-hour/12-hour light-dark cycle at 19-23°C, with water and normal chow diet (RM1, SDS) *ad libitum*. All procedures had local ethical approval and were performed in accordance with Home Office project licences (30/3056, 30/3057, P4155EEE0) under the United Kingdom Animals (Scientific Procedures) Act (1986). All mice detailed in the following experiments were of the strain C57BL/6. Both male and female mice were used, but only same sex mice were used in each experiment. All mice were maintained at the Biomedical Research Facility, Southampton General Hospital, Southampton, UK.

2.1.2 Stereotaxic surgery

Brain homogenate (10% w/v), derived from either normal brain (NBH) or from endpoint ME7 prion-injected mouse brain (ME7), was directly injected into the dorsal hippocampi of mice using a stereotaxic frame. Mice were anaesthetised with a ketamine/rompun mixture (85 mg/kg and 13 mg/kg), and the incision area was shaved with hair clippers (Wella) and sterilised with 70% alcohol. Lacri-lube (Allergan) was applied to each eye to prevent drying that comes from the removal of the blink reflex under anaesthesia. The mouse was fitted to a stereotactic frame (Knopf instruments) using 45° atraumatic ear bars and an incisor bar (Knopf Instruments). A sagittal incision was made exposing the skull, allowing for the location of bregma and burr holes were drilled bilaterally into the skull using a dentist's drill, taking care not to damage the dura mater, at the appropriate coordinates: 2.0 mm posterior to bregma and ±1.7 mm lateral to the midline. A Hamilton syringe with a 26s-gauge needle (Hamilton) was inserted into the brain to a depth of 1.6 mm, and 1 µl of brain homogenate was injected at a flow rate of 1 µl/minute. The needle remained in place for two minutes to allow for bolus diffusion, before being slowly removed. The incision was closed with sutures before the mice were placed in a heated

chamber to recover. After recovery, mouse appearance was regularly checked over the following week, and weights were measured weekly thereafter, to ensure animal welfare was maintained.

2.1.3 Behavioural assessments

2.1.3.1 Burrowing

Plastic cylinders, 20 cm long and 6.8 cm in diameter, were filled with 190 g of normal chow food pellets (RM1, SDS) and placed in the cages. Mice were habituated once with a full tube in a group cage and then twice in individual cages with a full burrowing tube before weekly testing. For testing, mice were placed individually in cages overnight (16-18 hours total), and the remaining pellets at the end of each session were weighed and the amount displaced ("burrowed") was calculated. The mice were returned to their home cage after testing. Relative weight of pellets burrowed across successive weeks was compared to initial baseline and presented as percentage of baseline.

2.1.3.2 Automated open field locomotor activity

The open field tests were performed in ENV-510 chambers using Activity Monitor 5 software (Med Associates Inc.). The open field consisted of an aluminium base (27 x 27 cm) enclosed on four sides by 0.7 cm thick acrylic sheet with attached infrared sensors and surrounded by an opaque screen. The mice were placed in the corner of individual boxes, with this motion starting a recording period of 5 minutes, to measure the time ambulatory (seconds) and total distance travelled (cm). Analysis of total distance covered was controlled by measuring changes in average speed as an internal control of motor abilities. Mice were habituated to the open field box prior to weekly testing, with 2 x 5 minutes exposures on two consecutive days one week before the first session.

2.1.3.3 Manual Open field locomotor activity

Due to restrictions in Containment Level 2 facilities at the Biomedical Research Facility, no computer equipment was available for use. The open field tests were performed using the chambers for automated activity recordings (see Section 2.1.3.2). A camera was set up above the chamber with the whole enclosure contained in the viewing frame. Video was recorded at a resolution of 720x480 pixels and 30 frames per second (FPS) on a mobile recording device. Analysis of open field video was carried out to obtain total distance travelled during each 5-minute session.

Videos were converted to MP4 format for downstream processing at a resolution of 480x270 pixels @ 30 FPS encoded as x264 with a constant rate factor of 21 using the open-source video transcoder Handbrake (v1.3.1; https://handbrake.fr). Videos were trimmed to 9000 total frames (300 seconds) from the placement of the mouse in the arena using the Delete Frame command (Image > Video Editing > Delete Frame) in Fiji (http://fiji.sc, built on ImageJ v2) (Rueden et al., 2017; Schindelin et al., 2012). Processed videos were analysed using a plugin for tracking objects, originally developed for *Caenorhabditis elegans* (http://www.phage.dk/plugins/wrmtrck.html), and a modified version of the Mouse Behavior Tracker macro (Appendix A2) (Nussbaum-Krammer et al., 2015; Tungtur et al., 2017).

2.1.3.4 Horizontal bar motor test

The test was performed on a 38 cm long metal bar with a diameter of 0.2 cm that was supported by wooden struts to a height of 49 cm over a padded bench surface. Mice were held by the tail and allowed to grip the centre of the bar with their front paws only. The tail was released, and time taken to fall off (60 seconds) or to reach one of the wooden supports (forepaw contact; maximum 60 seconds) was recorded. This test is known to assess motor ability, limb strength and coordination (Guenther et al., 2001).

2.1.3.5 Inverted screen task

The inverted screen is a 43 cm^2 wire mesh consisting of 12 mm^2 of 1 mm diameter metal wire, surrounded by 4 cm of wooden beam, to prevent the mouse from escaping the screen. Each mouse was placed in the centre of the square and the screen inverted over a two second period, with the head of the mouse declining first. The screen was steadily held 40-50 cm above a padded surface. The time at which the mouse fell of the screen was noted, or the mouse was removed after reaching a maximum time for the assay (120 seconds). This test is known to assess motor ability and limb strength (Guenther et al., 2001).

2.1.4 Injection of mice with fusion protein

Mice received an intraperitoneal (i.p.) injection with a brain-penetrant anti-TfR-TNF inhibitor fusion protein ($8D3_{130}$ hIgG1 TM ΔK-mTNFR2), a non-brain penetrant TNF inhibitor (NIP228 hIgG1 TM ΔK-mTNFR2), a brain penetrant control ($8D3_{130}$ hIgG1 TM) or an isotype control antibody (NIP228 hIgG1 TM) at an equimolar dose of 54 µM (for dilutions see Table 2.1). All fusion proteins were formulated in 25 mM sodium acetate, 175 mM sodium chloride, pH 5.0 (Acetate pH 5.0 buffer; see Appendix A1 for recipe) and this buffer was dosed to vehicle-treated mice at 6-8 ml/kg. All proteins were produced and purified at AstraZeneca (Cambridge, UK).

Table 2.1 Dilution of fusion protein for injection

Protein	Molecular Weight (Da)	Formulated Concentration (µM)	Dilution Factor	Buffer added to 1ml (µl)
NIP228 hIgG1 TM	147,086	82.26	1.523	523.4
NIP228 hIgG1 TM ΔK-mTNFR2	196,671	60.15	1.114	113.9
$8D3_{130}$ hIgG1 TM	148,059	83.07	1.538	538.4
$8D3_{130}$ hIgG1 TM ΔK-mTNFR2	197,610	63.76	1.181	180.8

2.1.5 Systemic inflammatory challenge

2.1.5.1 Injection with lipopolysaccharide

Mice received a single intraperitoneal (i.p.) injection of 100 μg/kg LPS (*Salmonella enterica* serotype abortus equi; L5886, Sigma) in non-pyrogenic saline. This dose of LPS was chosen for its ability to induce cytokine responses within the brain (Teeling et al., 2010, 2007).

2.1.5.2 Infection with *S. typhimurium* SL3261

For experimental conditions, mice received a sublethal intraperitoneal (i.p.) injection of 1 x 10^6 colony forming units (cfu) of a live-attenuated vaccine strain of *S. typhimurium* SL3261 – *his* G46 (del) *aro*A 554 (Peters et al., 2010) – diluted in 200 μl non-pyrogenic saline (Kent Pharmaceuticals), or saline-only as a control. For *in vivo* safety test of fusion protein administration, mice received an i.p. injection of 1.8 x 10^6 cfu in 200 μl non-pyrogenic saline. These doses were selected because they result in increased brain cytokine production (Püntener et al., 2012).

Mouse body weight and appearance were monitored daily for the first 7 days and then weekly until the end of the experiment. Mice were culled if they showed signs of significant distress, or they suffered a decrease in body weight of 15% or more. Experiments were performed in a Containment Level 2 Facility within the Biomedical Research Facility and in accordance with Health and Safety Executive regulations.

2.1.6 Perfusion of mice and tissue collection

Experimental mice were terminally anaesthetised with 500 μl rat Avertin [3% (w/v) 2, 2, 2-tribromoethanol (Sigma-Aldrich, UK), 7.2% (w/v) ethanol (Fisher Scientific), 1.8% (w/v) tertiary amyl alcohol (Sigma Aldrich, UK) diluted in 0.9% w/v sodium chloride (Fisher Scientific)] by i.p. injection. The left atrium was punctured, and blood collected into sterile RNase/DNase-free Eppendorf tubes (Starlab). Mice were transcardially perfused with saline (0.9% sodium chloride w/v), or Dulbecco's PBS (D-PBS; Sigma Aldrich), containing 5 units per millilitre (U/ml) heparin sodium (CP Pharmaceuticals).

For immunohistochemistry, one hemisphere of brain was embedded in Optimal Cutting Temperature embedding medium (OCT; Fisher Scientific) and frozen on isopentane cooled on solid carbon dioxide. For qPCR, a coronal section enriched for the relevant brain region was taken, a tissue punch made and then snap frozen in liquid nitrogen. Blood was centrifuged at 4,000 x *g* for 10 minutes and serum was transferred to new Eppendorf tubes and stored at -20°C until use. Spleens of mice were weighed, to assess level of immune response following *S. typhimurium* infection, transferred to an Eppendorf tube and snap-frozen in liquid nitrogen before processing for ribonucleic acid (RNA) isolation, immunohistochemistry by dissection and embedding in OCT. All samples were kept at -80°C until use.

2.2 Ex vivo tissue analyses

2.2.1 Immunohistochemical analysis of mouse brain tissue

2.2.1.1 Sectioning of brain tissue

10 µm thick sections were cut from brains embedded in OCT using a cryostat (Leica) at -20°C to -16°C. Sections were transferred onto 3'-aminuteopropyltriethoxysilane (Sigma Aldrich) coated glass slides (Fisher Scientific, UK), which were air dried and then stored at -20°C until use.

2.2.1.2 DAB immunohistochemistry

Slides were thawed at 37°C for 40 minutes, fixed in 100% ethanol at 4°C for 10 minutes, before washing in PBS containing 0.01% (v/v) Triton X-100 (PBS-TX) on a rotating shaker platform for 3 x 5 minutes at room temperature (RT). Sections were isolated from each other using a hydrophobic barrier pen (Vector Laboratories). Endogenous peroxidase activity was quenched with PBS containing 1% (v/v) H_2O_2 (Fisher Scientific) for 10 minutes at RT. Sections were then washed 3 x 5 minutes in PBS-TX with shaking. Sections were blocked with 2% (w/v) bovine serum albumin (BSA) and 10% (w/v) normal animal serum (NAS) in PBS-TX for 60 minutes at RT. Sections were incubated with primary antibodies diluted 1:500 in PBS-TX (or PBS-TX only for controls) overnight at 4°C. Slides were then

washed 3 x 5 minutes in PBS-TX with shaking before incubation for 60 minutes at RT with secondary antibodies diluted 1:200 in PBS-TX. For NAS, primary and secondary antibody combinations see Table 2.2 below. Sections were washed 3 x 5 minutes in PBS-TX with shaking and then incubated with avidin-biotin complex (Vectorstain ABC Kit, Vector Laboratories) for 30 minutes at RT. Sections were washed 3 x 10 minutes in PBS-TX with shaking. Slides were then placed in 0.1 M phosphate buffer containing 0.05% (v/v) 3, 3'-diaminobenzidine (DAB; Sigma Aldrich) and 0.015% (v/v) H_2O_2 and reaction was developed until brown precipitate was visible, with no staining in control sections. Slides were counterstained with Harris haematoxylin (Sigma Aldrich) and differentiated in acid alcohol (70% (v/v) ethanol and 1% (v/v) HCl, both Fisher Scientific). Slides were dehydrated in increasing ethanol concentrations and xylene (Fisher Scientific) and mounted with DPX mounting medium (Fisher Scientific).

Table 2.2 Combinations of animal serum, primary and secondary antibodies used in DAB immunohistochemistry

Primary antibody	Clone/ Manufacturer (Product no.)	Primary host species	Animal Serum	Secondary antibody/ Manufacturer (Product no.)	Conjugate
CD11b	5C6/ ThermoFisher (MA5-16528)	Rat	Rabbit	Rabbit anti-rat IgG H+L/ Vector Laboratories (BA-4000)	Biotin
CD64/ FcγRI	AT152-9/ Bio-Rad (MCA5997)	Rat	Rabbit	Rabbit anti-rat IgG H+L/ Vector Laboratories (BA-4000)	Biotin
CD71/ TfR	YTA74.4/ ThermoFisher Scientific (MA1-80015)	Rat	Rabbit	Rabbit anti-rat IgG H+L/ Vector Laboratories (BA-4000)	Biotin
MHCII	M5/114.15.2/ ThermoFisher Scientific (14-5321-82)	Rat	Rabbit	Rabbit anti-rat IgG H+L (1:200)/ Vector Laboratories (BA-4000)	Biotin
NeuN	A60/ Chemicon (MAB377)	Mouse	Goat	Goat anti-mouse IgG H+L/ Vector Laboratories (BA-9200)	Biotin

2.2.1.3 Image analysis and quantification of staining

All images were captured using Leica Application Suite X software (Leica Microsystems). DAB immunohistochemistry images were taken on a Leica DM4B microscope and camera (Leica Microsystems). Quantification of DAB immunohistochemistry was performed using Fiji, built on ImageJ2 (Rueden et al., 2017; Schindelin et al., 2012). The average percentage area above threshold was determined using a colour deconvolution plugin (Ruifrok and Johnston, 2001). All DAB immunohistochemistry images were deconvoluted by splitting images into haematoxylin and DAB channels. The DAB staining was turned into a binary image, and a marker specific threshold was set. The threshold was selected from a random control image in which binary staining represented actual cellular staining. Quantification was automated using a custom macro (Appendix A3) and expressed as fold change of percentage area above threshold relative to control group.

2.2.2 Quantitative real-time PCR analysis of mouse brain samples

2.2.2.1 Total RNA isolation from mouse brain

For experiments involving bispecific mTNFR2 fusion protein treatment, total RNA was extracted from hippocampus/thalamus-enriched tissue using a Macherey-Nagel NucleoSpin RNA Isolation Kit (Fisher Scientific). 300 µl Buffer RA1 containing 1% β-mercaptoethanol (β-ME; Sigma Aldrich) was added to snap frozen hippocampal samples and the hippocampus was disrupted using a motorised pestle and then a further 300 µl RA1 buffer containing 1% β-ME was added. The lysate was transferred to a NucleoSpin filter column in a 2 ml collection tube and centrifuged at 11,000 x *g* for 1 minute. 1 volume of 70 % ethanol was added to the column flow-through and mixed by pipetting before transfer to a NucleoSpin RNA column. The mixture was centrifuged for 30 s at 11,000 x *g.* Column flow-through was discarded and column desalted ahead of DNA removal using 350 µl MDB solution. The column was centrifuged at 11,000 x *g* for 30 s. DNA removal mixture was prepared by adding 10 µl rDNase to 90 µl Reaction Buffer. 95 µl of DNA removal mixture was added to the NucleoSpin column and incubated at RT for 15 minutes. Column was washed with 200 µl RAW2 buffer and centrifuged at 11,000 x *g* for 30 s. NucleoSpin column was placed in a new collection tube and 600 µl RA3 buffer

was used to wash the column by centrifugation at 11,000 x *g* for 30 s. Flow-through was discarded before an additional 250 µl RA3 buffer was added to the column and centrifuged for 2 minutes at 11,000 x *g.* NucleoSpin column was then placed in a 1.5 ml RNase-free collection tube and 40 µl RNase-free water was added directly to the column membrane. RNA was eluted by centrifugation at 11,000 x *g* for 1 minute.

For all other experiments, RNA was extracted from homogenised hippocampus/thalamus-enriched tissue using the RNeasy Micro Kit (Qiagen). 300 µl Buffer RLT containing 1% β-ME was added to snap frozen hippocampal samples and the hippocampus was disrupted using a motorised pestle and then a further 300 µl RLT buffer containing 1% β-ME was added. Disrupted samples were added to QIAshredder homogenisers (Qiagen) and centrifuged for 3 minutes at 8,000 x *g*. 1 volume of 70% ethanol was added to the flow-through to precipitate RNA, which was then transferred to RNeasy MinElute spin columns and centrifuged for 15 s at 8,000 x *g*. Columns were washed with 700 µl of RW1 buffer and centrifuged for 15 s at 8,000 x *g*. Columns were then washed with 500 µl RPE buffer in 70 % ethanol centrifuged for 15 s at 8,000 x *g* and washed again with 500 µl RPE buffer in 70 % ethanol centrifuged for 2 minutes at 8,000 x *g*. Column was dried by transferring to a new collection tube and centrifuging for 1 minute at 8,000 x *g*. RNA was eluted in 30 µl RNase-free water and centrifuged 1 minute at 8,000 x *g*.

Sample concentrations were measured using a Nanodrop ND-1000 spectrophotometer (Fisher Scientific). Absorbance at 260 nm (A_{260}) was measured and converted to concentration (ng/µl) using the Beer-Lambert Law and the conversion factor: 1 A_{260} unit for ssRNA = 40 µg. Sample purity was determined using A_{260}:A_{280} and A_{260}:A_{230} ratios, with acceptable levels set at A_{260}:A_{280} above 1.80 and A_{260}:A_{230} above 1.90. Samples were stored at -80°C prior to further processing.

2.2.2.2 Reverse transcription PCR

For cDNA synthesis, all reagents were supplied by Applied Biosciences, unless stated otherwise. Reverse transcription (RT-PCR) was performed according to kit instructions for use with random hexamers. 10.4 µl of mastermix containing 1X RT buffer, 1.75 mM $MgCl_2$, 2.5 µM random hexamers, 2 mM dNTP mix (0.5 mM each), 1.0 U/µl RNase

inhibitor, and 2.5 U/µl Multiscribe RT was added to 0.2 ml PCR tubes (Starlab). 400 ng RNA diluted in 9.6 µl DNase/RNase-free water (Sigma Aldrich) was added to PCR tubes. Tubes were then placed in a Biometra UNO-thermoblock at 25°C for 10 minutes; 37°C for 30 minutes; 95°C for 5 minutes and then kept at 4°C. cDNA was diluted 1:5 in DNase/RNase-free water (Sigma Aldrich) and stored at -20°C until use.

2.2.2.3 Quantitative real-time PCR

Lyophilised primers, purified by desalting, were purchased from Sigma-Aldrich, and reconstituted to a 100 µM stock in DNase/RNase-free water and stored at -20°C. Primers were designed according to the specifications described in Table 2.3.

Table 2.3 Criteria used for design of primers using Primer-BLAST (NCBI)
One primer of each pair recognised an exon-exon boundary to prevent the amplification of genomic DNA

	Minimum	Optimum	Maximum
Product length (bp)	70		300
Melting temperature (°C)	57	60	63
Primer size (bp)	15	20	25
Max. self-complementarity	0	0	7
Max. self 3' complementarity	0	0	3
Primer GC content (%)	40	50	65

15 µl of mastermix containing 0.3 µM of forward and reverse primers (Sigma Aldrich) (Table 2.5) and 1X iTaq Universal SYBR green mastermix (Bio-Rad) in DNase/RNase-free water (Sigma Aldrich) was added to wells of a 96-well non-skirted low-profile PCR plate (Starlab). 5 µl of 1:5 diluted cDNA was added to each well in duplicate. DNase/RNase-free water without cDNA was added to wells as a negative control. Plates were covered with optical caps (Starlab) and placed in a C1000 thermal cycler with CFX96 detection module (both Bio-Rad). qPCR was carried out using the protocol outlined in Table 2.4, including generation of a melt curve in 0.2°C steps between 55°C to 90°C. Threshold cycle (Ct) values and melt curve traces for each sample were compiled to check specific primer amplification. Expression of the housekeeping genes, glyceraldehyde 3-phosphate dehydrogenase (*Gapdh*) or phosphoglycerate kinase 1 (*Pgk1*), were measured in each sample as a reference Ct value. Ct values for other genes were obtain and relative gene of

interest (GOI) expression levels were calculated by normalising GOI Ct values to reference Ct values using the formula:

$$\text{Relative expression} = 2^{-(Ct\ GOI - Ct\ ref)}$$

Fold change in expression in experimental animals was calculated by dividing relative expression by average expression of the control group.

Table 2.4 qPCR cycling conditions for expression of mRNA transcripts in mouse brain tissue

Step	Step type	Temperature (°C)	Time
1	Initial Denaturation	95	10 minutes
2	Denaturation	95	15 s
3	Annealing	60	60 s
4	Plate read; go to Step 2 – 49 times	-	-
5	Extension	72	10 minutes
6	Final denaturation	95	10 minutes
7	Melt curve – 0.2-degree steps	55 - 90	-
8	Cool	4	< 16 hours

Table 2.5 Primer sequences used for qPCR analysis of mRNA transcripts from mouse brain

Gene	Protein name/aliases	Strand	Primer Sequence (5' – 3')
Ccl2	Chemokine (C-C motif) ligand 2/ monocyte chemoattractant protein 1 (MCP-1)	Forward Reverse	AGCATCCACGTGTTGGCTC CCAGCCTACTCATTGGGATCAT
Gapdh	Glyceraldehyde 3-phosphate dehydrogenase	Forward Reverse	TCCACCACCCTGTTGCTGTA TGAACGGGAAGCTCACTGG
Grin2a	NMDA receptor subunit 2a	Forward Reverse	TTGTCTCTGCCATTGCTGTC ATATGGCTCCTCTGGGGCCT
Grm1	Metabotropic glutamate receptor 1 (mGluR1)	Forward Reverse	AGGCAAGGGCGATGCTTGAT AGCATCCATTCCACTCTCGC
Il1b	Interleukin 1-beta (IL-1β)	Forward Reverse	CAAAAGATGAAGGGCTGCTTCC ATGTGCTGCTGCGAGATTTG
Il6	Interleukin 6 (IL-6)	Forward Reverse	CTCTGCAAGAGACTTCCATCC TGAAGTCTCCTCTCCGGACT
Il10	Interleukin 10 (IL-10)	Forward Reverse	GGCCCAGAAATCAAGGAGCA ACAGGGGAGAAATCGATGACAG
Pgk1	Phosphoglycerate kinase 1	Forward Reverse	GTCGTGATGAGGGTGGACT TTTGATGCTTGGAACAGCAG
Syp	Synaptophysin	Forward Reverse	GAGAACAACAAAGGGCCAAT GCACATAGGCATCTCCTTGA
Tfrc	Transferrin receptor, type 1 (TfR)	Forward Reverse	TGGACATGCTCATCTAGGAACTG CCCTGATGACTGAGATGGCG
Tnf	Tumour necrosis factor alpha (TNF-α)	Forward Reverse	CGAGGACAGCAAGGGACTA GCCACAAGCAGGAATGAGAA

2.3 Recombinant production and purification of bispecific fusion proteins

Amino acid sequences for the heavy (V_H) and light (V_L) chain variable regions for cV1q, anti-TNF-α antibody, were kindly provided by Dr Cheng Chang (Massachusetts Institute of Technology, Boston, USA) and Prof. Peter Krammer (German Cancer Centre, Heidelberg, Germany). Primary sequences for constant and variable regions of antibodies and fusion proteins, along with physicochemical properties of the fusion proteins can be found in Appendix B.

All antibodies and fusion proteins discussed in this chapter were generated at AstraZeneca (Cambridge, UK) under the scheme outlined below and represented in Figure 2.1, with complete and comprehensive methodology reported in Section 4.2.

2.3.1 Assembly of expression vectors for bispecific fusion proteins

Genes coding for antibody variable domains or scFv fragments were codon optimised for expression in Chinese Hamster ovary (CHO) cells and designed and ordered from GeneArt. The genes from the GeneArt vectors were amplified by PCR (Section 4.2.1) for cloning into AstraZeneca expression vectors containing antibody constant regions. Antibody variable domains were cloned into their respective human IgG1 TM heavy (pEU1.4) or human kappa light chain (pEU3.4) constant region expression vectors using restriction enzyme digestion and ligation protocols (Section 4.2.1.2 and 4.2.1.3). Antibody scFv fragments were amplified by PCR using oligonucleotides containing overlaps with heavy chain expression vectors (Table 4.1) and assembled into expression plasmids using NEBuilder HiFi DNA assembly (Section 4.2.1.4). Expression vectors were checked for correct assembly of DNA using restriction enzyme digestion followed by separation and extraction from an agarose gel (Section 4.2.1.5). *E. coli* were transformed with expression vector known to contain the inserted sequences (Section 4.2.1.6) and screened for the presence of expression vector (Section 4.2.1.7). Expression vectors were extracted and purified from *E. coli* (Section 4.2.1.8) and the correct DNA sequence was confirmed by Sanger sequencing of the entire coding region using the oligonucleotides detailed in Table 4.6 (Section 4.2.1.9).

2.3.2 Expression and purification of bispecific fusion proteins

CHO cells were transiently co-transfected with heavy chain and light chain expression vectors at a final concentration of 1 μg/ml (Section 4.2.2.1). Seven days later CHO cells were removed by centrifugation and filtration, with IgG protein purified from the supernatant using Protein A-based affinity chromatography (Section 4.2.2.2). Selected protein-containing fractions were identified by ultraviolet (UV) absorbance at 280 nm, confirmed by sodium dodecyl sulphate–polyacrylamide gel electrophoresis (SDS-PAGE) (Section 4.2.2.4) and then pooled. If further purification was required, the pooled protein sample was separated by molecular weight using size exclusion chromatography (SEC) (Section 4.2.2.5) before being concentrated to the desired final concentration (Section 4.2.2.6). Final protein concentration was determined using UV absorbance at 280 nm on a Nanodrop ND-100 (Section 4.2.2.7). Proteins may be required in specific buffer formulations and samples were buffer exchanged as described in Section 4.2.2.3.

2.3.3 Characterisation and quality control of purified bispecific fusion proteins

Bio-layer interferometry (BLI) and/or AlphaScreen assays were used to confirm target binding *in vitro* (Sections 4.2.3.2 and 4.2.3.3). *In vitro* efficacy of mTNF-α neutralisation was measured using a mTNF-α-dependent murine L929 fibroblast cytotoxicity assay (Section 4.2.3.1). Fusion protein characteristics were determined using assays from the following panel of quality control tests: Limulus Amoebocyte Lysate (LAL) assay to quantify endotoxin levels (Section 4.2.4.1), high performance liquid chromatography (HPLC)-SEC to test for monomeric protein purity (Section 4.2.4.2) and ultra-performance liquid chromatography-mass spectrometry (UPLC-MS) for proteins that contain glycosylated residues (Sections 4.2.4.3).

Chapter 2

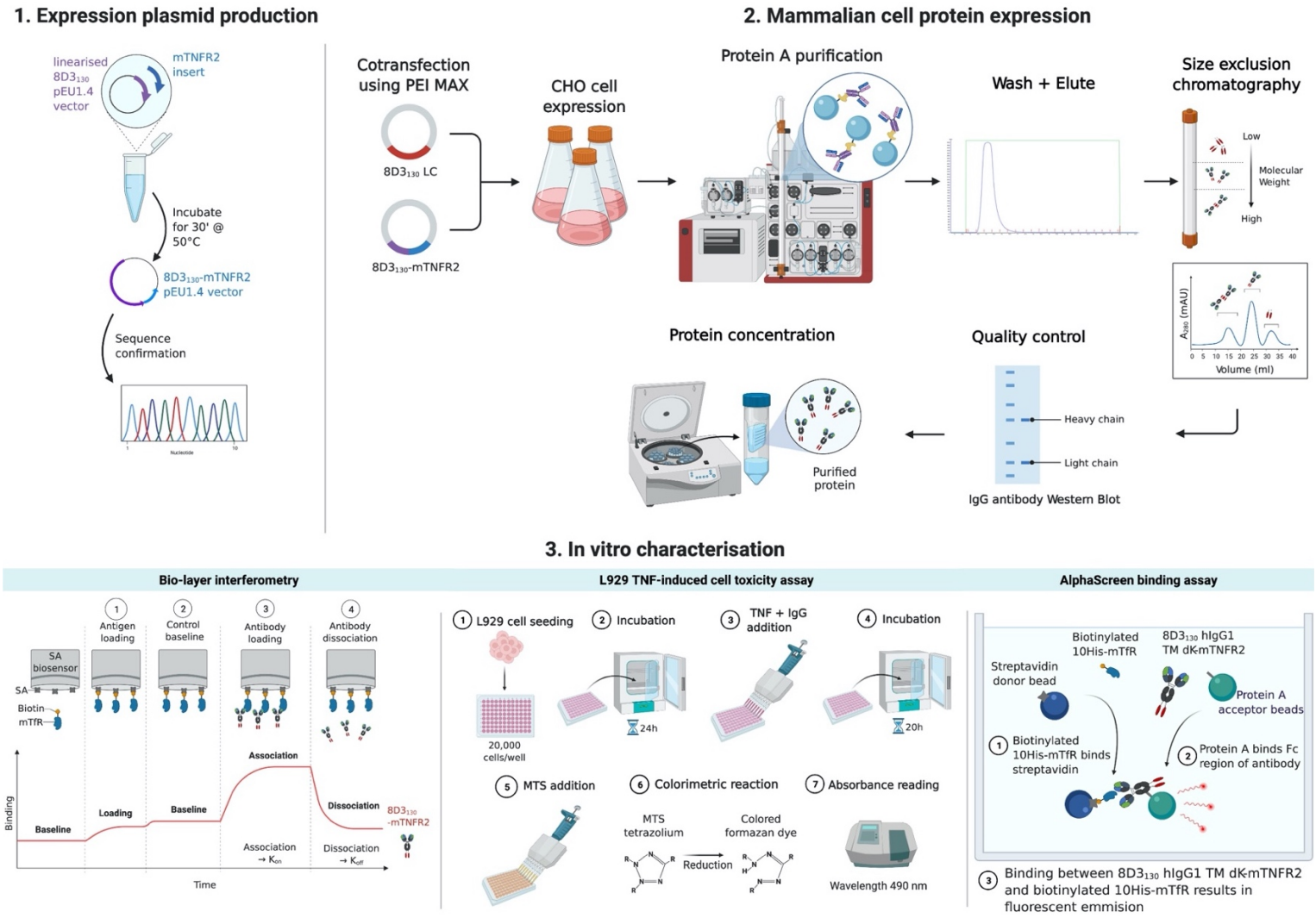

Figure 2.1 Schematic overview for protein production and characterisation of $8D3_{130}$ hIgG1 TM-mTNFR2

2.4 Statistical Analysis

Statistical analysis of data was performed using Prism 8 software (v 8.4.3, GraphPad). Data were first tested for normal and lognormal distribution using Shapiro-Wilk test. If data passed normality, they were analysed with appropriate parametric test depending on experimental design and number of independent variables – Students' t-test (between two groups), one-way analysis of variance (ANOVA) (for 3 or more groups with one independent variable); 2-way ANOVA (two independent variables). Holm-Sidak's multiple comparisons test was applied after a one-way ANOVA to reduce Type I error rates when comparing all groups to each other. For analysis of *in vivo* behavioural data, a 2-way repeated measures ANOVA was used to determine effects of both time and treatment on any changes with post-hoc analysis performed as appropriate.

If data failed normal distribution, but passed lognormality, data were log transformed and analysed with appropriate parametric test as described above. If normality was not met with log transformation, data were analysed using the appropriate non-parametric equivalent statistical tests – Mann-Whitney U for two groups or Kruskal-Wallis test for 3 or more groups with Dunn's multiple comparisons test. Data was graphed using Prism 8 software (v 8.4.3, GraphPad) and is presented as mean ± standard deviation (SD) from individual experiments or mean ± standard error of the mean (SEM) for combined data from replicated experiments.

Chapter 3 Characterising the murine ME7 prion model for anti-cytokine intervention in the presence and absence of systemic bacterial infection

3.1 Introduction

Clinical studies have shown that levels of cytokines in human sera for both IL-1β and TNF-α are significantly increased in AD patients compared to healthy controls, as well as in other neurodegenerative diseases (Dursun et al., 2015; Ott et al., 2018; Stoeck et al., 2014). Evidence of chronic inflammation and systemic inflammatory events in AD patients can modify neuropathology and is linked to a faster rate of cognitive decline in AD patients (Heneka et al., 2015; Holmes et al., 2003; Ide et al., 2016; Rakic et al., 2018). Furthermore, serum TNF-α levels are also increased in AD patients and this has been shown to contribute to faster progression, with inhibition using etanercept slowing this rate of decline (Butchart et al., 2015; Holmes et al., 2011, 2009). Therefore, TNF-α presents an interesting target for novel therapeutic strategies for the treatment of neurodegenerative diseases. One of the remaining questions is whether systemic or central cytokine expression is responsible for the effects of systemic inflammation on disease progression. To investigate this question, one requires an experimental model where both central cytokine expression and systemic inflammation can impact on disease progression, such as the murine ME7 prion model of chronic neurodegeneration (Chouhan et al., 2017).

Cytokine expression in the murine ME7 prion model have been measured around the onset of disease-associated symptoms (e.g. from 18 wpi onwards), with both IL-1β and TNF-α transcripts increased compared to NBH control mice (Cunningham, Wilcockson, Campion, *et al.*, 2005; Field *et al.*, 2010; Murray, Skelly and Cunningham, 2011). The changes in cytokine expression during the asymptomatic phase of the disease is relatively unknown. In addition, current data on cytokine expression after systemic inflammatory challenge in the murine ME7 prion model is limited to studies using the bacterial mimetic LPS (Lunnon *et al.*, 2011; Murray, Skelly and Cunningham, 2011; Hennessy, Griffin and Cunningham, 2015; Skelly *et al.*, 2018). Understanding how a live bacterial infection alters

disease progression, including behavioural changes and cytokine expression, would better reflect the circumstances under which systemic inflammation affects the progression of AD patients.

The aim of this results chapter was to characterise expression of inflammatory markers, by qPCR and histology, throughout the course of the murine ME7 prion model and the effects of live bacterial infection on these inflammatory markers. Time points were selected based on their relevance to pathological changes that are known to occur during disease progression (Chouhan et al., 2017). The 8 wpi time point was chosen as this is the earliest time point at which microglia activation is detected prior to synaptic loss at 12 wpi, but cytokine expression levels at this time remain unknown (Betmouni et al., 1996). The 12 wpi and 16 wpi time points were selected because these correspond to changes in behaviour and understanding biochemical changes at these time points could help identify the most appropriate time point for therapeutic intervention (Cunningham et al., 2009; Griffin et al., 2013; Hennessy et al., 2017; Murray et al., 2012). The last 18 wpi time point was chosen as this is when neuronal loss is evident and is usually coincident with early symptom onset (Cunningham et al., 2005c, 2005b; Felton et al., 2005).

ME7 prion injected (ME7) mice infected with *S. typhimurium* were also analysed to assess the effects of systemic inflammation on microglial activation, cytokines, and synaptic marker expression during progression of ME7 prion disease. The effect of *S. typhimurium* was assessed four weeks after infection as there is sustained production of cytokines in the brain at this time point following systemic bacterial infection (Püntener et al., 2012). Overall, it is expected that the data in this chapter will inform about the most suitable time point for anti-cytokine therapies in the murine ME7 prion model in the absence and presence of systemic bacterial infection. Enhanced delivery of antibodies into the CNS can be achieved through targeting TfR-mediated transcytosis (Pardridge, 2015; Paterson and Webster, 2016; Pulgar, 2019; Yu and Watts, 2013). However, TfR expression has not been described in the murine ME7 prion model and it is not known if neuropathology and/or neuroinflammation impact on its expression. Therefore, protein and transcript levels of TfR will be measured in ME7 prion mice with and without systemic bacterial infection.

3.2 Methods

Female C57BL/6 mice (10-12 weeks old) were placed in a stereotaxic frame and injected bilaterally in the dorsal hippocampus with either ME7 prion or normal brain (NBH) homogenate and assessed for disease progression by examination of behaviour and motor functions (Sections 2.1.2 and 2.1.3). ME7 mice were sacrificed at either 8 wpi or 18 wpi, and NBH mice were sacrificed at 18 wpi (n=4 for all groups). Mice were transcardially perfused with saline containing 5 U/ml heparin sodium and brains dissected (Section 2.1.6). The right hemisphere was embedded in OCT for histological analysis of microglial activation, neurodegeneration and TfR expression (Section 2.2.1). Tissue punches enriched for the hippocampus and thalamus from the left hemisphere were taken for qPCR analysis of TNF-α, IL-1β and TfR transcript levels (Section 2.2.2).

Archived samples, generated by Dr Ursula Püntener and Mr Steven Booth, include RNA isolated from ME7 and NBH mice culled at 12 wpi and 16 wpi; RNA isolated from ME7 mice challenged with *S. typhimurium*. Tissues from these mice was collected four weeks after systemic infection at 8 wpi (12 wpi) and at 12 wpi (16 wpi) (n=4-5/group). RNA samples were used to assess the effects of systemic bacterial infection on cytokine expression in the murine ME7 prion model. Immunohistochemical staining in the hippocampus and thalamus following systemic infection with *S. typhimurium* ($1x10^6$ cfu) or saline was performed by Steven Booth.

3.3 Results

3.3.1 Confirmation of prion disease progression through behavioural assessment

Disease progression was assessed by behavioural changes in ME7 prion-injected (ME7) mice compared to NBH-injected (NBH) mice (Figure 3.1). The first behavioural differences between ME7 and NBH mice are seen in burrowing, with ME7 mice displacing less pellets than NBH mice over time and are present from 14 wpi onwards (Figure 3.1A). There is a significant main effect of both 'treatment' ($F(1, 6) = 99.34$; $p < 0.0001$) and 'time after injection' ($F(10, 60) = 30.79$; $p < 0.0001$), with an interaction between 'time after injection' and 'treatment' in burrowing behaviour ($F(10, 60) = 30.79$; $p < 0.0001$). The next differences in behaviour between ME7 and NBH mice are seen in open field locomotion, with ME7 mice showing a significant increase in total distance covered from 16 wpi (Figure 3.1B). There was a significant interaction between 'treatment' and 'time after injection' ($F(10, 60) = 7.201$; $p < 0.0001$), with a significant main effect for both 'treatment' ($F(1, 6) = 6.599$; $p = 0.0424$) and 'time after injection' ($F(10, 60) = 7.391$; $p < 0.0001$). From 17 wpi we begin to see a decrease motor function in ME7 mice compared to NBH mice from the horizontal bar task and then deficits in the inverted screen test (Figure 3.1). There is a significant main effect of 'treatment' in both the horizontal bar task ($F(1, 6) = 48.73$; $p = 0.0004$) and the inverted screen test ($F(1, 6) = 14.84$; $p = 0.0084$). There is also a significant interaction between 'treatment' and 'time after injection' for both tests ($p <= 0.0001$), suggesting that ability to perform motor tasks is affected in the later stages of asymptomatic ME7 prion disease. Overall, these data show that disease progression significantly affects performance in a battery of behavioural tests that assess mood and motor function.

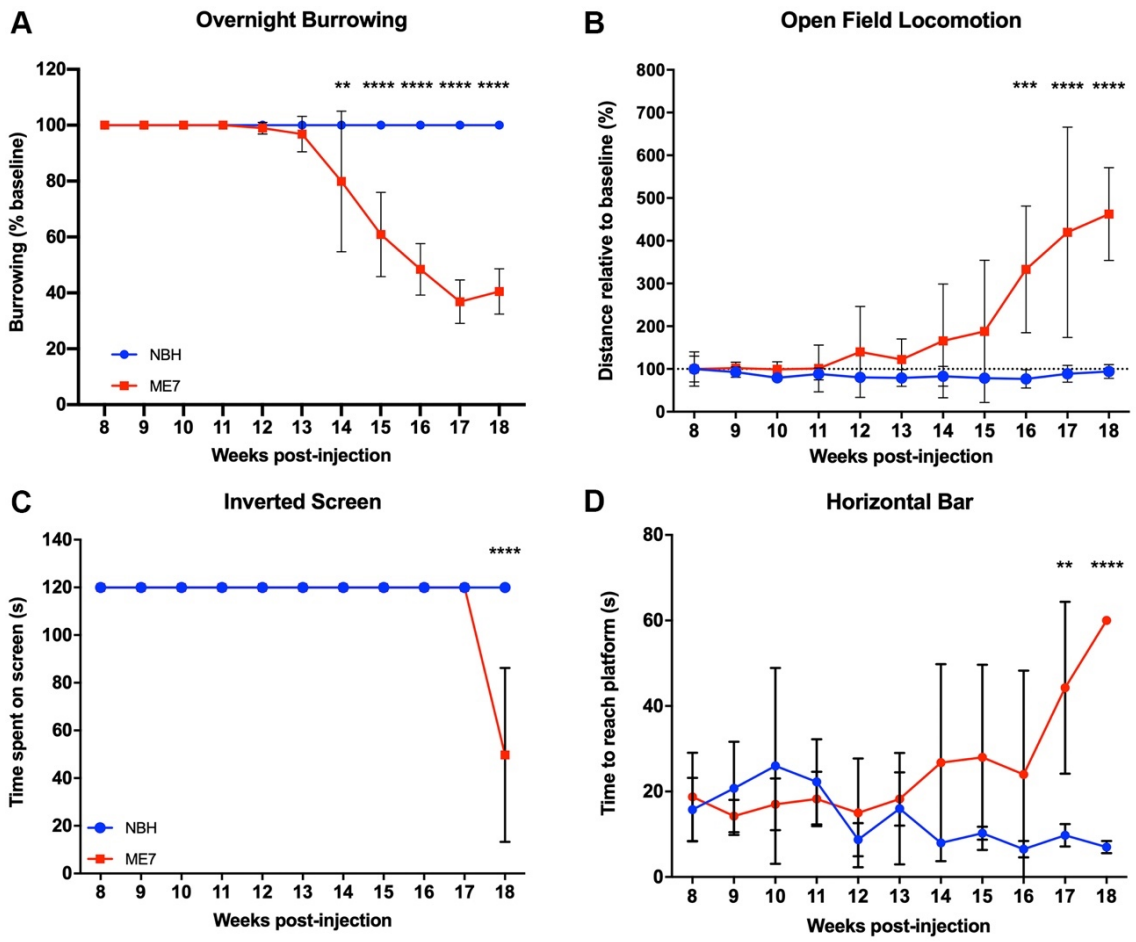

Figure 3.1 Changes in behaviour during progression of ME7 prion disease

ME7 prion-induced changes in (A) overnight burrowing, (B) open field locomotion, (C) horizontal bar task and (D) inverted screen. The onset of behavioural changes is dependent on the task with burrowing deficits from 14 wpi; open field from 16 wpi and motor tasks from 17 wpi. Data presented as mean ± SD, n = 4/ group. **, $p < 0.01$; ****, $p < 0.0001$ denotes statistically significant difference from NBH-injected mice using a two-way ANOVA with Holm-Sidak's multiple comparisons test.

3.3.2 Confirmation of ME7 prion disease pathology by immunohistochemical analysis

To investigate the kinetics of neuropathology and neuroinflammation in the murine ME7 prion model, expression levels of the neuronal marker NeuN and microglial activation marker CD11b were measured (Figure 3.2 and Figure 3.3).

3.3.2.1 Neuronal cell loss in the CA1 layer of the hippocampus of ME7 mice

The number of NeuN+ cells per mm^2 in the pyramidal cell layer of the hippocampal CA1 is significantly reduced in ME7 mice at 18 wpi compared to age matched NBH controls (113.9 ± 24.09 vs. 160.6 ± 29.87; $p = 0.0045$). Whereas there is no difference between NBH and 8 wpi ME7 mice ($p > 0.05$; Figure 3.2).

3.3.2.2 Activation of hippocampal microglia in ME7 mice

CD11b expression in the hippocampus, expressed as area covered relative to NBH mice, is significantly increased in ME7 mice at 18 wpi compared to NBH mice (31.96% vs. 15.60%; $p < 0.0001$) and ME7 mice at 8 wpi (31.96% vs. 11.27%; $p < 0.0001$). There is no significant difference in area covered between NBH and ME7 8 wpi mice (Figure 3.3). However, CD11b staining of ME7 mice at 18wpi identifies microglia with an activated phenotype, with a rounded cell body and shorter, thicker processes compared to microglia in NBH mice (Figure 3.3E/F).

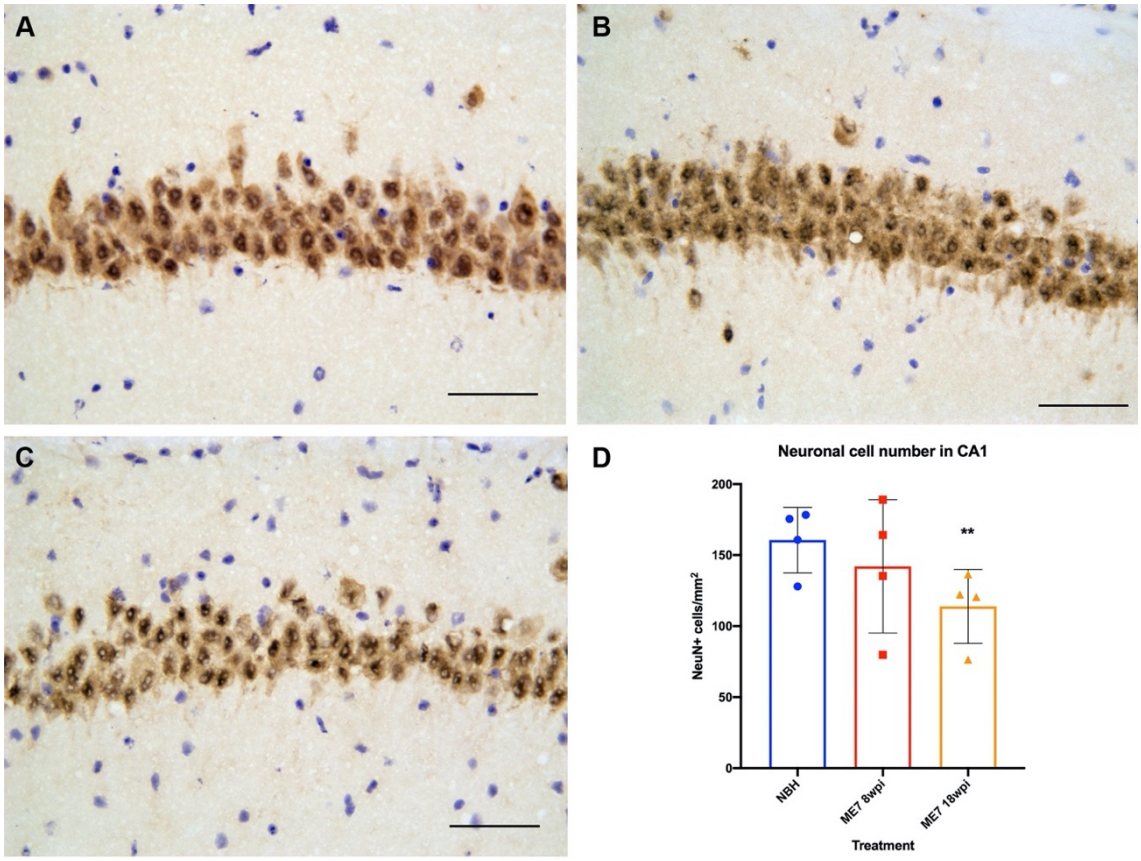

Figure 3.2 Evident neurodegeneration in the hippocampus of ME7 mice

The number of NeuN+ in the pyramidal CA1 layer is reduced in ME7 prion-injected (ME7) mice 18 weeks post-injection (wpi) compared to age-matched normal brain homogenate (NBH)-injected mice. (A-C) Representative images of NeuN staining in CA1 of the hippocampus from NBH mice at 18 wpi (A) and ME7 mice at 8 wpi (B) and at 18 wpi (C). (D) Quantification of NeuN+ cells in the CA1 pyramidal layer shows a significant reduction in ME7 mice at 18 wpi compared to NBH mice. n = 4 mice per group, with 3 technical replicates from each mouse. Data presented as mean ± SD. **, $p < 0.01$ denotes a statistical difference from NBH mice analysed with one-way ANOVA and Holm-Sidak's multiple comparisons test. Representative images were taken with a 40x objective; scale bar = 50 µm.

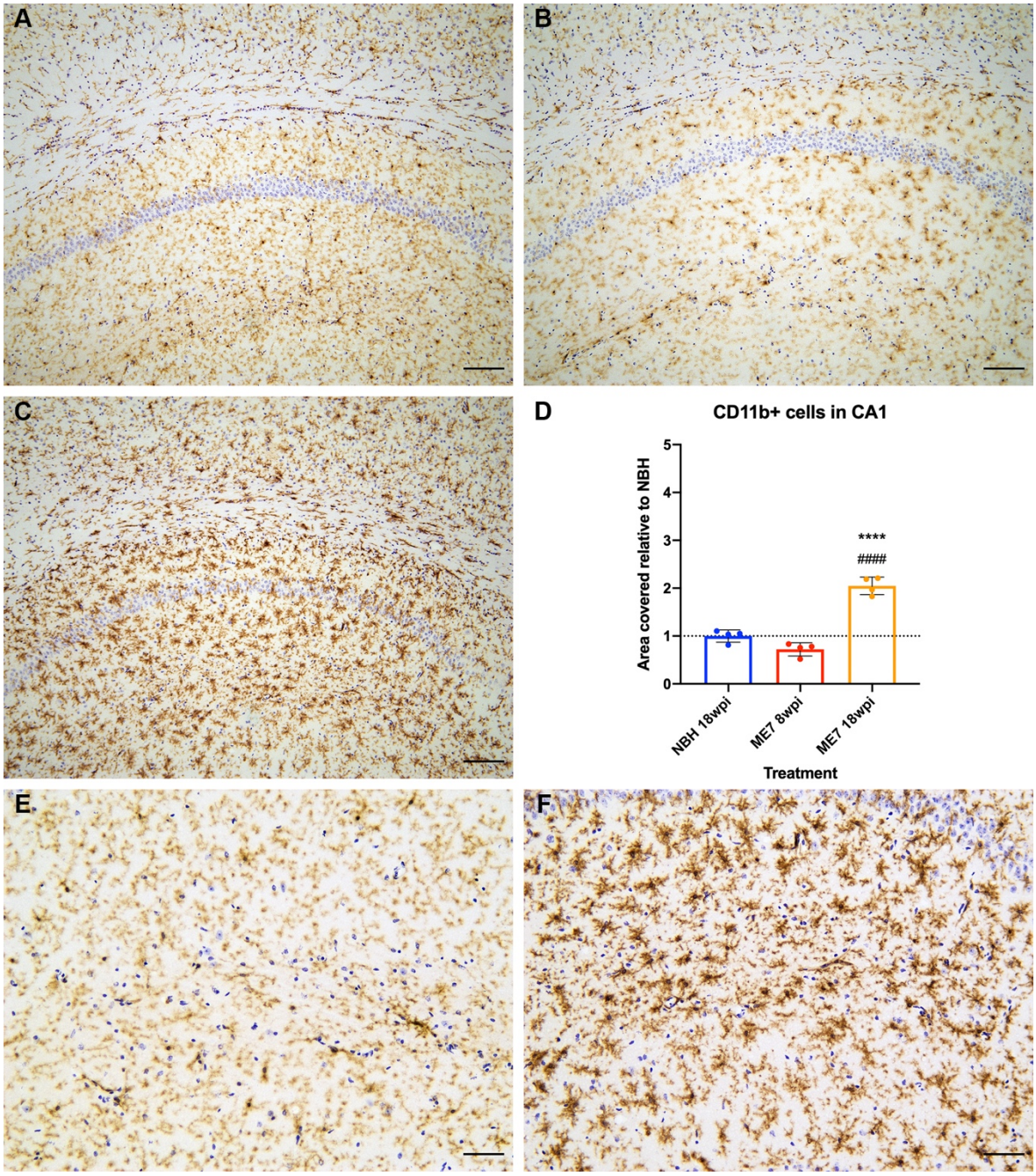

Figure 3.3 Microglial activation in the hippocampus of ME7 mice

Immunohistochemical analysis of CD11b expression in hippocampal sections identifies microglia of an activated phenotype in ME7 prion-injected (ME7) mice at 18 weeks post-injection (wpi) compared to age-matched normal brain homogenate (NBH)-injected control animals. (A-C) Representative images of CD11b staining within the hippocampal CA1 from NBH mice at 18 wpi (A) and ME7 mice at 8 wpi (B) and at 18 wpi (C). (D) Quantification of area covered by CD11b staining using DAB deconvolution relative NBH mice shows a significant increase in CD11b expression in ME7 18 wpi mice compared to both NBH controls and ME7 8 wpi mice. (E-F) Representative images of CD11b staining show microglia with a ramified morphology in NBH-injected mice (E) compared to activate microglia, with thicker cell body and processes, in ME7-injected mice at 18 wpi (F). n = 4 mice per group. Data presented as mean ± SD of fold change compared to NBH mice at 18 wpi. ****, $p < 0.0001$ compared to NBH; ####, $p < 0.0001$ compared to ME7 8 wpi analysed by one-way ANOVA with Holm-Sidak's multiple comparisons test. Representative images were taken with a 10x (A-C) or 20x (E-F) objective; scale bar = 100 μm (A-C); 50 μm (E-F).

3.3.2.3 Thalamic microglia activation in ME7 mice

The same pattern of increased CD11b expression in ME7 mice at 18 wpi compared to NBH mice (39.59% vs 9.83%; $p < 0.0001$) and ME7 mice at 8 wpi (39.59% vs 7.45%; $p < 0.0001$) is also evident in the thalamus (Figure 3.4). Moreover, there was no significant difference in expression between ME7 mice at 8 wpi and NBH mice (7.45% vs 9.83%; $p = 0.1866$).

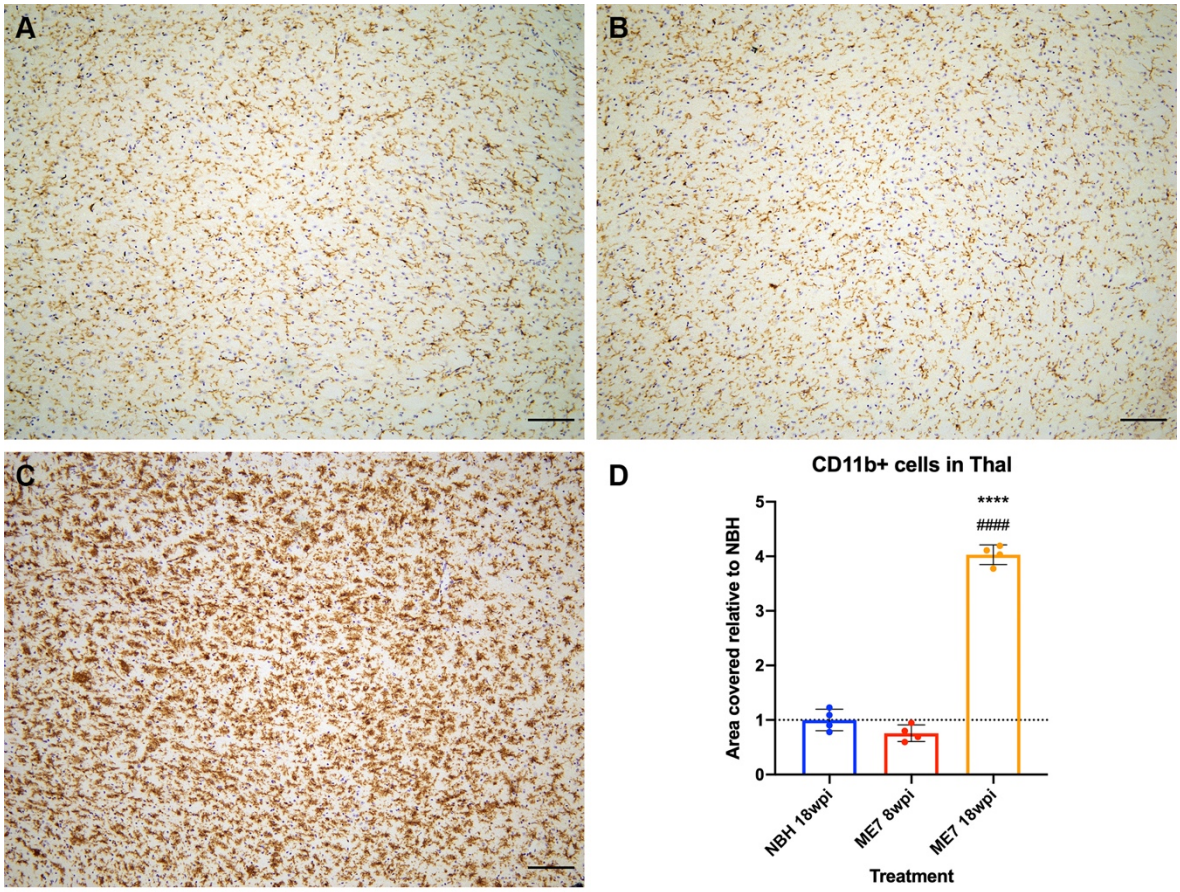

Figure 3.4 Microglial activation in the thalamus of ME7 mice

Immunohistochemical analysis of CD11b expression in thalamus identifies microglia of an activated phenotype in ME7 mice at 18 weeks post-injection (wpi) compared to age-matched normal brain homogenate (NBH)-injected control animals. (A-C) Representative images of CD11b staining within the thalamus from NBH mice at 18 wpi (A) and ME7 mice at 8 wpi (B) and at 18 wpi (C). (D) Quantification of area covered by CD11b staining using DAB deconvolution relative to NBH mice shows a significant increase in CD11b expression in ME7 18 wpi mice compared to both NBH controls and ME7 8 wpi mice. n = 4 mice per group. Data presented as mean ± SD of fold change compared to NBH mice at 18 wpi. ****, $p < 0.0001$ compared to NBH; ####, $p < 0.0001$ compared to ME7 8 wpi analysed by one-way ANOVA with Holm-Sidak's multiple comparisons test. Representative images were taken with a 10x objective; scale bar = 100 µm.

3.3.3 Cytokine expression during ME7 prion disease progression

Characterising the expression pro-inflammatory cytokines during disease progression will enable therapeutic study design to target these inflammatory proteins. Analysis of tissue from a range of time-points after ME7 prion injection (from 8 wpi to 18 wpi) was performed to measure changes in neuroinflammation linked to disease progression. mRNA transcripts levels of *Il1b* (Figure 3.5) and *Tnf* (Figure 3.6) in the hippocampus/thalamus of NBH and ME7 mice were assessed by qPCR.

The earliest time point measure, 8 wpi, showed a significant decrease in expression compared to NBH control mice ($t = 2.982$, $df = 9$, $p = 0.0455$; Figure 3.5C). At 12 wpi, Students' t-test analysis indicated no difference in mRNA transcript levels of *Il1b* between ME7 mice and NBH controls ($t = 1.687$, $df = 8$, $p = 0.1300$). At 16 wpi, *Il1b* transcript levels are significantly increased in ME7 mice compared to NBH mice after Students' t-test ($t = 3.240$, $df = 6$, $p = 0.0177$). One-way ANOVA analysis at 18 wpi shows no difference in *Il1b* transcripts levels between NBH and ME7 mice ($t = 0.3934$, $df = 9$, $p = 0.7032$). These data provide evidence for peak *Il1b* transcript levels at 16 wpi during ME7 disease progression (Figure 3.5).

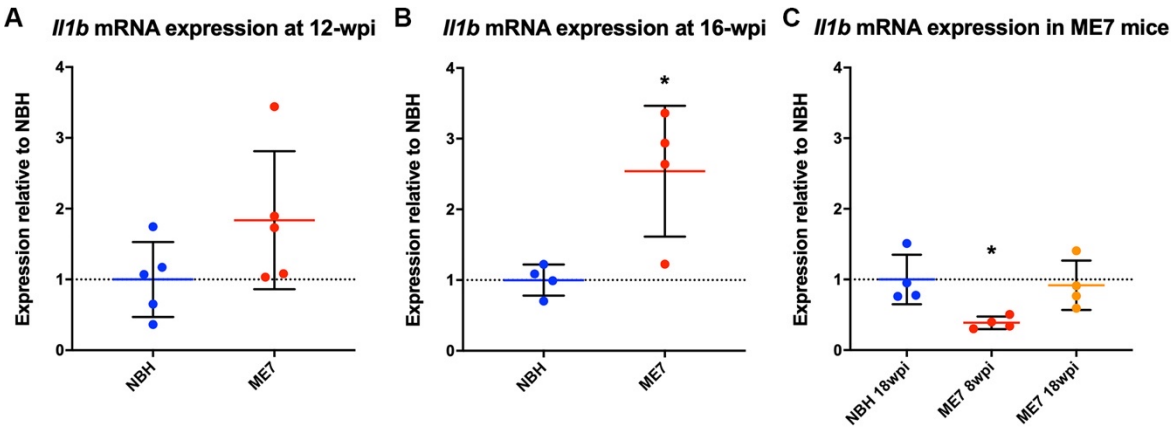

Figure 3.5 *Il1b* expression during progression of murine ME7 prion disease

mRNA expression of *Il1b* in hippocampus-enriched tissue from NBH and ME7 mice at (A) 12wpi, (B) 16 wpi and (C) at 8 and 18 wpi. n = 4-5 mice per group. *, $p < 0.05$ versus NBH. Data are presented as the mean ± SD (n = 4-5/group) of fold change compared to NBH after normalisation of expression to *Gapdh*. Tissue collection and RNA isolation of ME7 mice at 12 wpi and 16 wpi was performed by Dr Ursula Püntener and Steven Booth.

Analysis of *Tnf* transcript levels in ME7 mice at 8 wpi showed no change compared to NBH mice (t = 1.565, df = 9, p = 0.2809; Figure 3.6C). At 12 wpi, *Tnf* mRNA transcript levels are significantly increased in ME7-injected mice compared to NBH-injected control mice (t = 6.279, df = 8; p = 0.0002). At 16 wpi, there was a no significant difference in *Tnf* transcript levels between ME7 and NBH mice (U (12,24) = 2; p = 0.1143). At 18 wpi, *Tnf* mRNA expression showed no change compared to NBH mice (t = 1.525, df = 9, p = 0.2809). These data suggest that peak *Tnf* expression is at 12 wpi during ME7 prion disease compared to NBH controls, and levels return to control levels from 16 wpi onwards (Figure 3.6).

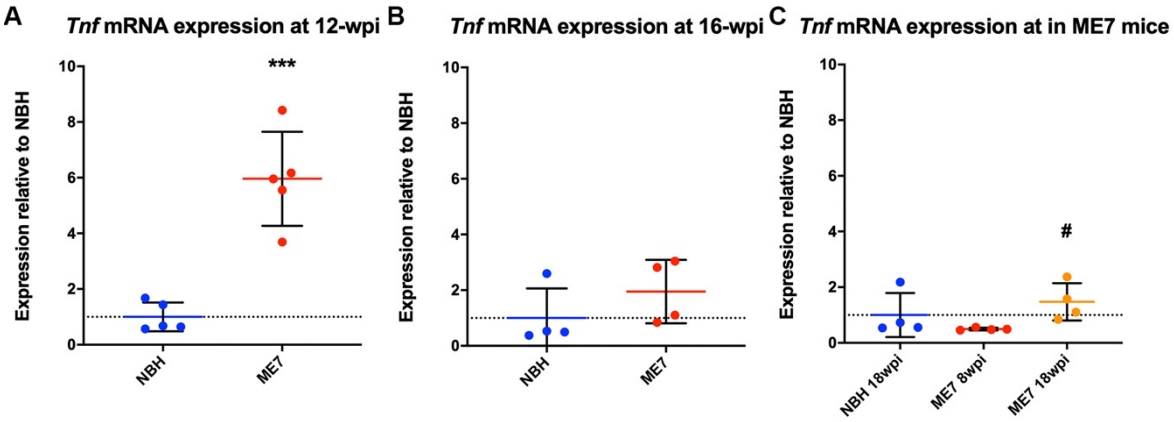

Figure 3.6 *Tnf* expression during progression of murine ME7 prion disease

mRNA expression of *Tnf* in hippocampus-enriched tissue from NBH and ME7 mice at (A) 12wpi, (B) 16 wpi and (C) at 8 and 18 wpi. n = 4-5 mice per group. ***, $p < 0.01$ denotes significant difference after a two-tailed unpaired Students' t-test. #, $p < 0.05$ versus ME7 8 wpi after one-way ANOVA with Holm-Sidak's multiple comparisons test. Data are presented as the mean ± SD (n = 4-5/group) of fold change compared to NBH after normalisation of expression to *Gapdh*. Tissue collection and RNA isolation of ME7 mice at 12 wpi and 16 wpi was performed by Dr Ursula Püntener and Steven Booth.

3.3.4 Effect of systemic bacterial infection on cytokine expression in ME7 prion disease

Systemic inflammation can have a detrimental effect on progression of neurodegenerative diseases, therefore elucidating any superimposed effects on microglial activation and cytokine expression in ME7 prion disease will allow for improved understanding of how these changes, if any, could be targeted in a model that reflects aspects of clinical disease.

Systemic infection with *S. typhimurium* SL3261 (1 x 10^6 cfu) in ME7 mice at 8 wpi had no effect on hippocampal/thalamic *Il1b* mRNA transcript levels measured after 4 weeks (t = 0.08024, df = 8, p = 0.4690) (12 wpi; Figure 3.7). At the same 12 wpi time point, there is a trend towards increased *Tnf* mRNA transcript levels following systemic bacterial infection (t = 1.464, df = 8, p = 0.0907). In contrast, infection of ME7 mice at 12 wpi and measurement of cytokine transcript levels 4 weeks later (16 wpi) shows that systemic bacterial infection results in a significant induction of *Il1b* transcripts (t = 2.090, df = 7, p = 0.0375) and *Tnf* transcripts (t = 2.126, df = 9, p = 0.0355) compared to saline injected ME7 mice (Figure 3.8). Furthermore, analysis of transcript levels relative to expression in age matched NBH mice shows that four weeks following systemic inflammation at 16 wpi, *Il1b* and *Tnf* mRNA levels are significantly increased, whereas only *Tnf* is increased at 12 wpi (Table 3.1).

Overall, these data suggest a differential response of ME7 mice to *S. typhimurium* dependent on disease progression, with ME7 mice later in disease progression at time of infection showing an exaggerated response to *S. typhimurium*.

Table 3.1 Fold change relative to NBH for cytokine genes in the hippocampus/thalamus of ME7 prion mice with and without systemic inflammatory challenge

ME7 timepoint	*Il1b*	*Tnf*
8 wpi	0.389[#]	0.498
12 wpi	1.84	5.96**
12 wpi + SL3261	1.88	8.43***
16 wpi	2.54*	1.95
16 wpi + SL3261 [a]	**4.25****	**4.78****
18 wpi	0.919	1.47

[#] $p < 0.05$ significant decrease vs NBH 18 wpi

* $p < 0.05$; ** $p < 0.01$; *** $p < 0.001$ significant increase vs NBH at relevant timepoint

[a] Numerals in bold also show significant increase over ME7 mice at 16 wpi ($0.01 < p < 0.05$)

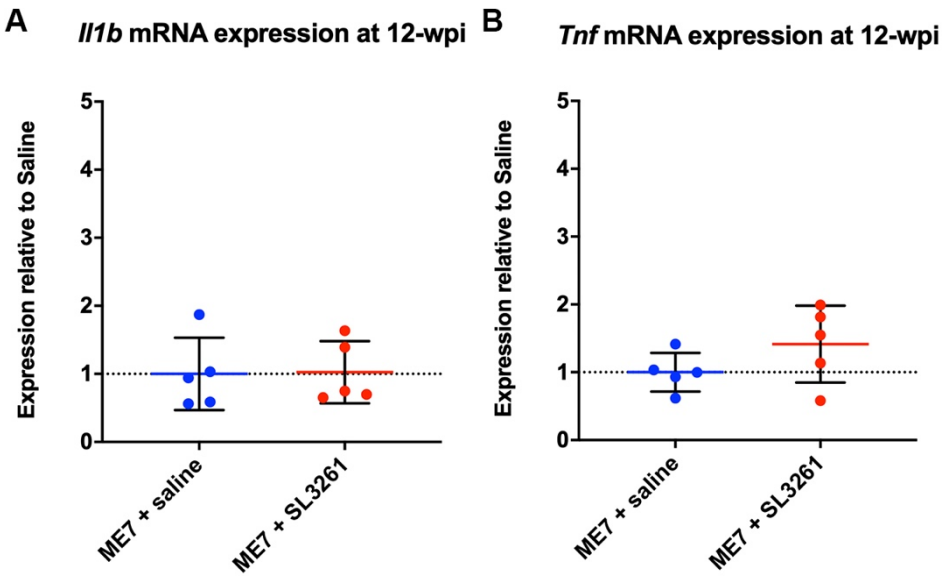

Figure 3.7 Cytokine expression in ME7 mice four weeks after systemic bacterial infection at 8 wpi

ME7-injected mice were infected with 1x10^6 colony forming units of *S. typhimurium* SL3261 (i.p.) at 8 wpi and tissue collected four weeks later at 12 wpi. Hippocampal expression of *Il1b* (A) and *Tnf* (B) transcripts show no change compared to saline injected ME7 mice. Data are presented as the mean ± SD (n = 5/group) of fold change compared to ME7 + saline after normalisation of expression to *Gapdh*. Tissue collection and RNA isolation of ME7 mice at 12 wpi was performed by Dr Ursula Püntener and Steven Booth.

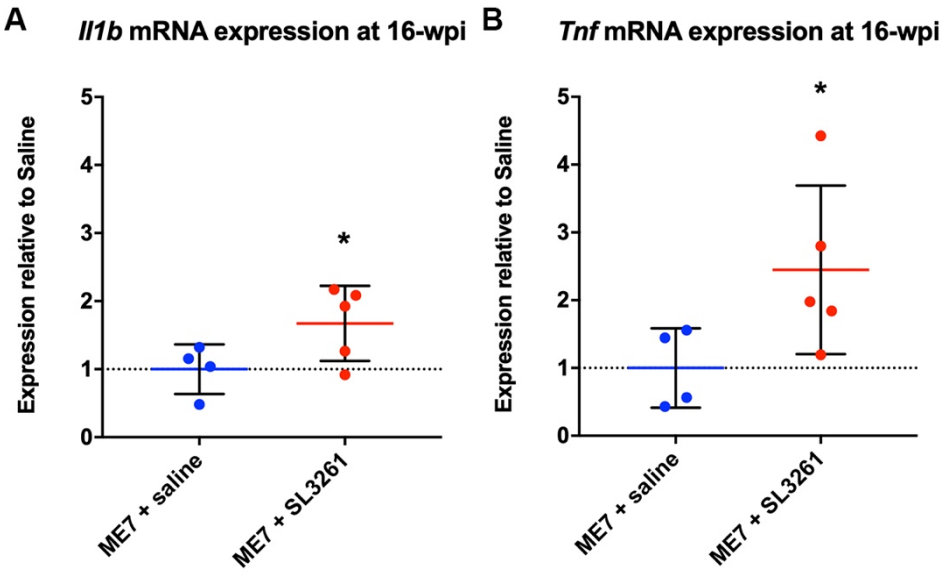

Figure 3.8 Cytokine expression in ME7 mice four weeks after systemic bacterial infection at 12 wpi

ME7-injected mice were infected with 1x10^6 colony forming units of *S. typhimurium* SL3261 (i.p.) at 12 wpi and tissue collected four weeks later at 16 wpi. Hippocampal expression of *Il1b* (A) and *Tnf* (B) transcripts show significantly increased levels compared to saline injected ME7 mice. *, $p < 0.05$ denotes significant difference after a one-tailed unpaired Students' t-test compared to Naive ME7 mice. Data are presented as the mean ± SD (n = 4-5/group) of fold change compared to ME7 + saline after normalisation of expression to *Gapdh*. Tissue collection and RNA isolation of ME7 mice at 16 wpi was performed by Dr Ursula Püntener and Steven Booth.

3.3.5 Vascular and microglial activation after systemic bacterial infection in ME7 mice

Systemic challenge with inflammatory modulators is known to activate the vasculature (Skelly et al., 2013; Uchikado et al., 2004; Varatharaj and Galea, 2017). In addition, activation of the vasculature following bacterial infection can lead to further activation of microglia and cytokine production long after initial challenge (Püntener et al., 2012). Expression of MHCII and CD11b in the hippocampus and thalamus from ME7 mice challenged with *S. typhimurium* was measured using DAB immunohistochemistry and subsequent quantification of staining.

3.3.5.1 MHCII expression in the hippocampus and thalamus of ME7 mice after systemic bacterial infection

Systemic infection with *S. typhimurium* at 8 wpi resulted in a significant increase ($U(15, 30) = 0$; $p = 0.0079$) in MHCII expression in the hippocampus and thalamus of ME7 mice four weeks later when compared to saline injection (Figure 3.9C). In contrast, systemic challenge at 12 wpi has no significant effect ($U(8, 13) = 2$; $p = 0.200$) on MHCII expression analysed four weeks later (Figure 3.9F).

MHCII is expressed on both microglia and endothelial cells following infection with *S. typhimurium* in C57Bl/6 mice (Püntener et al., 2012). Salmonella infected ME7 mice at 12 wpi show more vascular MHCII staining compared to ME7 mice at 16 wpi (arrowheads; Figure 3.10).

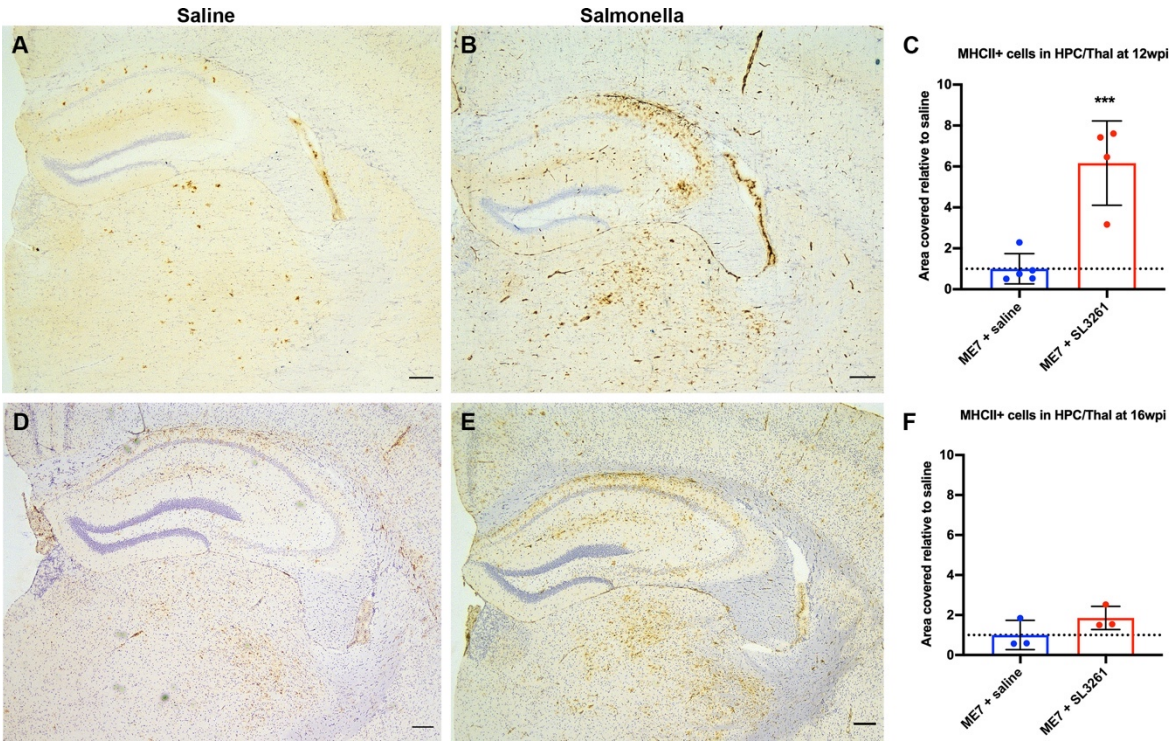

Figure 3.9 MHCII expression in ME7 mice following systemic bacterial infection
ME7 mice were administered *S. typhimurium* SL3261 ($1x10^6$ cfu) or non-pyrogenic saline (i.p.) at 8 wpi or 12 wpi and brains collected four weeks later. (A-B) Representative images of MHCII staining four weeks after administration of saline (A) or *S. typhimurium* (B) at 8 wpi. (C) Quantification of MHCII staining shows a significant increase four weeks after *S. typhimurium* infection compared to saline injection in ME7 mice. (D-E) Representative images of MHCII staining four weeks after administration of saline (D) or *S. typhimurium* (E) at 12 wpi. (F) Quantification of MHCII staining shows no significant difference four weeks after *S. typhimurium* infection compared to saline injection in ME7 mice. n = 3-5 mice per group. ***, $p < 0.001$ denotes significant difference after a one-tailed unpaired Students' t-test. Data are presented as mean ± SD relative to ME7 + saline expression. Images taken with a 2.5x objection; scale bar = 200 μm. Tissue collection and histology performed by Dr Ursula Püntener and Steven Booth.

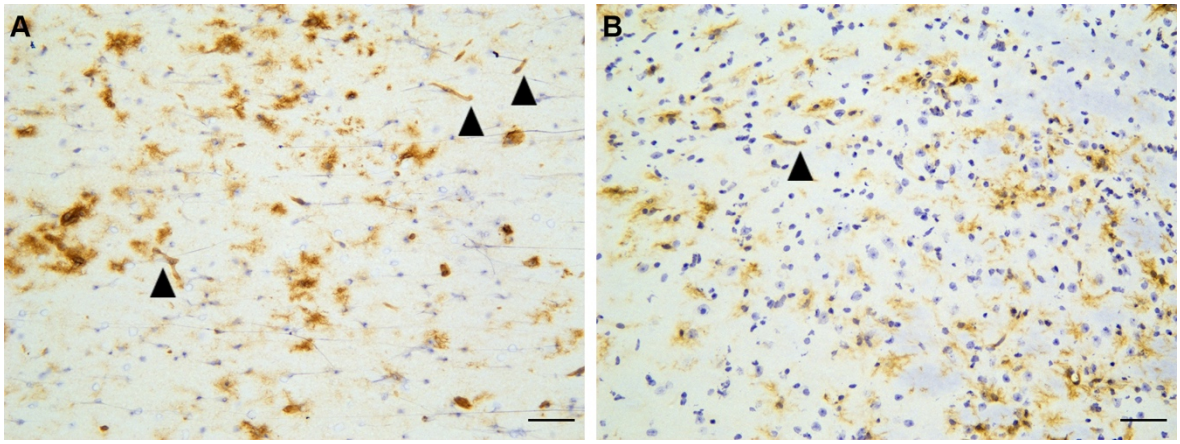

Figure 3.10 Vascular MHCII expression in the thalamus four weeks after bacterial infection in ME7 mice

Representative images of MHCII staining four weeks after infection with *S. typhimurium* SL3261 ($1x10^6$ cfu, i.p.) at 8 wpi (A) or 12 wpi (B) in ME7 mice. Vascular MHCII (arrowheads) in the thalamus is more evident in ME7 mice at 12 wpi (A) than at 16 wpi (B) four weeks after systemic bacterial challenge. Images taken with a 20x objection; scale bar = 50 μm. Tissue collection and histology performed by Dr Ursula Püntener and Steven Booth.

3.3.5.2 CD11b expression in the hippocampus and thalamus of ME7 mice after systemic bacterial infection

CD11b expression is significantly increased (t (8) = 2.683; p = 0.0139) in the hippocampus and thalamus four weeks after *S. typhimurium* infection in ME7 mice at 8 wpi when compared to expression in saline injected ME7 mice (Figure 3.11C). When challenged with *S. typhimurium* at 12 wpi, CD11b expression is significantly increased (U (6, 15) = 0; p = 0.05) four weeks later within the hippocampus and thalamus (Figure 3.11F). Microglia in the thalamus show an activated phenotype at both 12 wpi and 16 wpi, however there is no difference between microglia from brains of Naive and *Salmonella*-infected ME7 mice (Figure 3.12).

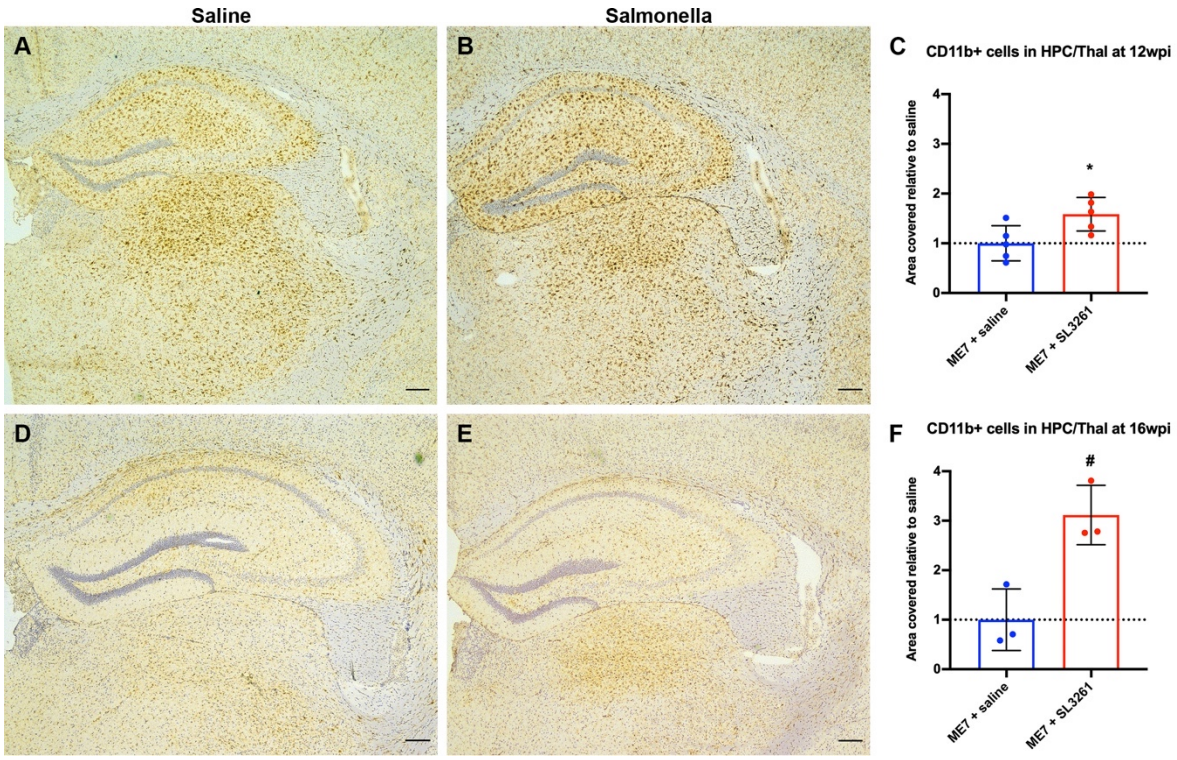

Figure 3.11 CD11b expression in ME7 prion mice following systemic infection with *S. typhimurium*

ME7-injected mice were administered *S. typhimurium* SL3261 ($1x10^6$ cfu) or non-pyrogenic saline (i.p.) at 8 wpi or 12 wpi and tissue collected four weeks later. (A-B) Representative images of CD11b staining four weeks after administration of saline (A) or *S. typhimurium* (B) at 8 wpi. (C) Quantification of CD11b staining shows a significant increase four weeks after *S. typhimurium* infection compared to saline injection in ME7 mice. (D-E) Representative images of CD11b staining four weeks after administration of saline (D) or *S. typhimurium* (E) at 12 wpi. (F) Quantification of CD11b staining shows no significant difference four weeks after *S. typhimurium* infection compared to saline injection in ME7 mice. n = 3-5 mice per group. *, $p < 0.05$ denotes significant difference after a one-tailed unpaired Students' t-test. #, $p = 0.05$ denotes significant difference after a one-tailed Mann-Whitney U test. Data are presented as mean ± SD relative to ME7 + saline expression. Images taken with a 2.5x objection; scale bar = 200 μm. Tissue collection and histology performed by Dr Ursula Püntener and Steven Booth.

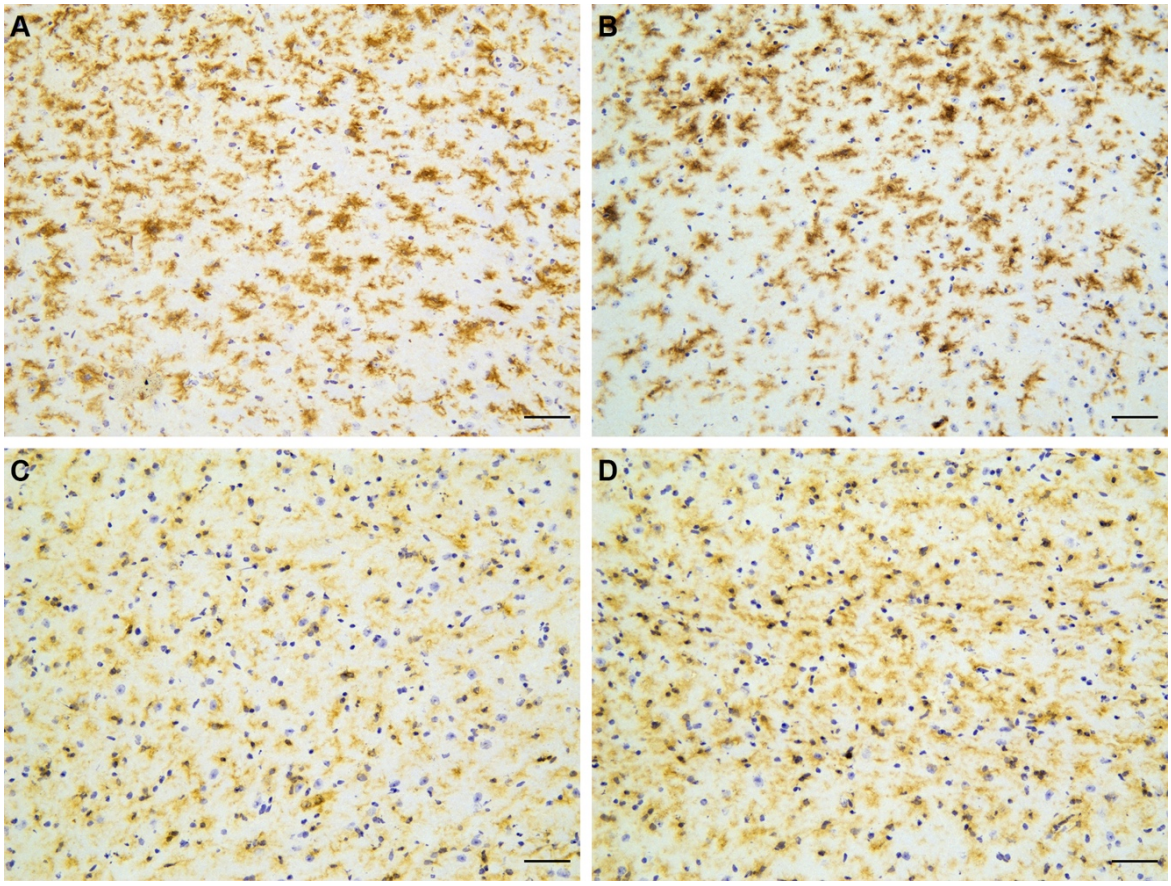

Figure 3.12 Microglial morphology in the thalamus four weeks after bacterial infection in ME7 mice

(A-B) Representative higher magnification images of CD11b staining shows no difference in microglial morphology four weeks after infection with *S. typhimurium* SL3261 ($1x10^6$ cfu, i.p.) in ME7 mice (B) compared to injection of non-pyrogenic saline (A) at 12 wpi. (C-D) Representative higher magnification images of CD11b staining four weeks after injection of *S. typhimurium* (D) at 16 wpi show no changes in microglial morphology compared to Naive ME7 mice (C). Images taken with a 20x objection; scale bar = 50 μm. Tissue collection and histology performed by Dr Ursula Püntener and Steven Booth.

3.3.6 Synaptic changes in the ME7 prion model in the presence and absence of systemic bacterial infection

To investigate expression of synaptic markers mRNA transcript levels of synaptophysin (*Syp*), metabotropic glutamate receptor type 1, mGluR1, (*Grm1*) and NMDA receptor subunit N2A (*Grin2a*) were measured in hippocampal/thalamic tissue samples from ME7 mice at 12 wpi and 16 wpi (Figure 3.13). The effects of systemic inflammation on expression were also analysed in tissues four weeks after systemic bacterial infection with *S. typhimurium* SL3261.

Analysis of *Syp* mRNA transcript levels at 12 wpi showed no significant changes in expression in ME7 mice compared to NBH control mice, nor any effect of systemic infection ($F(2,12) = 0.9821$, $p = 0.4027$; Figure 3.13A). Analysis of *Grm1* mRNA transcript levels at 12 wpi showed a significant main effect between conditions ($F(2,12) = 7.306$, $p = 0.0084$), with a significant decrease in expression four weeks after systemic bacterial infection compared to NBH control mice ($t(12) = 3.822$, $p = 0.0073$; Figure 3.13B). A similar effect was seen on expression of *Grin2a*, with a significant main effect ($F(2,12) = 4.964$, $p = 0.0269$) and a significant decrease in expression following systemic bacterial infection ($t(12) = 3.123$, $p = 0.0262$; Figure 3.13C).

Analysis of *Syp* expression in ME7 mice at 16wpi four weeks after systemic bacterial infection showed a significant decrease in mRNA transcript levels compared to NBH control mice ($t(10) = 3.134$, $p = 0.0315$) (Figure 3.13D). However, there was no difference between ME7 mice and NBH mice ($t(10) = 1.484$, $p = 0.2736$) at 16 wpi. *Grm1* mRNA transcript levels were significantly decrease in ME7 mice at 16 wpi compared to NBH mice and were also decreased following systemic bacterial infection compared to NBH mice ($F(2,10) = 5.843$, $p = 0.0209$) (Figure 3.13E). Expression of *Grin2a* at 16 wpi showed no changes in ME7 mice compared to NBH mice nor following systemic bacterial infection ($F(2,10) = 0.8174$, $p = 0.4690$) (Figure 3.13F).

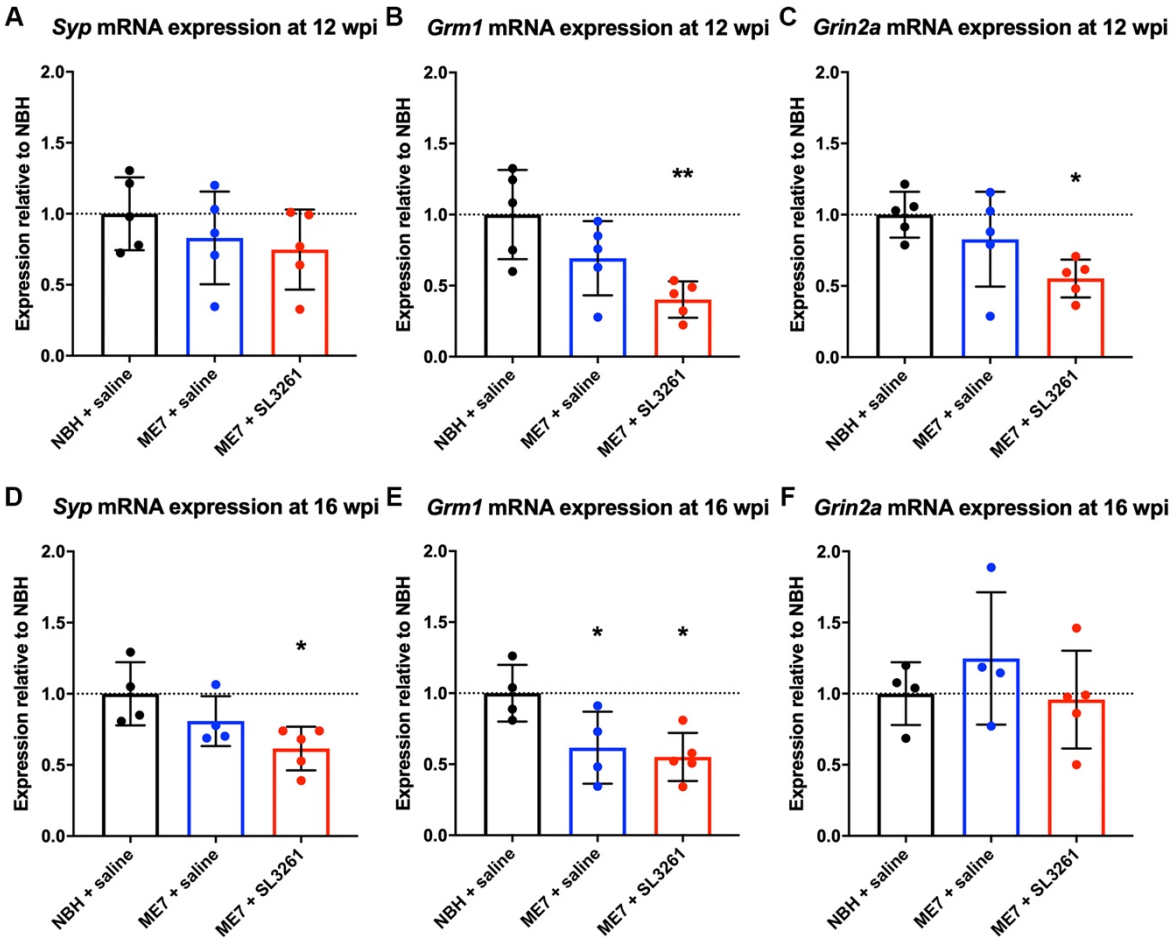

Figure 3.13 Expression of synaptic markers in ME7 mice following systemic bacterial infection
ME7-injected mice were infected with *S. typhimurium* SL3261 ($1x10^6$ cfu, i.p.) at 8 wpi (A-C) or 12 wpi (D-F) and tissue collected four weeks later. (A-C) Hippocampal expression of synaptophysin (*Syp*; A), metabotropic glutamate receptor type 1 (*Grm1*; B) and NMDA receptor subunit N2a (*Grin2a*; C) transcripts show no change in saline injected ME7 mice compared to NBH control mice at 12 wpi. Systemic bacterial challenge results in decreased expression of *Grm1* and *Grin2a* four weeks later compared to NBH mice. (D) Hippocampal expression of *Syp* after *s*ystemic bacterial infection results in decreased expression four weeks later compared to NBH mice. (E) *Grm1* expression is decreased four weeks after administration of saline or *S. typhimurium* in ME7 mice compared to saline injected NBH mice. (F) *Grin2a* expression is unchanged in ME7 mice at 16 compared to NBH mice and expression remains unaltered four weeks after systemic bacterial infection. Data are presented as the mean ± SD (n = 4-5/group) of fold change compared to NBH + saline after normalisation of expression to *Gapdh*. *, $p < 0.05$; **, $p < 0.01$ using one-way ANOVA with Holm-Sidak's multiple comparisons test versus NBH + saline. Tissue collection and RNA isolation of ME7 mice was performed by Dr Ursula Püntener and Steven Booth.

3.3.7 Transferrin receptor expression during ME7 prion disease progression

Characterising the changes in TfR expression during ME7 prion disease will provide valuable insight in to whether enhanced antibody delivery across the BBB could be affected because of neuropathology and/or neuroinflammation. Hippocampal/thalamic TfR mRNA transcript levels were measured by qPCR in ME7 mice at 8, 12, 16 and 18 wpi and in NBH control mice (Figure 3.14).

At 8 wpi, TfR transcript levels are not significantly different from NBH mice ($t = 0.5942$, $df = 9$, $p = 0.9188$). There is no difference in TfR transcript levels in ME7 mice at 12 wpi ($t = 0.3792$, $df = 8$, $p = 0.7144$). However, there is a trend towards reduction in TfR transcript levels in ME7 mice at 16 wpi compared to age matched NBH control mice ($t = 2.109$, $df = 6$, $p = 0.0795$). At 18 wpi, TfR transcripts levels are not significantly different compared to NBH mice ($t = 0.3193$, $df = 9$, $p = 0.9409$).

Overall, these data suggest that TfR mRNA transcript levels are stable throughout ME7 prion disease progression and but may decrease at later stages.

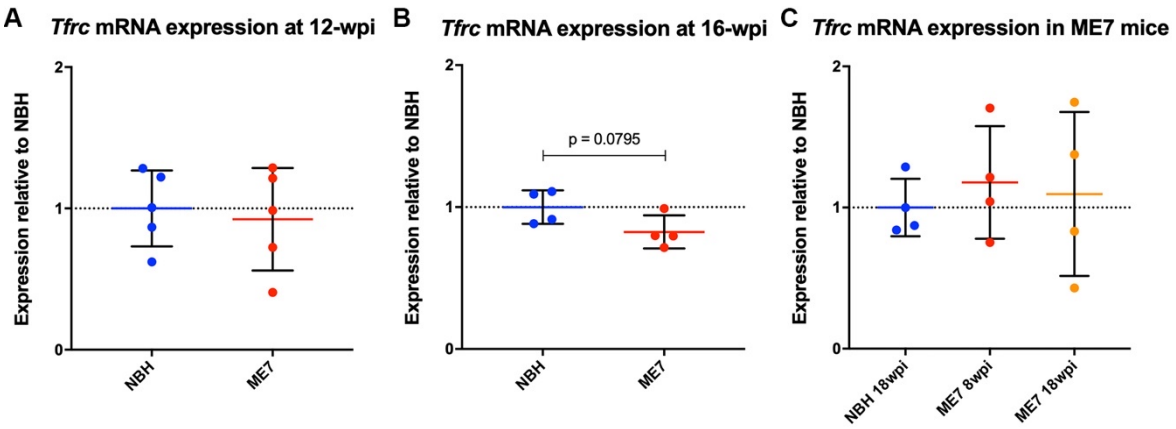

Figure 3.14 *Tfrc* expression during progression of murine ME7 prion
mRNA expression of *Tfrc* in hippocampus/thalamus-enriched tissue from NBH and ME7 mice at (A) 12wpi, (B) 16 wpi and (C) at 8 and 18 wpi. n = 4-5 mice per group. Data are presented as the mean ± SD (n = 4-5/group) of fold change compared to NBH after normalisation of expression to *Gapdh*. Tissue collection and RNA isolation of ME7 mice at 12 wpi and 16 wpi was performed by Dr Ursula Püntener and Steven Booth.

3.3.8 Effects of systemic bacterial infection on TfR expression in ME7 prion disease

Understanding the effects of systemic inflammation on TfR expression in ME7 mice will help to establish whether ME7 mice are a suitable model to show enhanced delivery of antibodies to the CNS. Hippocampal/thalamic TfR mRNA transcript levels were measured four weeks after systemic challenge with *S. typhimurium* at 8 wpi (12 wpi) or at 12 wpi (16 wpi) (Figure 3.15). *S. typhimurium* infected ME7 mice showed no changes in TfR mRNA transcript levels compared to saline injected ME7 mice four weeks later at 12 wpi (U (18,27) = 8, p = 0.7302) or at 16 wpi (U (31,24) = 9, p = 0.5476). Overall, these data suggest that TfR mRNA expression is unaltered in ME7 mice four weeks after systemic bacterial infection.

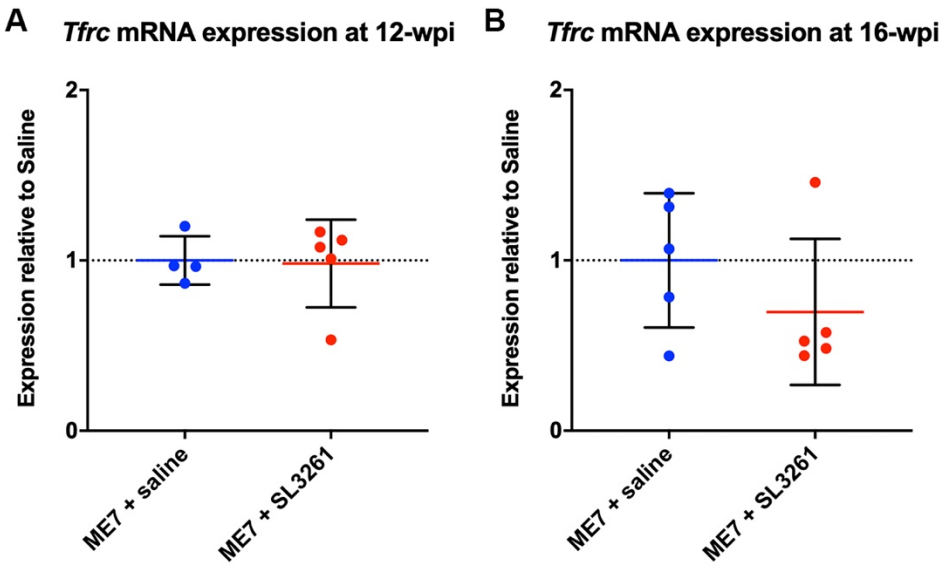

Figure 3.15 *Tfrc* expression in murine ME7 prion disease after systemic bacterial infection
ME7-injected mice were infected with *S. typhimurium* SL3261 ($1x10^6$ cfu, i.p.) at 8 or 12 wpi and tissue collected four weeks later at 12 wpi (A) or 16 wpi (B). Expression of *Tfrc* mRNA transcripts is unaltered four weeks after systemic bacterial challenge. Data are presented as the mean ± SD (n = 4-5/group) of fold change compared to saline after normalisation of expression to *Gapdh*. Tissue collection and RNA isolation of ME7 mice at 16 wpi was performed by Dr Ursula Püntener and Steven Booth.

3.3.9 Histological analysis of Transferrin receptor protein expression in ME7 prion disease

Analysis of TfR expression was assessed by immunohistochemistry and differences in coverage between NBH and ME7 mice was compared (Figure 3.16). Quantitative analysis using a one-way ANOVA, showed a significant decrease in expression in ME7 mice at 8 wpi and 18 wpi compared to NBH mice ($F(2, 9) = 15.40$; $p = 0.0012$). These data suggest that enhanced delivery of therapeutic antibodies across the BBB might be impaired due to reduced TfR1 expression within the hippocampus of ME7 prion mice. TfR is expressed on both blood vessels (arrowhead) and neuronal cell bodies (asterisks) in both NBH and ME7 mice (Figure 3.16). However, neuronal staining in the CA1 is less prominent in ME7 mice at 8 and 18 wpi.

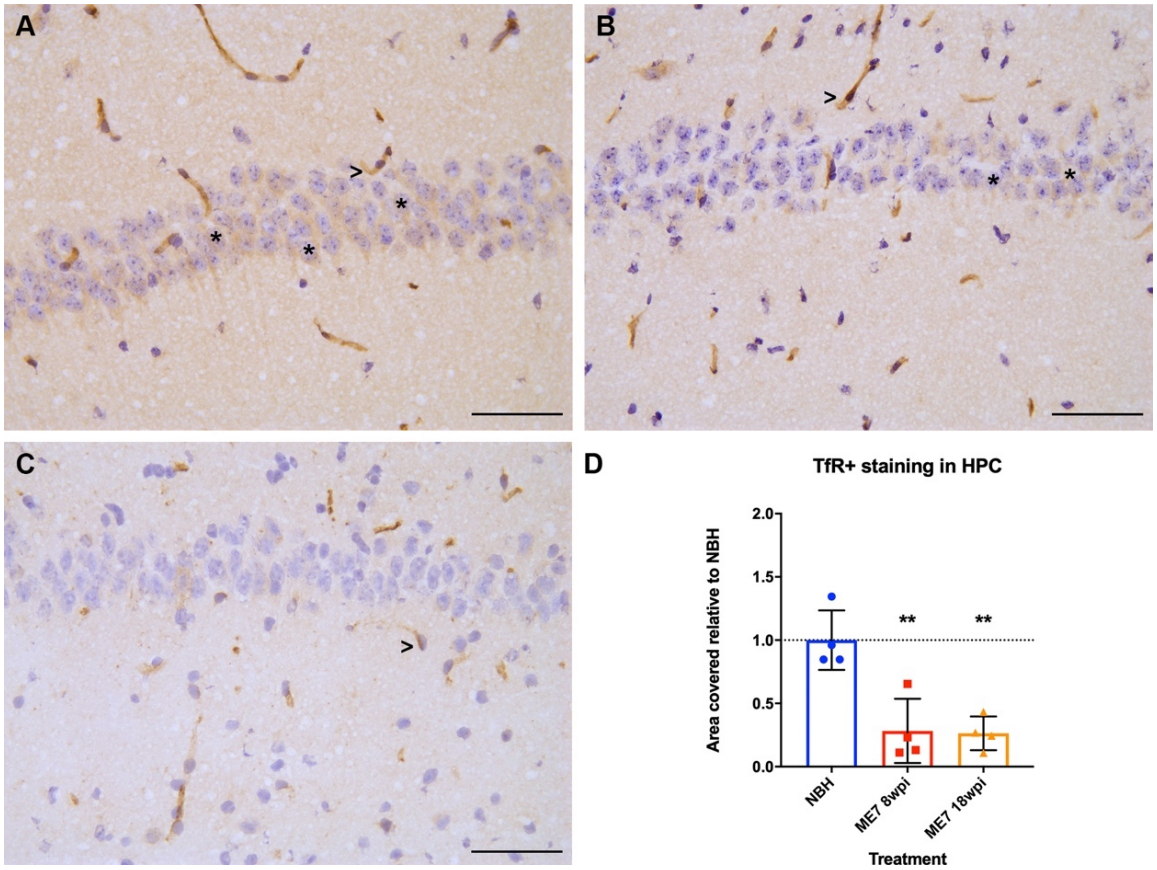

Figure 3.16 Transferrin receptor expression in hippocampus during ME7 prion disease
(A-C) TfR1 (transferrin receptor) expression in the CA1 is present on both the vasculature (arrowheads) and neuronal cell bodies (asterisks) in NBH-injected animals (A). Whereas neuronal staining in ME7-injected mice at 8 wpi (B) and 18 wpi (C) is severely reduced. (D) Quantitative analysis using one-way ANOVA showed a significant decrease in TfR1 staining in ME7 mice compared to NBH mice. **, $p<0.01$ versus NBH after one-way ANOVA with Holm-Sidak's multiple comparisons test. n = 4 mice per group; data are presented as mean ± SD. Representative images were taken with a 40x objective; scale bar = 50 μm.

3.4 Discussion

Induction of ME7 prion following injection of ME7 brain homogenate results in the expected observable changes in mouse behaviours and neuroinflammation. Increases in microglial activation markers and proinflammatory cytokines are observed from 12 wpi for TNF-α and 16 wpi for IL-1β, along with decreases in synaptic glutamate receptor expression. Systemic bacterial infection at 8 wpi results in exacerbation of neuroinflammatory changes observed in ME7 mice when measured four weeks later. Whilst systemic inflammation significantly decreased expression in synaptic markers four weeks after infection with *S. typhimurium*. Expression of TfR may be altered in ME7 mice, however this appears to not affect the vasculature and thus enhanced delivery of biologics via targeting of TfR is unlikely to be disrupted in ME7 mice compared to control mice.

3.4.1 Behavioural and histopathological progression of murine ME7 prion disease

ME7 prion-injected (ME7) mice show a specific pattern of behavioural changes during the asymptomatic phase of disease that have been well established previously (Betmouni et al., 1999b; Deacon et al., 2001; Guenther et al., 2001). These behavioural changes are also present in the data described in this chapter (Figure 3.1); with a decrease in burrowing evident from 14 wpi, hyperactivity in open field locomotion from 16 wpi, and deficits in both the inverted screen and horizontal bar from 17 wpi. The replication of these behavioural changes shows that this is a robust experimental model that behaves as predicted in a repeated fashion. This battery of behavioural tests highlights the progression of the disease that correspond to different histopathological events. Burrowing is considered a species-specific behaviour that reflects an affective deficit in ME7 mice compared to NBH-injected (NBH) mice. With the earlier appearance of this behavioural deficit compared to other tests, and given that burrowing appears to be a species-specific behaviour that requires organisation and executive function, this assay provides an opportunity to assess efficacy of treatments on hippocampal functions in ME7 mice (Deacon et al., 2001). Hyper-reactivity in the open-field test is known to be affected by hippocampal function, and its onset from 15-16 wpi is thought to correlate

with a decrease in synaptic density in the hippocampus and is suggestive of potential compensatory mechanisms (Cunningham et al., 2003; Felton et al., 2005; Guenther et al., 2001; Hilton et al., 2013). Deficits in motor function and coordination, as assessed by the inverted screen and horizontal bar tests, appear from 17 wpi onwards, and are thought to be associated with neuronal loss (Betmouni et al., 1999b; Cunningham et al., 2003; Hilton et al., 2013). Further study into motor function and coordination as well as open field activity highlight the relationship between the two tasks, that suggests as motor function declines the compensatory effects of open-field hyper-reactivity as a result of hippocampal degeneration are no longer present from 19 wpi as speed decreases (Felton et al., 2005; Guenther et al., 2001). The large variation at the onset of these behavioural changes suggests that a greater n number would help to improve accurate detection of the onset, especially when considering the use of this model in the context of drug discovery.

The expected pathological changes in ME7 mice at 18 wpi compared to NBH mice are also apparent, with a decrease in neuronal cells in the CA1 (Figure 3.2) and increased expression of CD11b (Figure 3.3). CD11b immunoreactivity was chosen to show changes in both microglial morphology and increases in microglial number. However, these two changes may have been better identified through separate use of specific activation and morphology markers, such as ionized calcium-binding adapter molecule 1 (IBA-1) and CD68 respectively (Betmouni et al., 1996; Gómez-Nicola et al., 2014, 2013). Evidence of detectable changes in microglial morphology from 8 wpi in the CA1 of ME7 mice (Figure 3.3), is consistent with phenotypic changes and increased expression of microglial activation markers (Betmouni et al., 1996; Gómez-Nicola et al., 2014, 2013). In addition, there is a significant increase in thalamic microglial activation at 18 wpi (Figure 3.4), which is known to result from increased microglial proliferation from 12 wpi onwards (Gómez-Nicola et al., 2013). The most prominent change within the hippocampus at 18 wpi is the evident neurodegeneration within the pyramidal layer of the hippocampal CA1 (Figure 3.2), that shows the expected pathology induced by injection of ME7 brain homogenate and is in line with that reported in the literature (Cunningham et al., 2005a, 2003). This loss in hippocampal neurons is the one aspect of this model that differs from genetic models of neurodegeneration, such as those for familial AD and primary tauopathies, and therefore provides replication of additional characteristics of human neurodegeneration

which can be investigated (Hsiao et al., 1996; Lord et al., 2006; Oddo et al., 2003; Terwel et al., 2005).

3.4.2 Cytokine expression during ME7 prion pathogenesis

Both TNF-α and IL-1β have been implicated as part of the neuroinflammatory response that contributes to the progression of neurodegenerative diseases (Ransohoff, 2016b). There's very little documented literature on the expression of cytokines in the brains of ME7 mice at 8 wpi, with a single study reporting no changes in thalamic transcript levels of TNF-α and IL-1β at 60 dpi (~8.5 wpi) (Carroll et al., 2016). Biochemical analysis corroborates the work of Carroll and colleagues when considering hippocampal/thalamic-enriched tissues, with neither TNF-α or IL-1β showing a significant change in expression at 8 wpi in ME7 mice compared to NBH mice (Table 3.1). IL-1β transcript levels steadily increase in ME7 mice compared to NBH mice over time until reaching a significant 2.54-fold increase at 16 wpi. In contrast, TNF-α transcript levels peak at 12 wpi with a significant 5.96-fold increase over NBH mice before decreasing over time (Table 3.1).

Transcript expression levels for TNF-α and IL-1β have been reported previously, with only TNF-α increased at 12 wpi in the hippocampus and thalamus (Cunningham et al., 2009; Murray et al., 2012). However, one study that compared the expression of neuroinflammatory genes in the thalamus throughout progression of ME7 prion disease showed a significant 2.7-fold increase in IL-1β transcript levels over mock-injected mice and a statistically non-significant 2.9-fold increase in TNF-α transcript levels at 80 dpi (~11.5 wpi) (Carroll et al., 2016). These data suggest that although both the hippocampus and thalamus are affected by ME7 prion disease they may be differentially affected, and the study of combined tissues may dilute any changes present in the individual regions.

As disease progresses, it has been shown that transcripts levels of TNF-α in the hippocampus and thalamus are significantly increased over NBH or mock-injected mice at 16 wpi (Carroll et al., 2016; Cunningham et al., 2005c; Hennessy et al., 2017). Tissue analysis at 16 wpi showed no significant increase in TNF-α transcript levels, although there was a 1.95-fold increase compared to NBH mice (Figure 3.6B). At this same timepoint there is a significant 2.54-fold increase in IL-1β transcripts levels compared to

NBH mice (Figure 3.5B), and this is similar to other studies that also report significantly increased IL-1β levels (Carroll et al., 2016; Cunningham et al., 2005c; Hennessy et al., 2017; Skelly et al., 2018).

In ME7 mice at 18 wpi, there is no significant difference in expression of IL-1β and TNF-α mRNA transcripts compared to NBH mice (Table 3.1). This data is in agreement with a recent publication by Obst and colleagues, however this is in contrast to previous studies that report disease-associated increases in both transcripts at 18wpi (Cunningham et al., 2005c, 2005b; Field et al., 2010; Obst et al., 2018). A previous investigation in temporal expression of proinflammatory cytokine mRNA transcripts in ME7 mice showed that both TNF-α and IL-1β are consistently increasing until 18 wpi where IL-1β levels begin to plateau before TNF-α levels plateau at 20 and 22 wpi (Cunningham et al., 2005b). The reasons for these differences are not obvious but it could reflect relative severity of disease across reports. Evidence from tissue histology shows clear vacuolation in ME7 brain tissue from other studies, whereas vacuolation is less frequent in the current cohort of ME7 mice at 18 wpi (Figure 3.2) (Cunningham et al., 2005c, 2003; Field et al., 2010). However, there is the consideration that vacuolation is solely an artefact of the embedding and fixation processed using in preparation for histology (Betmouni et al., 1999a), and thus is a possible explanation for the lack of vacuolation observed in the fresh-fixed tissue used in this thesis.

Overall, the data presented in this chapter show that TNF-α expression is significantly increased at 12 wpi and IL-1β expression peaks at 16 wpi, but these increases in expression return to NBH levels by later stages of disease progression at 18 wpi. Therefore, interventions targeted against these cytokines would likely be more effective in the progression of murine ME7 prion disease between 12 and 16 wpi.

3.4.3 The effects of *S. typhimurium* infection on microglial activation and cytokine expression in ME7 prion disease

Previous studies investigating the response of ME7 prion mice to systemic inflammation have used the bacterial mimetic, LPS. These studies have looked at the

neuroinflammatory and neuronal response in the hippocampus at various timepoints during disease progression, with exaggerated neuronal loss and acute changes to cytokine expression reported (Combrinck et al., 2002; Cunningham et al., 2009, 2005c; Griffin et al., 2013; Lunnon et al., 2011; Murray et al., 2012, 2011). These studies have proposed that microglia are primed by the concurrent ME7 prion-driven neuropathology and therefore respond with a greater potency to inflammatory stimuli compared to naïve, unprimed microglia (Cunningham et al., 2009; Griffin et al., 2013; Murray et al., 2012; Skelly et al., 2018).

It has been shown previously that there's a prolonged neuroinflammatory response that peaks 21 days after systemic challenge with the live bacteria *S. typhimurium* SL3261 and both microglia and the activated vasculature are a potential source for cytokine production (Püntener et al., 2012). Therefore, it could be predicted that infection with *S. typhimurium* in ME7 mice would increase IL-1β and TNF-α transcript levels. Interestingly, systemic challenge with *S. typhimurium* at an early timepoint during disease progression (8 wpi) did not induce a significant change in hippocampal/thalamic cytokine expression measured four weeks later. However, systemic challenge at 12 wpi with *S. typhimurium* in ME7 mice resulted in a significant increase in both IL-1β and TNF-α transcripts four weeks later (Table 3.1).

From 12 wpi in the ME7 prion disease there is deposition of PrP^{Sc} within the hippocampus as well as evident alterations to the neuronal networks, specifically a loss in synaptophysin density within the molecular layers of the CA1 (Cunningham et al., 2003; Hilton et al., 2013). These changes in synaptic density and protein accumulation will activate local resident microglia, prime them towards a secondary stimulus and this therefore could contribute to the greater production of cytokines after systemic challenge with *S. typhimurium* at 12 wpi. This may also explain the lack of cytokine production observed after systemic bacterial challenge at 8 wpi. Thus, the exaggerated microglial response to *S. typhimurium* could be explained by the loss of synaptic density in the hippocampus and the presence of primed microglia at 12 wpi, which would not have occurred at 8 wpi. It is also thought that microglia in the healthy brain can resolve inflammation more effectively than primed microglia (Lim et al., 2015; Neher and Cunningham, 2019). Thus, it is possible that unprimed microglia in ME7 mice at 8 wpi could show a temporal profile of cytokine production similar to a naïve mouse. In the

naïve mouse brain, the central cytokine expression peaks at 21 days following systemic bacterial challenge (Püntener et al., 2012), and it is possible that measurement after four weeks in ME7 mice does not capture this response. Analysis of central cytokine production at weekly intervals in ME7 mice following challenge with *S. typhimurium* at 8 wpi could elucidate this possibility. In addition, if performed in ME7 mice challenged at 12 wpi it could show that the observed cytokine production is prolonged in these mice because of primed microglia.

Another potential reason for the relative differences in cytokine response between the two timepoints is the relative microglial number and activation state at 8 wpi and 12 wpi. Increased expression of microglial activation markers and related morphological changes are detected in ME7 mice at both 8 wpi and at 12 wpi (Betmouni *et al.*, 1996; Gómez-Nicola *et al.*, 2013). This increased microglial activation is seen when staining for pan-macrophage marker CD11b (Figure 3.11). In this chapter, the data shows a greater increase in microglial activation as disease progresses, with a 3.1-fold increase in expression over saline-injected ME7 prion mice at 16 wpi, compared to a 1.6-fold increase at 12 wpi (Figure 3.11). Furthermore, microglial numbers in the hippocampus and thalamus are increasing in ME7 mice from 12 wpi (Gómez-Nicola et al., 2013). The differences in cytokine production four weeks after systemic bacterial infection in ME7 mice challenged at 8 wpi and 12 wpi could be explained by an increase in microglia numbers within the hippocampus and thalamus. Moreover, an increase in microglia could mean an increased number of primed microglia present to response to a secondary insult and results in exaggerated proinflammatory cytokine production from a greater number of cells. This possibility could be investigated by co-staining of MHCII with either CD11c or Dectin-1, markers known to be expressed and upregulated in primed microglia (Holtman et al., 2015; Norden and Godbout, 2013).

Further to the direct microglial response to systemic inflammation, another aspect of the immune response to a live bacterial infection is the response of the endothelial cells. Cerebral endothelial cells are activated following systemic challenge with *S. typhimurium*, which is in contrast to challenge with LPS, and remain activated for up to 21 days after challenge (Püntener et al., 2012). The activation of the endothelial cells after *S. typhimurium* challenge contributes to the crosstalk between the peripheral and central immune responses, with increased expression of cytokines and chemokines (van Sorge et

al., 2011). Therefore, the activation of the vasculature may contribute to the neuropathology and neuroinflammation observed following infection with *S. typhimurium* as a potential source of cytokine expression. Analysis of MHCII expression in the hippocampus and thalamus after systemic challenge with *S. typhimurium* showed there's a differential response depending on disease progression (Figure 3.9). When challenged at 8 wpi, ME7 mice four weeks later show increased expression of MHCII on both the vasculature, which results from infection, and on microglia. This contrasts with a challenge at 12 wpi where four weeks later there is no difference between saline-injected and *S. typhimurium*-infected ME7 mice, but most of the expression is on microglia and not the vasculature (Figure 3.10). The difference in MHCII response in ME7 mice at 12 and 16 wpi could be influenced by the exposure of primed microglia to a secondary inflammatory stimulus. Secondary challenge with intracerebral LPS four weeks after *S. typhimurium* infection resulted in expression of MHCII on both endothelial cells and microglia, suggesting that prior exposure can alter microglial responses (Püntener et al., 2012). Furthermore, this altered distribution of MHCII expression could contribute to the difference in cytokine production between ME7 mice at the two different timepoints, with a greater number of activated and primed microglia at the later timepoint showing an exaggerated response. Together, these data suggest that the exacerbatory effects of systemic inflammation on cytokine production in the ME7 prion model are only present when there is concurrent protein deposition and synaptic pathology.

3.4.4 Effects of systemic bacterial infection on expression of synaptic markers in ME7 prion disease

Understanding the expression of synaptic markers can help to elucidate the role that systemic inflammation has on exacerbating disease pathology. Synaptic dysfunction is seen early on disease progression, with synaptic density in the hippocampal CA1 decreased from 12-13 wpi, and is present when behavioural deficits appear (Hilton et al., 2013; Jeffrey et al., 2000). Decreased density of synaptophysin staining in the *stratum radiatum* of the hippocampal CA1 has been reported at 12 and 13 wpi in ME7 mice. However, western blot analysis of hippocampal homogenates showed no change in synaptophysin compared to NBH in ME7 12 wpi samples (Gray et al., 2009). These data

suggest that although relative density may be altered, there is no effect on overall expression. This may explain why synaptophysin mRNA transcript levels are unaffected at 12 wpi in ME7 compared to NBH mice (Figure 3.13). Synaptic loss has been described preferentially in the pre-synaptic compartment compared to the post-synaptic department, however alterations to the post-synaptic density are also observed (Gray et al., 2009; Sisková et al., 2010; Šišková et al., 2009). Expression of NMDAR subunits in the mouse hippocampus has shown that N2A subunits are both expressed in post-synaptic densities of γ-aminobutyric acid (GABA)-ergic synapses and on pyramidal cell bodies in the CA1 (Szabadits et al., 2011; Thompson et al., 2002). Previous analysis of NMDARs shows no change in expression compared to NBH at 12 wpi in ME7 mice (Gray et al., 2009). This was corroborated by analysing mRNA transcript levels for the N2a NMDAR subunit (*Grin2a*) in ME7 mice at 12 wpi. However, *Grin2a* expression in ME7 mice four weeks after systemic bacterial infection is significantly decreased compared to NBH mice (Figure 3.13). This response is also shown by mGluR1 (*Grm1*), which shows a significant decrease in expression after systemic bacterial challenge in ME7 mice at 12 wpi (Figure 3.13). mGluR1 is expressed at the synapse in neurons and induction of persistent long-term potentiation (LTP) in the hippocampus is dependent on activation of Type I mGluRs, including mGluR1 (Cheyne and Montgomery, 2008; Ferraguti and Shigemoto, 2006; Mukherjee and Manahan-Vaughan, 2013; Van Dam et al., 2004). Deficits in hippocampal long-term potentiation occur in ME7 prion mice from as early as 12 wpi and open field hyper-reactivity is only present after these deficits have started (Chiti et al., 2006). These data suggest a negative effect of systemic inflammation on glutamate receptor expression at an early time point and could be reflective of the acute behavioural deficits in ME7 mice after systemic inflammatory challenge (Cunningham et al., 2009).

Synaptic function in ME7 mice at 16 wpi has been shown to also be dysregulated, with changes in synaptic plasticity and membrane depolarisation concurrent with deficits in hippocampal-dependent behaviours (Chiti et al., 2006). Expression of synaptophysin and mGluR1 at 16 wpi is significantly decreased in the hippocampus of ME7 mice compared to NBH mice which suggest a change in the presynaptic compartment (Figure 3.13). In contrast, *Grin2a* transcript levels are unaltered in ME7 mice at 16 wpi, even after systemic bacterial infection (Figure 3.13). The differences in expression are unexpected given the progression of disease and the more prevalent synaptic dysfunction, with an increasing

number of degenerating synapses in ME7 mice at 16 wpi compared with 12 wpi (Caleo et al., 2012). However, these differences could be reflective of specific changes in the hippocampus. Increases in post-synaptic density area are evident at 16 wpi in ME7 mice, but these morphological alterations may not effect receptor expression (Sisková et al., 2010). Loss of the perineuronal net is also evident in ME7 mice at 16 wpi, with a decrease in perisomatic *Wisteria floribunda* agglutinin staining (Franklin et al., 2008). Given that profile array data (0) shows decreases in *Ncam1*, GABA receptor (GABAR) α5 subunit and α-amino-3-hydroxy-5-methyl-4-isoxazolepropionic acid (AMPA) receptor (AMPAR) subunit expression, along with increased *Mmp9* expression, it could be postulated that these are all indicative of early perineuronal net breakdown in ME7 mice four weeks after systemic bacterial challenge at 8 wpi (Franklin et al., 2008; McRae and Porter, 2012). Therefore, early loss of the perineuronal net may detrimentally affect extra-synapse glutamate receptor expression (e.g., *Grm1*) as opposed to post-synaptic receptors (e.g., *Grin2a*) (Figure 3.13). Together, these data do suggest that synaptic expression of glutamate receptors is altered in ME7 mice at 16 wpi, in the presence and absence of systemic bacterial infection, and this may have a role in the behavioural deficits that occur at this time point. To fully elucidate the effects on glutamate receptor expression immunohistochemical localisation and measurement of protein levels would provide more detail on the effects of systemic inflammation on synaptic function in ME7 mice.

3.4.5 Transferrin receptor expression in murine ME7 prion disease

One limitation with immunotherapies for CNS disorders is the limited delivery of therapeutics across the BBB and transport systems at the BBB have been targeted in order to improve delivery to the brain (Pardridge, 2012; Yu and Watts, 2013). TfR is one such target because it undergoes transcytosis at the level of the BBB and is significantly expressed on cerebral endothelial cells (Daneman et al., 2010; Zhang et al., 2014). There is also evidence of neuronal expression in the hippocampus and thalamus (Lein et al., 2007; Moos, 1996; Sunkin et al., 2013).

In ME7 mice there is stable expression of TfR transcript levels within the hippocampus and thalamus throughout disease progression. Although, there was a trend towards decreased expression at 16 wpi (Figure 3.14). Analysis of a previously published

microarray database from ME7 mice at 18 wpi shows that TfR transcripts levels are decreased compared to NBH controls in hippocampal-enriched tissues (Lunnon *et al.*, 2011). However, brain TfR expression has been measured in multiple mouse models of neurodegeneration, including the APP-PS2 model of AD, $SOD1^{G93A}$ model of MS and P301L and P301S models of tauopathy, without any alterations to expression compared to wild-type littermates (Bien-Ly et al., 2015). A difference between these models and the ME7 prion model is the presence or lack of neuronal loss (Lewis et al., 2000; Ozmen et al., 2009; Yoshiyama et al., 2007). Therefore, a possible explanation for a decrease in TfR transcripts levels in the ME7 mice at 16 wpi could be explained by the specific loss of synapses and neuronal dysfunction within the hippocampus and thalamus caused by the deposition of ME7 prion aggregates. However, in ME7 mice there is also a decrease in staining at 8 wpi, which suggests that although transcript levels do not change throughout disease progression there is altered protein expression early on. It could be postulated that given the role of TfR to provide iron for cells and its expression in hippocampal neurons, the loss of TfR early in ME7 prion disease could contribute to neuronal dysfunction.

Iron homeostasis is known to be altered in disease-affected regions in neurodegeneration, with aggregation in Aβ plaques associated with AD and accumulation in the substantia nigra during PD (Liu et al., 2018; Ward et al., 2014). Alterations in iron homeostasis are known to control expression of TfR transcripts through iron response elements, with increased cellular iron resulting in decreased TfR expression (Erlitzki et al., 2002). Furthermore, it has been shown that iron accumulation and loss of TfR in neurons results in neuronal death (Li et al., 2019; Matak et al., 2016). A decrease in TfR staining in the hippocampus and thalamus in ME7 mice at 18 wpi appears to corroborate this possibility, with a qualitative decrease in neuron-associated staining (asterisks; Figure 3.16). In support of this data, analysis of TfR expression in the striatum of a rodent model of PD showed a progressive reduction in TfR+ cells in the substantia nigra after injection of 6-hydroxydopamine (6-OHDA) (He et al., 1999). Interestingly, there was no effect on microvessel expression of TfR in these rats at any time point (He et al., 1999). This phenomenon was also observed in ME7 mice throughout disease course (Figure 3.16).

TfR expression in human AD brains has been reported in whole cortical samples or from isolated brain microvessels which suggest no change in expression compared to healthy

controls (Bien-Ly et al., 2015; Bourassa et al., 2019). However, very few studies have looked specifically at extra-vascular TfR expression. One such study in human AD brains showed reduced transferrin binding in the hippocampus compared to healthy controls, whilst vascular binding remained unchanged (Kalaria et al., 1992). This could suggest that changes in TfR expression may be limited to non-vascular cell types, in line with what is reported in this chapter. Interestingly, decreased neuronal TfR expression may prove beneficial for certain therapeutics where the target is either a cell surface marker or found in the extracellular space, such as proinflammatory cytokines. The reduction in neuronal TfR expression would reduce the likelihood of off-target engagement for soluble, extracellular targets and limit the sequestration and degradation of therapeutics. Furthermore, there is evidence that TfR undergoes constant cell surface recycling independent of transferrin binding (Watts, 1985), opening up the possibility that enhanced delivery across the BBB could still be achieved even with reduced protein expression within the hippocampus as seen in the murine ME7 prion model. However, the quantification presented here is disease-associated region specific rather than cell-type specific. Further analysis of the cell-type specific effects of ME7 prion disease on TfR expression would provide greater insights and help to elucidate the potential for enhanced delivery of immunotherapies into the CNS using TfR-mediated transcytosis across the BBB.

3.4.6 Transferrin receptor expression in ME7 mice after systemic inflammatory challenge

During infection one function of the host immune response is to remove iron from circulation and sequester it in the reticuloendothelial system, this is done to reduce the availability of the essential nutrient for the growth of pathogens, such as bacteria (Weiss, 2005). Macrophages are known to store iron during infections, and this is in part coordinated through cytokine production and modulation of iron homeostasis, and regulation of TfR expression (Weiss, 2005). In ME7 mice an additional systemic inflammatory challenge with *S. typhimurium* has no effect on hippocampal/thalamic expression of TfR transcripts four weeks after infection, regardless of concurrent neuropathology and neuroinflammation (Figure 3.15). Although, the large variation

following systemic infection at 16 wpi ultimately results in a non-significant decrease in TfR expression. Unfortunately, further tissue from *S. typhimurium* infected ME7 mice was not available to investigate this possibility and should be considered in future studies to address this lack of data.

The only previous data on TfR expression in the ME7 prion model after systemic inflammatory challenge involved the use of LPS at a later stage of disease progression, 18 wpi (Lunnon *et al.*, 2011). Analysis of microarray data suggests that LPS results in an acute decrease in TfR transcripts in hippocampal-enriched tissue six hours after peripheral injection. The difference in results following systemic challenge with LPS and *S. typhimurium* could be attributed to the nature of the models: LPS is an acute mimetic of infection, whereas *S. typhimurium* is a live infection that is known to persist in tissues for at least 21 days (Broz and Monack, 2011; Jackson et al., 2010; Rosche et al., 2015). Furthermore, LPS has been shown to induce a reduction in TfR expression on neuroblastoma cells and microglia *in vitro*, and this is reproduced following disruption of iron homeostasis and cellular iron accumulation (McCarthy et al., 2018; Reis et al., 2006). It is also of note that the response of macrophages to LPS is in contrast to that of microglia, where peripheral macrophages actually show increased TfR mRNA expression following exposure to LPS (Ludwiczek et al., 2003; Mulero and Brock, 1999; Tacchini et al., 2008).

In addition, it has been reported in the literature that *in vitro* infection of macrophages with *S. typhimurium* had no effect on TfR mRNA or protein expression within the first 36 hours (Nairz et al., 2008, 2007). These acute LPS-induced effects and analysis of *S. typhimurium* four weeks later means that we are unable to compare acute responses associated with *S. typhimurium* to the LPS response. However, there is evidence that after oral exposure, *S. typhimurium* can enter the brain and induce neurological changes (Brown et al., 2010; Chaudhuri et al., 2018; Wickham et al., 2007). In this case, it is possible that direct invasion of microglia may produce a similar acute effect on TfR expression to peripheral macrophages. In the current study, *S. typhimurium* was given through i.p. injection and although it has not been reported previously, because bacterial neuroinvasion was not investigated, the possibility that it has occurred in ME7 mice cannot be ruled out.

Overall, this chapter presents the first reports of hippocampal/thalamic TfR expression following infection with *S. typhimurium* in the murine ME7 prion model and identifies that there are differences in response compared to common models of systemic inflammation, such as LPS, and potentially between microglia and peripheral macrophages.

3.4.7 Summary

The murine ME7 prion model of neurodegeneration is a robust, reproducible model that can be followed non-invasively through the monitoring of behavioural tests and allows for assessment of therapeutic interventions with respect to neuroinflammation. The elucidation of cytokine expression throughout disease progression also enables the selection of timepoints at which possible interventions may prove most successful in the model. The characterisation of the model's response to live bacterial infection provides vital information in understanding the interactions between neuroinflammation, ongoing neurodegeneration and systemic inflammation. The *in vivo* responses of ME7 mice to live bacterial infection differs from healthy, naïve animals or *in vitro* models because of the underlying pathology at the time of challenge and therefore has the potential for variability in specific scenarios.

Overall, given that this model recapitulates many characteristics of human neurodegeneration and shows exaggerated neuroinflammatory changes in response to systemic bacterial challenge, this suggests that the murine ME7 prion model is an attractive model for drug discovery. Therefore, modulating the cytokine response through therapeutic intervention could prove useful in furthering our understanding in how to limit the co-morbid effects of systemic inflammation in patients with dementia.

Chapter 4 Generating brain-penetrant fusion proteins for neutralising central TNF-α

4.1 Introduction

The aim of this thesis is to test the hypothesis that enhanced delivery of an anti-cytokine therapeutic to the brain is beneficial and can delay disease progression in a murine model of chronic neurodegeneration. Anti-cytokine treatments exist in different forms, either as an antibody to directly neutralise the cytokine (e.g., infliximab, adalimumab for anti-TNF-α therapy) or in the form of a biologic with the aim to prevent binding to the natural receptor (e.g., anakinra for IL-1β). Antibodies that bind more than one target are known as bispecific antibodies and can be generated by combining variable domains of individual antibodies together in one molecule (Brinkmann and Kontermann, 2017). The aim of the work in this chapter was to produce and characterise bispecific antibodies and antibody fusion proteins which bind both mouse transferrin receptor (mTfR) and mouse TNFα (mTNF-α) to choose the best molecule format to take forward to *in vivo* studies.

Fusion of IL-1RA to the C-terminal end of the heavy chain of an anti-mTfR antibody was shown to effectively increase brain penetrance and proved efficacious in a model of neuropathic pain (Webster et al., 2017). A similar approach will be used here in the design of fusion proteins where an anti-mTfR antibody will be fused with a mTNF-α neutraliser. Both TNF-α and IL-1β are proinflammatory cytokines implicated in the effects of systemic inflammation on progression of dementia (Ransohoff, 2016b). Investigation using direct *in vivo* bioassays and models of systemic inflammation showed that an anti-mTfR-IL-1RA fusion protein failed to provide any benefits in peripheral response or cytokine transcript levels and as a result it was decided to proceed with targeting mTNF-α (Appendix D). Anti-mTNF-α bispecific fusion proteins were designed to have increased brain-penetrance through binding to mTfR (Figure 4.1). Control isotype fusion proteins were generated that i) bind mTNF-α but do not bind mTfR, ii) that do not bind mTNF-α, but do bind to mTfR and iii) that do not bind to mTNF-α or mTfR (Figure 4.1C). All the fusion proteins were characterised *in vitro* to determine if their target binding characteristics and biophysical profiles made them suitable candidates for *in vivo* studies.

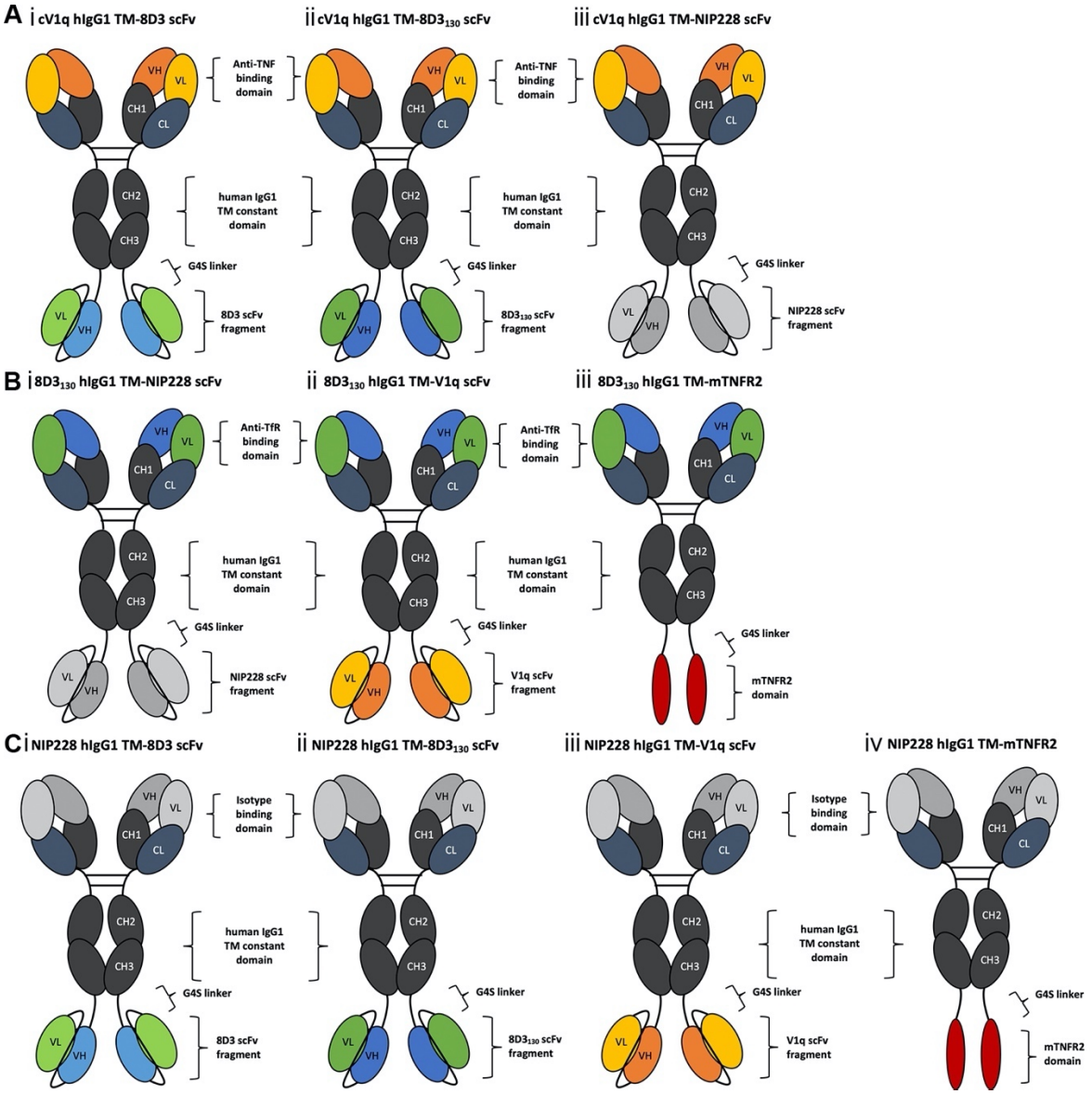

Figure 4.1 Schematic representation of anti-mTNF-α bispecific fusion proteins

(A) Anti-mTNF-α-mTfR bispecific heavy chain-scFv fusions that bind mTNF-α through cV1q variable regions (V_H and V_L) and are predicted to show increased brain penetrance through binding to mTfR via (i) 8D3 scFv or (ii) $8D3_{130}$ scFv, and (iii) a non-brain penetrant version with NIP228 isotype scFv. (B) Anti-mTfR-mTNF-α bispecific heavy chain-scFv fusions that bind mTfR via (i) $8D3_{130}$ variable regions (V_H and V_L) for increased brain penetrance with a non-mTNF-α binding isotype NIP228 scFv and bind mTNF-α through either (ii) V1q scFv or (iii) mTNFR2. (C) Isotype control heavy chain-scFv fusions that exhibit either binding to mTfR via (i) 8D3 scFv or (ii) $8D3_{130}$ scFv or bind mTNF-α through (iii) V1q scFv or (iv) mTNFR2, but not both.

4.2 Methods

Primary sequences for constant and variable regions of antibodies and fusion proteins and physicochemical properties of fusion proteins can be found in Appendix B.

4.2.1 Recombinant generation of bispecific fusion protein expression vectors

4.2.1.1 PCR amplification of antibody fragments for cloning into expression vectors

All sequences were codon optimised for expression in *Crictulus griseus* CHO cells, synthesised by GeneArt and supplied in standard GeneArt vectors (Thermo Fisher Scientific). 200 ng of DNA plasmid encoding the amino acid sequence for either mTfR, mTNFR2, single chain variable fragment (scFv), heavy chain variable region (V_H) or light chain variable region (V_L) was amplified by PCR. Specific DNA oligonucleotides (Sigma Aldrich) with overlapping nucleotides to the expression vector containing the appropriate heavy or light chain constant regions, (Persic *et al*, 1997), were designed for use with Q5 High-Fidelity 2X PCR Master Mix (New England Biolabs). Oligonucleotides were used at a final concentration of 0.4 µM in a 50 µl reaction volume. Individual oligonucleotides sequences and annealing temperatures are reported in Table 4.1, with PCR cycling conditions shown in Table 4.2. After PCR cycling, DNA products were separated using agarose gel electrophoresis and the band corresponding to the desired product was excised from the gel and DNA extracted (Section 4.2.1.5).

The pEU3.4 expression vector, encoding the human IgG kappa light chain constant region was used for cloning in V_L fragments for antibody expression. The pEU1.4 expression vector, encoding the constant region of the human IgG, subclass 1 (hIgG1) TM heavy chain, was used for cloning in mouse TNFR2 (mTNFR2), scFv and V_H fragments for the expression of antibodies and antibody fusion proteins. This hIgG1 TM heavy chain contains a triple mutation (TM) at positions L234F/L235E/P331S and has been engineered to reduced antibody-dependent cell-mediated cytotoxicity (ADCC) and complement-dependent cytotoxicity (CDC) (Oganesyan et al., 2008).

Table 4.1 Oligonucleotide sequences used for PCR amplification

Oligonucleotide Name	Sequence (5'-3')	Insert	Vector	Annealing Temperature (°C)
GAFor	GAAGGAAGGCCGTCAAGGCCACGT	V_H and V_L	pEU1.4; pEU3.4	60
GAVHRev	TTCCCGACTGGAAAGCGGGCAGTG	V_H	pEU1.4	60
GAKapRev	GGCCAGTCTTGTGCTCCAGGTACC	V_L	pEU3.4	60
CH3-G4S For	TCTCCCTGTCTCCGGGTAAAGGAG GCGGAGGATCCGGC	8D3, $8D3_{130}$, NIP228, V1q scFv	cV1q, $8D3_{130}$, NIP228 pEU1.4	67
SCFV Rev	GGCTGATTATGATCTCTAGACTAT CATCTCTT			67
VectorLink For	TCCCTGTCTCCGGGTAAAGGAGGC GGAGGATCCGGCGGAGGCGGATCT GGTGGCGGTGGATCTGTTCCAGCT CAGGTTGTG	mTNFR2	$8D3_{130}$, NIP228 pEU1.4	68
TNFR2-XbaI Rev	GTATGGCTGATTATGATCTCTAGA TTATTAGCCGCCTTTGGTAGACTG			68
V1q scFv HC For	TCTCCCTGTCTCCGGGTAAAGGTG GCGGAGGATCTGGC	V1q scFv	$8D3_{130}$, NIP228 pEU1.4	68
V1qF-K	CTCTCCCTGTCTCCGGGTGGTGGC GGAGGATCTGGCGGA	ΔK-V1q scFv	$8D3_{130}$, NIP228 pEU1.4	68
TNFR2NEBF-ΔK	CTCTCCCTGTCTCCGGGTGGAGGC GGAGGATCCGGCGGAGGCGGATCT GGTGGCGGTGGATCTGTTCCAGCT CAGGTTGTG	ΔK-mTNFR2	$8D3_{130}$, NIP228 pEU1.4	68
TNFR2-XbaI	GTATGGCTGATTATGATCTCTAGA TTATTAGCCGCCTTTGGTAGACTG			68
mTfRBssHIIF	TCTTGTCCGCGGTACCGGCGCGCA CTCACACCA	10His-mTFR	pEU1.4	65
mTfRXbaIR	TGAGGCCAGTCTTGTGCTCCGAGC TCTCTA			65

Table 4.2 PCR cycling conditions for insert amplification

Step	Step type	Temperature (°C)	Time
1	Initial Denaturation	98	30 s
2	Denaturation	98	5-10 s
3	Annealing	*50-72**	10-30 s
4	Extension	72	20-30 s /kb
5	Go to Step 2 – 25-30 times		
6	Final Extension	72	2 minutes
7	Cool	10	< 16 hours

* See Table 4.1 for specific annealing temperatures for individual oligonucleotides

4.2.1.2 Restriction enzyme digestion of expression vectors

To isolate inserts for ligation and linearise vectors, restriction digests were performed on expression vectors. Restriction enzymes used are detailed in Table 4.3. 50 µl reaction mixtures were made up as follows: 20 units (2 µl) of restriction enzyme (see Table 4.3), one unit (1 µl) of recombinant shrimp alkaline phosphatase (New England Biolabs), 5 µl 10X CutSmart buffer (New England Biolabs) and 1 or 2 µg expression vector diluted in nuclease-free water. If vectors were used for subsequent ligation reactions, recombinant shrimp alkaline phosphatase was not included. Heavy chain expression vectors (pEU1.4) were digested using the restriction enzymes BssHII and BstEII and light chain expression vectors (pEU3.4) were digested with ApaLI and PacI restriction enzymes. If double digests were required and could not be performed at the same temperature, then successive digest were performed. Following restriction digest, DNA products were separated using agarose gel electrophoresis and the required DNA fragment was excised and extracted from the gel (Section 4.2.1.5). For cloning using NEBuilder HiFi DNA assembly, target vectors were linearised using XbaI digestion (Section 4.2.1.4).

Table 4.3 Restriction enzymes and conditions used for digestion of expression vector

Restriction Enzyme	Target Sequence	Digestion Conditions (°C, minutes)	Target expression vector	Provider, Catalogue No
ApaLI	5′…G|TGCAC…3′ 3′…CACGT|G…5′	37, 60	pEU3.4	New England Biolabs, R0507S
BssHII	5′…G|CGCGC…3′ 3′…CGCGC|G…5′	50, 60	pEU1.4	New England Biolabs, R0199S
BstEII	5′…C|GTNACC…3′ 3′…CCANTG|G…5′	37, 60	pEU1.4	New England Biolabs, R3162S
PacI	5′…TTAAT|TAA…3′ 3′…AAT|TAATT…5′	37, 60	pEU3.4	New England Biolabs, R0547S
XbaI	5′…T|CTAGA…3′ 3′…AGATC|T…5′	37, 30	pEU1.4	New England Biolabs, R0145S

4.2.1.3 Ligation of inserts into expression vectors

To ligate inserts into the appropriate vector, both inserts and vectors were digested by restriction enzymes and DNA extracted as described in Section 4.2.1.2. The extracted DNA fragments were ligated using Instant Sticky-end Ligation 2X Master Mix (New England Biolabs) as per manufacturer's instructions. Briefly, a 3-fold molar excess of insert was combined with 50 - 100 ng of linearised expression vector and volume adjusted to 5 µl with nuclease-free water. 5 µl Instant sticky-end 2X Ligation Master Mix was added and mixed thoroughly by pipetting up and down 7-10 times. Ligated expression vector was transformed into Stellar Competent Cells (Takara Bio) as described in Section 4.2.1.6.

4.2.1.4 DNA assembly of scFv and mTNFR2 into expression vectors

Assembly of scFv and mTNFR2 with the appropriate heavy chain expression vector in the BsAb3 format (Dimasi *et al*, 2009) was achieved using NEBuilder HiFi DNA Assembly 2X Master Mix (New England Biolabs). The genes encoding the amino acid sequence for a $(G_4S)_3$ linker followed by either a scFv or mTNFR2 were PCR amplified and products extracted as described in Sections 4.2.1 and 4.2.1.5 respectively. PCR products were combined at a 2:1 molar ratio with 60 ng of appropriate linearised heavy chain expression vector in a total volume of 10 µl nuclease-free water. 10 µl NEBuilder HiFi DNA Assembly Master Mix was combined with vector, insert and reaction mixture incubated at 50°C for 30 minutes. Stellar Competent cells (Takara Bio) were transformed with 2 µl of DNA assembly reaction mix as described in Section 4.2.1.6.

4.2.1.5 Extraction of DNA fragments from agarose gel

PCR or restriction digest products were separated by agarose gel electrophoresis using 1% (w/v) agarose (Life Technologies) in 1X Tris-acetate-ethylenediaminetetraacetic acid (TAE) buffer (Laboratory Support Services, AstraZeneca) containing SYBR Safe DNA stain (1:10,000 dilution; Life Technologies) to visualise DNA. 10 µl 6X Purple Gel Loading Dye (New England Biolabs) was added to PCR reaction product and 50 µl was loaded directly into the gel, unless stated otherwise. 1kB Plus DNA ladder (Life Technologies) was run in parallel for size comparison, and DNA bands containing the correct size amplicon were

excised using a scalpel and extracted DNA purified using QIAquick Gel extraction kit (Qiagen) as per the manufacturer's directions. Briefly, excised DNA bands were weighed and three gel volumes of Buffer QG were added to the gel and incubated at 50°C until the gel had dissolved. One gel volume of 100% isopropanol was added, and the sample was applied to a spin column and centrifuged at 13,000 rpm for 1 minute. The column was washed using consecutive washes with 500 µl Buffer QG and 750 µl Buffer PE. Residual wash buffer was removed with further centrifugation at 13,000 rpm for 1 minute. DNA was eluted into a new microcentrifuge tube after the addition of 35 µl nuclease-free water and incubation at room temperature for 2 minutes before a final centrifugation step at 13,000 rpm for 1 minute.

4.2.1.6 Transformation of *E. coli* with expression vectors

For effective assembly of heavy chain-scFv expression vectors, plasmid DNA was grown in modified *Escherichia coli* (*E. coli*) lacking deoxyadenosine methylase and m5C DNA methyltransferase (*dam*$^-$/*dcm*$^-$) to ensure that no DNA methylation was present, as this would prevent plasmid digestion by the restriction enzyme XbaI (Marinus and Morris, 1973; Nelson et al., 1984). Methylation-free DNA plasmids were obtained by transformation of plasmid DNA into One Shot INV110 Competent *E. coli* (Invitrogen) using the following steps. Plasmid DNA was diluted to 100 pg/µl and 2 µl was added to 25 µl of thawed *E. coli* and incubated on ice for 30 minutes. *E. coli* were heat shocked at 42°C for exactly 60 seconds and placed on ice. 250 µl of SOC outgrowth media (New England Biolabs) was added to *E. coli* before incubation at 37°C, 220 rpm for 60 minutes. 100 µl of *E. coli*-containing media was plated on 2XTY agar petri containing glucose and the appropriate antibiotic selection, ampicillin (100 µg/ml) or kanamycin (50 µg/ml) (Laboratory Support Services, AstraZeneca). Plates were incubated at 37°C overnight.

For standard transformation of ligation or DNA assembly reaction mixtures and expression vectors, Stellar Competent *E. coli* (Takara Bio) were used as described below. 2 µl plasmid DNA was added to 25 µl of thawed *E. coli* and incubated on ice for 30 minutes. *E. coli* were heat shocked at 42°C for 60 s and placed on ice. 250 µl of SOC outgrowth media (New England Biolabs) was added to *E. coli* before incubation at 37°C, 220 rpm for

60 minutes. 100 µl of *E. coli*-containing media was plated on antibiotic selection agar petri dishes and plates were incubated at 37°C overnight.

4.2.1.7 Colony screening using PCR

To determine which colonies had the insert correctly incorporated in the expression vector after assembly of scFv/mTNFR2 with appropriate heavy chain, a colony screen was performed using PCR. Single *E. coli* colonies were selected and mixed with 30 µl nuclease-free water and 2 µl was added to a PCR reaction mix containing oligonucleotides to amplify the insert, described in Table 4.4, and 2X ReddyMix PCR Master Mix (ThermoFisher Scientific). PCR cycling conditions used for confirmation of insertion are shown in Table 4.5. 10 µl of PCR product was directly run on a 1% (w/v) agarose gel in TAE buffer and a 1kB Plus DNA ladder (Life Technologies) was used for size comparison and confirmation of expected amplicon size. Insert containing colonies were grown overnight in 5 ml 2xTY broth containing 100 µg/ml ampicillin (Laboratory Support Services, AstraZeneca) before expression vector was purified as described in Section 4.2.1.7.

Table 4.4 Oligonucleotide sequences used for colony screening

Oligonucleotide Name	Sequence (5'-3')	Region	Vector	Annealing Temperature
CH3 FOR	ACTACACGCAGAAGAGCCTC	scFv/mTNFR2	pEU1.4	62
VECT REV	TTTATGTTTCAGGTTCAGGG			62
IgGFor2	AACAGTAGCAGGCTTGAGG	10H-mTfR		58
pEURev	TCTTTCCGCCTCAGAAGCCA			58

Table 4.5 PCR cycling conditions for insert confirmation

Step	Step type	Temperature (°C)	Time
1	Initial Denaturation	95	2 minutes
2	Denaturation	95	25 seconds
3	Annealing	62	35 seconds
4	Extension	72	60 seconds/kb
5	Go to Step 2 – 30-40 times		
6	Final Extension	72	5-10 minutes
7	Cool	10	< 16 hours

4.2.1.8 Purification of bispecific fusion protein expression vectors

Expression vectors were purified from overnight 5 ml cultures of *E. coli* using QIAprep Spin Miniprep kits (Qiagen), respectively, according to manufacturer's instructions. Briefly, 5 ml *E. coli* cultures in 2xTY broth containing 100 µg/ml ampicillin (Laboratory Support Services, AstraZeneca) were centrifuged at 4000 rpm for 5 minutes and the pellet was re-suspended in 250 µl buffer P1. Re-suspended *E. coli* were transferred to a microcentrifuge tube and 250 µl of the lysis buffer P2 was added. After 5 minutes incubation at RT, the lysis reaction was stopped with buffer N3, and tubes were spun at 13,000 rpm for 10 minutes. The supernatant was transferred into a DNA binding column, spun at 13,000 rpm for 1 minute, and flow through discarded. Column was washed using 500 µl Buffer PB, followed by 750 µl Buffer PE. Residual wash buffer was removed with a final spin at 13,000 rpm for 1 minute. The spin column was transferred to a fresh microcentrifuge tube and 50 µl nuclease-free water was added. Columns were incubated at room temperature for 2 minutes before DNA was eluted by centrifugation at 13,000 rpm for 1 minute.

To prepare DNA for transfection of CHO cells, expression vectors were purified from 400 ml overnight cultures of *E. coli* in 2xTY broth containing 100 µg/ml ampicillin (Laboratory Support Services, AstraZeneca) using a Plasmid *Plus* Giga kit (Qiagen) according to manufacturer's directions. Briefly, 5 ml *E. coli* cultures were grown for 8 hours at 37°C and 250 rpm before spiking of a 400 ml culture using a 1:1000 dilution. 400 ml *E. coli* cultures were pelleted by centrifugation at 6,000-*g* for 10 minutes at 4°C after an overnight incubation at 37°C and 220 rpm. Pelleted bacteria were resuspended in 100 ml Buffer P1 and 100 ml Buffer P2 was added and gently mix by inverting and lysis reaction allowed to proceed RT for 5 minutes. The lysis reaction was stopped by addition of 100 ml Buffer S3 and immediately mixing. Lysate was transferred to a QIAfilter cartridge and incubated at RT for 10 minutes. Cell lysate was filtered by vacuum and applied to a QIAGEN Plasmid Plus spin column with tube extender attached to a QIAvac 24 Plus (Qiagen). DNA was bound to spin column by applying -300 mbar vacuum and drawing through filtrate. DNA was washed with consecutive application of 80 ml Buffer ETR and 50 ml Buffer PE. Residual wash buffer was removed by placing Plasmid Plus spin column in a 50 ml collection tube and centrifugation at 4500 rpm for 10 minutes. DNA was eluted by adding

5 ml nuclease-free water and transferring spin column to a fresh 50 ml collection tube and incubating at RT for 2 minutes before centrifugation for 4 minutes at 4500 rpm.

4.2.1.9 Sequencing of bispecific fusion protein expression vectors

Samples of expression vector, at 100 ng/µl, were sent to Source BioScience (Cambridge, UK) for performance of Sanger sequencing using the oligonucleotides described in Table 4.6. Sequencing data was analysed using Sequencher v5.4.1 (Gene Codes Corporation) with individual bases manually compared to chromatograms and any ambiguous bases were corrected if chromatogram showed presence of correct base. Primary sequences for constant and variable regions of antibodies and fusion proteins can be found in Appendix B.

Table 4.6 Oligonucleotides used for sequencing bispecific fusion protein expression vectors

Oligonucleotide	Region	Sequence (5'-3')	Vector
MHM HHF	Heavy chain, CH1	GCCACCATGGGATGGAGCTGTATCA	All heavy chain pEU1.4 vectors
CH1 rev		AGACCCTCTCCCTGAGCATGAGTGG	
Hinge for	Heavy chain, hinge and CH2	GAGGACCCTGCCCCTGACCTAAGCC	
CH2 rev		CCTCTGTCCATGTGGCCCTC	
CH3 for	Heavy chain, CH3	GAGGGCCACATGGACAGAGG	
MHM HHR		TAATGCGCCGCTACAGGGCGCGTGG	
CH3-G4S For	Linker + scFv/mTNFR2	ACTACACGCAGAAGAGCCTC	
VECT REV		TTTATGTTTCAGGTTCAGGG	
SCFV VL FOR		GTAGGCCTATCGCGATCTAG	
SCFV VH REV		AACCTCCGCCAGATGTAGAT	
HLKC for1	Kappa light chain, CL	ATCTGGGATAAGCATGCTG	All light chain pEU3.4 vectors
HLKC rev		AGGTGAAAGATGAGCTGGAGGACCG	

4.2.2 Purification of bispecific fusion proteins

4.2.2.1 Transfection of CHO cells with expression vectors

Modified CHO cells (Daramola et al., 2014) were diluted to 4 x 10^6 cells/ml in cell culture medium (Laboratory Support Services, AstraZeneca). Flasks (1-6/protein) containing 500 ml cells were co-transfected with 250 µg bispecific heavy chain expression vector and 250 µg light chain expression vector, or with 500 µg vector encoding 10His-mTfR. DNA was prepared at 31.25 µg/ml in 8200 µl 150 mM NaCl, then an equal volume of PEI MAX (40,000 MW, Polysciences) diluted to 187.5 µg/ml in 150 mM NaCl (Laboratory Support Services, AstraZeneca) was added and vortexed for 10 s. The mixture was incubated for 1 minute before adding to cells. Cells were incubated at 37°C in a humidified shaking incubator (5% $C0_2$; 140 rpm) for 4 hours before addition of F009 feed (3.4% v/v) and F010 feed (0.2% v/v) (both Laboratory Support Services, AstraZeneca) and transfer to a humidified shaking incubator at 34°C for 7 days. Cells were given additional feed on Day 3 and 6 after transfection – F009 feed (6.8% v/v) and F010 feed (0.4% v/v) – before supernatant was harvested on Day 7 after transfection. Seven days after transfection, CHO cells were centrifuged at 4000 rpm for 45 minutes and supernatant passed through a 0.22 µm filter (Stericup).

4.2.2.2 Protein A affinity chromatography-based IgG purification

IgG containing fusion proteins were purified from crude CHO cell supernatant using Protein A-based affinity chromatography HiTrap MabSelect SuRe columns (GE Healthcare) on an AKTA Pure system (GE Healthcare). Sample was loaded onto the column at 2 ml/minute using a sample pump until air was detected in the system and then D-PBS (Sigma Aldrich) was run to load remaining sample on to the column. The column was then washed with 40 column volumes (CV) of D-PBS to remove any unbound protein, and system flow-through was collected. Protein was eluted in 20 CV 0.1 M sodium citrate, pH 3.0 buffer and collected in 2 ml fractions in a 96-deep well plate. Column was sanitised with 10 CV 0.1 M NaOH followed by equilibration in 20 CV D-PBS between runs. Protein containing fractions, as determined by absorbance at 280 nm, were pooled.

4.2.2.3 Buffer exchange of fusion proteins

Proteins were buffer exchanged using the gravity protocol of PD-10 desalting columns (GE Healthcare). Buffer desalting columns were equilibrated with 25 ml of desired buffer, and 2.5 ml of sample was loaded onto column. Elution buffer (3.5 ml) was added, and protein was eluted in desired buffer. Protein concentration was determined using absorbance at 280 nm (Section 4.2.2.7).

4.2.2.4 Sodium dodecyl sulphate–polyacrylamide gel electrophoresis (SDS-PAGE)

5 µl 4X Bolt LDS Sample buffer (ThermoFisher) was added to 15 µl sample. The sample was mixed and 10 µl was loaded directly into the well of a Bolt 4-12% Bis-Tris gel (ThermoFisher). 5 µl See Blue Plus2 Prestained protein standard (ThermoFisher) was loaded on each gel. Gels were run at 200 V for 25 minutes in 1X Bolt MES SDS Running buffer (ThermoFisher). Gel was stained in Instant Blue (Expedeon) for 2 - 3 hours before being destained in MilliQ water overnight.

4.2.2.5 Size exclusion chromatography (SEC)

Pooled protein samples were loaded on to a HiLoad 26/600 Superdex 200pg column (GE Healthcare) at a flow rate of 1 ml/minute via a 20 ml superloop. Protein was eluted in 1 CV of desired buffer, either 1x D-PBS (Sigma Aldrich) or Acetate pH 5.0 buffer (Appendix A1) (Laboratory Support Services, AstraZeneca) and collected in 2 ml fractions in a 96-deep well plate. Selected protein-containing fractions, as determined by absorbance at 280 nm and SDS-PAGE (Section 4.2.2.4), were pooled as a final protein pool.

4.2.2.6 Concentration of fusion proteins

Bispecific fusion protein pools were concentrated using either a Vivacell 100, 10 kDa MWCO (Sartorius) or Vivaspin 20, 30 kDa MWCO (Sartorius) depending on final protein pool volume. Concentration was achieved by centrifugation at 2,000 x *g* for Vivacell 100 or 3,000 x *g* for Vivaspin 20, and total centrifugation time was related to protein size and

starting volume. Final protein volume was determined by downstream requirements of protein and final concentration was determined by absorbance at 280 nm (Section 4.2.2.7).

4.2.2.7 Nanodrop measurement of fusion protein concentration

Purified protein concentration was calculated by absorbance at 280 nm using the Beer-Lambert Law: $A_{280} = \varepsilon cl$; where ε is the molar extinction coefficient (M^{-1} cm^{-1}); c is the molar concentration and l is the pathlength in cm (l = 1 cm). An average of four absorbance measurements was used to calculate protein concentration. The molar extinction coefficient was calculated based on the amino acid sequence of the protein (Pace et al, 1995). Physicochemical properties, including molecular mass and molar extinction coefficients, of fusion proteins can be found in Appendix Table E.

4.2.3 *In vitro* characterisation of bispecific fusion proteins

4.2.3.1 Neutralisation of mTNF-α induced cytotoxicity

Neutralisation of mouse TNF-α by fusion proteins was determined by measuring cell viability levels in L929 mouse fibroblasts after incubation with mouse TNF-α in the presence of Actinomycin D (Goodall et al., 2015). Actinomycin D, an mRNA synthesis inhibitor, was included as a sensitizer of L929 cells; this is achieved through inhibition cell growth and reducing effects of cell density on assay sensitivity (Flick and Gifford, 1984; Trost and Lemasters, 1994).

For neutralisation of TNF-α, L929 cells were seeded in a 96-well plate at 400,00 cells/ml in Dulbecco's Modified Eagle's Media (DMEM) containing 10% (v/v) heat-inactivated and gamma irradiated fetal bovine serum (FBS) (both Sigma) and incubated for 24 hours in a humidified atmosphere (95% O_2, 5% CO_2) at 37°C. Mouse TNF-α was diluted to 200 pg/ml in assay media and bispecific fusion proteins were serially diluted 1:3 in DMEM containing 10% (v/v) FBS and 1 µg/ml Actinomycin D (Sigma); final concentration range of 15.24 pM - 100 nM for V1q scFv-containing fusion proteins, or 457 fM - 3 nM for mTNFR2-containing fusion proteins. Mouse TNF-α, Actinomycin D and bispecific fusion protein were pre-

incubated for 30 minutes at 37°C before addition to L929 fibroblasts and a further incubation in a humidified atmosphere (95% O_2, 5% CO_2) at 37°C for 20 hours. 20 µl Cell Titre 96 AQ_{ueous} One Solution reagent (Promega) was added to each well and incubated for 4 hours in a humidified atmosphere (95% O_2, 5% CO_2) at 37°C. Cell viability was calculated from absorbance values measured at 490 nm on an Envision plate reader (Perkin Elmer) using the equation:

$$\text{Percentage cell viability} = \frac{\text{absorbance at 490nm}}{\text{average absorbance of negative control}} \times 100;$$

where negative control wells contain L929 fibroblast cells in DMEM containing 10% (v/v) FBS and 1 µg/ml Actinomycin D only.

Increased cell viability was considered effective neutralisation of mTNF-α and IC_{50} values were calculated using the Nonlinear fit: sigmoidal, 4PL, log(concentration) with least-squares regression function in Prism 8 (v4.2.3, Graphpad).

4.2.3.2 Bio-layer interferometry kinetics measurements of bispecific fusion proteins to target proteins

Additional experiments with mTfR were performed with assistance from Alan Sandercock and Susan Fowler at AstraZeneca (Cambridge, UK).

Binding and affinity measurements were determined using bio-layer interferometry (BLI) kinetic assays using an Octet RED384 system (Forte Bio). For all kinetics assays antibody or fusion protein was immobilised using Anti-Human IgG Fc Capture biosensors (Forte Bio). Fusion proteins were diluted to 50 or 100 nM in D-PBS containing 1 mg/ml BSA and 0.01% v/v Tween 20 (all Sigma Aldrich) and a titration (ranging from 7.8125 to 1000 nM) of antigen - recombinant mouse TNF-α (Peprotech) or 10His-mTfR (Section 4.2.3.4.1) - was achieved through a 1:2 or 1:3 serial dilution in in D-PBS containing 0.1% (v/v) BSA and 0.01% (v/v) Tween 20. For all kinetic assays, 100 µl of fusion protein/antigen/buffer was added to the required wells of a tilted well 384-well plate (Forte Bio). Plate and sensors were equilibrated at 30°C for 10 minutes with continual agitation at 1000 rpm before initiation of kinetic measurements. Assay was set up with a 60 s baseline reading, a fusion protein-loading step of 120 s followed by a second 60 s baseline reading, before association with antigen for 300 s and dissociation of antigen in buffer for 600 s. Raw data

was processed using subtraction of reference wells, with an inter-step correction for dissociation, before analysis using a local R_{max} fit with a 1:1 binding model for all fusion protein concentrations to generate affinity for the antigen.

4.2.3.3 AlphaScreen binding measurements of bispecific fusion proteins to mTfR

Binding between mTfR and fusion proteins was measured using the AlphaScreen principle (Peppard et al., 2003). Biotinylated 10His-mTfR (Section 4.2.3.4.2) was diluted to 100 nM (4X concentrate) in D-PBS containing 0.1% BSA and 0.01% Tween-20 (all Sigma Aldrich) before 2.5 μl was added to the required wells of a 384-well plate (Corning). Fusion proteins were titrated across an 8-point 1:2 serial dilution in D-PBS containing 0.1% BSA and 0.01% Tween-20with a final well concentration range of 7.8 nM - 1 μM. 2.5μl fusion protein dilution was added to the plate before adding 10 μl of a streptavidin-coated donor beads and Protein A-coated acceptor beads mix (both Perkin Elmer) at a final concentration of 20 μg/ml for each bead. Reaction mix was incubated in the dark at room temperature for 4 hours before fluorescence was read at 570 nm using an Envision plate reader (Perkin Elmer).

Wells containing mTfR and beads only were included as a non-specific binding control and an average reading was used to calculate specific binding from assay wells:

$$\text{Specific binding} = \frac{\text{absorbance at 570nm}}{\text{average absorbance of non-specific binding}}$$

Specific biding values were graphed using the Nonlinear fit: sigmoidal, 4PL, log(concentration) with least-squares regression function in Prism 8 (v4.2.3, Graphpad). Relative assay signal was determined by using the maximal response for that protein as 100% and then calculating the proportional response from the other concentrations:

$$\frac{specific\ binding\ response}{maximal\ binding\ response} \times 100$$

4.2.3.4 Generation of biotinylated 10His-mTfR

4.2.3.4.1 Purification of 10His-mTfR

CHO cells were transfected as described in Section 4.2.2.1. Seven days after transfection, CHO cells were spun at 4000 rpm for 45 minutes and supernatant filtered through a 0.22 µm filter (Stericup). Protein was purified from crude CHO cell supernatant using immobilised metal ion affinity chromatography HisTrap Excel columns (GE Healthcare) on an AKTA Pure system (GE Healthcare). Sample was loaded on to the column at a flow rate of 5 ml/minute using a sample pump and was washed with 20 CV 2X D-PBS (Laboratory Support Services, AstraZeneca). Protein was eluted using the following multi-step elution program: Column wash with 45 CV of 30 mM Imidazole in 2X D-PBS (Laboratory Support Services, AstraZeneca) with fractions collected every 45 ml, followed by a gradient elution of protein using 30-400 mM Imidazole in 2X D-PBS over 10 CV, with fractions collected every 2 ml. Column was washed with 400 mM imidazole in 2X D-PBS (Laboratory Support Services, AstraZeneca) after elution of protein. Protein containing fractions, as determined by absorbance at 280 nm, were pooled and concentrated using a Vivaspin 20 centrifugal concentrator to a final volume of 6 ml and loaded on to a HiLoad 16/600 Superdex 200pg column (GE Healthcare) at a flow rate of 1 ml/minute. Protein was eluted in 1 CV of 1X D-PBS (Sigma Aldrich) and collected in 2 ml fractions. Protein fractions were analysed by SDS-PAGE and concentration of pooled protein was determined by absorbance at 280 nm.

4.2.3.4.2 Biotinylation of 10His-mTfR

Biotinylation of 10His-mTfR (2 moles per mole of protein) was achieved by incubation of protein with an 80-fold molar excess of EZ-Link Sulfo-NHS-LC biotin (Thermo Scientific) reconstituted in nuclease-free water (VWR) for 30 minutes at room temperature. Excess biotin was removed by buffer exchange of solution into 1X D-PBS (Sigma Aldrich) using a 2 ml Zeba Spin Desalting column (Thermo Scientific), with a 7 kDa molecular weight cut-off. Spin column was equilibrated with 3 CV of 1X D-PBS before addition of protein sample, and protein was eluted by centrifugation at 1,000 x *g* for 2 minutes. Protein concentration was calculated from absorbance at 280 nm using Beer-Lambert equation. Incorporation of biotin was quantified using a Pierce Biotin Quantification kit (Thermo Scientific), will

volumes for the cuvette method adjusted to reduce sample usage. Briefly, displacement of HABA from HABA-avidin complex by biotin results in a decrease in absorbance at 490/500 nm. The difference in absorbance is used to calculate the moles of biotin per mole of protein using the following sequence of equations:

$$1.\ \text{Concentration of biotin} = \frac{\Delta A490\ (H/A - H/A/B)}{\varepsilon};\ \varepsilon = 34{,}000\ M^{-1}\ cm^{-1}$$

$$2.\ \text{biotin:protein molar ratio} = \frac{[\text{biotin}]\ \text{x dilution factor}}{[protein]}$$

4.2.4 Quality Control analysis of fusion proteins

4.2.4.1 Quantitative endotoxin testing

Limulus Amoebocyte Lysate (LAL) endotoxin quantification of fusion proteins was performed by Jennifer Spooner at AstraZeneca (Cambridge, UK) using the Limulus Amoebocyte Lysate (LAL) Kinetic-QCL kit (Lonza) as per manufacturer's instructions. Briefly, samples were measured for reaction time taken, where time is inversely proportional to endotoxin levels, using an increase in 0.2 absorbance units at 405 nm. A standard curve is used to calculate the amount of endotoxin present in the samples and was generated in the range of 0.005 to 5 EU/ml through 1:10 serial dilutions, with vigorous vortexing for 1 minute between dilutions.

4.2.4.2 High performance liquid chromatography-size exclusion chromatography (HPLC-SEC)

Protein analysis by HPLC-SEC was performed by Jennifer Spooner at AstraZeneca (Cambridge, UK) as described below.

HPLC-SEC (Agilent Systems) was performed by loading 70 µl of sample onto a TSKgel G3000SWXL (Sigma); 5 µm, 7.8 mm x 300 mm column using a flow rate of 1 ml/minute and 0.1 M sodium phosphate dibasic anhydrous + 0.1 M sodium sulphate, pH 6.8 as the isocratic running buffer. A gel filtration standard (Bio-Rad) and a NIP228 hIgG1 TM control are also run for quality control and comparative purposes.

4.2.4.3 Ultra-performance liquid chromatography-mass spectrometry (UPLC-MS)

UPLC-MS analysis of glycosylated and deglycosylated fusion proteins, as described below, was performed by Esther Martin at AstraZeneca (Cambridge, UK).

Experiments were performed using an ACQUITY I-Class UPLC coupled to a Xevo G2-XS Q-TOF instrument (Waters); both operated using UNIFI Scientific Information System. For the LC system, Solvent A was water with 0.1% formic acid and solvent B was acetonitrile with 0.1% formic acid (both UPLC-MS grade, BioSolve). The UV detector was set to measure at wavelengths of 220 nm and 280 nm and the vials placed in a sample chamber maintaining a temperature of 4°C. The protein was diluted to 0.1 mg/ml, placed in an LC-MS vial, and then put into the auto-sampler. A volume of 1 µl was injected onto a reverse phase ACQUITY UPLC Protein BEH C4 Column, 300 Å-pore column (Waters) and proteins were eluted using an increasing gradient of solvent B. The mass spectrometer was calibrated from 500-5000 m/z by infusing 2 µg/µl sodium iodide in 50% 2-propanol and the lockspray was 200 pg/µl Leucine Enkephalin. The instrument was operated in positive ionisation mode and sensitivity analyser mode with the following key settings: capillary voltage = 3.0 V; sample cone voltage = 40 V; source temperature = 120°C; desolvation temperature = 450°C; cone gas flow = 120 L/h; desolvation gas flow = 1000 L/h; mass range = 500-5000 m/z, scan time = 1.0 second. Data were processed in UNIFI software. The spectra were combined from the retention time in the chromatogram where the protein of interest eluted. The raw data was background subtracted and deconvoluted using MaxEnt1 algorithm for large molecules. The experimental data was compared to the mass of theoretical sequences that took into consideration disulfide bonds for non-reduced analysis and free cysteines for reduced analysis.

4.2.4.3.1 Deglycosylation of protein samples for UPLC-MS

Deglycosylation of fusion proteins, as described below, was performed by Esther Martin at AstraZeneca (Cambridge, UK).

Deglycosylation was carried out using Protein Deglycosylation Mix II (New England Biolabs) which removes both N-linked and O-linked glycans. For denaturing/reducing

reaction conditions, 100 µg of protein was prepared in 40 µl of water. 5 µl of Deglycosylation Mix Buffer 2 was added and incubated at 75°C for 10 minutes in a heating block. The sample was cooled down and 5 µl of Deglycosylation Mix II added to the protein. The reaction was incubated at 25°C for 30 minutes and then transferred to a 37°C incubator for a further hour. For native/non-reducing reaction conditions (to keep fusion proteins intact), 100 µg of protein was prepared in 40 µl of water and 5 µl of Deglycosylation Mix Buffer 1 was added. The reaction was incubated at 25°C for 30 minutes and then transferred to a 37°C incubator for 16 hours.

4.3 Results

4.3.1 Production of cV1q hIgG1 TM antibody

The anti-mTNF-α antibody, V1q, is only commercially available as a rat IgD antibody (Abcam; ab8097). To generate a recombinant hIgG1 TM version of this antibody (cV1q hIgG1 TM), the amino acid sequences for the V_H and V_L regions are required (Appendix B). The biological activity of the IgD format antibody has been previously described in the literature (Echtenacher et al., 1990; Gatti et al., 1993).

4.3.1.1 Generation of cV1q heavy and light chain expression vectors

DNA sequences for the V_H and V_L regions were amplified from GeneArt supplied vectors by PCR amplification for cloning into hIgG1 TM heavy chain (pEU1.4) and kappa light chain (pEU3.4) expression vectors which already contained the genes coding the antibody constant regions. Expression plasmids were linearised by restriction enzyme digestion and variable domain sequences were ligated into the appropriate expression vectors (Table 4.3; Section 4.2.1.2).

E. coli was transformed with either heavy chain or light chain expression vectors and bacterial colonies were screened for vector containing the inserted DNA and checked for the correct heavy and light chain sequences. Successful insertion of variable domain DNA was confirmed using agarose gel electrophoresis and the presence of a DNA band between 300 and 400 base pairs (Figure 4.2). All selected colonies (#1 - #4) for cV1q V_H contained the correct sequences, whilst only colonies #2 and #3 for cV1q V_L contained the correct sequence. For purification of cV1q hIgG1 TM, cV1q pEU1.4 colony #1 containing the cV1q V_H expression vector and cV1q pEU3.4 colony #2 containing cV1q V_L expression vector were used (both highlighted in Figure 4.2).

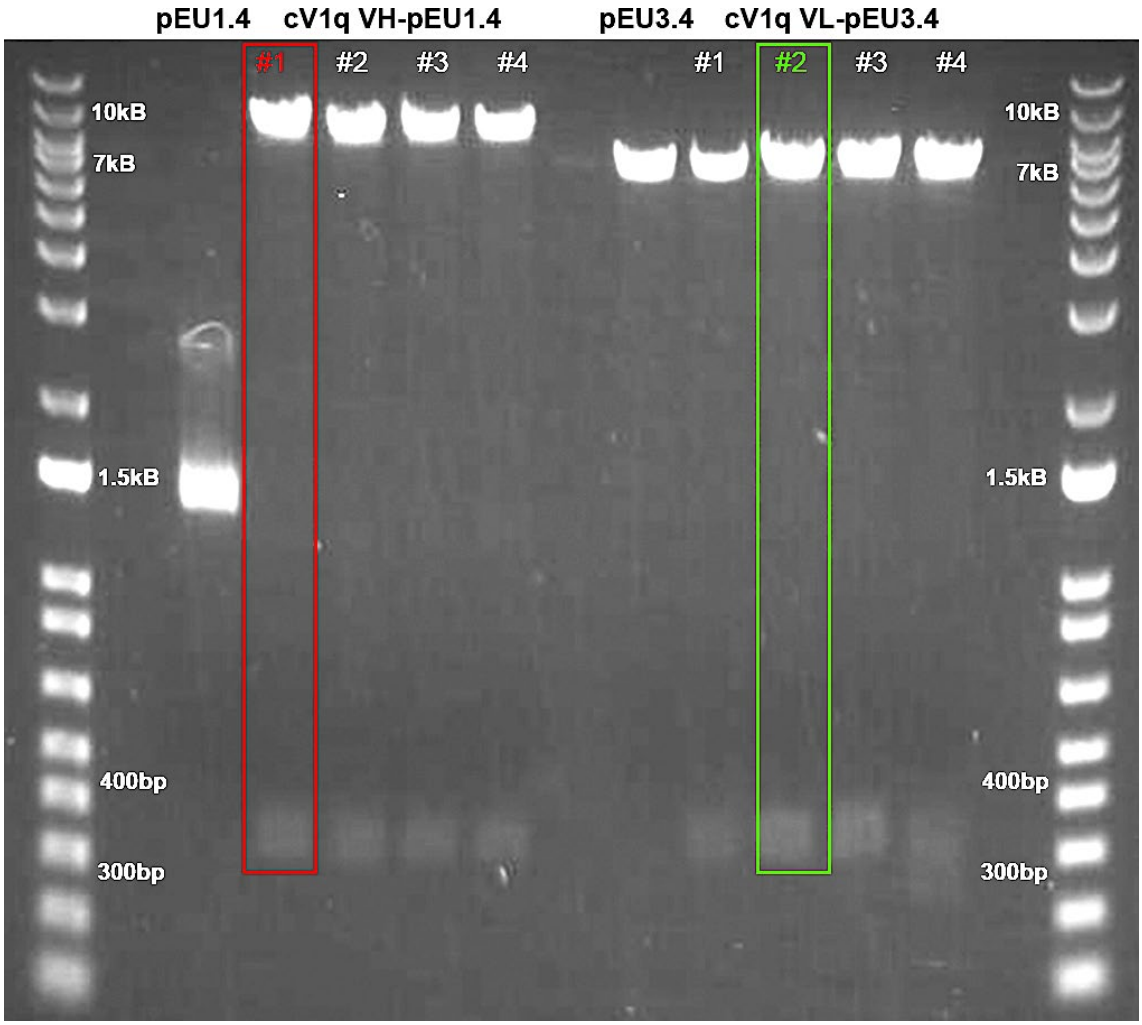

Figure 4.2 Insert confirmation by restriction digestion and DNA separation

Heavy chain expression vectors were digested with BstEII and BssHII, and kappa light chain pEU3.4 expression vectors were digested with ApaLI and PacI. 1µg DNA was separated on a 1% agarose gel run at a constant voltage of 100 V for 45 minutes. DNA bands highlighted at ~350bp represent the variable fragment inserts, confirming successful ligation and production of cV1q V_H pEU1.4 (colonies #1 - #4) and cV1q V_L pEU3.4 (colonies #1 - #4) expression vector. Digested expression vectors incubated without heavy (pEU1.4) or light (pEU3.4) chain insert were run as controls for insertion. Highlighted positive colonies for cV1q V_H pEU1.4 (red) and cV1q V_L pEU3.4 (green) were selected for antibody purification.

4.3.1.2 Purification of cV1q hIgG1 TM antibody

CHO cells were transfected with expression vectors for cV1q heavy and light chain and protein was purified from the supernatant seven days later. Protein was eluted using Protein A-based affinity chromatography (Figure 4.3A). Select protein-containing fractions were pooled and buffer exchanged into 1X D-PBS, pH 7.4 and analysed by SDS-PAGE and HPLC-SEC for correct molecular weight and monomeric protein (Figure 4.3). cV1q hIgG1 TM is used throughout this chapter as a control for binding, affinity measurements and neutralisation of mTNF-α when assessing bispecific fusion protein function.

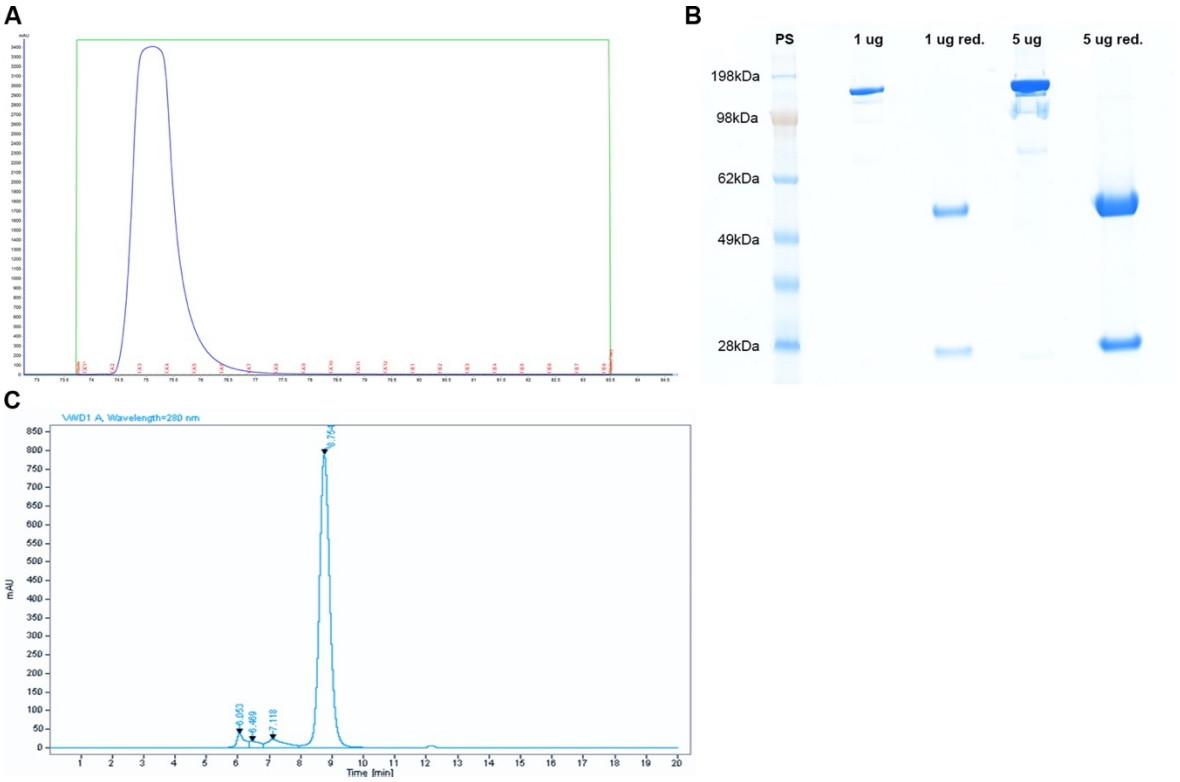

Figure 4.3 Protein analysis of cV1q hIgG1 TM
(A) cV1q hIgG1 TM antibody was eluted in 10 CV 100% 0.1 M sodium citrate pH 3.0 (green line). Protein was collected in 0.5 ml fractions (red annotations) and selected protein containing fractions, as determined by absorbance at 280 nm (purple line), were pooled and buffer exchanged into 1X D-PBS. (B) Reducing SDS-PAGE confirmation of cV1q hIgG1 TM purification, with protein reduction confirming heavy chain (50 kDa) and light chain (25 kDa) molecular weights when compared to protein standard (PS). (C) HPLC-SEC trace confirming monomeric protein peak at 8.754 minutes. HPLC-SEC experiments and analyses were performed by Jennifer Spooner at AstraZeneca (Cambridge, UK).

4.3.2 Production of brain-penetrant cV1q hIgG1 TM bispecific heavy chain-scFv fusion proteins

Bispecific heavy chain-scFv fusion proteins were designed to bind both mTfR and mTNF-α by introducing a second binding region C-terminal to the IgG heavy chain (Figure 4.4) (Dimasi *et al.*, 2009). A scFv of either a high affinity (8D3) or low affinity ($8D3_{130}$) anti-mTfR antibody, or isotype control antibody (NIP228), is attached to the C-terminus of an anti-mTNF-α antibody via a 15 amino acid linker (GGGGSGGGGSGGGGS). Brain penetrant non-mTNF-α binding NIP228 isotype control antibody-scFv fusions were produced in parallel (Figure 4.4). The scFv formats of 8D3, $8D3_{130}$ and NIP228 were designed based on previous methods used to generate an scFv of 8D3 (Hultqvist et al., 2017). The heavy

chain variable region was located N-terminal to the light chain variable region and is separated by an 18 amino acid linker (GSTSGGGSGGGSGGGGSS).

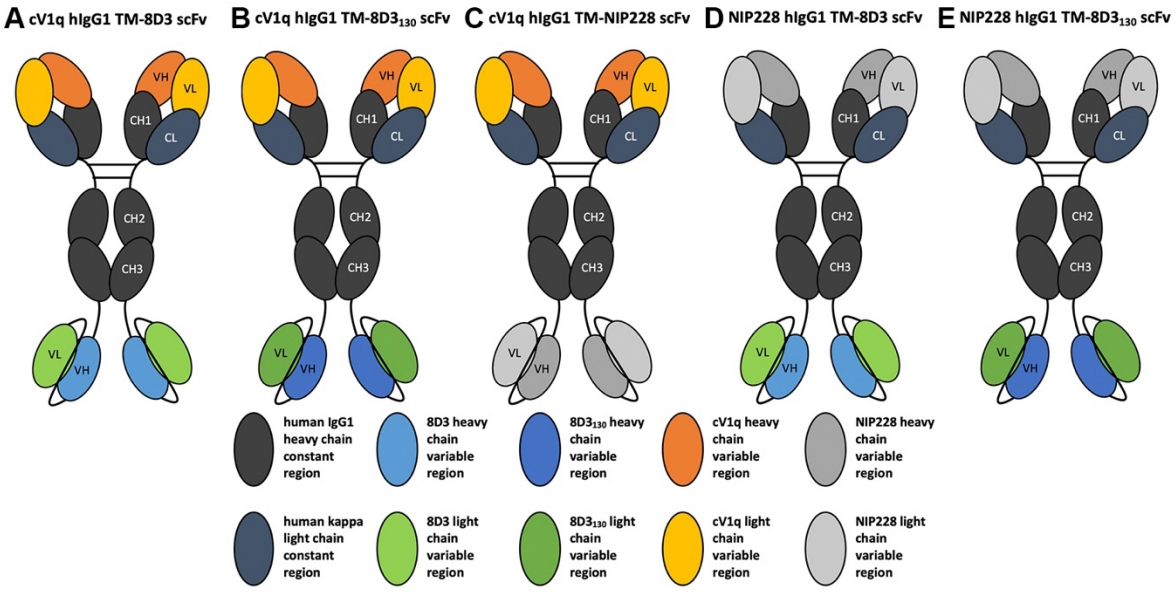

Figure 4.4 Schematic representation of anti-mTNF-α-anti-mTfR bispecific heavy chain-scFv fusion proteins

(A-C) An anti-mTNF-α antibody, cV1q hIgG1 TM fused to either (A) 8D3 scFv or (B) $8D3_{130}$ scFv, for enhanced brain penetration, or (C) a non-brain penetrant version with NIP228 isotype scFv. (D-E) A non-mTNF-α binding isotype control bispecific antibody, NIP228 hIgG1 TM, fused with either (D) 8D3 scFv or (E) $8D3_{130}$ scFv, for enhanced brain penetration.

4.3.2.1 Generation of bispecific heavy chain-scFv expression vectors

Anti-mTfR and isotype control heavy chain-scFv fusion expression vectors were generated using NEBuilder HiFi DNA assembly (Section 4.2.1.4) and selected colonies were screened for insertion of DNA encoding scFv (Figure 4.5). Expression vector purified from colonies NIP228 hIgG1 TM-$8D3_{130}$ scFv pEU1.4 #2, NIP228 hIgG1 TM-8D3 scFv pEU1.4 #1, cV1q hIgG1 TM -NIP228 scFv pEU1.4 #3, cV1q hIgG1 TM-$8D3_{130}$ scFv pEU1.4 #5 and cV1q hIgG1 TM-8D3 scFv pEU1.4 #4 were used for transfection of CHO cells.

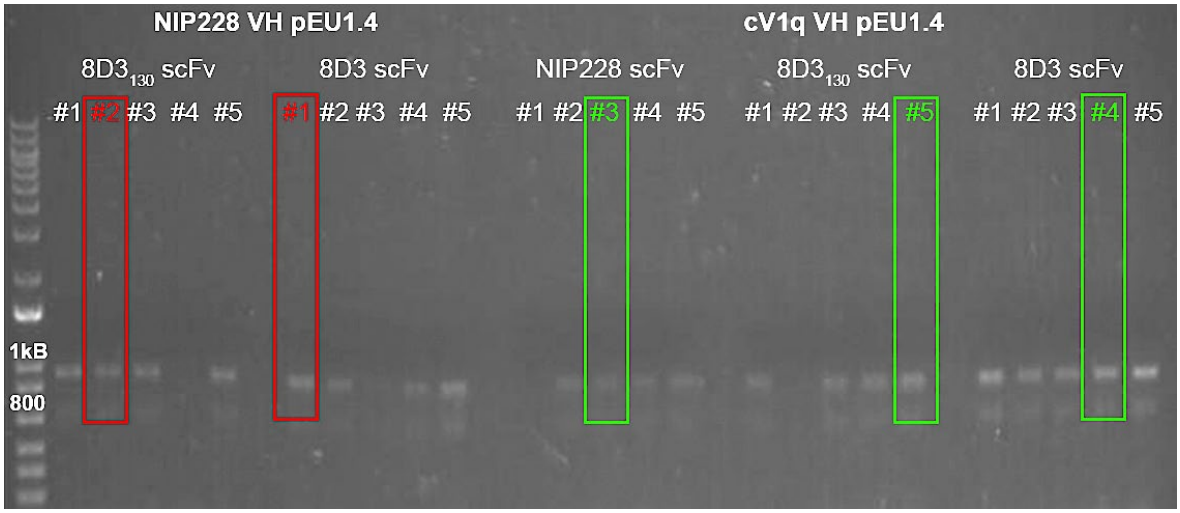

Figure 4.5 Insert confirmation by PCR amplification and agarose gel electrophoresis
NIP228 hIgG1 TM-8D3$_{130}$ scFv pEU1.4 colonies #1 - #5, NIP228 hIgG1 TM-8D3 scFv pEU1.4 colonies #1 - #5, cV1q hIgG1 TM-NIP228 scFv pEU1.4 colonies #1 - #5, cV1q hIgG1 TM-8D3$_{130}$ scFv pEU1.4 colonies #1 - #5 and cV1q hIgG1 TM-8D3 scFv pEU1.4 colonies #1 - #5 were PCR amplified and products were separated on a 1% agarose gel run at a constant voltage of 100 V for 45 minutes. DNA bands highlighted at ~900 bp represent the insert in heavy chain expression plasmids and confirms successful insertion and assembly. Highlighted positive colonies for NIP228 V_H pEU1.4 constructs (red) and cV1q V_H pEU1.4 constructs (green) were selected for antibody purification.

4.3.2.2 Purification of NIP228 and cV1q hIgG1 TM bispecific heavy chain-scFv fusion proteins

Bispecific heavy chain-scFv fusion proteins were purified from CHO cell supernatant using Protein A-affinity chromatography. Bispecific heavy chain-scFv fusion proteins were initially buffer exchanged into D-PBS pH 7.4 from elution buffer, 0.1 M sodium citrate pH 3.0. However, precipitation was evident after overnight storage at 4°C. Precipitation suggests instability in D-PBS pH 7.4 and bispecific heavy chain-scFv fusion proteins were buffer exchanged into 50 mM sodium acetate, 100 mM sodium chloride pH 5.5 to attempt solubilisation of protein. However, precipitation was again evident after an overnight storage at 4°C. Bispecific heavy chain-scFv fusion proteins were buffer exchanged into 25 mM sodium acetate, 175 mM sodium chloride, pH 5.0 (Acetate pH 5.0 buffer) and the resulting higher salt concentration and lower pH had a positive effect on solubility with no precipitate visible after an overnight storage at 4°C.

With a stable buffer formulation identified, protein purification was repeated, and eluted bispecific fusion proteins were immediately buffer exchanged into Acetate pH 5.0 buffer. Protein size in eluted fractions was confirmed by SDS-PAGE and monomeric protein purity of the sample preparation was determined by HPLC-SEC analysis (Figure 4.6). Protein

concentration, as determined using a molar extinction coefficient based on the amino acid sequence (Appendix Table E), and initial monomeric protein HPLC-SEC analysis showed that current samples showed sufficient yield for scalability ahead of production for *in vivo* use (Table 4.7). However, high aggregate levels suggest that further separation of monomeric protein, using size exclusion chromatography (SEC), is required following affinity chromatography (Figure 4.6C). Further HPLC-SEC analysis confirmed that the additional SEC step was sufficient to ensure suitable removal of aggregates prior to *in vitro* characterisation of bispecific heavy chain-scFv fusion proteins (Figure 4.6D; Table 4.8).

In addition, the endotoxin level in each bispecific heavy chain-scFv fusion protein preparation was determined using a quantitative LAL assay (Table 4.7). Measured endotoxin levels are significantly below the limit for (1.5 EU/ml) and preclinical bolus injections in humans (0.5 EU/mg) (Dawson, 2017; Malyala and Singh, 2008), suggesting that the preparation methods used result in proteins suitable for *in vivo* administration.

Table 4.7 Summary of bispecific heavy chain-scFv fusion protein characterisation
Protein purity was determined by HPLC-SEC and endotoxin levels by LAL assay with experiments and analyses performed by Jennifer Spooner at AstraZeneca (Cambridge, UK).

Bispecific heavy chain-scFv fusion protein	Concentration (mg/ml)	Monomeric protein purity (%)	Endotoxin (EU/ml)	Endotoxin (EU/mg)
cV1q hIgG1 TM-8D3$_{130}$ scFv	2.40	66.28	0.08	0.03
cV1q hIgG1 TM-8D3 scFv	2.08	64.20	0.08	0.04
cV1q hIgG1 TM-NIP228 scFv	1.31	82.72	0.08	0.06
NIP228 hIgG1 TM-8D3$_{130}$ scFv	1.23	73.39	0.08	0.07
NIP228 hIgG1 TM-8D3 scFv	2.12	67.77	0.10	0.05

Table 4.8 Summary of properties for SEC purified bispecific heavy chain-scFv fusion proteins
Protein purity was determined by HPLC-SEC with experiments and analyses performed by Jennifer Spooner at AstraZeneca (Cambridge, UK).

Bispecific heavy chain-scFv fusion protein	Concentration (mg/ml)	Monomeric protein purity (%)
cV1q hIgG1 TM-8D3$_{130}$ scFv	1.19	96.44
cV1q hIgG1 TM-8D3 scFv	0.64	98.63
cV1q hIgG1 TM-NIP228 scFv	1.44	97.62
NIP228 hIgG1 TM-8D3$_{130}$ scFv	0.71	96.31
NIP228 hIgG1 TM-8D3 scFv	1.81	98.49

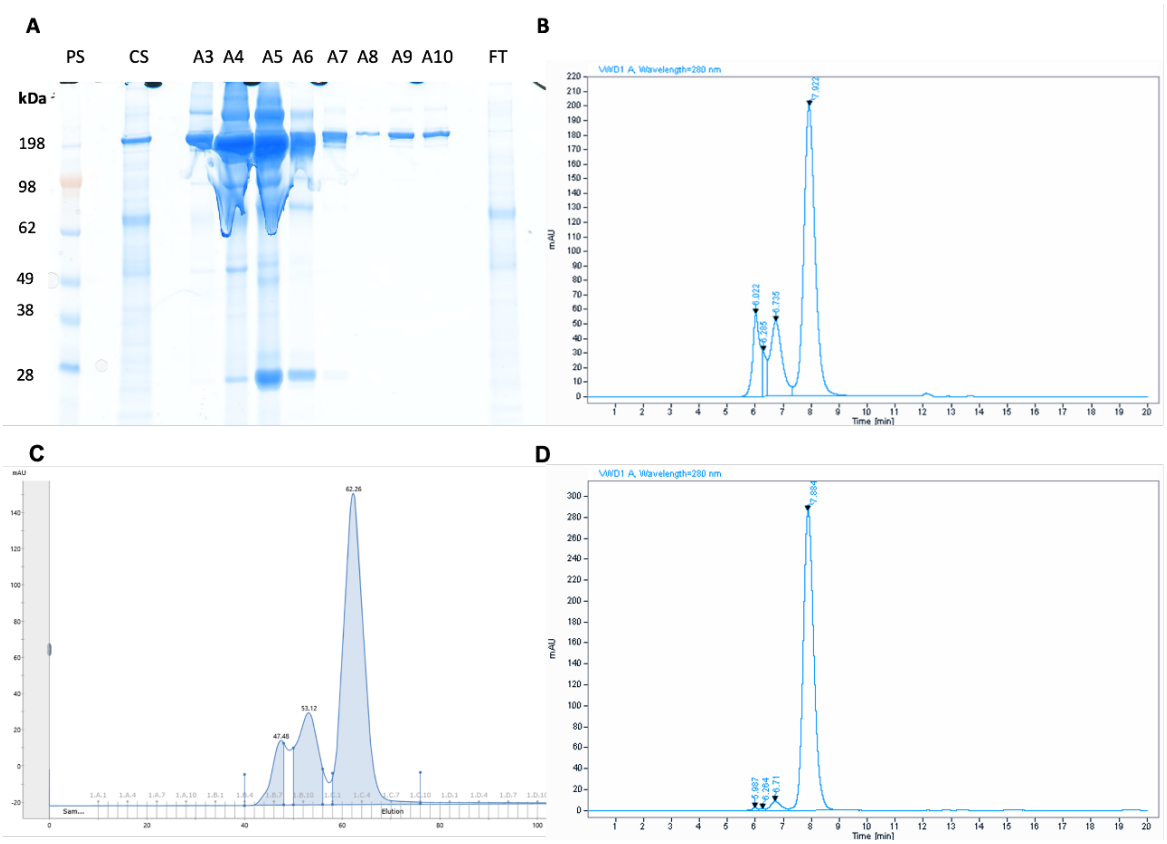

Figure 4.6 Quality control analysis of purified cV1q hIgG1 TM-8D3$_{130}$ scFv bispecific fusion protein

(A) SDS-PAGE analysis of protein in elution fractions A3-A10 for cV1q hIgG1 TM-8D3$_{130}$ scFv and crude supernatant (CS) and column flow through samples (FT). Protein size in CS and elution samples was confirmed by comparison to protein standard (PS) with intact protein size expected at ~200 kDa and evidence of aggregates at molecular weights above 200 kDa. Lack of corresponding protein bands in FT sample suggests efficient protein binding and elution. (B) HP-SEC analysis of cV1q hIgG1 TM-8D3$_{130}$ scFv bispecific fusion protein shows both aggregated protein and monomeric protein peaks. C-D) Clean-up process for bispecific fusion proteins. (C) SEC elution trace for cV1q hIgG1 TM-8D3$_{130}$ scFv shows separation of proteins based on size, with heavier molecular weight proteins eluting first. (D) HPLC-SEC analysis of pooled SEC fractions confirms removal of aggregated proteins in cV1q hIgG1 TM-8D3$_{130}$ scFv sample, with protein peak at 7.884 minutes used to calculate monomeric protein purity. HPLC-SEC experiments and analyses were performed by Jennifer Spooner at AstraZeneca (Cambridge, UK).

4.3.2.3 Characterisation of bispecific heavy chain-scFv fusion proteins

An important property to confirm for these bispecific heavy chain-scFv fusion proteins is binding and affinity to mTfR. Affinity of anti-TfR antibodies for mTfR within the low nanomolar range is sufficient for BBB transport, with 8D3 hIgG1 TM and 8D3$_{130}$ hIgG1 TM having respective affinities of < 1 nM and 130 nM (Webster et al., 2017). However, reformatting the variable domains of these anti-mTfR antibodies as scFv fragments may result in altered binding to mTfR.

To test for this possibility the binding of bispecific heavy chain-scFv fusion proteins to mTfR was determined by bio-layer interferometry (BLI). Bispecific heavy chain-scFv fusion proteins were immobilised using anti-human Fc capture sensors with mTfR in solution for measurement of association and dissociation kinetics (Figure 4.7). Binding of 8D3 scFv-containing bispecific fusion proteins, cV1q hIgG1 TM-8D3 scFv and NIP228 hIgG1 TM-8D3 scFv, resulted in a 1.17-fold and 1.19-fold reduction in binding response compared to parent antibody, 8D3 hIgG1 TM (Table 4.9). Binding by $8D3_{130}$ scFv-containing fusion proteins to mTfR was also reduced compared to its parent antibody, $8D3_{130}$ hIgG1 TM, with a 2.50-fold and 1.90-fold decrease in binding response for NIP228 hIgG1 TM-$8D3_{130}$ scFv and cV1q hIgG1 TM-$8D3_{130}$ scFv, respectively (Table 4.9). The isotype control antibody, cV1q hIgG1 TM-NIP228 scFv, showed no measurable binding to mTfR as expected (Figure 4.7G).

Overall, these data suggest that the reformatting of anti-mTfR antibodies 8D3 and $8D3_{130}$ as scFv results in a reduction in binding to mTfR that is likely to negatively impact its ability to increase brain penetrance compared to non-mTfR targeted control antibodies *in vivo*. These data suggest that enhanced BBB transport of anti-mTNF-α antibody would be better achieved by having anti-mTfR binding domains in the Fab arms of the IgG and either reformatting cV1q as a scFv (V1q scFv) or by generating an anti-mTfR-mouse TNFR2 (mTNFR2) bispecific fusion protein, similar to previously published constructs (Zhou *et al.*, 2011).

Table 4.9 Binding responses in BLI for bispecific heavy chain-scFv fusion proteins for mTfR

Bispecific fusion protein	Response (nm)	Estimated K_D (nM)	K_{on} (M^{-1} s^{-1}), x10^4	K_{off} (s^{-1}), x10^{-3}
NIP228 hIgG1 TM-$8D3_{130}$ scFv	0.3891	357	2.61	9.32
NIP228 hIgG1 TM-8D3 scFv	1.1852	151	3.21	4.85
cV1q hIgG1 TM-$8D3_{130}$ scFv	0.2945	353	2.79	9.86
cV1q hIgG1 TM-8D3 scFv	1.2076	112	3.09	3.46
cV1q hIgG1 TM-NIP228 scFv	0.01	n.d.	n.d.	n.d.
$8D3_{130}$ hIgG1 TM	0.7389	185	3.80	7.02
8D3 hIgG1 TM	1.4138	76.9	5.68	4.36

n.d., not determined.

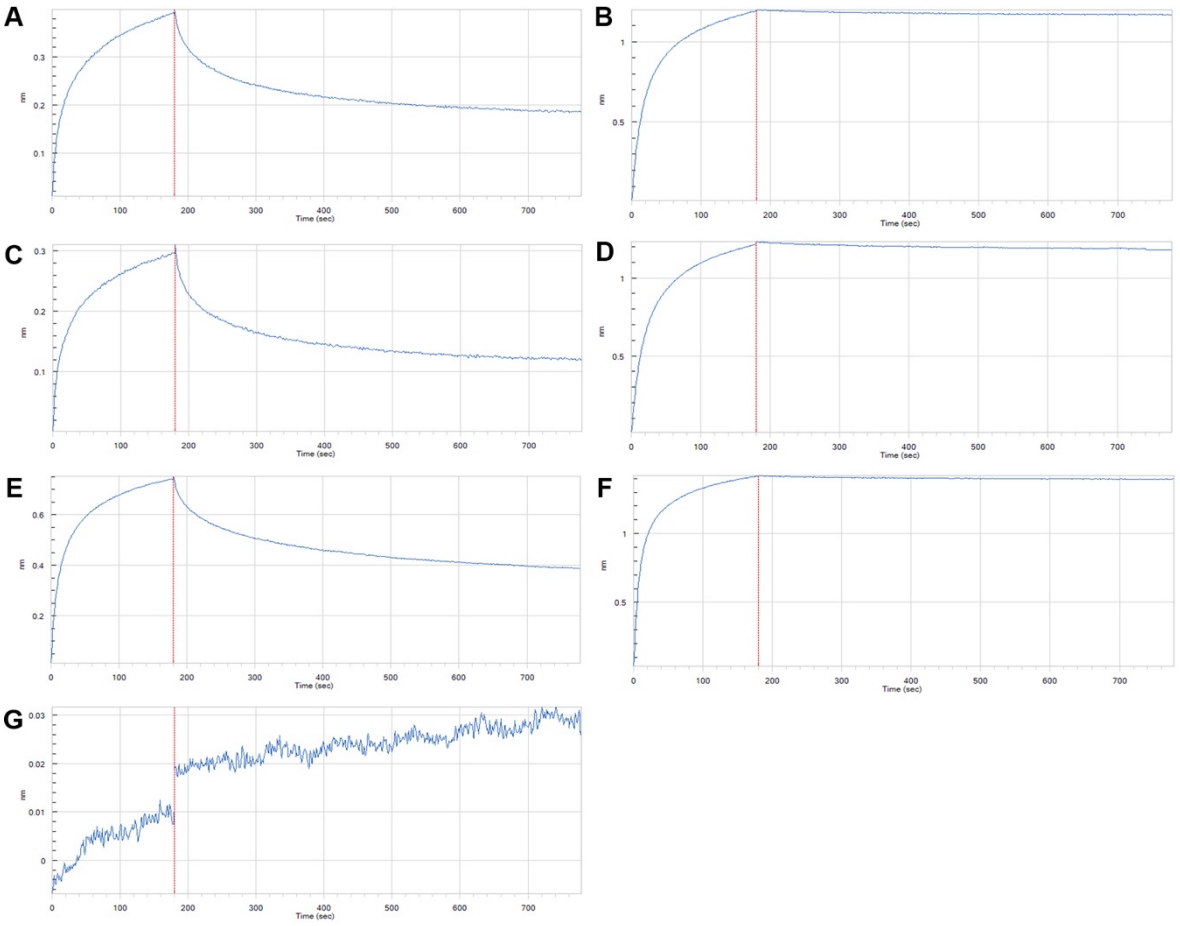

Figure 4.7 Binding responses of bispecific heavy chain-scFv fusion proteins to mTfR
(A-G) Representative association and dissociation traces for Fc-immobilised bispecific heavy chain-scFv fusion proteins (50 nM) binding to mTfR (1μM) using BLI. (A-F) Heavy chain-scFv variants NIP228 hIgG1 TM-8D3$_{130}$ scFv (A), NIP228 hIgG1 TM-8D3 scFv (B), cV1q hIgG1 TM-8D3$_{130}$ scFv (C) and cV1q hIgG1 TM-8D3 scFv (D) show reduced binding compared to parent IgG, 8D3$_{130}$ hIgG1 TM (E) and 8D3 hIgG1 TM (F). (G) Isotype control heavy chain-scFv fusion, cV1q hIgG1 TM-NIP228 scFv, shows no binding to mTfR. Experiment performed by Alan Sandercock at AstraZeneca (Cambridge, UK).

4.3.3 Production of brain penetrant V1q scFv and mTNFR2 bispecific fusion proteins

V1q scFv and mTNFR2 bispecific fusion proteins were generated in a similar manner to bispecific fusion proteins (Figure 4.8). V1q scFv and mTNFR2 DNA sequences were assembled into $8D3_{130}$ hIgG1 TM and NIP228 hIgG1 TM heavy chain expression vectors after XbaI digestion using NEBuilder HiFi DNA assembly. *E. coli* were transformed with assembled DNA and selected colonies were PCR screened for presence of the insert and products separated by agarose gel electrophoresis. The expression vector purified from the following positive colonies were selected for production of fusion proteins: $8D3_{130}$ hIG1 TM-V1q scFv pEU1.4 #2, NIP228 hIG1 TM-V1q scFv pEU1.4 #3, $8D3_{130}$ hIG1 TM-mTNFR2 pEU1.4 #2, and NIP228 hIG1 TM-mTNFR2 pEU1.4 #1. Expression vectors for heavy and light chains were co-transfected into CHO cells and bispecific fusion proteins were purified from CHO cell supernatant using Protein A-affinity chromatography, followed by SEC. Profiles of protein elution from SEC column showed that bispecific V1q scFv fusion proteins had a higher proportion of aggregation and recovery of expressed protein is reduced compared to bispecific mTNFR2 fusion proteins (Figure 4.9). Quality control analysis for monomeric protein content by HPLC-SEC and endotoxin levels measured by LAL assay are summarised in Table 4.10.

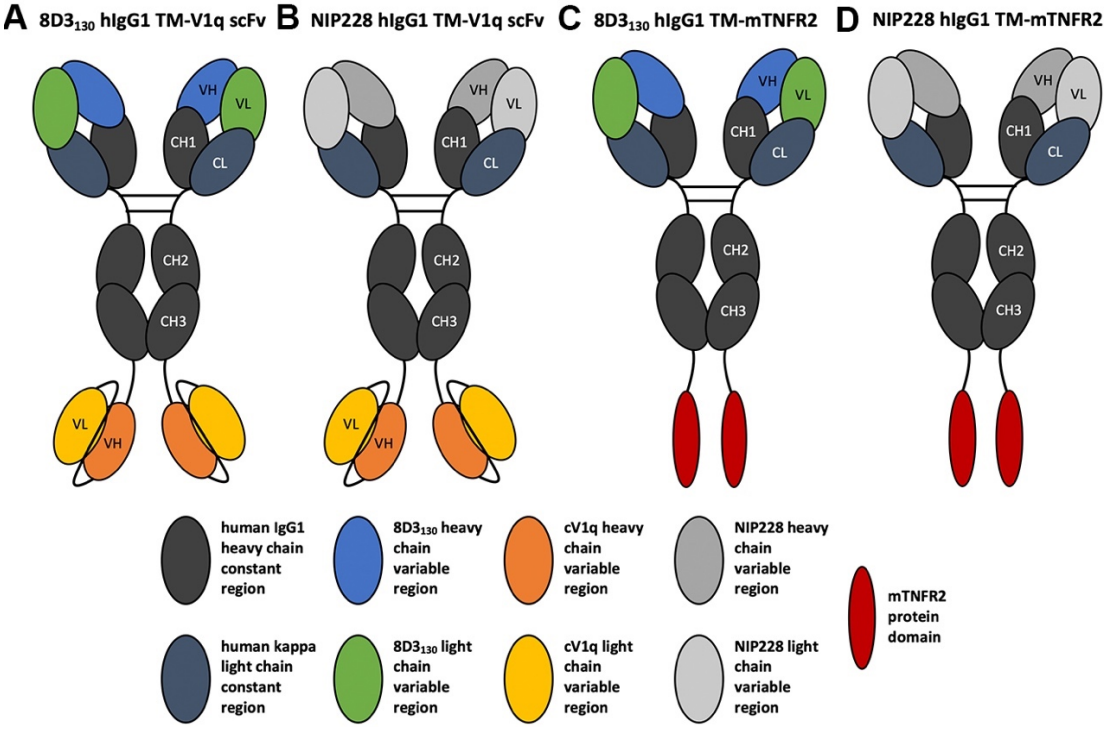

Figure 4.8 Schematic representation of anti-mTNF-α fusion protein formats
(A-B) Anti-mTNF-α binding bispecific containing V1q scFv which either (A) crosses the blood-brain barrier through $8D3_{130}$ binding domains, or (B) acts peripherally through NIP228 binding domains (B). (C-D) Anti-mTNF-α neutralising fusion protein containing mTNFR2 which either (C) acts centrally through $8D3_{130}$ binding domains, or (D) shows no brain penetration through NIP228 binding domains.

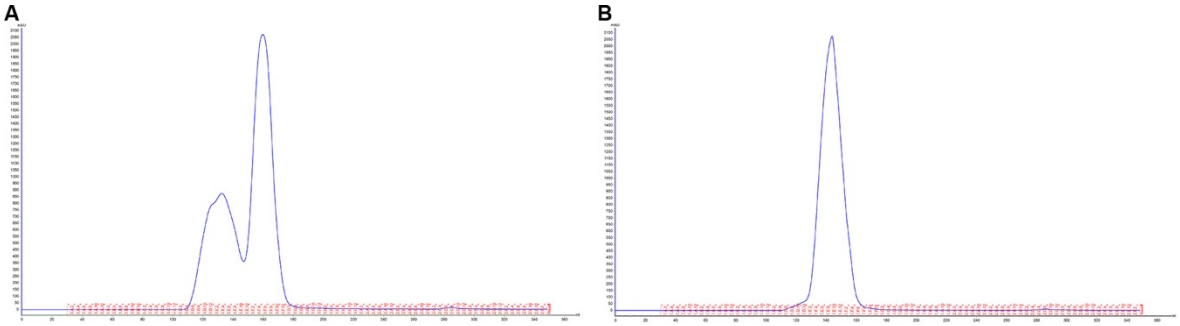

Figure 4.9 SEC elution traces for bispecific fusion proteins
Traces of SEC elution for $8D3_{130}$ hIgG1 TM-V1q scFv (A) shows greater proportion of higher molecular weight protein (left most peak) compared to $8D3_{130}$ hIgG1 TM-mTNFR2 (B).

Table 4.10 Quality control summary for bispecific fusion proteins
Protein purity was determined by HPLC-SEC and endotoxin levels by LAL assay. Experiments and analyses were performed by Jennifer Spooner at AstraZeneca (Cambridge, UK).

Bispecific fusion protein	Concentration (mg/ml)	Monomeric protein purity (%)	Endotoxin (EU/ml)	Endotoxin (EU/mg)
$8D3_{130}$ hIgG1 TM-V1q scFv	4.48	92.45	0.08	0.02
NIP228 hIgG1 TM-V1q scFv	5.77	89.28	0.08	0.01
$8D3_{130}$ hIgG1 TM-mTNFR2	11.78	98.58	0.08	<0.01
NIP228 hIgG1 TM-mTNFR2	5.50	97.46	0.12	0.02

4.3.4 *In vitro* analysis of bispecific anti-mTNF-α fusion proteins

4.3.4.1 Confirmation of mTNF-α binding

Reformatting V1q as an scFv required confirmation of binding to mTNF-α using BLI and was performed alongside the bispecific mTNFR2 fusion proteins. Titrations of mTNF-α were used to generate kinetic measurements against a fixed concentration of fusion protein (100 nM), and cV1q hIgG1 TM was used as positive control for mTNF-α binding.

Analysis of kinetic measurements show that $8D3_{130}$ hIgG1 TM-V1q scFv and NIP228 hIgG1 TM-V1q scFv have a similar binding profile, with equitable maximal binding responses (Figure 4.10). However, there is an increased dissociation rate which relates to an approximate 193-fold and a 129-fold decrease in affinity for $8D3_{130}$ hIgG1 TM-V1q scFv and NIP228 hIgG1 TM-V1q scFv, respectively, compared to cV1q hIgG1 TM (Table 4.11). These data suggest that reformatting of V1q as a scFv has altered its binding kinetics to mTNF-α compared to its parent IgG format.

$8D3_{130}$ hIgG1 TM-mTNFR2 and NIP228 hIgG1 TM-mTNFR2 fusion proteins show a reduced maximal binding response compared to cV1q hIgG1 TM (Figure 4.10). The binding kinetics for mTNFR2 fusion proteins show an increased association and dissociation rate, which reflects an approximate 20-fold and 24-fold decrease in affinity for mTNF-α compared to cV1q hIgG1 TM (Table 4.11). It should be noted that kinetics measurements for soluble mTNFR2 were not made, and thus the exact effect of adding mTNFR2 to an anti-TfR antibody on binding mTNF-α compared to soluble mTNFR2 is not fully investigated here.

Overall, these data suggest that mTNFR2-containing bispecific fusion proteins show greater affinity for mTNF-α compared to V1q scFv-containing bispecific fusion proteins. However, both fusion proteins show reduced affinity compared to cV1q hIgG1 TM.

Table 4.11 Estimated K_D values for bispecific anti-mTNF-α fusion proteins against mTNF-α in BLI

Bispecific fusion protein	Response (nm)	Estimated K_D (pM)	K_{on}, x10^5 (M^{-1} s^{-1})	K_{off}, x10^{-6} (s^{-1})
cV1q hIgG1 TM	0.5298	16.79	1.25	2.09
8D3$_{130}$ hIgG1 TM-V1q scFv	0.4365	3235	1.33	429
NIP228 hIgG1 TM-V1q scFv	0.2526	2170	2.18	473
8D3$_{130}$ hIgG1 TM-mTNFR2	0.1814	367.6	5.71	210
NIP228 hIgG1 TM-mTNFR2	0.2517	410.2	4.48	184

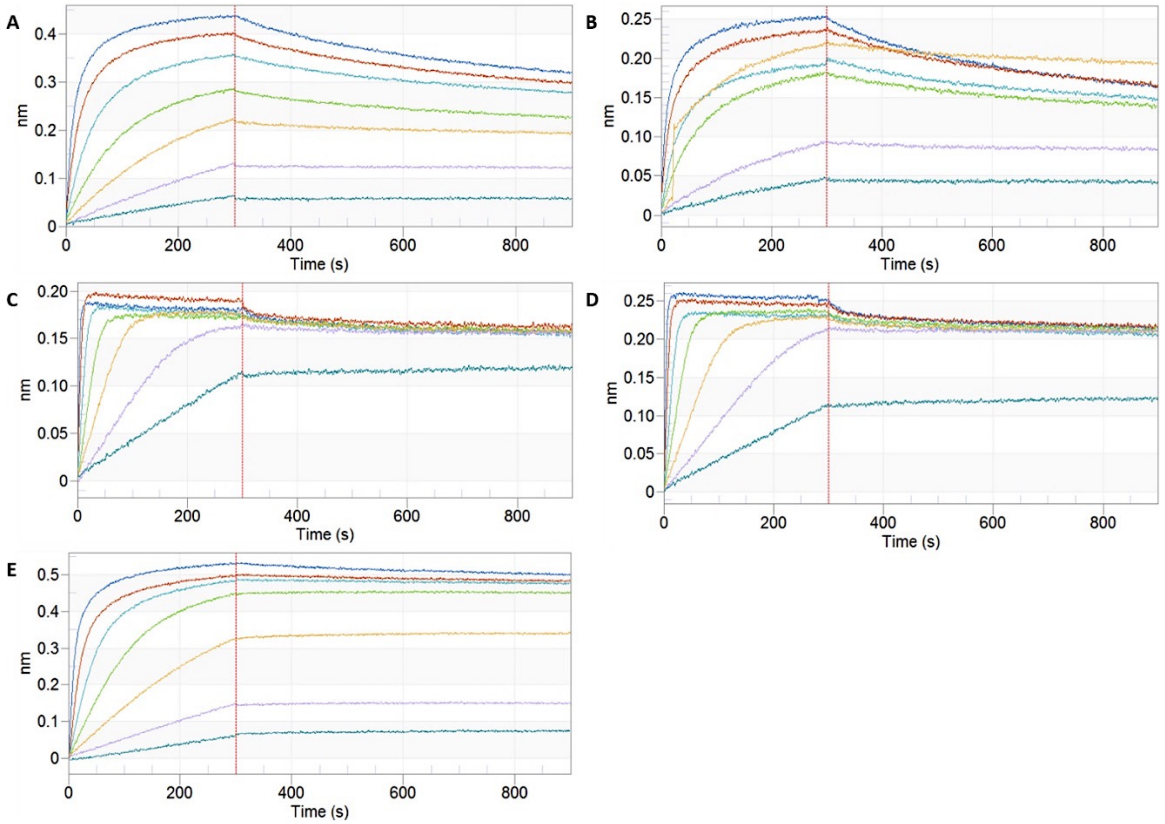

Figure 4.10 Kinetic measurements of anti-mTNF-α bispecific fusion proteins for mTNF-α
Immobilisation of 100 nM bispecific fusion protein with anti-Human Fc capture biosensors and addition of varying concentrations of mTNF-α results in binding (upward trace) for (A) 8D3$_{130}$ hIgG1 TM-V1q scFv, (B) NIP228 hIgG1 TM-V1q scFv, (C) 8D3$_{130}$ hIgG1 TM-mTNFR2, (D) NIP228 hIgG1 TM-mTNFR2 and (E) cV1q hIgG1 TM. mTNFR2 fusion proteins (C and D) show faster association (left of red line) with mTNF-α compared to V1q scFv fusion proteins (A and B). Subsequent removal from mTNF-α (right of red line) results in observed dissociation (downward trace) for all fusion proteins, except cV1q hIgG1 TM (E). Mouse TNF-α concentrations: blue = 500 nM, red = 250 nM, turquoise = 125 nM, green = 62.5 nM, yellow = 31.25 nM, lilac = 15.625 nM, teal = 7.8125 nM.

4.3.4.2 Determining neutralisation of mTNF-α

V1q scFv and mTNFR2 fusion protein were tested *in vitro*, alongside their respective anti-mTNF-α parent proteins, for their ability to neutralise mTNF-α using a TNF-α-induced L929 fibroblast cytotoxicity assay, adapted from previous experimental methods to utilise colorimetric analysis of cytotoxicity (Goodall *et al*., 2015). Mouse TNF-α, in combination with the cell cycle inhibitor actinomycin D, was added to L929 fibroblasts and incubated for 20 hours. Cell viability was measured using the principle of a colourimetric assay, where a coloured formazan product is produced after reduction in metabolically active cells and absorbance is directly proportional to the number of viable cells present in a well (Promega Corporation, 2012). Effective neutralisation of mTNF-α by fusion protein will result in increased cell viability compared to mTNF-α alone, and cV1q hIgG1 TM and soluble mTNFR2 were included as positive controls for their respective fusion proteins.

Analysis of neutralisation from initial experiments showed that mTNFR2 fusion proteins are a more potent neutraliser of mTNF-α compared to V1q scFv fusion proteins, with dilutions beginning at 100 nM for V1q scFv fusion proteins and mTNFR2 fusion proteins starting from 3 nM (Figure 4.11). mTNFR2 fusion proteins showed equivalent neutralisation to soluble mTNFR2, whilst V1q scFv fusion proteins showed a similar profile to its parent antibody, cV1q hIgG1 TM (Figure 4.11). IC_{50} values were calculated to directly compare neutralisation of mTNF-α between fusion proteins and mTNFR2 fusion proteins were approximately 10-fold more potent neutralisers of mTNF-α than V1q scFv fusion proteins (Table 4.12). In addition, both V1q scFv and mTNFR2 fusion proteins were more potent than their parent proteins. Overall, these data suggest that mTNFR2 fusion proteins would be a more suitable option for neutralising mTNF-α compared to V1q scFv fusion proteins.

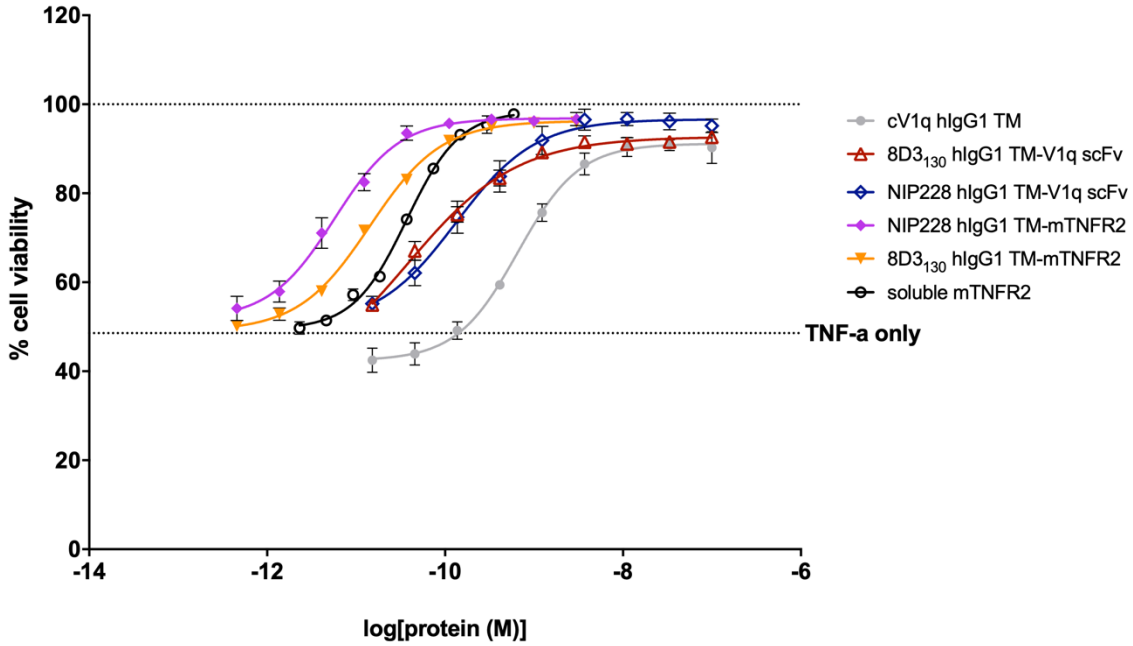

Figure 4.11 Neutralisation of mTNF-α by bispecific anti-mTNF-α fusion proteins
Bispecific anti-mTNF-α fusion proteins and parent proteins were titrated using a 1:3 serial dilution and pre-incubated for 30 minutes with 200 pg/ml mTNF-α before addition to murine L929 fibroblasts to test neutralising ability of mTNF-α-induced cytotoxicity. V1q scFv fusion proteins also show effective neutralisation comparable with cV1q hIgG1 TM. Bispecific mTNFR2 fusion proteins show similar neutralising ability as recombinant soluble mTNFR2 and are more potent than V1q scFv fusion proteins. Data represented as mean ± SEM, with n=6 per concentration.

Table 4.12 IC_{50} values for bispecific anti-mTNF-α fusion proteins in a mTNF-α-induced L929 cytotoxicity assay

Bispecific fusion protein	IC_{50} (pM)
cV1q hIgG1 TM	827.3
$8D3_{130}$ hIgG1 TM-V1q scFv	109.7
NIP228 hIgG1 TM-V1q scFv	243.3
Soluble mTNFR2	36.82
$8D3_{130}$ hIgG1 TM-mTNFR2	7.436
NIP228 hIgG1 TM-mTNFR2	11.33

4.3.5 Purification of bispecific mTNFR2 fusion proteins for *in vivo* experiments

It has previously been noted that the C-terminal Lysine residue of hIgG1 antibodies is not present during protein isolation from mammalian cells (Harris et al. 1990; Harris, 1995). Cleavage of this C-terminal Lysine is a result of carboxypeptidase activity within CHO cell cultures and is known to separate Fc-peptide fusion proteins (Kleemann et al., 2008). In addition, there's evidence that *in vivo* only 0.02% of circulating serum antibodies have a C-terminal lysine residue and that cleavage of this C-terminal lysine occurs rapidly with a half-life of 62 minutes (Cai et al., 2011). The potential for cleavage of this residue *in vivo* presents a liability for delivery of the therapeutic fusion protein across the BBB and therefore, bispecific mTNFR2 fusion proteins were re-engineered to remove the C-terminal lysine residue (denoted hIgG1 TM ΔK). DNA sequences encoding mTNFR2 were assembled into $8D3_{130}$ hIgG1 TM and NIP228 hIgG1 TM heavy chain expression vectors after XbaI digestion using NEBuilder HiFi DNA assembly with forward primers lacking bases coding the C-terminal Lys residue (Table 2.4). *E. coli* colonies transformed with expression vectors were screened, sequenced and the following positive colonies were used for protein expression and purification as described before: $8D3_{130}$ hIgG1 TM ΔK-mTNFR2 pEU1.4 #1 and NIP228 hIgG1 TM ΔK-mTNFR2 pEU1.4 #1.

4.3.6 Quality control analysis of bispecific mTNFR2 fusion proteins

Bispecific mTNFR2 fusion protein molecular weight was analysed by reducing SDS-PAGE and showed no evidence for cleavage liability (Figure 4.12). HPLC-SEC analysis of both heavy chain ΔK-mTNFR2 fusion proteins showed a single elution peak at 6.7 minutes (Figure 4.13). Area under the curve analysis of these elution peaks gave a monomeric protein concentration of greater than 99% for heavy chain ΔK-mTNFR2 fusion proteins (Table 4.13).

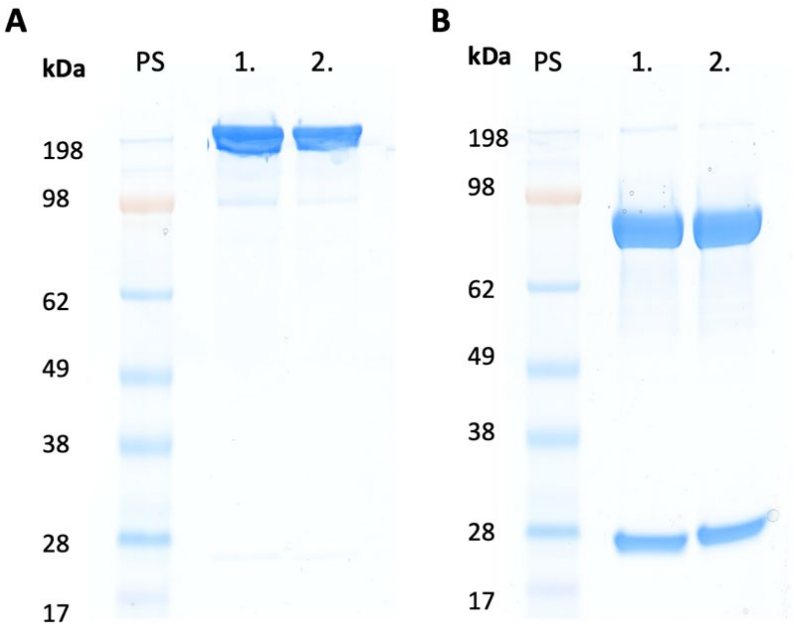

Figure 4.12 SDS-PAGE analysis of bispecific mTNFR2 fusion proteins
(A) Non-reducing SDS-PAGE analysis of 5 μg bispecific fusion protein, $8D3_{130}$ hIgG1 TM ΔK-mTNFR2 (1) and NIP228 hIgG1 TM ΔK-mTNFR2 (2) shows single band at correct size of ~198 kDa. (B) Reducing SDS-PAGE analysis of 5 μg bispecific fusion protein shows correct molecular weights for light chain (~25 kDa) and heavy chain-mTNFR2 fusion (~75 kDa) of both $8D3_{130}$ hIgG1 TM ΔK-mTNFR2 (1) and NIP228 hIgG1 TM-ΔK mTNFR2 (2) without evidence of mTNFR2 cleavage.

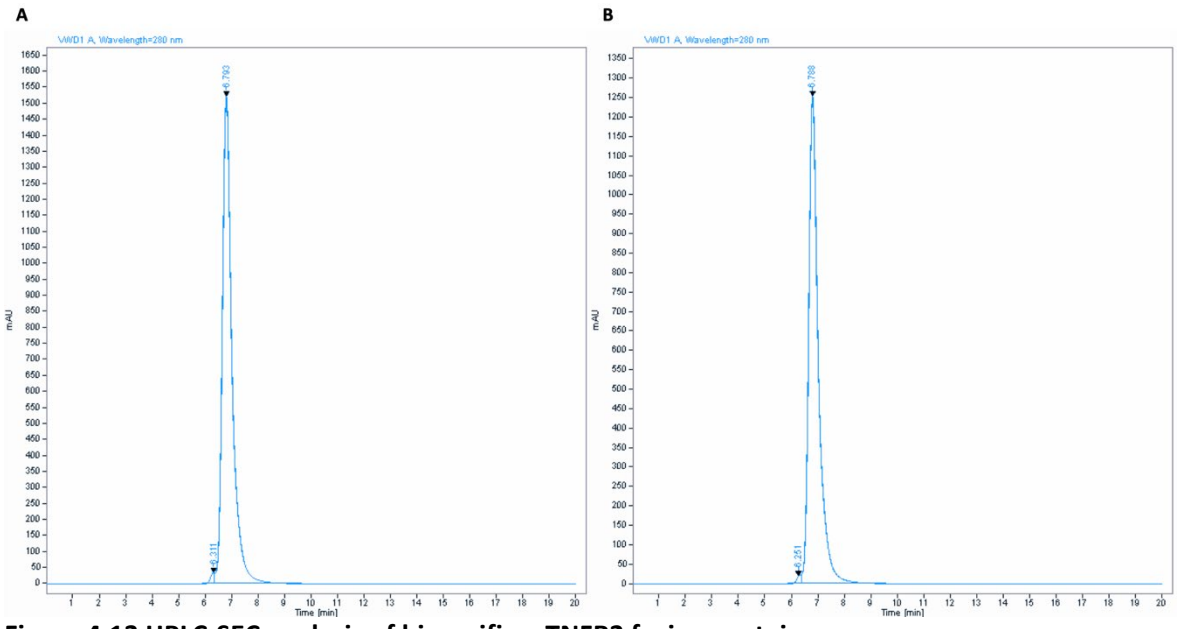

Figure 4.13 HPLC-SEC analysis of bispecific mTNFR2 fusion proteins
HP-SEC traces of $8D3_{130}$ hIgG1 TM ΔK-mTNFR2 (A) and NIP228 hIgG1 TM ΔK-mTNFR2 (B). Arrowheads represent monomeric protein peaks used to determine protein purity. HPLC-SEC experiments and analysis were performed by Jennifer Spooner at AstraZeneca (Cambridge, UK).

Final protein pool was concentrated in Acetate pH 5.0 buffer and used for quality control analyses. The concentration of the fusion proteins was measured by absorbance at 280 nm and the endotoxin levels in each sample was measured using the LAL quantitation assay (data summarised in Table 4.13). The parent antibodies, $8D3_{130}$ hIgG1 TM and NIP228 hIgG1 TM, will be used as control antibodies for *in vivo* experiments and they were buffer exchanged into Acetate pH 5.0 buffer and protein concentration, purity and endotoxin levels were quantified in parallel (Table 4.13).

Table 4.13 Summary of mTNFR2 fusion proteins and isotype control properties
Protein purity was determined by HPLC-SEC and endotoxin levels by LAL assay with experiments and analyses performed by Jennifer Spooner at AstraZeneca (Cambridge, UK).

Fusion protein	Concentration (mg/ml)	Monomer Purity (%)	Endotoxin (EU/ml)	Endotoxin (EU/mg)
$8D3_{130}$ hIgG1 TM ΔK-mTNFR2	12.58	99.1	1.35	0.11
NIP228 hIgG1 TM ΔK-mTNFR2	11.81	99.2	1.32	0.11
$8D3_{130}$ hIgG1 TM	12.34	99.4	<0.12	<0.01
NIP228 hIgG1 TM	12.07	99.5	0.484	0.04

Glycosylation of biologics is known to impact on many of their functions, including stability, immunogenicity and serum half-life (Beck et al., 2013; Zhou and Qiu, 2019). Etanercept, a human TNFR2 biologic shows evidence of glycosylation in the C-terminal domain of TNFR2 and this contributes heavily to the overall molecular weight of the Fc-fusion protein (Gur and Oktayoglu, 2010; Montacir et al., 2018). Although, sequence homology between mTNFR2 and human TNFR2 extracellular domains is only 56%, the sequence does predict similar glycosylation sites for mTNFR2 (Bateman, 2019). Therefore, it is important to determine if glycosylation is present in the bispecific mTNFR2 fusion proteins produced in this chapter.

Protein mass was confirmed using UPLC-MS with deglycosylated protein under reducing and non-reducing conditions. Under non-reducing conditions, both mTNFR2 fusion proteins had a mass 2.8kDa heavier than expected, suggesting that there was incomplete deglycosylation (Table 4.14; Figure 4.14A/B). Under reducing conditions, analysis of the heavy chain ΔK-mTNFR2 fragments identified the presence of remaining glycosylation moieties. As these glycosylation moieties existed alongside the whole fragment, it is likely

that these glycosylation sites remain on the mTNFR2 (Table 4.15; Figure 4.14C/D). All human kappa light chains had the expected mass for their respective antibodies (Table 4.15; Figure 4.14E/F).

Table 4.14 Summary of observed molecular mass for bispecific mTNFR2 fusion proteins
Molecular mass was determined by UPLC-MS under reducing and non-reducing conditions following protein deglycosylation. Experiments and analyses were performed by Esther Martin at AstraZeneca (Cambridge, UK).

Bispecific fusion protein	Expected Mass (Da)	Observed mass (Da)
$8D3_{130}$ hIgG1 TM ΔK-mTNFR2	**197,610**	**200,469**
Heavy chain fusion	75,420	75,424
Light chain	23,385	23,385
NIP228 hIgG1 TM ΔK-mTNFR2	**196,671**	**199,497**
Heavy chain fusion	75,127	75,132
Light chain	23,191	23,191

Table 4.15 Summary of observed glycosylation moieties for heavy chain ΔK-mTNFR2 fragments
Molecular mass was determined by UPLC-MS under reducing conditions following protein deglycosylation. Experiments and analyses were performed by Esther Martin at AstraZeneca (Cambridge, UK).

Bispecific fusion protein	Expected Mass (Da)	Observed mass (Da)
$8D3_{130}$ heavy chain fusion	**75,420**	**75,424**
1) +1 HexNAc		75,626
2) +1 HexNAc-Hex		75,789
3) +1 HexNAc-Hex; +1 HexNAc		75,992
4) +2 HexNAc-Hex		76,155
NIP228 heavy chain fusion	**75,144**	**75,132**
1) +1 HexNAc		75,331
2) +1 HexNAc-Hex		75,496
3) +1 HexNAc-Hex; +1 HexNAc		75,700
4) +2 HexNAc-Hex		75,884

Hex: mannose/galactose; NAc: N-acetylgalactosamine/N-acetylglucosamine

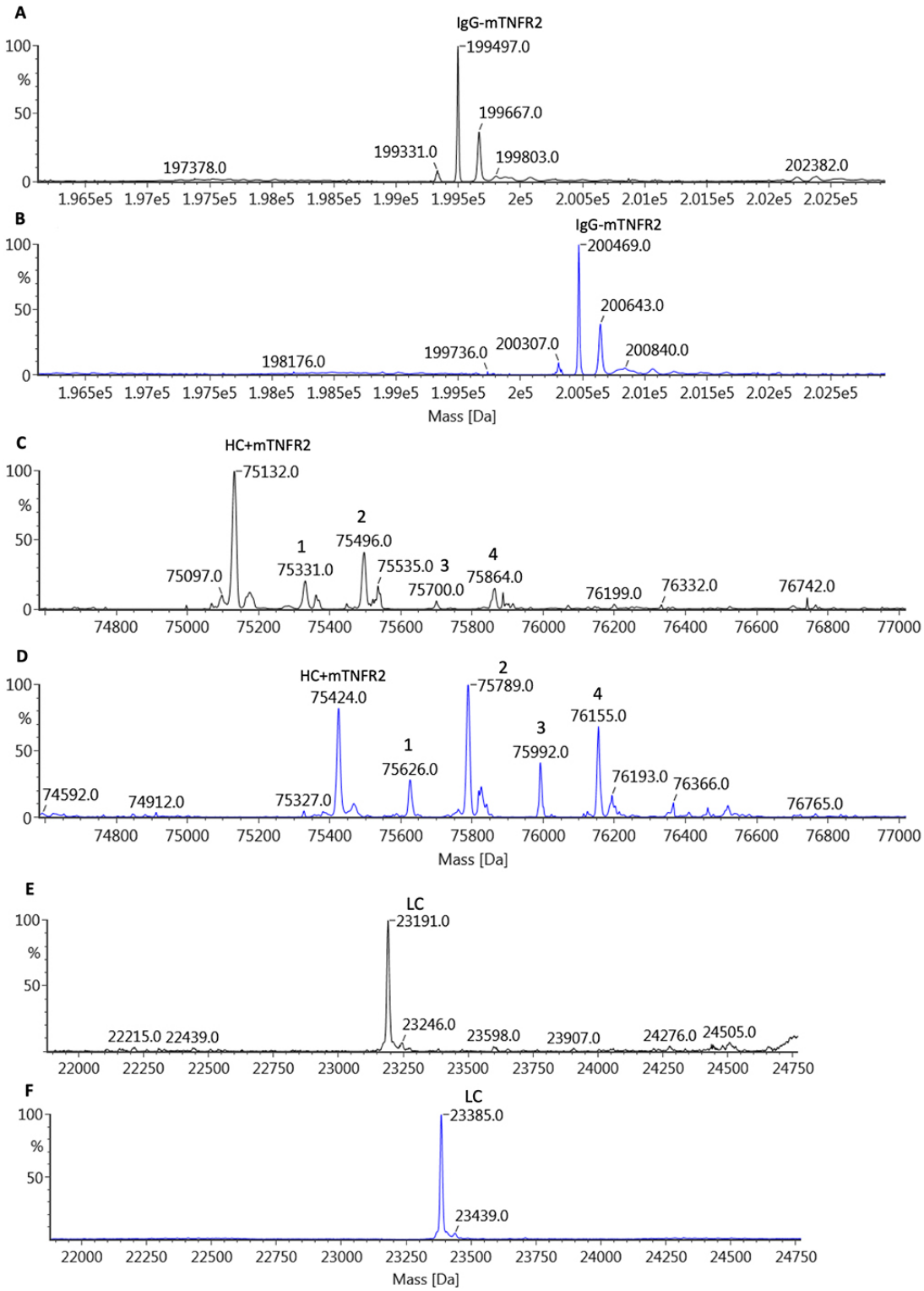

Figure 4.14 UPLC-MS analysis of bispecific mTNFR2 fusion proteins

(A-B) Mass analysis of deglycosylated protein under non-reducing conditions identified higher than expected masses for NIP228 hIgG1 TM ΔK-mTNFR2 (A) and $8D3_{130}$ hIgG1 TM ΔK-mTNFR2 (B). (C-F) Mass analysis of deglycosylated protein under reducing conditions highlighted the presence of different glycosylation moieties (1-4) on heavy chain ΔK-mTNFR2 fusions of both NIP228 hIgG1 TM ΔK-mTNFR2 (C) and $8D3_{130}$ hIgG1 TM ΔK-mTNFR2 (D). Light chains for NIP228 hIgG1 TM ΔK-mTNFR2 (E) and $8D3_{130}$ hIgG1 TM ΔK-mTNFR2 (F) showed expected masses. Glycosylation moieties identified by UPLC-MS: 1) +1 HexNAc; 2) +1 HexNAc-Hex; 3) +1 HexNAc-Hex, +1 HexNAc; 4) +2 HexNAc-Hex. Hex: mannose/galactose; NAc: N-acetylgalactosamine/N-acetylglucosamine. UPLC-MS experiments and analysis were performed by Esther Martin at AstraZeneca (Cambridge, UK).

4.3.7 *In vitro* characterisation of bispecific mTNFR2 fusion proteins

4.3.7.1 Binding of mTNF-α by bispecific mTNFR2 fusion proteins

Binding of mTNFR2 fusion proteins to mTNF-α was confirmed by BLI; fusion proteins were immobilised using anti-human Fc capture biosensors and kinetics measurements were performed using a titration of mTNF-α (7.8125-500 nM). Kinetics profiles were similar between repeat experiments and produced estimated K_D values within a similar pM range to previous purified protein batches (Table 4.16 vs Table 4.11). With both mTNFR2 fusion proteins showing similar binding profiles and responses for mTNF-α (Figure 4.15).

Table 4.16 Estimated K_D values of bispecific mTNFR2 fusion proteins for mTNF-α in BLI

Bispecific fusion protein	Response (nm)	Estimated K_D (nM)	K_{on} (M^{-1} s^{-1}), x105	K_{off} (s^{-1}), $x10^{-6}$
$8D3_{130}$ hIgG1 TM ΔK-mTNFR2	0.1951	213.6	6.62	14.13
NIP228 hIgG1 TM ΔK-mTNFR2	0.222	127.7	6.39	8.15

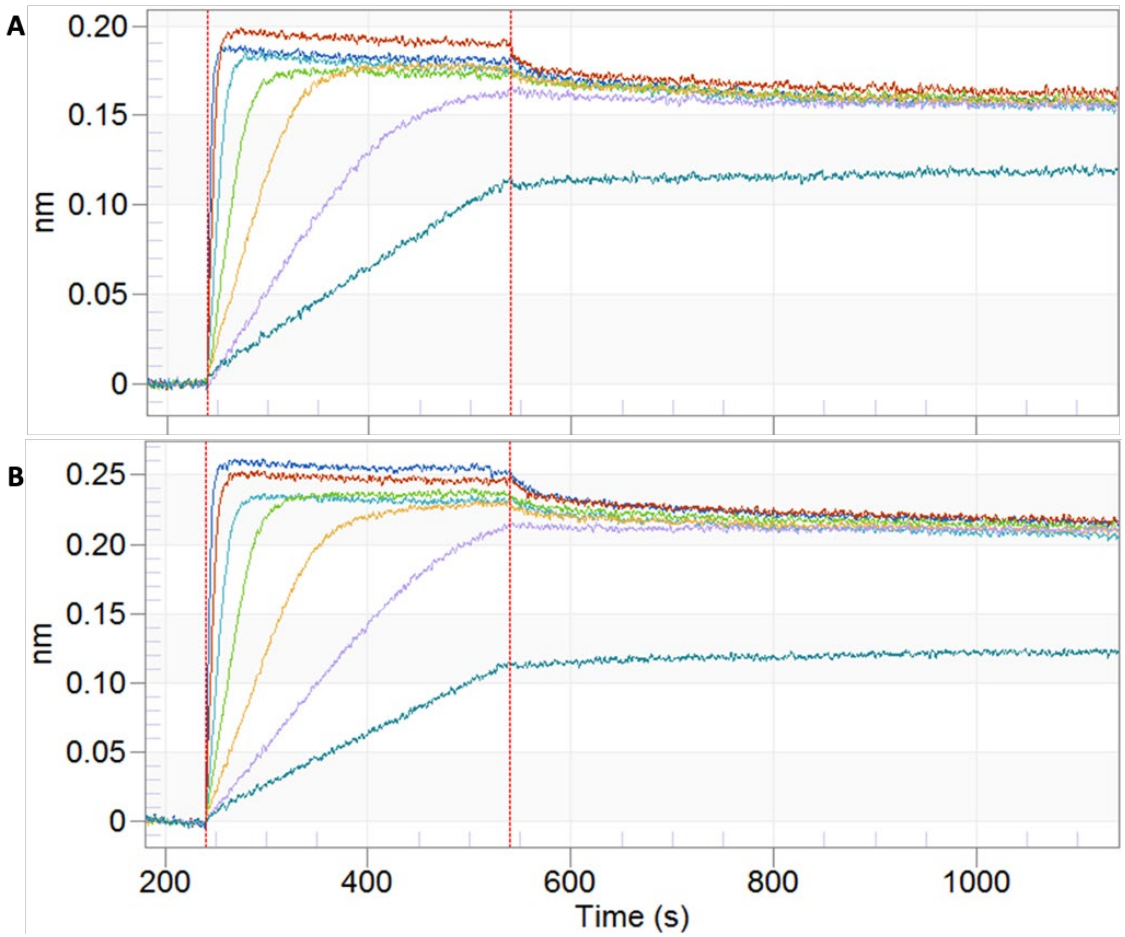

Figure 4.15 Kinetic measurements of bispecific mTNFR2 fusion proteins for mTNF-α
Binding of bispecific $8D3_{130}$ hIgG1 TM ΔK-mTNFR2 (A) or NIP228 hIgG1 TM ΔK-mTNFR2 (B) to mTNF-α was confirmed by BLI. Association and dissociation kinetics of the two fusion proteins show similar profiles, with similar maximal binding responses. Mouse TNF-α concentrations: blue = 500 nM, red = 250 nM, turquoise = 125 nM, green = 62.5 nM, yellow = 31.25 nM, lilac = 15.625 nM, teal = 7.8125 nM.

4.3.7.2 Neutralisation of mTNF-α by bispecific mTNFR2 fusion proteins

$8D3_{130}$ hIgG1 TM ΔK-mTNFR2, NIP228 hIgG1 TM ΔK-mTNFR2 and control parent antibodies, $8D3_{130}$ hIgG1 TM and NIP228 hIgG1 TM, were titrated against mTNF-α in an L929 mouse fibroblast cytotoxicity assay, with soluble mTNFR2 included as a positive control for neutralisation of mTNF-α. Both mTNFR2 fusion proteins showed similar neutralisation profiles to previous small batch productions and to soluble mTNFR2 (Figure 4.16 vs Figure 4.11). Calculated IC_{50} values for $8D3_{130}$ hIgG1 TM ΔK-mTNFR2 and NIP228 hIgG1 TM ΔK-mTNFR2 were within a similar range to soluble mTNFR2 (Table 4.17). The isotype control antibodies showed no efficacy in the cell assay, and as such IC_{50} values were not determined. These data confirm that bispecific mTNFR2 fusion proteins, produced for *in vivo* experiments, show potent neutralisation of mTNF-α *in vitro* equivalent to soluble mTNFR2.

Table 4.17 IC_{50} values for bispecific mTNFR2 fusion proteins in a mTNF-α-induced L929 cytotoxicity assay

Bispecific fusion protein	IC_{50} (pM)
Soluble mTNFR2	48
$8D3_{130}$ hIgG1 TM ΔK-mTNFR2	44.1
NIP228 hIgG1 TM ΔK-mTNFR2	82.9
$8D3_{130}$ hIgG1 TM	n.d.
NIP228 hIgG1 TM	n.d.

n.d. = not determined

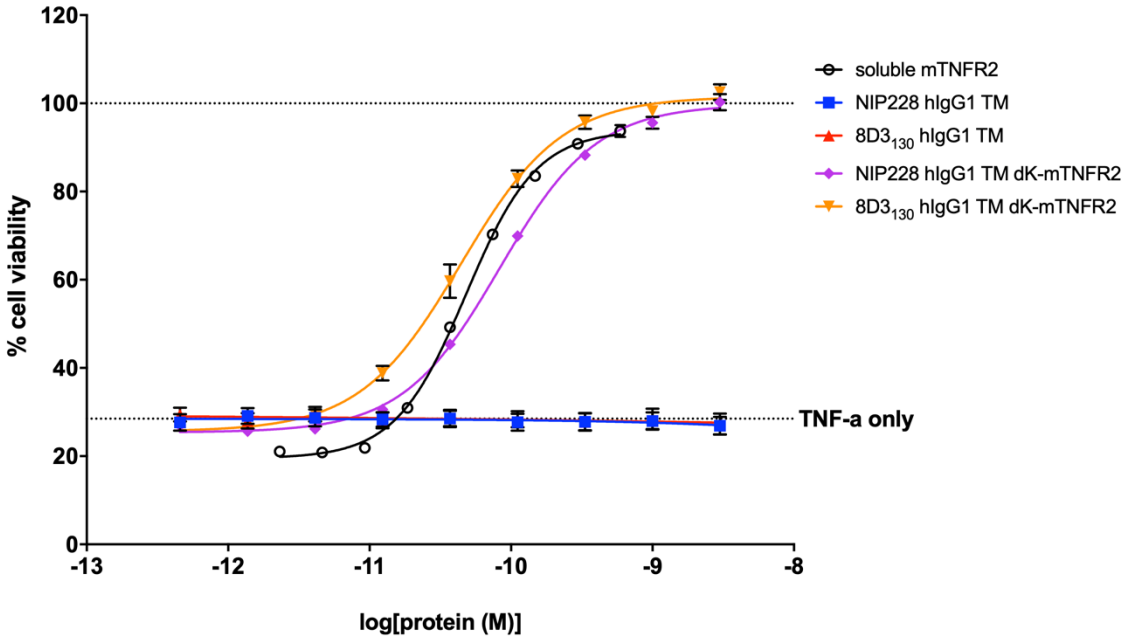

Figure 4.16 Neutralisation of mTNF-α by bispecific mTNFR2 fusion proteins

Bispecific mTNFR2 fusion proteins and their isotype control antibodies were titrated using a 1:3 serial dilution to test neutralising ability of mTNF-α-induced cytotoxicity in L929 mouse fibroblasts. Bispecific mTNFR2 fusion proteins show similar neutralising ability as recombinant soluble mTNFR2, with isotype control antibodies having no effect on mTNF-α-induced cytotoxicity. Data represented as mean ± SEM, with n=6 per concentration.

4.3.7.3 Confirmation of mTfR binding by bispecific mTNFR2 fusion proteins

Binding of mTfR was determined by immobilising $8D3_{130}$ hIgG1 TM or $8D3_{130}$ hIgG1 TM ΔK-mTNFR2 on anti-human Fc capture biosensors at a concentration of 50 nM. Loading of $8D3_{130}$ hIgG1 TM ΔK-mTNFR2 on to biosensor was reduced when compared to $8D3_{130}$ hIgG1 TM (Figure 4.17A). Both proteins showed similar binding profiles with mTfR during association and dissociation with either 1000 nM or 333 nM mTfR using BLI (Figure 4.17B). However, the maximal response at the same mTfR concentration was severely reduced with the bispecific mTNFR2 fusion compared to its parent IgG (Figure 4.17B).

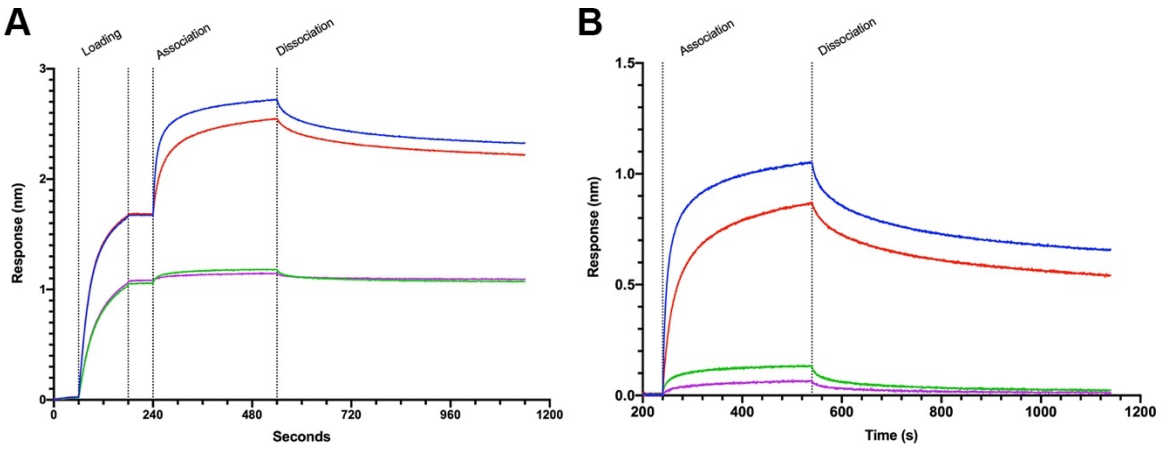

Figure 4.17 Binding for mTfR against immobilised anti-mTfR IgG fusion proteins
Binding responses for association mTfR (blue/green = 1000 nM; red/purple = 333 nM) and 50 nM $8D3_{130}$ hIgG1 TM (blue/red) or 50 nM $8D3_{130}$ hIgG1 TM ΔK-mTNFR2 (green/purple).
(A) Difference in initial loading between $8D3_{130}$ hIgG1 TM ΔK-mTNFR2 and $8D3_{130}$ hIgG1 TM is clearly observable in full traces. (B) mTfR shows association (from 240 s) and dissociation (from 540 s) with both proteins with similar profiles. However, maximal binding response is severely reduced with $8D3_{130}$ hIgG1 TM ΔK-mTNFR2 compared to $8D3_{130}$ hIgG1 TM. Experiment performed by Susan Fowler at AstraZeneca (Cambridge, UK).

As affinity to mTfR could not be determined using BLI, we sought to use another method to confirm similar response profiles when measuring target binding between the fusion protein, $8D3_{130}$ hIgG1 TM ΔK-mTNFR2, or its parent antibody, $8D3_{130}$ hIgG1 TM, and biotinylated mTfR. Binding was assayed using an AlphaScreen where binding is measured through the transfer of singlet oxygen species between acceptor and donor beads that bind separate components of the binding reaction. Reagent conditions for AlphaScreen were optimised using 8D3 hIgG1 to confirm positive binding between antibody and receptor, with concentrations set at 1 μM and 25 nM respectively. Both $8D3_{130}$ hIgG1 TM and $8D3_{130}$ hIgG1 TM ΔK-mTNFR2 were able to generate AlphaScreen signals, although the maximal signal for $8D3_{130}$ hIgG1 TM was 17.5-fold stronger than $8D3_{130}$ hIgG1 TM ΔK-mTNFR2 (Figure 4.18A). Calculated EC_{50} for $8D3_{130}$ hIgG1 TM is 164 nM, close to its published affinity, and $8D3_{130}$ hIgG1 TM ΔK-mTNFR2 is 212 nM, which is within an acceptable range of its parent IgG (Table 4.18). NIP228 hIgG1 TM and NIP228 hIgG1 TM ΔK-mTNFR2 were also assayed, and as expected showed no signal above background (Figure 4.18A). Relative AlphaScreen signal allows us to assess the binding profile exhibited by $8D3_{130}$ hIgG1 TM containing proteins, irrespective of the maximal binding response (Figure 4.18B). This identifies that both $8D3_{130}$ hIgG1 TM ΔK-mTNFR2 and $8D3_{130}$ hIgG1 TM share similar responses, relative to their maximum response.

Given the binding profiles of $8D3_{130}$ hIgG1 TM and $8D3_{130}$ hIgG1 TM ΔK-mTNFR2 in both BLI and AlphaScreen are relatively similar, it can be suggested that the bispecific mTNFR2 fusion protein would have similar BBB transport to its parent antibody, and thus presents a suitable *in vivo* solution for enhanced delivery of an anti-mTNF-α neutraliser to the brain.

Table 4.18 EC_{50} values for binding of bispecific mTNFR2 fusion proteins to mTfR using AlphaScreen

Bispecific fusion protein	EC_{50} (nM)
$8D3_{130}$ hIgG1 TM ΔK-mTNFR2	212
NIP228 hIgG1 TM ΔK-mTNFR2	n.d.
$8D3_{130}$ hIgG1 TM	164
NIP228 hIgG1 TM	n.d.

n.d. = not determined

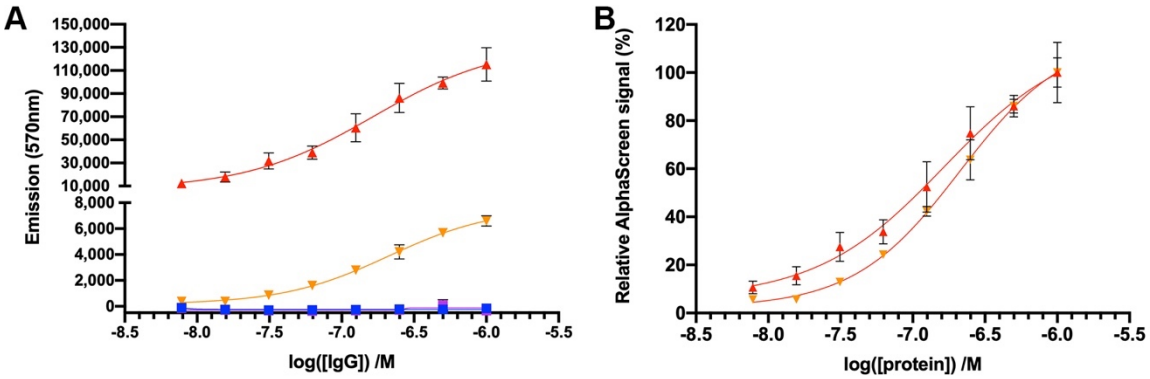

Figure 4.18 AlphaScreen responses for binding of bispecific mTNFR2 fusion proteins to mTfR
(A) Raw emission results from a dose-response of binding between biotinylated mTfR and $8D3_{130}$ hIgG1 TM (red) or $8D3_{130}$ hIgG1 TM ΔK-mTNFR2 (orange). $8D3_{130}$ hIgG1 TM shows a greater maximal response than its bispecific fusion. NIP228 hIgG1 TM (blue) and NIP228 hIgG1 TM ΔK-mTNFR2 (purple) show no binding to mTfR (B) Relative binding profiles of $8D3_{130}$ hIgG1 TM (red) and $8D3_{130}$ hIgG1 TM ΔK-mTNFR2 (orange), with maximal emission for each protein equivalent to 100%. Data are presented as mean ± SD, n=2 per concentration.

4.4 Discussion

Generation of a bispecific anti-mTfR-mTNF-α fusion protein, $8D3_{130}$ hIgG1 TM ΔK-mTNFR2, was achieved through combining a low-affinity anti-mTfR antibody, $8D3_{130}$ hIgG1 TM, with the mTNF-α neutralising protein, mTNFR2. *In vitro* analysis showed that $8D3_{130}$ hIgG1 TM ΔK-mTNFR2 effectively and potently neutralises mTNF-α in a model of TNF-α-induced cytotoxicity and that it binds to mTfR with a similar affinity to its parent antibody, indicative of suitability for use in *in vivo* models.

4.4.1 Identifying the most suitable anti-mTNF-α fusion protein for *in vivo* experiments

One major focus of developing technologies to overcome the BBB has been the "Molecular Trojan horse" approach (Pardridge, 2012, 2006), where antibodies bind to a receptor expressed on the surface of endothelial cells and are transported and released on the opposite side, e.g. from blood to brain. It has been shown that low-affinity mTfR-specific antibodies show greater brain penetrance compared to non-mTfR targeted antibodies (Lee *et al.*, 2000). These findings presented an attractive method for overcoming the challenges posed by the BBB in treating CNS-based disorders.

$8D3_{130}$ hIgG1 TM is an engineered antibody against mTfR with reduced affinity for mTfR compared to its parent antibody, 8D3 (Kissel et al., 1998; Webster et al., 2017). Enhanced delivery of therapeutics to the CNS has been shown using anti-mTfR antibody-fusion proteins in mice, rats and cynomolgus monkeys with evidence of therapeutic target engagement (Thom et al., 2018; Webster et al., 2017; Yu et al., 2014). In addition to full IgG antibodies, scFv and single Fab formats of anti-mTfR antibodies have also been successfully used to improve brain penetration of therapeutic antibodies (Bien-Ly et al., 2014; Hultqvist et al., 2017; Niewoehner et al., 2014; Yu et al., 2014, 2011). For example reformatting an anti-human TfR antibody as a scFv resulted in equivalent target engagement as an anti-human TfR antibody, and increased delivery of GAL4 DNA to tumour cells as a TfRscFv-GAL4 fusion protein (Ye et al., 2012). Also, addition of 8D3 as a scFv C-terminal to the constant domain of the light chain of an anti-Aβ antibody resulted

in efficient binding to mTfR in a monovalent fashion and a 10-fold increase in delivery two hours after a 10 mg/kg systemic administration (Hultqvist et al., 2017). Furthermore, use of an anti-TfR single Fab domain (BS domain) C-terminal to the heavy chain of an anti-Aβ antibody resulted in a 12.4-fold increase in brain concentration of detectable antibody after 14 weekly systemic injections in a mouse model of amyloidopathy (Weber et al., 2018).

By using anti-mTfR antibodies in a scFv format it was expected that this would enable generation of a novel format for brain penetration that would lead to greater flexibility in targeting mTNF-α – since both the anti-mTfR and therapeutic moieties could be used in the parent IgG format depending on the efficacy of reformatting the antibody. Here I have shown that reformatting of 8D3 and $8D3_{130}$ variable domains as scFv fragments is possible, however the antibody-scFv fusions were highly aggregation prone which was a concern for producing them at scale for *in vivo* studies and for concentrating them to the required levels for dosing in the models (> 10 mg/ml). In addition, there is an apparent reduction in binding of 8D3 and $8D3_{130}$ scFv in the IgG-scFv format (Table 4.9). A possible reason for the reduction in maximal binding between anti-mTfR antibodies and anti-mTfR scFv could be linked to the nature of expected binding *in vivo*, whereby the antibody is expected to interact with the receptor in a bivalent manner. When mTfR is expressed on cell membranes it is present as a homodimer, whereas the recombinant protein used in this assay is monomeric and this difference in protein structure could mean that the true interaction between mTfR and an anti-mTfR antibody is not fully reproduced under these specific assay conditions. However, mTfR binding data comparing free 8D3 scFv and 8D3 scFv fused to the C-terminus of each light chain of an anti-Aβ antibody, RmAb158-8D3scFv, suggests monovalent interactions between anti-mTfR scFv and the receptor (Hultqvist et al., 2017). This is because the monovalent scFv showed a two-fold decrease in affinity compared to the fusion protein which, relative to binding sites per molecule, would indicate no change to binding. In the binding analysis in the chapter however, a proportional reduction in binding with 8D3 scFv was not observed when compared to its parent IgG, nor for $8D3_{130}$ scFv either (Figure 4.7). Therefore, it is possible that this may represent a real reduction in affinity or an artefact of how the IgG-scFv fusion protein is immobilised on the Octet chip (Section 4.4.3). Unfortunately, a working *in vitro* transcytosis model was not available at the time of these experiment to understand if the

reformatting influenced function so the exact impact of reformatting 8D3 hIgG1 TM and $8D3_{130}$ hIgG1 TM as scFv fragments on enhanced brain delivery cannot be fully determined in this thesis.

As discussed above, reformatting anti-mTfR antibodies as a scFv may impact on their binding to mTfR and as a result their delivery across the BBB. This potential issue means that the bispecific anti-mTNF-α-anti-mTfR scFv fusion proteins may not be suitable for *in vivo* experiments based on the *in vitro* data available. Although other studies have shown that brain delivery is still achievable, even with reduced binding compared to parent IgG formats (Hultqvist et al., 2017; Niewoehner et al., 2014), a risk-averse approach was taken to increase the likelihood that enhanced brain penetrance will be achieved *in vivo*. $8D3_{130}$ hIgG1 TM was selected as the IgG component of the bispecific antibody because there is already evidence that, as an anti-cytokine fusion protein, this format shows enhanced brain delivery and efficacy *in vivo* (Webster et al., 2017).

The anti-mTNF-α specific antibody, V1q, has potent mTNF-α neutralising activity in an *in vivo* mouse model of peritonitis and zymosan-induced multiple organ dysfunction syndrome in mice (Echtenacher et al., 1990; Jansen et al., 1998). Having shown *in vivo* neutralising activity, V1q presented as a useful tool for generating a novel brain penetrant anti-mTNF-α-mTfR fusion protein. Chimeric versions of V1q have been generated by changing the constant regions from its native rat IgD format, and are denoted as cV1q antibodies (Scallon et al., 2004). cV1q antibodies have been used to neutralise mTNF-α in mouse models of skin carcinoma and muscular dystrophy (Piers et al., 2011; Radley et al., 2008; Scott et al., 2003). The decision was made to produce bispecific fusion proteins with an anti-mTfR antibody and V1q as a scFv. V1q has not been reported in scFv form, and to address the risk that reformatting might alter its binding properties, an alternative, contingent fusion protein was considered to ensure that both characteristics of mTNF-α neutralisation and mTfR binding would be met. A brain penetrant TNF-α neutralising biologic has been generated previously (Chang et al., 2017; Sumbria et al., 2013; Qing Hui Zhou et al., 2011b), and a fusion protein containing $8D3_{130}$ hIgG1 TM and mTNFR2 was made in parallel to V1q scFv-containing bispecific fusion proteins.

4.4.2 Determining efficacy of bispecific anti-mTNF-α fusion proteins

To determine potency of anti-mTNF-α bispecific fusion proteins, neutralisation of mTNF-α *in vitro* was measured using a L929 mouse fibroblast cell line where cytotoxicity is induced by incubating cells with mTNF-α, in the presence of the cell cycle inhibitor actinomycin D. This process has previously been used to test the neutralisation of anti-TNF-α antibodies with a similar procedure throughout (Luchese et al., 2018; Qian et al., 2014; J. Wang et al., 2014). I have shown that mTNF-α can reproducibly induce cytotoxicity in L929 cells, and that this can be inhibited by anti-mTNF-α antibodies, including cV1q as a hIgG1 TM (Figure 4.11). Both V1q variable domain-containing fusion proteins and mTNFR2 fusion proteins show mTNF-α neutralising activity. However, V1q fusion proteins – in their full IgG or scFv formats – showed a ~10-fold lower potency compared to mTNFR2 fusion proteins. The results are similar to reported differences in TNF neutralisation between clinically approved TNFR2 receptor fusion, etanercept, and anti-TNF antibodies, infliximab and adalimumab, in L929 cells (Shen et al., 2017). The reasoning behind the observed reduction in potency of V1q scFv containing-fusion proteins compared to mTNFR2 fusion proteins was investigated further by performing kinetic binding studies. BLI experiments identified a difference in binding kinetics between fusion proteins, with mTNFR2-containing fusion proteins showing faster association and slower dissociation compared to V1q scFv-containing fusion proteins (Figure 4.10). These data could explain the difference in potency given that all fusion proteins were initially incubated with mTNF-α prior to addition to L929 fibroblasts, and faster association of mTNFR2 with mTNF-α could infer increased neutralisation compared to V1q.

It has been shown previously that the binding kinetics and the stability of complexes formed between TNF and two human TNF-α antagonists, infliximab and etanercept, contribute to their different neutralising potentials, in an *in vitro* assay of TNF-induced E-selectin expression (Scallon et al., 2002). Therefore, the difference in potency could also be explained by the specific binding of V1q and mTNFR2 to mTNF-α. TNFR2 binds all components of the TNF trimers, preventing the interaction of TNF with its receptor (Mukai et al., 2010). In contrast, the binding of a cV1q has been shown to be limited to a single TNF-α trimer, with no difference between a Fab fragment of V1q and the intact antibody (Scallon et al., 2004). These differences indicate a lack of avidity effects (e.g.,

formation of higher order protein/TNF-α complexes) with cV1q that could be responsible for the reduced potency compared to soluble mTNFR2. The possible lack of polyvalent binding of cV1q molecules to mTNF-α was suggested after the addition of anti-mouse Fc antibody was able to increase the neutralising potency of cV1q in an *in vitro* assay of TNF-induced cell death (Scallon et al., 2004). These data suggest that the introduction of cross-linking via anti-mouse Fc antibodies enabled the cV1q to bind to two TNF-α trimers simultaneously. In support of this data, V1q scFv fusion proteins are more potent at neutralising mTNF-α than cV1q hIgG1 TM (Figure 4.11). This may be due to the flexibility of the G4S linker present in the antibody-scFv fusion protein that could enable simultaneous binding to multiple mTNF-α trimers.

An additional factor that makes bispecific mTNFR2 fusion proteins a more suitable tool for *in vivo* experiments was identified during protein purification. Compared to bispecific V1q scFv fusion proteins they showed a reduced propensity to form higher molecular weight species, as identified during SEC (Figure 4.9). The increased aggregation was a concern for recovery of monomeric protein when considering large scale purification of *in vivo* material and therefore selection of bispecific mTNFR2 fusion proteins would reduce the possibility of aggregation during concentration steps and ensure a greater yield of final purified product from CHO cell supernatant compared to bispecific V1q scFv fusion proteins.

4.4.3 Limitations with determining bispecific anti-mTfR antibody-protein fusion affinity for mTfR

Kinetic measurements and affinity of anti-mTfR antibodies for mTfR have been described using BLI (Webster et al, 2017). In this chapter, kinetic measurements to establish binding of bispecific anti-mTfR-anti-mTNF-α fusion proteins using BLI proved challenging. Immobilisation of purified antibodies using anti-Human Fc capture biosensors to measure binding kinetics with a fixed concentration of mTfR showed that reformatting anti-mTfR antibodies as scFv resulted in reduced maximal binding responses to mTfR compared to the full IgG (Figure 4.7). The scFv fused to the C-terminal of the antibody will be closer in space than the binding interfaces on the end of the Fab domains in the $8D3_{130}$ hIgG1 TM antibody and will be more conformationally restricted. This may have impacted the ability

of the antibody-scFv fusion to bind two mTfR molecules simultaneously and led to a loss in binding avidity compared to the full IgG. A reduction in maximal binding response was also evident when measuring binding of mTfR to $8D3_{130}$ hIgG1 TM ΔK-mTNFR2 when compared to 8D3 hIgG1 TM (Figure 4.17B). A potential reason for this result could be due to reduced loading on the biosensor due to the size of the bispecific anti-mTfR fusion proteins, at ~200 kDa with the additional protein domain, compared to the smaller parent IgG (Figure 4.17A). Furthermore, immobilisation of such a large protein via its Fc domain may result in steric hinderance that could prevent accessibility of mTfR to the binding domains.

As quantification of binding kinetics was not achieved through BLI, alternative assays designed to measure protein-protein interactions were investigated to provide additional information on mTfR binding with bispecific anti-mTfR fusion proteins. The AlphaScreen combines both binding and avidity properties of proteins to improve sensitivity of low affinity interactions (Peppard et al., 2003). In addition, as both proteins remain in solution and with the effective transfer of singlet oxygen species over a 200 nm range it can be predicted that the relative effects of antigen presentation and protein size on binding measurements may be reduce compared to BLI. Indeed, sufficient binding was measured with both $8D3_{130}$ hIgG1 TM and $8D3_{130}$ hIgG1 TM ΔK-mTNFR2 and a similar binding profile to mTfR was observed for the two proteins (Figure 4.18). However, the size of the fusion proteins may still have affected the maximal responses measured in this assay with a clear reduction observed with $8D3_{130}$ hIgG1 TM ΔK-mTNFR2 compared to $8D3_{130}$ hIgG1 TM.

These binding assays predict that the biophysical properties required for enhanced brain delivery *in vivo*, specifically nanomolar affinity of an anti-mTfR IgG for mTfR, are retained in a bispecific anti-mTfR-mTNFR2 fusion protein and therefore provides a suitable solution for *in vivo* testing.

4.4.4 Summary

In summary, protein production and purification of various anti-mTfR-TNF-α fusion proteins and subsequent *in vitro* characterisation ensured that the most suitable bispecific fusion protein was chosen for *in vivo* experiments. As a result, $8D3_{130}$ hIgG1 TM ΔK-mTNFR2 and NIP228 hIgG1 TM ΔK-mNTFR2 will be used, alongside their respective parent antibodies as controls, to test the hypothesis that enhanced brain penetration of a mTNF-α neutraliser would delay disease progression in a model of chronic neurodegeneration.

Chapter 5 Inhibition of TNF-alpha using bispecific mTNFR2 fusion proteins in ME7 prion mice

5.1 Introduction

There is evidence that TNF-α is increased in the CSF of multiple sclerosis (MS) and AD patients – both of which are progressive neuroinflammatory/neurodegenerative diseases – and that these increased levels are linked to progression of disease (Ott et al., 2018; Rossi et al., 2014; Tarkowski et al., 2003). A single dose with a clinically used TNF-α neutraliser, etanercept, showed a positive trend towards slowing cognitive decline in mild-to-moderate AD patients over a six-month follow-up period compared to placebo-treated patients (Butchart et al., 2015). However, evidence with oral ME7 prion models suggests that genetic ablation of TNF-α increases resistance to infection (Mabbott et al., 2000). Yet, peripheral pharmacological intervention with a peripherally acting TNF-α inhibitor has no effect on prion pathology progression (Mabbott et al., 2002). One limiting factor with treating CNS disorders is effective delivery of a biologic to the brain parenchyma. It is thought that improvements in TNF therapy for CNS disorders can be achieved by enhancing delivery across the BBB. By using antibody engineering to target both mTfR and a therapeutic target, increased brain penetrance can be achieved in animal models of AD (Bien-Ly et al., 2014; Hultqvist et al., 2017; Niewoehner et al., 2014; Yu et al., 2014, 2011). The clinical evidence does suggest that targeting TNF-α, with peripherally acting TNF inhibitors, could have benefits in progressive neurodegenerative diseases. However, there is a need to understand the effects of anti-TNF treatment in ME7 prion to help elucidate the mechanisms that may be targeted prior to treatment in the presence of systemic inflammation.

In this chapter, I will assess the effects of treating mice with bispecific mTNFR2 fusion proteins on disease progression and neuroinflammation in ME7 prion disease as understanding the contributions of TNF-α to disease progression will allow for better elucidation of the interplay between systemic inflammation and TNF-α inhibition on disease progression in future chapters. To investigate this possibility, ME7 mice were

treated from 12 wpi with weekly injections of fusion protein, detailed in Table 5.1, over four weeks and animal behaviour was monitored from 8 wpi until 16 wpi. Neuroinflammation was measured through analysis of proinflammatory cytokine transcript levels and immunohistochemistry for microglial activation markers in the hippocampus and thalamus. Mouse TfR levels were measured by histology to ensure effective expression for enhanced delivery across the BBB and synaptic markers were analysed by qPCR. Furthermore, systemic challenge with LPS was used to determine whether bispecific mTNFR2 fusions show effective *in vivo* neutralisation of TNFR signalling through qPCR analysis of downstream cytokine expression.

Table 5.1 Biological properties of fusion proteins used in this chapter

Protein	Binds mTfR	Binds mTNF-α	Properties
NIP228 hIgG1 TM	No	No	Peripheral isotype control
NIP228 hIgG1 TM ΔK-mTNFR2	No	Yes	Peripheral TNF neutraliser
8D3$_{130}$ hIgG1 TM	Yes	No	BBB-crossing isotype
8D3$_{130}$ hIgG1 TM ΔK-mTNFR2	Yes	Yes	BBB-crossing TNF neutraliser

5.2 Methods

5.2.1 Treatment of ME7 mice with bispecific mTNFR2 fusion proteins

Male C57Bl/6 mice (12-14 weeks old) were placed in a stereotaxic frame and injected bilaterally with ME7 brain homogenate in the dorsal hippocampus (Section 2.1.2). Disease progression was monitored through assessment of overnight burrowing (Section 2.1.3.1) and automated open field locomotor activity from 9 wpi (Section 2.1.3.2). ME7 mice (n=7-8/group) were treated with bispecific mTNFR2 fusion protein or isotype control antibody for four weeks from 12 wpi. Mice received a weekly i.p. injection of 54 μM fusion protein or vehicle (6 ml/kg) (Section 2.1.4). Mice were sacrificed at 16 wpi, 7 days after final i.p. injection and perfused with D-PBS containing heparin sodium (5 U/ml) before brains, spleens and sera were collected for downstream analysis (Section 2.1.6). Spleens were weighed and then snap frozen in liquid nitrogen for analysis of cytokines and immune cell markers. The right hemisphere was processed for immunohistochemistry: embedded brain tissues were sectioned and stained for expression of CD64, MHCII and TfR by DAB immunohistochemistry (Section 2.2.1). A tissue punch enriched for the hippocampus and thalamus from the left hemisphere was snap frozen then homogenised and processed for qPCR analysis of cytokine and synaptic marker transcript levels (Section 2.2.2).

5.2.2 Efficacy of bispecific mTNFR2 fusion proteins following systemic challenge with LPS

In vivo neutralisation of TNF-α was determined in 12-week-old female C57BL/6 mice with injection of bispecific mTNFR2 fusion proteins (54 μM, i.p.) 24 hours prior to systemic challenge with LPS (100 μg/kg, i.p.) (Section 2.1.5.1). Mice were perfused two hours after LPS injection with D-PBS (Section 2.1.6), and the hippocampus/thalamus were removed as described above for analysis of cytokine expression (Section 2.2.2). Spleens were weighed to measure fusion protein-induced changes.

5.3 Results

5.3.1 Peripheral changes following systemic administration of bispecific mTNFR2 fusion proteins in ME7 mice

Mice bodyweights following weekly administration of bispecific mTNFR2 fusion proteins were no different than following weekly vehicle injections (Figure 5.1A). Statistical analysis showed a main effect of 'time after first injection' ($F(2.831, 87.77) = 4.653$, $p = 0.0054$) over the four-week period as expected for growth of ME7 mice. However, there was no main effect of 'treatment' ($F(4, 31) = 0.8137$, $p = 0.5261$) or an interaction between 'time after first injection x treatment' ($F(16, 124) = 0.7507$, $p = 0.7371$) using a two-way ANOVA.

Analysis of spleen weights from ME7 mice at 16 wpi after a four-week dosing regimen showed a significant increase in spleen weights in ME7 mice that were treated with $8D3_{130}$ hIgG1 TM compared to vehicle-treated ME7 mice ($t = 5.707$, $df = 17$, $p = 0.0001$). Mice receiving the mTfR-targeting control antibody showed on average 5-fold increase in spleen weights; whilst no other treatment groups showed any difference to vehicle-treated ME7 mice (Figure 5.1B).

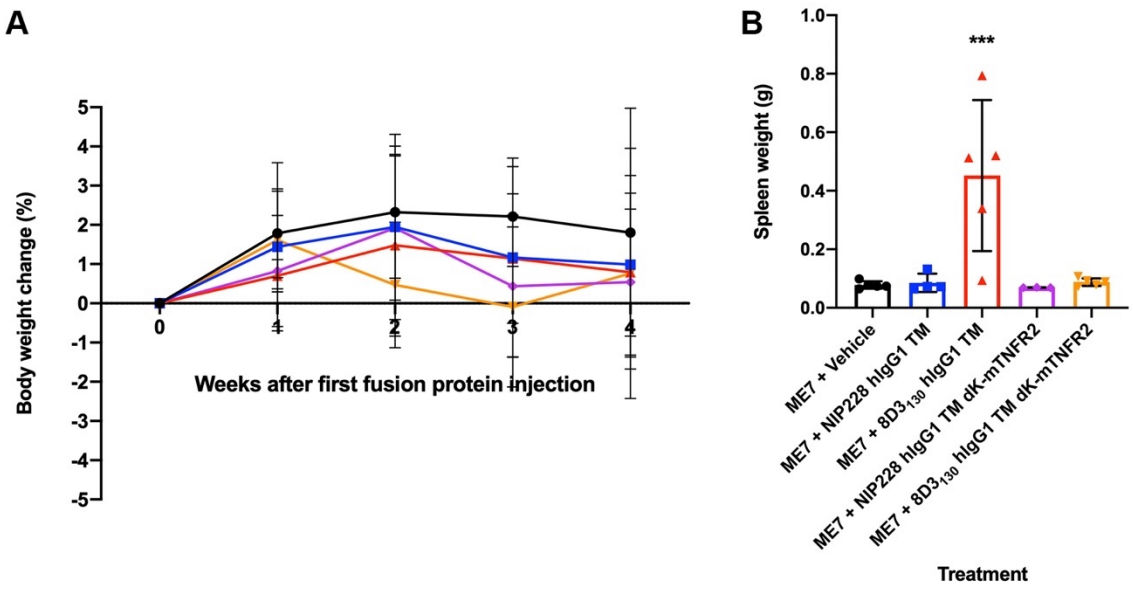

Figure 5.1 Body and spleen weight changes following administration of bispecific mTNFR2 fusion proteins in ME7 mice

ME7 mice were injected weekly with mTNFR2 fusion protein or isotype control antibody (54 μM, i.p.) from 12 wpi and tissue collected 7 days after final injection at 16 wpi. (A) Mouse body weights are not significantly different over time between treatment groups. vehicle = black; NIP228 hIgG1 TM = blue; $8D3_{130}$ hIgG1 TM = red; NIP228 hIgG1 TM ΔK-mTNFR2 = purple; $8D3_{130}$ hIgG1 TM ΔK-mTNFR2 = orange. (B) Terminal spleen weights in $8D3_{130}$ hIgG1 TM-treated ME7 mice are significantly increased over vehicle-treated ME7 mice. ***, $p < 0.0001$ versus vehicle-treated ME7 mice following one-way ANOVA with Holm-Sidak's multiple comparisons test. Data presented as mean ± SD; n = 3-5 per group.

5.3.2 TfR expression following systemic administration of bispecific mTNFR2 fusion proteins in ME7 mice

TfR expression was analysed to determine the effects of 4 weekly fusion protein injections on expression within pathologically affected brain regions in ME7 mice.

Expression of TfR in the hippocampus can be detected on brain endothelial cells and neurons in both naïve control mice and ME7 mice (Figure 5.2). TfR expression in ME7 mice at 16 wpi shows a non-significant increase (average 1.68-fold) compared to naïve control mice using one-way ANOVA ($F(5, 11) = 1.097$, $p = 0.4150$) (Figure 5.2G). However, neuronal TfR expression within the CA1 pyramidal layer is qualitatively reduced in ME7 mice compared to Naïve mice (asterisks; Figure 5.2). Treatment of ME7 mice from 12 wpi with bispecific mTNFR2 fusion proteins has no effect on TfR expression in the hippocampus compared to vehicle-treated ME7 mice ($F(4, 10) = 0.3884$, $p = 0.8123$) (Figure 5.2H).

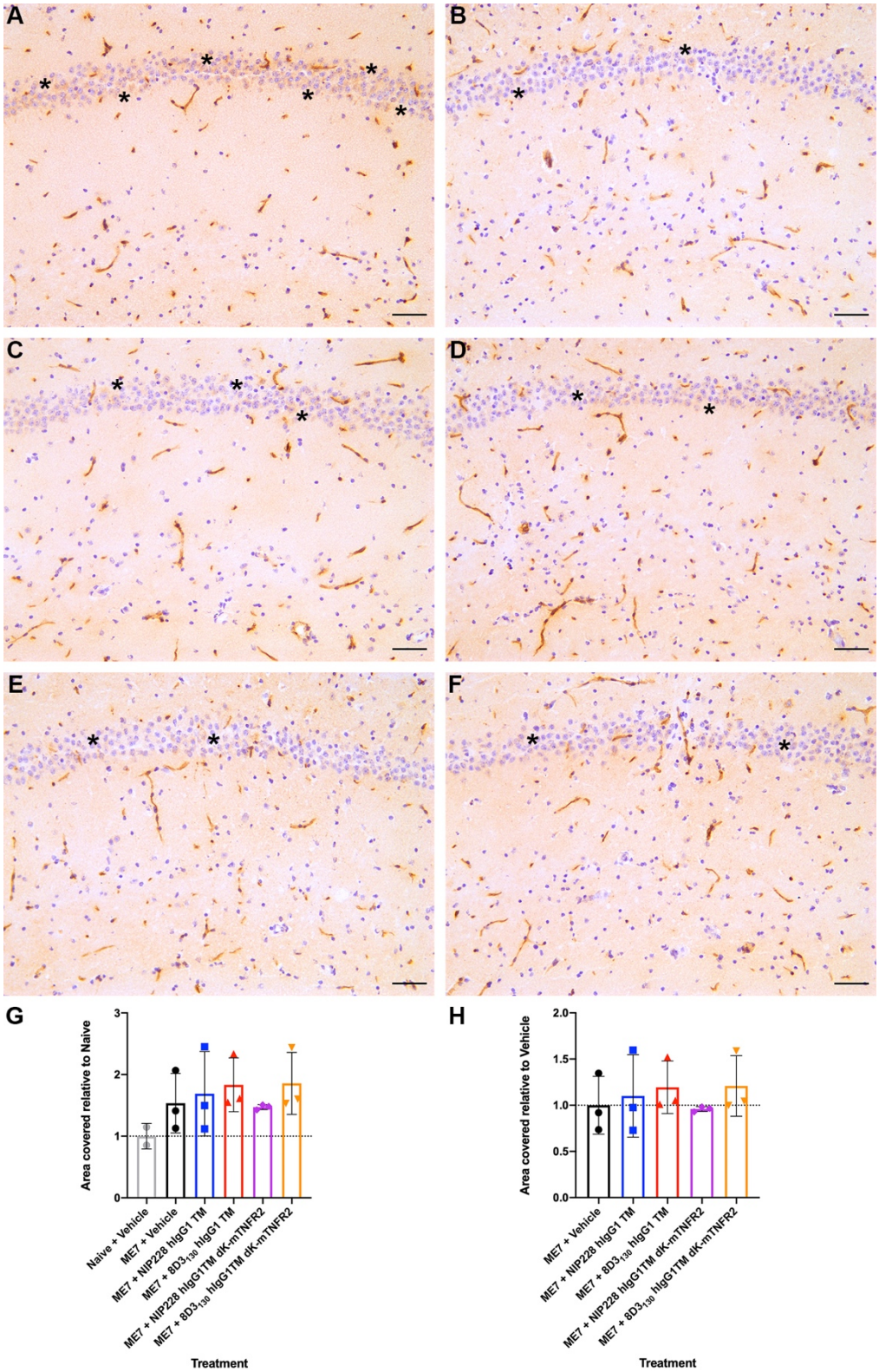

Figure 5.2 TfR expression in ME7 mice following bispecific mTNFR2 fusion protein administration

(A-F) Representative images of hippocampal TfR staining (asterisks = neuronal) in naïve control mice (A) and ME7 mice at 16 wpi following weekly injections from 12 wpi with vehicle (B), NIP228 hIgG1 TM (C), $8D3_{130}$ hIgG1 TM (D), NIP228 hIgG1 TM ΔK-mTNFR2 (E) and $8D3_{130}$ hIgG1 TM ΔK-mTNFR2 (F). (G-H) Analysis of TfR expression 7 days after final injection in ME7 mice. (G) Expression in ME7 mice is unchanged compared to naïve control mice. (H) Bispecific mTNFR2 fusion protein treatment has no effect on TfR expression in ME7 mice when compared to vehicle-treated mice following one-way ANOVA. Data is presented as mean ± SD, n = 2-3/group. Images were taken with a 20x objective; scale bar = 50 μm.

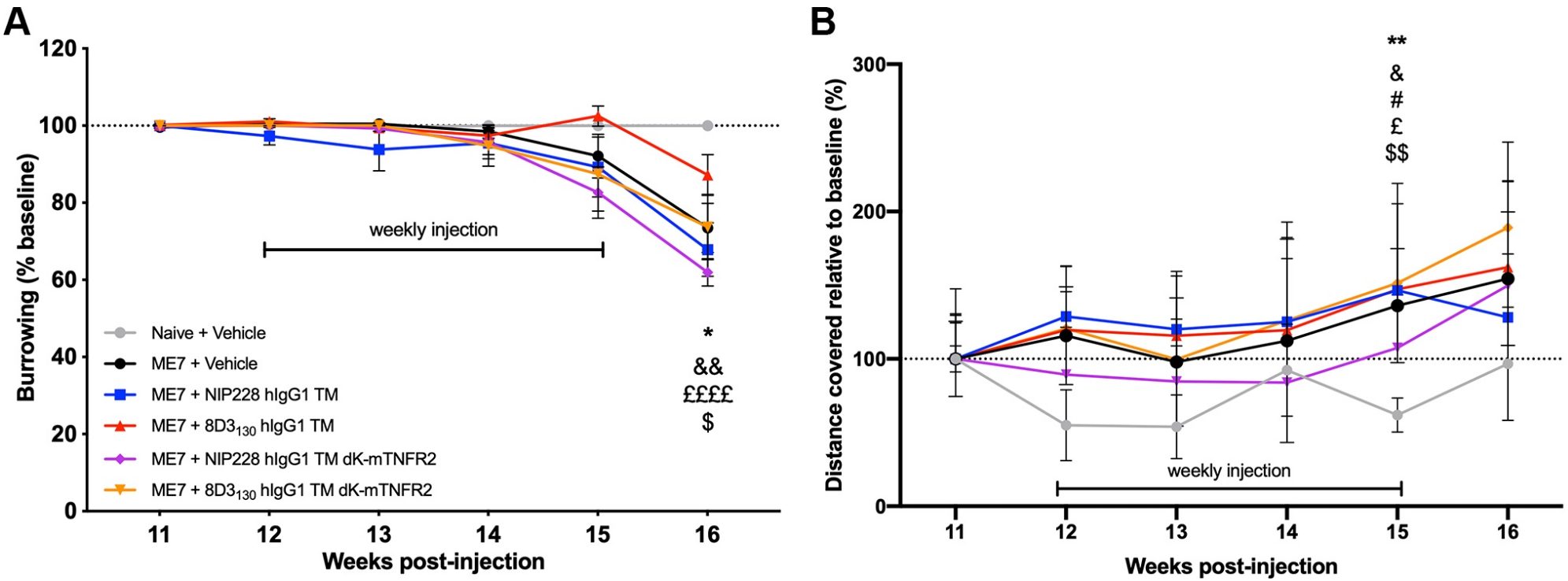

Figure 5.3 Behavioural assessment of ME7 mice following administration of bispecific mTNFR2 fusion proteins

ME7 mice were monitored in burrowing (A) and open field (B) behaviours to determine disease progression before and during weekly treatment with bispecific mTNFR2 fusion protein or isotype control (54 μM, i.p.) from 12 wpi. (A) Changes in burrowing behaviour between naïve controls and ME7 mice are present from 15 wpi, but mTNFR2 fusion protein treatment has no significant effect on behaviour compared to vehicle-treated ME7 mice. (B) Open field locomotor activity in ME7 mice shows an initial decrease compared to naïve control mice at 11 wpi. ME7 mice then show increasing locomotion until significance at 15 wpi. Treatment with mTNFR2 fusion proteins has no significant effect compared to vehicle-treated ME7 mice. Data are presented as mean ± SD; Naïve mice, n = 4; ME7 mice, n =7-8/group. *, $p < 0.05$, **, $p < 0.01$ for ME7 + Vehicle; &, $p < 0.05$, &&, $p < 0.01$ for ME7 + NIP228 hIgG1 TM; #, $p < 0.05$ for ME7 + $8D3_{130}$ hIgG1 TM; £, $p < 0.05$, ££££, $p < 0.0001$ for ME7 + NIP228 hIgG1 TM ΔK-mTNFR2; $, $p < 0.05$, $$, $p < 0.01$ for ME7 + $8D3_{130}$ hIgG1 TM ΔK-mTNFR2 versus Naïve + Vehicle following a two-way ANOVA and Dunnett's multiple comparisons.

5.3.3 Effect of TNF neutralisation on behavioural assessment of ME7 mice

Baseline measurements for behaviours were established at 8 wpi and this time point was used to measure relative changes over time. Age-matched, non-injected C57Bl/6 (Naïve) mice were included as behavioural controls to follow progression of ME7 prion disease (Figure 5.3).

ME7 mice began showing decreased burrowing from 15 wpi (7-17%) compared to Naïve control mice, but this decrease was only significant at 16 wpi (Figure 5.3A). Two-way repeated measures ANOVA analysis of burrowing behaviour showed a significant main effect of 'time after injection' ($F(2.219, 82.11) = 30.53$, $p < 0.0001$) and a significant interaction between 'time after injection x treatment' ($F(35, 259) = 1.987$, $p = 0.0014$). Treatment with bispecific mTNFR2 fusion did not modify ME7-induced burrowing changes and there was no main effect of 'treatment' ($F(5, 37) = 1.705$, $p = 0.1578$). At 16 wpi, $8D3_{130}$ hIgG1 TM-treated ME7 mice burrowed more food pellets than any other treatment group (88% compared to 62-74%) and were not significantly different from naïve control mice at 16 wpi following Dunnett's multiple comparisons test ($q = 2.223$, $df = 7$, $p = 0.1562$) (Figure 5.3A).

ME7 mice show stable locomotion from 11 to 14 wpi, whereas Naïve control mice show an initial decrease in locomotion, with the nadir between 12-13 wpi, before increases from 14 wpi (Figure 5.3B). Analysis of open field locomotor activity using two-way repeated measures ANOVA identified a significant main effect of 'time (wpi)' ($F(3.403, 125.9) = 8.534$, $p < 0.0001$; $\varepsilon = 0.6805$) and 'treatment' ($F(5, 37) = 2.773$, $p = 0.0317$), but no significant interaction between the two 'time x treatment' ($F(25, 185) = 0.8992$, $p = 0.6064$). At 15 wpi locomotion in all treated ME7 mice is significantly increased over Naïve control mice following Dunnett's multiple comparisons ($0.0028 < p < 0.0339$) (Figure 5.3B).

5.3.4 Biochemical analysis of synaptic markers following administration of bispecific mTNFR2 fusion proteins in ME7 mice

Synaptophysin (*Syp*) mRNA transcripts expression in the hippocampus and thalamus is significantly different between groups ($F(5,36) = 2.944$, $p = 0.025$). Post-hoc analysis showed significant decreases (average 25% decrease) in *Syp* expression between NIP228 hIgG1 TM, NIP228 hIgG1 TM ΔK-mTNFR2 and $8D3_{130}$ hIgG1 TM ΔK-mTNFR2 treated ME7 mice compared to Naïve control mice (Figure 5.4A). Treatment with bispecific mTNFR2 fusion had no effect on ME7-induced changes with no significant differences ($F(4,34) = 1.838$, $p = 0.1443$) between treatment groups in ME7 mice (Figure 5.4C).

Expression of *Grm1* transcripts was unchanged in ME7 mice compared to naïve control mice ($F(5, 36) = 1.507$, $p = 0.2119$) (Figure 5.4B). However, post-hoc multiple comparisons identified a trend towards decreased expression (average 32% decrease) in all ME7 mice compared to Naïve control mice ($p = 0.0824$ for all groups). Analysis with one-way ANOVA between treatment groups in ME7 mice showed no significant differences in means ($F(4, 34) = 0.05881$, $p = 0.9933$) (Figure 5.4D).

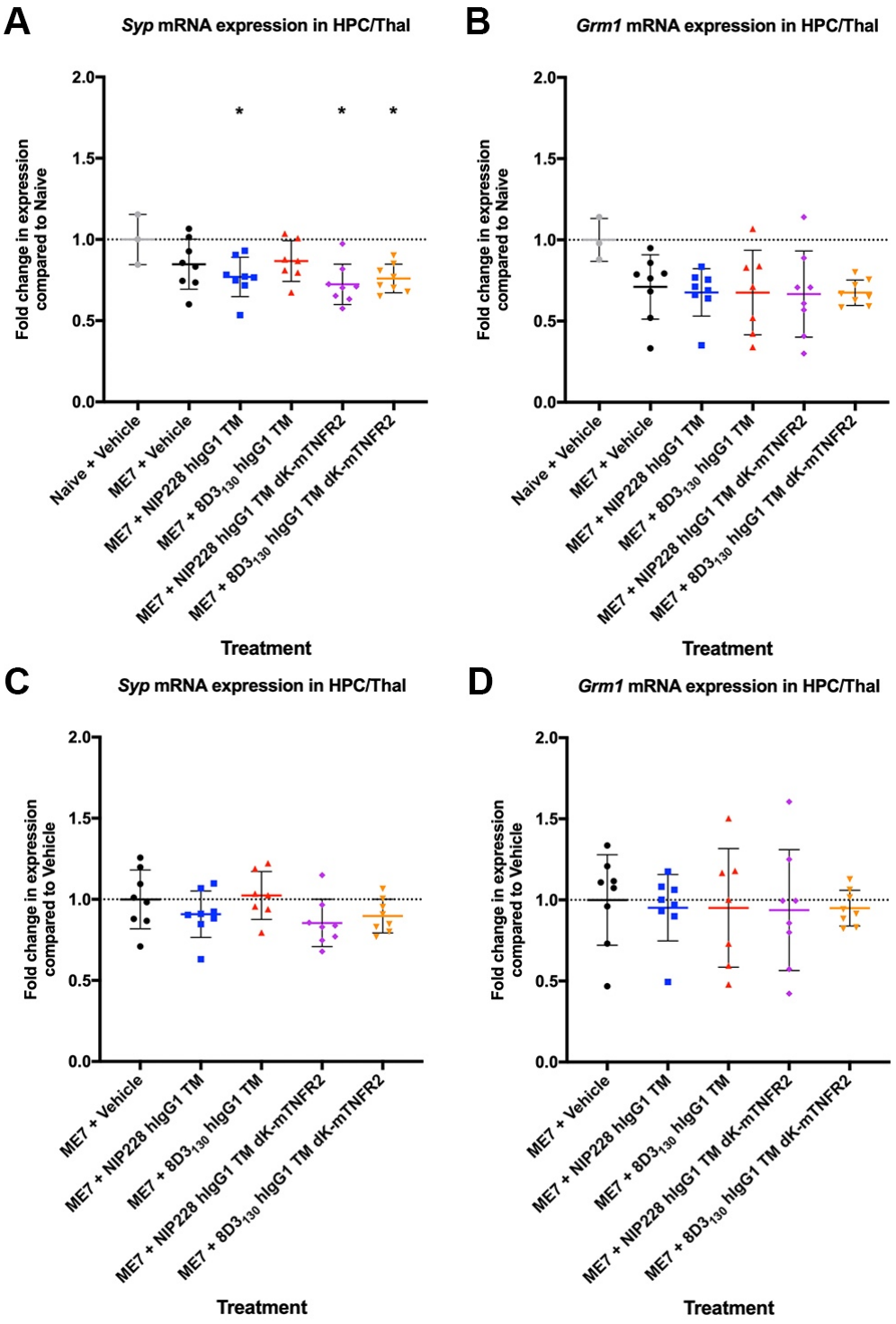

Figure 5.4 Expression of synaptic markers in hippocampus/thalamus in ME7 mice after bispecific mTNFR2 fusion protein treatment

(A) Expression of synaptophysin (*Syp*) mRNA transcripts in the hippocampus and thalamus of 16 wpi ME7 mice shows decreased expression relative to age-matched naïve control mice. (B) mGluR1 (*Grm1*) expression in the hippocampus and thalamus of 16 wpi ME7 mice shows no change relative to age-matched Naïve mice. (C-D) *Syp* (C) and *Grm1* (D) mRNA transcripts levels remain unchanged following weekly systemic administration of bispecific mTNFR2 fusion proteins from 12 wpi in ME7 mice. Data are presented as the mean ± SD (Naïve mice, n = 4; ME7 mice, n =7-8/group) of fold change compared to naïve control or vehicle after normalisation of expression to *Pgk1.* *, $p < 0.05$ versus Naïve + Vehicle following one-way ANOVA with Holm-Sidak's multiple comparisons test.

5.3.5 Microglial activation in ME7 mice following systemic administration of bispecific mTNFR2 fusion proteins

Microglial activation in the brains of ME7 mice 7 days after final fusion protein injection was measured by CD64 (FcγRI) and MHCII expression in the hippocampus (Figure 5.5, Figure 5.7) and thalamus (Figure 5.6, Figure 5.8).

5.3.5.1 Hippocampal CD64 expression

CD64 staining was increased an average 8.98-fold in the hippocampus of ME7 mice at 16 wpi compared to age-matched naïve control mice (Figure 5.5). Analysis of staining using one-way ANOVA showed a significant difference between group means ($F(5, 11) = 7.055$, $p = 0.0035$). Post-hoc analysis showed increased staining compared to Naïve control mice for all treatment groups in ME7 mice ($0.0054 < p < 0.0068$), with $8D3_{130}$ hIgG1 TM-treated mice showing the greatest increase ($t = 5.764$, $df = 11$, $p = 0.0006$) (Figure 5.5G). Treatment of ME7 mice with bispecific mTNFR2 fusion proteins has no effect on CD64 expression in the hippocampus compared to vehicle-treated ME7 mice ($F(4, 10) = 1.829$, $p = 0.1999$) (Figure 5.5H).

5.3.5.2 Thalamic CD64 expression

An increase in CD64 expression (average 17.2-fold) was evident in the thalamus of ME7 mice at 16 wpi, irrespective of treatment, compared to age-matched Naïve control mice (Figure 5.6). Analysis of staining using one-way ANOVA showed a significant difference between group means ($F(5, 11) = 5.645$, $p = 0.0081$). Holm-Sidak multiple comparisons post-hoc analysis identified a significant increase in thalamic CD64 expression in all ME7 treatments compared to Naïve control mice for all treatment groups in ME7 mice ($0.0036 < p < 0.0039$) (Figure 5.6G). Treatment of ME7 mice with bispecific mTNFR2 fusion proteins had no effect on CD64 expression in the thalamus compared to vehicle-treated ME7 mice ($F(4, 10) = 0.1322$, $p = 0.9669$) (Figure 5.6H).

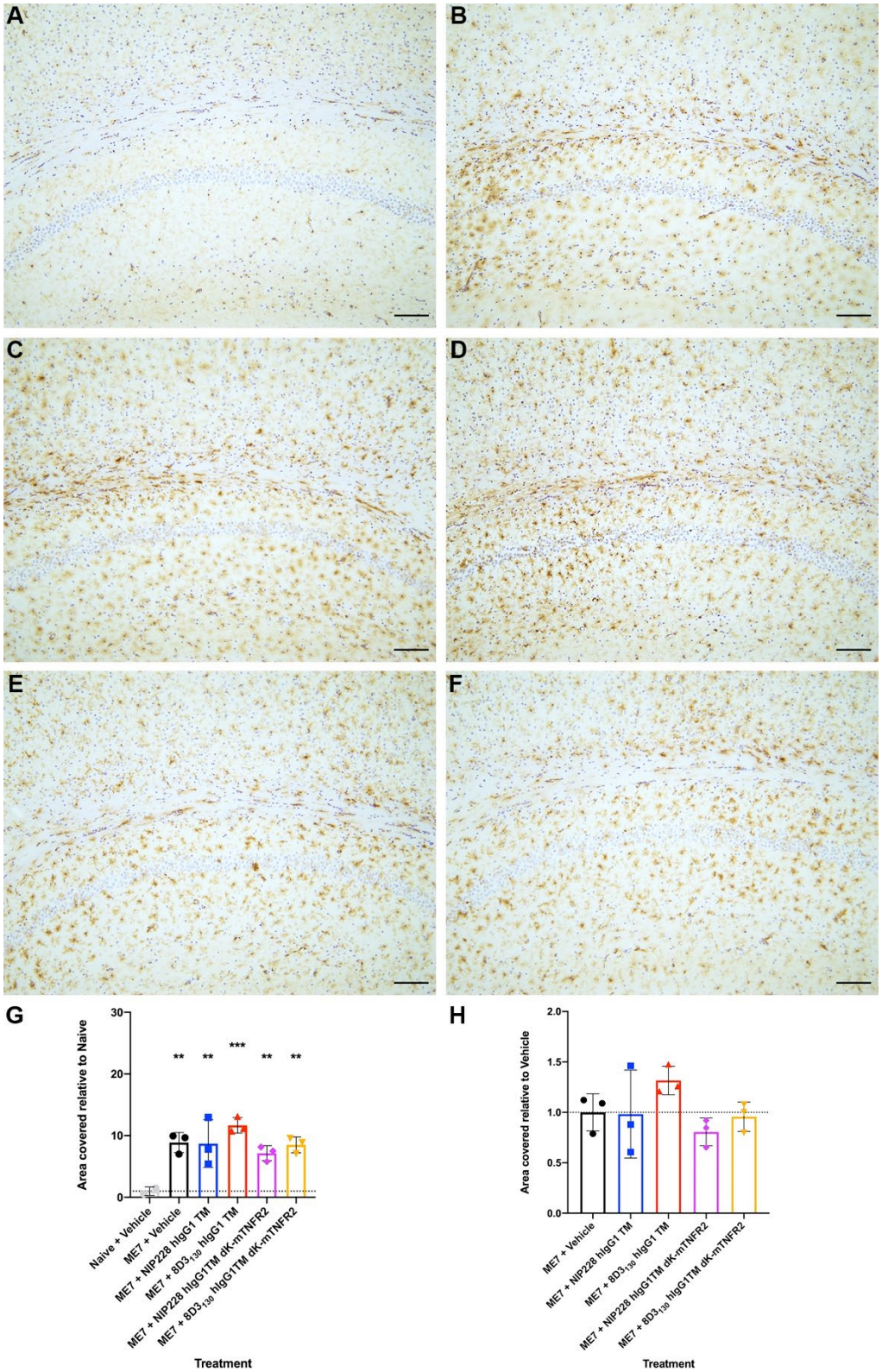

Figure 5.5 Hippocampal CD64 expression in ME7 prion mice after bispecific mTNFR2 fusion protein administration

(A-F) Hippocampal CD64 staining in naïve control mice (A) and ME7 mice at 16 wpi following weekly injections from 12 wpi with vehicle (B), NIP228 hIgG1 TM (C), $8D3_{130}$ hIgG1 TM (D), NIP228 hIgG1 TM ΔK-mTNFR2 (E) and $8D3_{130}$ hIgG1 TM ΔK-mTNFR2 (F). (G) Analysis of hippocampal CD64 expression in ME7 mice shows a significant increase compared to Naïve control mice when measured 7 days after final injection. (H). Bispecific mTNFR2 fusion protein treatment does not alter ME7-induced changes in CD64 expression when compared to vehicle-treated ME7 mice. Data is presented as mean ± SD, n = 3/group. **, $p < 0.01$, ***, $p < 0.001$ versus Naïve + Vehicle using one-way ANOVA with Holm-Sidak's multiple comparisons test. Images were taken with a 10x objective lens; scale bar = 100 μm.

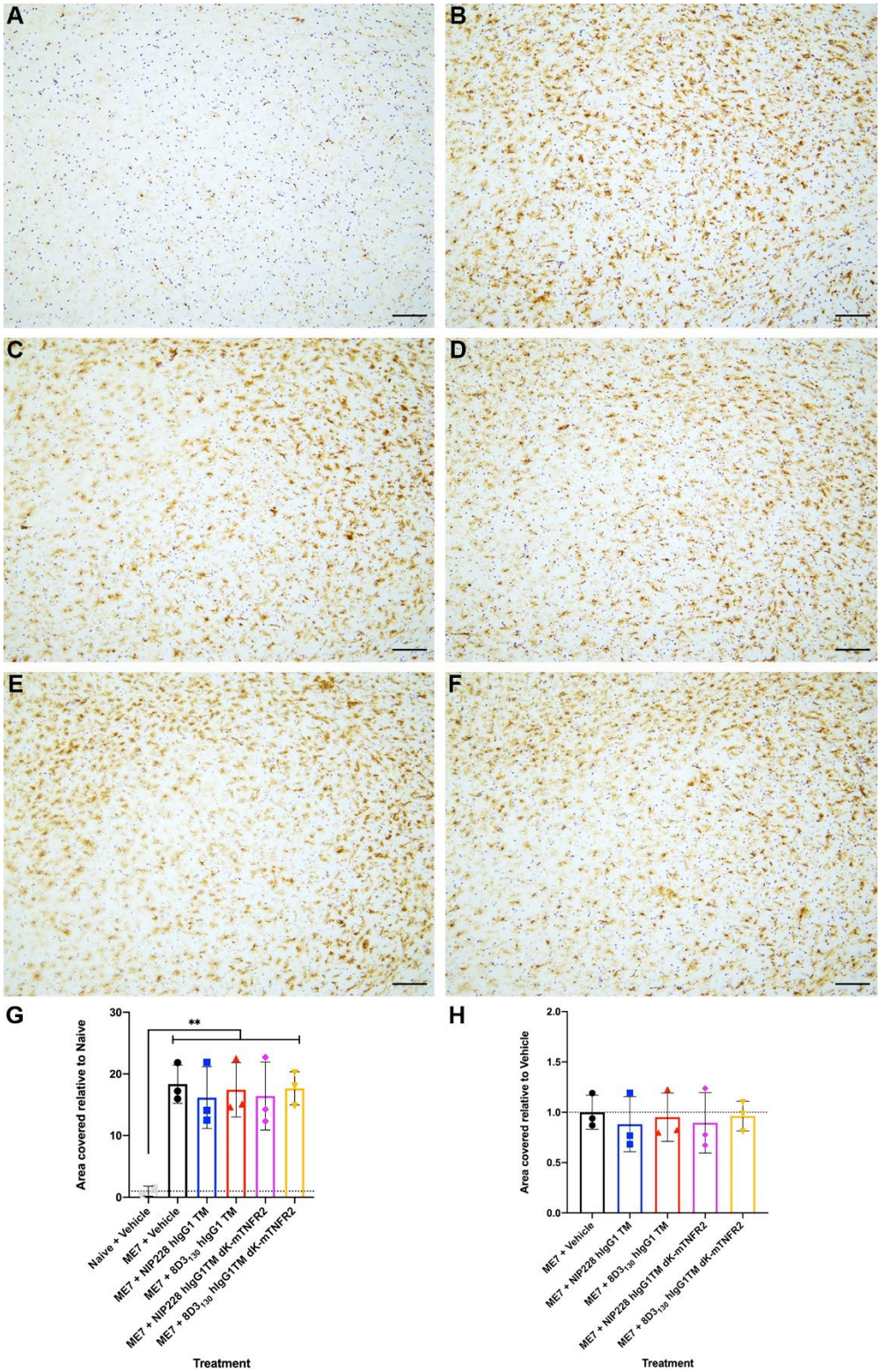

Figure 5.6 CD64 staining in thalamus of ME7 mice following bispecific mTNFR2 fusion protein administration

(A-F) Representative images of thalamic CD64 staining in naïve control mice (A) and ME7 mice at 16 wpi following weekly injections from 12 wpi with vehicle (B), NIP228 hIgG1 TM (C), $8D3_{130}$ hIgG1 TM (D), NIP228 hIgG1 TM ΔK-mTNFR2 (E) and $8D3_{130}$ hIgG1 TM ΔK-mTNFR2 (F). (G-H) Analysis of thalamic CD64 expression 7 days after final injection in ME7 mice. (G) Expression in ME7 mice is significantly increased compared to Naïve control mice. (H) Treatment with bispecific mTNFR2 fusion proteins has no effect on ME7-induced increases on thalamic CD64 expression when compared to vehicle treatment. Data is presented as mean ± SD, n = 3/group. **, $p < 0.01$ versus Naïve + Vehicle using one-way ANOVA with Holm-Sidak's multiple comparisons test. Images taken with a 10x objective lens; scale bar = 100 μm.

5.3.5.3 Hippocampal MHCII expression

Increased staining of MHCII was also seen in ME7 mice at 16 wpi in the hippocampus compared to age-matched naïve control mice (Figure 5.7). This increased staining is significant following analysis with one-way ANOVA ($F(5, 11) = 7.247$, $p = 0.0031$). Interestingly, a significant difference was only recorded between vehicle-treated ME7 mice and Naïve control mice ($q = 5.019$, $df = 11$, $p = 0.0015$) (Figure 5.7G). Analysis of staining within ME7 mice showed a significant reduction (average 74% decrease) in hippocampal MHCII expression in NIP228 hIgG1 TM-, NIP228 hIgG1 TM ΔK-mTNFR2- and $8D3_{130}$ hIgG1 TM ΔK-mTNFR2 treated ME7 mice compared to vehicle-treated ME7 mice ($F(4, 10) = 6.416$, $p = 0.0080$) (Figure 5.7H).

5.3.5.4 Thalamic MHCII expression

Increased MHCII expression (average 218.8-fold) was also seen in the thalamus of ME7 mice at 16 wpi compared to age-matched Naïve control mice (Figure 5.8). However, large variation, measured with coefficient of variation (%CV) ranged from 51.1% to 110% in expression of MHCII in ME7 mice meant these increases were not significant following analysis with a Kruskal-Wallis test ($H(6, 17) = 6.386$, $p = 0.2705$) (Figure 5.8G). Analysis of staining between treatment groups in ME7 mice showed no effect of bispecific mTNFR2 treatment on hippocampal MHCII expression compared to vehicle-treated ME7 mice ($H(5, 15) = 1.767$, $p = 0.8203$) (Figure 5.8H).

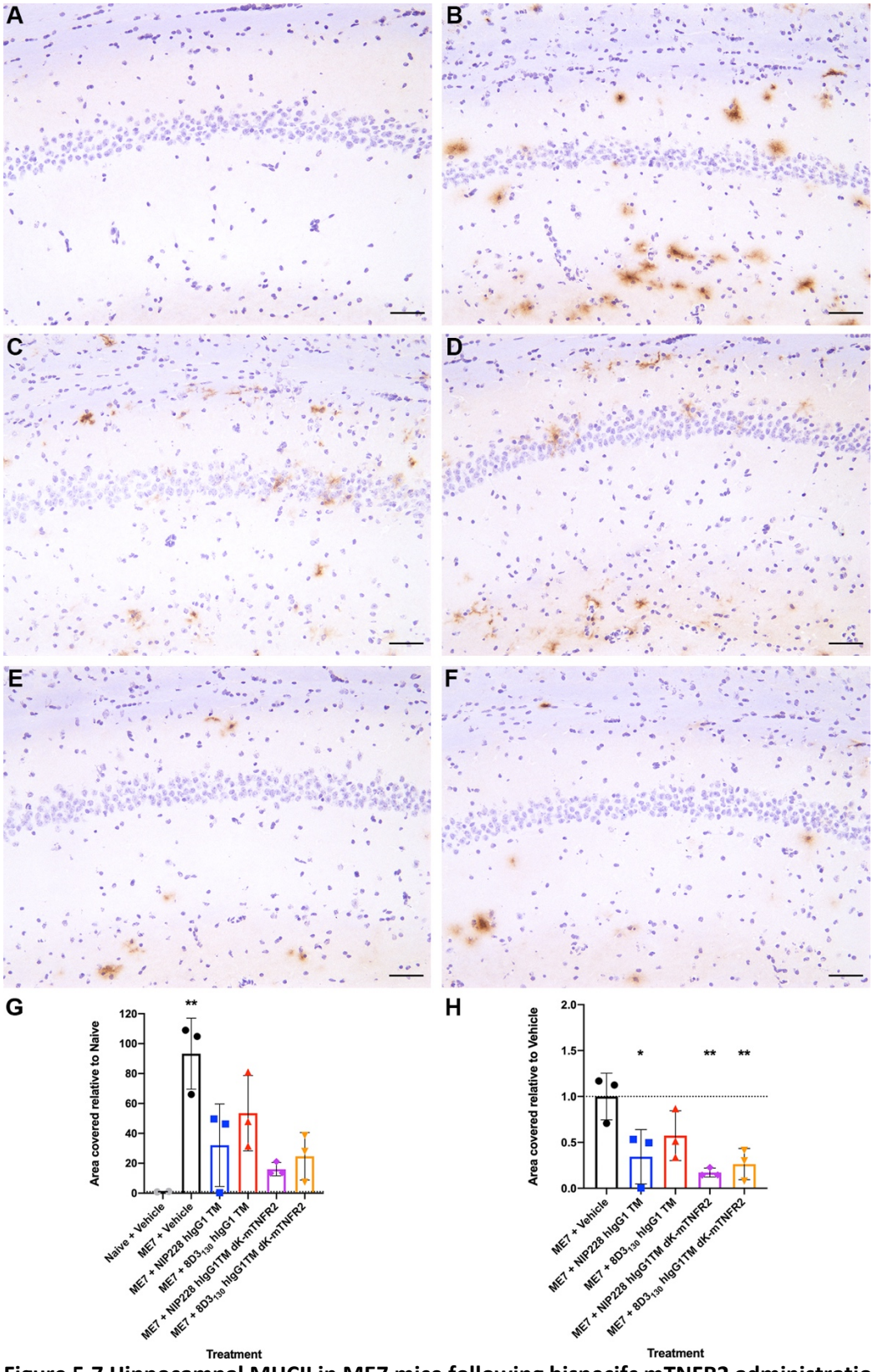

Figure 5.7 Hippocampal MHCII in ME7 mice following bispecifc mTNFR2 administration
(A-F) Hippocampal MHCII staining in naïve control mice (A) and ME7 mice at 16 wpi following weekly injections from 12 wpi with vehicle (B), NIP228 hIgG1 TM (C), $8D3_{130}$ hIgG1 TM (D), NIP228 hIgG1 TM ΔK-mTNFR2 (E) and $8D3_{130}$ hIgG1 TM ΔK-mTNFR2 (F). (G-H) Analysis of hippocampal MHCII expression in vehicle-treated ME7 mice shows an increase compared to Naïve control mice 7 days after final injection in ME7 mice (G). Bispecific mTNFR2 fusion protein treatment reduces MHCII expression in ME7 mice when compared to vehicle-treated ME7 mice following one-way ANOVA (H). Data is presented as mean ± SD, n = 3/group. Images were taken with a 20x objective lens; scale bar = 50 μm.

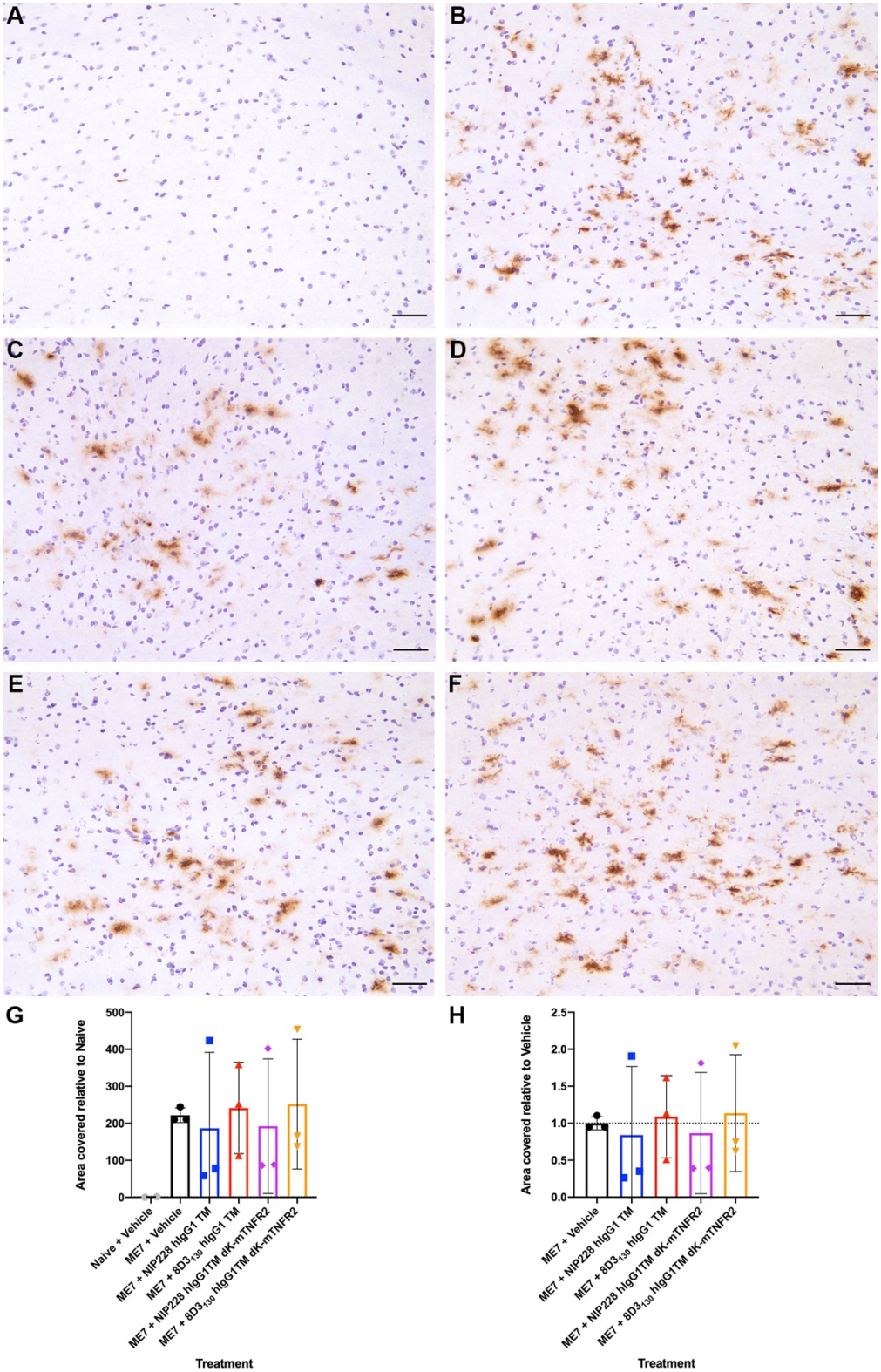

Figure 5.8 MHCII staining in thalamus of ME7 mice following bispecific mTNFR2 fusion protein administration

(A-F) Representative images of thalamic MHCII staining in naïve mice (A) and ME7 mice at 16 wpi following weekly injections from 12 wpi with vehicle (B), NIP228 hIgG1 TM (C), $8D3_{130}$ hIgG1 TM (D), NIP228 hIgG1 TM ΔK-mTNFR2 (E) and $8D3_{130}$ hIgG1 TM ΔK-mTNFR2 (F). (G) Analysis of thalamic MHCII expression in ME7 mice. Showed no changed compared to Naïve control mice 7 days after final injection. (H) Bispecific mTNFR2 fusion protein treatment has no effect on MHCII expression in ME7 mice when compared to vehicle-treated mice following one-way ANOVA. Data is presented as mean ± SD, n = 3/group. Images taken with a 20x objective lens; scale bar = 50 μm.

5.3.6 Biochemical analysis of cytokines in ME7 mice following fusion protein administration

Analysis of cytokine transcripts from hippocampus/thalamus-enriched tissue from ME7 mice showed that expression of *Tnf* is increased, but not significantly different from Naïve control mice after Kruskal-Wallis test (H (6, 42) = 8.332, p = 0.1389). However, Dunn's post-hoc multiple comparisons identified significant differences in NIP228 hIgG1 TM-treated and $8D3_{130}$ hIgG1 TM-treated ME7 mice compared to Naïve control mice (Figure 5.9A).

Il1b expression is significantly increased in ME7 mice at 16 wpi compared to age-matched Naïve mice (F (5, 36) = 4.810, p = 0.0018). ME7 mice treated with $8D3_{130}$ hIgG1 TM showed a greater increase in expression (5.23-fold versus average 4.15-fold increase) than other treatment groups compared to Naïve control mice (Figure 5.9B).

Ccl2 expression is significantly increased (average 14.5-fold) in ME7 mice compared to Naïve control mice following analysis with one-way ANOVA (F (5, 36) = 3.876, p = 0.0065). Interestingly, there was a significant difference between standard deviations of the groups (F (5, 36) = 3.535, p = 0.0106) following Brown-Forsythe test and this is reflected by the different levels of significance between treatments in ME7 mice and Naïve control mice (Figure 5.9C).

Analysis of bispecific mTNFR2 fusion protein treatment in ME7 mice showed that treatment had no effect on cytokine expression when compared to vehicle-treated ME7 mice (Figure 5.9D-F). There was no significant difference between treatment groups for expression of *Tnf* transcripts (H (5, 39) = 0.1955, p = 0.9955), *Il1b* transcripts (F (4, 34) = 1.364, p = 0.2671) or *Ccl2* transcripts (F (4, 34) = 1.418, p = 0.2490) when compared to vehicle-treated ME7 mice (Figure 5.9D-F). Again, a significant difference between standard deviations was reported for *Ccl2*transcripts in ME7 mice (F (4, 34) = 3.486, p = 0.0173) following analysis with Brown-Forsythe test (Figure 5.9F).

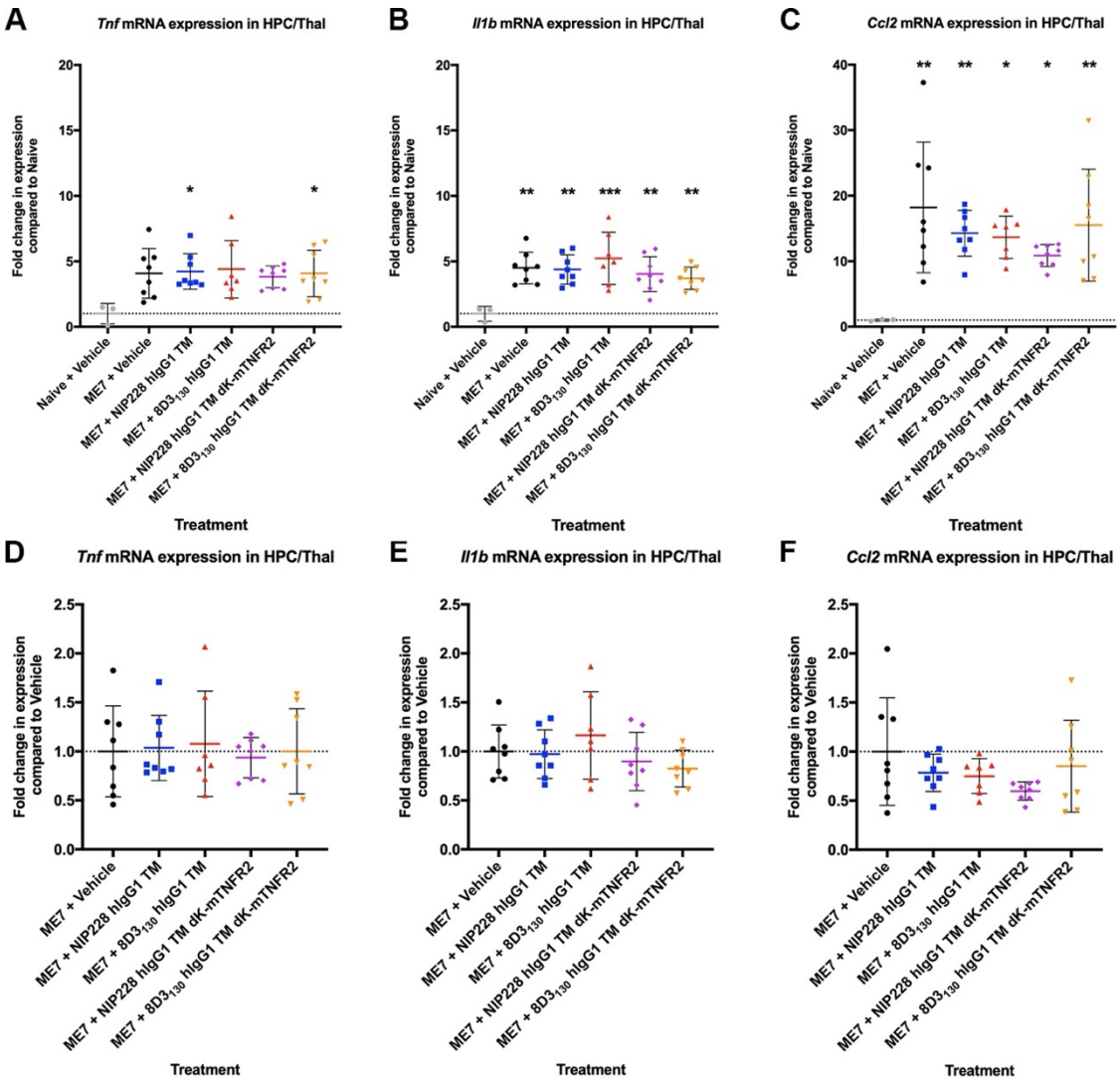

Figure 5.9 Cytokine expression in ME7 mice after bispecific mTNFR2 fusion protein treatment
(A-C) Expression of *Tnf* (A), *Il1b* (B) and *Ccl2* (C) mRNA transcripts in the hippocampus and thalamus of 16 wpi ME7 mice shows increased expression relative to age-matched Naïve control mice. (D-F) *Tnf* (D), *Il1b* (E) and *Ccl2* (F) mRNA transcripts levels remain unchanged following weekly systemic administration of bispecific mTNFR2 fusion proteins from 12 wpi in ME7 mice. Data are presented as the mean ± SD (Naïve mice, n = 4; ME7 mice, n =7-8/group) of fold change compared to Naïve control or vehicle treatment after normalisation of expression to *Pgk1*. *, $p < 0.05$ versus Naïve + Vehicle for *Tnf* using Dunn's multiple comparisons following Kruskal-Wallis test; *, $p < 0.05$, **, $p < 0.01$, ***, $p < 0.001$ versus Naïve + Vehicle following a one-way ANOVA with Holm-Sidak's multiple comparisons test.

5.3.7 Efficacy of TNF inhibition with bispecific mTNFR2 fusion proteins following systemic inflammatory challenge

The *in vivo* efficacy of TNF-α inhibition using bispecific mTNFR2 fusion proteins was investigated by injecting C57Bl/6 mice with a 54 μM dose (i.p.) 24 hours prior to systemic challenge with 100 μg/kg LPS. Mice showed no adverse effects following injection with bispecific mTNFR2 fusion protein compared to vehicle. Following LPS injection, piloerection and lethargy were noted during a 30-minute observation period, however there was no difference between behaviours in mice that received bispecific mTNFR2 fusion proteins and vehicle.

5.3.7.1 Splenic response to administration of bispecific mTNFR2 fusion proteins

Analysis of spleen weights from mice 26 hours after injection of fusion proteins showed a significant difference between medians following Kruskal-Wallis test ($W(5, 20) = 10.61$; $p = 0.0314$) (Figure 5.10). Post-hoc comparison with Dunn's multiple comparison correction identified that spleens from $8D3_{130}$ hIgG1 TM + LPS-injected mice were increased compared to spleens from vehicle + LPS-injected mice ($Z(4,4) = 2.723$, $p = 0.0259$). Treatment with other fusion proteins did not affect spleen weights compared to vehicle + LPS-injected mice ($p > 0.9999$).

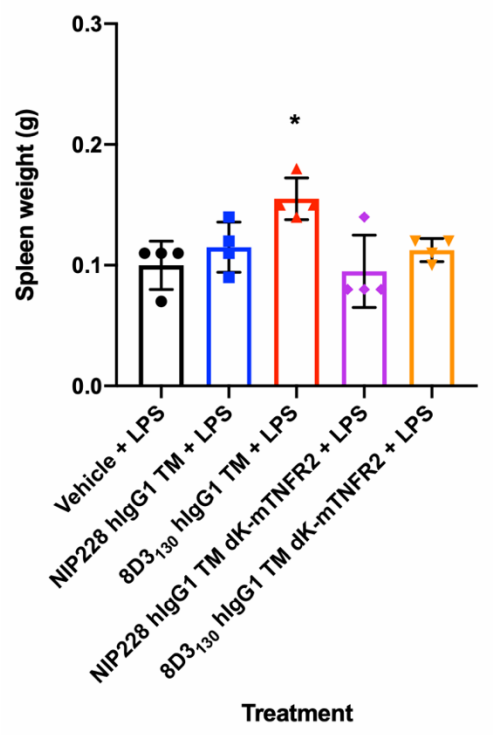

Figure 5.10 Spleen weights following fusion protein treatment and LPS challenge
Spleen weights of mice 26 hours after injection with fusion protein (54 μM, i.p.) and 2 hours after LPS challenge. Spleens from mice injected with $8D3_{130}$ hIgG1 TM + LPS are increased compared to vehicle + LPS-injected mice. Data are presented as mean ± SD (n=4/group). *, $p < 0.05$ for $8D3_{130}$ hIgG1 TM + LPS versus vehicle + LPS following Dunn's correction for multiple comparisons after a Kruskal-Wallis test.

5.3.7.2 Cytokine production in the brain following systemic challenge with LPS

Analysis of cytokine transcripts from hippocampus/thalamus-enriched tissue showed that expression of *Tnf* is not significantly different 2 hours after systemic challenge with LPS between treatment groups following one-way ANOVA ($F(4, 15) = 1.480$, $p = 0.2575$) (Figure 5.11A). However, there was a significant difference in the standard deviations between all treatment groups as determined by Brown-Forsythe test ($F(4, 15) = 3.468$, $p = 0.0339$). These data reflect the high variation present within vehicle + LPS-injected mice (%CV = 87.27%) and $8D3_{130}$ hIgG1 TM + LPS-injected mice (%CV = 100.4%) compared to the other treatment groups (average %CV = 35.7%)

Analysis of IL-1β transcript levels by one-way ANOVA showed that mean expression is not significantly different across treatment groups 2 hours after systemic challenge with LPS ($F(4, 15) = 1.947$, $p = 0.1548$) (Figure 5.11B). Again, standard deviations between all treatment groups were significantly different ($F(4, 15) = 4.953$, $p = 0.0095$) and vehicle + LPS-injected mice (%CV = 72.85%) and $8D3_{130}$ hIgG1 TM + LPS-injected mice (%CV = 108.9%) showed the greatest variation.

Analysis of CCL2 expression using Kruskal-Wallis test identified that median values are not significantly different between treatment groups 2 hours after LPS challenge ($W(5, 20) = 4.771$, $p = 0.3116$) (Figure 5.11C). Vehicle + LPS-injected mice (%CV = 67.55%) and $8D3_{130}$ hIgG1 TM + LPS-injected mice (%CV = 111.9%) again showed the greatest variation within treatment groups.

Analysis of IL-6 transcript levels by one-way ANOVA showed that mean expression is not significantly different between treatment groups 2 hours after systemic LPS challenge ($F(4, 15) = 1.250$, $p = 0.3323$) (Figure 5.11D). However, standard deviations between all treatment groups were not significantly different ($F(4, 15) = 2.228$, $p = 0.1149$).

Analysis of IL-10 expression using Kruskal-Wallis test identified that median values are not significantly different between treatment groups 2 hours after LPS challenge ($W(5, 20) = 5.786$, $p = 0.2157$) (Figure 5.11E). There was a trend towards decreased expression when comparing $8D3_{130}$ hIgG1 TM + LPS-injected mice to vehicle + LPS-injected mice with Dunn's multiple comparisons ($Z(4,4) = 2.271$, $p = 0.0926$).

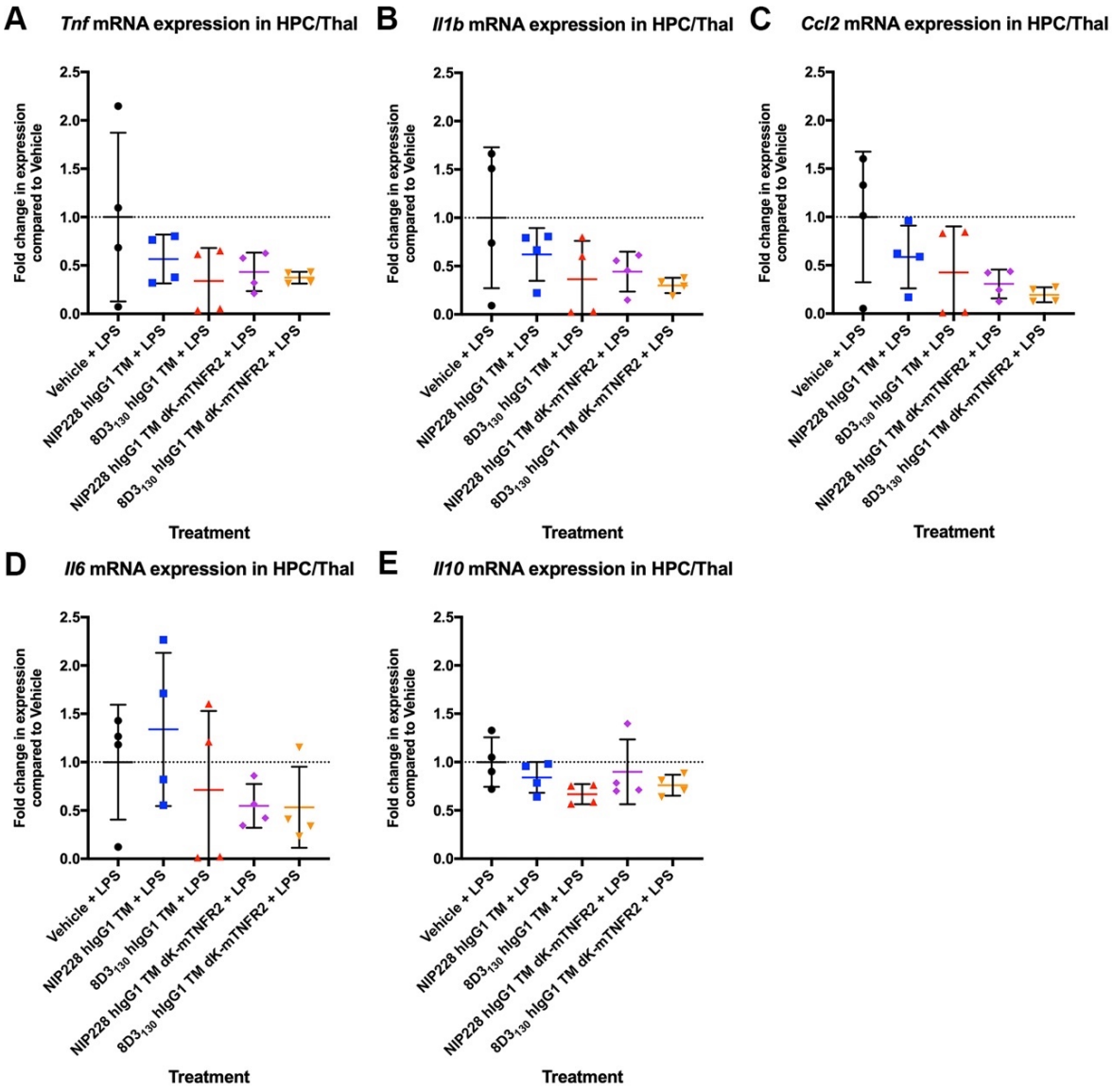

Figure 5.11 Cytokine transcript levels in hippocampus/thalamus following systemic challenge with LPS

Hippocampus/thalamus enriched brain tissue were analysed for expression of cytokines downstream of TNFR1 two hours after injection of LPS (100 μg/kg). Mice were injected with bispecific mTNFR2 fusion protein or control antibody (54 μM, i.p.).24 hours prior to LPS challenge. Transcript levels for *Tnf* (A), IL-1β (B), CCL2 (C), IL-6 (D) and IL-10 (E) in response to LPS are not altered by prior treatment with bispecific mTNFR2 fusion protein. Data are presented as mean ± SD (n=4) for fold change compared to vehicle after normalisation of expression to the housekeeping gene, *Pgk1*.

5.4 Discussion

Administration of bispecific anti-TNF fusion proteins in ME7 mice had no effect on the progression of disease, as monitored by burrowing and open field behaviours, nor was there a significant alteration in the expression of proinflammatory cytokines or synaptic markers, or the levels of microglial activation markers, except MHCII in the hippocampus.

Pre-treatment of mice prior to LPS exposure with bispecific anti-TNF fusion proteins suggested a trend towards to a reduced expression in proinflammatory cytokines induced downstream of TNFR activation suggesting potential *in vivo* neutralisation of mTNF-α.

5.4.1 Behavioural changes in ME7 mice after bispecific mTNFR2 administration

Significant changes in burrowing were not observed until 16 wpi in ME7 mice; this in contrast to previous studies where deficits are frequently observed from 14 or 15 wpi (Felton et al., 2005; Gómez-Nicola et al., 2014, 2013; Obst et al., 2018). This delayed onset in burrowing deficits is not due to neutralisation of TNF-α because bispecific mTNFR2 fusion protein-treated ME7 mice show no difference in burrowing compared to vehicle-treated ME7 mice (Figure 5.3). Interestingly, $8D3_{130}$ hIgG1 TM treated ME7 mice showed less deficit in burrowing and were not significantly different from naïve control mice. This apparent protective effect is also evident in open field locomotion, with $8D3_{130}$ hIgG1 TM treated mice not showing any difference in behaviour compared to naïve control mice at 16 wpi. All mice showed habituation to the open field arena during early disease stages (9-11 wpi; not shown) but once a baseline was established from 11 wpi activity across all ME7 groups increased week on week (Figure 5.3). Hyper-reactivity in the open field was observed in vehicle-, NIP228 hIgG1 TM- and $8D3_{130}$ hIgG1 TM ΔK-mTNFR2 treated ME7 mice at 15 wpi, but no difference was seen between $8D3_{130}$ hIgG1 TM treated ME7 mice and naïve control mice. A possible reason for this could be because of a peripheral response to the antibody (e.g., splenomegaly) conferring some protection in these mice. This coincides with analysis of mRNA transcripts for the presynaptic protein, synaptophysin (*Syp*), where $8D3_{130}$ hIgG1 TM treated ME7 mice did not show a significant decrease compared to naïve control mice (Figure 5.4). As burrowing behaviour is

inherently linked to hippocampal function – with hippocampal lesions causing specific deficits in burrowing behaviour (Cunningham, 2005; Deacon et al., 2001) – this preservation of synaptic function through normal levels of synaptophysin is a likely reason for why ME7 mice treated with $8D3_{130}$ hIgG1 TM do not show any burrowing deficits at 16 wpi compared to Naïve mice. This also supported by a lack of change in mGluR1 (*Grm1*) expression between ME7 mice and naïve control (Figure 5.4), especially given that mGluR1 expression can play a role in induction and maintenance of LTP in the hippocampus (Cheyne and Montgomery, 2008; Ferraguti and Shigemoto, 2006; Mukherjee and Manahan-Vaughan, 2013; Van Dam et al., 2004).

The data presented in this chapter show that there is a separation in burrowing deficits between the peripherally acting NIP228 hIgG1 TM ΔK-mTNFR2 and the brain-penetrant $8D3_{130}$ hIgG1 TM ΔK-mTNFR2 (62.24% versus 73.80%), suggesting that delivery of mTNFR2 across the BBB may contribute to this result. It would be important to design future experiments in which the fusion protein can be detected in the hippocampus and test if treatment with bispecific mTNFR2 fusion proteins results in delayed progression when followed later in disease from 16-20 wpi.

5.4.2 Neuroinflammatory response in ME7 mice after bispecific mTNFR2 administration

Induction of a neuroinflammatory response was observed in all ME7 mice, with a significant increase in expression of CD64 and MHCII in both the hippocampus and thalamus compared to naïve control mice. These data reflect previous reports that show increased microglia numbers and expression of activation markers in ME7 mice compared to control mice from 12 wpi onwards (Gómez-Nicola et al., 2013; Griffin et al., 2013). MHCII expression on microglia is representative of activation and could be associated with a priming response (Neher and Cunningham, 2019; Perry and Holmes, 2014). In ME7 mice following treatment with bispecific mTNFR2 fusion proteins, there is a differential microglial response in the hippocampus and thalamus.

All ME7 mice showed a significant upregulation of CD64 expression in the hippocampus compared to Naïve mice, however there is a greater increase in $8D3_{130}$ hIgG1 TM-treated mice (Figure 5.5). Within the thalamus all ME7 mice show increased expression of CD64 compared to naïve mice, irrespective of treatment group (Figure 5.6). These data from both regions reflect previous observations of increased microglia activation in ME7 mice from 12 wpi and are most likely associated with increased proliferation (Gómez-Nicola et al., 2013; Griffin et al., 2013; Murray et al., 2012). It is possible that the splenomegaly observed after dosing with $8D3_{130}$ hIgG1 TM is a result of immune cell activation in the periphery, which would result in immune-to-brain communication, and may account for the increased hippocampal CD64 expression, although the underlying mechanisms remains unclear. An alternative explanation for the observed effects of $8D3_{130}$ hIgG1 TM is that increased delivery across the BBB and uptake by neurons (Yu et al., 2011), could result in dysfunction that induces further microglial activation. This response could be TNF-α dependent as $8D3_{130}$ hIgG1 TM ΔK-mTNFR2 treated ME7 mice do not show this response. Furthermore, NIP228 hIgG1 TM ΔK-mTNFR2 also show a decrease in CD64 expression relative to their isotype control treatment, NIP228 hIgG1 TM (Figure 5.5).

Within the CA1 field of the hippocampus, MHCII expression is significantly reduced in ME7 mice that received either NIP228 hIgG1 TM ΔK-mTNFR2 or $8D3_{130}$ hIgG1 TM ΔK-mTNFR2, as well as NIP228 hIgG1 TM, compared to vehicle-treated ME7 mice (Figure 5.7). Within the thalamus increased expression of MHCII is observed but there is no difference following treatment with any of the bispecific mTNFR2 fusion proteins (Figure 5.8). The neuroinflammatory response in ME7 prion within the dorsal thalamus is independent of sub-region with respect to PrP^{Sc} deposition and microglial activation at later disease stages (Gómez-Nicola et al., 2013; Hilton et al., 2013; Reis et al., 2015). However, neurodegenerative changes are sub-region specific - significant neuronal loss occurs in the posterior nuclei yet is sparse in the ventral posteromedial and ventral posterolateral nuclei; whilst the opposite is observed with respect to synaptic density loss (Cunningham et al., 2005a; Davis et al., 2015; Nazmi et al., 2019; Reis et al., 2015). Thus, it is possible that as disease progresses subregion-specific effects become less defined. At the current point of analysis (16 wpi), there is a visual difference in the microglial response within the dorsal thalamus, which spares the posterior nuclei. Interestingly, this subregion specificity is not observed for CD64, possibly suggesting a coordinated response of MHCII-positive

microglia within the thalamus. Alternatively, a simpler explanation for the relative differences in expression of MHCII in the hippocampus and thalamus is one of variation, with significant variation observed in all ME7 mice within the thalamus (Figure 5.8). Addition of greater numbers for histological analysis, and introduction of alternative quantification methods, such as cell count as opposed to protein load, would identify if variation is the true cause of these regional differences or if there is perhaps a biological process that underlies these observations.

5.4.3 Proinflammatory cytokine production in ME7 mice after bispecific mTNFR2 fusion protein treatment

Analysis of cytokine mRNA transcripts was performed on tissue punches enriched for both the hippocampus and thalamus. Transcript levels of *Tnf* and *Il1b* were both significantly upregulated in all ME7 mice compared to Naïve mice, an average 4.12-fold and 4.36-fold increase respectively (Figure 5.9). However, treatment of ME7 mice with bispecific mTNFR2 fusion proteins had no effect cytokine production with transcript levels remaining similar to those in vehicle-treated ME7 mice. The regional differences in microglial response between the hippocampus and thalamus may explain this lack of effect on cytokine production. In addition*, Ccl2* transcript levels were substantially increased in all ME7 mice over naïve control mice, with an average 14.5-fold increase in expression. Interestingly, ME7 mice treated with the peripherally acting NIP228 hIgG1 TM ΔK-mTNFR2 showed a trend towards reduced *Ccl2* transcript expression compared to vehicle-treated mice, and this lack of significance is most likely in part due to the large variation with the vehicle-treated group (Figure 5.9). The difference in variation between the two mTNFR2 fusion proteins with respect to *Ccl2* transcript levels could be associated with functional differences in relative distribution throughout the organism, with $8D3_{130}$ hIgG1 TM ΔK-mTNFR2 less likely to act in the circulation, because of mTfR targeting that would re-distribute the fusion protein to both the brain and other TfR-expression organs, such as the spleen. CCL2 is an important chemokine in the peripheral immune system and therefore neutralisation of TNF-α in the periphery could modulate brain expression through immune-to-brain signalling. However, this association between peripheral and central inflammation and the effects of TNF-α inhibition in the periphery is only really

reflected by a decrease in MHCII expression within the hippocampus, as discussed above. Therefore, one could postulate that combined analyses of both hippocampus and thalamus may dilute any subtle differences between subregions. As such future analysis should prioritise dissection of these structures to achieve an accurate picture of the specific neuroinflammatory state within each brain region. These analyses would add to the neuroinflammatory picture and provide greater detail as to which aspects, if any, of the immune response to ME7 prion deposition in the brain is altered by delivery of mTNFR2 to the brain parenchyma.

5.4.4 Determining efficacy of *in vivo* TNF-α inhibition

As treatment with mTNFR2 fusion proteins in ME7 mice had no significant effect on disease progression or cytokine transcript levels in the hippocampus/thalamus, *in vivo* efficacy of the bispecific mTNFR2 fusion proteins was tested by pre-treating C57BL/6 mice with fusion protein 24 hours prior to systemic challenge with LPS. Injection of low dose LPS (100 μg/kg) induces an acute peripheral and neuroinflammatory response in mice (Teeling et al., 2010, 2007). The production of proinflammatory cytokines, including mTNF-α, is detectable in the hippocampus and hypothalamus two hours after systemic LPS administration (Skelly et al., 2013; Teeling et al., 2010).

Proinflammatory cytokine expression induced by administration of LPS suggests an effect for mTNF-α inhibition as transcript levels in the hippocampus/thalamus are attenuated following pre-treatment with NIP228 hIgG1 TM ΔK-mTNFR2 and $8D3_{130}$ hIgG1 TM ΔK-mTNFR2 fusion proteins (Figure 5.11). However, large variation in cytokine expression within the vehicle + LPS-injected mice limit our interpretation. As all antibody/fusion protein treatment groups show reduced cytokine expression compared to vehicle + LPS-injected mice it also possible that non-specific IgG effects are responsible for the observed reductions and not a specific effect of mTNF-α neutralisation. The role of cytokines other than mTNF-α in initiating a neuroinflammatory response following systemic challenge with LPS could be a reason why there is not complete inhibition of cytokine expression with bispecific mTNFR2 fusion proteins. It has been shown that endothelial cells produce prostaglandins in response to systemic IL-1β, induced by LPS, in order to mediate immune-to-brain signalling (Konsman, 2016; Layé et al., 2000; Quan and

Banks, 2007). Interestingly, induction of proinflammatory cytokines in the brain can also be attenuated by subdiaphragmatic vagotomy following systemic LPS administration (Laye et al., 1995). Therefore, it could be postulated that pre-treatment with bispecific mTNFR2 fusion proteins may result in a decreased production of central cytokines directly induced by mTNF-α without affecting production resulting from other activation pathways, such as IL-1β. To determine whether inhibition of immune-to-brain signalling contributes to the results observed, staining of prostaglandin production in endothelial cells and measuring prostaglandin and cyclooxygenase enzyme induction via qPCR would establish whether treatment with an mTNFR2 fusion protein causes a reduction in expression of prostaglandins following LPS (Griffin et al., 2013; Skelly et al., 2013).

If immune-to-brain communication is responsible for the production of cytokines in the brain, then you might predict that there would be a differential response between brain-penetrant and peripherally acting mTNFR2 fusion proteins. It is possible that the re-distribution of $8D3_{130}$ hIgG1 TM ΔK-mTNFR2 within the brain could limit its peripheral inhibitory effect on immune-to-brain signalling, therefore potentially being a less effective inhibitor of peripheral immune challenge. However, this is unlikely to be the case given that only ~1.5% of injected fusion protein is expected to enter the brain within 24 hours (Webster et al., 2017). The reduced expression of the anti-inflammatory cytokine IL-10, and similar effect of NIP228 hIgG1 TM ΔK-mTNFR2 and $8D3_{130}$ hIgG1 TM ΔK-mTNFR2 (0.89-fold and 0.76-fold vehicle response), suggests attenuation of systemic inflammatory response after LPS (Figure 5.11). Furthermore, as IL-10 production following systemic inflammation is induced to act as a negative regulator and is independent of TNF-α and NF-κB activation (Liu et al., 2017; Saraiva and O'Garra, 2010). Stable IL-10 expression after mTNFR2 fusion protein treatment suggests specific inhibition and points to reduced TNFR activation and downstream induction of NF-κB. Investigating levels of activated NF-κB through western blot analysis of hippocampal tissue and measuring systemic cytokine levels within the sera would confirm whether an attenuated inflammatory response was observed following systemic challenge with LPS in these mice.

Further analysis could elucidate whether a lack of mTNF-α inhibition was due to increased clearance of bispecific mTNFR2 fusion proteins compared to isotype control antibodies. Previous studies that have used anti-mTfR antibodies as transport molecules for the delivery of therapeutics to the CNS have shown that repeated dosing results in increased

clearance in rhesus monkeys (Pardridge et al., 2018b). Also, there are various reports as to the presence of ADAs that are raised against the binding regions of the anti-mTfR antibody following multiple doses in mice (Chang et al., 2017; Qing Hui Zhou et al., 2011a, 2011b). If ADAs are present, and different between bispecific mTNFR2 fusion proteins, this may help elucidate differences in responses. ADAs were measured in mouse serum using an indirect ELISA (Appendix A4). Pilot experiments showed there was no difference in detection of ADAs between vehicle-treated mice and mice injected with NIP228 hIgG1 TM fusion protein (Appendix F). These data suggest that ADAs might not be expected after administration of hIgG1 TM proteins, either after a single injection or multiple injections. Additional ADA ELISAs using sera from $8D3_{130}$ hIgG1 TM ΔK-mTNFR2 treated mice showed a higher response compared to sera from NIP228 hIgG1 TM treated mice from the same experiments (Appendix F). However, dilution ranges were different between the two pilot experiments and further protocol optimisation is needed to determine whether there are differences between anti-mTfR targeted antibodies and bispecific fusion proteins compared to NIP228 hIgG1 TM treated and naïve control mice. Increased clearance of bispecific mTNFR2 fusion proteins will decrease circulating levels available for transport across the BBB and thus reduce brain exposure. Analysis of brain penetrance could be achieved through detection of human IgG in the brain parenchyma using immunohistochemistry or through ELISA on homogenised brain samples.

Overall, these data in part suggest an attenuation of transcript levels downstream of TNFR activation following treatment with anti-TNF-α fusion proteins prior to LPS challenge. However, significant additional work is required to address whether successful inhibition of TNF-α was achieved and whether this significantly differed between systemic and central compartments.

5.4.5 Peripheral response to multiple injections of bispecific mTNFR2 fusion proteins in ME7 mice

Mouse body weights were monitored weekly from 8 wpi to 16 wpi in ME7 mice to determine any adverse effects that may occur because of multiple injections of

antibody/fusion protein. As discussed in more detail below, quantification and analysis of spleen weights showed that treatment with $8D3_{130}$ hIgG1 TM for four weeks in ME7 mice resulted in splenomegaly, whilst other treatments did not. There was no significant difference in body weights between treatments in ME7 mice following each weekly injection (Figure 5.1). However, after the second and third injections, ME7 mice treated with either NIP228 hIgG1 TM ΔK-mTNFR2 or $8D3_{130}$ hIgG1 TM ΔK-mTNFR2 showed a sharp decrease in body weights (1.2% and 1.4% decrease respectively). These decreases never dropped weights to below pre-injection levels and did not limit expected growth compared to vehicle-injected ME7 mice over the final few weeks but do suggest a possible effect from inhibiting mTNF-α. At termination of ME7 mice, there was an obvious difference in spleen sizes in certain animals and all spleens were collected for histology and qPCR analysis after weighing. Overall, these data suggest that multiple doses of bispecific mTNFR2 fusion proteins do not induce behavioural changes and are tolerated by ME7 mice.

Expression levels of mTfR within the hippocampus was not affected by treatment with anti-mTfR antibodies compared to vehicle-treated ME7 mice (Figure 5.2). These data contrast with previous analysis that showed mTfR expression to be decreased at 8 and 18 wpi (Figure 3.16). This is most likely due to both neuronal and vascular expression of TfR remaining at 16 wpi (asterisks; Figure 5.2). These analyses do suggest that expected delivery of mTNFR2 across the BBB with $8D3_{130}$ hIgG1 TM ΔK-mTNFR2 would not have been compromised by a reduction in mTfR expression on brain endothelial cells.

5.4.6 Anti-TfR antibody-induced splenomegaly in ME7 prion and LPS-injected mice

$8D3_{130}$ hIgG1 TM treatment in ME7 mice resulted in splenomegaly, with spleen sizes 5-fold larger compared to all other treatments (Figure 5.1). A 1.5-fold increase in spleen weight was also observed in mice given a single injection of $8D3_{130}$ hIgG1 TM, prior to systemic challenge with LPS, compared to other treatments (Figure 5.10).

Splenomegaly could be caused by an effect of $8D3_{130}$ hIgG1 TM, an anti-mTfR antibody, on its target antigen, by disrupting its role in erythropoiesis. TfR is involved in the late stages of erythroblast maturation, specifically the enucleation step, and it has been

shown that anti-mTfR antibodies can reduce enucleation of erythroblasts by preventing internalisation of the receptor (Aoto et al., 2019). Furthermore, it has been shown that anti-mTfR antibodies can reduce reticulocyte numbers in the blood 24 hours after injection (Couch et al., 2013; Lo et al., 2017). Loss of reticulocytes has been shown to result in decreased erythrocyte output from the bone marrow and, as a result induces compensatory haematopoiesis. Extramedullary, or stress, haematopoiesis (EMH), which is negligible under homeostasis, is induced under such conditions and is characterised by splenomegaly (Klei et al., 2017; Liu et al., 2013; Paulson et al., 2020). Couch *et al* observed that loss of reticulocytes was mediated through both antibody-dependent cell-mediated cytotoxicity (ADCC) and complement-dependent cytotoxicity (CDC), with removal of all FcγR and complement interactions attenuating reticulocyte loss (Couch et al., 2013; Lo et al., 2017). The $8D3_{130}$ hIgG1 TM antibody used in this present study has been engineered to contain three mutations ("TM") with in the Fc region that significantly reduce binding to various effector molecules known to contribute to ADCC and CDC (Borrok et al., 2017; Oganesyan et al., 2008). It is possible however that at high doses these antibodies induce complement-dependent responses that reduce reticulocyte numbers, as seen with other anti-mTfR antibodies that lack Fc effector function (Couch et al., 2013; Gadkar et al., 2016). As reticulocyte numbers were not investigated in the current study, we cannot confirm whether a loss of reticulocytes may have contributed to the splenomegaly observed after treatment with $8D3_{130}$ hIgG1 TM.

A direct effect on the spleen is also a possible reason for the observed splenomegaly, with anti-mTfR antibodies known to distribute to the spleen, as well as the bone marrow, following systemic administration and can show cytotoxicity *in vitro* (Sehlin et al., 2017; Shimosaki et al., 2017; Sugyo et al., 2017). Therefore, to investigate which cell populations could be responsible for the observed splenomegaly, spleens were cut and stained for the macrophage markers CD64, CD68 and CD11b (Appendix E). It has been shown that splenomegaly results in clear disorganisation of both the red and white pulp in histological sections (Schubert et al., 2008). Histology of spleen tissue from ME7 mice showed visible disorganisation of the red and white pulp in spleens from ME7 mice treated with $8D3_{130}$ hIgG1 TM compared to $8D3_{130}$ hIgG1 TM ΔK-mTNFR2-treated ME7 mice (Appendix E). Further analysis highlighted a reduction in CD11b-positive cells in the

red pulp and the marginal zone of spleens from ME7 mice treated with $8D3_{130}$ hIgG1 TM, whilst CD68 expression remained stable (Appendix E). Binding of anti-mTfR antibodies to circulating reticulocytes can cause cross-linking which either results in cell death or targets cells for complement-dependent removal (Daniels-Wells and Penichet, 2016; Neiveyans et al., 2019). Therefore, as red pulp macrophages are involved in the removal of opsonised cells from the spleen these changes could be reflective of a decrease in complement receptor expression on red pulp macrophages or on a subset of splenic dendritic cells involved in antigen presentation (Bronte and Pittet, 2013; Lewis et al., 2019). However, increased expression of CD64-positive cells within the red pulp of spleens from ME7 mice treated with $8D3_{130}$ hIgG1 TM was also observed and this may suggest an increase in myeloid cells as opposed to increases in the reticulocyte population as suggested above (Appendix E).

Splenomegaly was not observed following injection of $8D3_{130}$ hIgG1 TM ΔK-mTNFR2 (Figure 5.1, Figure 5.10). There could be a couple of potential reasons for this phenomenon: 1) the structure of the antibody-protein fusion prevents any form of immune response being raised against it, or 2) activity of mTNFR2 prevents induction of splenomegaly either directly or indirectly via inhibition of mTNF-α. Recent evidence suggests that orientation and size of a fusion protein can contribute to induction of ADCCs. Conjugation of Fab protein domains to the C-terminal end of an antibody with Fc effector function (mBS-2Fab/dBS-2Fab) results in attenuation of FcγR-mediated ADCC compared to the native IgG construct (anti-mTfR), and shows a similar response as a mutated Fc designed to remove FcγR effector function (anti-TfR PGLALA) (Weber et al., 2018). Therefore, as $8D3_{130}$ hIgG1 TM ΔK-mTNFR2 is an antibody-protein fusion that uses the C-terminal conjugation of mTNFR2 to its native antibody $8D3_{130}$ hIgG1 TM, it could be suggested that a similar effect might be expected to exist here and thus could explain the lack of splenomegaly seen in mice treated with $8D3_{130}$ hIgG1 TM ΔK-mTNFR2. There is also evidence to suggest that mTNF-α can play an active role in inhibiting haematopoiesis, by directly inducing apoptosis of progenitor cells and indirectly by inhibiting Gata1 dependent gene expression (Chen et al., 2015; Diederich et al., 2009; Paulson et al., 2020). This would initiate EMH within the spleen to compensate for loss of progenitor cells in the bone marrow (Paulson et al., 2020). Therefore, it is possible that $8D3_{130}$ hIgG1

TM ΔK-mTNFR2 actively prevents the induction of splenomegaly by inhibiting mTNF-α and limiting the effects of anti-mTfR antibodies on haematopoiesis. Furthermore, exogenous administration of soluble TNFR2 is known to inhibit the biological activity of mTNF-α in response to LPS (Guo et al., 2009; Mohler et al., 1993). This could be confirmed by adding serum from mice injected with LPS to murine L929 cells and determine the cytotoxic effect of serum mTNF-α. If inhibition of mTNF-α was achieved, then serum from $8D3_{130}$ hIgG1 TM ΔK-mTNFR2-treated mice would show little to no cytotoxic activity in murine L929 cell cultures compared to $8D3_{130}$ hIgG1 TM-treated mice and would provide evidence of *in vivo* neutralisation. In addition, cytotoxicity measurements could be supported by serum mTNF-α levels, because soluble mTNFR2 is known to bind and act as a TNF carrier (Guo et al., 2009; Mohler et al., 1993; Yli-Karjanmaa et al., 2019), and this would result in higher serum levels in $8D3_{130}$ hIgG1 TM ΔK-mTNFR2-treated mice compared to $8D3_{130}$ hIgG1 TM-treated mice.

In future studies, measuring both the circulating and bone marrow erythrocyte populations would provide additional information to the exact erythrocyte/reticulocyte response after administration of anti-TfR antibodies. Reticulocyte numbers can be measured in a few ways using fluorescence-associated cell sorting, with thiazole orange staining of freshly isolated red blood cells from circulation and bone marrow, as well as isolated splenocytes, and subpopulations of erythrocytes can be identified via labelling with anti-Ter119 and anti-CD71 antibodies, combined with forward scatter to determine cell size (Altamura et al., 2020; Bhardwaj and Saxena, 2015; Rhodes et al., 2016). In addition, targeted histological analysis of red pulp splenocytes could also identify cell populations responsible for splenomegaly, which could include erythrocyte subpopulations. Understanding the effects of anti-TfR antibodies will help to determine the safety profile for use in human studies, specifically with reference to reticulocyte numbers and Fc effector function. Moreover, if antibodies require Fc effector function for their therapeutic effects additional knowledge will enable careful consideration for the use of enhanced brain delivery technology for different therapeutic targets.

5.4.7 Summary

The data presented in this chapter show that systemic administration of bispecific mTNFR2 fusion proteins is tolerated by ME7 mice after multiple injections. Proinflammatory cytokines produced following systemic LPS challenge were attenuated in mice pre-treated with bispecific mTNFR2 fusion protein, suggesting that bispecific mTNFR2 fusion proteins show effective inhibition of mTNF-α *in vivo*, with additional work needed to fully confirm. However, they have no effect on disease progression in ME7 mice that may interact with additional systemic inflammation as determined through changes in mouse behaviours, microglial activation, and synaptic marker expression.

Chapter 6 Targeting of TNF-alpha using bispecific mTNFR2 fusion proteins after systemic bacterial challenge in ME7 prion mice

6.1 Introduction

Chronic inflammatory conditions, such as rheumatoid arthritis (RA), are associated with an increased incidence of neurodegenerative diseases, such as Parkinson's disease (PD) and AD (Chou et al., 2016; Peter et al., 2018; Zhou et al., 2020). There is evidence that SIEs are associated with increased serum cytokines and an increased rate of cognitive decline; whilst high serum TNF-α levels themselves are correlated with a four-fold increase in the rate of cognitive decline in AD (Holmes et al., 2011, 2009; Ide et al., 2016). In line with these findings, treatment with TNF inhibitors in RA and sarcoidosis results in improved cognition (Chen et al., 2010; Elfferich et al., 2010). Treatment of inflammatory bowel disease (IBD) patients with anti-TNF therapy results in a significant reduction in the incidence of PD (Peter et al., 2018). And the use of anti-TNF blocking agents is also linked to reduced incidence of AD (Chou et al., 2016; Zhou et al., 2020). Furthermore, in Chapter 3 I have reported that systemic inflammation, induced by bacterial infection, potentiates the neuroinflammatory response in the ME7 prion model of neurodegeneration. Based on these data I predict that treatment with a TNF-α blocker will have protective effects on the exacerbatory consequences of a systemic inflammatory challenge on disease progression in ME7 prion disease.

In this chapter, I will assess the benefits of treatment with bispecific mTNFR2 fusion proteins in a model of chronic neurodegeneration and systemic inflammation. I hypothesise that treatment with mTNFR2 fusion proteins after systemic bacterial challenge will reduce cytokine production in the brain. To investigate this hypothesis, ME7 prion mice will be subjected to infection with *S. typhimurium* SL3261 at 8 wpi and then treated with weekly mTNFR2 fusion protein from 12 wpi for four weeks. Neuroinflammatory response will be measured through microglial activation markers and

cytokine production in the hippocampus, whilst disease progression will be monitored by non-invasive behavioural tests.

Use of TNF-α inhibitors following systemic infection with *S. typhimurium* results in increased infectivity suggesting that TNF-α is integral to suppressing growth of intracellular bacteria (Gulig et al., 1997; Mastroeni et al., 1993b; Mastroeni et al., 1995). As *Salmonella* can persist in the spleen and liver of mice up to 60 days after infection (Mastroeni, 2002; Monack et al., 2004a), and increased infectivity can cause a relapse of infection, it is essential to ensure that administration of mTNFR2 fusion proteins is tolerated by *Salmonella* infected mice. To determine whether mTNF-α inhibition with these specific fusion proteins is safe and does not induce any adverse effects, mice were dosed with mTNFR2 fusion proteins 10 days after *Salmonella* challenge. This timepoint was selected because it is after formation of granulomas and plateauing of bacterial growth and more reflective of persistent infection (Mastroeni, 2002; Monack et al., 2004b).

6.2 Methods

6.2.1 Treatment of ME7 prion mice with bispecific mTNFR2 fusion proteins following systemic bacterial challenge

Female C57Bl/6 mice (11-13 weeks old) were injected bilaterally with ME7 prion brain homogenate (10% w/v) in the dorsal hippocampus using a stereotaxic frame (Section 2.1.2). Disease progression was monitored through assessment of overnight burrowing (Section 2.1.3.1) and manual open field locomotor activity from 7 wpi (Sections 2.1.3.3). ME7-injected mice (n=5-6/group) were systemically challenged with 1 x 10^6 cfu *S. typhimurium* at 8 wpi (Section 2.1.5.2). ME7 mice were treated for four weeks from 12 wpi and received a weekly i.p. injection (54 μM) of bispecific mTNFR2 fusion protein or isotype control antibody (Section 2.1.4). Mice were sacrificed at 17 wpi by transcardial perfusion with D-PBS containing heparin sodium (5 U/ml) and brains and spleens collected for tissue analysis (Section 2.1.6). A tissue punch enriched for hippocampus/thalamus from the left hemisphere was taken and snap frozen in liquid nitrogen; the right hemisphere was embedded in OCT. Spleens were weighed and snap frozen in liquid nitrogen for future processing. Embedded brain tissues were sectioned and stained for expression of CD64, MHCII and TfR by DAB immunohistochemistry (Section 2.2.1). Enriched hippocampus/thalamus tissue punches were homogenised and processed, alongside samples from Naïve + vehicle controls (Chapter 5), for qPCR analysis of cytokine and synaptic marker transcript levels (Section 2.2.2).

6.2.2 *In vivo* safety and tolerability of bispecific mTNFR2 fusion proteins after systemic challenge with *S. typhimurium*

In vivo safety profile of bispecific mTNFR2 fusion proteins was assessed by a single i.p. injection (54 μM) in 12-week-old male C57BL/6 mice 10 days after infection with 1.8 x 10^6 cfu *S. typhimurium* SL3261 (Section 2.1.5.2). Mice were monitored for 7 days before brain and spleen tissues were collected by transcardial perfusion with D-PBS containing heparin sodium (5 U/ml) (Section 2.1.6). Spleens were weighed and processed for cytokine expression by qPCR along with hippocampus/thalamus enriched tissues (Section 2.2.2).

6.3 Results

6.3.1 Peripheral response following systemic bacterial challenge and bispecific mTNFR2 administration in ME7 mice

Experiments involving *S. typhimurium* infection were impacted by Covid-19 enforced restrictions on animal experiments. Consequently, the number of treatments and size of each experimental group was significantly reduced. A vehicle treatment was omitted as in ME7 mice, treatment with NIP288 hIgG1 TM had no significant impact on disease pathology or behavioural changes relative to vehicle treatment (Figure 5.3). Analysis was compared to previously obtained Naïve + vehicle samples were appropriate.

6.3.1.1 Body weight responses to *S. typhimurium* infection

ME7 mice were randomly assigned to a treatment group and then challenged with *S. typhimurium* SL3261 (ME7/SL3261) at 8 wpi and systemic responses were monitored through body and spleen weight measurements (Figure 6.1). ME7/SL3261 mice showed a typical response to *S. typhimurium* infection with an average body weight loss of 6.56% one day after and recovery by seven days after (Figure 6.1A).

6.3.1.2 Body weight responses to administration of fusion proteins

ME7/SL3261 mice were assessed for any adverse effects associated with repeated injections through monitoring of body weight over the duration of treatment. Weights of ME7/SL3261 mice from all treatment groups increased over the course of multiple injections, in line with expected growth (Figure 6.1B). Analysis using a 2-way ANOVA identified a significant main effect of 'time after first injection' on body weight changes ($F(1.510, 28.69) = 8.087$, $p = 0.0034$; $\varepsilon = 0.3020$). There was no main effect of 'treatment' ($F(3, 19) = 0.3546$, $p = 0.7864$), nor an interaction between 'time after first injection and treatment' ($F(15, 95) = 0.4979$, $p = 0.9363$).

6.3.1.3 Spleen weigh responses to *S. typhimurium* infection and administration of fusion proteins

Spleen weights were measured at the time of tissue collection, nine weeks after systemic challenge with *S. typhimurium*. Spleen weights from Naïve control mice, who also received weekly vehicle injections, were included for comparison (Figure 6.1C). Average spleen weights between groups ranged from 110-230 mg across groups, with average weights from ME7/SL3261 mice increased over Naïve control mice (110 mg versus 148 mg). There was a significant difference between means following a one-way ANOVA ($F(4, 22) = 2.842$, $p = 0.0486$), with a significant difference between Naïve control spleens and spleens from ME7/SL3261 mice treated with NIP228 hIgG1 TM ΔK-mTNFR2 ($t = 2.724$, $df = 22$, $p = 0.0486$) (Figure 6.1B). Spleens from $8D3_{130}$ hIgG1 TM injected ME7/SL3261 mice showed a trend towards increased weight compared to naïve control spleens ($t = 2.310$, $df = 22$, $p = 0.0891$).

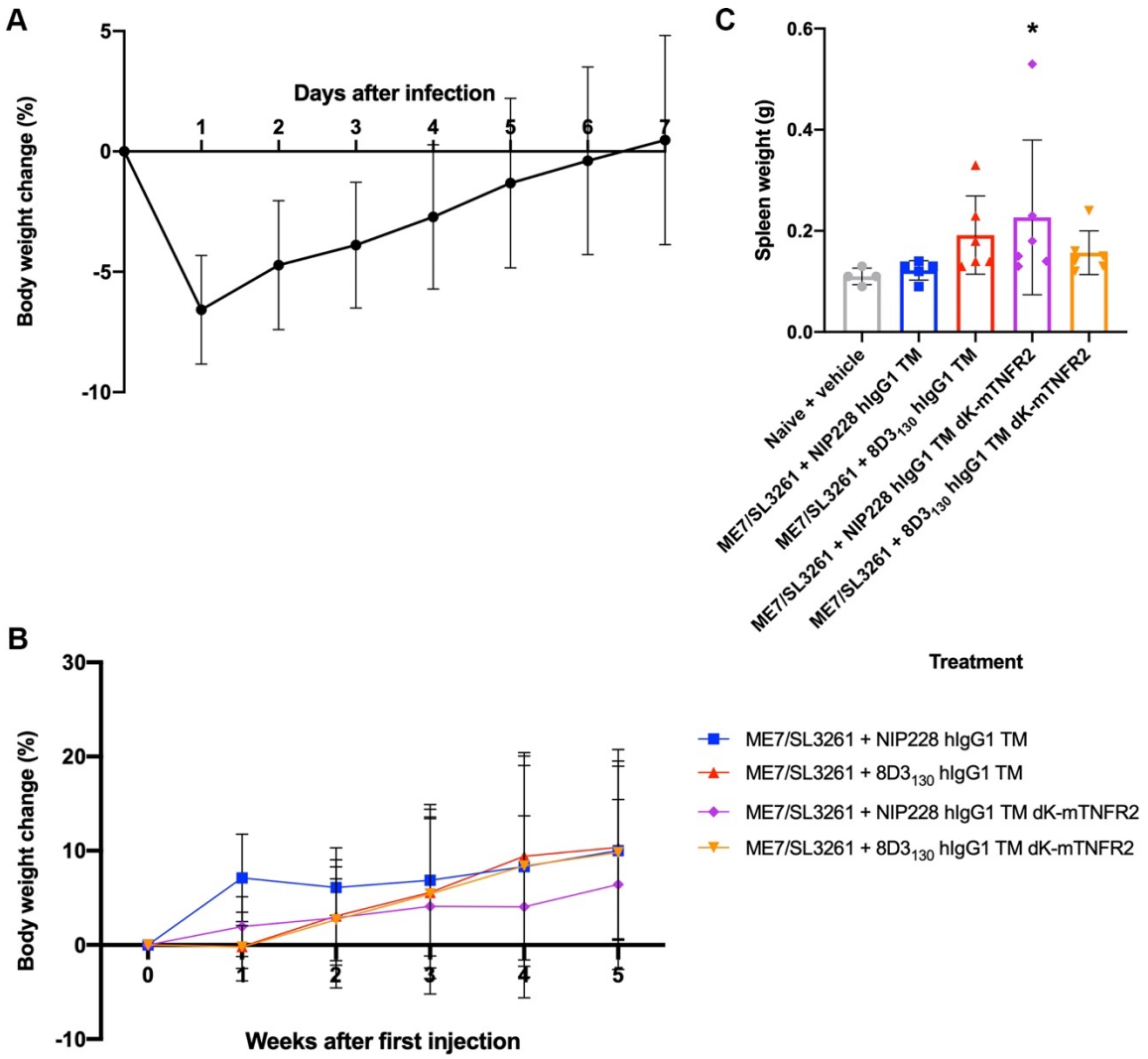

Figure 6.1 Peripheral responses following challenge with *S. typhimurium* in ME7 mice at 8 wpi and administration of bispecific mTNFR2 fusion proteins

ME7 mice were challenged with *S. typhimurium* SL3261 (1 x 10^6 cfu, i.p.) at 8 wpi and were monitored for weight changes before weekly injections of bispecific mTNFR2 fusion protein from 12 wpi and tissue collection at 17 wpi. (A) Mouse body weights decrease in the first days after systemic challenge and recover after seven days. (B) Fusion protein injection did not have a negative impact on body weight growth over the duration of treatment. (C) Spleen weights nine weeks after systemic challenge with *S. typhimurium* were recorded from all treatment groups. Data presented as mean ± SD, n = 4-6 per group. *, $p < 0.05$ versus Naïve + Saline following one-way ANOVA with Holm-Sidak's multiple comparisons test.

6.3.2 TfR expression in ME7 mice following systemic bacterial challenge and bispecific mTNFR2 fusion protein administration

TfR expression was analysed in the hippocampus to determine if there are any long-term effects resulting from systemic bacterial challenge in ME7 mice.

Staining of TfR in the hippocampus is seen on brain endothelial cells and neurons (asterisks; Figure 6.2) in both naïve controls and ME7/SL3261 mice challenged with *S. typhimurium* at 8 wpi. Analysis of TfR expression using Kruskal-Wallis test shows no significant difference between median values ($F(5, 15) = 6.367$, $p = 0.1706$) between Naïve control mice and ME7 mice nine weeks after injection with *S. typhimurium* (Figure 6.2F).

Analysis of mRNA transcript levels for *Tfrc* in the hippocampus and thalamus showed no significant changes in expression between Naïve controls and ME7 mice ($F(4,22) = 1.286$, $p = 0.3058$) (Figure 6.2G), nor between treatment groups within ME7 mice ($F(3,19) = 1.553$, $p = 0.2336$) (Figure 6.2H).

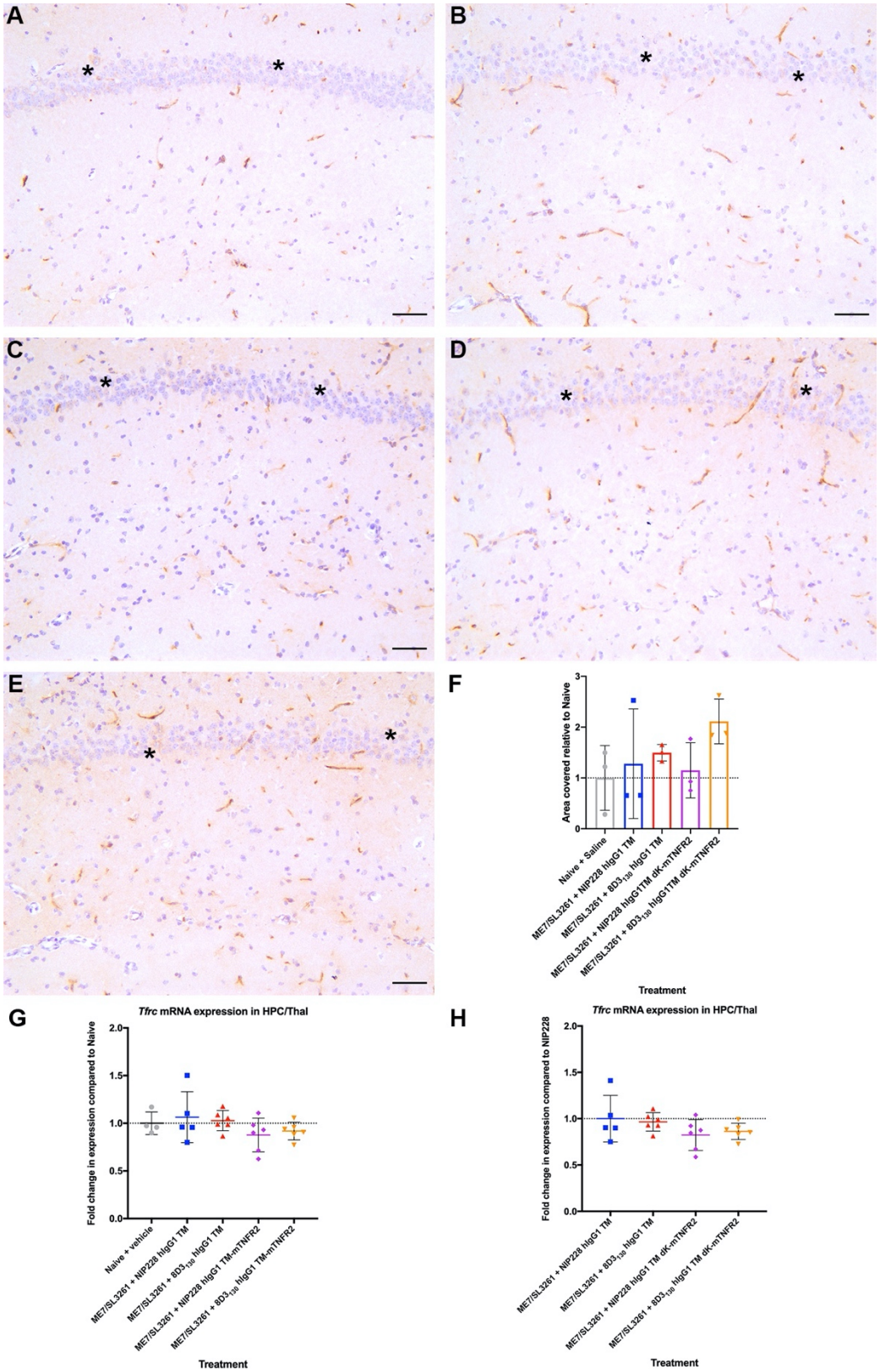

Figure 6.2 Hippocampal TfR expression in ME7 mice challenged with *S. typhimurium* and treated with bispecific mTNFR2 fusion proteins

(A-E) Representative images of hippocampal TfR staining in naïve control mice (A) and ME7/SL3261 mice nine weeks after systemic challenge with *S. typhimurium* SL3261 ($1x10^6$ cfu, i.p.) and following four weekly injections, from 12 wpi, with NIP228 hIgG1 TM (B), $8D3_{130}$ hIgG1 TM (C), NIP228 hIgG1 TM ΔK-mTNFR2 (D), and $8D3_{130}$ hIgG1 TM ΔK-mTNFR2 (E). Asterisks highlight areas of neuronal TfR staining in CA1 layer. (F) Analysis of hippocampal TfR expression in ME7/SL3261 mice shows no change compared to Naïve control mice. Data is presented as mean ± SD, n = 3/group. Images were taken with a 2x objective lens; scale bar = 50 μm.

6.3.3 Effect of TNF neutralisation on behavioural assessment of ME7 mice after systemic bacterial challenge

Behavioural analysis of ME7/SL3261 mice compared to Naïve mice was not possible in this experiment due to Covid-19 enforced restrictions on animal experiments during the collection of these data. Therefore, weekly behavioural analysis was reduced to collect data at key time points only – one week before and after *S. typhimurium* infection and before, during and after treatment with bispecific mTNFR2 fusion proteins. Behaviours are consistent with baseline readings throughout an ME7 study and are unaffected by multiple injections (Figure 5.4). Therefore, ME7/SL3261 mice were compared to baseline readings at 7 wpi prior to challenge with *S. typhimurium* for all behavioural analysis (Figure 6.3).

Food pellets burrowed by ME7/SL3261 mice decrease over time compared to baseline and this decrease is significant at 16 and 17 wpi (Figure 6.3A). Analysis using a 2-way ANOVA confirmed a significant main effect of 'time after injection' ($F(2.657, 50.48) = 91.79$, $p < 0.0001$). However, there was no main effect of 'treatment' ($F(3, 19) = 0.6751$, $p = 0.5779$) nor interaction between 'time after injection x treatment' ($F(21, 133) = 0.6420$, $p = 0.8805$). Post-hoc analysis did not identify any significant differences between bispecific mTNFR2 fusion treatment and NIP228 hIgG1 TM treated ME7/SL3261 mice at any time point.

Distance covered in the open field arena showed an increase over time in ME7/SL3261 mice compared to baseline, and this increase becomes significant at 16 wpi (Figure 6.3B). Analysis using a 2-way ANOVA confirmed a significant main effect of 'time after injection' ($F(2.917, 55.42) = 22.39$, $p < 0.0001$). However, there was no main effect of 'treatment' ($F(3, 19) = 1.097$, $p = 0.3815$) or interaction between 'time after injection x treatment' ($F(21, 133) = 1.272$, $p = 0.2055$). Post-hoc analysis showed no significant differences between bispecific mTNFR2 fusion protein treated and NIP228 hIgG1 TM treated ME7/SL3261 mice at any time point.

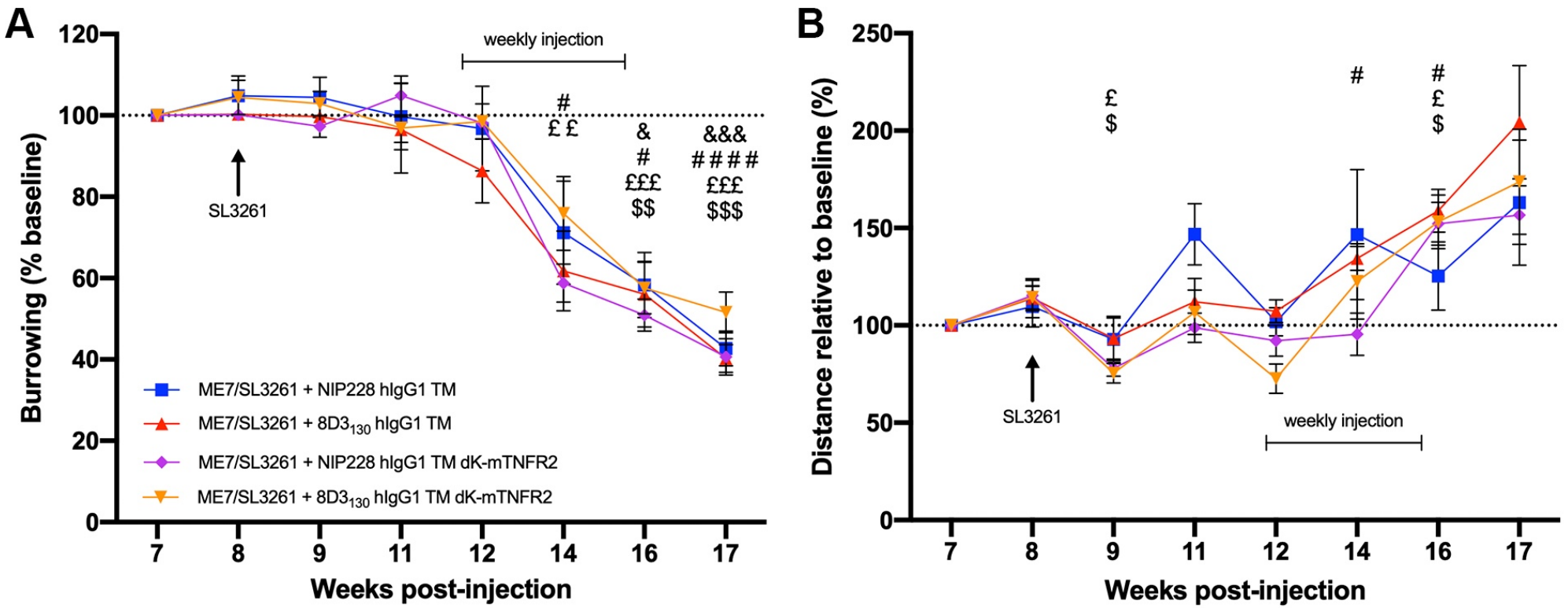

Figure 6.3 Behavioural assessment of ME7 mice following systemic bacterial challenge at 8 wpi

ME7 prion mice were assessed in burrowing (A) and open field (B) behaviours to monitor disease progression following systemic challenge with *S. typhimurium* SL3261 ($1x10^6$ cfu; i.p.) and four weekly injections, from 12 wpi, with bispecific mTNFR2 fusion protein or isotype control (54 μM, i.p.). (A) Changes in burrowing behaviour in ME7/SL3261 mice are present from 14 wpi, but mTNFR2 fusion protein treatment has no significant effect on behaviour compared to NIP228 hIgG1 TM-treated ME7/SL3261 mice. (B) Open field locomotor activity in ME7/SL3261 mice show increasing locomotion until significance at 16 wpi. Data are presented as mean ± SD, n = 5-6/group. &, $p < 0.05$, &&&, $p < 0.001$ for NIP228 hIgG1 TM; #, $p < 0.05$, ####, $p < 0.0001$ for $8D3_{130}$ hIgG1 TM; £, $p < 0.05$, ££, $p < 0.01$, £££, $p < 0.001$ for NIP228 hIgG1 TM ΔK-mTNFR2; $, $p < 0.05$, $$, $p < 0.01$, $$$, $p < 0.001$ for $8D3_{130}$ hIgG1 TM ΔK-mTNFR2 versus 7wpi baseline following a two-way ANOVA and Dunnett's multiple comparisons test.

6.3.4 Biochemical analysis of synaptic markers in ME7 mice after systemic bacterial challenge and administration of bispecific mTNFR2 fusion proteins

Expression of synaptophysin (*Syp*) in the hippocampus and thalamus of ME7/SL3261 mice showed a trend towards decreased expression compared to Naïve control mice with a Kruskal-Wallis test ($W(5, 27) = 8.119$, $p = 0.0873$) (Figure 6.4A). Post-hoc analysis showed a significant decrease in Syp expression in NIP228 hIgG1 TM ΔK-mTNFR2 treated ME7/SL3261 mice ($Z(4, 6) = 2.603$, $p = 0.0370$). However, when comparing treatments in ME7/SL3261 mice showed no significant differences compared to NIP228 hIgG1 TM treated mice ($W(4, 23) = 2.078$, $p = 0.5564$) (Figure 6.4B).

Analysis of mGluR1 (*Grm1*) transcript levels showed a trend towards decreased expression between ME7/SL3261 mice and Naïve control mice using one-way ANOVA ($F(4, 22) = 2.738$, $p = 0.0547$) (Figure 6.4C). Post-hoc analysis identified significant decreases in mGLuR1 expression in $8D3_{130}$ hIgG1 TM ($t = 2.699$, $p = 0.0388$) and $8D3_{130}$ hIgG1 TM ΔK-mTNFR2 ($t = 2.1987$, $p = 0.0269$) treated ME7/SL3261 mice compared to Naïve control mice. Analysis with one-way ANOVA between treatment groups in ME7/SL3261 mice showed no significant differences in means ($F(3, 19) = 0.9052$, $p = 0.4570$) (Figure 6.4D).

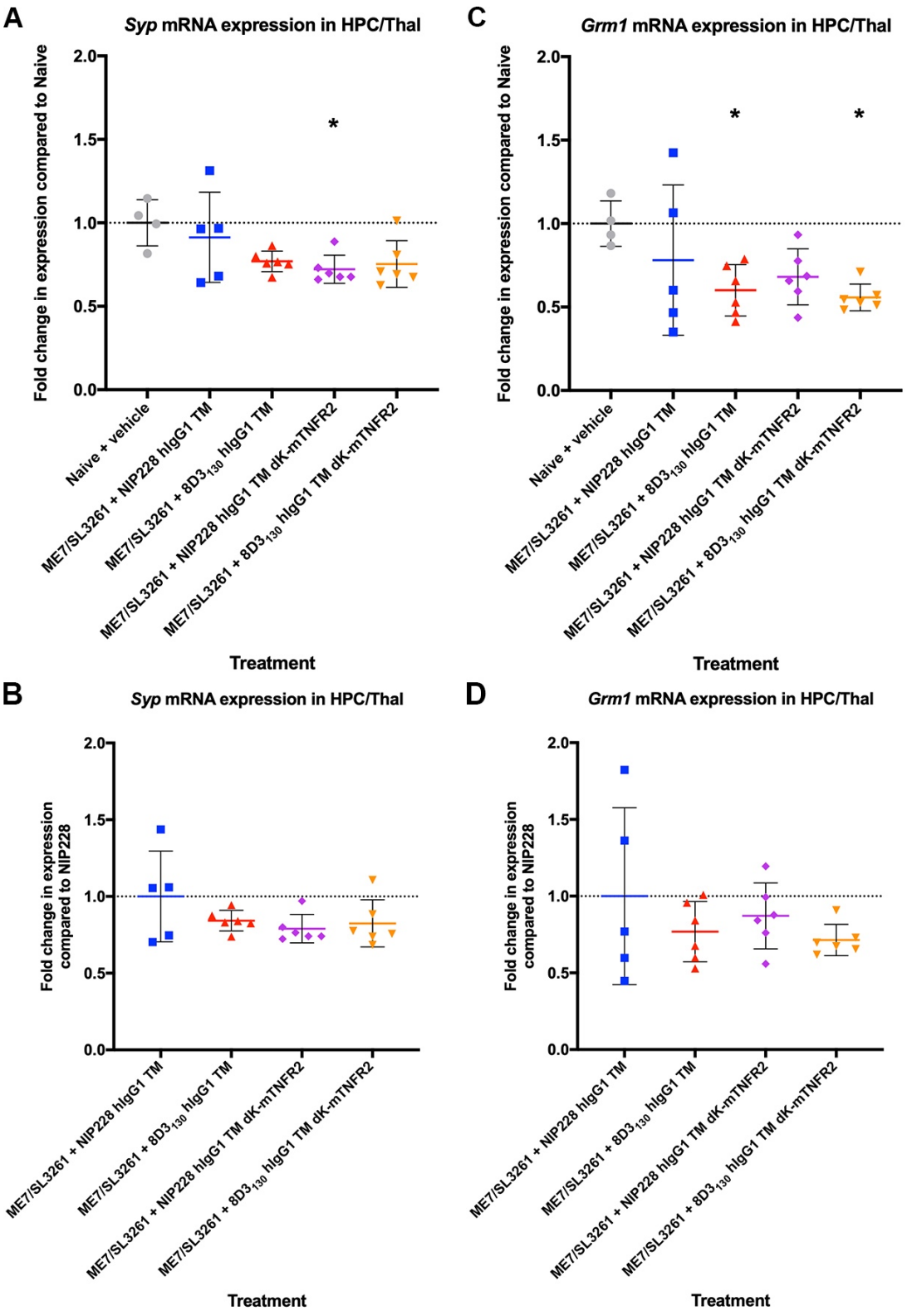

Figure 6.4 Expression of synaptic markers in hippocampus/thalamus in ME7 mice after systemic bacterial challenge and bispecific mTNFR2 fusion proteins treatment

Synaptic marker mRNA transcripts in the hippocampus and thalamus of ME7/SL3261 mice nine weeks after systemic challenge with *S. typhimurium* SL3261 ($1x10^6$ cfu, i.p.) and four weekly bispecific fusion protein injections from 12 wpi. (A-B) Expression of synaptophysin (*Syp*) mRNA transcripts in ME7/SL3261 relative to Naïve controls (A) and relative to NIP228 hIgG1 TM-treated ME7/SL3261 (B). (C-D) Expression of metabotropic glutamate receptor type 1 (*Grm1*) mRNA transcripts in ME7/SL3261 relative to Naive controls (C) and relative to NIP228 hIgG1 TM-treated ME7/SL3261 (D). Data are presented as mean ± SD (n=4-6/group) for expression after normalisation to *Pgk1*. *, $p < 0.05$ versus Naïve + vehicle following one-way ANOVA WITH Holm-Sidak's multiple comparisons test.

6.3.5 Microglial activation in ME7 mice following systemic bacterial challenge and administration of bispecific mTNFR2 fusion proteins

Microglial activation in the brains of ME7/SL3261 mice at 17 wpi was measured by immunohistochemistry for CD64 (FcγRI) and MHCII in the hippocampus (Figure 6.5, Figure 6.6) and thalamus (Figure 6.7, Figure 6.8). Previously generated tissue from age-matched Naive control mice (Naïve + vehicle) were included as a comparison for induction of expected ME7 pathology.

6.3.5.1 Hippocampal CD64 expression

Increased staining of CD64 was evident in the hippocampus of all ME7/SL3261 mice compared to Naïve control mice (Figure 6.5). Analysis of area covered by one-way ANOVA showed a significant difference between group means ($F(4, 10) = 28.57$, $p < 0.0001$). Post-hoc analysis showed increased staining compared to Naïve control mice for all treatment groups in ME7/SL3261 mice ($p < 0.0001$) (Figure 6.5F). Treatment of ME7/SL3261 mice with bispecific mTNFR2 fusion proteins has no effect on CD64 expression in the hippocampus compared to NIP228 hIgG1 TM-treated ME7/SL3261 mice ($F(3, 8) = 1.426$, $p = 0.3052$) (Figure 6.5G).

6.3.5.2 Hippocampal MHCII expression

Hippocampal expression of MHCII is increased in ME7/SL3261 mice compared to Naïve control mice (Figure 6.6). Analysis of area covered by Kruskal-Wallis test showed a significant difference in group medians ($W(5, 15) = 10.50$, $p = 0.0044$). Post-hoc analysis identifies a trend towards significant increases in ME7/SL3261 mice treated with $8D3_{130}$ hIgG1 TM, NIP228 hIgG1 TM ΔK-mTNFR2 and $8D3_{130}$ hIgG1 TM ΔK-mTNFR2 groups (all $z = 2.465$, $p = 0.0548$) compared to Naïve control mice (Figure 6.6F). In addition, there is a trend towards a significant difference between NIP228 hIgG1 TM and other treatments in ME7/SL3261 mice ($W(4, 12) = 6.231$, $p = 0.0877$) (Figure 6.6G).

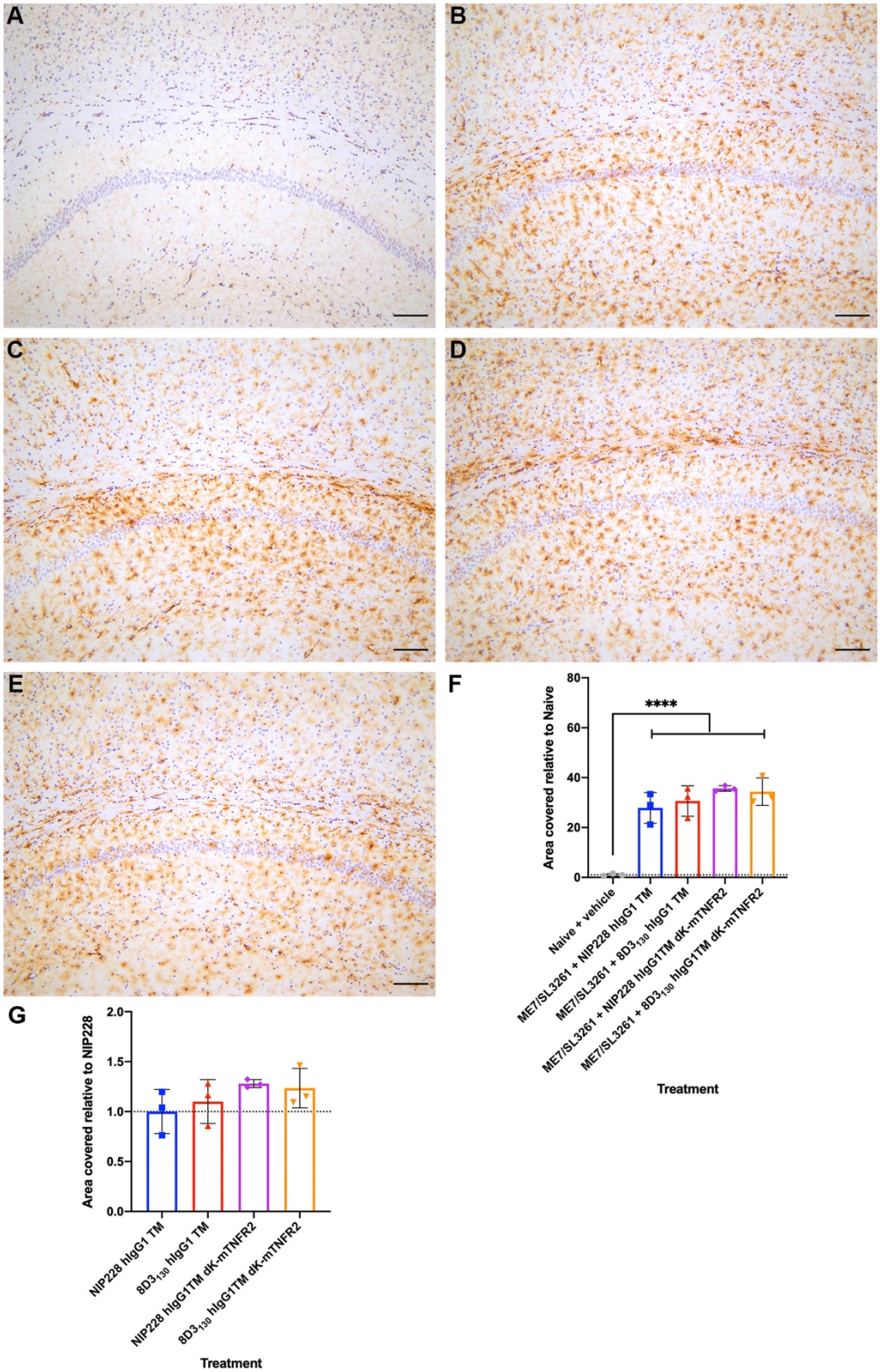

Figure 6.5 CD64 expression in the hippocampal CA1 of ME7 mice challenged with *S. typhimurium* and treated with bispecific mTNFR2 fusion proteins

(A-E) Representative images of hippocampal CD64 staining in Naive control mice (A) and ME7/SL3261 mice nine weeks after systemic challenge with *S. typhimurium* SL3261 ($1x10^6$ cfu, i.p.) and four weekly injections of NIP228 hIgG1 TM (B), $8D3_{130}$ hIgG1 TM (C), NIP228 hIgG1 TM ΔK-mTNFR2 (D), or $8D3_{130}$ hIgG1 TM ΔK-mTNFR2 (E) from 12 wpi. (F) Analysis of hippocampal CD64 expression in ME7/SL3261 mice shows a significant increase compared to Naïve control mice. (G) Treatment with bispecific mTNFR2 fusion protein treatment has no effect on hippocampal CD64 expression in ME7/SL3261 mice when compared to NIP228hIgG1 TM -treated mice. Data is presented as mean ± SD, n = 3/group. ****, $p < 0.0001$ versus Naïve + vehicle using one-way ANOVA with Holm-Sidak's multiple comparisons test. Images were taken with a 10x objective lens; scale bar = 100 μm.

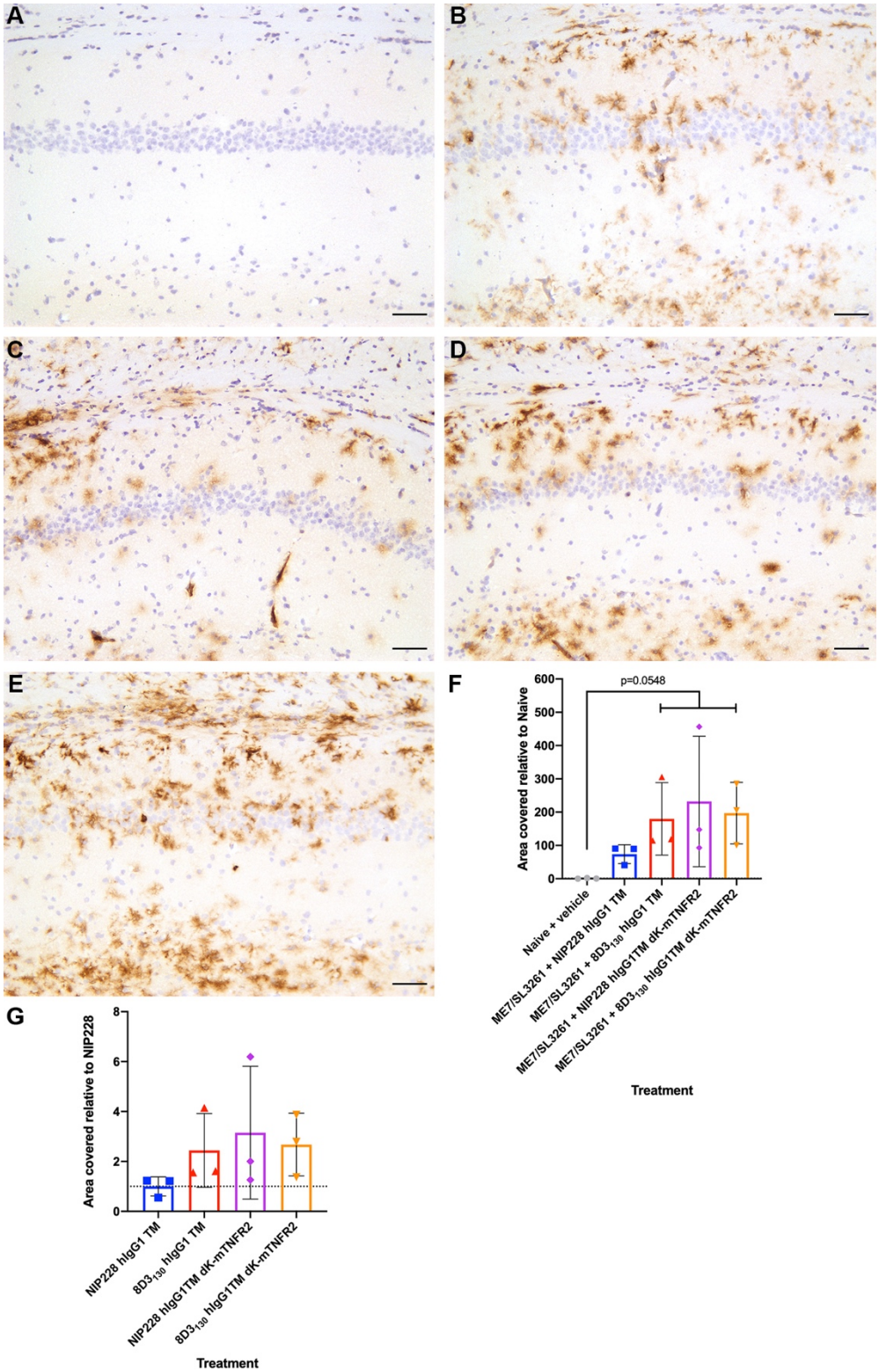

Figure 6.6 Hippocampal MHCII in ME7 mice challenged with *S. typhimurium* and treated with bispecific mTNFR2 fusion proteins

(A-E) Hippocampal MHCII staining in Naive control mice (A) and ME7/SL3261 mice nine weeks after systemic challenge with *S. typhimurium* SL3261 ($1x10^6$ cfu, i.p.) and four weekly injections with NIP228 hIgG1 TM (B), $8D3_{130}$ hIgG1 TM (C), NIP228 hIgG1 TM ΔK-mTNFR2 (D), or $8D3_{130}$ hIgG1 TM ΔK-mTNFR2 (E) from 12 wpi. (F) Analysis of hippocampal MHCII expression in ME7/SL3261 mice shows a trend towards increased expression compared to Naïve control mice. (G) Treatment with bispecific mTNFR2 fusion protein treatment has no effect on MHCII expression in ME7/SL3261 mice when compared to NIP228-treated mice. Data is presented as mean ± SD, n = 2-3/group. p = 0.0548 versus Naïve + vehicle using one-way ANOVA with Holm-Sidak's multiple comparisons test. Images were taken with a 20x objective lens; scale bar = 50 μm.

6.3.5.3 Thalamic CD64 expression

Increased CD64 staining was evident in the thalamus of ME7/SL3261 mice, irrespective of treatment, to age-matched Naïve control mice (Figure 6.7). Analysis of area covered using one-way ANOVA showed a significant difference between group means ($F(4, 10) = 62.81$, $p < 0.0001$). Holm-Sidak multiple comparisons post-hoc analysis identified a significant increase in thalamic CD64 expression in all ME7/SL3261 treatments compared to Naïve control mice for all treatment groups in ME7/SL3261 mice ($p < 0.0001$) (Figure 6.7F). Analysis of ME7/SL3261 mice showed no significant difference between means compared to NIP228 hIgG1 TM treatment ($F(3, 8) = 1.035$, $p = 0.4275$) (Figure 6.7G).

6.3.5.4 Thalamic MHCII expression

MHCII staining in the thalamus is increased in ME7/SL3261 mice compared to expression in Naïve control mice (Figure 6.8). Analysis of area covered with one-way ANOVA showed a significant difference in group means ($F(4, 10) = 68.78$, $p < 0.0001$). Post-hoc analysis showed that area covered is significantly increased in all ME7/SL3261 mice, except 8D3130 hIgG1 ΔK-mTNFR2 treated mice, compared to Naïve control mice ($p < 0.0001$) (Figure 6.8F). However, there is no significant difference between treatment groups in ME7/SL3261 mice ($F(3, 8) = 1.153$, $p = 0.3854$) (Figure 6.8G).

Overall, systemic bacterial infection in ME7 mice induced significant expression of CD64 and MHCII in the hippocampus and thalamus, however treatment with bispecific mTNFR2 fusion proteins had no effect on expression levels.

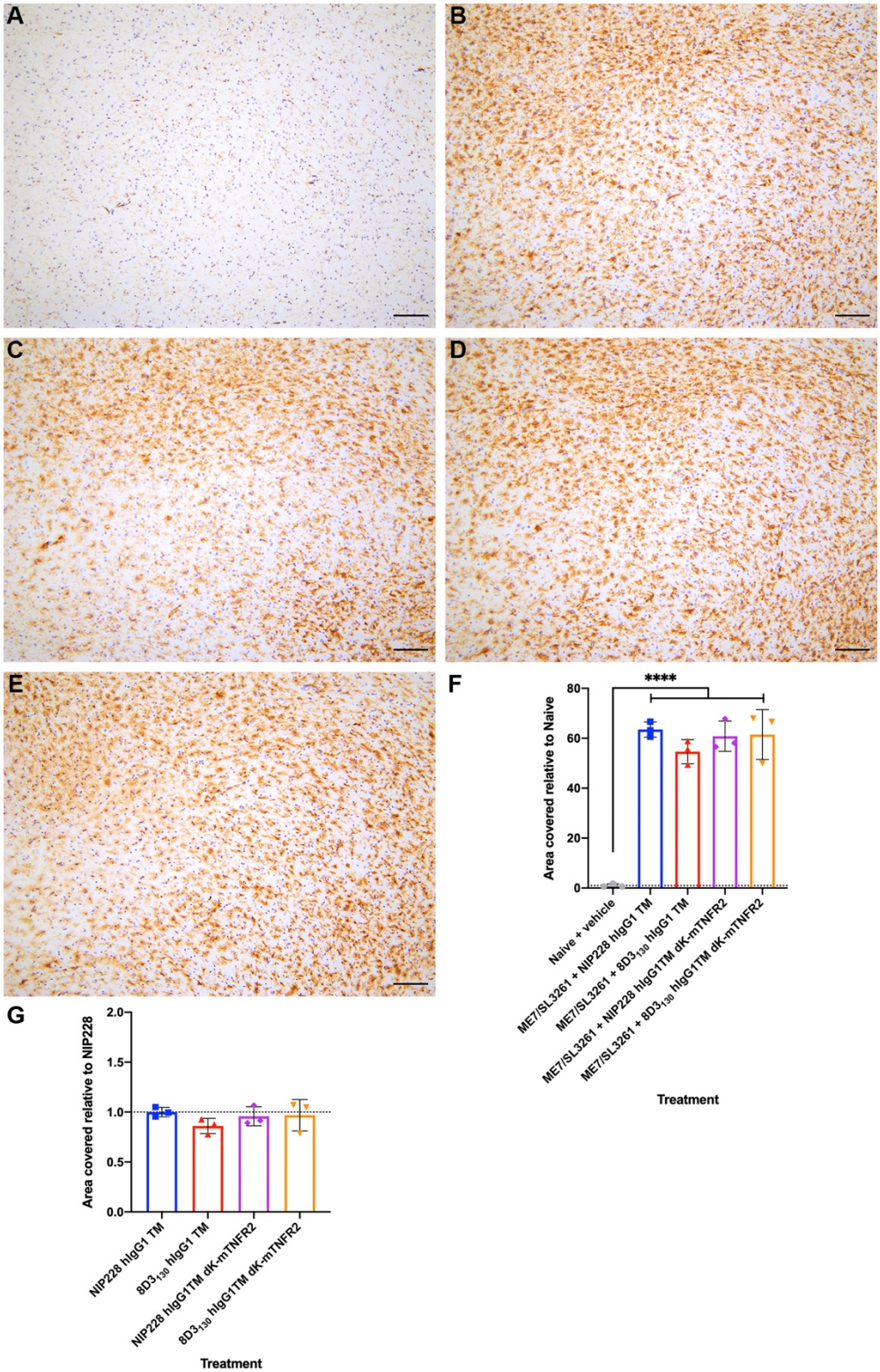

Figure 6.7 CD64 staining in thalamus of ME7 mice following systemic bacterial challenge and bispecific mTNFR2 fusion protein administration

(A-E) Representative images of thalamic CD64 staining in Naive control mice (A) and ME7/SL3261 mice nine weeks after systemic challenge with *S. typhimurium* SL3261 ($1x10^6$ cfu, i.p.) and four weekly injections of NIP228 hIgG1 TM (B), $8D3_{130}$ hIgG1 TM (C), NIP228 hIgG1 TM ΔK-mTNFR2 (D), or $8D3_{130}$ hIgG1 TM ΔK-mTNFR2 (E) from 12 wpi. (F) Analysis of hippocampal CD64 expression in ME7 mice shows a significant increase compared to Naïve control mice. (G) Treatment with bispecific mTNFR2 fusion protein treatment has no effect on CD64 expression in ME7/SL3261 mice when compared to NIP228-treated mice. Data is presented as mean ± SD, n = 3/group. ****, $p < 0.0001$ versus Naïve + vehicle using one-way ANOVA with Holm-Sidak's multiple comparisons test. Scale bar = 100 μm.

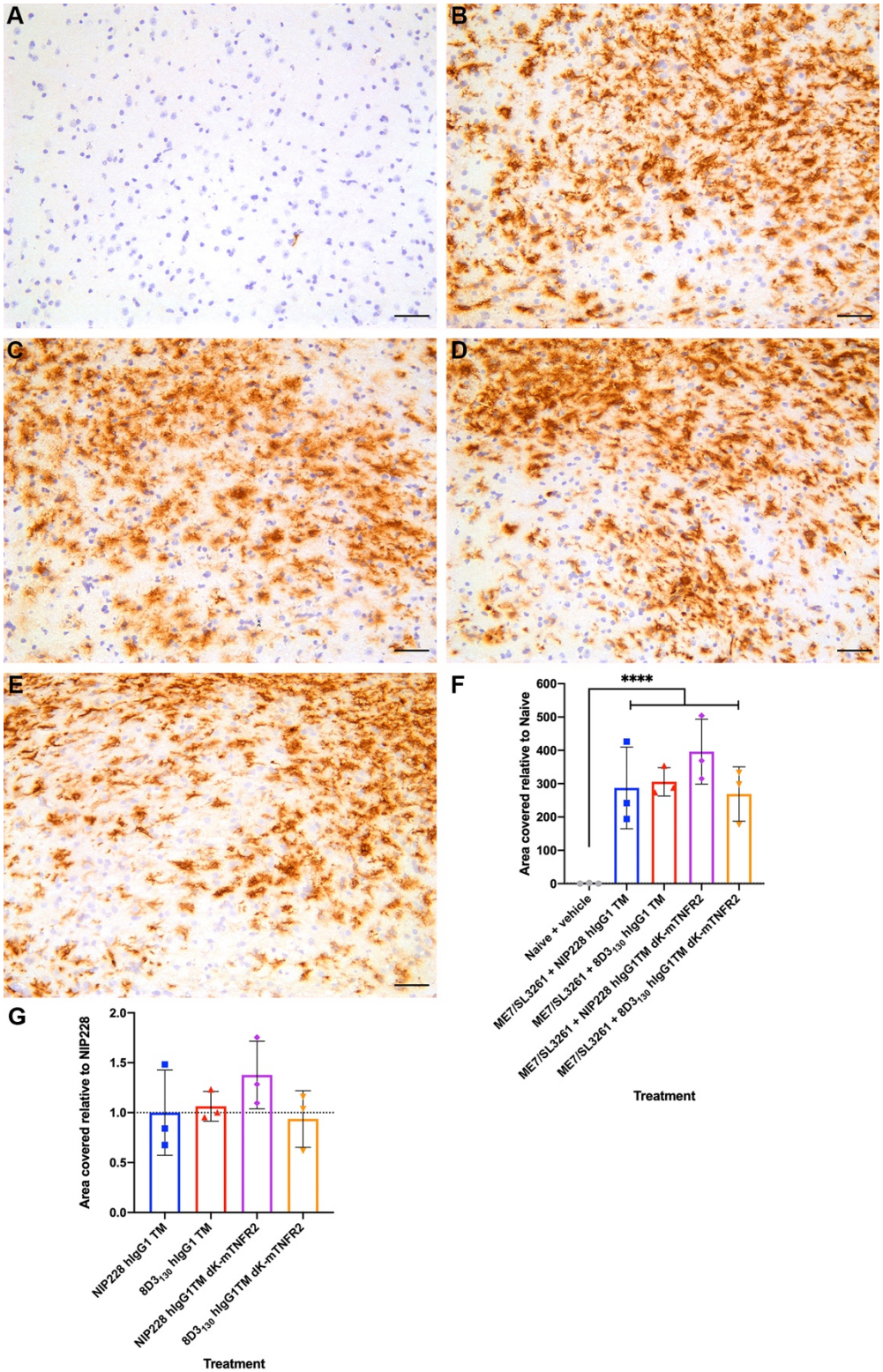

Figure 6.8 Thalamic MHCII in ME7 mice challenged with *S. typhimurium* and treated with bispecific mTNFR2 fusion proteins

(A-E) Thalamic MHCII staining in Naive control mice (A) and ME7/SL3261 mice nine weeks after systemic challenge with *S. typhimurium* SL3261 ($1x10^6$ cfu, i.p.) and four weekly injections of NIP228 hIgG1 TM (B), $8D3_{130}$ hIgG1 TM (C), NIP228 hIgG1 TM ΔK-mTNFR2 (D), or $8D3_{130}$ hIgG1 TM ΔK-mTNFR2 (E) from 12 wpi. (F) Analysis of thalamic MHCII expression in ME7/SL3261 mice shows a significant increase compared to Naïve control mice. (G) Treatment with bispecific mTNFR2 fusion protein treatment has no effect on MHCII expression in ME7/SL3261 mice when compared to NIP228-treated mice. Data is presented as mean ± SD, n = 2-3/group. **, $p < 0.01$ versus Naïve + vehicle using one-way ANOVA with Holm-Sidak's multiple comparisons test. Images were taken with a 20x objective lens; scale bar = 50 μm.

6.3.6 Biochemical analysis of cytokines in ME7 prion mice following fusion protein administration

Analysis of cytokine transcripts from hippocampus/thalamus-enriched tissue showed that expression of *Tnf* is significantly increased in ME7/SL3261 mice compared to Naïve control mice ($F(4, 22) = 5.243$, $p = 0.0040$) (Figure 6.9A). *Il1b* expression shows a significant increase in ME7/SL3261 mice compared to Naïve control mice ($F(4, 22) = 19.27$, $p < 0.0001$) (Figure 6.9B).

Ccl2 expression is significantly increased in ME7/SL3261 mice following analysis with one-way ANOVA ($F(4, 22) = 10.51$, $p < 0.0001$). There was a significant difference between ME7/SL3261 mice when compared to Naïve control mice, with NIP228 hIgG1 TM (40.1-fold; $p = 0.0012$) and $8D3_{130}$ hIgG1 TM ΔK-mTNFR2 (38.7-fold; $p = 0.0011$) treated ME7 showing smaller increases compared to $8D3_{130}$ hIgG1 TM (54.96-fold; $p < 0.0001$) and NIP228 hIgG1 TM ΔK-mTNFR2 treated ME7/SL3261 mice (48.89-fold; $p < 0.0001$) (Figure 6.9C).

When analysing differences in cytokine expression between treatments in ME7/SL3261 mice, there was no significant differences in expression of *Tnf* ($H(5,39) = 0.1955$, $p = 0.9955$), *Il1b* ($F(4,34) = 1.364$, $p = 0.2761$) or *Ccl2* ($F(4,34) = 1.418$, $p = 0.2490$) when compared to NIP228 hIgG1 TM-treated ME7/SL3261 mice (Figure 6.9D-F).

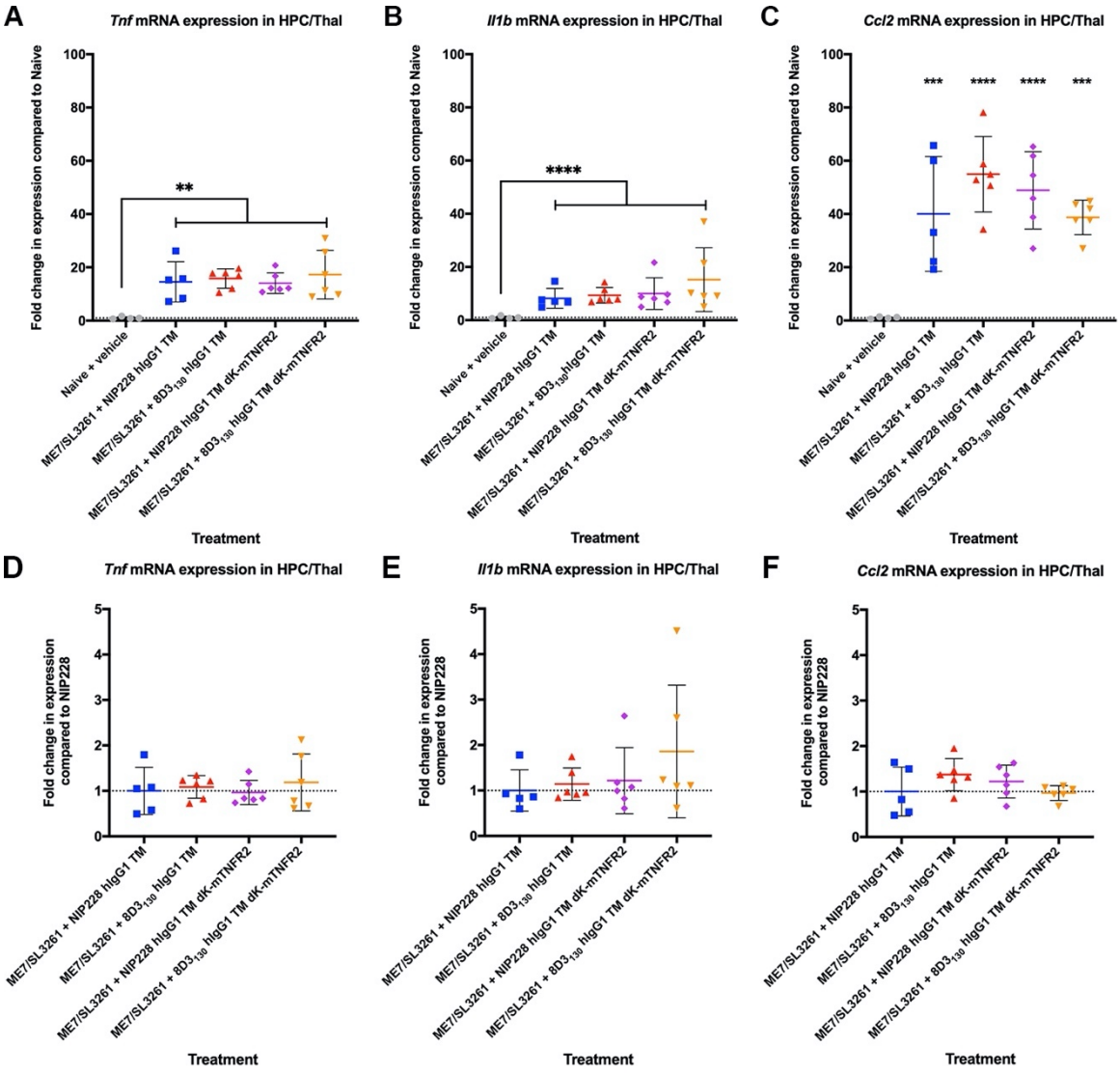

Figure 6.9 Cytokine expression in ME7 mice after systemic bacterial challenge and bispecific mTNFR2 fusion protein treatment

(A-C) Cytokine mRNA transcripts in the hippocampus and thalamus of ME7/SL3261 mice nine weeks after systemic challenge with *S. typhimurium* (1 x 10^6 cfu, i.p.) and weekly bispecific fusion protein injection for four weeks from 12 wpi. Expression of *Tnf* (A), *Il1b* (B), and *Ccl2* (C), show significantly increased expression in ME7/SL3261 mice relative to Naïve control mice. (D-F) *Tnf* (D), *Il1b* (E), and *Ccl2* (F), transcripts levels in ME7 mice remained unchanged compared to NIP228 hIgG1 TM treated mice. Data are presented as mean ± SD (n=4-6/group) for expression after normalisation to *Pgk1*. **, $p < 0.01$; ***, $p < 0.001$; ****, $p < 0.0001$ versus Naïve + vehicle following a one-way ANOVA with Holm-Sidak's multiple comparisons test.

6.3.7 Safety analysis of bispecific mTNFR2 fusion proteins after administration of *S. typhimurium*

The safety of administering bispecific anti-mTfR-mTNFR2 fusion proteins during *S. typhimurium* infection was tested by giving a single 54 μM dose of fusion protein or isotype control 10 days after infection. Mice body weights were monitored across to confirm response to *S. typhimurium* and to monitor any adverse effects from administration of fusion proteins (Figure 6.10).

Mice were randomly placed in treatment groups, with no significant difference in starting weight between treatment groups. All mice showed the expected weight change after injection of *S. typhimurium*, with an average 6% loss in body weight one day after infection that recovers to 2% body weight loss seven days after (Figure 6.10A). All spleens showed the expected response of splenomegaly after injection of *S. typhimurium* with increased spleen weights. However, there was no significant difference between treatment groups ($F(4,14) = 0.7889$; $p = 0.5514$) (Figure 6.10B). Body weights of mice after treatment with fusion proteins remained stable and there was no effect of treatment group on weight change ($F(4, 14) = 0.1634$; $p = 0.9534$) (Figure 6.10C).

Analysis of MHCII and CD64 expression confirmed the expected neuroinflammatory response following infection with *S. typhimurium* (0).

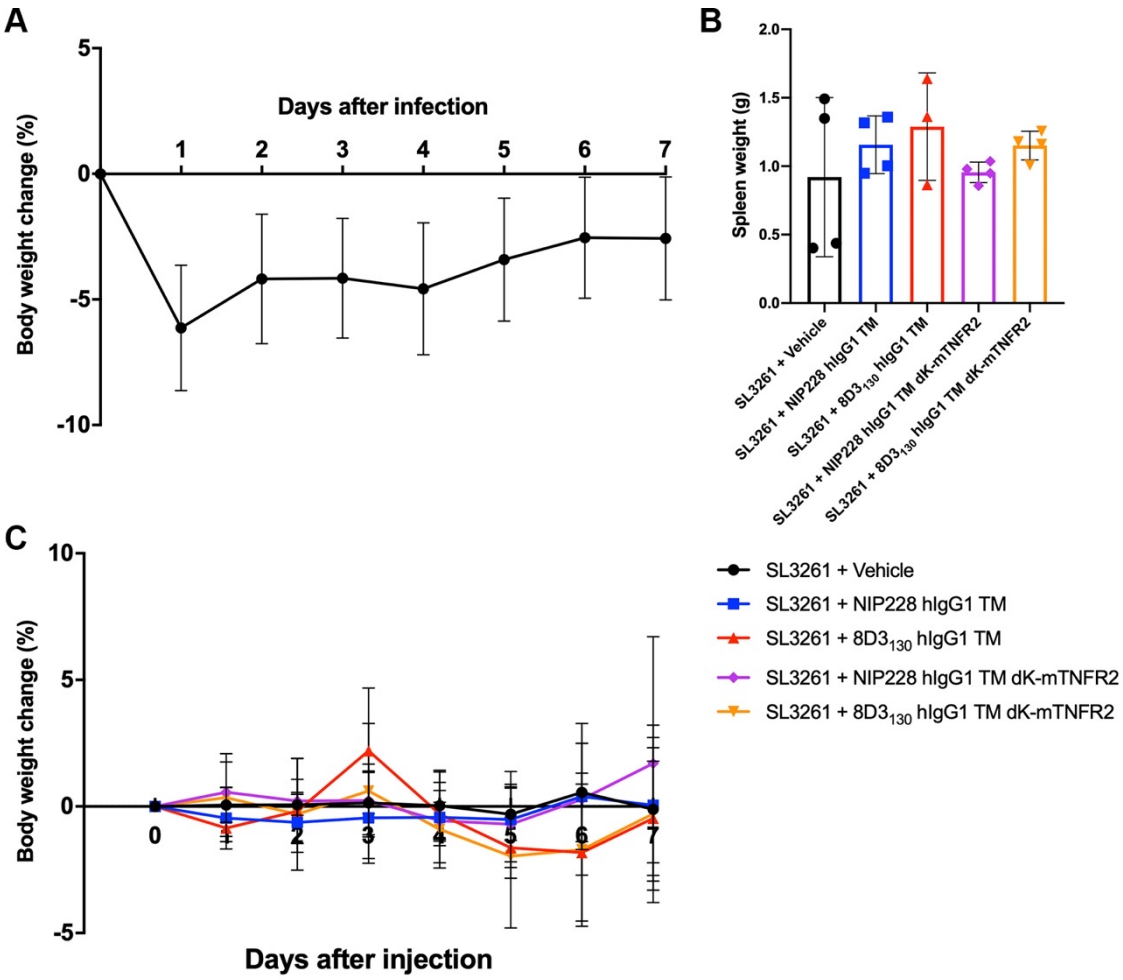

Figure 6.10 Systemic responses following *S. typhimurium* and fusion protein administration
(A) Body weight changes in response to injection of 1.8 x 10^6 cfu *S. typhimurium* SL3261 over the course of seven days. Data are presented as mean ± SD (n = 20/day). (B) Spleen weights of mice at the end of experiment, 17 days after SL3261 injection. (C) Changes in body weight after administration of a single injection of fusion protein (54 μM; i.p.) followed for seven days. Data are presented as mean ± SD (n=3-4/group).

6.4 Discussion

Systemic bacterial infection in ME7 mice at 8 wpi results in the onset of behavioural deficits associated with disease progression appearing earlier, but this is not attenuated by treatment with bispecific mTNFR2 fusion proteins. Furthermore, increased expression of MHCII and CD64 in the hippocampus and thalamus following systemic bacterial infection is associated with increased expression of *Tnf*, *Il1b* and *Ccl2* mRNA transcripts nine weeks later. However, these associated neuroinflammatory changes are not prevented by treatment of *S. typhimurium* infected ME7 mice with bispecific mTNFR2 fusion proteins.

6.4.1 Temporal considerations for mTNFR2 fusion protein treatment in *S. typhimurium* infected ME7 mice

The experimental hypothesis that inhibition of TNF-α following systemic inflammation will reduce cytokine production needs to be carefully investigated with the correct experimental design. Each variable - ME7 prion progression, systemic infection, anti-TNF-α treatment – will interact and influence each other, for example, later infection in ME7 prion results in increased cytokine expression and microglial activation; earlier anti-TNF treatment following *Salmonella* infection can be detrimental to survival; longer sampling time for output measurements may show differences in cytokine expression due to expected resolution of infection. Therefore, the decisions as to when to manipulate each individual variable will impact on the outcome of the experiment. There are three main considerations: 1) At what time during ME7 prion disease progression do you infect with *S. typhimurium*? 2) When after *S. typhimurium* infection do you give anti-TNF-α treatment? 3) How long is the anti-TNF-α treatment and when after final administration do you measure your endpoint?

If we take the first question, then based on the data reported previously in this thesis (Sections 3.4.2 and 3.4.3), we know that infection earlier during disease progression at 8 wpi results in a reduced neuroinflammatory response compared to that when infection is initiated at 12 wpi. Thus, the optimum time to induce infection would be 12 wpi as this is

known to significantly affect the brain microenvironment during ME7 prion disease. This approach was unfortunately not used in the current experimental plan (Figure 6.11) because of the COVID-19 pandemic and subsequent alterations to facility access. These changes meant that to investigate the hypothesis with respect to systemic inflammation an earlier infection was required to complete the experiment within a suitable timeframe. Infection at 8 wpi was chosen given that this time point had been used previously and therefore some reference to the neuroinflammatory response was available.

Questions 2 and 3 can be considered concurrently. We could expect that earlier intervention with respect to TNF-α would be most appropriate, due to its peak in expression at 12 wpi (Figure 3.6). However, intervening at this time point did not have any effect on ME7 prion progression, as observed through mouse behaviours (Figure 5.3). Therefore, it is unlikely that inhibition of TNF-α in the ME7 prion model, without additional systemic inflammation, effects disease progression. Thus, the timing of infection will greatly influence at which point anti-TNF-α treatment is initiated. It has previously been reported that inhibition of TNF-α, using anti-TNF-α antibodies, after *S. typhimurium* infection results in increased bacterial growth and increased mortality when administered between one and seven days post-infection (Mastroeni et al., 1993b, 1992b). However, administration of a TNF-α neutraliser 48 days after *S. typhimurium* infection had no adverse effects on mice (Van Diepen et al., 2007). This suggests that safe administration of anti-TNF-α treatments exists between 7- and 48-days post-infection. A timepoint of four weeks post-infection, at 12 wpi, was selected for beginning mTNFR2 fusion protein administration both because this was within the safe administration period and because central cytokine expression peaks at this timepoint, allowing for the investigation of central inhibition of TNF-α following systemic infection. Furthermore, initiating treatment at 12 wpi allowed for comparison with data from the previous chapter (Section 5.3), as well as allowing for flexibility in the experimental approach given the ever-changing restrictions during the COVID-19 pandemic.

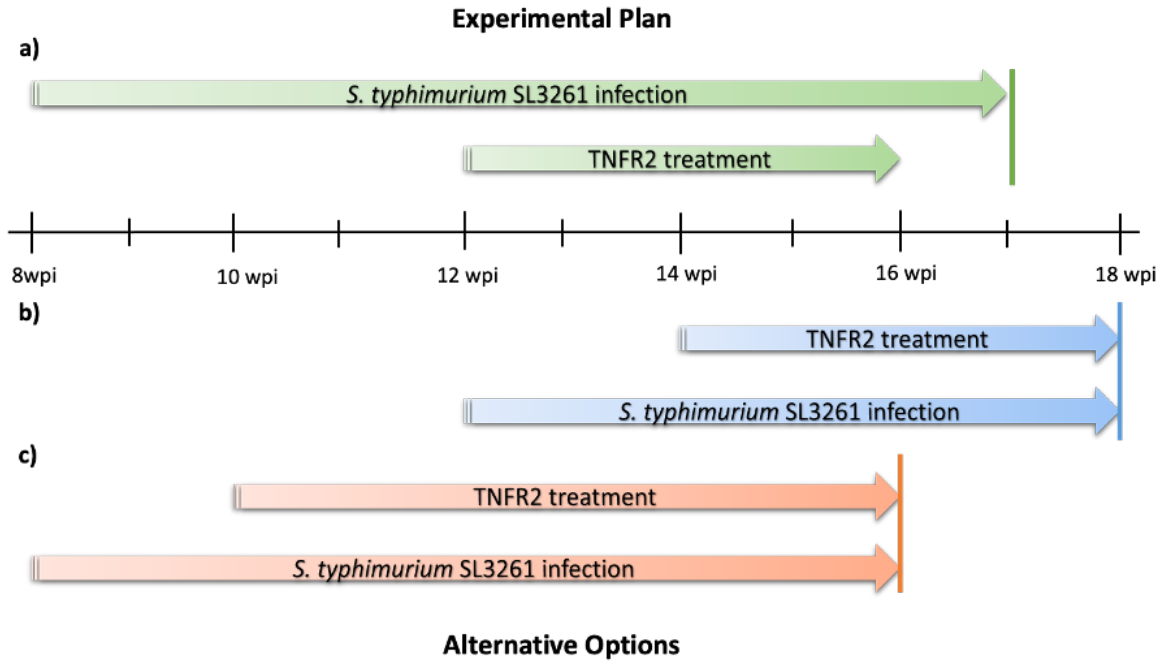

Figure 6.11 Schematic representation of experimental plan timeline
(A) Timeline of *S. typhimurium* infection and anti-TNF-α treatment as used in ME7 mice for this experiment. (B-C) Potential alternative experimental approaches that consider both the optimum timing for infection based on previous experimentation (B) and ideal duration for anti-TNF-α treatment throughout infection course (C) in the murine ME7 prion model, along with the most suitable endpoint for analysis (vertical lines).

Alternative approaches should involve investigation following systemic bacterial infection at 12 wpi, with intervention starting two weeks later, with the added information that administration is safe and tolerable 10 days after infection (Figure 6.10) and continues for 4 weeks with an experimental end point at 18 wpi (Figure 6.11B). This would hopefully provide a suitable timeframe for disruption of systemic response to bacterial infection and limit central cytokine production, whilst also ensuring that monitoring of behaviours could be completed following onset and establishment of deficits, especially within burrowing. Alternatives should also consider whether anti-TNF-α is required throughout the duration of the study and could therefore be initiated earlier during disease progression as end point collection of tissues following final administration would be able to analyse delivery of fusion protein across the BBB. Furthermore, given the current data that systemic infection at 8 wpi does result in significantly increased levels of CD64, MHCII and proinflammatory cytokines within the hippocampus and thalamus, the possibility that repeating the current experimental plan but with earlier and prolonged anti-TNF-α treatment cannot be excluded from potential future investigations (Figure 6.11C). In addition, studies into safety and tolerability of pre-treatment with mTNFR2 fusion

proteins prior to infection with *S. typhimurium* would also provide clear indication whether a prophylactic intervention is at all viable within the context of *S. typhimurium* infection in ME7 mice. Ideally, any approach that brings the induction of systemic inflammation and TNF-α intervention closer together should be considered the most optimal future study and should maximise treatment duration to ascertain whether TNF has any role in disease progression following systemic bacterial infection.

6.4.2 Behavioural and synaptic changes in ME7 mice following systemic bacterial challenge

The acute effects of systemic challenge with *S. typhimurium* in ME7 mice at 8 wpi has no effect on burrowing behaviour, which remained unchanged one week after infection. This is in line with burrowing data from naïve mice which show stable burrowing behaviour up to three weeks after systemic challenge with *S. typhimurium* (Püntener et al., 2012). Initial decreases in number of food pellets burrowed was recorded at 14 wpi with an average 33% decrease across all treatment groups (Figure 6.3A). Onset of this burrowing deficit is in line with previous reports of ME7 mice (Borner et al., 2011; Obst et al., 2018). However, burrowing deficits were observed earlier than non-infected ME7 mice treated with bispecific fusion proteins suggesting that systemic bacterial challenge may contribute to earlier onset of behavioural deficits (Figure 6.3 vs Figure 5.3). This decrease in burrowing behaviour continued as disease progressed and from 16 wpi all treatment groups showed a significant decrease compared to baseline (Figure 6.3). $8D3_{130}$ hIgG1 TM ΔK-mTNFR2 treated ME7/SL3261 mice consistently showed a smaller reduction in burrowing behaviour from 14 wpi compared to NIP228 hIgG1 TM ΔK-mTNFR2 treated ME7/SL3261 mice (10% difference on average). However, this was not significant at any time point and it would be interesting to see whether this separation widened if disease was allowed to progress further. Open field locomotion shows a decrease one week after systemic challenge with *S. typhimurium* in ME7 mice (Figure 6.3). These data represent the first report of open field locomotion in *Salmonella*-infected ME7 mice. Compared to non-infected ME7 mice (Figure 5.3), the onset of open field hyperactivity is earlier in ME7/SL3261, but is in line with previous reports on or after 16 wpi (Chiti et al., 2006; Cunningham et al., 2005a; Felton et al., 2005; Gómez-Nicola et al., 2014). There is an

evident upward trend in open field locomotion for all ME7/SL3261 treatment groups from 14 wpi (Figure 6.3B). However, a continuation of this study further into disease progression might not show any specific differences between bispecific mTNFR2 fusion protein treated ME7/SL3261 mice and their isotype controls due to the large variation in groups at the later time points (%CV = 23-44% across groups at 17 wpi).

The earlier onset of behavioural deficits in ME7/SL3261 mice could be associated with the effects of systemic inflammation on behaviours in ME7 mice. Systemic challenge with LPS does not induce an earlier onset but rather worsens decline after induction of acute deficits (Cunningham et al., 2009; Davis et al., 2015; Murray et al., 2012). However, the majority of systemic inflammatory challenges, with LPS or proinflammatory cytokines, in ME7 prion disease have been on mice at later stages (14-18 wpi) of disease progression (Griffin et al., 2013; Hennessy et al., 2017, 2015; Lunnon et al., 2011; Murray et al., 2011). In the current study, underlying pathology is minimal at the time of systemic challenge and thus the greater level of pathology in previous studies may contribute to the difference in reported effects between *S. typhimurium* and LPS in ME7 mice. However, given that these data come from different cohorts of animals it possible that the difference in onset of behaviours is simply due to variation between cohorts and is not *Salmonella*-induced.

Systemic bacterial challenge in ME7 mice results in significant changes to expression of genes associated with synaptic plasticity and function, including synaptophysin and mGluR1 (0). Analysis of synaptic markers by qPCR identified a trend towards decreased expression in ME7/SL3261 mice compared to Naive control mice for both markers (Figure 6.4). The average decreases in expression compared to controls for synaptophysin and mGluR1 were similar in size to those observed in non-infected ME7 mice (Figure 5.4). This suggests that *S. typhimurium* infection had no significant effect on expression measured nine weeks after infection. These data do not support findings in Chapter 3 (Figure 3.13), where bacterial infection in ME7 mice at 8 wpi resulted in a significant decrease in *Grm1* transcript levels four weeks later compared to saline injected NBH mice. A potential reason for this difference is that any effects induced by *S. typhimurium* after four weeks

may not result in long-term changes and these changes are resolved between four and nine weeks after infection, and thus are no longer observed.

6.4.3 Microglial activation and cytokine expression following systemic bacterial challenge

Systemic bacterial challenge in ME7 results in significant upregulation of MHCII in the thalamus compared to Naive control mice (Figure 6.8). Large variation in MHCII expression in the hippocampus limits statistical analysis to a trend towards increased expression. Although increased microglial expression within the CA1 is evident when compared to Naive mice (Figure 6.6). The average increase in hippocampal MHCII compared to control mice is approximately four-fold greater for ME7/SL3261 mice than in non-infected ME7 mice (Figure 5.7 vs Figure 6.6). A similar phenomenon is observed in the thalamus, where the increased expression observed compared to control mice is ~10-fold greater compared to non-infected ME7 mice (Figure 5.8 vs Figure 6.8). This change in expression level could be from direct exposure of microglia to *S. typhimurium*. Bacterial contact with splenic dendritic cells resulted in increased cytokine production ex vivo, as well as antigen presentation specific to *S. typhimurium* via MHCI and MHCII (Yrlid and Wick, 2002). However, neuroinvasion with *S. typhimurium* has only ever been reported following oral infection, including with the grandparent strain of SL3261, SL1344 (Bauler et al., 2017; Chaudhuri et al., 2018; Kaur et al., 2020; Wickham et al., 2007). Therefore, this suggests that direct exposure to microglia is unlikely but investigating this possibility via histology following i.p. injection would determine if it has occurred in ME7/SL3261 mice.

CD64 expression within the hippocampus and thalamus is significantly increased in ME7/SL3261 mice compared to Naïve mice (Figure 6.5, Figure 6.7). The response in both brain regions is the same, and not different between treatment groups. In addition, the greater increase in CD64 expression when compared to unchallenged ME7 mice (Figure 5.5, Figure 5.6) is the same for both brain regions (ca. three-fold). However, there are subtle differences between regions with respect to treatments in ME7/SL3261 mice. Hippocampal CD64 expression shows a trend towards being increased with mTNFR2-containing fusion proteins (Figure 6.5G). This could be due to the fact that inhibition of

TNF-α during *Salmonella* infection can attenuate granuloma formation and result in unsuppressed growth of bacteria (Mastroeni et al., 1993b; Mastroeni et al., 1995). These changes would then result in an increased and continued systemic response that may translate to increased microglial activation within the hippocampus. Analysis of serum cytokines between treatments in ME7/SL3261 mice could also identify whether there was an increased systemic response in mTNFR2-treated ME7/SL3261 mice. Interestingly, this possible effect on bacterial growth by TNF-α inhibition has no effect on thalamic expression of CD64 (Figure 6.7). This may be because of regional differences in response to *S. typhimurium*, where the hypothalamus/thalamus is involved in the anorexic response via gut-to-brain axis and Vagus nerve transmission (Rao et al., 2017; Wang et al., 2002). However, because there are no differences in weights between mTNFR2-treated ME7/SL3261 mice and other treatments (Figure 6.1C), this would suggest a lack of possible reactivation of *S. typhimurium* in the spleen although could be confirmed by culturing of spleen extracts. Surprisingly, treatment of ME7/SL3261 mice with $8D3_{130}$ hIgG1 TM resulted in a significant decrease in CD64 expression in the thalamus compared to ME7/SL3261 mice treated with NIP228 hIgG1 TM (Figure 6.7G). One possible explanation for this could result from the effects of $8D3_{130}$ hIgG1 TM on reticulocytes as discussed previously (Section 5.4.6). Reticulocyte numbers are known to be reduced following administration with anti-mTfR antibodies (Couch et al., 2013). This results in a shift in haematopoiesis towards extramedullary sites (Paulson et al., 2020), and it is possible that the compensatory increase in erythropoiesis and subsequent decrease in myelopoiesis effectively reduces the circulating monocyte population in $8D3_{130}$ hIgG1 TM-treated ME7/SL3261 mice compared to treatment with NIP228 hIgG1 TM.

Both *Tnf* and *Il1b* mRNA transcript levels in the hippocampus and thalamus are significantly increased nine weeks after infection with *S. typhimurium* in ME7 mice, with a 15.4- and 10.7-fold increase over Naïve control mice, respectively (Figure 6.9). These increases are approximately a three-fold increase in the levels observed in ME7 mice alone at 16 wpi (Figure 5.9) and suggest an exacerbated neuroinflammatory response following systemic bacterial infection. It must be noted that these differences may not be solely due to *S. typhimurium* infection and may be associated, in part, with inter-cohort variation.

Analysis of *Ccl2* transcript levels showed that levels are increased in all ME7/SL3261 mice compared to Naïve control mice by an average of 45.7-fold (Figure 6.9). Interestingly, $8D3_{130}$ hIgG1 TM ΔK-mTNFR2-treated ME7/SL3261 mice showed a reduction in *Ccl2* levels compared to its isotype control, suggesting that a TNF-α dependent effect was responsible for this difference. However, this was not observed with NIP228 hIgG1 TM ΔK-mTNFR2-treated ME7/SL3261. This may be due to peripheral effects of TNF-α inhibition in *S. typhimurium* infected mice, whereby removal of TNF-α can induce proliferation of bacteria within secondary lymphoid tissues, such as the spleen (Gulig et al., 1997; Mastroeni et al., 1991; Mastroeni et al., 1993b; Mastroeni et al., 1995; Rossi et al., 2017). The possibility of TNF-α inhibition induced proliferation may be evidenced by increases in spleen weights, as was observed in spleens from NIP228 hIgG1 TM ΔK-mTNFR2-treated ME7/SL3261 mice compared to Naïve controls (Figure 6.1).

Overall, the increased expression of CD64 and MHCII in both the hippocampus and thalamus, along with significant increases in proinflammatory cytokine expression, in ME7/SL3261 mice compared to NBH mice and ME7 mice alone suggests an exacerbatory effect of systemic inflammation on microglial activation during ongoing neurodegeneration, but that this is not altered by administration of anti-TNF fusion proteins four weeks after systemic bacterial infection.

6.4.4 Peripheral response to systemic bacterial challenge and bispecific mTNFR2 fusion protein treatment in ME7 mice

Weight changes in ME7 mice following infection with *S. typhimurium* SL3261 showed a monophasic response characterised by an initial decrease one day after injection followed by recovery to pre-injection weight seven days later (Figure 6.1). This response is akin to that observed in wild-type C57Bl/6 mice and is most likely mediated by the presence of LPS in the serum as this follows a similar pattern as weight loss (Püntener et al., 2012). Multiple injections of fusion protein in ME7/SL3261 mice had no effect on body weight, with all treatments showing an average week-on-week increase after the first injection (Figure 6.1). This suggests no long-term effects of *S. typhimurium* on food intake after the

initial acute anorexic response. Hippocampal TfR expression in ME7 mice was not changed by systemic bacterial infection (Figure 6.2), suggesting that availability of TfR following infection with *S. typhimurium* is not a limiting factor for delivery across the BBB in ME7 mice.

6.4.4.1 Splenic response to systemic bacterial challenge and bispecific mTNFR2 fusion protein treatment in ME7 mice

Systemic inflammation and proinflammatory cytokine production is known to induce EMH, shifting production towards myelopoiesis, and results in splenomegaly (Paulson et al., 2020). Increases in proinflammatory cytokines in the serum following *Salmonella* infection have been reported for IFNγ, IL-1β and TNF-α (Brown et al., 2013; Püntener et al., 2012). IL-1β has been shown to act directly on multipotential progenitor cells through increased expression of the transcription factor PU.1 to engage the production of myeloid cells and shifts cell fate away from erythrocyte production (Diederich et al., 2009; Pietras, 2017; Pietras et al., 2016). IFNγ has been shown to limit iron availability following *S. typhimurium* infection and also to increase PU.1 expression and erythrocyte turnover following chronic expression (Libregts et al., 2011; Nairz et al., 2008). TNF-α is known to limit erythropoiesis and facilitate the increased myelopoiesis necessary for the immune response through direct inhibition of Gata1-dependent transcription induces apoptosis in erythroid progenitors and decreases differentiation of erythrocytes (Papadaki et al., 2002; Rusten and Jacobsen, 1995; Tsopra et al., 2009; Xiao et al., 2002).

Analysis of spleens from ME7/SL3261 mice showed that only spleens from NIP228 hIgG1 TM ΔK-mTNFR2 treated mice showed a significant increase in weight when compared to Naïve spleens (Figure 6.1). Therefore, splenomegaly observed in NIP228 hIgG1 TM ΔK-mTNFR2 treated ME7/SL3261 mice could be due to direct mTNF-α inhibition and the effect this has within the spleen and on bacterial growth. It has been reported that treatment of *S. typhimurium* infected mice with anti-TNF treatments has resulted in expansion of bacteria within the spleen, and also within the liver, and thus could result in further splenomegaly (Gulig et al., 1997; Mastroeni et al., 1991; Mastroeni et al., 1993b; Mastroeni et al., 1995; Rossi et al., 2017). However, splenomegaly was not seen in spleens from $8D3_{130}$ hIgG1 TM ΔK-mTNFR2 treated ME7/SL3261 mice and could be due to

a differential distribution of fusion protein in the spleen given the role of the spleen in peripheral pharmacokinetics (Cataldi et al., 2017). TfR is expressed in the spleen and anti-TfR antibodies significantly distribute within the spleen compared to administration of transferrin or citrate (Sugyo et al., 2017). In future, analysis to assess bacterial load within the spleen by culturing spleen extracts from ME7/SL3261 mice and determining changes in bacterial colony formation between treatment groups would elucidate whether peripheral inhibition of mTNF-α results in growth of bacteria within the spleen.

$8D3_{130}$ hIgG1 TM treated ME7/SL3261 mice showed a trend towards a significant increase in spleen weight compared to Naïve mice (Figure 6.1). An increase in spleen size was observed in ME7 mice treated with $8D3_{130}$ hIgG1 TM, not challenged with *S. typhimurium* (Figure 5.1) and there are several possible reasons for this observation. Firstly, the transient effect of anti-mTfR antibodies on reticulocytes, with reticulocyte numbers returning to pre-injection levels after seven days following four weekly injections (Couch et al., 2013). It is possible that analysis 14 days after final injection allows for a return to homeostatic haematopoiesis and as a result a reduction in EMH. Secondly, systemic bacterial challenge with *S. typhimurium* appears to mask the effects of $8D3_{130}$ hIgG1 TM on the spleen, with no increase in spleen weight compared to other treatments seven days after final injection (Figure 6.10). Infection with *S. typhimurium* results in increased circulating reticulocytes and an increase in immature erythrocyte populations in the spleen, suggestive of EMH (Hyland et al., 2005; Jackson et al., 2010). This suggests that infection-induced splenomegaly could also contribute to the change in spleen weight seen and combined with a reduction in anti-mTfR-induced EMH, could explain the mild splenomegaly found in $8D3_{130}$ hIgG1 TM treated ME7/SL3261 mice. Finally, inhibition of mTNF-α could limit induction of EMH following bacterial infection, and anti-mTfR treatment, by preventing the effects of TNF-α on bone marrow haematopoiesis (Paulson et al., 2020). Thus, contributing to the difference in spleen weights between $8D3_{130}$ hIgG1 TM and $8D3_{130}$ hIgG1 TM ΔK-mTNFR2 treated ME7/SL3261, with the latter spleens no different in weight compared to spleens from ME7/SL3261 mice treated with NIP228 hIgG1 TM (Figure 6.1).

6.4.5 Safety and tolerability of bispecific mTNFR2 fusion proteins after systemic inflammatory challenge

The *in vivo* safety experiment using *S. typhimurium* was designed to test for the likelihood of any adverse effects if with administration of the fusion proteins was attempted earlier than four weeks after infection with *S. typhimurium*. The timing of intervention at 10 days after *S. typhimurium* infection was selected because this allowed for granuloma formation and establishment of a plateau in bacterial growth, which have been shown to be associated with TNF-α function and are significantly affected by inhibition (Mastroeni et al., 1992; Mastroeni et al., 1993b).

Systemic infection with *S. typhimurium* resulted in a significant decrease in body weight for all mice one day after injection which is in line with previous findings (Püntener et al., 2012) (Figure 6.10). All mice showed increased spleen weights compared to naïve mice (1.08 g versus 0.11 g; Figure 6.10, Figure 6.1) suggestive of splenomegaly observed following infection with *S. typhimurium* SL3261, albeit with large variation (Peters et al., 2010). Interestingly, two spleens from the vehicle-injected mice showed a relatively smaller degree of splenomegaly compared to all other mice (401 mg average versus 1162 mg average; Figure 6.10). This suggests a lower activation of the innate and adaptive immune response and could be reflective of a smaller initial weight loss. The two vehicle-injected mice that had smaller spleens at termination, lost an average of 2.50% body weight one day after infection with *S. typhimurium* compared to an average of 6.56% for all other mice. However, this is unlikely to have affected overall observations of adverse effects.

The experiment was designed to look for changes in mouse body weight and home cage behaviour through daily monitoring to judge if mTNF-α inhibition induced any adverse effects. There was no change in mouse body weights in the first three days after fusion protein or control treatments. However, from three days after injection there was a decrease in body weights in mice injected with anti-mTfR targeting fusion proteins, $8D3_{130}$ hIgG1 TM and $8D3_{130}$ hIgG1 TM ΔK-mTNFR2, but not isotype control fusion proteins. This would indicate a specific effect from binding to mTfR, independent of mTNF-α function, possibly on reticulocytes as discussed earlier (Section 5.4.6). Although, no changes to normal mouse behaviour were noted, it is possible that these were not observed during

the daily monitoring periods. Together, the body weight data and lack of alterations to normal mouse behaviours suggests that administration of bispecific mTNFR2 fusion proteins during ongoing systemic bacterial infection does not adversely affect mice. Thus, interventions against TNF-α could be attempted at earlier timepoints following *S. typhimurium* infection in ME7 mice in future experimentation without the expectation of adverse effects.

Analysis of CD64 and MHCII expression within the hippocampus confirmed induction of expected response following infection with *S. typhimurium* SL3261 (0). Analysis of brain cytokine expression showed no difference between treatment groups seven days after administration in *S. typhimurium*-infected mice, with considerable variation observed (Appendix G4). Analysis of TfR expression in the hippocampus of mice following systemic challenge with *S. typhimurium* was conducted to assess potential confounding issues with enhanced delivery across the blood-brain barrier. TfR expression remained unchanged between treatment groups suggesting that enhanced delivery across the BBB is not limited by an ongoing inflammatory response (Appendix G3). TfR mRNA expression in the spleen was also unaffected by systemic bacterial infection (Appendix H1). Further analysis of spleens was completed to investigate changes at the cellular and molecular level that could be attributed to inhibition of mTNF-α. Analysis of macrophage markers (CD68, CD11b) showed no differences between treatment groups, and this was also observed for analysis of cytokine immune markers (TNF-α, IL-1, IL-10, IL-12) induced following systemic *S. typhimurium* infection (0). It is possible that measuring spleen mRNA levels seven days after administration and 17 days after infection does not reflect protein levels which are increased two weeks after *S. typhimurium* (Püntener et al., 2012). Therefore, investigation of protein levels in both the periphery and the brain would help to identify *in vivo* neutralisation of mTNF-α after bacterial infection with *S. typhimurium*.

Overall, these data suggest that administration of bispecific mTNFR2 fusion proteins is unlikely to induce adverse events in C57BL/6 mice when administered 10 days post-infection with *S. typhimurium* and thus suggests that earlier intervention in models of systemic inflammation combined with neurodegeneration could be investigated, as discussed previously.

6.4.6 Summary

Systemic bacterial challenge in ME7 mice results in exaggerated neuroinflammation compared to non-infected ME7 mice. However, treatment with bispecific mTNFR2 fusion proteins had no effect on disease progression or neuropathology. This lack of modulation is possibly due to timing of administration with first injection given four weeks after infection. It is possible that this time point was too late, and it may be more important to limit systemic response prior to induction of central cytokine production and this should be investigated in future works. Furthermore, administration of bispecific mTNFR2 fusion proteins 10 days following systemic challenge with *S. typhimurium* had no adverse effects on weight loss or normal mouse behaviours in naïve C57BL/6 mice suggesting that earlier intervention could be tolerated.

Chapter 7 General Discussion

Alzheimer's disease (AD) is the most common neurodegenerative diseases, which currently has no disease-modifying treatment available. This is also the case for other neurodegenerative diseases, and whilst the underlying pathophysiology of these diseases are different, they have a common factor: neuroinflammation. Neuroinflammation has been suggested to contribute to disease progression and therefore presents a common target for multiple neurodegenerative diseases. Furthermore, there is evidence that systemic inflammation can negatively impact on cognitive function and hasten decline in patients with AD. The main aim of this thesis was to investigate the role of neuroinflammation in a model of neurodegeneration and the effects of systemic bacterial infection on neuroinflammation. In addition, this rationale allowed for identification of suitable cytokine targets for intervention in a model of chronic neurodegeneration in the presence and absence of systemic bacterial infection.

7.1 Targeting neuroinflammation in neurodegeneration

The transcript levels for the proinflammatory cytokines, TNF-α and IL-1β, in the hippocampus and thalamus are increased in ME7 mice over NBH mice as disease progresses, with peak expression for TNF-α at 12 and at 16 wpi for IL-1β. Following peak expression both cytokines show decreases in expression to similar levels as observed in NBH or Naïve at 18 wpi (Section 3.3.3). This time course of changes in central cytokine expression for TNF-α and IL-1β have been reported in other strains of murine prion disease, including RML and 22L, suggesting a common neuroinflammatory response in models of neurodegeneration (Carroll et al., 2016, 2015; Carroll and Chesebro, 2019). Evidence from mouse prion models also shows a possible role for IL-1β in disease progression, with genetic ablation of IL-1RI resulting in attenuated astrogliosis and increased incubation times following intracerebral inoculation with prion strain 139A (Schultz et al., 2004). Genetic ablation of TNF-α had no effect on incubation times following intracerebral inoculation of ME7 compared to WT controls (Mabbott et al., 2000). Whilst modulating TNF signalling, through ablation of TNFRs, resulted in decreased

incubation times following inoculation with RML prion (Tamgüney et al., 2008). Furthermore, *in vivo* testing of a brain-penetrant IL-1RA fusion protein in inflammatory models failed to have any effect on central cytokine production and therefore suggested that inhibiting central IL-1β would not prove beneficial (Appendix D; Daniel Cohn, personal communication). Although, these IL-1RA fusion protein experiments were conducted in the absence of neurodegeneration, it may be that under conditions of inflammation and neurodegeneration combination therapy against multiple cytokines may be beneficial.

Microglia are the resident immune cells of the brain and are known to produce cytokines in response to both central and peripheral inflammation (Perry and Teeling, 2013; Rivest, 2003; Teeling and Perry, 2009). TNF-α expression in the brains of Tg2576 mice and post-mortem AD brain is found in glial cells associated with amyloid plaques (Benzing et al., 1999; Zhao et al., 2003). Therefore, microglia are an attractive neuroinflammatory target in neurodegeneration. Peripheral administration of a CSF1R inhibitor, that blocks microglial proliferation, in ME7 mice resulted in a delayed onset of behavioural deficits and decreased hippocampal neurodegeneration compared to Vehicle-treated ME7 mice (Gómez-Nicola et al., 2013). In addition, treatment of APP/PS1 mice with GW2580 improved performance in memory and behavioural tasks as well as preventing synaptic degeneration, without affecting neuropathology (Olmos-Alonso et al., 2016). It is possible that the targeting of TNF-α producing cells, such as microglia, may be more beneficial for ameliorating cognitive and behavioural deficits than inhibiting signalling by TNF-α in models of neurodegeneration.

7.1.1 The role of TNF in early neurodegeneration

The changes in TNF-α expression in ME7 mice can be correlated to changes in disease pathology, with peak expression coinciding with onset of burrowing changes and sustained expression continuing through synaptic dysfunction and locomotor deficits (Section 3.3) (Chouhan et al., 2017). The changes in behaviour and synaptic function observed during the asymptomatic phase of ME7 prion disease may reflect subjective changes in the human population, akin to mild cognitive impairment (MCI). Functional pathway analysis identified 'TNF signalling' as correlated with phosphorylated Tau levels

in the cerebrospinal fluid (CSF) of MCI patients in both cross-sectional and longitudinal cohorts (Pillai et al., 2019). However, studies that have investigated CSF levels of TNF-α in MCI/AD have shown mixed results with TNF-α being reported as not changing or being up- or downregulated depending on the study (Brosseron et al., 2014; de la Monte et al., 2017; Swardfager et al., 2010). However, although CSF TNF-α levels themselves did not correlate with disease severity, when combined with markers of neurodegeneration in CSF samples, such as oligomeric α-synuclein and phosphorylated tau, TNF-α can be predictive of risk for PD in asymptomatic subjects (Delgado-Alvarado et al., 2017; Majbour et al., 2020). These data suggest that higher levels of TNF-α appear to be associated with evident cognitive dysfunction, rather than being predictive of progression to more severe cognitive decline from MCI to AD. The above studies in human patients would propose that increasing levels of TNF-α may have a role in the progression of neurodegeneration and warrants targeting (Decourt et al., 2017; Ekert et al., 2018; Shamim and Laskowski, 2017; Torres-Acosta et al., 2020). However, they also suggest the role of TNF-α in neurodegeneration is complex and differential depending on disease-type as well as stage of disease progression and therefore may not be straightforward to target in neurodegeneration.

Previous studies have reported that in mice genetically deficient for TNF-α prevents development of scrapie in a peripherally induced model and pharmacological inhibition with a huTNFR:Fc fusion protein prior to ME7 prion inoculation delays transfer of prions to the brain (Mabbott et al., 2002, 2000). However, peripheral administration of a huTNFR:Fc fusion protein before intracerebral inoculation had no effect on incubation period and suggests that establishment of disease within the CNS is not affected by inhibition of TNF-α signalling in the periphery (Mabbott et al., 2002). These results could be explained by a lack of brain penetration by the huTNFR:Fc fusion protein and thus improving delivery to the brain could have resulted in better outcomes. These studies suggests that enhanced delivery of anti-TNF therapeutics to the brain might improve the possibility of delaying disease progression in ME7 prion.

7.1.2 Targeting TNF in neurodegeneration

In this thesis, I describe the neuroinflammatory changes in the ME7 prion model and the effect of blocking TNF-α in neurodegeneration alone. Neutralisation of TNF-α from 12 wpi in ME7 mice had no significant effects on mouse behaviours, proinflammatory cytokine production nor synaptic marker expression (Section 5.3). When given at 12 wpi for four weeks bispecific mTNFR2 fusion proteins, which are engineered for enhanced delivery across the BBB, had no effect on onset of behavioural deficits in ME7 mice compared to isotype controls (Figure 5.3). This may because intervention was started at the peak of transcriptional expression, when synaptic dysfunction is already observed (Chiti et al., 2006). Thus, although TNF-α may be inhibited after this point the downstream processes involved in synaptic dysfunction may not be altered by changes in TNF-α levels. This would ultimately limit the effects of TNF-α inhibition to changes occurring after administration and therefore may be too late to repair any effects on behaviour and synaptic dysfunction. Therefore, additional clinical and experimental investigations are required to fully understand the benefits of targeting TNF-α and at what stage of disease would it be most beneficial. Analysis of synaptic function, beyond transcriptional expression of limited markers, was not possible due to the tissue processing methods used in this thesis which were chosen to prioritise the analysis of microglial function. A further understanding of the effects of TNF-α inhibition in ME7 mice on synaptic functions, such as LTP, would determine whether there are any beneficial effects, irrespective of disease progression, that could inform improved therapeutic regimen. In addition to the behavioural tests associated with monitoring disease progression, testing of behaviours linked to hippocampal function and cognition could be investigated. For example, the alternating Y/T-maze would add value to the current experimental outputs as it is altered in ME7 mice and affected by systemic inflammatory challenge (Davis et al., 2015; Griffin et al., 2013; Hennessy et al., 2017; Murray et al., 2012). Further investigation would be highly valuable for determining a better time point for intervention in the murine ME7 prion model to protect cognitive functions.

The testing of multiple dosing regimens was not investigated in this thesis. The tested treatment of four weekly injections of bispecific mTNFR2 fusion protein had no effect in ME7 mice. It is possible that the intervention against TNF-α was too late and that earlier intervention from 8 wpi could prove more beneficial in the murine ME7 prion model. An

earlier intervention would delay peak expression of TNF-α and could delay the onset of behavioural changes and alter disease progression. It is also possible that prolonged TNF-α inhibition, for example continued administration of mTNFR2 fusion proteins, is required to prevent any increases in TNF-α expression.

7.1.3 Alternative TNF-α interventions

Currently approved anti-TNF-α therapies are licensed for a variety of inflammatory diseases such as RA, IBD, Crohn's disease (CrD) and psoriasis. These therapies include infliximab, adalimumab and golimumab, which are monoclonal antibodies against TNF-α; certolizumab pegol, which is a polyethylene glycol-conjugated Fab domain of an anti-TNF-α antibody; and etanercept, a hIgG1 Fc-TNFR2 fusion protein (Fischer et al., 2015; Steeland et al., 2018). All therapies prevent signalling at both receptors by interacting with TNF-α directly, albeit with different affinities, and inhibition of tmTNF-α occurs at lower affinities than sTNF-α (Billmeier et al., 2016; Kaymakcalan et al., 2009). Etanercept has a greater affinity for sTNF-α than anti-TNF-α antibodies, however its binding is saturated with lower concentrations of TNF-α (Kaymakcalan et al., 2009). Furthermore, it is apparent that different effector mechanisms, mediated by FcγR interactions and outside-in signalling are important for efficacy in certain diseases, such as CrD and IBD (Dong et al., 2015; Steeland et al., 2018). Outside-in signalling, or reverse signalling, is triggered by binding of anti-TNF-α therapeutic to tmTNF-α and induction of apoptosis (Kirchner et al., 2004b, 2004a). Etanercept has a lower affinity for tmTNF-α compared to anti-TNF-α antibodies and it is this property that may limit its efficacy in some conditions (Billmeier et al., 2016; Steeland et al., 2018). A recent study reported that the introduction of two mutations (W89Y/E92N) in the TFNR2 domain of etanercept, designated T0001, results in increased affinity for sTNF-α and greater neutralisation of TNF-α-induced cytotoxicity and at ameliorating symptoms of CIA compared to etanercept (Shen et al., 2017; Yang et al., 2010). Compared to $8D3_{130}$ hIgG1 TM ΔK-mTNFR2, which is a brain-penetrant etanercept-like therapeutic, the increased activity shown by T0001 may prove beneficial as this would direct TNF-α activity towards TNFR2 signalling and its neuroprotective effects.

Increasingly there is a drive towards activating TNFR2 signalling as a therapeutic approach in neurodegeneration, which comes from evidence that TNFR2 signalling in the brain is neuroprotective (Dong et al., 2015; Ortí-Casañ et al., 2019). Experimental evidence has shown that deletion or silencing of TFNR2 can exacerbate pathology in 3xTg-AD mice; whilst deletion of TNFR1 attenuated pathology (He et al., 2007; Montgomery et al., 2013, 2011). However, in models of PD, the role of TNFRs is somewhat disputed with double TNFR KO being protective from 1-methyl-4-phenyl-1,2,3,6-tetrahydropyridine (MPTP)-induced neurodegeneration, whilst individual TFNR1 or TNFR2 KO having no effect on disease pathology (Leng et al., 2005; Sriram et al., 2006, 2002). However, selective activation of TNFR2 in an *in vitro* model of PD was protective of dopaminergic neurons in the substantia nigra (Fischer et al., 2011). Clinical evidence also shows that TNF-α levels in the brains of AD and PD patients is increased (Kouchaki et al., 2018; Zhao et al., 2003). Moreover TNF-α may have a greater affinity for TFNR1 than TNFR2 in AD brains compared to non-demented controls (Cheng et al., 2010). This complex involvement of TNF-α in cognitive function and disease progression may explain why intervention in ME7 prion with bispecific mTNFR2 fusion proteins had no effect on behavioural changes nor microglial activation.

It may be that alternative approaches for targeting TNFR2 signalling are required for efficacy in neurodegenerative diseases. Selective inhibition of TNFR1 signalling using dominant-negative inhibition of sTNF-α with mutein TNF-α monomers (dnTNFs) has been investigated in models of AD and PD (Fischer et al., 2015; McCoy and Tansey, 2008; Steeland et al., 2018). XPro1595, also known as XENP1595, and XENP345 are examples of dnTNFs that show significantly impaired binding to TNFRs and reduce TNF-induced caspase activity due to the introduction of specific mutations (Steed et al., 2003; Zalevsky et al., 2007). In the 6-OHDA model of PD in rats, direct infusion of XENP345 for three weeks or lentiviral expression of XPro1595 in the substantia nigra from the time of lesion resulted in protection of dopaminergic neurons and reduction in behavioural deficits (McCoy et al., 2008, 2006). Furthermore, peripheral administration of XPro1595 initiated either three or 14 days after 6-OHDA injection resulted in reduced gliosis five weeks after lesion. However, only treatment from three days after lesion was able to protect significant numbers of tyrosine hydroxylase-positive neurons in the substantia nigra compared to saline-treated 6-OHDA animals (Barnum et al., 2014). In a model of

amyloidopathy, peripheral administration of XPro1595 prior to deposition of amyloid plaques was able to prevent the later development of synaptic dysfunction induced by increased glutamate excitability (Cavanagh et al., 2016). When given after deposition of extracellular amyloid in the 5xFAD model of AD, peripheral treatment with XPro1595 between five and seven months was able to ameliorate LTP impairments in 5xFAD mice compared to non-transgenic controls, but only modestly reduced amyloid plaque deposition and *Ccl2* transcript levels (MacPherson et al., 2017). These effects could be mediated through alterations in the immune cell profile in both the periphery and the brain. XPro1595 treatment was able to reduce MHCII+ cells in resting and activated microglial populations and also modulated T cell populations (MacPherson et al., 2017). In 3xTg-AD mice, XENP345 was able to prevent amyloid deposition when administered i.c.v. via osmotic pump during repeated LPS challenge (McAlpine et al., 2009). Combined these experiments suggest that targeting of sTNF-α could be beneficial in models of neurodegeneration, but strongly highlight the need for early interventions for these beneficial effects. Moreover, it may be through modulation of T cell populations that XPro1595 treatment had it effects after onset of pathology in 5xFAD mice. The effects of bispecific mTNFR2 fusion protein administration on T cell populations in ME7 mice should be investigated and the results may elucidate why this treatment proved unsuccessful both in unchallenged ME7 mice but also following systemic bacterial challenge.

7.1.4 Summary

Targeting of TNF-α, although guided by evidence from clinical studies that implicated elevated CSF levels with disease progression and increased expression in ME7 mice prior to onset of behavioural deficits, proved unsuccessful in ME7 mice using bispecific mTNFR2 fusion proteins. It is possible that earlier intervention and additional behavioural outputs, specifically focused on cognition, may be required to observe efficacy of TNF-α inhibition in ME7 prion disease. Furthermore, alternative anti-TNF-α approaches that direct signalling towards TNFR2 and modulation of immune cell populations, through combination therapy with other cytokines, could also prove beneficial and should be investigated.

7.2 Systemic inflammation, TNF-α and neurodegeneration

7.2.1 Effects of systemic inflammation on neuroinflammation

It has been shown that peripheral infection-induced inflammation, from bacteria such as *P. gingivalis*, in patients can increase disease risk and drive disease progression, whilst in in animal models of neurodegeneration systemic inflammation can exacerbate disease pathology (Giridharan et al., 2019; Ide et al., 2016; Lim et al., 2015; Machado et al., 2011; O'Banion, 2014; Olsen et al., 2020). In Chapter 3, I show that a peripheral challenge with an attenuated strain of *S. typhimurium* results in a robust neuroinflammatory response, with increased microglial activation and cytokine production in the brain four weeks after challenge in ME7 mice. Furthermore, there was an exaggerated neuroinflammatory response when ME7 mice were infected at 12 wpi compared to 8 wpi, suggesting that when underlying neuropathology is more advanced (e.g., in older mice) a greater effect is observed in the brain (Section 3.3.4). In ME7 mice this exaggerated response could be due to increased glial numbers as microglial and astrocytic proliferation is a key component of disease progression during the two timepoint when systemic challenge was administered (Gómez-Nicola et al., 2013).

When looking at the role of gliosis in modulating the effects of systemic inflammation on neuroinflammation during neurodegeneration, it is apparent that underlying glial pathology is important in the neuroinflammatory response. Interestingly, intracerebroventricular injection of α-synuclein oligomers one month after peripheral injection of LPS induced a reduction in hippocampal LTP, exaggerated microglial activation and synaptic dysfunction when compared to α-synuclein oligomer administration alone (La Vitola et al., 2021). This suggests that activation of microglial prior to a pathological treatment can detrimentally exaggerate future insults and may also worsen cognitive function. Furthermore, in mice overexpressing A53T mutant human α-synuclein, systemic challenge with LPS results in significant reductions in novel object recognition, Morris water maze and Y-maze behaviours, as well as reduced tyrosine hydroxylase immunoreactivity in the substantia nigra that appear alongside increased IBA-1 expression (Gao et al., 2011; La Vitola et al., 2021).

Microglial priming is characterised by expression of CD11c and Dectin-1, as well as MHCII , and is evidenced through exaggerated responses to secondary activating stimuli during neurodegeneration (Neher and Cunningham, 2019; Perry and Holmes, 2014). Additionally, it has also been reported after infection with *S. typhimurium* (Püntener et al., 2012). Evidence that priming has occurred in ME7/SL3261 mice comes from increased expression of MHCII and CD64 and exaggerated cytokine production within the hippocampus and thalamus compared to non-infected ME7 mice (Figure 6.9 vs Figure 5.9). These data suggest that an initial insult has provided microglia with an immune memory response that is trained, or primed, for a secondary stimulus and results in an enhanced response over that expected in naïve unprimed microglia. In the current scenario, systemic bacterial challenge in ME7 mice with *S. typhimurium* at 8 wpi is the primary insult, due to the lack of pathology and microglial activation at this time point (Betmouni et al., 1996; Betmouni and Perry, 1999; Gómez-Nicola et al., 2013). The second activating stimulus that results in a trained, or priming, response is the deposition of pathological prion protein, synaptic dysfunction, and resultant microglial activation. It has been reported that extravascular expression of MHCII, activation of microglia and increased expression of proinflammatory cytokines are archetypal responses from primed microglia (Cunningham et al., 2005; Cunningham et al., 2009; Lunnon et al., 2011; Püntener et al., 2012). Furthermore, evidence of a trained response comes from decreased production of IL-10. Transcripts levels of *Il10* in the hippocampus have not been investigated in this study but could help to understand in part whether a trained response is being observed in ME7/SL3261 mice nine weeks after initial bacterial challenge. In addition, understanding the transcriptomic and epigenetic changes associated with this exaggerated response would help elucidate whether this is indeed a trained, or primed, microglial response, as observed before (Neher and Cunningham, 2019; Wendeln et al., 2018).

7.2.2 Safety of TNF-α inhibition during systemic bacterial infection

Previous reports have shown that anti-TNF treatment during the first two weeks of bacterial infection with *S. typhimurium* can increase infection severity and thus presents a safety concern when investigating the effects of anti-TNF-α treatment following bacterial

challenge. Here I have shown that a single dose of bispecific mTNFR2 fusion protein ten days after systemic bacterial challenge with *S. typhimurium* SL3261 is safely tolerated in naïve C57BL/6 mice. Neutralisation of TNF-α prior to systemic bacterial infection has not been investigated in ME7 prion mice. Therefore, to avoid unexpected adverse effects in neurologically compromised mice, the treatment regimen used reflected that given to ME7 mice without additional inflammatory challenge. In future it will be necessary to determine safety of pre-treatment with anti-TNF-α treatment in naive *S. typhimurium* SL3261-challenged mice before considering an alternative dosing regimen for ME7/SL3261 mice.

7.2.3 Efficacy of targeting TNF-α following systemic bacterial infection in a model of neurodegeneration

The most convincing data for targeting TNF-α in neurodegeneration come from studies that look at the effect of anti-TNF-α treatment in patients with an increased risk of AD and PD. The incidence of AD and PD is significantly increased in patients with chronic inflammatory conditions, such as RA, CrD, IBD and psoriasis, compared to the general population (Zhou et al., 2020). This increased risk is significantly reduced in patients that have been exposed to anti-TNF-α treatments, whether that be in the form of direct immunotherapy, such as adalimumab and infliximab, or indirect neutralisation with etanercept (Chou et al., 2016; Elfferich et al., 2010; Park et al., 2019; Peter et al., 2018; Zhou et al., 2020). In addition, SIEs can have a negative impact on disease onset and/or progression and that increased serum TNF-α is associated with an increased rate of cognitive decline (Holmes et al., 2011, 2009, 2003).

Moreover, the effects of systemic TNF-α on neuroinflammation may not be limited to acute systemic inflammatory events as peripheral TNF-α levels are increased in neurodegenerative diseases. Increased serum TNF-α levels were measured in a cohort of MCI patients compared to age-matched cognitively normal controls, and also correlated to a reduction in hippocampal functional connectivity (Magalhães et al., 2017; Shen et al., 2019). Furthermore, serum TNF-α has been shown to be increased in both early and late-onset AD patients and was associated with cognitive impairment in a population of elderly patients (Gezen-Ak et al., 2013; Huang et al., 2020). In addition, increased serum

TNF-α levels are observed in PD and MS, with a correlation to progressive forms of MS and severity and duration of disease in PD; as well as being associated with categorization of PD patients from healthy controls (Eidson et al., 2017; Fresegna et al., 2020; Kouchaki et al., 2018). Interestingly, peripheral levels of IL-1β in AD patients do not correlate with changes in cognition, even though they are found to be frequently increased (Dursun et al., 2015; Lai et al., 2017; Ng et al., 2018). These data suggest that the targeting of both systemic and central TNF-α should have a therapeutic benefit.

A bacterial challenge at an early stage of ME7 prion disease, prior to overt neuropathology, was selected to test if a microbial infection influences disease progression. Such a scenario would be most attractive as a therapeutic strategy and intervention with bispecific mTNFR2 fusion proteins was investigated. Systemic bacterial challenge with *S. typhimurium* in ME7 mice at 8 wpi resulted in increased cytokine production when compared to levels of non-infected ME7 mice at a similar time point (Figure 6.9 vs Figure 5.9). This suggests that an early systemic bacterial challenge can have long-lasting effects on the neuroinflammatory status of ME7 mice. Furthermore, systemic challenge resulted in an earlier onset of behavioural deficits compared to non-infected ME7 mice (Figure 6.3 vs Figure 5.3). These neuroinflammatory and behavioural changes have also been observed following challenge with LPS in ME7 mice, although at later timepoints due to the acute effects of LPS (Davis et al., 2015; Griffin et al., 2013; Hennessy et al., 2015; Murray et al., 2011).

Intervention with bispecific mTNFR2 fusion proteins starting at 12 wpi, which was four weeks after *S. typhimurium* infection, had no effect on disease progression in ME7 mice. However, I have shown that treatment of mice with mTNFR2 fusion protein prior to challenge with LPS results in a trend towards reduced proinflammatory cytokine production, this identifies *in vivo* inhibition from mTNFR2 treatment (Figure 5.11). It is likely that the inflammation-induced changes to cytokine production and microglial activation in ME7 mice are already established four weeks after challenge and therefore inhibition of TNF-α has no impact on disease progression. Although intrahippocampal infusion with anti-TNF therapeutic, XENP345, can prevent LPS-induced increases in amyloid plaque immunoreactivity in 3xTgAD mice (McAlpine et al., 2009). The administration of anti-TNF and LPS was concurrent and therefore this may have contributed to the effects observed. Furthermore a systemic bacterial challenge evokes

neuroinflammatory responses that are observed later and this profile is more akin to the clinical setting (Hoogland et al., 2018). Challenge with *P. gingivalis* in APP transgenic mice results in increased amyloid and plaque loads, as well as increases in brain levels of TNF-α and IL-1β (Ishida et al., 2017). Furthermore, time spent investigating novel object was also decreased following peripheral administration of *P. gingivalis* (Ishida et al., 2017). In addition, bacterial challenge with another Gram-negative bacterium, *Helicobacter pylori*, can increase $A\beta_{42}$ production and affect cognition in rats, whilst direct challenge with *S. typhimurium* in the brain of 5XFAD mice results in Aβ deposits (Kumar et al., 2016; X.-L. Wang et al., 2014). Moreover, *Salmonella*-induced colitis can increase susceptibility to oral prion disease by 2.3-fold in C57Bl/6 mice (Sigurdson et al., 2008). Interestingly, a common allelic mutation in *Lrkk2* associated with PD results in reduced bacterial growth and increased survival following *S. typhimurium* infection in mice (Shutinoski et al., 2019).

S. typhimurium activates both an innate and adaptive immune response as opposed to LPS challenge and therefore there are multiple activation pathways that can contribute to its effects on ME7 mice and the establishment of these effects prior to TNF-α inhibition. These data suggest that live bacterial infections have a multitude of differential effects on mice and that targeting after systemic inflammation may require interventions in multiple pathways, not just single cytokines. Measurements of cytokines protein levels in the brain and periphery following systemic infection were not investigated in the current study. Evaluating the time course of cytokine protein levels in the brain following infection with *S. typhimurium* could help identify a better time point for intervention as the current treatment starting four weeks later had no effect on cytokine transcript levels. Furthermore, T-cell infiltration has been reported in ME7 mice (Ursula Püntener, unpublished observations) and therefore understanding the interplay between microglia and T cells both in ME7 prion disease and following systemic bacterial infection could elucidate potential changes in microglial function, such as immune suppression, and could identify other read-outs for future therapeutic interventions.

As is observed in the clinic, systemic inflammation is sometimes unpreventable in patients prior to development of AD and these may still be exacerbatory during disease (Davis et al., 2015). The data presented in this thesis suggests that anti-TNF-α treatment after systemic bacterial challenge is unlikely to limit the co-morbid effects or delay disease progression in a mouse model of chronic neurodegeneration. It has previously been

reported that a single dose of etanercept has possible benefits in limiting cognitive decline in mild-to-moderate AD patients, but inflammatory status of patients compared to placebo was not different (Butchart et al., 2015). This suggests that treatment prior to systemic inflammatory challenge could still be beneficial in the context of neurodegeneration. Therefore, investigating whether a treatment course started before or concurrent with *S. typhimurium* challenge in ME7 mice would provide valuable information as to whether TNF-α inhibition alone is sufficient to prevent the exacerbatory effects of systemic inflammation on neuroinflammation in models of neurodegeneration.

7.2.4 Summary

Systemic bacterial challenge in ME7 mice results in cytokine production in the brain four weeks later. This cytokine response is exaggerated with increased neuropathology during disease progression. Inhibition of TNF-α using bispecific mTNFR2 fusion proteins following systemic bacterial challenge in ME7 prion had no effect on disease progression. It may be necessary to prevent increased cytokine production in the brain during systemic inflammation to see a therapeutic benefit and therefore, timing of intervention should be reconsidered in future experiments.

7.3 Enhanced brain delivery of therapeutics for AD

7.3.1 Application of enhanced delivery of biologics in AD

Adjusting the delivery route of therapeutics was considered a viable option to improve delivery to the brain, with direct administration into the CSF via perispinal/intrathecal or intracerebroventricular (i.c.v.) injection. Perispinal injection of etanercept in clinical settings has reputably shown both acute and sustained improvements in patients following weekly treatments (Tobinick et al., 2006; Tobinick and Gross, 2008). It was thought that this delivery to the CSF would improve outcomes compared to traditional subcutaneous administration which failed to show any benefit over placebo (Bohac et al., 2002). However, intrathecal or i.c.v. delivery of a therapeutic only results in accumulation in the lateral ventricles and at the choroid plexus, and not parenchymal distribution as

would be desired for treatment of CNS disorders (Tobinick et al., 2009; Yadav et al., 2017). Furthermore, efficacy of therapeutic delivery to the CSF has only been observed where the target is located either on the surface of the brain, accessible via the spinal column, or within diffusion range of the injection site (Pardridge, 2020b).

It is thought however that engineering immunotherapies to take advantage of natural transport mechanisms, such as RMT, across the BBB and improve delivery to the brain parenchyma would overcome distribution issues and increase the likelihood of effective treatments for CNS disorders. Using RMT to improve delivery across the BBB was considered an important factor in study design in this thesis with the aim of testing whether enhanced brain penetration with a bispecific mTNFR2 fusion protein can alter disease progression. There was no effect on disease progression in the ME7 prion model of chronic neurodegeneration using this approach though, as discussed previously – with timing of intervention perhaps being a contributing factor. However, a similar approach was shown to reduce microgliosis, Aβ levels and improve cognition in a mouse model of AD when compared to its peripherally acting analogue, etanercept (Chang et al., 2017).

Effective delivery of fusion protein across the BBB *in vivo* has not been established in this thesis and should be investigated in future through detection of human IgG Fc within mouse brain tissue. Bispecific mTNFR2 fusion proteins were designed to show enhanced brain penetration by targeting mTfR and *in vitro* they possess the required characteristics for enhanced delivery *in vivo*. Observations of a trend towards greater inhibition of hippocampal TNF production following LPS challenge with $8D3_{130}$ hIgG1 TM ΔK-mTNFR2 compared to NIP228 hIgG1 TM ΔK-mTNFR2 suggest successful delivery. However, preliminary evidence from detection of ADAs suggests there could be a difference in clearance between isotype control antibodies and fusion proteins (Appendix F), and this could impact on the pharmacokinetics and brain delivery. Furthermore, in ME7 mice systemic inflammatory challenge with LPS results in significant extravasation of IgG into the brain parenchyma compared to NBH control mice (Lunnon et al., 2011). Whether this phenomenon occurs following systemic bacterial infection should also be investigated as this could effectively render enhanced delivery unnecessary if BBB permeability to IgG is increased and brain delivery of biologics also increases. The effects of *S. typhimurium* infection in ME7 mice on BBB permeability could be investigated by immunohistochemistry for IgG and fibrinogen extravasation.

All future approaches to treat CNS disorders need to include the consideration of improved brain penetrance for future generations of drug development to improve the chance of clinical approval. Safe and tolerable administration of BBB-penetrating fusion proteins following systemic administration (i.v.) has been reported in open-label clinical trials in patients with mucopolysaccharidosis (MPS) Type I and II (Giugliani et al., 2018; Okuyama et al., 2020, 2019). In both patient populations safety end-points were met, with additional reporting that neurocognitive developmental issues were either maintained or showed some improvement in patients over the course of the studies (Giugliani et al., 2018; Okuyama et al., 2020). Therefore, these studies provide evidence for efficacious treatment of CNS-dependent symptoms due to successful brain penetration with re-engineered therapeutic proteins.

In line with this, Roche have entered the first RMT-targeted anti-Aβ antibody, with a single Fab domain of an anti-human TfR antibody fused to the C-terminus of Gantenerumab (RO7126209; ClinicalTrials.gov - NCT04639050). An initial Phase 1a trial was completed with RO7126209 in July 2020, but results have yet to be reported (ClinicalTrials.gov - NCT04023994). In addition, a multi-level dose Phase 1b/2a clinical trial has entered the recruitment phase and is designed to determine safety, tolerability, pharmacokinetic and pharmacodynamic properties of the bispecific antibody in prodromal/mild-to-moderate AD patients; with results expected in 2024. The results from studies with RO7126209, when they are reported, will hopefully provide evidence that enhanced delivery of antibodies across the BBB is safely tolerated and leads to improvements in biomarker outcomes. Furthermore, these data should support the requirement of BBB-transport mechanisms for CNS therapeutics and lead to an increase in re-engineering of potential AD therapeutics and clinical investigations in patients. Moreover, recent clinical trials are beginning to focus on early/preclinical AD patients, based on amyloid positron emission tomography levels, with the aim to follow cognitive decline (ClinicalTrials.gov - NCT01767311; NCT03887455; NCT04468659). If earlier intervention proves successful with traditional immunotherapies, it may be that enhanced delivery is required for patients further along in disease progression and could have more efficacy in these cohorts over non-BBB penetrating immunotherapies.

7.3.2 Non-immunotherapy approaches to improve brain delivery of therapeutics

In addition to immunotherapy approaches, various other technologies have been researched to combat the problem of the BBB in CNS disorders. For examples, recent reports suggest that serotypes of adeno-associated viruses (AAV) – AAV9, AAVrh8, AAVrh10 – have also shown conclusive evidence of crossing the BBB and robust CNS expression following systemic administration (Stanimirovic et al., 2018). Furthermore, the development of nano-drug delivery applications, including nanoparticles, polymeric liposomes, and carbon nanotubes, in combination with RMT targets has shown that directed delivery across the BBB is achievable (Johnsen et al., 2019; Karthivashan et al., 2018; Pardridge, 2020b). With TfR-targeted liposomes enabling the delivery of tyrosine hydroxylase or glial-derived neurotrophic factor in the 6-OHDA model of PD, with enzymatic activity normalised in three days (Pardridge, 2020b). However, due to limited *in vivo* investigations these approaches have yet to translate to the clinic, with increased understanding of pharmacokinetics and extent of transport efficiency still needed (Johnsen et al., 2019; Karthivashan et al., 2018; Pulgar, 2019).

7.3.3 Summary

The rationale behind enhanced delivery of immunotherapies across the BBB is based on unsuccessful clinical trials and limitations in these studies. Increasing experimental evidence suggests that approaches that target TfR are suitable for increasing brain penetrance and translation into the clinic is beginning. However, greater commitment to this approach is required if clinical benefits are to be seen with CNS disorders.

7.4 Conclusions

The murine ME7 prion model of neurodegeneration is a robust model that shares hallmarks of human neurodegenerative disease, such as neuroinflammation and neurodegeneration. There's evidence that systemic inflammation can exacerbate neurodegeneration and here I have shown that systemic bacterial infection with *S. typhimurium* results in increased microglial activation, proinflammatory cytokine production and decreased expression of synapse-associated proteins in ME7 mice. This increased microglial activation due to *S. typhimurium* infection is exacerbated by underlying disease pathology with a greater increase in cytokine production when ME7 mice are challenged under neuropathological conditions. To address the combined effects of systemic inflammation and neuroinflammation in a model of neurodegeneration, I purified and characterised a bispecific fusion protein that can effectively neutralise mTNF-α and has the properties for enhanced delivery across the BBB *in vivo* via targeting of mTfR. Treatment of ME7 mice at 12 wpi with bispecific mTNFR2 fusion protein did not have any effect on mouse behaviour, microglial activation or proinflammatory cytokine production. Furthermore, treatment of ME7 mice with bispecific mTNFR2 fusion protein following systemic bacterial infection with *S. typhimurium* did not modulate disease progression or modify neuropathology. As systemic bacterial infection activates multiple pathways, it may be that a combination of treatments is required for a therapeutic benefit. The current data do not provide evidence that improved delivery across the BBB of an anti-TNF-α biologic results in improved therapy compared to a peripherally acting anti-TNF-α biologic and further work is needed to address the limitations of this study.

Appendix A Additional Methodologies

A1 Recipe for Acetate pH 5.0 formulation buffer

2.761 g anhydrous sodium acetate, 20.454 g sodium chloride, 0.981 ml acetic acid was weighed and added to 1600 ml water for irrigation (Baxter), then pH adjusted to pH 5.0. Additional water was added to a total of 2 litres, giving a final concentration of 25 mM sodium acetate, 175 mM sodium chloride, before filter sterilisation (0.22 um Stericup).

A2 Manual analysis of mouse open field locomotor activity using a modified macro in FIJI

The Mouse Behavior Tracker macro executes the following commands to isolate the mouse in the video from any background objects: An MP4 format file is opened in Fiji using the FFMPEG plugin and then converted to an 8-bit video. A background image of the arena was generated by using the Z-project command (Image > Stack > Z-project) and selecting “Average intensity” as projection type. This background image is then subtracted from all frames of the video using the Image Calculator (Process > Image Calculator…) and selecting “Difference” as the operation and “Creating a New Window” as an option. The resulting video shows the mouse as a binary object, in this case a white object on a black background. To remove any selection of the arena edges in further analysis these objects were removed using the Gaussian filter command (Process > Filters > Gaussian Blur…) with a radius of 3.0 pixels and processing the whole stack. The binary video was then thresholded to select the mouse in all frames, this was achieved using the Threshold command (Image > Adjust > Threshold…) and setting the mode as Yen, with dark background selected, and applying the limits of 140, 255.

The macro then uses the wrMTrck plugin to track the mouse in the thresholded binary video through all frames. Size parameters are selected based on the minimum thresholded area required to successfully track the mouse in all frames. Velocity parameters are based on movement of the mouse across the arena within a frame; this is then doubled to allow for variation in speed between individual mice. All other

parameters are shown in Appendix Figure A, with any parameters for tracking *Caenorhabditis elegans* disabled (bendThreshold and bendDetect).

Mouse Behavior Tracker generates six files: the “Res_(file name).xls” file describing the raw data, the “Sum_(file name).xls” file showing the summarised data, the “Path_(file name).tif” file showing the traced results, the “Result of (file name) labels.avi” video file showing the mouse tracking with the object identifier number, the “Result of (file name).avi” video file showing the mouse in binary image, and the “Avg_(file name).tif” file showing the background cage image without the mouse. The "Length" parameter in the “Res_(file name).xls” file corresponds to the distance travelled by the mouse.

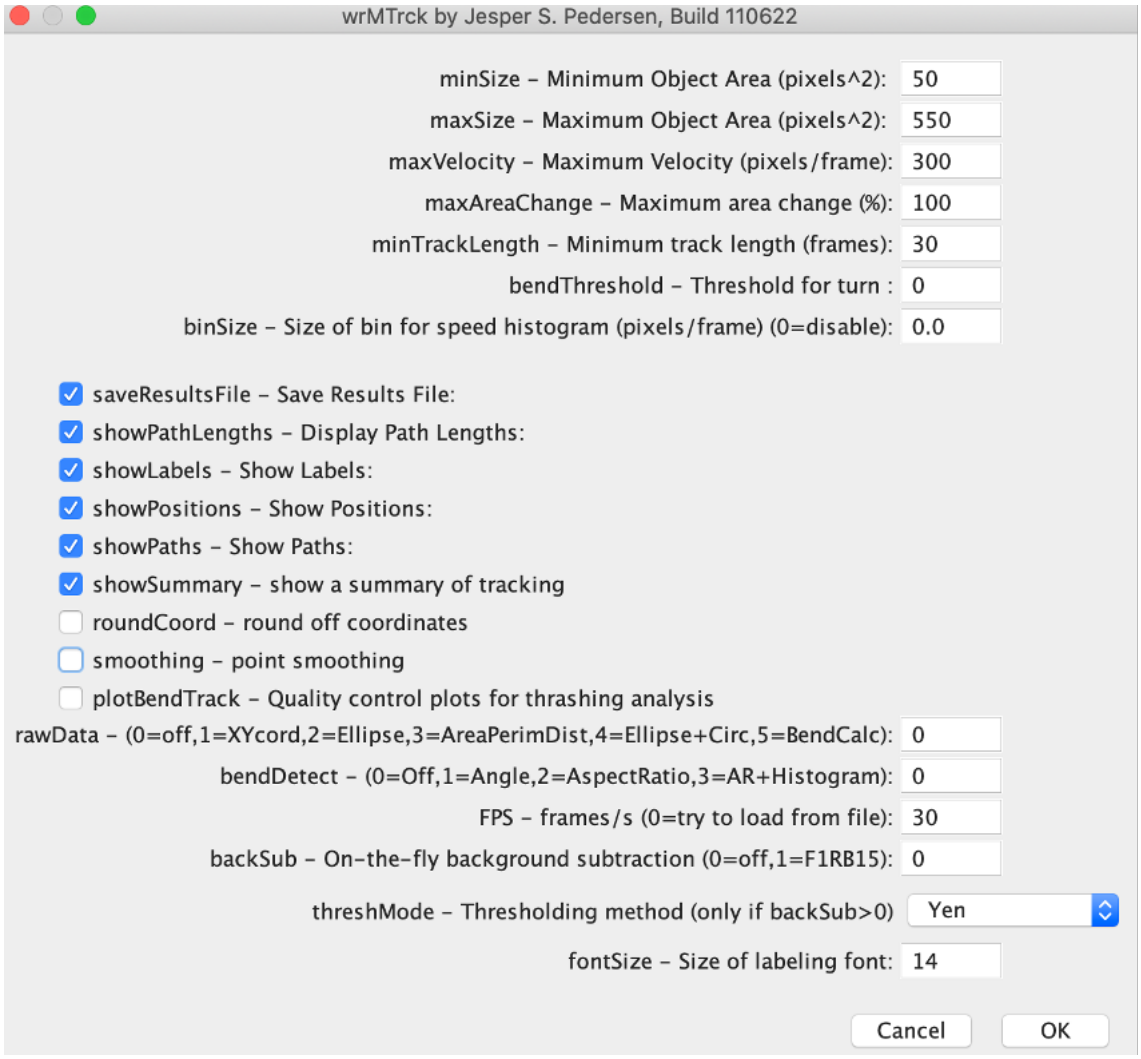

Appendix Figure A Parameters used to track mice during manual open field analysis
The parameter settings in the wrMTrck plugin used to track mouse movement from processed open field locomotor activity videos.

A3 Batch macro processing of images for color deconvolution quantification in FIJI

The following commands were added to FIJI startup macros (Plugins > Macros > Startup macros).

```
//Batch DAB to Deconvoluted Image
macro "Batch DAB to Deconvoluted Image... [F10] " {
dir1 = getDirectory("Choose Source Directory ");
dir2 = getDirectory("Choose Destination Directory ");
list = getFileList(dir1);
setBatchMode(true);
for (i=0; i<list.length; i++) {
showProgress(i+1, list.length);
filename = dir1 + list[i];
if (endsWith(filename, "tif")) {
open(filename);
//Color deconvolution values set using H DAB, with DAB as
channel 1
run("Colour Deconvolution", "vectors=[User values]
[r1]=0.26814753 [g1]=0.57031375 [b1]=0.77642715
[r2]=0.6500286 [g2]=0.704031 [b2]=0.2860126 [r3]=0.7110272
[g3]=0.42318153 [b3]=0.5615672");
run("Close");
run("Close");
run("Restore Selection");
saveAs("TIFF", dir2+list[i]);
close();
}
}
}
```

```
//Batch Deconvoluted Image to Binary Image
macro "Batch Deconvoluted to Binary Image... [F11] " {
dir1 = getDirectory("Choose Source Directory ");
dir2 = getDirectory("Choose Destination Directory ");
list = getFileList(dir1);
setBatchMode(true);
for (i=0; i<list.length; i++) {
showProgress(i+1, list.length);
filename = dir1 + list[i];
if (endsWith(filename, "tif")) {
open(filename);
setAutoThreshold("Default");
run("Threshold...");
//CHANGE SECOND THRESHOLD NUMBER BELOW
setThreshold(0, xxx);
run("Convert to Mask");
run("Despeckle");
saveAs("TIFF", dir2+list[i]);
close();
}
}
}
```

```
//Binary Image Quantification
macro "Batch Binary Image Quantification...[F12]" {
dir = getDirectory("Choose a Directory ");
list = getFileList(dir);
if (getVersion>="1.40e")
 setOption("display labels", true);
setBatchMode(true);
for (i=0; i<list.length; i++) {
path = dir+list[i];
showProgress(i, list.length);
if (!endsWith(path,"/")) open(path);
if (nImages>=1) {
run("Analyze Particles...", "size=0-Infinity clear
summarize");
}
}
}
```

A4 Detection of anti-drug antibodies (ADAs) in mouse sera

Treatment fusion protein acted as capture antigen (15nM, 50 μl/well) and was incubated overnight in all wells of a clear, flat-bottomed 96-well MaxiSorp plate (Nunc). Wells were washed three times with PBS containing 0.1% (v/v) Tween 20 (PBS-T). Wells were blocked with PBS-T containing 3% BSA for 60 minutes on an orbital shaker at 700 rpm. Wells were washed three times with PBS-T before addition of serum samples. All dilution steps were made in PBS-T containing 1% (w/v) BSA. Serum samples from experimental mice were serially diluted 1 in 3 before incubation at RT with shaking for 60 minutes. Serum from naïve control mice were diluted and run alongside normal animal serum as controls where available. Wells were washed three times with PBS-T before addition of rat anti-mouse IgG (1:1000; Jackson, 415-005-166) and incubation for 60 minutes at RT with shaking. Wells were washed with PBS-T three times before incubation with biotinylated rabbit anti-rat IgG (1:500; Vector, BA-9401) for 45 minutes at RT with shaking. Wells were washed with PBS-T three times before incubation with Streptavidin-HRP (1:40; R&D Systems, DY998) for 30 minutes at RT with shaking. Wells were washed three times with PBS-T. TMB substrate (Life Technologies) was added undiluted, and reaction allowed to develop for 5 minutes at RT before addition of 1N H_2SO_4 to stop the reaction. Plates were read using a Tecan infinite F200 Pro plate reader and I-control 2.0 software (Tecan) at 450 nm and 570 nm. Readings at 570 nm were subtracted from 450 nm to equate for plate variations. Data were plotted using the Nonlinear fit: sigmoidal, 4PL, log(concentration) with least-squares regression function in Prism 8 (v4.2.3, Graphpad).

Appendix B Bispecific fusion protein domain sequences and physicochemical properties

Appendix Table A Constant region sequences for human IgG1 TM Kappa isotype

Constant region	Primary sequence
Human IgG1 TM heavy chain (ΔK)	ASTKGPSVFPLAPSSKSTSGGTAALGCLVKDYFPEPVTVSWNSGALTSGVHTFPAVLQ SSGLYSLSSVVTVPSSSLGTQTYICNVNHKPSNTKVDKRVEPKSCDKTHTCPPCPAPEFE GGPSVFLFPPKPKDTLMISRTPEVTCVVVDVSHEDPEVKFNWYVDGVEVHNAKTKPR EEQYNSTYRVVSVLTVLHQDWLNGKEYKCKVSNKALPASIEKTISKAKGQPREPQVYT LPPSREEMTKNQVSLTCLVKGFYPSDIAVEWESNGQPENNYKTTPPVLDSDGSFFLYS KLTVDKSRWQQGNVFSCSVMHEALHNHYTQKSLSLSPG(K)
Human Kappa light chain	TVAAPSVFIFPPSDEQLKSGTASVVCLLNNFYPREAKVQWKVDNALQSGNSQESVTE QDSKDSTYSLSSTLTLSKADYEKHKVYACEVTHQGLSSPVTKSFNRGEC

Appendix Table B Heavy chain variable region (VH) sequences

Protein	Primary sequence
8D3$_{130}$	EVQLVESGGGLVQPGNSLTLSCVASGFTFSNYGMHWIRQAPKKGLEWIAMIYYDSSK MNYADTVKGRFTISRDNSKNTLYLEMNSLRSEDTAMYYCAVPTSHAVVDVWGQGV WVTVSS
NIP228	QVNLRESGGGVVQPGRSLRLSCAASGFTFSSYGMHWVRQAPGEGLEWVSAISGSGG STYYADSVKGRFTISRDNSKNTLYLQMNSLRAEDTAVYYCAKRFGEFAFDIWGRGTTV TVSS
V1q	QVQLKESGPGLVQPSQTLSLTCTVSGFSLTSYNVHWVRQPPGKGLEWMGRMRYNG DTSYNSALKSRLSISRDTSKNQVFLKMNSLQTDDTGTYYCTRDRFSWASYFDYWGQG VMVTVSS

Appendix Table C Light chain variable domain (VL) sequences

Protein	Primary sequence
8D3$_{130}$	DIQMTQSPASLSASLEEIVTITCQASQDIGNWLAWYQQKPGKSPQLLIYGATSLADGV PSRFSGSRSGTQFSLKISRVQVEDIGIYYCLAAYNTPWTFGGGTKLELKR
NIP228	AIRMTQSPSSLSASVGDRVTITCRASQSISSYLNWYQQKPGKAPKLLIYAASSLQSGVPS RFSGSGSGTDFTLTISSLQPEDFATYYCQQSYSTPLTFGGGTKVEIKR
V1q	NIQLTQSPSLLSASVGDRVTLSCKGSQNINNFLAWYQQELGEAPKLLIYNTNSLQTGIP SRFTGSGSGTDYTLTISSLQPEDVATYFCYQYNNGNTFGVGTKLELKR

Appendix Table D Sequences for mTNFR2 and scFv with antibody linker

Fusion protein	Primary sequence with linker
mTNFR2 ECD	GGGGSGGGGSGGGGSVPAQVVLTPYKPEPGYECQISQEYYDRKAQMCCAKCPPGQ YVKHFCNKTSDTVCADCEASMYTQVWNQFRTCLSCSSSCTTDQVEIRACTKQQNRV CACEAGRYCALKTHSGSCRQCMRLSKCGPGFGVASSRAPNGNVLCKACAPGTFSDTT SSTDVCRPHRICSILAIPGNASTDAVCAPESPTLSAIPRTLYVSQPEPTRSQPLDQEPGPS QTPSILTSLGSTPIIEQSTKGG
V1q scFv	GGGGSGGGGSGGGGSQVQLKESGPGLVQPSQTLSLTCTVSGFSLTSYNVHWVRQPP GKGLEWMGRMRYNGDTSYNSALKSRLSISRDTSKNQVFLKMNSLQTDDTGTYYCTR DRFSWASYFDYWGQGVMVTVSSGSTSGGGSGGGSGGGGSSNIQLTQSPSLLSASVG DRVTLSCKGSQNINNFLAWYQQELGEAPKLLIYNTNSLQTGIPSRFTGSGSGTDYTLTIS SLQPEDVATYFCYQYNNGNTFGVGTKLELKR
NIP228 scFv	GGGGSGGGGSGGGGSQVNLRESGGGVVQPGRSLRLSCAASGFTFSSYGMHWVRQ APGEGLEWVSAISGSGGSTYYADSVKGRFTISRDNSKNTLYLQMNSLRAEDTAVYYCA KRFGEFAFDIWGRGTTVTVSSGSTSGGGSGGGSGGGGSSAIRMTQSPSSLSASVGDR VTITCRASQSISSYLNWYQQKPGKAPKLLIYAASSLQSGVPSRFSGSGSGTDFTLTISSLQ PEDFATYYCQQSYSTPLTFGGGTKVEIKR
8D3$_{130}$ scFv	GGGGSGGGGSGGGGSEVQLVESGGGLVQPGNSLTLSCVASGFTFSNYGMHWIRQA PKKGLEWIAMIYYDSSKMNYADTVKGRFTISRDNSKNTLYLEMNSLRSEDTAMYYCA VPTSHAVVDVWGQGVWVTVSSGSTSGGGSGGGSGGGGSSDIQMTQSPASLSASLE EIVTITCQASQDIGNWLAWYQQKPGKSPQLLIYGATSLADGVPSRFSGSRSGTQFSLKI SRVQVEDIGIYYCLAAYNTPWTFGGGTKLELKR
8D3 scFv	GGGGSGGGGSGGGGSEVQLVESGGGLVQPGNSLTLSCVASGFTFSNYGMHWIRQA PKKGLEWIAMIYYDSSKMNYADTVKGRFTISRDNSKNTLYLEMNSLRSEDTAMYYCA VPTSHYVVDVWGQGVSVTVSSGSTSGGGSGGGSGGGGSSDIQMTQSPASLSASLEEI VTITCQASQDIGNWLAWYQQKPGKSPQLLIYGATSLADGVPSRFSGSRSGTQFSLKIS RVQVEDIGIYYCLQAYNTPWTFGGGTKLELKR

Appendix Table E Physicochemical properties of bispecific fusion proteins

Protein	Molecular mass (Da)	Molar Extinction Coefficient (M^{-1} cm^{-1})	pI
cV1q hIgG1 TM	148,589	209,420	8.94
8D3$_{130}$ hIgG1 TM	148,059	228,440	7.77
NIP228 hIgG1 TM	147,086	195,440	9.36
cV1q hIgG1 TM-8D3 scFv	200,072	314,660	8.82
cV1q hIgG1 TM-8D3$_{130}$ scFv	199,972	322,680	8.82
cV1q hIgG1 TM-NIP228 scFv	198,858	289,680	9.39
NIP228 hIgG1 TM-8D3 scFv	198,366	300,680	9.15
NIP228 hIgG1 TM-8D3$_{130}$ scFv	198,266	308,700	9.15
8D3$_{130}$ hIgG1 TM-V1q scFv	200,026	322,680	9.00
NIP228 hIgG1 TM-V1q scFv	194,074	275,575	9.39
8D3$_{130}$ hIgG1 TM-mTNFR2	197,867	266,030	9.04
NIP228 hIgG1 TM-mTNFR2	196,927	233,030	9.51
8D3$_{130}$ hIgG1 TM ΔK-mTNFR2	197,610	266,030	8.94
NIP228 hIgG1 TM ΔK-mTNFR2	196,671	233,030	9.46

Appendix C Focused analysis of synaptic plasticity markers in ME7 prion disease

Appendix Table F Fold change in expression of synaptic plasticity genes compared to NBH mice

Analysis of synaptic plasticity genes in NBH mice, ME7 mice at 8wpi, ME7 mice four weeks after infection with *S. typhimurium* SL3261 ($1x10^6$ colony forming units) was conducted using an RT^2 Profiler PCR Array Mouse Synaptic Plasticity (QIAGEN, UK) and performed by Steven Booth.

Gene	Description	ME7 + saline	ME7 + Salmonella
Adam10	A disintegrin and metallopeptidase domain 10	0.936921447	0.895025071
Adcy1	Adenylate cyclase 1	0.856188285	0.574349177
Adcy8	Adenylate cyclase 8	0.714992493	0.411795509
Akt1	Thymoma viral proto-oncogene 1	0.681129017	0.823591017
Arc	Activity regulated cytoskeletal-associated protein	0.990342872	0.926588062
Bdnf	Brain derived neurotrophic factor	0.832775771	0.737134609
Camk2a	Calcium/calmodulin-dependent protein kinase II alpha	0.838568184	0.823591017
Camk2g	Calcium/calmodulin-dependent protein kinase II gamma	0.815637493	0.768437591
Cdh2	Cadherin 2	0.821310701	0.659753955
Cebpb	CCAAT/enhancer binding protein (C/EBP), beta	1.061423209	1.021012126
Cebpd	CCAAT/enhancer binding protein (C/EBP), delta	1.665551542	1.424050196
Cnr1	Cannabinoid receptor 1 (brain)	0.85027416	0.747424624
Creb1	CAMP responsive element binding protein 1	0.653382627	0.683020128
Crem	CAMP responsive element modulator	0.681129017	0.801069878
Dlg4	Discs, large homolog 4 (Drosophila)	0.771640088	0.687770909
Egr1	Early growth response 1	0.976708529	0.668963777
Egr2	Early growth response 2	1.522033381	0.895025071
Egr3	Early growth response 3	0.750539549	0.692554734

Gene	Description	ME7 + saline	ME7 + Salmonella
Egr4	Early growth response 4	0.85027416	0.812252396
Ephb2	Eph receptor B2	0.719965659	0.524858342
Fos	FBJ osteosarcoma oncogene	0.750539549	0.692554734
Gabra5	Gamma-aminobutyric acid (GABA) A receptor, subunit alpha 5	0.564873607	0.641712949
Gnai1	Guanine nucleotide binding protein (G protein), alpha inhibiting 1	0.724973416	0.562529242
Gria1	Glutamate receptor, ionotropic, AMPA1 (alpha 1)	0.609627547	0.570381858
Gria2	Glutamate receptor, ionotropic, AMPA2 (alpha 2)	0.950000383	0.939522749
Gria3	Glutamate receptor, ionotropic, AMPA3 (alpha 3)	0.719965659	0.550952558
Gria4	Glutamate receptor, ionotropic, AMPA4 (alpha 4)	0.745355193	0.602903914
Grin1	Glutamate receptor, ionotropic, NMDA1 (zeta 1)	0.936921447	0.952637998
Grin2a	Glutamate receptor, ionotropic, NMDA2A (epsilon 1)	0.714992493	0.570381858
Grin2b	Glutamate receptor, ionotropic, NMDA2B (epsilon 2)	0.76630998	0.747424624
Grin2c	Glutamate receptor, ionotropic, NMDA2C (epsilon 3)	0.777007269	0.692554734
Grin2d	Glutamate receptor, ionotropic, NMDA2D (epsilon 4)	0.777007269	0.650670928
Grip1	Glutamate receptor interacting protein 1	0.810003474	0.668963777
Grm1	Glutamate receptor, metabotropic 1	0.527045712	0.381564802
Grm2	Glutamate receptor, metabotropic 2	1.114193651	0.77916458
Grm3	Glutamate receptor, metabotropic 3	0.85027416	0.858565436
Grm4	Glutamate receptor, metabotropic 4	0.810003474	0.535886731
Grm5	Glutamate receptor, metabotropic 5	0.990342872	0.801069878
Grm7	Glutamate receptor, metabotropic 7	0.880259014	0.590496331
Grm8	Glutamate receptor, metabotropic 8	0.671751713	0.611320139
Homer1	Homer homolog 1 (Drosophila)	0.832775771	0.668963777

Appendix C

Gene	Description	ME7 + saline	ME7 + Salmonella
Igf1	Insulin-like growth factor 1	0.613867842	0.678302164
Inhba	Inhibin beta-A	1.083725967	0.757858283
Jun	Jun oncogene	0.838568184	0.578344092
Junb	Jun-B oncogene	0.639936207	0.768437591
Kif17	Kinesin family member 17	1.083725967	0.712025098
Klf10	Kruppel-like factor 10	0.787853886	0.829319546
Mapk1	Mitogen-activated protein kinase 1	0.810003474	0.920187651
Mmp9	Matrix metallopeptidase 9	1.202469249	0.732042848
Ncam1	Neural cell adhesion molecule 1	0.810003474	0.602903914
Nfkb1	Nuclear factor of kappa light polypeptide gene enhancer in B-cells 1, p105	0.844400887	0.840896415
Nfkbib	Nuclear factor of kappa light polypeptide gene enhancer in B-cells inhibitor, beta	1.688801775	1.01395948
Ngf	Nerve growth factor	1.076240125	0.692554734
Ngfr	Nerve growth factor receptor (TNFR superfamily, member 16)	0.676424116	0.641712949
Nos1	Nitric oxide synthase 1, neuronal	0.545631939	0.598739352
Nptx2	Neuronal pentraxin 2	0.898755127	0.823591017
Nr4a1	Nuclear receptor subfamily 4, group A, member 1	0.804408371	0.882702996
Ntf3	Neurotrophin 3	0.588861395	0.558643569
Ntf5	Neurotrophin 5	0.553248677	0.303548721
Ntrk2	Neurotrophic tyrosine kinase, receptor, type 2	0.710053679	0.574349177
Pcdh8	Protocadherin 8	1.145517898	1
Pick1	Protein interacting with C kinase 1	0.750539549	0.763129604
Pim1	Proviral integration site 1	1.106497353	0.590496331
Plat	Plasminogen activator, tissue	0.844400887	0.692554734
Plcg1	Phospholipase C, gamma 1	0.85027416	0.846745312

Gene	Description	ME7 + saline	ME7 + Salmonella
Ppp1ca	Protein phosphatase 1, catalytic subunit, alpha isoform	0.671751713	0.721964598
Ppp1cc	Protein phosphatase 1, catalytic subunit, gamma isoform	0.695440986	0.697371833
Ppp1r14a	Protein phosphatase 1, regulatory (inhibitor) subunit 14A	1.083725967	0.882702996
Ppp2ca	Protein phosphatase 2 (formerly 2A), catalytic subunit, alpha isoform	1.061423209	0.628506687
Ppp3ca	Protein phosphatase 3, catalytic subunit, alpha isoform	0.85027416	0.615572207
Prkca	Protein kinase C, alpha	0.777007269	0.716977624
Prkcc	Protein kinase C, gamma	0.892546971	0.668963777
Prkg1	Protein kinase, cGMP-dependent, type I	0.740206649	0.611320139
Rab3a	RAB3A, member RAS oncogene family	0.681129017	0.624165274
Rela	V-rel reticuloendotheliosis viral oncogene homolog A (avian)	1.011152081	0.864537231
Reln	Reelin	0.690637224	0.697371833
Rgs2	Regulator of G-protein signaling 2	0.676424116	0.835087919
Rheb	Ras homolog enriched in brain	0.924022572	0.806641759
Sirt1	Sirtuin 1 (silent mating type information regulation 2, homolog) 1 (S. cerevisiae)	0.690637224	0.61985385
Srf	Serum response factor	0.777007269	0.726986259
Synpo	Synaptopodin	0.898755127	0.895025071
Timp1	Tissue inhibitor of metalloproteinase 1	1.939923821	1.214194884
Tnf	Tumor necrosis factor	9.164143184	9.447941291
Ywhaq	Tyrosine 3-monooxygenase/tryptophan 5-monooxygenase activation protein, theta polypeptide	0.740206649	0.570381858

Appendix D *In vivo* inhibition of IL-1β using an anti-mTfR-IL-1RA antibody-protein fusion

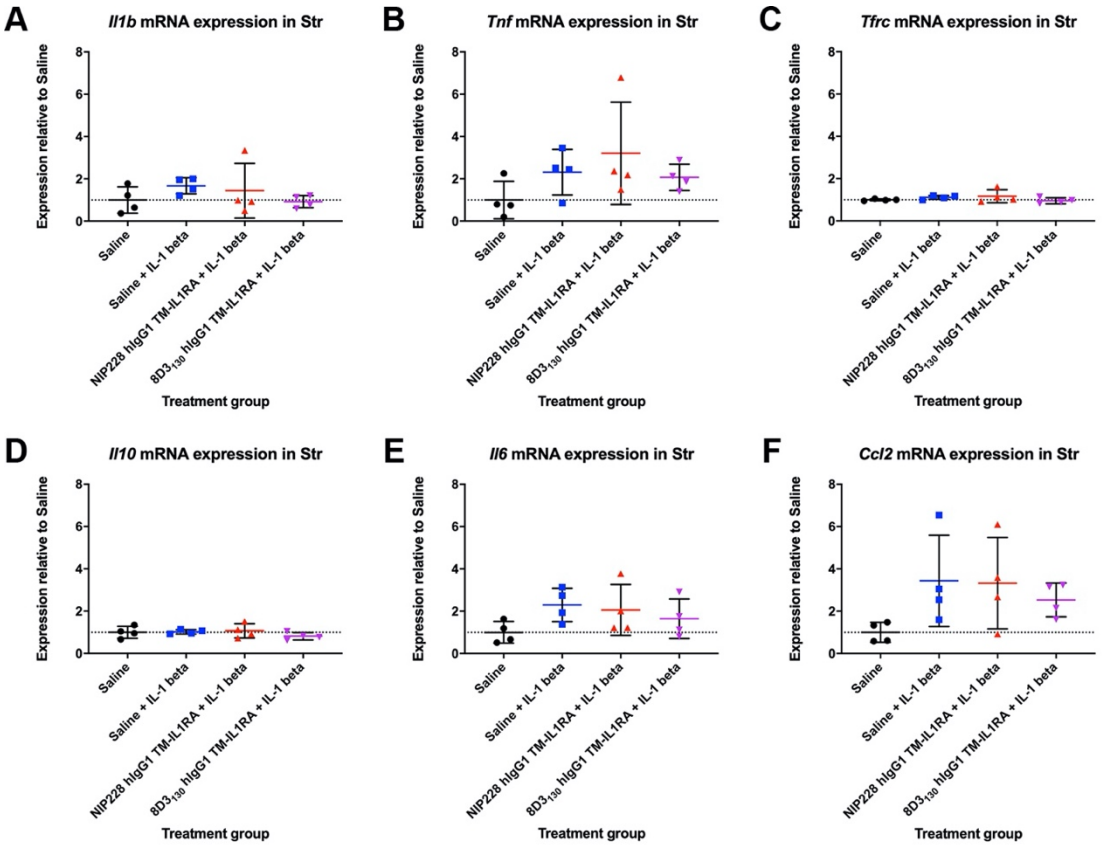

Appendix Figure B Biochemical analysis of cytokine and protein markers by qPCR following treatment with anti-mTfR-IL-1RA fusion proteins

Analysis of mRNA expression of *Tnf* (A), *Il1b* (B), *Tfrc* (C), *Il10* (D), *Il6* (E) and *Ccl2* (F) in the striatum 3 hours after intrastriatal injection with 1 µl saline or 1 ng/µl recombinant mouse IL-1β. Mice were injected (i.p.) 1 hour prior to intrastriatal injection with saline or IL-1RA fusion protein (NIP228 hIgG1 TM-IL1RA/ $8D3_{130}$ hIgG1 TM-IL1RA; 54 µM). Striatal mRNA expression was analysed by SYBR green qPCR (Section 2.2.2.3). Values are displayed as average gene expression relative to Saline-treated animals, after normalisation to the housekeeping gene *Pgk1*. Data were analysed by one-way ANOVA with Holm-Sidak's multiple comparisons test. Graphs are presented as mean ± SD.

Appendix E Peripheral responses in ME7 prion mice treated with bispecific mTNFR2 fusion proteins

E1 Cytokine expression in the spleen of ME7 prion mice after bispecific mTNFR2 fusion protein treatment

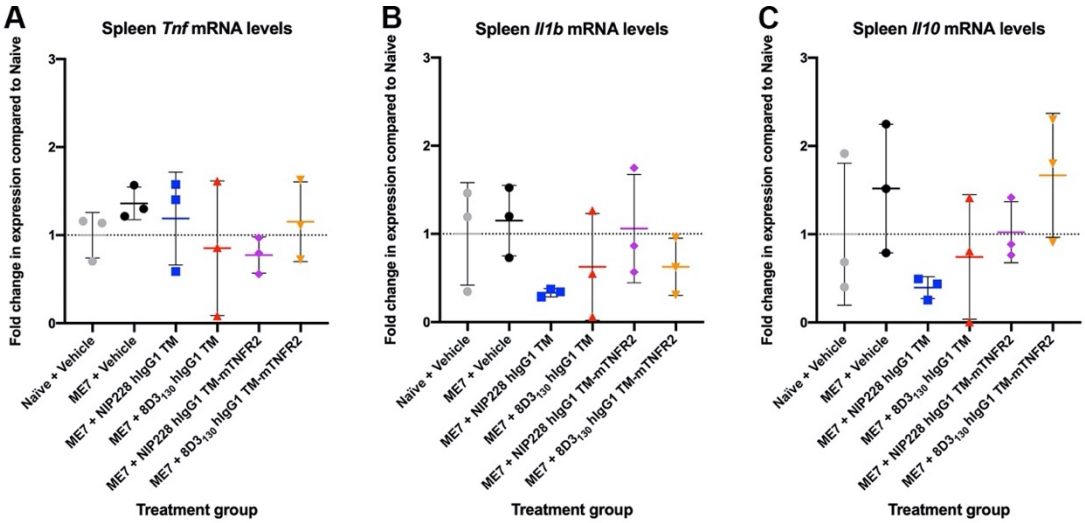

Appendix Figure C Spleen cytokine expression after bispecific mTNFR2 fusion protein treatment in ME7 prion mice

Analysis of *Tnf* (A), *Il1b* (B), and *Il10* (C) in the spleen of ME7 prion mice at 16 wpi by SYBR green qPCR (Section 2.2.2.3). Mice were treated with isotype control or bispecific anti-mTNF-α fusion protein (54 μM, i.p.) weekly from 12 wpi to 15 wpi and tissue collected 7 days later. Values are displayed as average gene expression relative to Naïve control, after normalisation to the housekeeping gene *Gapdh*. Data were analysed by one-way ANOVA with Holm-Sidak's multiple comparisons test. Data are presented as the mean ± SD (n = 3/group) of fold change compared to naïve control after normalisation of expression to *Pgk1.* These data were generated by an MBioSci student, Ms. Hanna Davies.

E2 CD64 expression in the spleen of ME7 prion mice after bispecific mTNFR2 fusion protein treatment

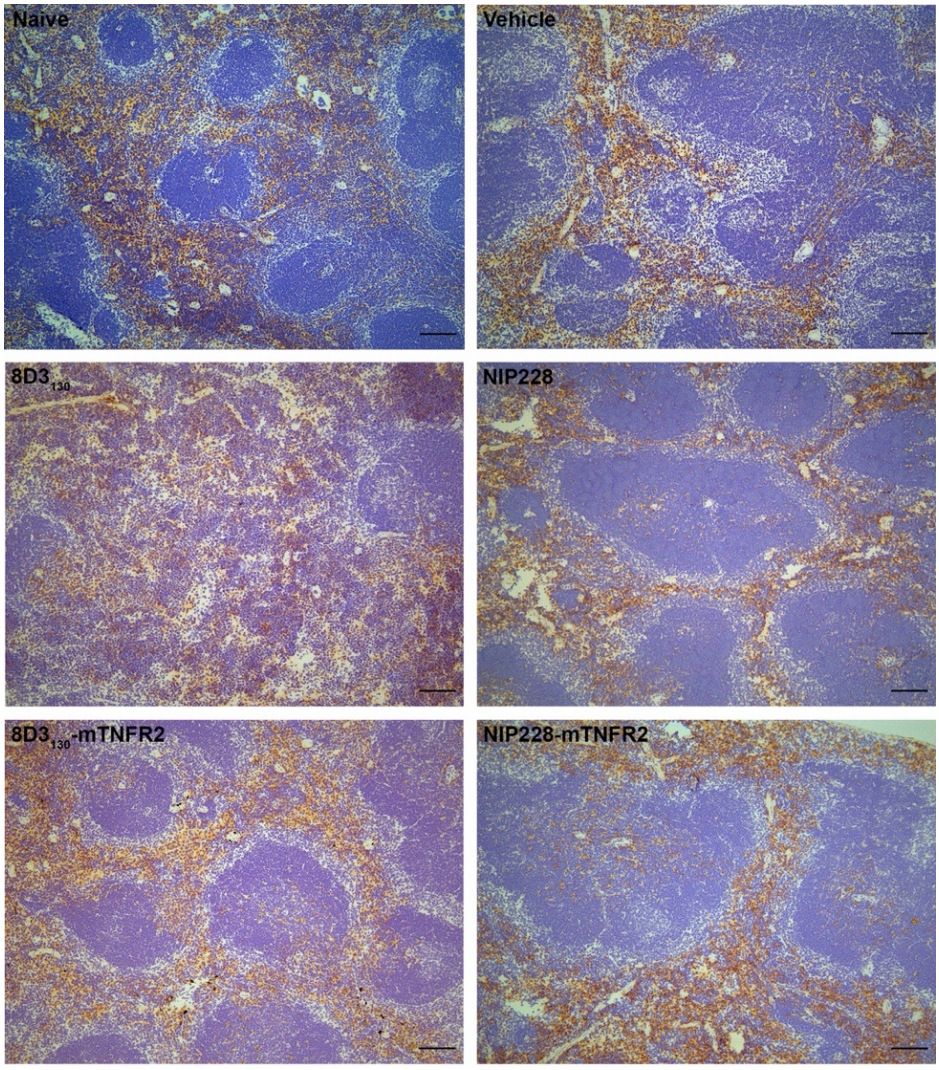

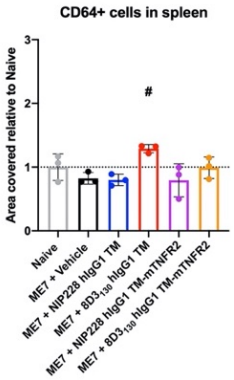

Appendix Figure D Spleen CD64 expression after bispecific mTNFR2 fusion protein treatment in ME7 prion mice

Analysis of CD64 expression in the spleen of ME7 prion mice at 16 wpi. Mice were treated with isotype control or bispecific anti-mTNF-α fusion protein (54 μM, i.p.) weekly from 12 wpi to 15 wpi and tissue collected 7 days later. Values are displayed as average area covered relative to expression in vehicle-treated ME7 prion mice as determined by custom macro analysis in FIJI (Appendix A3). Data were analysed by one-way ANOVA with Holm-Sidak's multiple comparisons test; #, $p < 0.05$ versus ME7 + vehicle. Graphs are presented as mean ± SD; n = 2-3/group. Staining and imaging were performed by an MBioSci student, Ms. Hanna Davies.

E3 CD11b expression in the spleen of ME7 prion mice after bispecific mTNFR2 fusion protein treatment

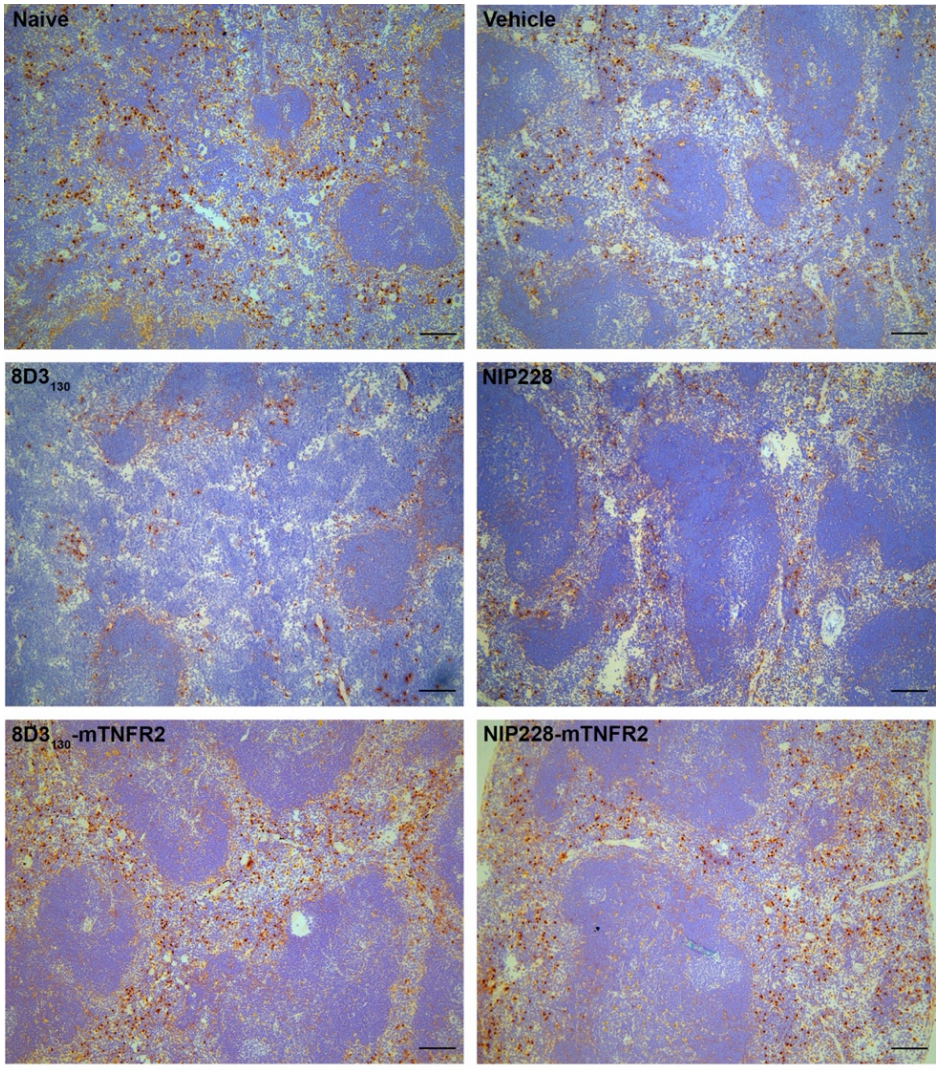

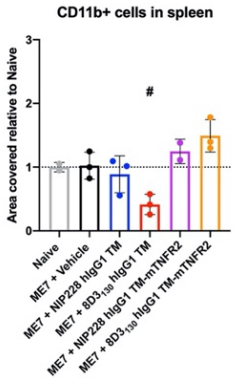

Appendix Figure E Spleen CD11b expression after bispecific mTNFR2 fusion protein treatment in ME7 prion mice

Analysis of CD11b expression in the spleen of ME7 prion mice at 16 wpi. Mice were treated with isotype control or bispecific anti-mTNF-α fusion protein (54 μM, i.p.) weekly from 12 wpi to 15 wpi and tissue collected 7 days later. Values are displayed as average area covered relative to expression in vehicle-treated ME7 prion mice as determined by custom macro analysis in FIJI (Appendix A3). Data were analysed by one-way ANOVA with Holm-Sidak's multiple comparisons test; #, $p < 0.05$ versus ME7 + vehicle. Graphs are presented as mean ± SD; n = 2-3/group. Staining and imaging were performed by an MBioSci student, Ms. Hanna Davies.

E4 CD68 expression in the spleen of ME7 prion mice after bispecific mTNFR2 fusion protein treatment

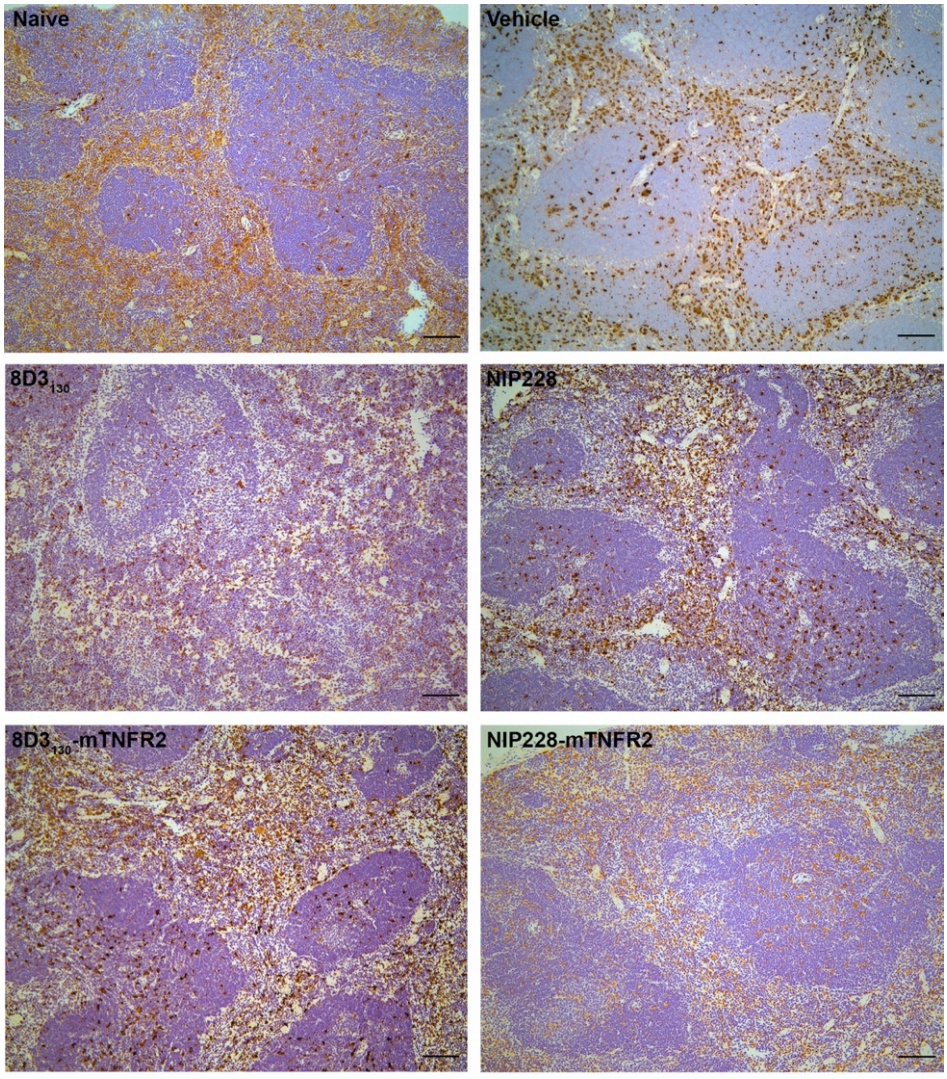

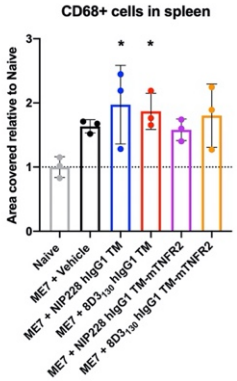

Appendix Figure F Spleen CD68 expression after bispecific mTNFR2 fusion protein treatment in ME7 prion mice

Analysis of CD68 expression in the spleen of ME7 prion mice at 16 wpi. Mice were treated with isotype control or bispecific anti-mTNF-α fusion protein (54 μM, i.p.) weekly from 12 wpi to 15 wpi and tissue collected 7 days later. Values are displayed as average area covered relative to expression in vehicle-treated ME7 prion mice as determined by custom macro analysis in FIJI (Appendix A3). Data were analysed by one-way ANOVA with Holm-Sidak's multiple comparisons test; *, $p < 0.05$ versus naïve control mice. Graphs are presented as mean ± SD; n = 2-3/group. Staining and imaging were performed by an MBioSci student, Ms. Hanna Davies.

Appendix F Immunogenicity response in ME7 prion mice treated with bispecific mTNFR2 fusion proteins

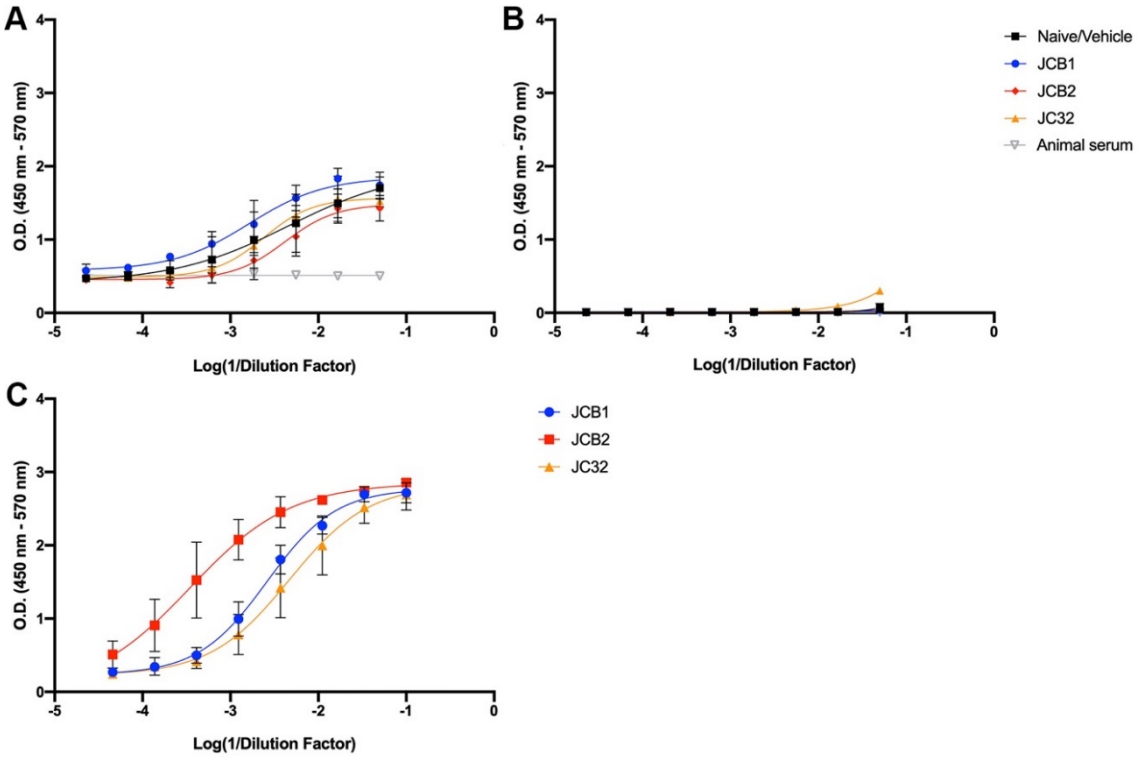

Appendix Figure G ADA detection in experimental mice after antibody/fusion protein treatment
Anti-drug antibodies (ADAs) were detected in mouse serum using an indirect ELISA (see Appendix A4). Experimental mice (n = 2-3/group) from JCB1 (blue; Chapter 5: ME7 + fusion protein), JCB2 (red; ME7/SL3261 + fusion protein), JC32 (orange; SL3261 + fusion protein). Serum from Vehicle-injected/naïve control mice (black) were diluted and run alongside normal horse serum (grey) as controls where available. (A-B) Sera from NIP228 hIgG1 TM-injected mice was serially diluted 1 in 3 from a starting dilution of 1:200. (A) NIP228 hIgG1 TM was used as the capture antigen and mouse IgG was detected in all serum samples, except animal serum. (B) BSA was used as capture antigen to confirm specific binding and detection of mouse IgG. Serum mice from NIP228 hIgG1 TM-injected mice from JCB1, JCB2 and JC32 and from Vehicle-injected/Naïve mice showed no response suggesting no non-specific detection of mouse IgG binding to BSA at the same concentration as NIP228 hIgG1 TM. (C) Sera from $8D3_{130}$ hIgG1 TM ΔK-mTNFR2 injected mice were serially diluted 1 in 3 from a starting concentration of 1:10 and added to wells coated with $8D3_{130}$ hIgG1 TM ΔK-mTNFR2 (15 nM). All samples showed detection of mouse IgG above plate background.

Appendix G Central responses to mTNFR2 fusion protein administration after *S. typhimurium* infection

G1 Biochemical analysis of cytokine markers within the brain after *S. typhimurium* infection and mTNFR2 fusion protein treatment

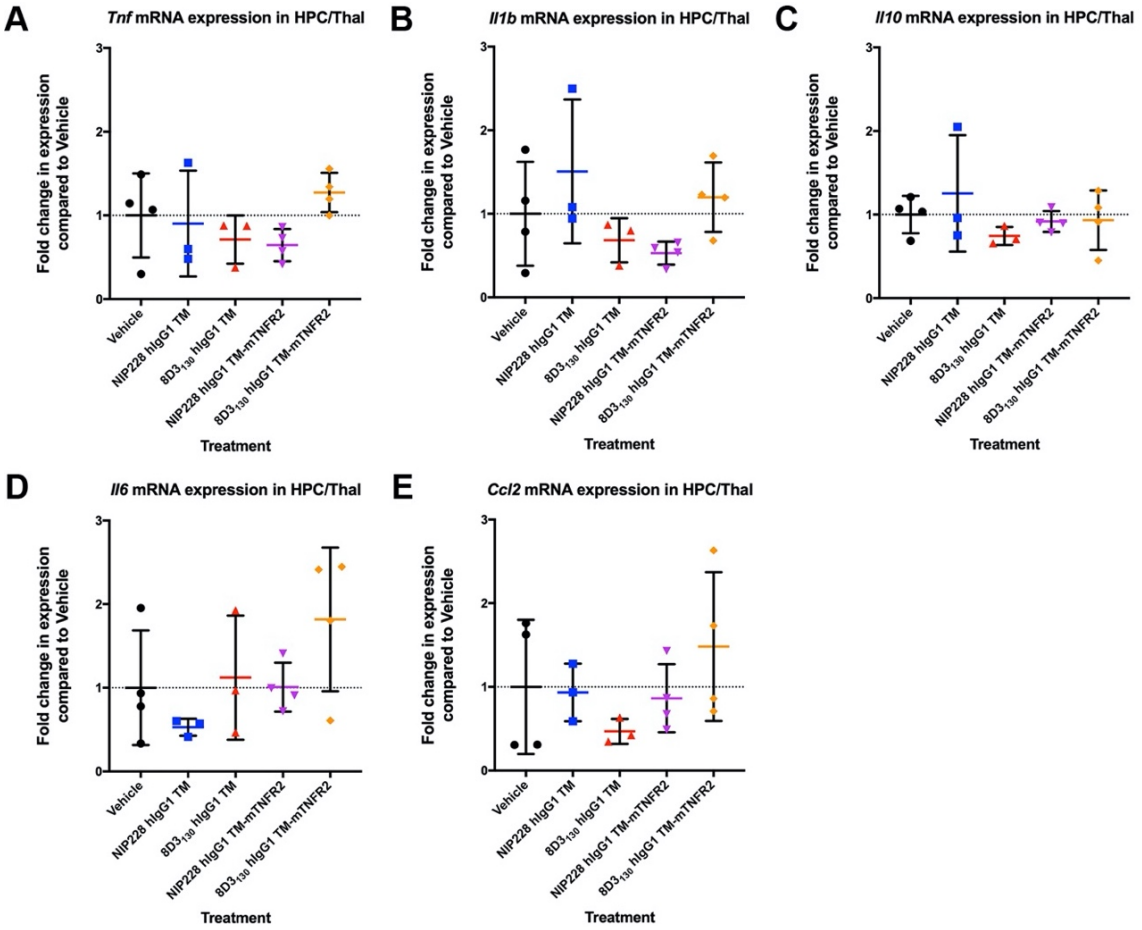

Appendix Figure H Brain cytokine expression after bispecific mTNFR2 fusion protein treatment in *S. typhimurium* SL3261-infected mice

Analysis of expression of specific cytokine markers downstream of TNF-α in the brain 17 days after injection with 1.8 x 10^6 colony forming units of *S. typhimurium* SL3261. Mice were treated 10 days after *S. typhimurium* injection with bispecific anti-mTNF-α fusion protein, or isotype control (54 μM, i.p.), and tissue collected 7 days later. Hippocampal/thalamic mRNA expression of *Tnf* (A), *Il1b* (B), *Il10* (C), *Il6* (D) and *Ccl2* (E) was analysed by SYBR green qPCR (Section 2.2.2.3). Data are presented as the mean ± SD (n = 3-4/group) of fold change compared to naïve control after normalisation of expression to *Pgk1.* Data were analysed by one-way ANOVA with Holm-Sidak's multiple comparisons test.

G2 CD64 expression in the hippocampus/thalamus after *S. typhimurium* infection and mTNFR2 fusion protein treatment

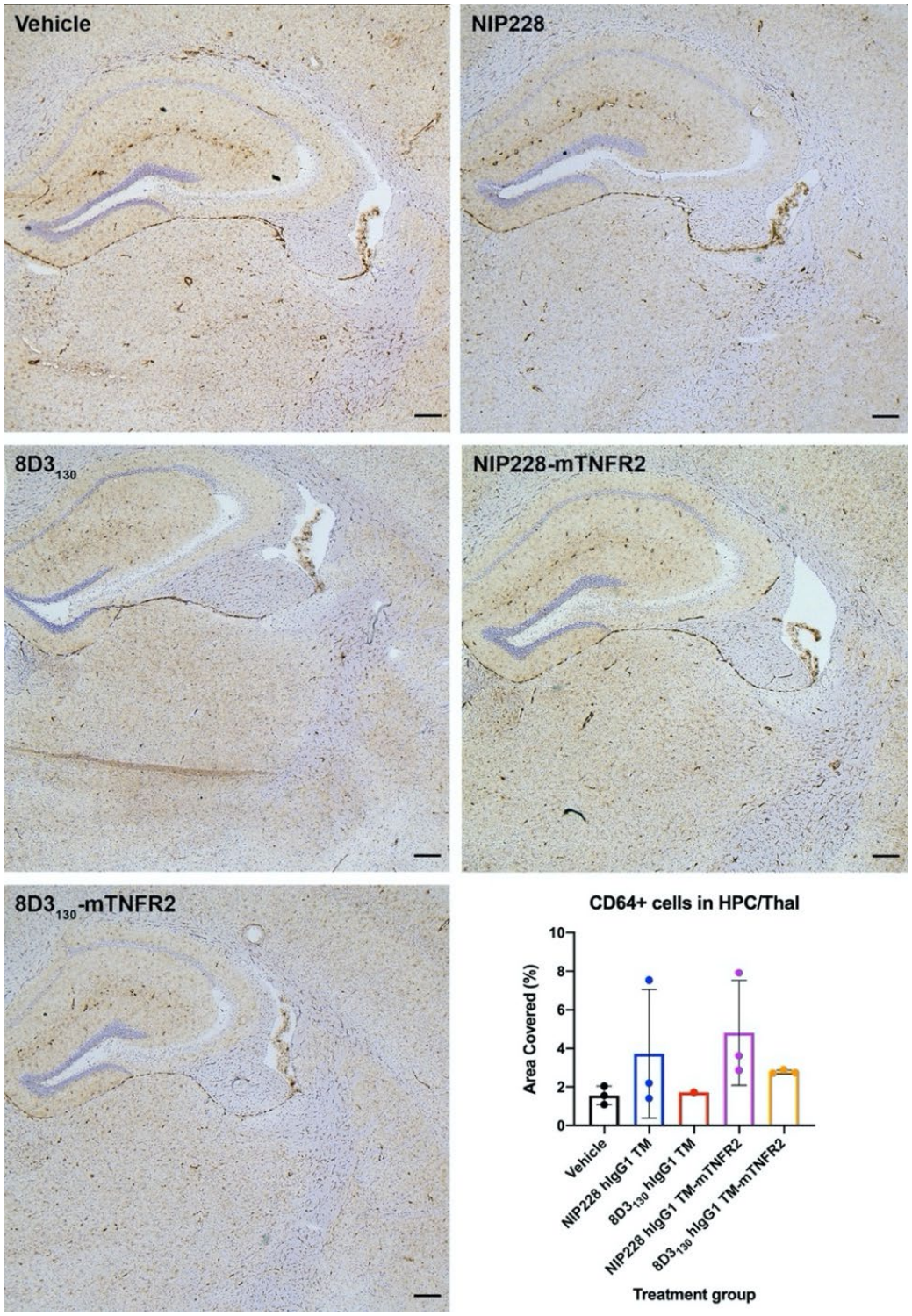

Appendix Figure I Brain CD64 expression after bispecific mTNFR2 fusion protein treatment in *S. typhimurium* SL3261-infected mice

Analysis of CD64 expression in the brain 17 days after injection with 1.8 x 10^6 colony forming units of *S. typhimurium* SL3261. Mice were treated with isotype control or bispecific anti-mTNF-α fusion protein (54 μM, i.p.) 10 days after *S. typhimurium* injection and tissue collected 7 days later. Values are displayed as average area covered as determined by custom macro analysis in FIJI (Appendix A3). Data were analysed by one-way ANOVA with Holm-Sidak's multiple comparisons test. Graphs are presented as mean ± SD; n = 3-4/group.

G3 MHCII expression in the hippocampus/thalamus after *S. typhimurium* infection and mTNFR2 fusion protein treatment

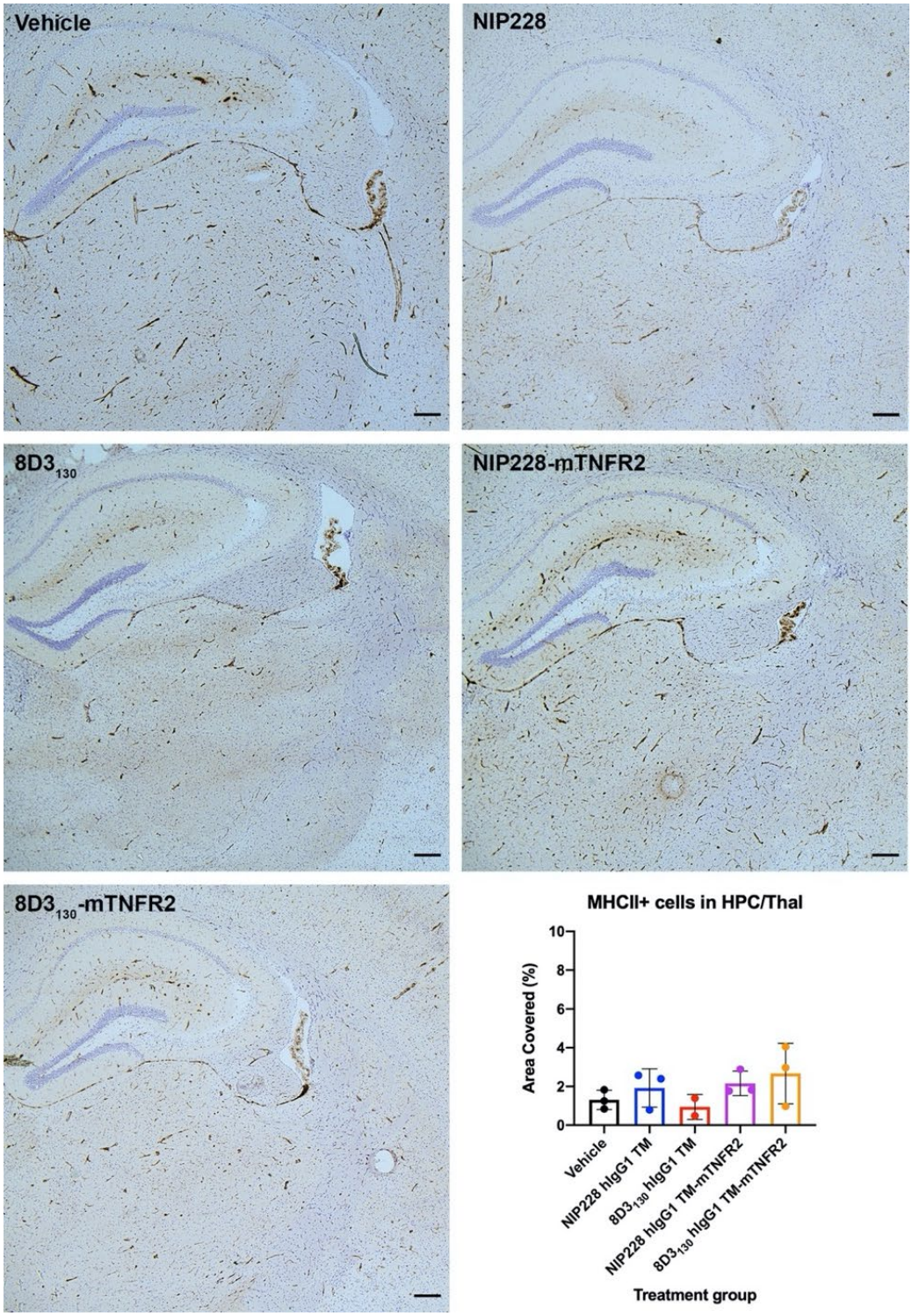

Appendix Figure J Brain MHCII expression after bispecific mTNFR2 fusion protein treatment in *S. typhimurium* SL3261-infected mice

Analysis of MHCII expression in the brain 17 days after injection with 1.8 x 10^6 colony forming units of *S. typhimurium* SL3261. Mice were treated with isotype control or bispecific anti-mTNF-α fusion protein (54 μM, i.p.) 10 days after *S. typhimurium* injection and tissue collected 7 days later. Values are displayed as average area covered as determined by custom macro analysis in FIJI (Appendix A3). Data were analysed by one-way ANOVA with Holm-Sidak's multiple comparisons test. Graphs are presented as mean ± SD; n = 3-4/group.

G4 TfR expression in the hippocampus/thalamus after *S. typhimurium* infection and mTNFR2 fusion protein treatment

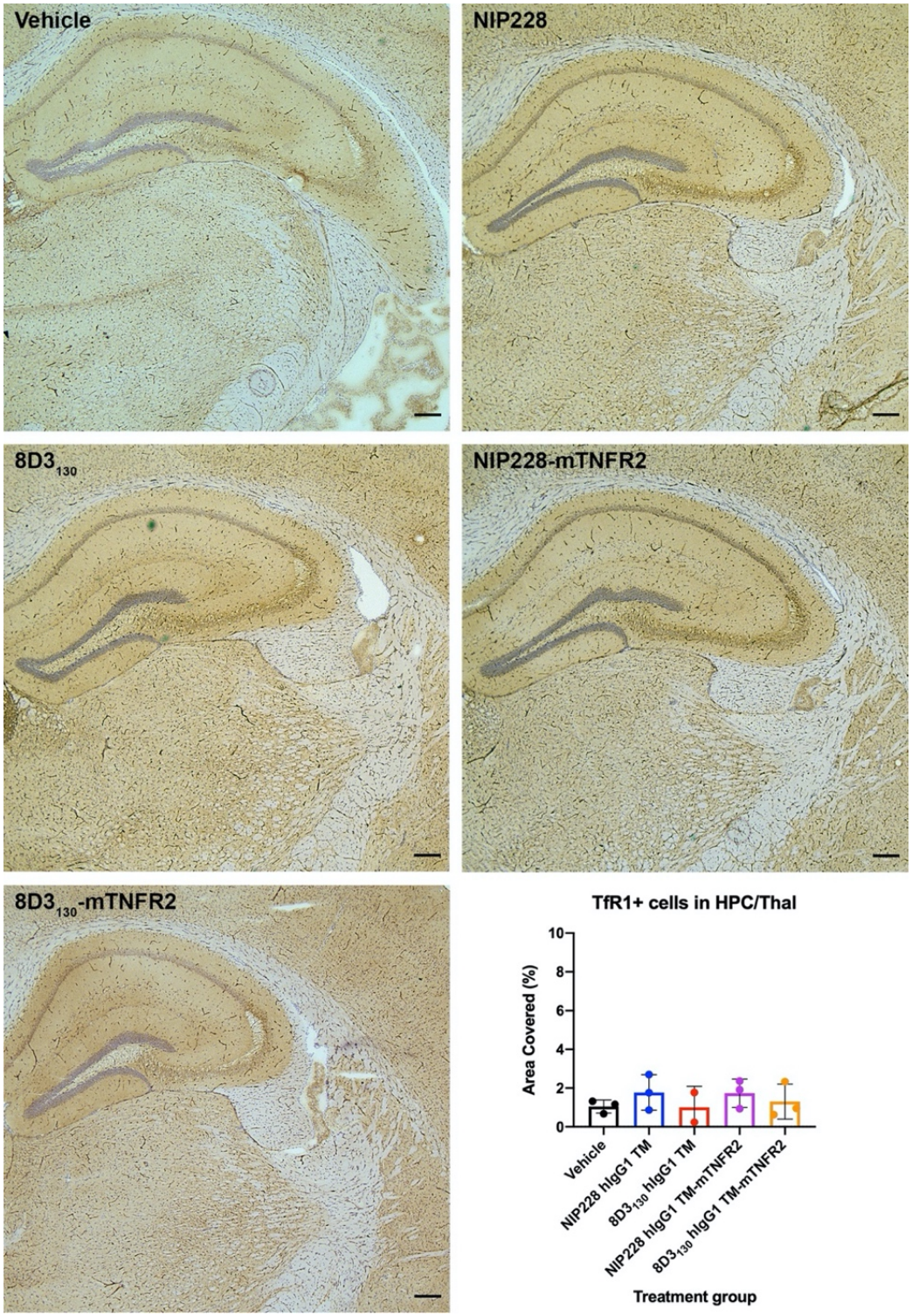

Appendix Figure K Brain TfR expression after bispecific mTNFR2 fusion protein treatment in *S. typhimurium* SL3261-infected mice

Analysis of TfR expression in the brain 17 days after injection with 1.8 x 10^6 colony forming units of *S. typhimurium* SL3261. Mice were treated with isotype control or bispecific anti-mTNF-α fusion protein (54 μM, i.p.) 10 days after *S. typhimurium* injection and tissue collected 7 days later. Values are displayed as average area covered as determined by custom macro analysis in FIJI (Appendix A3). Data were analysed by one-way ANOVA with Holm-Sidak's multiple comparisons test. Graphs are presented as mean ± SD; n = 3-4/group.

Appendix H Splenic response to *S. typhimurium* after administration of bispecific mTNFR2 fusion proteins

H1 Biochemical analysis of cytokine and protein markers within the spleen after *S. typhimurium* infection and mTNFR2 fusion treatment

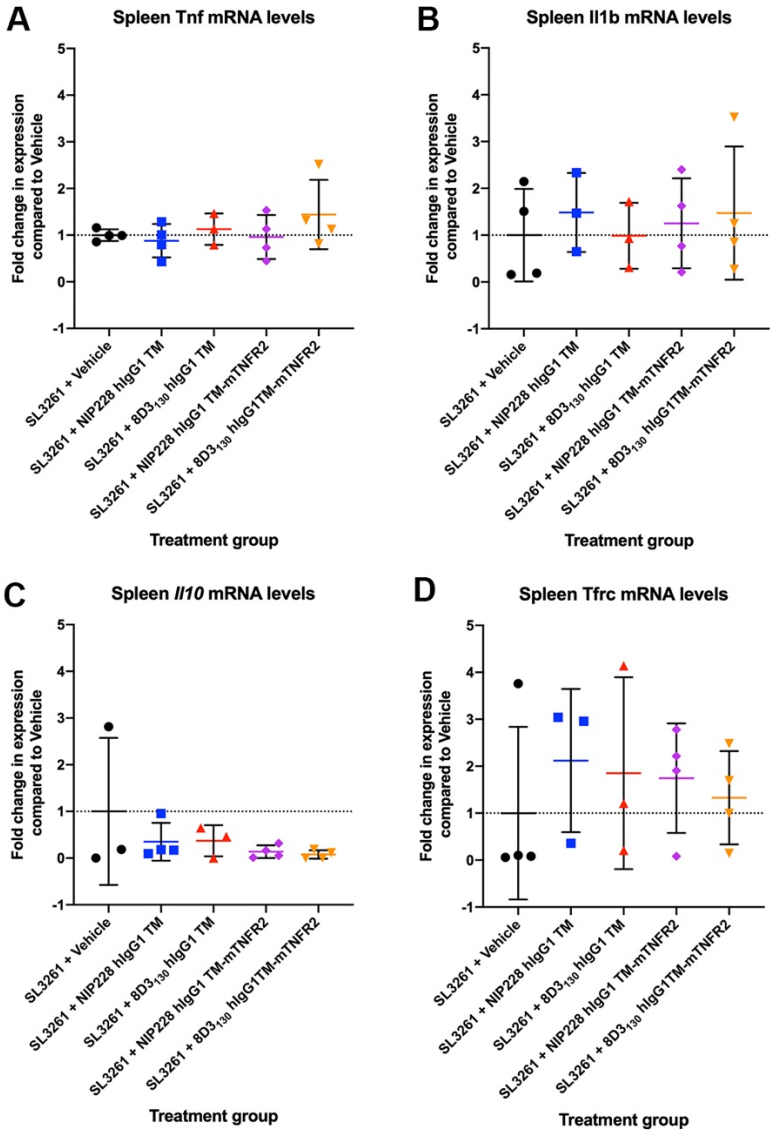

Appendix Figure L Spleen cytokine expression after bispecific mTNFR2 fusion protein treatment in *S. typhimurium* SL3261-infected mice

Analysis of expression of specific cytokine and protein markers downstream of TNF-α in the spleen 17 days after injection with 1.8 x 10^6 colony forming units of *S. typhimurium* SL3261. Mice were treated 10 days after *S. typhimurium* injection with isotype control or bispecific anti-mTNF-α fusion protein (54 μM, i.p.) and tissue collected 7 days later. Spleen mRNA expression of *Tnf* (A), *Il1b* (B), *Il10* (C), *Tfrc* (D) was analysed by SYBR green qPCR (Section 2.2.2.3). Data are presented as the mean ± SD (n = 3-4/group) of fold change compared to SL3261 + vehicle mice after normalisation of expression to *Pgk1.* Data were analysed by one-way ANOVA with Holm-Sidak's multiple comparisons test. These data were generated by an MBioSci student, Ms. Hanna Davies.

H2 CD64 expression in the spleen after *S. typhimurium* infection and mTNFR2 fusion protein treatment

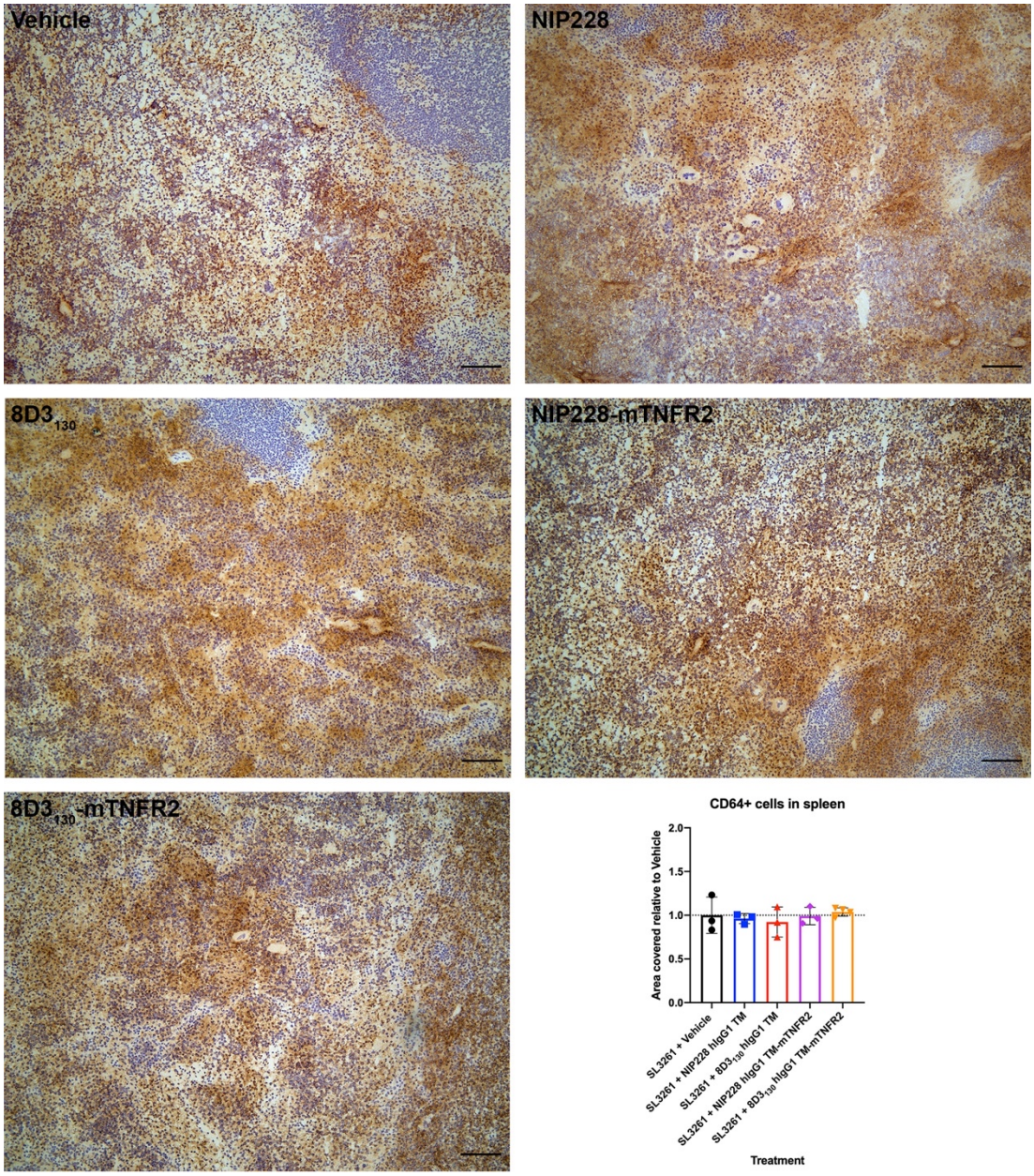

Appendix Figure M Spleen CD64 expression after bispecific mTNFR2 fusion protein treatment in *S. typhimurium* SL3261-infected mice

Analysis of CD64 expression in the spleen 17 days after injection with 1.8 x 10^6 colony forming units of *S. typhimurium* SL3261. Mice were treated with isotype control or bispecific anti-mTNF-α fusion protein (54 μM, i.p.) 10 days after *S. typhimurium* injection and tissue collected 7 days later. Values are displayed as average area covered relative to Vehicle-treated mice as determined by custom macro analysis in FIJI (Appendix A3). Data were analysed by one-way ANOVA with Holm-Sidak's multiple comparisons test. Graphs are presented as mean ± SD; n = 3-4/group. Staining and imaging were performed by an MBioSci student, Ms. Hanna Davies.

H3 CD11b expression in the spleen after *S. typhimurium* infection and mTNFR2 fusion protein treatment

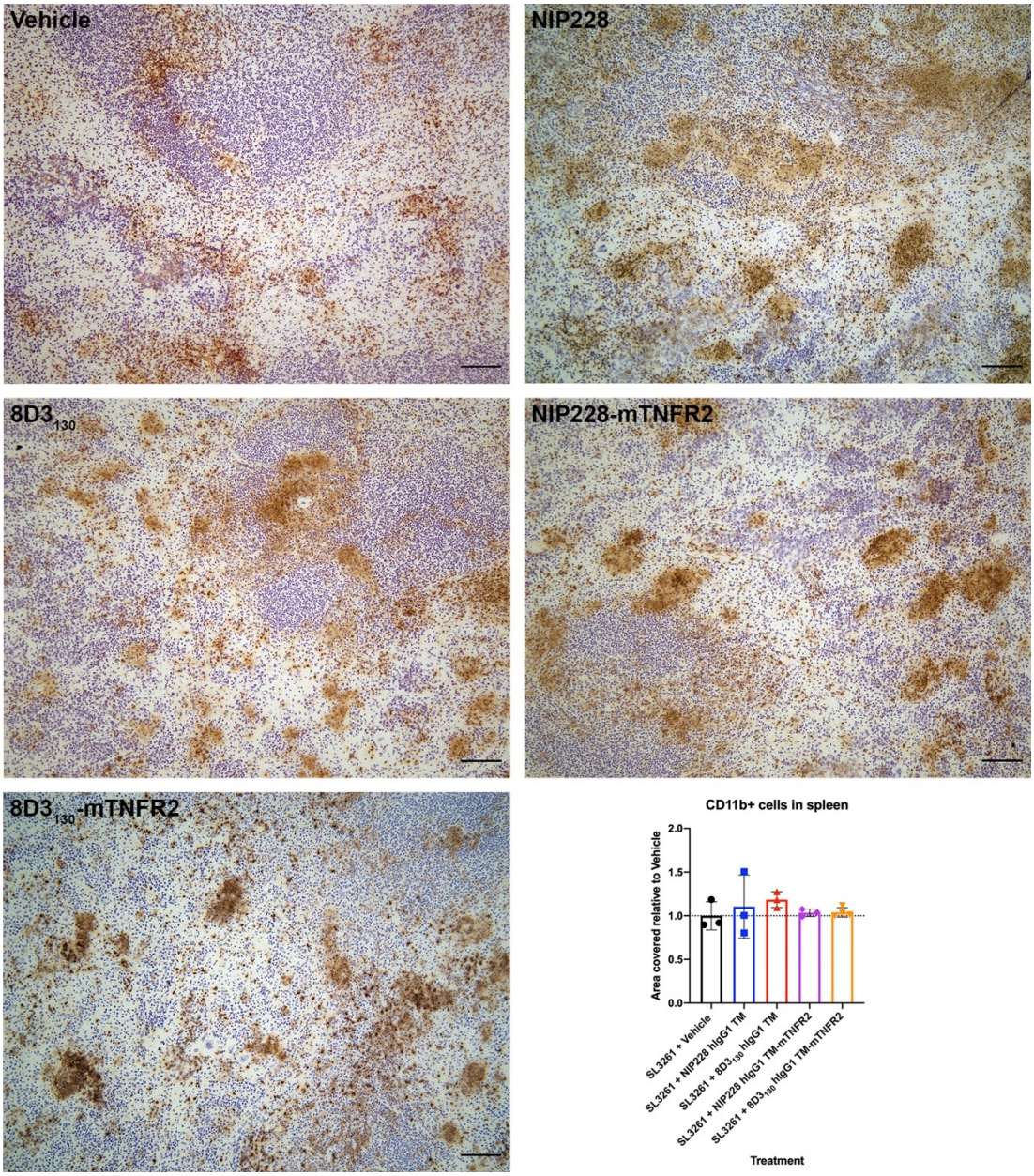

Appendix Figure N Spleen CD11b expression after bispecific mTNFR2 fusion protein treatment in *S. typhimurium* SL3261-infected mice

Analysis of CD11b expression in the spleen 17 days after injection with 1.8 x 10^6 colony forming units of *S. typhimurium* SL3261. Mice were treated with isotype control or bispecific anti-mTNF-α fusion protein (54 μM, i.p.) 10 days after *S. typhimurium* injection and tissue collected 7 days later. Values are displayed as average area covered relative to Vehicle-treated mice as determined by custom macro analysis in FIJI (Appendix A3). Data were analysed by One-way ANOVA with Dunnett's correction for multiple comparisons. Graphs are presented as mean ± SD; n = 3-4/group. Staining and imaging were performed by an MBioSci student, Ms. Hanna Davies.

H4 CD68 expression in the spleen after *S. typhimurium* infection and mTNFR2 fusion protein treatment

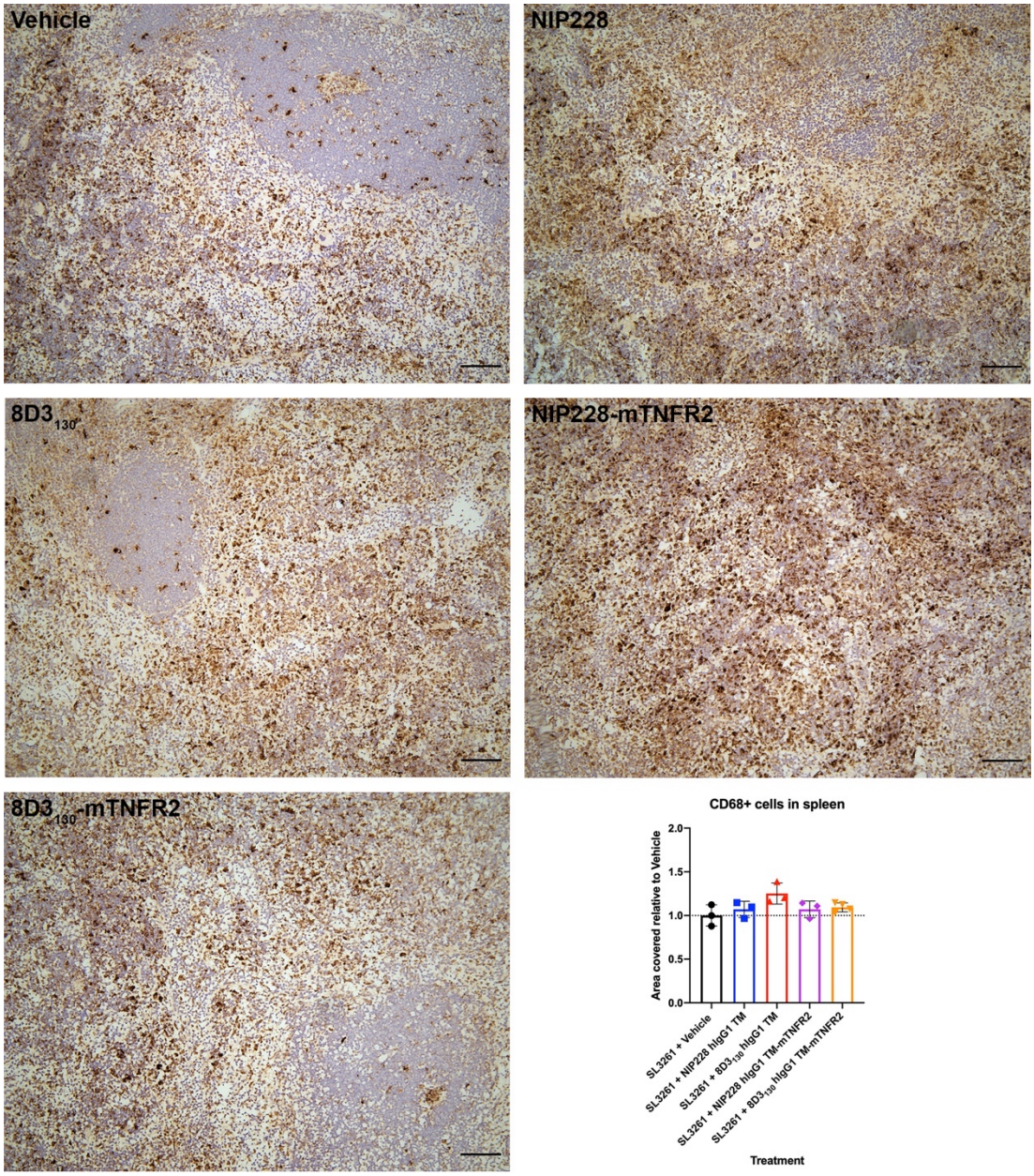

Appendix Figure O Spleen CD68 expression after bispecific mTNFR2 fusion protein treatment in *S. typhimurium* SL3261-infected mice

Analysis of CD68 expression in the spleen 17 days after injection with 1.8 x 10^6 colony forming units of *S. typhimurium* SL3261. Mice were treated with isotype control or bispecific anti-mTNF-α fusion protein (54 μM, i.p.) 10 days after *S. typhimurium* injection and tissue collected 7 days later. Values are displayed as average area covered relative to Vehicle-treated mice as determined by custom macro analysis in FIJI (Appendix A3). Data were analysed by One-way ANOVA with Dunnett's correction for multiple comparisons. Graphs are presented as mean ± SD; n = 3-4/group. Staining and imaging were performed by an MBioSci student, Ms. Hanna Davies.

Bibliography

Abbott, N.J., 2013. Blood-brain barrier structure and function and the challenges for CNS drug delivery. J. Inherit. Metab. Dis. 36, 437–449. https://doi.org/10.1007/s10545-013-9608-0

Abbott, N.J., Patabendige, A.A.K., Dolman, D.E.M., Yusof, S.R., Begley, D.J., 2010. Structure and function of the blood-brain barrier. Neurobiol. Dis. 37, 13–25. https://doi.org/10.1016/j.nbd.2009.07.030

Ajami, B., Bennett, J.L., Krieger, C., Tetzlaff, W., Rossi, F.M.V., 2007. Local self-renewal can sustain CNS microglia maintenance and function throughout adult life. Nat. Neurosci. 10, 1538–1543. https://doi.org/10.1038/nn2014

Alibhai, J., Blanco, R.A., Barria, M.A., Piccardo, P., Caughey, B., Perry, V.H., Freeman, T.C., Manson, J.C., 2016. Distribution of Misfolded Prion Protein Seeding Activity Alone Does Not Predict Regions of Neurodegeneration. PLOS Biol. 14, e1002579. https://doi.org/10.1371/journal.pbio.1002579

Altamura, S., Vegi, N.M., Hoppe, P.S., Schroeder, T., Aichler, M., Walch, A., Okreglicka, K., Hültner, L., Schneider, M., Ladinig, C., Kuklik-Roos, C., Mysliwietz, J., Janik, D., Neff, F., Rathkolb, B., de Angelis, M.H., Buske, C., da Silva, A.R., Muedder, K., Conrad, M., Ganz, T., Kopf, M., Muckenthaler, M.U., Bornkamm, G.W., 2020. Glutathione peroxidase 4 and vitamin E control reticulocyte maturation, stress erythropoiesis and iron homeostasis. Haematologica 105, 937–950. https://doi.org/10.3324/haematol.2018.212977

Annunziato, F., Cosmi, L., Liotta, F., Maggi, E., Romagnani, S., 2012. Defining the human T helper 17 cell phenotype. Trends Immunol. 33, 505–512. https://doi.org/10.1016/j.it.2012.05.004

Aoto, M., Iwashita, A., Mita, K., Ohkubo, N., Tsujimoto, Y., Mitsuda, N., 2019. Transferrin receptor 1 is required for enucleation of mouse erythroblasts during terminal differentiation. FEBS Open Bio 9, 291–303. https://doi.org/10.1002/2211-5463.12573

Arnaiz, E., Almkvist, O., 2003. Neuropsychological features of mild cognitive impairment and preclinical Alzheimer's disease. Acta Neurol. Scand. 107, 34–41.

Askew, K., Li, K., Olmos-Alonso, A., Garcia-Moreno, F., Liang, Y., Richardson, P., Tipton, T., Chapman, M.A., Riecken, K., Beccari, S., Sierra, A., Molnár, Z., Cragg, M.S., Garaschuk, O., Perry, V.H., Gomez-Nicola, D., 2017. Coupled Proliferation and Apoptosis Maintain the Rapid Turnover of Microglia in the Adult Brain. Cell Rep. 18, 391–405. https://doi.org/10.1016/j.celrep.2016.12.041

Association, A., 2015. 2015 Alzheimer's disease facts and figures. Alzheimer's Dement. 11, 332–384. https://doi.org/10.1016/j.jalz.2015.02.003

Bibliography

Atwal, J.K., Chen, Y., Chiu, C., Mortensen, D.L., Meilandt, W.J., Liu, Y., Heise, C.E., Hoyte, K., Luk, W., Lu, Y., Peng, K., Wu, P., Rouge, L., Zhang, Y., Lazarus, R.A., Scearce-Levie, K., Wang, W., Wu, Y., Tessier-Lavigne, M., Watts, R.J., 2011. A therapeutic antibody targeting BACE1 inhibits amyloid-β production in vivo. Sci. Transl. Med. 3. https://doi.org/10.1126/scitranslmed.3002254

Ayloo, S., Gu, C., 2019. Transcytosis at the blood–brain barrier. Curr. Opin. Neurobiol. 57, 32–38. https://doi.org/10.1016/j.conb.2018.12.014

Balaram, P., Kien, P.K., Ismail, A., 2009. Toll-like receptors and cytokines in immune responses to persistent mycobacterial and Salmonella infections. Int. J. Med. Microbiol. 299, 177–185. https://doi.org/10.1016/j.ijmm.2008.08.004

Banks, W.A., 2008. Developing drugs that can cross the blood-brain barrier: applications to Alzheimer's disease. BMC Neurosci. 9, 1–4. https://doi.org/10.1186/1471-2202-9-s3-s2

Banks, W.A., Erickson, M.A., 2010. The blood-brain barrier and immune function and dysfunction. Neurobiol. Dis. 37, 26–32. https://doi.org/10.1016/j.nbd.2009.07.031

Banks, W.A., Robinson, S.M., 2010. Minimal penetration of lipopolysaccharide across the murine blood-brain barrier. Brain. Behav. Immun. 24, 102–109. https://doi.org/10.1016/j.bbi.2009.09.001

Banks, W.A., Terrell, B., Farr, S.A., Robinson, S.M., Nonaka, N., Morley, J.E., 2002. Passage of amyloid β protein antibody across the blood–brain barrier in a mouse model of Alzheimer's disease. Peptides 23, 2223–2226. https://doi.org/10.1016/s0196-9781(02)00261-9

Barnum, C.J., Chen, X., Chung, J., Chang, J., Williams, M., Grigoryan, N., Tesi, R.J., Tansey, M.G., 2014. Peripheral administration of the selective inhibitor of soluble tumor necrosis factor (TNF) XPro®1595 attenuates nigral cell loss and glial activation in 6-OHDA hemiparkinsonian rats. J. Parkinsons. Dis. 4, 349–360. https://doi.org/10.3233/JPD-140410

Barr, T.A., Brown, S., Mastroeni, P., Gray, D., 2010. TLR and B Cell Receptor Signals to B Cells Differentially Program Primary and Memory Th1 Responses to Salmonella enterica . J. Immunol. 185, 2783–2789. https://doi.org/10.4049/jimmunol.1001431

Bateman, A., 2019. UniProt: A worldwide hub of protein knowledge. Nucleic Acids Res. 47, D506–D515. https://doi.org/10.1093/nar/gky1049

Bauler, T.J., Starr, T., Nagy, T.A., Sridhar, S., Scott, D., Winkler, C.W., Steele-Mortimer, O., Detweiler, C.S., Peterson, K.E., 2017. Salmonella Meningitis Associated with Monocyte Infiltration in Mice. Am. J. Pathol. 187, 187–199. https://doi.org/10.1016/j.ajpath.2016.09.002

Bechmann, I., Galea, I., Perry, V.H., 2007. What is the blood-brain barrier (not)? Trends Immunol. 28, 5–11. https://doi.org/10.1016/j.it.2006.11.007

Beck, A., Diemer, H., Ayoub, D., Debaene, F., Wagner-Rousset, E., Carapito, C., Van Dorsselaer, A., Sanglier-Cianférani, S., 2013. Analytical characterization of biosimilar antibodies and Fc-fusion proteins. TrAC - Trends Anal. Chem. 48, 81–95. https://doi.org/10.1016/j.trac.2013.02.014

Bell, R.D., Winkler, E.A., Sagare, A.P., Singh, I., LaRue, B., Deane, R., Zlokovic, B. V., 2010. Pericytes Control Key Neurovascular Functions and Neuronal Phenotype in the Adult Brain and during Brain Aging. Neuron 68, 409–427. https://doi.org/10.1016/j.neuron.2010.09.043

Benjamin, W.H., Hall, P., Roberts, S.J., Briles, D.E., 1990. The primary effect of the Ity locus is on the rate of growth of Salmonella typhimurium that are relatively protected from killing. J. Immunol. 144, 3143–3151.

Benzing, W.C., Wujek, J.R., Ward, E.K., Shaffer, D., Ashe, K.H., Younkin, S.G., Brunden, K.R., 1999. Evidence for glial-mediated inflammation in aged APP(SW) transgenic mice. Neurobiol. Aging 20, 581–589. https://doi.org/10.1016/S0197-4580(99)00065-2

Berthoud, H.-R., Neuhuber, W.L., 2000. Functional and chemical anatomy of the afferent vagal system. Auton. Neurosci. 85, 1–17. https://doi.org/10.1016/S1566-0702(00)00215-0

Bertram, L., Lill, C.M., Tanzi, R.E., 2010. The genetics of alzheimer disease: Back to the future. Neuron 68, 270–281. https://doi.org/10.1016/j.neuron.2010.10.013

Betmouni, S., Clements, J., Perry, V.H., 1999a. Vacuolation in murine prion disease: An informative artifact. Curr. Biol. 9, 677–679. https://doi.org/10.1016/S0960-9822(99)80437-0

Betmouni, S., Deacon, R.M.J., Rawlins, J.N.P., Perry, V.H., 1999b. Behavioral consequences of prion disease targeted to the hippocampus in a mouse model of scrapie. Psychobiology 27, 63–71. https://doi.org/10.3758/BF03332100

Betmouni, S., Perry, V.H., 1999. The acute inflammatory response in CNS following injection of prion brain homogenate or normal brain homogenate. Neuropathol. Appl. Neurobiol. 25, 20–8. https://doi.org/10.1046/j.1365-2990.1999.00153.x

Betmouni, S., Perry, V.H., Gordon, J.L., 1996. Evidence for an early inflammatory response in the central nervous system of mice with scrapie. Neuroscience 74, 1–5. https://doi.org/10.1016/0306-4522(96)00212-6

Bhardwaj, N., Saxena, R.K., 2015. Selective loss of younger erythrocytes from blood circulation and changes in erythropoietic patterns in bone marrow and spleen in mouse anemia induced by poly-dispersed single-walled carbon nanotubes. Nanotoxicology 9, 1032–1040. https://doi.org/10.3109/17435390.2014.998307

Bickel, U., 2005. How to measure drug transport across the blood-brain barrier. NeuroRx 2, 15–26. https://doi.org/10.1602/neurorx.2.1.15

Bibliography

Bien-Ly, N., Boswell, C.A., Jeet, S., Beach, T.G., Hoyte, K., Luk, W., Shihadeh, V., Ulufatu, S., Foreman, O., Lu, Y., DeVoss, J., van der Brug, M., Watts, R.J., 2015. Lack of Widespread BBB Disruption in Alzheimer's Disease Models: Focus on Therapeutic Antibodies. Neuron 88, 289–297. https://doi.org/10.1016/j.neuron.2015.09.036

Bien-Ly, N., Yu, Y.J., Bumbaca, D., Elstrott, J., Boswell, C.A., Zhang, Y., Luk, W., Lu, Y., Dennis, M.S., Weimer, R.M., Chung, I., Watts, R.J., 2014. Transferrin receptor (TfR) trafficking determines brain uptake of TfR antibody affinity variants. J. Exp. Med. 211, 233–44. https://doi.org/10.1084/jem.20131660

Billmeier, U., Dieterich, W., Neurath, M.F., Atreya, R., 2016. Molecular mechanism of action of anti-tumor necrosis factor antibodies in inflammatory bowel diseases. World J. Gastroenterol. 22, 9300–9313. https://doi.org/10.3748/wjg.v22.i42.9300

Biswas, S.K., Lopez-Collazo, E., 2009. Endotoxin tolerance: new mechanisms, molecules and clinical significance. Trends Immunol. 30, 475–487. https://doi.org/10.1016/j.it.2009.07.009

Blamire, A.M., Anthony, D.C., Rajagopalan, B., Sibson, N.R., Perry, V.H., Styles, P., 2000. Interleukin-1beta -induced changes in blood-brain barrier permeability, apparent diffusion coefficient, and cerebral blood volume in the rat brain: A magnetic resonance study [In Process Citation]. J Neurosci 20, 8153–8159.

Bluthe, R.-M., Michaud, B., Kelley, K.W., Dantzer, R., 1996. Vagotomy attenuates behavioural effects of interleukin-1 injected peripherally but not centrally. Neuroreport 7, 1485–1488. https://doi.org/10.1097/00001756-199606170-00008

Boado, R.J., Zhou, Q., Lu, J.Z., Hui, E.K., Pardridge, W.M., 2010. Pharmacokinetics and Brain Uptake of a Genetically Engineered Bifunctional Fusion Antibody Targeting the Mouse Transferrin Receptor. Mol. Pharm. 7, 237–244. https://doi.org/10.1021/mp900235k

Bohac, D., Burke, W., Cotter, R., Zheng, J., Potter, J., 2002. A 24-Week Randomized, Double-Blind, Placebo-Controlled Study Of The Efficacy And Tolerability Of Tnfr: Fc (Etanercept) In The Treatment Of Dementia Of The Alzheimer Type. Neurobiol. Aging 23, S83. https://doi.org/10.1016/s0197-4580(02)00052-0

Bohrmann, B., Baumann, K., Benz, J., Gerber, F., Huber, W., Knoflach, F., Messer, J., Oroszlan, K., Rauchenberger, R., Richter, W.F., Rothe, C., Urban, M., Bardroff, M., Winter, M., Nordstedt, C., Loetscher, H., 2012. Gantenerumab: A novel human anti-Aβ antibody demonstrates sustained cerebral amyloid-β binding and elicits cell-mediated removal of human amyloid-β. J. Alzheimer's Dis. 28, 49–69. https://doi.org/10.3233/JAD-2011-110977

Borner, R., Bento-Torres, J., Souza, D.R.V., Sadala, D.B., Trevia, N., Farias, J.A., Lins, N., Passos, A., Quintairos, A., Diniz, J.A., Perry, V.H., Vasconcelos, P.F., Cunningham, C., Picanço-Diniz, C.W., 2011. Early behavioral changes and quantitative analysis of neuropathological features in murine prion disease. Prion 5, 215–227. https://doi.org/10.4161/pri.5.3.16936

Borovikova, L. V., Ivanova, S., Zhang, M., Yang, H., Botchkina, G.I., Watkins, L.R., Wang, H., Abumrad, N., Eaton, J.W., Tracey, K.J., 2000. Vagus nerve stimulation attenuates the systemic inflammatory response to endotoxin. Nature 405, 458–462. https://doi.org/10.1038/35013070

Borrok, M.J., Mody, N., Lu, X., Kuhn, M.L., Wu, H., Dall'Acqua, W.F., Tsui, P., 2017. An "Fc-Silenced" IgG1 Format With Extended Half-Life Designed for Improved Stability. J. Pharm. Sci. 106, 1008–1017. https://doi.org/10.1016/j.xphs.2016.12.023

Bourassa, P., Alata, W., Tremblay, C., Paris-Robidas, S., Calon, F., 2019. Transferrin Receptor-Mediated Uptake at the Blood-Brain Barrier Is Not Impaired by Alzheimer's Disease Neuropathology. Mol. Pharm. 16, 583–594. https://doi.org/10.1021/acs.molpharmaceut.8b00870

Boyko, A., Troyanova, N., Kovalenko, E., Sapozhnikov, A., 2017. Similarity and Differences in Inflammation-Related Characteristics of the Peripheral Immune System of Patients with Parkinson's and Alzheimer's Diseases. Int. J. Mol. Sci. 18, 2633. https://doi.org/10.3390/ijms18122633

Braak, H., Thal, D.R., Ghebremedhin, E., Tredici, K. Del, 2011. Stages of the Pathologic Process in Alzheimer Disease : Age Categories From 1 to 100 Years Stages of the Pathologic Process in Alzheimer Disease : Age Categories From 1 to 100 Years. J. Neuropathol. Exp. Neurol. 70, 960–969. https://doi.org/10.1097/NEN.0b013e318232a379

Bret-Dibat, J.L., Bluthe, R.M., Kent, S., Kelley, K.W., Dantzer, R., 1995. Lipopolysaccharide and interleukin-1 depress food-motivated behavior in mice by a vagal-mediated mechanism. Brain Behav. Immun. https://doi.org/10.1006/brbi.1995.1023

Brinkmann, U., Kontermann, R.E., 2017. The making of bispecific antibodies. MAbs 9, 182–212. https://doi.org/10.1080/19420862.2016.1268307

Bronte, V., Pittet, M.J., 2013. The spleen in local and systemic regulation of immunity. Immunity 39, 806–818. https://doi.org/10.1016/j.immuni.2013.10.010

Brosseron, F., Krauthausen, M., Kummer, M., Heneka, M.T., 2014. Body Fluid Cytokine Levels in Mild Cognitive Impairment and Alzheimer???s Disease: a Comparative Overview. Mol. Neurobiol. 50, 534–544. https://doi.org/10.1007/s12035-014-8657-1

Brown, D.E., Libby, S.J., Moreland, S.M., McCoy, M.W., Brabb, T., Stepanek, A., Fang, F.C., Detweiler, C.S., 2013. Salmonella enterica Causes More Severe Inflammatory Disease in C57/BL6 Nramp1G169 Mice Than Sv129S6 Mice. Vet. Pathol. 50, 867–876. https://doi.org/10.1177/0300985813478213

Brown, D.E., McCoy, M.W., Pilonieta, M.C., Nix, R.N., Detweiler, C.S., 2010. Chronic murine typhoid fever is a natural model of secondary hemophagocytic lymphohistiocytosis. PLoS One 5. https://doi.org/10.1371/journal.pone.0009441

Broz, P., Monack, D.M., 2011. Molecular mechanisms of inflammasome activation during microbial infections. Immunol. Rev. 243, 174–190. https://doi.org/http://dx.doi.org/10.1111/j.1600-065X.2011.01041.x

Bibliography

Broz, P., Ohlson, M.B., Monack, D.M., 2012. Innate immune response to Salmonella typhimurium, a model enteric pathogen. Gut Microbes 3, 62–70. https://doi.org/10.4161/gmic.19141

Burdo, J.R., Antonetti, D.A., Wolpert, E.B., Connor, J.R., 2003. Mechanisms and regulation of transferrin and iron transport in a model blood-brain barrier system. Neuroscience 121, 883–890. https://doi.org/10.1016/S0306-4522(03)00590-6

Buss, N.A.P.S., Henderson, S.J., McFarlane, M., Shenton, J.M., De Haan, L., 2012. Monoclonal antibody therapeutics: History and future. Curr. Opin. Pharmacol. 12, 615–622. https://doi.org/10.1016/j.coph.2012.08.001

Busse, M., Michler, E., Von Hoff, F., Dobrowolny, H., Hartig, R., Frodl, T., Busse, S., 2017. Alterations in the Peripheral Immune System in Dementia. J. Alzheimer's Dis. 58, 1303–1313. https://doi.org/10.3233/JAD-161304

Butchart, J., Brook, L., Hopkins, V., Teeling, J., Puntener, U., Culliford, D., Sharples, R., Sharif, S., McFarlane, B., Raybould, R., Thomas, R., Passmore, P., Perry, V.H., Holmes, C., 2015. Etanercept in Alzheimer disease: A randomized, placebo-controlled, double-blind, phase 2 trial. Neurology 84, 2161–2168. https://doi.org/10.1212/WNL.0000000000001617

Cabal-Hierro, L., Lazo, P.S., 2012. Signal transduction by tumor necrosis factor receptors. Cell. Signal. 24, 1297–1305. https://doi.org/10.1016/j.cellsig.2012.02.006

Cai, B., Pan, H., Flynn, G.C., 2011. C-terminal lysine processing of human immunoglobulin G2 heavy chain in vivo. Biotechnol. Bioeng. 108, 404–412. https://doi.org/10.1002/bit.22933

Caleo, M., Restani, L., Vannini, E., Siskova, Z., Al-Malki, H., Morgan, R., O'Connor, V., Perry, V.H., 2012. The Role of Activity in Synaptic Degeneration in a Protein Misfolding Disease, Prion Disease. PLoS One 7, e41182. https://doi.org/10.1371/journal.pone.0041182

Canault, M., Peiretti, F., Mueller, C., Deprez, P., Bonardo, B., Bernot, D., Juhan-Vague, I., Nalbone, G., 2004. Proinflammatory properties of murine aortic endothelial cells exclusively expressing a non cleavable form of TNFα. Thromb. Haemost. 92, 1428–1437. https://doi.org/10.1160/th04-06-0344

Carroll, J.A., Chesebro, B., 2019. Neuroinflammation, microglia, and cell-association during prion disease. Viruses 11. https://doi.org/10.3390/v11010065

Carroll, J.A., Striebel, J.F., Race, B., Phillips, K., Chesebro, B., 2015. Prion infection of mouse brain reveals multiple new upregulated genes involved in neuroinflammation or signal transduction. J Virol 89, 2388–2404. https://doi.org/10.1128/JVI.02952-14

Carroll, J.A., Striebel, J.F., Rangel, A., Woods, T., Phillips, K., Peterson, K.E., Race, B., Chesebro, B., 2016. Prion Strain Differences in Accumulation of PrPSc on Neurons and Glia Are Associated with Similar Expression Profiles of Neuroinflammatory Genes: Comparison of Three Prion Strains. PLOS Pathog. 12, e1005551. https://doi.org/10.1371/journal.ppat.1005551

Carter, P.J., 2011. Introduction to current and future protein therapeutics: A protein engineering perspective. Exp. Cell Res. 317, 1261–1269. https://doi.org/10.1016/j.yexcr.2011.02.013

Cataldi, M., Vigliotti, C., Mosca, T., Cammarota, M.R., Capone, D., 2017. Emerging role of the spleen in the pharmacokinetics of monoclonal antibodies, nanoparticles and exosomes. Int. J. Mol. Sci. 18. https://doi.org/10.3390/ijms18061249

Cavanagh, C., Tse, Y.C., Nguyen, H.B., Krantic, S., Breitner, J.C.S., Quirion, R., Wong, T.P., 2016. Inhibiting tumor necrosis factor-α before amyloidosis prevents synaptic deficits in an Alzheimer's disease model. Neurobiol. Aging 47, 41–49. https://doi.org/10.1016/j.neurobiolaging.2016.07.009

Chang, R., Knox, J., Chang, J., Derbedrossian, A., Vasilevko, V., Cribbs, D., Boado, R.J., Pardridge, W.M., Sumbria, R.K., 2017. Blood–Brain Barrier Penetrating Biologic TNF-α Inhibitor for Alzheimer's Disease. Mol. Pharm. 14, 2340–2349. https://doi.org/10.1021/acs.molpharmaceut.7b00200

Chaudhuri, D., Roy Chowdhury, A., Biswas, B., Chakravortty, D., 2018. Salmonella Typhimurium Infection Leads to Colonization of the Mouse Brain and Is Not Completely Cured With Antibiotics. Front. Microbiol. 9, 1–12. https://doi.org/10.3389/fmicb.2018.01632

Chen, Y., Zou, Z., Wu, Z., Zhao, Z., Luo, X., Xie, C., Liang, Y., 2015. TNF-α-induced programmed cell death in the pathogenesis of acquired aplastic anemia. Expert Rev. Hematol. 8, 515–526. https://doi.org/10.1586/17474086.2015.1049593

Chen, Y.M., Chen, H.H., Lan, J.L., Chen, D.Y., 2010. Improvement of cognition, a potential benefit of anti-TNF therapy in elderly patients with rheumatoid arthritis. Jt. Bone Spine 77, 366–367. https://doi.org/10.1016/j.jbspin.2010.01.017

Chen, Z., Ljunggren, H.G., Bogdanovic, N., Nennesmo, I., Winblad, B., Zhu, J., 2002. Excitotoxic neurodegeneration induced by intranasal administration of kainic acid in C57BL/6 mice. Brain Res. 931, 135–145. https://doi.org/10.1016/S0006-8993(02)02268-0

Cheng, X., Yang, L., He, P., Li, R., Shen, Y., 2010. Differential activation of tumor necrosis factor receptors distinguishes between brains from Alzheimer's disease and non-demented patients. J. Alzheimer's Dis. 19, 621–630. https://doi.org/10.3233/JAD-2010-1253

Cheyne, J.E., Montgomery, J.M., 2008. Plasticity-dependent changes in metabotropic glutamate receptor expression at excitatory hippocampal synapses. Mol. Cell. Neurosci. 37, 432–439. https://doi.org/10.1016/j.mcn.2007.10.015

Chiti, Z., Knutsen, O.M., Betmouni, S., Greene, J.R.T., 2006. An integrated, temporal study of the behavioural, electrophysiological and neuropathological consequences of murine prion disease. Neurobiol. Dis. 22, 363–373. https://doi.org/10.1016/j.nbd.2005.12.002

Bibliography

Chou, R.C., Kane, M., Ghimire, S., Gautam, S., Gui, J., 2016. Treatment for Rheumatoid Arthritis and Risk of Alzheimer's Disease: A Nested Case-Control Analysis. CNS Drugs 30, 1111–1120. https://doi.org/10.1007/s40263-016-0374-z

Chouhan, J.K., Fowler, S.B., Webster, C.I., Teeling, J.L., 2017. The ME7 prion model of neurodegeneration as a tool to understand and target neuroinflammation in Alzheimer's disease. Drug Discov. Today Dis. Model. 25–26, 45–52. https://doi.org/10.1016/j.ddmod.2018.10.004

Cicha, I., Urschel, K., 2015. TNF-alpha: in the cardiovascular system: from physiology to therapy. Int. J. Interf. Cytokine Mediat. Res. 7, 9. https://doi.org/10.2147/IJICMR.S64894

Clark, A.J., Davis, M.E., 2015. Increased brain uptake of targeted nanoparticles by adding an acid-cleavable linkage between transferrin and the nanoparticle core. Proc. Natl. Acad. Sci. 112, 12486–12491. https://doi.org/10.1073/pnas.1517048112

Combrinck, M.I., Perry, V.H., Cunningham, C., 2002. Peripheral infection evokes exaggerated sickness behaviour in pre-clinical murine prion disease. Neuroscience 112, 7–11. https://doi.org/10.1016/S0306-4522(02)00030-1

Cosmi, L., Maggi, L., Santarlasci, V., Liotta, F., Annunziato, F., 2014. T helper cells plasticity in inflammation. Cytom. Part A 85, 36–42. https://doi.org/10.1002/cyto.a.22348

Couch, J.A., Yu, Y.J., Zhang, Y., Tarrant, J.M., Fuji, R.N., Meilandt, W.J., Solanoy, H., Tong, R.K., Hoyte, K., Luk, W., Lu, Y., Gadkar, K., Prabhu, S., Ordonia, B.A., Nguyen, Q., Lin, Y., Lin, Z., Balazs, M., Scearce-Levie, K., Ernst, J.A., Dennis, M.S., Watts, R.J., 2013. Addressing Safety Liabilities of TfR Bispecific Antibodies That Cross the Blood-Brain Barrier. Sci. Transl. Med. 5, 183ra57-183ra57. https://doi.org/10.1126/scitranslmed.3005338

Cullen, P.J., Steinberg, F., 2018. To degrade or not to degrade: mechanisms and significance of endocytic recycling. Nat. Rev. Mol. Cell Biol. 19, 679–696. https://doi.org/10.1038/s41580-018-0053-7

Cunningham, A.F., Gaspal, F., Serre, K., Mohr, E., Henderson, I.R., Scott-Tucker, A., Kenny, S.M., Khan, M., Toellner, K.-M., Lane, P.J.L., MacLennan, I.C.M., 2007. Salmonella Induces a Switched Antibody Response without Germinal Centers That Impedes the Extracellular Spread of Infection . J. Immunol. 178, 6200–6207. https://doi.org/10.4049/jimmunol.178.10.6200

Cunningham, C., 2013. Microglia and neurodegeneration: The role of systemic inflammation. Glia 61, 71–90. https://doi.org/10.1002/glia.22350

Cunningham, C., 2005. Mouse Behavioural Studies and What They Can Teach Us about Prion Diseases, in: Brown, D.R. (Ed.), Neurodegeneration and Prion Disease. Springer US, Boston, MA, pp. 111–137. https://doi.org/10.1007/0-387-23923-5_5

Cunningham, C., Campion, S., Lunnon, K., Murray, C.L., Woods, J.F.C., Deacon, R.M.J., Rawlins, J.N.P., Perry, V.H., 2009. Systemic Inflammation Induces Acute Behavioral and Cognitive Changes and Accelerates Neurodegenerative Disease. Biol. Psychiatry 65, 304–312. https://doi.org/10.1016/j.biopsych.2008.07.024

Cunningham, C., Deacon, R., Wells, H., Boche, D., Waters, S., Diniz, C.P., Scott, H., Rawlins, J.N.P., Perry, V.H., 2003. Synaptic changes characterize early behavioural signs in the ME7 model of murine prion disease. Eur. J. Neurosci. 17, 2147–2155. https://doi.org/10.1046/j.1460-9568.2003.02662.x

Cunningham, C., Deacon, R.M.J., Chan, K., Boche, D., Rawlins, J.N.P., Perry, V.H., 2005a. Neuropathologically distinct prion strains give rise to similar temporal profiles of behavioral deficits. Neurobiol. Dis. 18, 258–269. https://doi.org/10.1016/j.nbd.2004.08.015

Cunningham, C., Wilcockson, D.C., Boche, D., Perry, V.H., 2005b. Comparison of Inflammatory and Acute-Phase Responses in the Brain and Peripheral Organs of the ME7 Model of Prion Disease. J. Virol. 79, 5174–5184. https://doi.org/10.1128/JVI.79.8.5174-5184.2005

Cunningham, C., Wilcockson, D.C., Campion, S., Lunnon, K., Perry, V.H., 2005c. Central and Systemic Endotoxin Challenges Exacerbate the Local Inflammatory Response and Increase Neuronal Death during Chronic Neurodegeneration. J. Neurosci. 25, 9275–9284. https://doi.org/10.1523/JNEUROSCI.2614-05.2005

D'Anna, L., Abu-Rumeileh, S., Fabris, M., Pistis, C., Baldi, A., Sanvilli, N., Curcio, F., Gigli, G.L., D'Anna, S., Valente, M., 2017. Serum Interleukin-10 Levels Correlate with Cerebrospinal Fluid Amyloid Beta Deposition in Alzheimer Disease Patients. Neurodegener. Dis. 17, 227–234. https://doi.org/10.1159/000474940

D'Mello, C., Swain, M.G., 2016. Immune-to-Brain Communication Pathways in Inflammation-Associated Sickness and Depression, in: Brain Imaging in Behavioral Neuroscience. pp. 73–94. https://doi.org/10.1007/7854_2016_37

Dagher, N.N., Najafi, A.R., Kayala, K.M.N., Elmore, M.R.P., White, T.E., Medeiros, R., West, B.L., Green, K.N., 2015. Colony-stimulating factor 1 receptor inhibition prevents microglial plaque association and improves cognition in 3xTg-AD mice. J. Neuroinflammation 12, 1–14. https://doi.org/10.1186/s12974-015-0366-9

Daneman, R., Zhou, L., Agalliu, D., Cahoy, J.D., Kaushal, A., Barres, B.A., 2010. The mouse blood-brain barrier transcriptome: A new resource for understanding the development and function of brain endothelial cells. PLoS One 5, 1–16. https://doi.org/10.1371/journal.pone.0013741

Daniels-Wells, T.R., Penichet, M.L., 2016. Transferrin receptor 1: A target for antibody-mediated cancer therapy. Immunotherapy 8, 991–994. https://doi.org/10.2217/imt-2016-0050

Dantzer, R., 2004. Cytokine-induced sickness behaviour: a neuroimmune response to activation of innate immunity. Eur. J. Pharmacol. 500, 399–411. https://doi.org/10.1016/j.ejphar.2004.07.040

Dantzer, R., 2001. Cytokine-Induced Sickness Behavior: Mechanisms and Implications. Ann. N. Y. Acad. Sci. 933, 222–234. https://doi.org/10.1111/j.1749-6632.2001.tb05827.x

Bibliography

Dantzer, R., O'Connor, J.C., Freund, G.G., Johnson, R.W., Kelley, K.W., 2008. From inflammation to sickness and depression: When the immune system subjugates the brain. Nat. Rev. Neurosci. 9, 46–56. https://doi.org/10.1038/nrn2297

Daramola, O., Stevenson, J., Dean, G., Hatton, D., Pettman, G., Holmes, W., Field, R., 2014. A high-yielding CHO transient system: Coexpression of genes encoding EBNA-1 and GS enhances transient protein expression. Biotechnol. Prog. 30, 132–141. https://doi.org/10.1002/btpr.1809

Datta-Mannan, A., Witcher, D.R., Tang, Y., Watkins, J., Wroblewski, V.J., 2007. Monoclonal antibody clearance: Impact of modulating the interaction of IgG with the neonatal Fc receptor. J. Biol. Chem. 282, 1709–1717. https://doi.org/10.1074/jbc.M607161200

Davis, D.H.J., Skelly, D.T., Murray, C., Hennessy, E., Bowen, J., Norton, S., Brayne, C., Rahkonen, T., Sulkava, R., Sanderson, D.J., Rawlins, J.N., Bannerman, D.M., MacLullich, A.M.J., Cunningham, C., 2015. Worsening cognitive impairment and neurodegenerative pathology progressively increase risk for delirium. Am. J. Geriatr. Psychiatry 23, 403–415. https://doi.org/10.1016/j.jagp.2014.08.005

Dawson, M., 2017. Endotoxin Limits For Parenteral Drug Products. BET White Pap. 1, 1–7.

de la Monte, S.M., Daiello, L.A., Hapel, A.J., Tong, M., 2017. Altered Serum and Cerebrospinal Fluid Inflammatory Cascades in Mild Cognitive Impairment and Alzheimer ' s Disease. J. Neuroinflammation Neurodegener. Dis. 1, 1–24.

Deacon, R.M., Raley, J.M., Perry, V.H., Rawlins, J.N., 2001. Burrowing into prion disease. Neuroreport 12, 2053–2057.

Deacon, R.M.J., Croucher, A., Rawlins, J.N.P., 2002. Hippocampal cytotoxic lesion effects on species-typical behaviours in mice. Behav. Brain Res. 132, 203–213. https://doi.org/10.1016/S0166-4328(01)00401-6

Deacon, R.M.J., Rawlins, J.N.P., 2005. Hippocampal lesions, species-typical behaviours and anxiety in mice. Behav. Brain Res. 156, 241–249. https://doi.org/10.1016/j.bbr.2004.05.027

Decourt, B., Lahiri, D.K., Sabbagh, M.N., 2017. Targeting Tumor Necrosis Factor Alpha for Alzheimer's Disease. Curr. Alzheimer Res. 14, 1–14. https://doi.org/10.2174/1567205013666160930

Delgado-Alvarado, M., Gago, B., Gorostidi, A., Jiménez-Urbieta, H., Dacosta-Aguayo, R., Navalpotro-Gómez, I., Ruiz-Martínez, J., Bergareche, A., Martí-Massó, J.F., Martínez-Lage, P., Izagirre, A., Rodríguez-Oroz, M.C., 2017. Tau/α-synuclein ratio and inflammatory proteins in Parkinson's disease: An exploratory study. Mov. Disord. 32, 1066–1073. https://doi.org/10.1002/mds.27001

Descamps, L., Dehouck, M.P., Torpier, G., Cecchelli, R., 1996. Receptor-mediated transcytosis of transferrin through blood-brain barrier endothelial cells. Am. J. Physiol. 270, H1149–H1158. https://doi.org/10.1152/ajpheart.1996.270.4.H1149

Diederich, M., Morceau, F., Dicato, M., 2009. Pro-inflammatory cytokine-mediated anemia: Regarding molecular mechanisms of erythropoiesis. Mediators Inflamm. 2009. https://doi.org/10.1155/2009/405016

Dimasi, N., Gao, C., Fleming, R., Woods, R.M., Yao, X.T., Shirinian, L., Kiener, P.A., Wu, H., 2009. The Design and Characterization of Oligospecific Antibodies for Simultaneous Targeting of Multiple Disease Mediators. J. Mol. Biol. 393, 672–692. https://doi.org/10.1016/j.jmb.2009.08.032

Diniz, B.S., Teixeira, A.L., Ojopi, E.B., Talib, L.L., Mendonça, V.A., Gattaz, W.F., Forlenza, O.V., 2010. Higher serum sTNFR1 level predicts conversion from mild cognitive impairment to Alzheimer's disease. J. Alzheimer's Dis. 22, 1305–1311. https://doi.org/10.3233/JAD-2010-100921

Dominy, S.S., Lynch, C., Ermini, F., Benedyk, M., Marczyk, A., Konradi, A., Nguyen, M., Haditsch, U., Raha, D., Griffin, C., Holsinger, L.J., Arastu-Kapur, S., Kaba, S., Lee, A., Ryder, M.I., Potempa, B., Mydel, P., Hellvard, A., Adamowicz, K., Hasturk, H., Walker, G.D., Reynolds, E.C., Faull, R.L.M., Curtis, M.A., Dragunow, M., Potempa, J., 2019. Porphyromonas gingivalis in Alzheimer's disease brains: Evidence for disease causation and treatment with small-molecule inhibitors. Sci. Adv. 5, eaau3333. https://doi.org/10.1126/sciadv.aau3333

Dong, Y., Dekens, D., De Deyn, P., Naudé, P., Eisel, U., 2015. Targeting of Tumor Necrosis Factor Alpha Receptors as a Therapeutic Strategy for Neurodegenerative Disorders, Antibodies. https://doi.org/10.3390/antib4040369

Dougan, G., John, V., Palmer, S., Mastroeni, P., 2011. Immunity to salmonellosis. Immunol. Rev. 240, 196–210. https://doi.org/10.1111/j.1600-065X.2010.00999.x

Dursun, E., Gezen-Ak, D., Hanağası, H., Bilgiç, B., Lohmann, E., Ertan, S., Atasoy, İ.L., Alaylıoğlu, M., Araz, Ö.S., Önal, B., Gündüz, A., Apaydın, H., Kızıltan, G., Ulutin, T., Gürvit, H., Yılmazer, S., 2015. The interleukin 1 alpha, interleukin 1 beta, interleukin 6 and alpha-2-macroglobulin serum levels in patients with early or late onset Alzheimer's disease, mild cognitive impairment or Parkinson's disease. J. Neuroimmunol. 283, 50–57. https://doi.org/10.1016/j.jneuroim.2015.04.014

Echtenacher, B., Falk, W., Mannel, D.N., Krammer, P.H., 1990. Requirement of endogenous tumor necrosis factor / cachectin for recovery from experimental peritonitis. J. Immunol. 145, 3762–3766.

Eidson, L.N., Kannarkat, G.T., Barnum, C.J., Chang, J., Chung, J., Caspell-Garcia, C., Taylor, P., Mollenhauer, B., Schlossmacher, M.G., Ereshefsky, L., Yen, M., Kopil, C., Frasier, M., Marek, K., Hertzberg, V.S., Tansey, M.G., 2017. Candidate inflammatory biomarkers display unique relationships with alpha-synuclein and correlate with measures of disease severity in subjects with Parkinson's disease. J. Neuroinflammation 14, 1–16. https://doi.org/10.1186/s12974-017-0935-1

Ek, M., Kurosawa, M., Lundeberg, T., Ericsson, A., 1998. Activation of vagal afferents after intravenous injection of interleukin-1β: Role of endogenous prostaglandins. J. Neurosci. 18, 9471–9479. https://doi.org/10.1523/jneurosci.18-22-09471.1998

Ekert, J.O., Gould, R.L., Reynolds, G., Howard, R.J., 2018. TNF alpha inhibitors in alzheimer's disease: A systematic review. Int. J. Geriatr. Psychiatry 33, 688–694. https://doi.org/10.1002/gps.4871

Bibliography

Elfferich, M.D., Nelemans, P.J., Ponds, R.W., De Vries, J., Wijnen, P.A., Drent, M., 2010. Everyday cognitive failure in sarcoidosis: The prevalence and the effect of anti-TNF-α treatment. Respiration 80, 212–219. https://doi.org/10.1159/000314225

Engelhardt, B., 2008. The Blood-Central Nervous System Barriers Actively Control Immune Cell Entry into the Central Nervous System. Curr. Pharm. Des. 14, 1555–1565. https://doi.org/10.2174/138161208784705432

Erickson, M.A., Banks, W.A., 2013. Blood–Brain Barrier Dysfunction as a Cause and Consequence of Alzheimer's Disease. J. Cereb. Blood Flow Metab. 33, 1500–1513. https://doi.org/10.1038/jcbfm.2013.135

Erickson, M.A., Banks, W.A., 2011. Cytokine and chemokine responses in serum and brain after single and repeated injections of lipopolysaccharide: Multiplex quantification with path analysis. Brain. Behav. Immun. 25, 1637–1648. https://doi.org/10.1016/j.bbi.2011.06.006

Erlitzki, R., Long, J.C., Theil, E.C., 2002. Multiple, conserved iron-responsive elements in the 3'-untranslated region of transferrin receptor mRNA enhance binding of iron regulatory protein 2. J. Biol. Chem. 277, 42579–42587. https://doi.org/10.1074/jbc.M207918200

Esther van de Vosse, Ottenhoff, T.H.M., 2006. Human host genetic factors in mycobacterial and Salmonella infection: lessons from single gene disorders in IL-12/IL-23-dependent signaling that affect innate and adaptive immunity. Microbes Infect. 8, 1167–1173. https://doi.org/10.1016/j.micinf.2005.10.032

Felton, L.M., Cunningham, C., Rankine, E.L., Waters, S., Boche, D., Perry, V.H., 2005. MCP-1 and murine prion disease: Separation of early behavioural dysfunction from overt clinical disease. Neurobiol. Dis. 20, 283–295. https://doi.org/10.1016/j.nbd.2005.03.008

Ferraguti, F., Shigemoto, R., 2006. Metabotropic glutamate receptors. Cell Tissue Res. 326, 483–504. https://doi.org/10.1007/s00441-006-0266-5

Field, R., Campion, S., Warren, C., Murray, C., Cunningham, C., 2010. Systemic challenge with the TLR3 agonist poly I: C induces amplified IFNα/β and IL-1β responses in the diseased brain and exacerbates chronic neurodegeneration. Brain. Behav. Immun. 24, 996–1007. https://doi.org/10.1016/j.bbi.2010.04.004

Fillatreau, S., 2011. Novel regulatory functions for Toll-like receptor-activated B cells during intracellular bacterial infection. Immunol. Rev. 240, 52–71. https://doi.org/10.1111/j.1600-065X.2010.00991.x

Fischer, R., Kontermann, R., Maier, O., 2015. Targeting sTNF/TNFR1 Signaling as a New Therapeutic Strategy. Antibodies 4, 48–70. https://doi.org/10.3390/antib4010048

Fischer, R., Maier, O., Siegemund, M., Wajant, H., Scheurich, P., Pfizenmaier, K., 2011. A TNF receptor 2 selective agonist rescues human neurons from oxidative stress-induced cell death. PLoS One 6. https://doi.org/10.1371/journal.pone.0027621

Fishman, J.B., Rubin, J.B., Handrahan, J. V, Connor, J.R., Fine, R.E., 1987. Receptor-Mediated Transcytosis of Transferrin Across the Blood-Brain Barrier. J. Neurosci. Res. 18, 299–304.

Flick, D.A., Gifford, G.E., 1984. Comparison of in vitro cell cytotoxic assays for tumor necrosis factor. J. Immunol. Methods 68, 167–175. https://doi.org/10.1016/0022-1759(84)90147-9

Franklin, S.L., Love, S., Greene, J.R.T., Betmouni, S., 2008. Loss of perineuronal net in ME7 prion disease. J. Neuropathol. Exp. Neurol. 67, 189–199. https://doi.org/10.1097/NEN.0b013e3181654386

Fresegna, D., Bullitta, S., Musella, A., Rizzo, F.R., De Vito, F., Guadalupi, L., Caioli, S., Balletta, S., Sanna, K., Dolcetti, E., Vanni, V., Bruno, A., Buttari, F., Stampanoni Bassi, M., Mandolesi, G., Centonze, D., Gentile, A., 2020. Re-Examining the Role of TNF in MS Pathogenesis and Therapy. Cells 9, 2290. https://doi.org/10.3390/cells9102290

Gabriel Knoll, J., Krasnow, S.M., Marks, D.L., 2017. Interleukin-1β signaling in fenestrated capillaries is sufficient to trigger sickness responses in mice. J. Neuroinflammation 14, 1–21. https://doi.org/10.1186/s12974-017-0990-7

Gadkar, K., Yadav, D.B., Zuchero, J.Y., Couch, J.A., Kanodia, J., Kenrick, M.K., Atwal, J.K., Dennis, M.S., Prabhu, S., Watts, R.J., Joseph, S.B., Ramanujan, S., 2016. Mathematical PKPD and safety model of bispecific TfR/BACE1 antibodies for the optimization of antibody uptake in brain. Eur. J. Pharm. Biopharm. 101, 53–61. https://doi.org/10.1016/j.ejpb.2016.01.009

Galea, I., Bechmann, I., Perry, V.H., 2007. What is immune privilege (not)? Trends Immunol. 28, 12–18. https://doi.org/10.1016/j.it.2006.11.004

Gao, H.M., Zhang, F., Zhou, H., Kam, W., Wilson, B., Hong, J.S., 2011. Neuroinflammation and α-synuclein dysfunction potentiate each other, driving chronic progression of neurodegeneration in a mouse model of Parkinson's disease. Environ. Health Perspect. 119, 807–814. https://doi.org/10.1289/ehp.1003013

Gatti, S., Faggioni, R., Echtenacher, B., Ghezzi, P., 1993. Role of tumour necrosis factor and reactive oxygen intermediates in lipopolysaccharide-induced pulmonary oedema and lethality. Clin. Exp. Immunol. 91, 456–461. https://doi.org/10.1111/j.1365-2249.1993.tb05924.x

Gaykema, R.P.A., Balachandran, M.K., Godbout, J.P., Johnson, R.W., Goehler, L.E., 2007. Enhanced neuronal activation in central autonomic network nuclei in aged mice following acute peripheral immune challenge. Auton. Neurosci. Basic Clin. 131, 137–142. https://doi.org/10.1016/j.autneu.2006.07.005

Gezen-Ak, D., Dursun, E., Hanağasi, H., Bilgiç, B., Lohman, E., Araz, Ö.S., Atasoy, I.L., Alaylioğlu, M., Önal, B., Gürvit, H., Yilmazer, S., 2013. BDNF, TNFα, HSP90, CFH, and IL-10 serum levels in patients with early or late onset Alzheimer's disease or mild cognitive impairment. J. Alzheimer's Dis. 37, 185–195. https://doi.org/10.3233/JAD-130497

Bibliography

Ghetie, V., Hubbard, J.G., Kim, J.-K., Tsen, M.-F., Lee, Y., Ward, E.S., 1996. Abnormally short serum half-lives of IgG in β2-microglobulin-deficient mice. Eur. J. Immunol. 26, 690–696. https://doi.org/10.1002/eji.1830260327

Ghetie, V., Popov, S., Borvak, J., Radu, C., Matesoi, D., Medesan, C., Ober, R.J., Ward, E.S., 1997. Increasig the serum persistence of an IgG frament by random mutagenesis. Nat. Biotechnol. 15, 637–640.

Ginhoux, F., Greter, M., Leboeuf, M., Nandi, S., See, P., Gokhan, S., Mehler, M.F., Conway, S.J., Ng, L.G., Stanley, E.R., Samokhvalov, I.M., Merad, M., 2010. Primitive Macrophages. Science (80-.). 701, 841–845.

Ginhoux, F., Prinz, M., 2015. Origin of microglia: Current concepts and past controversies. Cold Spring Harb. Perspect. Biol. 7, 1–16. https://doi.org/10.1101/cshperspect.a020537

Giridharan, V.V., Masud, F., Petronilho, F., Dal-Pizzol, F., Barichello, T., 2019. Infection-Induced Systemic Inflammation Is a Potential Driver of Alzheimer's Disease Progression. Front. Aging Neurosci. 11, 122. https://doi.org/10.3389/FNAGI.2019.00122

Giugliani, R., Giugliani, L., De Oliveira Poswar, F., Donis, K.C., Corte, A.D., Schmidt, M., Boado, R.J., Nestrasil, I., Nguyen, C., Chen, S., Pardridge, W.M., 2018. Neurocognitive and somatic stabilization in pediatric patients with severe Mucopolysaccharidosis Type i after 52 weeks of intravenous brain-penetrating insulin receptor antibody-iduronidase fusion protein (valanafusp alpha): An open label phase 1-2 trial. Orphanet J. Rare Dis. 13, 1–11. https://doi.org/10.1186/s13023-018-0849-8

Godinez, I., Haneda, T., Raffatellu, M., George, M.D., Paixão, T.A., Rolán, H.G., Santos, R.L., Dandekar, S., Tsolis, R.M., Bäumler, A.J., 2008. T cells help to amplify inflammatory responses induced by Salmonella enterica serotype Typhimurium in the intestinal mucosa. Infect. Immun. 76, 2008–2017. https://doi.org/10.1128/IAI.01691-07

Gómez-Nicola, D., Fransen, N.L., Suzzi, S., Perry, V.H., Gomez-Nicola, D., Fransen, N.L., Suzzi, S., Perry, V.H., 2013. Regulation of Microglial Proliferation during Chronic Neurodegeneration. J. Neurosci. 33, 2481–93. https://doi.org/10.1523/JNEUROSCI.4440-12.2013

Gomez-Nicola, D., Perry, V.H., 2015. Microglial dynamics and role in the healthy and diseased brain: A paradigm of functional plasticity. Neuroscientist 21, 169–184. https://doi.org/10.1177/1073858414530512

Gómez-Nicola, D., Schetters, S.T.T., Hugh Perry, V., 2014. Differential role of CCR2 in the dynamics of microglia and perivascular macrophages during prion disease. Glia 62, 1041–1052. https://doi.org/10.1002/glia.22660

Goodall, L.J., Ovecka, M., Rycroft, D., Friel, S.L., Sanderson, A., Mistry, P., Davies, M.L., Stoop, A.A., 2015. Pharmacokinetic and pharmacodynamic characterisation of an anti-mouse TNF receptor 1 domain antibody formatted for in vivo half-life extension. PLoS One 10, 1–16. https://doi.org/10.1371/journal.pone.0137065

Gray, B.C., Siskova, Z., Perry, V.H., O'Connor, V., 2009. Selective presynaptic degeneration in the synaptopathy associated with ME7-induced hippocampal pathology. Neurobiol. Dis. 35, 63–74. https://doi.org/10.1016/j.nbd.2009.04.001

Gregori, M., Orlando, A., Re, F., Sesana, S., Nardo, L., Salerno, D., Mantegazza, F., Salvati, E., Zito, A., Malavasi, F., Masserini, M., Cazzaniga, E., 2016. Novel Antitransferrin Receptor Antibodies Improve the Blood-Brain Barrier Crossing Efficacy of Immunoliposomes. J. Pharm. Sci. 105, 276–283. https://doi.org/10.1016/j.xphs.2015.11.009

Grell, M., Lohden, M., Clauss, M., Lesslauer, W., Kollias, S.G., Pfizenmaier, K., Scheurich, P., 1995. The Transmembrane Form of Tumor Necrosis Factor Is the Prime Activating Ligand of the 80 kDa Tumor Necrosis Factor Receptor. Cell 83, 793–802.

Griffin, E.W., Skelly, D.T., Murray, C.L., Cunningham, C., 2013. Cyclooxygenase-1-Dependent Prostaglandins Mediate Susceptibility to Systemic Inflammation-Induced Acute Cognitive Dysfunction. J. Neurosci. 33, 15248–15258. https://doi.org/10.1523/JNEUROSCI.6361-11.2013

Guenther, K., Deacon, R.M.J., Perry, V.H., Rawlins, J.N.P., 2001. Early behavioural changes in scrapie-affected mice and the influence of dapsone. Eur. J. Neurosci. 14, 401–409. https://doi.org/10.1046/j.0953-816X.2001.01645.x

Gulig, P.A., Doyle, T.J., Clare-Salzler, M.J., Maiese, R.L., Matsui, H., 1997. Systemic infection of mice by wild-type but not Spv- Salmonella typhimurium is enhanced by neutralization of gamma interferon and tumor necrosis factor alpha. Infect. Immun. 65, 5191–5197.

Guo, Z., Wang, S., Jiao, Q., Xu, M., Xu, Z., 2009. Soluble TNFR II/IgG1 Fc fusion protein treatment in the LPS-mediated septic shock of rats. Biomed. Pharmacother. 63, 537–542. https://doi.org/10.1016/j.biopha.2008.08.012

Gur, A., Oktayoglu, P., 2010. Advances in Biologic Agents for the Treatment of Rheumatoid Arthritis. Antiinflamm. Antiallergy. Agents Med. Chem. 9, 24–34. https://doi.org/10.2174/187152310790711656

Gurbaxani, B., Dela Cruz, L.L., Chintalacharuvu, K., Morrison, S.L., 2006. Analysis of a family of antibodies with different half-lives in mice fails to find a correlation between affinity for FcRn and serum half-life. Mol. Immunol. 43, 1462–1473. https://doi.org/10.1016/j.molimm.2005.07.032

Halliday, M.R., Rege, S. V., Ma, Q., Zhao, Z., Miller, C.A., Winkler, E.A., Zlokovic, B. V., 2015. Accelerated pericyte degeneration and blood-brain barrier breakdown in apolipoprotein E4 carriers with Alzheimer's disease. J. Cereb. Blood Flow Metab. 36, 1–9. https://doi.org/10.1038/jcbfm.2015.44

Hammond, T.R., Marsh, S.E., Stevens, B., 2019. Immune Signaling in Neurodegeneration. Immunity 50, 955–974. https://doi.org/10.1016/j.immuni.2019.03.016

Bibliography

Hansen, M.K., Daniels, S., Goehler, L.E., Gaykema, R.P.A., Maier, S.F., Watkins, L.R., 2000. Subdiaphragmatic vagotomy does not block intraperitoneal lipopolysaccharide-induced fever. Auton. Neurosci. Basic Clin. 85, 83–87. https://doi.org/10.1016/S1566-0702(00)00224-1

Harris, R.J., 1995. Processing of C-terminal lysine and arginine residues of proteins isolated from mammalian cell culture. J. Chromatogr. A 705, 129–134. https://doi.org/10.1016/0021-9673(94)01255-D

Harris, R.J., Wagner, K.L., Spellman, M.W., 1990. Structural characterization of a recombinant CD4-IgG hybrid molecule. Eur. J. Biochem. 194, 611–620. https://doi.org/10.1111/j.1432-1033.1990.tb15660.x

He, P., Zhong, Z., Lindholm, K., Berning, L., Lee, W., Lemere, C., Staufenbiel, M., Li, R., Shen, Y., 2007. Deletion of tumor necrosis factor death receptor inhibits amyloid β generation and prevents learning and memory deficits in Alzheimer's mice. J. Cell Biol. 178, 829–841. https://doi.org/10.1083/jcb.200705042

He, Y., Lee, T., Leong, S.K., 1999. Time-course and localization of transferrin receptor expression in the substantia nigra of 6-hydroxydopamine-induced parkinsonian rats. Neuroscience 91, 579–585. https://doi.org/10.1016/S0306-4522(98)00669-1

Heneka, M.T., Carson, M.J., Khoury, J. El, Landreth, G.E., Brosseron, F., Feinstein, D.L., Jacobs, A.H., Wyss-Coray, T., Vitorica, J., Ransohoff, R.M., Herrup, K., Frautschy, S.A., Finsen, B., Brown, G.C., Verkhratsky, A., Yamanaka, K., Koistinaho, J., Latz, E., Halle, A., Petzold, G.C., Town, T., Morgan, D., Shinohara, M.L., Perry, V.H., Holmes, C., Bazan, N.G., Brooks, D.J., Hunot, S., Joseph, B., Deigendesch, N., Garaschuk, O., Boddeke, E., Dinarello, C.A., Breitner, J.C., Cole, G.M., Golenbock, D.T., Kummer, M.P., 2015. Neuroinflammation in Alzheimer's disease. Lancet Neurol. 14, 388–405. https://doi.org/10.1016/S1474-4422(15)70016-5

Hennessy, E., Gormley, S., Lopez-Rodriguez, A.B., Murray, Caoimhe, Murray, Carol, Cunningham, C., 2017. Systemic TNF-alpha produces acute cognitive dysfunction and exaggerated sickness behavior when superimposed upon progressive neurodegeneration. Brain. Behav. Immun. 59, 233–244. https://doi.org/10.1016/j.bbi.2016.09.011

Hennessy, E., Griffin, E.W., Cunningham, C., 2015. Astrocytes Are Primed by Chronic Neurodegeneration to Produce Exaggerated Chemokine and Cell Infiltration Responses to Acute Stimulation with the Cytokines IL-1 and TNF-. J. Neurosci. 35, 8411–8422. https://doi.org/10.1523/JNEUROSCI.2745-14.2015

Heppner, F.L., Ransohoff, R.M., Becher, B., 2015. Immune attack: the role of inflammation in Alzheimer disease. Nat. Rev. Neurosci. 16, 358–372. https://doi.org/10.1038/nrn3880

Hess, J., Ladel, C., Miko, D., Kaufmann, S.H., 1996. Salmonella typhimurium aroA- infection in gene-targeted immunodeficient mice: major role of CD4+ TCR-alpha beta cells and IFN-gamma in bacterial clearance independent of intracellular location. J. Immunol. 156, 3321–6.

Hill, J.M., Ruff, M.R., Weber, R.J., Pert, C.B., 1985. Transferrin receptors in rat brain: neuropeptide-like pattern and relationship to iron distribution. Proc. Natl. Acad. Sci. U. S. A. 82, 4553–7. https://doi.org/10.1073/pnas.82.13.4553

Hilton, K.J., Cunningham, C., Reynolds, R.A., Perry, V.H., 2013. Early Hippocampal Synaptic Loss Precedes Neuronal Loss and Associates with Early Behavioural Deficits in Three Distinct Strains of Prion Disease. PLoS One 8, e68062. https://doi.org/10.1371/journal.pone.0068062

Hoiseth, S.K., Stocker, B.A.D., 1981. Aromatic-dependent Salmonella typhimurium are non-virulent and effective as live vaccines. Nature 291, 238–239.

Holmes, C., Cunningham, C., Zotova, E., Culliford, D., Perry, V.H., 2011. Proinflammatory cytokines, sickness behavior, and Alzheimer disease. Neurology 77, 212–218. https://doi.org/10.1212/WNL.0b013e318225ae07

Holmes, C., Cunningham, C., Zotova, E., Woolford, J., Dean, C., Kerr, S., Culliford, D., Perry, V.H., 2009. Systemic inflammation and disease progression in Alzheimer disease. Neurology 73, 768–774. https://doi.org/10.1212/WNL.0b013e3181b6bb95

Holmes, C., El-Olk, M., Williams, A.L., Cunningham, C., Wilcockson, D., Perry, V.H., 2003. Systemic infection, interleukin 1β, and cognitive decline in Alzheimer's disease. J Neurol Neurosurg Psychiatry 74, 788–790. https://doi.org/10.1136/jnnp.74.6.788

Holtman, I.R., Raj, D.D., Miller, J.A., Schaafsma, W., Yin, Z., Brouwer, N., Wes, P.D., Möller, T., Orre, M., Kamphuis, W., Hol, E.M., Boddeke, E.W.G.M., Eggen, B.J.L., 2015. Induction of a common microglia gene expression signature by aging and neurodegenerative conditions: a co-expression meta-analysis. Acta Neuropathol. Commun. 3, 31. https://doi.org/10.1186/s40478-015-0203-5

Hoogland, I.C.M., Westhoff, D., Engelen-Lee, J.Y., Melief, J., Valls Serón, M., Houben-Weerts, J.H.M.P., Huitinga, I., van Westerloo, D.J., van der Poll, T., van Gool, W.A., van de Beek, D., 2018. Microglial activation after systemic stimulation with lipopolysaccharide and Escherichia coli. Front. Cell. Neurosci. 12, 1–10. https://doi.org/10.3389/fncel.2018.00110

Hsiao, K., Chapman, P., Nilsen, S., Eckman, C., Harigaya, Y., Younkin, S., Yang, F., Cole, G., 1996. Correlative Memory Deficits, Abeta Elevation, and Amyloid Plaques in Transgenic Mice. Science (80-.). 274, 7–10.

Huang, H.H., Chang, J.C.Y., Liu, H.C., Yang, Z.Y., Yang, Y.J., Chen, L.K., Yen, D.H.T., 2020. Handgrip strength, tumor necrosis factor-α, interlukin-6, and visfatin levels in oldest elderly patients with cognitive impairment. Exp. Gerontol. 142, 111138. https://doi.org/10.1016/j.exger.2020.111138

Hultqvist, G., Syvänen, S., Fang, X.T., Lannfelt, L., Sehlin, D., 2017. Bivalent Brain Shuttle Increases Antibody Uptake by Monovalent Binding to the Transferrin Receptor. Theranostics 7, 308–318. https://doi.org/10.7150/thno.17155

Huwyler, J., Pardridge, W.M., 1998. Examination of blood-brain barrier transferrin receptor by confocal fluorescent microscopy of unfixed isolated rat brain capillaries. J. Neurochem. 70, 883–886. https://doi.org/10.1046/j.1471-4159.1998.70020883.x

Bibliography

Hyland, L., Villarreal-Ramos, B., Clarke, B., Baaten, B., Hou, S., 2005. Bone marrow immunosuppression in Salmonella-infected mice is prolonged following influenza virus infection. Exp. Hematol. 33, 1477–1485. https://doi.org/10.1016/j.exphem.2005.09.005

Ide, M., Harris, M., Stevens, A., Sussams, R., Hopkins, V., Culliford, D., Fuller, J., Ibbett, P., Raybould, R., Thomas, R., Puenter, U., Teeling, J., Perry, V.H., Holmes, C., 2016. Periodontitis and Cognitive Decline in Alzheimer's Disease. PLoS One 11, e0151081. https://doi.org/10.1371/journal.pone.0151081

Inoue, W., Matsumura, K., Yamagata, K., Takemiya, T., Shiraki, T., Kobayashi, S., 2002. Brain-specific endothelial induction of prostaglandin E2 synthesis enzymes and its temporal relation to fever. Neurosci. Res. 44, 51–61. https://doi.org/10.1016/S0168-0102(02)00083-4

Ishida, N., Ishihara, Y., Ishida, K., Tada, H., Funaki-Kato, Y., Hagiwara, M., Ferdous, T., Abdullah, M., Mitani, A., Michikawa, M., Matsushita, K., 2017. Periodontitis induced by bacterial infection exacerbates features of Alzheimer's disease in transgenic mice. npj Aging Mech. Dis. 3, 1–7. https://doi.org/10.1038/s41514-017-0015-x

Jackson, A., Nanton, M.R., O'Donnell, H., Akue, A.D., McSorley, S.J., 2010. Innate Immune Activation during Salmonella Infection Initiates Extramedullary Erythropoiesis and Splenomegaly . J. Immunol. 185, 6198–6204. https://doi.org/10.4049/jimmunol.1001198

Jaeger, L.B., Dohgu, S., Sultana, R., Lynch, J.L., Owen, J.B., Erickson, M.A., Shah, G.N., Price, T.O., Fleegal-Demotta, M.A., Butterfiled, D.A., Banks, W.A., 2009. Lipopolysaccharide alters the blood-brain barrier transport of amyloid beta protein: A mechanism for inflammation in the progression of Alzheimer's disease. Brain. Behav. Immun. 23, 507–517. https://doi.org/10.1016/j.bbi.2009.01.017

Janelsins, M.C., Mastrangelo, M.A., Park, K.M., Sudol, K.L., Narrow, W.C., Oddo, S., LaFerla, F.M., Callahan, L.M., Federoff, H.J., Bowers, W.J., 2008. Chronic Neuron-Specific Tumor Necrosis Factor-Alpha Expression Enhances the Local Inflammatory Environment Ultimately Leading to Neuronal Death in 3xTg-AD Mice. Am. J. Pathol. 173, 1768–1782. https://doi.org/10.2353/ajpath.2008.080528

Jansen, M.J., Hendriks, T., Hermsen, R., Van der Meer, J.W., Goris, R.J., 1998. A monoclonal antibody against tumour necrosis factor-alpha improves survival in experimental multiple organ dysfunction syndrome. Cytokine 10, 904–10. https://doi.org/10.1006/cyto.1998.0374

Jantsch, J., Chikkaballi, D., Hensel, M., 2011. Cellular aspects of immunity to intracellular Salmonella enterica. Immunol. Rev. 240, 185–195. https://doi.org/10.1111/j.1600-065X.2010.00981.x

Jeffrey, M., Halliday, W.G., Bell, J., Johnston, A.R., Macleod, N.K., Ingham, C., Sayers, A.R., Brown, D.A., Fraser, J.R., 2000. Synapse loss associated with abnormal PrP precedes neuronal degeneration in the scrapie-infected murine hippocampus. Neuropathol. Appl. Neurobiol. 26, 41–54. https://doi.org/10.1046/j.1365-2990.2000.00216.x

Jiang, J., Natarajan, K., Margulies, D.H., 2019. MHC Molecules, T cell Receptors, Natural Killer Cell Receptors, and Viral Immunoevasins—Key Elements of Adaptive and Innate Immunity, in: Jin, T., Yin, Q. (Eds.), Advances in Experimental Medicine and Biology, Advances in Experimental Medicine and Biology. Springer Singapore, Singapore, pp. 21–62. https://doi.org/10.1007/978-981-13-9367-9_2

Jiang, Y., Woronicz, J.D., Liu, W., Goeddel, D. V, 1999. Prevention of constitutive TNF receptor 1 signaling by silencer of death domains [published erratum appears in Science 1999 Mar 19;283(5409):1852]. Science (80-.). 283, 543–546.

Johnsen, K.B., Burkhart, A., Thomsen, L.B., Andresen, T.L., Moos, T., 2019. Targeting the transferrin receptor for brain drug delivery. Prog. Neurobiol. 181, 101665. https://doi.org/10.1016/j.pneurobio.2019.101665

Junghans, R.P., Anderson, C.L., 1996. The protection receptor for IgG catabolism is the beta2-microglobulin-containing neonatal intestinal transport receptor. Proc Natl Acad Sci U S A 93, 5512–5516.

Kalaria, R.N., Sromek, S.M., Grahovac, I., Harik, S.I., 1992. Transferrin receptors of rat and human brain and cerebral microvessels and their status in Alzheimer's disease. Brain Res. 585, 87–93. https://doi.org/10.1016/0006-8993(92)91193-I

Kandel, E.R., Schwartz, J.H., Jessell, T.M., Siegelbaum, S.A., Hudspeth, A.J., 2013. Principles of Neural Science. McGraw-Hill.

Karthivashan, G., Ganesan, P., Park, S.Y., Kim, J.S., Choi, D.K., 2018. Therapeutic strategies and nano-drug delivery applications in management of ageing alzheimer's disease. Drug Deliv. 25, 307–320. https://doi.org/10.1080/10717544.2018.1428243

Kaur, A., Chopra, K., Kaur, I.P., Rishi, P., 2020. Salmonella Strain Specificity Determines Post-typhoid Central Nervous System Complications: Intervention by Lactiplantibacillus plantarum at Gut-Brain Axis. Front. Microbiol. 11. https://doi.org/10.3389/fmicb.2020.01568

Kaymakcalan, Z., Sakorafas, P., Bose, S., Scesney, S., Xiong, L., Hanzatian, D.K., Salfeld, J., Sasso, E.H., 2009. Comparisons of affinities, avidities, and complement activation of adalimumab, infliximab, and etanercept in binding to soluble and membrane tumor necrosis factor. Clin. Immunol. 131, 308–316. https://doi.org/10.1016/j.clim.2009.01.002

Kettenmann, H., Hanisch, U.K., Noda, M., Verkhratsky, A., 2011. Physiology of microglia. Physiol. Rev. 91, 461–553. https://doi.org/10.1152/physrev.00011.2010

Khan, A.I., Liu, J., Dutta, P., 2018. Iron transport kinetics through blood-brain barrier endothelial cells. Biochim. Biophys. Acta - Gen. Subj. 1862, 1168–1179. https://doi.org/10.1016/j.bbagen.2018.02.010

Kirchner, S., Boldt, S., Kolch, W., Haffner, S., Kazak, S., Janosch, P., Holler, E., Andreesen, R., Eissner, G., 2004a. LPS resistance in monocytic cells caused by reverse signaling through transmembrane TNF (mTNF) is mediated by the MAPK/ERK pathway. J. Leukoc. Biol. 75, 324–331. https://doi.org/10.1189/jlb.0703343

Kirchner, S., Holler, E., Haffner, S., Andreesen, R., Eissner, G., 2004b. Effect of different tumor necrosis factor (TNF) reactive agents on reverse signaling of membrane integrated TNF in monocytes. Cytokine 28, 67–74. https://doi.org/10.1016/j.cyto.2004.06.008

Kissel, K., Hamm, S., Schulz, M., Vecchi, A., Garlanda, C., Engelhardt, B., 1998. Immunohistochemical localization of the murine transferrin receptor (TfR) on blood-tissue barriers using a novel anti-TfR monoclonal antibody. Histochem. Cell Biol. 110, 63–72. https://doi.org/10.1007/s004180050266

Kitazawa, M., Cheng, D., Tsukamoto, M.R., Koike, M.A., Wes, P.D., Vasilevko, V., Cribbs, D.H., LaFerla, F.M., 2011. Blocking IL-1 Signaling Rescues Cognition, Attenuates Tau Pathology, and Restores Neuronal -Catenin Pathway Function in an Alzheimer's Disease Model. J. Immunol. 187, 6539–6549. https://doi.org/10.4049/jimmunol.1100620

Kitazawa, M., Oddo, S., Yamasaki, T.R., Green, K.N., LaFerla, F.M., 2005. Lipopolysaccharide-Induced Inflammation Exacerbates Tau Pathology by a Cyclin-Dependent Kinase 5-Mediated Pathway in a Transgenic Model of Alzheimer's Disease. J. Neurosci. 25, 8843–8853. https://doi.org/10.1523/JNEUROSCI.2868-05.2005

Kleemann, G.R., Beierle, J., Nichols, A.C., Dillon, T.M., Pipes, G.D., Bondarenko, P. V., 2008. Characterization of IgG1 immunoglobulins and peptide-Fc fusion proteins by limited proteolysis in conjunction with LC-MS. Anal. Chem. 80, 2001–2009. https://doi.org/10.1021/ac701629v

Klei, T.R.L., Meinderts, S.M., van den Berg, T.K., van Bruggen, R., 2017. From the cradle to the grave: The role of macrophages in erythropoiesis and erythrophagocytosis. Front. Immunol. 8. https://doi.org/10.3389/fimmu.2017.00073

Klein, M.A., Frigg, R., Flechsig, E., Raeber, A.J., Kalinke, U., Bluethmann, H., Bootz, F., Suter, M., Zinkernagel, R.M., Aguzzi, A., 1997. A crucial role for B cells in neuroinvasive scrapie. Nature 390, 687–690. https://doi.org/10.1038/37789

Klein, R.S., Hunter, C.A., 2017. Protective and Pathological Immunity during Central Nervous System Infections. Immunity 46, 891–909. https://doi.org/10.1016/j.immuni.2017.06.012

Kolaczkowska, E., Kubes, P., 2013. Neutrophil recruitment and function in health and inflammation. Nat. Rev. Immunol. 13, 159–175. https://doi.org/10.1038/nri3399

Konsman, J.P., 2016. Immune-to-brain signaling and substrates of altered behavior during inflammation. Neuroimmunol. Neuroinflammation 3, 207. https://doi.org/10.20517/2347-8659.2016.19

Konsman, J.P., Luheshi, G.N., Bluthé, R.M., Dantzer, R., 2000. The vagus nerve mediates behavioural depression, but not fever, in response to peripheral immune signals; a functional anatomical analysis. Eur. J. Neurosci. 12, 4434–4446. https://doi.org/10.1046/j.0953-816X.2000.01319.x

Kouchaki, E., Kakhaki, R.D., Tamtaji, O.R., Dadgostar, E., Behnam, M., Nikoueinejad, H., Akbari, H., 2018. Increased serum levels of TNF-α and decreased serum levels of IL-27 in patients with Parkinson disease and their correlation with disease severity. Clin. Neurol. Neurosurg. 166, 76–79. https://doi.org/10.1016/j.clineuro.2018.01.022

Krstic, D., Madhusudan, A., Doehner, J., Vogel, P., Notter, T., Imhof, C., Manalastas, A., Hilfiker, M., Pfister, S., Schwerdel, C., Riether, C., Meyer, U., Knuesel, I., 2012. Systemic immune challenges trigger and drive Alzheimer-like neuropathology in mice. J. Neuroinflammation 9, 699. https://doi.org/10.1186/1742-2094-9-151

Kumar, A., Singh, A., 2015. A review on Alzheimer's disease pathophysiology and its management : an update. Pharmacol. Reports 67, 195–203. https://doi.org/10.1016/j.pharep.2014.09.004

Kumar, D.K.V., Choi, S.H., Washicosky, K.J., Eimer, W.A., Tucker, S., Ghofrani, J., Lefkowitz, A., Mccoll, G., Goldstein, L.E., Tanzi, R.E., Moir, R.D., 2016. Amyloid-β peptide protects against microbial infection in mouse and worm models of Alzheimer's disease. Sci. Transl. Med. 8.

Kurtz, J.R., Goggins, J.A., McLachlan, J.B., 2017. Salmonella infection: Interplay between the bacteria and host immune system. Immunol. Lett. 190, 42–50. https://doi.org/10.1016/j.imlet.2017.07.006

La Vitola, P., Balducci, C., Baroni, M., Artioli, L., Santamaria, G., Castiglioni, M., Cerovic, M., Colombo, L., Caldinelli, L., Pollegioni, L., Forloni, G., 2021. Peripheral inflammation exacerbates α-synuclein toxicity and neuropathology in Parkinson's models. Neuropathol. Appl. Neurobiol. 47, 43–60. https://doi.org/10.1111/nan.12644

Lai, K.S.P., Liu, C.S., Rau, A., Lanctôt, K.L., Köhler, C.A., Pakosh, M., Carvalho, A.F., Herrmann, N., 2017. Peripheral inflammatory markers in Alzheimer's disease: A systematic review and meta-analysis of 175 studies. J. Neurol. Neurosurg. Psychiatry 88, 876–882. https://doi.org/10.1136/jnnp-2017-316201

Lajoie, J.M., Shusta, E. V., 2015. Targeting Receptor-Mediated Transport for Delivery of Biologics Across the Blood-Brain Barrier. Annu. Rev. Pharmacol. Toxicol. 55, 613–631. https://doi.org/10.1146/annurev-pharmtox-010814-124852

Lapaque, N., Walzer, T., Méresse, S., Vivier, E., Trowsdale, J., 2009. Interactions between Human NK Cells and Macrophages in Response to Salmonella Infection . J. Immunol. 182, 4339–4348. https://doi.org/10.4049/jimmunol.0803329

Lawson, L.J., Perry, V.H., Dri, P., Gordon, S., 1990. Heterogeneity in the distribution and morphology of microglia in the normal adult mouse brain. Neuroscience 39, 151–170. https://doi.org/10.1016/0306-4522(90)90229-W

Laye, S., Bluthe, R.M., Kent, S., Combe, C., Medina, C., Parnet, P., Kelley, K., Dantzer, R., 1995. Subdiaphragmatic vagotomy blocks induction of IL-1 beta mRNA in mice brain in response to peripheral LPS. Am. J. Physiol. Integr. Comp. Physiol. 268, R1327–R1331. https://doi.org/10.1152/ajpregu.1995.268.5.R1327

Bibliography

Layé, S., Gheusi, G., Cremona, S., Combe, C., Kelley, K., Dantzer, R., Parnet, P., 2000. Endogenous brain IL-1 mediates LPS-induced anorexia and hypothalamic cytokine expression. Am. J. Physiol. Regul. Integr. Comp. Physiol. 279, R93–R98. https://doi.org/10.1016/s0006-8993(98)00641-6

Laye, S., Parnet, P., Goujon, E., Dantzer, R., 1994. Peripheral administration of lipopolysaccharide induces the expression of cytokine transcripts in the brain and pituitary of mice. Brain Res Mol Brain Res 27, 157–162.

Lee, H.J., Engelhardt, B., Lesley, J., Bickel, U., Pardridge, W.M., 2000. Targeting rat anti-mouse transferrin receptor monoclonal antibodies through blood-brain barrier in mouse. J. Pharmacol. Exp. Ther. 292, 1048–1052. https://doi.org/10.1353/hcy.2011.0023

Lee, J., Lee, Y., Yuk, D., Choi, D., Ban, S., Oh, K., Hong, J., 2008. Neuro-inflammation induced by lipopolysaccharide causes cognitive impairment through enhancement of beta-amyloid generation. J. Neuroinflammation 5, 37. https://doi.org/10.1186/1742-2094-5-37

Lein, E.S., Hawrylycz, M.J., Ao, N., Ayres, M., Bensinger, A., Bernard, A., Boe, A.F., Boguski, M.S., Brockway, K.S., Byrnes, E.J., Chen, Lin, Chen, Li, Chen, T.M., Chin, M.C., Chong, J., Crook, B.E., Czaplinska, A., Dang, C.N., Datta, S., Dee, N.R., Desaki, A.L., Desta, T., Diep, E., Dolbeare, T.A., Donelan, M.J., Dong, H.W., Dougherty, J.G., Duncan, B.J., Ebbert, A.J., Eichele, G., Estin, L.K., Faber, C., Facer, B.A., Fields, R., Fischer, S.R., Fliss, T.P., Frensley, C., Gates, S.N., Glattfelder, K.J., Halverson, K.R., Hart, M.R., Hohmann, J.G., Howell, M.P., Jeung, D.P., Johnson, R.A., Karr, P.T., Kawal, R., Kidney, J.M., Knapik, R.H., Kuan, C.L., Lake, J.H., Laramee, A.R., Larsen, K.D., Lau, C., Lemon, T.A., Liang, A.J., Liu, Y., Luong, L.T., Michaels, J., Morgan, J.J., Morgan, R.J., Mortrud, M.T., Mosqueda, N.F., Ng, L.L., Ng, R., Orta, G.J., Overly, C.C., Pak, T.H., Parry, S.E., Pathak, S.D., Pearson, O.C., Puchalski, R.B., Riley, Z.L., Rockett, H.R., Rowland, S.A., Royall, J.J., Ruiz, M.J., Sarno, N.R., Schaffnit, K., Shapovalova, N. V., Sivisay, T., Slaughterbeck, C.R., Smith, S.C., Smith, K.A., Smith, B.I., Sodt, A.J., Stewart, N.N., Stumpf, K.R., Sunkin, S.M., Sutram, M., Tam, A., Teemer, C.D., Thaller, C., Thompson, C.L., Varnam, L.R., Visel, A., Whitlock, R.M., Wohnoutka, P.E., Wolkey, C.K., Wong, V.Y., Wood, M., Yaylaoglu, M.B., Young, R.C., Youngstrom, B.L., Yuan, X.F., Zhang, B., Zwingman, T.A., Jones, A.R., 2007. Genome-wide atlas of gene expression in the adult mouse brain. Nature 445, 168–176. https://doi.org/10.1038/nature05453

Leng, A., Mura, A., Feldon, J., Ferger, B., 2005. Tumor necrosis factor-alpha receptor ablation in a chronic MPTP mouse model of Parkinson's disease. Neurosci. Lett. 375, 107–111. https://doi.org/10.1016/j.neulet.2004.10.077

Levites, Y., Smithson, L.A., Price, R.W., Dakin, R.S., Yuan, B., Sierks, M.R., Kim, J., McGowan, E., Reed, D.K., Rosenberry, T.L., Das, P., Golde, T.E., 2006. Insights into the mechanisms of action of anti-Aβ antibodies in Alzheimer's disease mouse models. FASEB J. 20, 2576–2578. https://doi.org/10.1096/fj.06-6463fje

Lewis, J., McGowan, E., Rockwood, J., Melrose, H., Nacharaju, P., Van Slegtenhorst, M., Gwinn-Hardy, K., Murphy, M.P., Baker, M., Yu, X., Duff, K., Hardy, J., Corral, A., Lin, W.L., Yen, S.H., Dickson, D.W., Davies, P., Hutton, M., 2000. Neurofibrillary tangles, amyotrophy and progressive motor disturbance in mice expressing mutant (P301L)tau protein. Nat. Genet. 25, 402–405. https://doi.org/10.1038/78078

Lewis, S.M., Williams, A., Eisenbarth, S.C., 2019. Structure and function of the immune system in the spleen. Sci. Immunol. 4. https://doi.org/10.1126/sciimmunol.aau6085

Li, L.-B., Chai, R., Zhang, S., Xu, S.-F., Zhang, Y.-H., Li, H.-L., Fan, Y.-G., Guo, C., 2019. Iron Exposure and the Cellular Mechanisms Linked to Neuron Degeneration in Adult Mice. Cells 8, 198. https://doi.org/10.3390/cells8020198

Libregts, S.F., Gutiérrez, L., De Bruin, A.M., Wensveen, F.M., Papadopoulos, P., Van Ijcken, W., Özgür, Z., Philipsen, S., Nolte, M.A., 2011. Chronic IFN-γ production in mice induces anemia by reducing erythrocyte life span and inhibiting erythropoiesis through an IRF-1/PU.1 axis. Blood 118, 2578–2588. https://doi.org/10.1182/blood-2010-10-315218

Lim, S.L., Rodriguez-Ortiz, C.J., Kitazawa, M., 2015. Infection, systemic inflammation, and Alzheimer's disease. Microbes Infect. 17, 549–556. https://doi.org/10.1016/j.micinf.2015.04.004

Liu, J., Zhang, J., Ginzburg, Y., Li, H., Xue, F., De Franceschi, L., Chasis, J.A., Mohandas, N., An, X., 2013. Quantitative analysis of murine terminal erythroid differentiation in vivo:novelmethod to study normal and disordered erythropoiesis. Blood 121, 43–49. https://doi.org/10.1182/blood-2012-09-456079

Liu, J.L., Fan, Y.G., Yang, Z.S., Wang, Z.Y., Guo, C., 2018. Iron and Alzheimer's disease: From pathogenesis to therapeutic implications. Front. Neurosci. 12, 1–14. https://doi.org/10.3389/fnins.2018.00632

Liu, T., Zhang, L., Joo, D., Sun, S.-C.C., 2017. NF-κB signaling in inflammation. Signal Transduct. Target. Ther. 2, 17023. https://doi.org/10.1038/sigtrans.2017.23

Llano, D.A., Li, J., Waring, J.F., Ellis, T., Devanarayan, V., Witte, D.G., Lenz, R.A., 2012. Cerebrospinal Fluid Cytokine Dynamics Differ Between Alzheimer Disease Patients and Elderly Controls. Alzheimer Dis. Assoc. Disord. 26, 322–328. https://doi.org/10.1097/WAD.0b013e31823b2728

Lo, M., Kim, H.S., Tong, R.K., Bainbridge, T.W., Vernes, J.M., Zhang, Y., Lin, Y.L., Chung, S., Dennis, M.S., Zuchero, Y.J.Y., Watts, R.J., Couch, J.A., Meng, Y.G., Atwal, J.K., Brezski, R.J., Spiess, C., Ernst, J.A., 2017. Effector-attenuating substitutions that maintain antibody stability and reduce toxicity in mice. J. Biol. Chem. 292, 3900–3908. https://doi.org/10.1074/jbc.M116.767749

Lord, A., Kalimo, H., Eckman, C., Zhang, X.Q., Lannfelt, L., Nilsson, L.N.G., 2006. The Arctic Alzheimer mutation facilitates early intraneuronal Aβ aggregation and senile plaque formation in transgenic mice. Neurobiol. Aging 27, 67–77. https://doi.org/10.1016/j.neurobiolaging.2004.12.007

Bibliography

Luchese, M.D., Lopes dos Santos, M., Garbuio, A., Targino, R.C., Mansueli, C.P., Tsuruta, L.R., Quintilio, W., Moro, A.M., 2018. A new CHO (Chinese hamster ovary)-derived cell line expressing anti-TNFα monoclonal antibody with biosimilar potential. Immunol. Res. 66, 392–405. https://doi.org/10.1007/s12026-018-8997-4

Ludwiczek, S., Aigner, E., Theurl, I., Weiss, G., 2003. Cytokine-mediated regulation of iron transport in human monocytic cells. Blood 101, 4148–4154. https://doi.org/10.1182/blood-2002-08-2459

Lunnon, K., Teeling, J.L., Tutt, A.L., Cragg, M.S., Glennie, M.J., Perry, V.H., 2011. Systemic inflammation modulates Fc receptor expression on microglia during chronic neurodegeneration. J. Immunol. 186, 7215–7224. https://doi.org/10.4049/jimmunol.0903833

Lyman, M., Lloyd, D.G., Ji, X., Vizcaychipi, M.P., Ma, D., 2014. Neuroinflammation: The role and consequences. Neurosci. Res. 79, 1–12. https://doi.org/10.1016/j.neures.2013.10.004

Mabbott, N.A., McGovern, G., Jeffrey, M., Bruce, M.E., 2002. Temporary blockade of the tumor necrosis factor receptor signaling pathway impedes the spread of scrapie to the brain. J Virol 76, 5131–5139. https://doi.org/10.1128/JVI.76.10.5131

Mabbott, N.A., Williams, A., Farquhar, C.F., Pasparakis, M., Kollias, G., Bruce, M.E., 2000. Tumor necrosis factor alpha-deficient, but not interleukin-6-deficient, mice resist peripheral infection with scrapie. J Virol 74, 3338–3344. https://doi.org/10.1128/jvi.74.7.3338-3344.2000

Machado, A., Herrera, A.J., Venero, J.L., Santiago, M., De Pablos, R.M., Villarán, R.F., Espinosa-Oliva, A.M., Argüelles, S., Sarmiento, M., Delgado-Cortés, M.J., Maurio, R., Cano, J., 2011. Peripheral inflammation increases the damage in animal models of nigrostriatal dopaminergic neurodegeneration: Possible implication in parkinson's disease incidence. Parkinsons. Dis. 2011, 18–21. https://doi.org/10.4061/2011/393769

MacPherson, K.P., Sompol, P., Kannarkat, G.T., Chang, J., Sniffen, L., Wildner, M.E., Norris, C.M., Tansey, M.G., 2017. Peripheral administration of the soluble TNF inhibitor XPro1595 modifies brain immune cell profiles, decreases beta-amyloid plaque load, and rescues impaired long-term potentiation in 5xFAD mice. Neurobiol. Dis. 102, 81–95. https://doi.org/10.1016/j.nbd.2017.02.010

Magalhães, T.N.C., Weiler, M., Teixeira, C.V.L., Hayata, T., Moraes, A.S., Boldrini, V.O., dos Santos, L.M., de Campos, B.M., de Rezende, T.J.R., Joaquim, H.P.G., Talib, L.L., Forlenza, O. V., Cendes, F., Balthazar, M.L.F., 2017. Systemic Inflammation and Multimodal Biomarkers in Amnestic Mild Cognitive Impairment and Alzheimer's Disease. Mol. Neurobiol. https://doi.org/10.1007/s12035-017-0795-9

Majbour, N.K., Aasly, J.O., Hustad, E., Thomas, M.A., Vaikath, N.N., Elkum, N., Van De Berg, W.D.J., Tokuda, T., Mollenhauer, B., Berendse, H.W., El-Agnaf, O.M.A., 2020. CSF total and oligomeric α-Synuclein along with TNF-α as risk biomarkers for Parkinson's disease: A study in LRRK2 mutation carriers. Transl. Neurodegener. 9, 1–10. https://doi.org/10.1186/s40035-020-00192-4

Malyala, P., Singh, M., 2008. Endotoxin Limits in Formulations for Preclinical Research. J. Pharm. Sci. 97, 2041–2044. https://doi.org/10.1002/jps.21152

Marcos, G., Santabárbara, J., Lopez-Anton, R., De-la-Cámara, C., Gracia-García, P., Lobo, E., Pírez, G., Menchón, J.M., Palomo, T., Stephan, B.C.M., Brayne, C., Lobo, A., 2016. Conversion to dementia in mild cognitive impairment diagnosed with DSM-5 criteria and with Petersen's criteria. Acta Psychiatr. Scand. 133, 378–385. https://doi.org/10.1111/acps.12543

Marinus, M.G., Morris, N.R., 1973. Isolation of deoxyribonucleic acid methylase mutants of Escherichia coli K-12. J. Bacteriol. 114, 1143–1150.

Martin, J.B., 1999. Molecular Basis of the Neurodegenerative Disorders. N. Engl. J. Med. 340, 1970–1980. https://doi.org/10.1056/NEJM199906243402507

Martinet, L., Smyth, M.J., 2015. Balancing natural killer cell activation through paired receptors. Nat. Rev. Immunol. 15, 243–254. https://doi.org/10.1038/nri3799

Mastroeni, P., 2002. Immunity to systemic Salmonella infections. Curr. Mol. Med. 2, 393–406. https://doi.org/10.2174/1566524023362492

Mastroeni, P., Arena, A., Costa, G.B., Liberto, M.C., Bonina, L., Hormaeche, C.E., 1991. Serum TNFα in mouse typhoid and enhancement of a salmonella infection by anti-TNFα antibodies. Microb. Pathog. 11, 33–38. https://doi.org/10.1016/0882-4010(91)90091-N

Mastroeni, P., Grant, A., Restif, O., Maskell, D., 2009. A dynamic view of the spread and intracellular distribution of Salmonella enterica. Nat. Rev. Microbiol. 7, 73–80. https://doi.org/10.1038/nrmicro2034

Mastroeni, P., Harrison, J.A., Robinson, J.H., Clare, S., Khan, S., Maskell, D.J., Dougan, G., Hormaeche, C.E., 1998. Interleukin-12 is required for control of the growth of attenuated aromatic-compound-dependent salmonellae in BALB/c mice: Role of gamma interferon and macrophage activation. Infect. Immun. 66, 4767–4776. https://doi.org/10.1128/iai.66.10.4767-4776.1998

Mastroeni, P., Simmons, C., Fowler, R., Hormaeche, C.E., Dougan, G., 2000. Igh-6(-/-) (B-cell-deficient) mice fail to mount solid acquired resistance to oral challenge with virulent Salmonella enterica serovar Typhimurium and show impaired Th1 T-cell responses to Salmonella antigens. Infect. Immun. 68, 46–53. https://doi.org/10.1128/IAI.68.1.46-53.2000

Mastroeni, P., Skepper, J.N., Hormaeche, C.E., 1995. Effect of anti-tumor necrosis factor alpha antibodies on histopathology of primary Salmonella infections. Infect. Immun. 63, 3674–3682. https://doi.org/10.1017/S0030605306001098

Mastroeni, P., Villarreal-Ramos, B., Hormaeche, C.E., 1993a. Adoptive transfer of immunity to oral challenge with virulent salmonellae in innately susceptible BALB/c mice requires both immune serum and T cells. Infect. Immun. 61, 3981–3984. https://doi.org/10.1128/iai.61.9.3981-3984.1993

Bibliography

Mastroeni, P., Villarreal-Ramos, B., Hormaeche, C.E., 1993b. Effect of late administration of anti-TNα antibodies on a Salmonella infection in the mouse model. Microb. Pathog. 14, 473–480. https://doi.org/10.1006/mpat.1993.1046

Mastroeni, P., Villarreal-Ramos, B., Hormaeche, C.E., 1992a. Role of T cells, TNFα and IFNγ in recall of immunity to oral challenge with virulent salmonellae in mice vaccinated with live attenuated aro-salmonella vaccines. Microb. Pathog. 13, 477–491. https://doi.org/10.1016/0882-4010(92)90014-F

Mastroeni, P., Villarreal, B., de Hormaeche, R.D., Hormaeche, C.E., 1992b. Serum TNFα inhibitor in mouse typhoid. Microb. Pathog. 12, 343–349. https://doi.org/10.1016/0882-4010(92)90097-8

Matak, P., Matak, A., Moustafa, S., Aryal, D.K., Benner, E.J., Wetsel, W., Andrews, N.C., 2016. Disrupted iron homeostasis causes dopaminergic neurodegeneration in mice. Proc. Natl. Acad. Sci. U. S. A. 113, 3428–3435. https://doi.org/10.1073/pnas.1519473113

McAlpine, F.E., Lee, J.-K., Harms, A.S., Ruhn, K.A., Blurton-Jones, M., Hong, J., Das, P., Golde, T.E., LaFerla, F.M., Oddo, S., Blesch, A., Tansey, M.G., 2009. Inhibition of soluble TNF signaling in a mouse model of Alzheimer's disease prevents pre-plaque amyloid-associated neuropathology. Neurobiol. Dis. 34, 163–77.

McCarthy, R.C., Kosman, D.J., 2015. Mechanisms and regulation of iron trafficking across the capillary endothelial cells of the blood-brain barrier. Front. Mol. Neurosci. 8, 31. https://doi.org/10.3389/fnmol.2015.00031

McCarthy, R.C., Kosman, D.J., 2013. Ferroportin and exocytoplasmic ferroxidase activity are required for brain microvascular endothelial cell iron efflux. J. Biol. Chem. 288, 17932–17940. https://doi.org/10.1074/jbc.M113.455428

McCarthy, R.C., Kosman, D.J., 2012. Mechanistic analysis of iron accumulation by endothelial cells of the BBB. BioMetals 25, 665–675. https://doi.org/10.1007/s10534-012-9538-6

McCarthy, R.C., Sosa, J.C., Gardeck, A.M., Baez, A.S., Lee, C.H., Wessling-Resnick, M., 2018. Inflammation-induced iron transport and metabolism by brain microglia. J. Biol. Chem. 293, 7853–7863. https://doi.org/10.1074/jbc.RA118.001949

McCoy, M.K., Martinez, T.N., Ruhn, K.A., Szymkowski, D.E., Smith, C.G., Botterman, B.R., Tansey, K.E., Tansey, M.G., 2006. Blocking soluble tumor necrosis factor signaling with dominant-negative tumor necrosis factor inhibitor attenuates loss of dopaminergic neurons in models of Parkinson's disease. J. Neurosci. 26, 9365–9375. https://doi.org/10.1523/JNEUROSCI.1504-06.2006

McCoy, M.K., Ruhn, K.A., Martinez, T.N., McAlpine, F.E., Blesch, A., Tansey, M.G., 2008. Intranigral lentiviral delivery of dominant-negative TNF attenuates neurodegeneration and behavioral deficits in hemiparkinsonian rats. Mol. Ther. 16, 1572–1579. https://doi.org/10.1038/mt.2008.146

McCoy, M.K., Tansey, M.G., 2008. TNF signaling inhibition in the CNS: Implications for normal brain function and neurodegenerative disease. J. Neuroinflammation 5, 1–13. https://doi.org/10.1186/1742-2094-5-45

McRae, P.A., Porter, B.E., 2012. The perineuronal net component of the extracellular matrix in plasticity and epilepsy. Neurochem. Int. 61, 963–972. https://doi.org/10.1016/j.neuint.2012.08.007

McSorley, S.J., Jenkins, M.K., 2000. Antibody is required for protection against virulent but not attenuated Salmonella enterica serovar typhimurium. Infect. Immun. 68, 3344–3348. https://doi.org/10.1128/IAI.68.6.3344-3348.2000

Medesan, C., Matesoi, D., Radu, C., Ghetie, V., Ward, E.S., 1997. Delineation of the amino acid residues involved in transcytosis and catabolism of mouse IgG1. J. Immunol. 158, 2211–2217.

Micheau, O., Tschopp, J., 2003. Induction of TNF Receptor I-Mediated Apoptosis via Two Sequential Signaling Complexes. Cell 114, 181–190. https://doi.org/10.1016/S0092-8674(03)00521-X

Mildner, A., Schmidt, H., Nitsche, M., Merkler, D., Hanisch, U.K., Mack, M., Heikenwalder, M., Brück, W., Priller, J., Prinz, M., 2007. Microglia in the adult brain arise from Ly-6ChiCCR2+ monocytes only under defined host conditions. Nat. Neurosci. 10, 1544–1553. https://doi.org/10.1038/nn2015

Minett, T., Classey, J., Matthews, F.E., Fahrenhold, M., Taga, M., Brayne, C., Ince, P.G., Nicoll, J.A.R., Boche, D., 2016. Microglial immunophenotype in dementia with Alzheimer's pathology. J. Neuroinflammation 13, 135. https://doi.org/10.1186/s12974-016-0601-z

Minogue, A.M., Jones, R.S., Kelly, R.J., McDonald, C.L., Connor, T.J., Lynch, M.A., 2014. Age-associated dysregulation of microglial activation is coupled with enhanced blood-brain barrier permeability and pathology in APP/PS1 mice. Neurobiol. Aging 35, 1442–1452. https://doi.org/10.1016/j.neurobiolaging.2013.12.026

Mittrücker, H.-W., Raupach, B., Köhler, A., Kaufmann, S.H.E., 2000. Cutting Edge: Role of B Lymphocytes in Protective Immunity Against Salmonella typhimurium Infection . J. Immunol. 164, 1648–1652. https://doi.org/10.4049/jimmunol.164.4.1648

Mittrucker, H.W., Kaufmann, S.H.E., 2000. Immune response to infection with Salmonella typhimurium in mice. J. Leukoc. Biol. 67, 457–463. https://doi.org/10.1002/jlb.67.4.457

Mohler, K.M., Torrance, D.S., Smith, C.A., Goodwin, R.G., Stremler, K.E., Fung, V.P., Madani, H., Widmer, M.B., 1993. Soluble tumor necrosis factor (TNF) receptors are effective therapeutic agents in lethal endotoxemia and function simultaneously as both TNF carriers and TNF antagonists. J. Immunol. 151, 1548–61.

Monack, D.M., Bouley, D.M., Falkow, S., 2004a. Salmonella typhimurium Persists within Macrophages in the Mesenteric Lymph Nodes of Chronically Infected Nramp1+/+ Mice and Can Be Reactivated by IFNγ Neutralization. J. Exp. Med. 199, 231–241. https://doi.org/10.1084/jem.20031319

Monack, D.M., Mueller, A., Falkow, S., 2004b. Persistent bacterial infections: The interface of the pathogen and the host immune system. Nat. Rev. Microbiol. 2, 747–765. https://doi.org/10.1038/nrmicro955

Montacir, O., Montacir, H., Springer, A., Hinderlich, S., Mahboudi, F., Saadati, A., Parr, M.K., 2018. Physicochemical Characterization, Glycosylation Pattern and Biosimilarity Assessment of the Fusion Protein Etanercept. Protein J. 37, 164–179. https://doi.org/10.1007/s10930-018-9757-y

Montagne, A., Barnes, S.R., Sweeney, M.D., Halliday, M.R., Sagare, A.P., Zhao, Z., Toga, A.W., Jacobs, R.E., Liu, C.Y., Amezcua, L., Harrington, M.G., Chui, H.C., Law, M., Zlokovic, B. V., 2015. Blood-Brain barrier breakdown in the aging human hippocampus. Neuron 85, 296–302. https://doi.org/10.1016/j.neuron.2014.12.032

Montgomery, S.L., Bowers, W.J., 2012. Tumor necrosis factor-alpha and the roles it plays in homeostatic and degenerative processes within the central nervous system. J. Neuroimmune Pharmacol. 7, 42–59. https://doi.org/10.1007/s11481-011-9287-2

Montgomery, S.L., Mastrangelo, M.A., Habib, D., Narrow, W.C., Knowlden, S.A., Wright, T.W., Bowers, W.J., 2011. Ablation of TNF-RI/RII expression in Alzheimer's disease mice leads to an unexpected enhancement of pathology: Implications for chronic pan-TNF-α suppressive therapeutic strategies in the brain. Am. J. Pathol. 179, 2053–2070. https://doi.org/10.1016/j.ajpath.2011.07.001

Montgomery, S.L., Narrow, W.C., Mastrangelo, M.A., Olschowka, J.A., O'Banion, M.K., Bowers, W.J., 2013. Chronic neuron- and age-selective down-regulation of TNF receptor expression in triple-transgenic alzheimer disease mice leads to significant modulation of amyloid- and Tau-related pathologies. Am. J. Pathol. 182, 2285–2297. https://doi.org/10.1016/j.ajpath.2013.02.030

Moos, T., 1996. Immunohistochemical localization of intraneuronal transferrin receptor immunoreactivity in the adult mouse central nervous system. J. Comp. Neurol. 375, 675–692. https://doi.org/10.1002/(SICI)1096-9861(19961125)375:4<675::AID-CNE8>3.0.CO;2-Z

Morea, V., Lesk, A.M., Tramontano, A., 2000. Antibody modeling: Implications for engineering and design. Methods 20, 267–279. https://doi.org/10.1006/meth.1999.0921

Morimoto, K., Horio, J., Satoh, H., Sue, L., Beach, T., Arita, S., Tooyama, I., Konishi, Y., 2011. Expression profiles of cytokines in the brains of Alzheimer's disease (AD) patients compared to the brains of non-demented patients with and without increasing AD pathology. J. Alzheimer's Dis. 25, 59–76. https://doi.org/10.3233/JAD-2011-101815

Morris, C.M., Keith, A.B., Edwardson, J.A., Pullen, R.G., 1992. Uptake and distribution of iron and transferrin in the adult rat brain. J Neurochem 59, 300–306.

Mukai, Y., Nakamura, T., Yoshikawa, M., Yoshioka, Y., Tsunoda, S.I., Nakagawa, S., Yamagata, Y., Tsutsumi, Y., 2010. Solution of the structure of the TNF-TNFR2 complex. Sci. Signal. 3, 1–11. https://doi.org/10.1126/scisignal.2000954

Mukherjee, S., Manahan-Vaughan, D., 2013. Role of metabotropic glutamate receptors in persistent forms of hippocampal plasticity and learning. Neuropharmacology 66, 65–81. https://doi.org/10.1016/j.neuropharm.2012.06.005

Mulero, V., Brock, J.H., 1999. Regulation of iron metabolism in murine J774 macrophages: role of nitric oxide-dependent and -independent pathways following activation with gamma interferon and lipopolysaccharide. Blood 94, 2383–9.

Murphy, K., Weaver, C., 2017. Janeway's Immunobiology, Ninth Edition, Garland Science. Garland Science, Taylor & Francis Group.

Murray, C., Sanderson, D.J., Barkus, C., Deacon, R.M.J., Rawlins, J.N.P., Bannerman, D.M., Cunningham, C., 2012. Systemic inflammation induces acute working memory deficits in the primed brain: Relevance for delirium. Neurobiol. Aging 33, 603–616. https://doi.org/10.1016/j.neurobiolaging.2010.04.002

Murray, C.L., Skelly, D.T., Cunningham, C., 2011. Exacerbation of CNS inflammation and neurodegeneration by systemic LPS treatment is independent of circulating IL-1β and IL-6. J. Neuroinflammation 8, 50. https://doi.org/10.1186/1742-2094-8-50

Murray, M.E., Lowe, V.J., Graff-Radford, N.R., Liesinger, A.M., Cannon, A., Przybelski, S.A., Rawal, B., Parisi, J.E., Petersen, R.C., Kantarci, K., Ross, O.A., Duara, R., Knopman, D.S., Jack, C.R., Dickson, D.W., 2015. Clinicopathologic and ^{11}C-Pittsburgh compound B implications of Thal amyloid phase across the Alzheimer's disease spectrum. Brain 138, 1370–1381. https://doi.org/10.1093/brain/awv050

Nadeau, S., Rivest, S., 2000. Role of microglial-derived tumor necrosis factor in mediating CD14 transcription and nuclear factor κ B activity in the brain during endotoxemia. J. Neurosci. 20, 3456–3468. https://doi.org/10.1523/jneurosci.20-09-03456.2000

Nadeau, S., Rivest, S., 1999. Effects of circulating tumor necrosis factor on the neuronal activity and expression of the genes encoding the tumor necrosis factor receptors (p55 and p75) in the rat brain: A view from the blood-brain barrier. Neuroscience 93, 1449–1464. https://doi.org/10.1016/S0306-4522(99)00225-0

Nairz, M., Fritsche, G., Brunner, P., Talasz, H., Hantke, K., Weiss, G., 2008. Interferon-γ limits the availability of iron for intramacrophage Salmonella typhimurium. Eur. J. Immunol. 38, 1923–1936. https://doi.org/10.1002/eji.200738056

Nairz, M., Fritsche, G., Crouch, M.L. V., Barton, H.C., Fang, F.C., Weiss, G., 2009. Slc11a1 limits intracellular growth of Salmonella enterica sv. Typhimurium by promoting macrophage immune effector functions and impairing bacterial iron acquisition. Cell. Microbiol. 11, 1365–1381. https://doi.org/10.1111/j.1462-5822.2009.01337.x

Nairz, M., Theurl, I., Ludwiczek, S., Theurl, M., Mair, S.M., Fritsche, G., Weiss, G., 2007. The co-ordinated regulation of iron homeostasis in murine macrophages limits the availability of iron for intracellular Salmonella typhimurium. Cell. Microbiol. 9, 2126–2140. https://doi.org/10.1111/j.1462-5822.2007.00942.x

Nanton, M.R., Way, S.S., Shlomchik, M.J., McSorley, S.J., 2012. Cutting Edge: B Cells Are Essential for Protective Immunity against Salmonella Independent of Antibody Secretion . J. Immunol. 189, 5503–5507. https://doi.org/10.4049/jimmunol.1201413

Bibliography

Nazmi, A., Field, R.H., Griffin, E.W., Haugh, O., Hennessy, E., Cox, D., Reis, R., Tortorelli, L., Murray, C.L., Lopez-Rodriguez, A.B., Jin, L., Lavelle, E.C., Dunne, A., Cunningham, C., 2019. Chronic neurodegeneration induces type I interferon synthesis via STING, shaping microglial phenotype and accelerating disease progression. Glia 1–23. https://doi.org/10.1002/glia.23592

Neher, J.J., Cunningham, C., 2019. Priming Microglia for Innate Immune Memory in the Brain. Trends Immunol. 40, 358–374. https://doi.org/10.1016/j.it.2019.02.001

Neiveyans, M., Melhem, R., Arnoult, C., Bourquard, T., Jarlier, M., Busson, M., Laroche, A., Cerutti, M., Pugnière, M., Ternant, D., Gaborit, N., Chardès, T., Poupon, A., Gouilleux-Gruart, V., Pèlegrin, A., Poul, M.A., 2019. A recycling anti-transferrin receptor-1 monoclonal antibody as an efficient therapy for erythroleukemia through target up-regulation and antibody-dependent cytotoxic effector functions. MAbs 11, 593–605. https://doi.org/10.1080/19420862.2018.1564510

Nelson, M., Christ, C., Schildkraut, I., 1984. Alteration of apparent restriction endonuclease recognition specificities by DNA methylases. Nucleic Acids Res. 12, 5165–5173. https://doi.org/10.1093/nar/12.13.5165

Ng, A., Tam, W.W., Zhang, M.W., Ho, C.S., Husain, S.F., McIntyre, R.S., Ho, R.C., 2018. IL-1β, IL-6, TNF- α and CRP in Elderly Patients with Depression or Alzheimer's disease: Systematic Review and Meta-Analysis. Sci. Rep. 8, 1–12. https://doi.org/10.1038/s41598-018-30487-6

Niewoehner, J., Bohrmann, B., Collin, L., Urich, E., Sade, H., Maier, P., Rueger, P., Stracke, J.O., Lau, W., Tissot, A.C., Loetscher, H., Ghosh, A., Freskgård, P.-O., 2014. Increased Brain Penetration and Potency of a Therapeutic Antibody Using a Monovalent Molecular Shuttle. Neuron 81, 49–60. https://doi.org/10.1016/j.neuron.2013.10.061

Nimmerjahn, A., Kirchhoff, F., Helmchen, F., 2005. Resting microglial cells are highly dynamic surveillants of brain parenchyma in vivo. Neuroforum 11, 95–96. https://doi.org/10.1515/nf-2005-0304

Norden, D.M., Godbout, J.P., 2013. Review: Microglia of the aged brain: Primed to be activated and resistant to regulation. Neuropathol. Appl. Neurobiol. 39, 19–34. https://doi.org/10.1111/j.1365-2990.2012.01306.x

Nussbaum-Krammer, C.I., Neto, M.F., Brielmann, R.M., Pedersen, J.S., Morimoto, R.I., 2015. Investigating the Spreading and Toxicity of Prion-like Proteins Using the Metazoan Model Organism C. elegans. JoVE e52321. https://doi.org/doi:10.3791/52321

O'Banion, M.K., 2014. Does peripheral inflammation contribute to Alzheimer disease? Neurology 83, 480–481.

Ober, R.J., Radu, C.G., Ghetie, V., Ward, E.S., 2001. Differences in promiscuity for antibody-FcRn interactions across species: Implications for therapeutic antibodies. Int. Immunol. 13, 1551–1559. https://doi.org/10.1093/intimm/13.12.1551

Obst, J., Mancuso, R., Simon, E., Gomez-Nicola, D., 2018. PD-1 deficiency is not sufficient to induce myeloid mobilization to the brain or alter the inflammatory profile during chronic neurodegeneration. Brain. Behav. Immun. 73, 708–716. https://doi.org/10.1016/j.bbi.2018.08.006

Oddo, S., Caccamo, A., Shepherd, J.D., Murphy, M.P., Golde, T.E., Kayed, R., Metherate, R., Mattson, M.P., Akbari, Y., LaFerla, F.M., 2003. Triple-transgenic model of Alzheimer's Disease with plaques and tangles: Intracellular Aβ and synaptic dysfunction. Neuron 39, 409–421. https://doi.org/10.1016/S0896-6273(03)00434-3

Oganesyan, V., Gao, C., Shirinian, L., Wu, H., Dall'Acqua, W.F., 2008. Structural characterization of a human Fc fragment engineered for lack of effector functions. Acta Crystallogr. Sect. D Biol. Crystallogr. 64, 700–704. https://doi.org/10.1107/S0907444908007877

Okuyama, T., Eto, Y., Sakai, N., Minami, K., Yamamoto, T., Sonoda, H., Yamaoka, M., Tachibana, K., Hirato, T., Sato, Y., 2019. Iduronate-2-Sulfatase with Anti-human Transferrin Receptor Antibody for Neuropathic Mucopolysaccharidosis II: A Phase 1/2 Trial. Mol. Ther. 27, 456–464. https://doi.org/10.1016/j.ymthe.2018.12.005

Okuyama, T., Eto, Y., Sakai, N., Nakamura, K., Yamamoto, T., Yamaoka, M., Ikeda, T., So, S., Tanizawa, K., Sonoda, H., Sato, Y., 2020. Drug delivery across the blood-brain barrier: a phase 2/3 trial of pabinafusp alfa, iduronate-2-sulfatase fused with anti-human transferrin receptor antibody, targeting neurodegeneration in Mucopolysaccharidosis II. Mol. Ther. 29, 1–9. https://doi.org/10.1016/j.ymthe.2020.09.039

Olmos-Alonso, A., Schetters, S.T.T., Sri, S., Askew, K., Mancuso, R., Vargas-Caballero, M., Holscher, C., Perry, V.H., Gomez-Nicola, D., 2016. Pharmacological targeting of CSF1R inhibits microglial proliferation and prevents the progression of Alzheimer's-like pathology. Brain 139, 891–907. https://doi.org/10.1093/brain/awv379

Olsen, I., Kell, D.B., Pretorius, E., 2020. Is Porphyromonas gingivalis involved in Parkinson's disease? Eur. J. Clin. Microbiol. Infect. Dis. 39, 2013–2018. https://doi.org/10.1007/s10096-020-03944-2

Ortí-Casañ, N., Wu, Y., Naudé, P.J.W., De Deyn, P.P., Zuhorn, I.S., Eisel, U.L.M., 2019. Targeting TNFR2 as a novel therapeutic strategy for Alzheimer's disease. Front. Neurosci. 13, 1–8. https://doi.org/10.3389/fnins.2019.00049

Ott, B.R., Jones, R.N., Daiello, L.A., de la Monte, S.M., Stopa, E.G., Johanson, C.E., Denby, C., Grammas, P., 2018. Blood-Cerebrospinal Fluid Barrier Gradients in Mild Cognitive Impairment and Alzheimer's Disease: Relationship to Inflammatory Cytokines and Chemokines. Front. Aging Neurosci. 10, 1–12. https://doi.org/10.3389/fnagi.2018.00245

Ozmen, L., Albientz, A., Czech, C., Jacobsen, H., 2009. Expression of transgenic APP mRNA is the key determinant for beta-amyloid deposition in PS2APP transgenic mice. Neurodegener. Dis. 6, 29–36. https://doi.org/10.1159/000170884

Bibliography

Papadaki, H.A., Kritikos, H.D., Valatas, V., Boumpas, D.T., Eliopoulos, G.D., 2002. Anemia of chronic disease in rheumatoid arthritis is associated with increased apoptosis of bone marrow erythroid cells: improvement following anti–tumor necrosis factor-α antibody therapy. Blood 100, 474–482. https://doi.org/10.1182/blood-2002-01-0136

Parachikova, A., Agadjanyan, M.G., Cribbs, D.H., Blurton-Jones, M., Perreau, V., Rogers, J., Beach, T.G., Cotman, C.W., 2007. Inflammatory changes parallel the early stages of Alzheimer disease. Neurobiol. Aging 28, 1821–1833. https://doi.org/10.1016/j.neurobiolaging.2006.08.014

Pardon, M.C., 2015. Lipopolysaccharide hyporesponsiveness: Protective or damaging response to the brain? Rom. J. Morphol. Embryol. 56, 903–913.

Pardridge, W.M., 2020a. Treatment of alzheimer's disease and blood–brain barrier drug delivery. Pharmaceuticals 13, 1–25. https://doi.org/10.3390/ph13110394

Pardridge, W.M., 2020b. Blood-Brain Barrier and Delivery of Protein and Gene Therapeutics to Brain. Front. Aging Neurosci. 11, 1–27. https://doi.org/10.3389/fnagi.2019.00373

Pardridge, W.M., 2017. Delivery of Biologics Across the Blood–Brain Barrier with Molecular Trojan Horse Technology. BioDrugs 31, 503–519. https://doi.org/10.1007/s40259-017-0248-z

Pardridge, W.M., 2016. CSF, blood-brain barrier, and brain drug delivery. Expert Opin. Drug Deliv. 13, 963–975. https://doi.org/10.1517/17425247.2016.1171315

Pardridge, W.M., 2015. Blood–brain barrier drug delivery of IgG fusion proteins with a transferrin receptor monoclonal antibody. Expert Opin. Drug Deliv. 12, 207–222. https://doi.org/10.1517/17425247.2014.952627

Pardridge, W.M., 2012. Drug transport across the blood-brain barrier. J. Cereb. blood flow Metab. 32, 1959–72. https://doi.org/10.1038/jcbfm.2012.126

Pardridge, W.M., 2006. Molecular Trojan horses for blood-brain barrier drug delivery. Curr. Opin. Pharmacol. 6, 494–500. https://doi.org/10.1016/j.coph.2006.06.001

Pardridge, W.M., 2002. Drug and gene targeting to the brain with molecular trojan horses. Nat. Rev. Drug Discov. 1, 131–139. https://doi.org/10.1038/nrd725

Pardridge, W.M., Boado, R.J., Giugliani, R., Schmidt, M., 2018a. Plasma Pharmacokinetics of Valanafusp Alpha, a Human Insulin Receptor Antibody-Iduronidase Fusion Protein, in Patients with Mucopolysaccharidosis Type I. BioDrugs 32, 169–176. https://doi.org/10.1007/s40259-018-0264-7

Pardridge, W.M., Boado, R.J., Patrick, D.J., Hui, E.K.W., Lu, J.Z., 2018b. Blood-Brain Barrier Transport, Plasma Pharmacokinetics, and Neuropathology Following Chronic Treatment of the Rhesus Monkey with a Brain Penetrating Humanized Monoclonal Antibody Against the Human Transferrin Receptor. Mol. Pharm. 15, 5207–5216. https://doi.org/10.1021/acs.molpharmaceut.8b00730

Park, S., Kim, J., Chun, J., Han, K., Soh, H., Kang, E.A., Lee, H.J., Im, J.P., Kim, J.S., 2019. Patients with Inflammatory Bowel Disease Are at an Increased Risk of Parkinson's Disease: A South Korean Nationwide Population-Based Study. J. Clin. Med. 8, 1191. https://doi.org/10.3390/jcm8081191

Parker, D.C., 1993. T Cell-Dependent B Cell Activation. Annu. Rev. Immunol. 11, 331–360. https://doi.org/10.1146/annurev.iy.11.040193.001555

Paterson, J., Webster, C.I., 2016. Exploiting transferrin receptor for delivering drugs across the blood-brain barrier. Drug Discov. Today Technol. 20, 49–52. https://doi.org/10.1016/j.ddtec.2016.07.009

Paulson, R.F., Ruan, B., Hao, S., Chen, Y., 2020. Stress Erythropoiesis is a Key Inflammatory Response. Cells 9, 634. https://doi.org/10.3390/cells9030634

Peppard, J., Glickman, F., He, Y., Hu, S.I., Doughty, J., Goldberg, R., 2003. Development of a high-throughput screening assay for inhibitors of aggrecan cleavage using luminescent oxygen channeling (AlphaScreen^{TM}). J. Biomol. Screen. 8, 149–156. https://doi.org/10.1177/1087057103252308

Perl, D.P., 2010. Neuropathology of Alzheimer's Disease. Mt. Sinai J. Med. A J. Transl. Pers. Med. 77, 32–42. https://doi.org/10.1002/msj.20157

Perry, V.H., 2016. Microglia. Microbiol. Spectr. 4, 1–9. https://doi.org/10.1128/microbiolspec.MCHD-0003-2015

Perry, V.H., Holmes, C., 2014. Microglial priming in neurodegenerative disease. Nat. Rev. Neurol. 10, 217–24. https://doi.org/10.1038/nrneurol.2014.38

Perry, V.H., Teeling, J., 2013. Microglia and macrophages of the central nervous system: the contribution of microglia priming and systemic inflammation to chronic neurodegeneration. Semin. Immunopathol. 35, 601–612. https://doi.org/10.1007/s00281-013-0382-8

Persic, L., Roberts, A., Wilton, J., Cattaneo, A., Bradbury, A., Hoogenboom, H.R., 1997. An integrated vecctor system for the eukaryotic expression of antibodies or their fragments after selection from phage display libraries. Gene 187, 9–18.

Peruzzo, B., Pastor, F.E., Blázquez, J.L., Schöbitz, K., Peláez, B., Amat, P., Rodríguez, E.M., 2000. A second look at the barriers of the medial basal hypothalamus. Exp. Brain Res. 132, 10–26. https://doi.org/10.1007/s002219900289

Peter, I., Dubinsky, M., Bressman, S., Park, A., Lu, C., Chen, N., Wang, A., 2018. Anti-tumor necrosis factor therapy and incidence of Parkinson disease among patients with inflammatory bowel disease. JAMA Neurol. 75, 939–946. https://doi.org/10.1001/jamaneurol.2018.0605

Peters, S.E., Paterson, G.K., Bandularatne, E.S.D., Northen, H.C., Pleasance, S., Willers, C., Wang, J., Foote, A.K., Constantino-Casas, F., Scase, T.J., Blacklaws, B.A., Bryant, C.E., Mastroeni, P., Charles, I.G., Maskell, D.J., 2010. Salmonella enterica serovar typhimurium trxA mutants are protective against virulent challenge and induce less inflammation than the live-attenuated vaccine strain SL3261. Infect. Immun. 78, 326–336. https://doi.org/10.1128/IAI.00768-09

Bibliography

Petersen, A.M.W., Pedersen, B.K., 2005. The anti-inflammatory effect of exercise. J. Appl. Physiol. 98, 1154–1162. https://doi.org/10.1152/japplphysiol.00164.2004.

Petersen, R.C., 2016. Mild Cognitive Impairment. Contin. Lifelong Learn. Neurol. 22, 404–418. https://doi.org/10.1212/CON.0000000000000313

Piers, A.T., Lavin, T., Radley-Crabb, H.G., Bakker, A.J., Grounds, M.D., Pinniger, G.J., 2011. Blockade of TNF in vivo using cV1q antibody reduces contractile dysfunction of skeletal muscle in response to eccentric exercise in dystrophic mdx and normal mice. Neuromuscul. Disord. 21, 132–141. https://doi.org/10.1016/j.nmd.2010.09.013

Pietras, E.M., 2017. Inflammation: A key regulator of hematopoietic stem cell fate in health and disease. Blood 130, 1693–1698. https://doi.org/10.1182/blood-2017-06-780882

Pietras, E.M., Mirantes-Barbeito, C., Fong, S., Loeffler, D., Kovtonyuk, L. V., Zhang, S., Lakshminarasimhan, R., Chin, C.P., Techner, J.M., Will, B., Nerlov, C., Steidl, U., Manz, M.G., Schroeder, T., Passegué, E., 2016. Chronic interleukin-1 exposure drives haematopoietic stem cells towards precocious myeloid differentiation at the expense of self-renewal. Nat. Cell Biol. 18, 607–618. https://doi.org/10.1038/ncb3346

Pillai, J.A., Maxwell, S., Bena, J., Bekris, L.M., Rao, S.M., Chance, M., Lamb, B.T., Leverenz, J.B., 2019. Key inflammatory pathway activations in the MCI stage of Alzheimer's disease. Ann. Clin. Transl. Neurol. 6, 1248–1262. https://doi.org/10.1002/acn3.50827

Poltorak, M.P., Schraml, B.U., 2015. Fate mapping of dendritic cells. Front. Immunol. 6, 1–15. https://doi.org/10.3389/fimmu.2015.00199

Potkin, S.G., 2002. The ABC of Alzheimer's disease: ADL and improving day-to-day functioning of patients. Int. Psychogeriatrics 14, 7–26. https://doi.org/10.1017/s1041610203008640

Pott Godoy, M.C., Tarelli, R., Ferrari, C.C., Sarchi, M.I., Pitossi, F.J., 2008. Central and systemic IL-1 exacerbates neurodegeneration and motor symptoms in a model of Parkinson's disease. Brain 131, 1880–1894. https://doi.org/10.1093/brain/awn101

Preston, J.E., Joan Abbott, N., Begley, D.J., 2014. Transcytosis of macromolecules at the blood-brain barrier, 1st ed, Advances in Pharmacology. Elsevier Inc. https://doi.org/10.1016/bs.apha.2014.06.001

Prince, M., Prina, M., Guerchet, M., 2013. World Alzheimer Report 2013 Journey of Caring: An Analysis of Long-Term Care for Dementia. Alzheimer's Dis. Int.

Prince, M., Wimo, A., Guerchet, M., Gemma-Claire, A., Wu, Y.-T., Prina, M., 2015. World Alzheimer Report 2015: The Global Impact of Dementia - An analysis of prevalence, incidence, cost and trends. Alzheimer's Dis. Int. https://doi.org/10.1111/j.0963-7214.2004.00293.x

Promega Corporation, 2012. CellTiter 96® One Solution AQueous Cell Proliferation Assay Technical Bulletin #TB245.

Pulgar, V.M., 2019. Transcytosis to Cross the Blood Brain Barrier, New Advancements and Challenges. Front. Neurosci. 12, 1–9. https://doi.org/10.3389/fnins.2018.01019

Punt, J., Stranford, S.A., Jones, P., Owen, J.A., 2018. Kuby Immunology, Eighth Edition. W. H. Freeman and Company.

Püntener, U., Booth, S.G., Perry, V.H., Teeling, J.L., 2012. Long-term impact of systemic bacterial infection on the cerebral vasculature and microglia. J. Neuroinflammation 9, 146. https://doi.org/10.1186/1742-2094-9-146

Purves, D., Augustine, G.J., Fitzpatrick, D., Hall, W.C., LaMantia, A.-S., Mooney, R.D., Platt, M.L., White, L.E., 2018. Neuroscience. Oxford University Press.

Qian, H., Yuan, H., Wang, J., Du, Y., Zhang, X., Sun, Y., Li, Z., Zhao, W., 2014. A monoclonal antibody ameliorates local inflammation and osteoporosis by targeting TNF-α and RANKL. Int. Immunopharmacol. 20, 370–376. https://doi.org/10.1016/j.intimp.2014.03.017

Quan, N., Banks, W.A., 2007. Brain-immune communication pathways. Brain. Behav. Immun. 21, 727–735. https://doi.org/10.1016/j.bbi.2007.05.005

Quan, N., Whiteside, M., Herkenham, M., 1998. Time course and localization patterns of interleukin-1β messenger RNA expression in brain and pituitary after peripheral administration of lipopolysaccharide. Neuroscience 83, 281–293. https://doi.org/10.1016/S0306-4522(97)00350-3

Radley, H.G., Davies, M.J., Grounds, M.D., 2008. Reduced muscle necrosis and long-term benefits in dystrophic mdx mice after cV1q (blockade of TNF) treatment. Neuromuscul. Disord. 18, 227–238. https://doi.org/10.1016/j.nmd.2007.11.002

Rakic, S., Hung, Y.M.A., Smith, M., So, D., Tayler, H.M., Varney, W., Wild, J., Harris, S., Holmes, C., Love, S., Stewart, W., Nicoll, J.A.R., Boche, D., 2018. Systemic infection modifies the neuroinflammatory response in late stage Alzheimer's disease. Acta Neuropathol. Commun. 6, 88. https://doi.org/10.1186/s40478-018-0592-3

Ransohoff, R. M., 2016a. A polarizing question: Do M1 and M2 microglia exist. Nat. Neurosci. 19, 987–991. https://doi.org/10.1038/nn.4338

Ransohoff, R. M., 2016b. How neuroinflammation contributes to neurodegeneration. Science (80-.). 353, 168–175.

Ransohoff, R.M., Kivisäkk, P., Kidd, G., 2003. Three or more routes for leukocyte migration into the central nervous system. Nat. Rev. Immunol. 3, 569–581. https://doi.org/10.1038/nri1130

Rao, S., Schieber, A.M.P., O'Connor, C.P., Leblanc, M., Michel, D., Ayres, J.S., 2017. Pathogen-Mediated Inhibition of Anorexia Promotes Host Survival and Transmission. Cell 168, 503-516.e12. https://doi.org/10.1016/j.cell.2017.01.006

Raub, T.J., Newton, C.R., 1991. Recycling kinetics and transcytosis in primary cultures of bovine brain microvessel endothelial cells. J. Cell. Physiol. 149, 141–151.

Re, F., Strominger, J.L., 2001. Toll-like Receptor 2 (TLR2) and TLR4 Differentially Activate Human Dendritic Cells. J. Biol. Chem. 276, 37692–37699. https://doi.org/10.1074/jbc.M105927200

Reis, K., Hälldin, J., Fernaeus, S., Pettersson, C., Land, T., 2006. NADPH oxidase inhibitor diphenyliodonium abolishes lipopolysaccharide-induced down-regulation of transferrin receptor expression in N2a and BV-2 cells. J. Neurosci. Res. 84, 1047–1052. https://doi.org/10.1002/jnr.21005

Reis, R., Hennessy, E., Murray, C., Griffin, É.W., Cunningham, C., 2015. At the centre of neuronal, synaptic and axonal pathology in murine prion disease: degeneration of neuroanatomically linked thalamic and brainstem nuclei. Neuropathol. Appl. Neurobiol. 41, 780–797. https://doi.org/10.1111/nan.12232

Reisberg, B., Finkel, S., Overall, J., Schmidt-Gollas, N., Kanowski, S., Lehfeld, H., Hulla, F., Sclan, S.G., Wilms, H.-U., Heininger, K., Hindmarch, I., Stemmler, M., Poon, L., Kluger, A., Cooler, C., Bergener, M., Hugonot-Diener, L., Robert, P.H., Erzigkeit, H., 2001. The Alzheimer's Disease Activities of Daily Living International Scale (ADL-IS). Int. Psychogeriatrics 13, 163–181. https://doi.org/10.1017/S1041610201007566

Rhodes, M.M., Koury, S.T., Kopsombut, P., Alford, C.E., Price, J.O., Koury, M.J., 2016. Stress reticulocytes lose transferrin receptors by an extrinsic process involving spleen and macrophages. Am. J. Hematol. 91, 875–882. https://doi.org/10.1002/ajh.24421

Rivest, S., 2003. Molecular insights on the cerebral innate immune system. Brain. Behav. Immun. 17, 13–19. https://doi.org/10.1016/S0889-1591(02)00055-7

Roopenian, D.C., Christianson, G.J., Sproule, T.J., Brown, A.C., Akilesh, S., Jung, N., Petkova, S., Avanessian, L., Choi, E.Y., Shaffer, D.J., Eden, P.A., Anderson, C.L., 2014. The MHC Class I-Like IgG Receptor Controls Perinatal IgG Transport, IgG Homeostasis, and Fate of IgG-Fc-Coupled Drugs. J. Immunol. 170, 3528–3533. https://doi.org/10.4049/jimmunol.170.7.3528

Rosche, K.L., Aljasham, A.T., Kipfer, J.N., Piatkowski, B.T., Konjufca, V., 2015. Infection with Salmonella enterica Serovar Typhimurium Leads to Increased Proportions of F4/80+ Red Pulp Macrophages and Decreased Proportions of B and T Lymphocytes in the Spleen. PLoS One 10, e0130092. https://doi.org/10.1371/journal.pone.0130092

Rossi, O., Grant, A.J., Mastroeni, P., 2017. Effect of in vivo neutralization of tumor necrosis alpha on the efficacy of antibiotic treatment in systemic Salmonella enterica infections. Pathog. Dis. 75, 1–8. https://doi.org/10.1093/femspd/ftx002

Rossi, S., Motta, C., Studer, V., Barbieri, F., Buttari, F., Bergami, A., Sancesario, G., Bernardini, S., De Angelis, G., Martino, G., Furlan, R., Centonze, D., 2014. Tumor necrosis factor is elevated in progressive multiple sclerosis and causes excitotoxic neurodegeneration. Mult. Scler. J. 20, 304–312. https://doi.org/10.1177/1352458513498128

Ruano-Salguero, J.S., Lee, K.H., 2020. Antibody transcytosis across brain endothelial-like cells occurs nonspecifically and independent of FcRn. Sci. Rep. 10, 1–10. https://doi.org/10.1038/s41598-020-60438-z

Ruby, T., Mclaughlin, L., Gopinath, S., Monack, D., 2012. Salmonella's long-term relationship with its host. FEMS Microbiol. Rev. 36, 600–615. https://doi.org/10.1111/j.1574-6976.2012.00332.x

Rueden, C.T., Schindelin, J., Hiner, M.C., DeZonia, B.E., Walter, A.E., Arena, E.T., Eliceiri, K.W., 2017. ImageJ2: ImageJ for the next generation of scientific image data. BMC Bioinformatics 18, 1–26. https://doi.org/10.1186/s12859-017-1934-z

Ruifrok, A.C., Johnston, D.A., 2001. Quantification of histochemical staining by color deconvolution. Anal. Quant. Cytol. Histol. 23, 291–9.

Rusten, L.S., Jacobsen, S.E.W., 1995. Tumor necrosis factor (TNF)-α directly inhibits human erythropoiesis in vitro: Role of p55 and p75 TNF receptors. Blood 85, 989–996. https://doi.org/10.1182/blood.v85.4.989.bloodjournal854989

Santos, R.L., Zhang, S., Tsolis, R.M., Kingsley, R.A., Garry Adams, L., Bäumler, A.J., 2001. Animal models of Salmonella infections: Enteritis versus typhoid fever. Microbes Infect. 3, 1335–1344. https://doi.org/10.1016/S1286-4579(01)01495-2

Saraiva, M., O'Garra, A., 2010. The regulation of IL-10 production by immune cells. Nat. Rev. Immunol. 10, 170–181. https://doi.org/10.1038/nri2711

Scallon, B., Cai, A., Radewonuk, J., Naso, M., 2004. Addition of an extra immunoglobulin domain to two anti-rodent TNF monoclonal antibodies substantially increased their potency. Mol. Immunol. 41, 73–80. https://doi.org/10.1016/j.molimm.2004.01.006

Scallon, B., Cai, A., Solowski, N., Rosenberg, A., Song, X., Shealy, D., Wagner, C., 2002. Binding and Functional Comparisons of Two Types of Tumor Necrosis Factor Antagonists. J. Pharmacol. Exp. Ther. 301, 418–426. https://doi.org/10.1124/jpet.301.2.418

Schindelin, J., Arganda-Carreras, I., Frise, E., Kaynig, V., Longair, M., Pietzsch, T., Preibisch, S., Rueden, C., Saalfeld, S., Schmid, B., Tinevez, J.Y., White, D.J., Hartenstein, V., Eliceiri, K., Tomancak, P., Cardona, A., 2012. Fiji: An open-source platform for biological-image analysis. Nat. Methods 9, 676–682. https://doi.org/10.1038/nmeth.2019

Schlachetzki, F., Zhu, C., Pardridge, W.M., 2002. Expression of the neonatal Fc receptor (FcRn) at the blood-brain barrier. J. Neurochem. 81, 203–206. https://doi.org/10.1046/j.1471-4159.2002.00840.x

Schubert, T.E.O., Obermaier, F., Ogucsai, P., Männel, D.N., Echtenacher, B., Hofstädter, F., Haerle, P., 2008. Murine models of anaemia of inflammation: Extramedullary haematopoiesis represents a species specific difference to human anaemia of inflammation that can be eliminated by splenectomy. Int. J. Immunopathol. Pharmacol. 21, 577–584. https://doi.org/10.1177/039463200802100310

Schuetze, N., Schoeneberger, S., Mueller, U., Freudenberg, M.A., Alber, G., Straubinger, R.K., 2005. IL-12 family members: Differential kinetics of their TLR4-mediated induction by Salmonella Enteritidis and the impact of IL-10 in bone marrow-derived macrophages. Int. Immunol. 17, 649–659. https://doi.org/10.1093/intimm/dxh247

Bibliography

Schultz, J., Schwarz, A., Neidhold, S., Burwinkel, M., Riemer, C., Simon, D., Kopf, M., Otto, M., Baier, M., 2004. Role of interleukin-1 in prion disease-associated astrocyte activation. Am J Pathol 165, 671–678. https://doi.org/165/2/671 [pii]

Schulz, M., Engelhardt, B., 2005. The circumventricular organs participate in the immunopathogenesis of experimental autoimmune encephalomyelitis. Cerebrospinal Fluid Res. 2, 1–14. https://doi.org/10.1186/1743-8454-2-8

Scott, K. a, Moore, R.J., Arnott, C.H., East, N., Thompson, R.G., Scallon, B.J., Shealy, D.J., Balkwill, F.R., 2003. An anti-tumor necrosis factor-alpha antibody inhibits the development of experimental skin tumors. Mol. Cancer Ther. 2, 445–451.

Sehlin, D., Fang, X.T., Meier, S.R., Jansson, M., Syvänen, S., 2017. Pharmacokinetics, biodistribution and brain retention of a bispecific antibody-based PET radioligand for imaging of amyloid-β. Sci. Rep. 7, 17254. https://doi.org/10.1038/s41598-017-17358-2

Shamim, D., Laskowski, M., 2017. Inhibition of Inflammation Mediated Through the Tumor Necrosis Factor α Biochemical Pathway Can Lead to Favorable Outcomes in Alzheimer Disease. J. Cent. Nerv. Syst. Dis. 9, 17–20. https://doi.org/10.1177/1179573517722512

Shen, X.N., Lu, Y., Tan, C.T.Y., Liu, L.Y., Yu, J.T., Feng, L., Larbi, A., 2019. Identification of inflammatory and vascular markers associated with mild cognitive impairment. Aging (Albany. NY). 11, 2403–2419. https://doi.org/10.18632/aging.101924

Shen, Y., Li, G., Gu, C., Chen, B., Chen, A., Li, H., Gao, B., Liang, C., Wu, J., Yang, T., Jin, L., Su, Y., 2017. T0001, a variant of TNFR2-Fc fusion protein, exhibits improved Fc effector functions through increased binding to membrane-bound TNFα. PLoS One 12, 1–15. https://doi.org/10.1371/journal.pone.0177891

Sheng, J.G., Bora, S.H., Xu, G., Borchelt, D.R., Price, D.L., Koliatsos, V.E., 2003. Lipopolysaccharide-induced-neuroinflammation increases intracellular accumulation of amyloid precursor protein and amyloid β peptide in APPswe transgenic mice. Neurobiol. Dis. 14, 133–145. https://doi.org/10.1016/S0969-9961(03)00069-X

Shi, J.Q., Shen, W., Chen, J., Wang, B.R., Zhong, L.L., Zhu, Y.W., Zhu, H.Q., Zhang, Q.Q., Zhang, Y.D., Xu, J., 2011. Anti-TNF-α reduces amyloid plaques and tau phosphorylation and induces CD11c-positive dendritic-like cell in the APP/PS1 transgenic mouse brains. Brain Res. 1368, 239–247. https://doi.org/10.1016/j.brainres.2010.10.053

Shimosaki, S., Nakahata, S., Ichikawa, T., Kitanaka, A., Kameda, T., Hidaka, T., Kubuki, Y., Kurosawa, G., Zhang, L., Sudo, Y., Shimoda, K., Morishita, K., 2017. Development of a complete human IgG monoclonal antibody to transferrin receptor 1 targeted for adult T-cell leukemia/lymphoma. Biochem. Biophys. Res. Commun. 485, 144–151. https://doi.org/10.1016/j.bbrc.2017.02.039

Shutinoski, B., Hakimi, M., Harmsen, I.E., Lunn, M., Rocha, J., Lengacher, N., Zhou, Y.Y., Khan, J., Nguyen, A., Hake-Volling, Q., El-Kodsi, D., Li, J., Alikashani, A., Beauchamp, C., Majithia, J., Coombs, K., Shimshek, D., Marcogliese, P.C., Park, D.S., Rioux, J.D., Philpott, D.J., Woulfe, J.M., Hayley, S., Sad, S., Tomlinson, J.J., Brown, E.G., Schlossmacher, M.G., 2019. Lrrk2 alleles modulate inflammation during microbial infection of mice in a sex-dependent manner. Sci. Transl. Med. 11, 36–41. https://doi.org/10.1126/scitranslmed.aas9292

Sigurdson, C.J., Heikenwalder, M., Manco, G., Barthel, M., Schwarz, P., Stecher, B., Krautler, N.J., Hardt, W., Seifert, B., MacPherson, A.J.S., Corthesy, I., Aguzzi, A., 2008. Bacterial Colitis Increases Susceptibility to Oral Prion Disease. J. Infect. Dis. 199, 243–252. https://doi.org/10.1086/595791

Šišková, Z., Page, A., O'Connor, V., Perry, V.H., 2009. Degenerating synaptic boutons in prion disease: Microglia activation without synaptic stripping. Am. J. Pathol. 175, 1610–1621. https://doi.org/10.2353/ajpath.2009.090372

Sisková, Z., Sanyal, N.K., Orban, A., O'Connor, V., Perry, V.H., 2010. Reactive hypertrophy of synaptic varicosities within the hippocampus of prion-infected mice. Biochem. Soc. Trans. 38, 471–475. https://doi.org/10.1042/BST0380471

Skelly, D.T., Griffin, É.W., Murray, C.L., Harney, S., O'Boyle, C., Hennessy, E., Dansereau, M.-A., Nazmi, A., Tortorelli, L., Rawlins, J.N., Bannerman, D.M., Cunningham, C., 2018. Acute transient cognitive dysfunction and acute brain injury induced by systemic inflammation occur by dissociable IL-1-dependent mechanisms. Mol. Psychiatry https://doi.org/10.1038/s41380-018-0075-8. https://doi.org/10.1038/s41380-018-0075-8

Skelly, D.T., Hennessy, E., Dansereau, M.A., Cunningham, C., 2013. A Systematic Analysis of the Peripheral and CNS Effects of Systemic LPS, IL-1B, TNF-α and IL-6 Challenges in C57BL/6 Mice. PLoS One 8, 1–20. https://doi.org/10.1371/journal.pone.0069123

Sonoda, H., Morimoto, H., Yoden, E., Koshimura, Y., Kinoshita, M., Golovina, G., Takagi, H., Yamamoto, R., Minami, K., Mizoguchi, A., Tachibana, K., Hirato, T., Takahashi, K., 2018. A Blood-Brain-Barrier-Penetrating Anti-human Transferrin Receptor Antibody Fusion Protein for Neuronopathic Mucopolysaccharidosis II. Mol. Ther. 26, 1366–1374. https://doi.org/10.1016/j.ymthe.2018.02.032

Sriram, K., Matheson, J.M., Benkovic, S.A., Miller, D.B., Luster, M.I., O'Callaghan, J.P., 2006. Deficiency of TNF receptors suppresses microglial activation and alters the susceptibility of brain regions to MPTP-induced neurotoxicity: role of TNF-α 1 . FASEB J. 20, 670–682. https://doi.org/10.1096/fj.05-5106com

Sriram, K., Matheson, J.M., Benkovic, S.A., Miller, D.B., Luster, M.I., O'Callaghan, J.P., 2002. Mice deficient in TNF receptors are protected against dopaminergic neurotoxicity: implications for Parkinson's disease. FASEB J. 16, 1474–1476. https://doi.org/10.1096/fj.02-0216fje

Bibliography

St-Amour, I., Paré, I., Alata, W., Coulombe, K., Ringuette-Goulet, C., Drouin-Ouellet, J., Vandal, M., Soulet, D., Bazin, R., Calon, F., 2013. Brain Bioavailability of Human Intravenous Immunoglobulin and its Transport through the Murine Blood–Brain Barrier. J. Cereb. Blood Flow Metab. 33, 1983–1992. https://doi.org/10.1038/jcbfm.2013.160

Stanimirovic, D.B., Sandhu, J.K., Costain, W.J., 2018. Emerging Technologies for Delivery of Biotherapeutics and Gene Therapy Across the Blood–Brain Barrier. BioDrugs 32, 547–559. https://doi.org/10.1007/s40259-018-0309-y

Steed, P.M., Tansey, M.G., Zalevsky, J., Zhukovsky, E.A., Desjarlais, J.R., Szymkowski, D.E., Abbott, C., Carmichael, D., Chan, C., Cherry, L., Cheung, P., Chirino, A.J., Chung, H.H., Doberstein, S.K., Eivazi, A., Filikov, A. V., Gao, S.X., Hubert, R.S., Hwang, M., Hyun, L., Kashi, S., Kim, A., Kim, E., Kung, J., Martinez, S.P., Muchhal, U.S., Nguyen, D.H.T., O'Brien, C., O'Keefe, D., Singer, K., Vafa, O., Vielmetter, J., Yoder, S.C., Dahiyat, B.I., 2003. Inactivation of TNF signaling by rationally designed dominant-negative TNF variants. Science (80-.). 301, 1895–1898. https://doi.org/10.1126/science.1081297

Steeland, S., Libert, C., Vandenbroucke, R.E., 2018. A new venue of TNF targeting. Int. J. Mol. Sci. 19, 1–55. https://doi.org/10.3390/ijms19051442

Stewart, P.A., 2000. Endothelial vesicles in the blood-brain barrier: Are they related to permeability? Cell. Mol. Neurobiol. 20, 149–163. https://doi.org/10.1023/A:1007026504843

Stoeck, K., Schmitz, M., Ebert, E., Schmidt, C., Zerr, I., 2014. Immune responses in rapidly progressive dementia: a comparative study of neuroinflammatory markers in Creutzfeldt-Jakob disease, Alzheimer's disease and multiple sclerosis. J. Neuroinflammation 11, 170. https://doi.org/10.1186/s12974-014-0170-y

Stopschinski, B.E., Diamond, M.I., 2017. The prion model for progression and diversity of neurodegenerative diseases. Lancet Neurol. 4422, 1–10. https://doi.org/10.1016/S1474-4422(17)30037-6

Striebel, J.F., Race, B., Meade-White, K.D., LaCasse, R., Chesebro, B., 2011. Strain specific resistance to murine scrapie associated with a naturally occurring human prion protein polymorphism at residue 171. PLoS Pathog. 7, e1002275. https://doi.org/10.1371/journal.ppat.1002275

Sugyo, A., Tsuji, A.B., Sudo, H., Nomura, F., Satoh, H., Koizumi, M., Kurosawa, G., Kurosawa, Y., Saga, T., 2017. Uptake of 111In-labeled fully human monoclonal antibody TSP-A18 reflects transferrin receptor expression in normal organs and tissues of mice. Oncol. Rep. 37, 1529–1536. https://doi.org/10.3892/or.2017.5412

Sumbria, R.K., Zhou, Q.-H., Hui, E.K.-W., Lu, J.Z., Boado, R.J., Pardridge, W.M., 2013. Pharmacokinetics and Brain Uptake of an IgG-TNF Decoy Receptor Fusion Protein Following Intravenous, Intraperitoneal, and Subcutaneous Administration in Mice. Mol. Pharm. 10, 1425–1431. https://doi.org/10.1021/mp400004a

Sunkin, S.M., Ng, L., Lau, C., Dolbeare, T., Gilbert, T.L., Thompson, C.L., Hawrylycz, M., Dang, C., 2013. Allen Brain Atlas: An integrated spatio-temporal portal for exploring the central nervous system. Nucleic Acids Res. 41. https://doi.org/10.1093/nar/gks1042

Swardfager, W., Lanctt, K., Rothenburg, L., Wong, A., Cappell, J., Herrmann, N., 2010. A meta-analysis of cytokines in Alzheimer's disease. Biol. Psychiatry 68, 930–941. https://doi.org/10.1016/j.biopsych.2010.06.012

Sweeney, M.D., Zhao, Z., Montagne, A., Nelson, A.R., Zlokovic, B. V., 2019. Blood-brain barrier: From physiology to disease and back. Physiol. Rev. 99, 21–78. https://doi.org/10.1152/physrev.00050.2017

Szabadits, E., Cserép, C., Szonyi, A., Fukazawa, Y., Shigemoto, R., Watanabe, M., Itohara, S., Freund, T.F., Nyiri, G., 2011. NMDA receptors in hippocampal GABAergic synapses and their role in nitric oxide signaling. J. Neurosci. 31, 5893–5904. https://doi.org/10.1523/JNEUROSCI.5938-10.2011

Tacchini, L., Gammella, E., De Ponti, C., Recalcati, S., Cairo, G., 2008. Role of HIF-1 and NF-κB transcription factors in the modulation of transferrin receptor by inflammatory and anti-inflammatory signals. J. Biol. Chem. 283, 20674–20686. https://doi.org/10.1074/jbc.M800365200

Takeda, S., Sato, N., Ikimura, K., Nishino, H., Rakugi, H., Morishita, R., 2013. Increased blood-brain barrier vulnerability to systemic inflammation in an Alzheimer disease mouse model. Neurobiol. Aging 34, 2064–2070. https://doi.org/10.1016/j.neurobiolaging.2013.02.010

Talbot, S., Tötemeyer, S., Yamamoto, M., Akira, S., Hughes, K., Gray, D., Barr, T., Mastroeni, P., Maskell, D.J., Bryant, C.E., 2009. Toll-like receptor 4 signalling through MyD88 is essential to control Salmonella enterica serovar Typhimurium infection, but not for the initiation of bacterial clearance. Immunology 128, 472–483. https://doi.org/10.1111/j.1365-2567.2009.03146.x

Tamgüney, G., Giles, K., Glidden, D. V., Lessard, P., Wille, H., Tremblay, P., Groth, D.F., Yehiely, F., Korth, C., Moore, R.C., Tatzelt, J., Rubinstein, E., Boucheix, C., Yang, X., Stanley, P., Lisanti, M.P., Dwek, R.A., Rudd, P.M., Moskovitz, J., Epstein, C.J., Cruz, T.D., Kuziel, W.A., Maeda, N., Sap, J., Ashe, K.H., Carlson, G.A., Tesseur, I., Wyss-Coray, T., Mucke, L., Weisgraber, K.H., Mahley, R.W., Cohen, F.E., Prusiner, S.B., 2008. Genes contributing to prion pathogenesis. J. Gen. Virol. 89, 1777–1788. https://doi.org/10.1099/vir.0.2008/001255-0

Tarkowski, E., Andreasen, N., Tarkowski, A., Blennow, K., 2003. Intrathecal inflammation precedes development of Alzheimer's disease. J. Neurol. Neurosurg. Psychiatry 74, 1200–1205. https://doi.org/10.1136/jnnp.74.9.1200

Teeling, J.L., Cunningham, C., Newman, T.A., Perry, V.H., 2010. The effect of non-steroidal anti-inflammatory agents on behavioural changes and cytokine production following systemic inflammation: Implications for a role of COX-1. Brain. Behav. Immun. 24, 409–419. https://doi.org/10.1016/j.bbi.2009.11.006

Bibliography

Teeling, J.L., Felton, L.M., Deacon, R.M.J., Cunningham, C., Rawlins, J.N.P., Perry, V.H., 2007. Sub-pyrogenic systemic inflammation impacts on brain and behavior, independent of cytokines. Brain. Behav. Immun. 21, 836–850. https://doi.org/10.1016/j.bbi.2007.01.012

Teeling, J.L., Perry, V.H., 2009. Systemic infection and inflammation in acute CNS injury and chronic neurodegeneration: Underlying mechanisms. Neuroscience 158, 1062–1073. https://doi.org/10.1016/j.neuroscience.2008.07.031

Terwel, D., Lasrado, R., Snauwaert, J., Vandeweert, E., Van Haesendonck, C., Borghgraef, P., Van Leuven, F., 2005. Changed conformation of mutant tau-P301L underlies the moribund tauopathy, absent in progressive, nonlethal axonopathy of tau-4R/2N transgenic mice. J. Biol. Chem. 280, 3963–3973. https://doi.org/10.1074/jbc.M409876200

Thibeault, I., Laflamme, N., Rivest, S., 2001. Regulation of the gene encoding the monocyte chemoattractant protein 1 (MCP-1) in the mouse and rat brain in response to circulating lps and proinflammatory cytokines. J. Comp. Neurol. 434, 461–477. https://doi.org/10.1002/cne.1187

Thom, G., Burrell, M., Haqqani, A.S., Yogi, A., Lessard, E., Brunette, E., Delaney, C., Baumann, E., Callaghan, D., Rodrigo, N., Webster, C.I., Stanimirovic, D.B., 2018. Enhanced Delivery of Galanin Conjugates to the Brain through Bioengineering of the Anti-Transferrin Receptor Antibody OX26. Mol. Pharm. 15, 1420–1431. https://doi.org/10.1021/acs.molpharmaceut.7b00937

Thome, A.D., Faridar, A., Beers, D.R., Thonhoff, J.R., Zhao, W., Wen, S., Pascual, B., Masdeu, J.C., Appel, S.H., 2018. Functional alterations of myeloid cells during the course of Alzheimer's disease. Mol. Neurodegener. 13, 61. https://doi.org/10.1186/s13024-018-0293-1

Thompson, A., Nessler, R., Wisco, D., Anderson, E., WInckler, B., Sheff, D., 2007. Recycling Endosomes of Polarized Epithelial Cells Actively Sort Apical and Basolateral Cargos into Separate Subdomains. Mol. Biol. Cell 18, 2687–2697. https://doi.org/10.1091/mbc.E05–09–0873

Thompson, C.L., Drewery, D.L., Atkins, H.D., Stephenson, F.A., Chazot, P.L., 2002. Immunohistochemical localization of N-methyl-D-aspartate receptor subunits in the adult murine hippocampal formation: Evidence for a unique role of the NR2D subunit. Mol. Brain Res. 102, 55–61. https://doi.org/10.1016/S0169-328X(02)00183-3

Tobinick, E., 2007. Perispinal etanercept for treatment of Alzheimer's disease. Curr. Alzheimer Res. 4, 550–2. https://doi.org/10.2174/156720507783018217

Tobinick, E., Gross, H., Weinberger, A., Cohen, H., 2006. TNF-alpha Modulation for Treatment of Alzheimer's Disease: A 6-Month Pilot Study. MedGenMed 8, 25.

Tobinick, E.L., Chen, K., Chen, X., 2009. Rapid intracerebroventricular delivery of Cu-DOTA-etanercept after peripheral administration demonstrated by PET imaging. BMC Res. Notes 2, 1–5. https://doi.org/10.1186/1756-0500-2-28

Tobinick, E.L., Gross, H., 2008. Rapid cognitive improvement in Alzheimer's disease following perispinal etanercept administration. J. Neuroinflammation 5, 1–10. https://doi.org/10.1186/1742-2094-5-2

Tolnay, M., Probst, A., 1999. REVIEW: tau protein pathology in Alzheimer's disease and related disorders. Neuropathol. Appl. Neurobiol. 25, 171–87. https://doi.org/10.1046/j.1365-2990.1999.00182.x

Torres-Acosta, N., O'Keefe, J.H., O'Keefe, E.L., Isaacson, R., Small, G., 2020. Therapeutic Potential of TNF-α Inhibition for Alzheimer's Disease Prevention. J. Alzheimer's Dis. 78, 619–626. https://doi.org/10.3233/JAD-200711

Torres, K.C., Lima, G.S., Fiamoncini, C.M.I., Rezende, V.B., Pereira, P.A., Bicalho, M.A., Moraes, E.N., Romano-Silva, M.A., 2014. Increased frequency of cluster of differentiation 14 (CD14+) monocytes expressing interleukin 1 beta (IL-1β) in Alzheimer's disease patients and intermediate levels in late-onset depression patients. Int. J. Geriatr. Psychiatry 29, 137–143. https://doi.org/10.1002/gps.3973

Triguero, D., Buciak, J.B., Yang, J., Pardridge, W.M., 1989. Blood-brain barrier transport of cationized immunoglobulin G: enhanced delivery compared to native protein. Proc. Natl. Acad. Sci. U. S. A. 86, 4761–5. https://doi.org/10.1073/pnas.86.12.4761

Trost, L.C., Lemasters, J.J., 1994. A Cytotoxicity Assay for Tumor Necrosis Factor Employing a Multiwell Fluorescence Scanner. Anal. Biochem. https://doi.org/10.1006/abio.1994.1311

Tsopra, O.A., Ziros, P.G., Lagadinou, E.D., Symeonidis, A., Kouraklis-Symeonidis, A., Thanopoulou, E., Angelopoulou, M.K., Vassilakopoulos, T.P., Pangalis, G.A., Zoumbos, N.C., 2009. Disease-related anemia in chronic lymphocytic leukemia is not due to intrinsic defects of erythroid precursors: A possible pathogenetic role for tumor necrosis factor-alpha. Acta Haematol. 121, 187–195. https://doi.org/10.1159/000220331

Tulving, E., 2002. Episodic Memory: From Mind to Brain. Annu. Rev. Psychol. 53, 1–25. https://doi.org/10.1146/annurev.psych.53.100901.135114

Tungtur, S.K., Nishimune, N., Radel, J., Nishimune, H., 2017. Mouse Behavior Tracker: An economical method for tracking behavior in home cages. Biotechniques 63, 215–220. https://doi.org/10.2144/000114607

Uchikado, H., Akiyama, H., Kondo, H., Ikeda, K., Tsuchiya, K., Kato, M., Oda, T., Togo, T., Iseki, E., Kosaka, K., 2004. Activation of vascular endothelial cells and perivascular cells by systemic inflammation - An immunohistochemical study of postmortem human brain tissues. Acta Neuropathol. 107, 341–351. https://doi.org/10.1007/s00401-003-0815-x

Ulrich, J.D., Huynh, T.P., Holtzman, D.M., 2015. Re-evaluation of the Blood-Brain Barrier in the Presence of Alzheimer's Disease Pathology. Neuron 88, 237–239. https://doi.org/10.1016/j.neuron.2015.10.008

Bibliography

Van Dam, E.J.M., Kamal, A., Artola, A., De Graan, P.N.E., Gispen, W.H., Ramakers, G.M.J., 2004. Group I metabotropic glutamate receptors regulate the frequency-response function of hippocampal CA1 synapses for the induction of LTP and LTD. Eur. J. Neurosci. 19, 112–118. https://doi.org/10.1111/j.1460-9568.2004.03103.x

Van Der Willik, K.D., Fani, L., Rizopoulos, Di., Licher, S., Fest, J., Schagen, S.B., Ikram, M.K., Ikram, M.A., 2019. Balance between innate versus adaptive immune system and the risk of dementia: A population-based cohort study. J. Neuroinflammation 16, 1–9. https://doi.org/10.1186/s12974-019-1454-z

Van Der Zanden, E.P., Boeckxstaens, G.E., De Jonge, W.J., 2009. The vagus nerve as a modulator of intestinal inflammation. Neurogastroenterol. Motil. 21, 6–17. https://doi.org/10.1111/j.1365-2982.2008.01252.x

Van Diepen, A., Martina, C.A.E., Flierman, R., Janssen, R., Van Dissel, J.T., 2007. Treatment with anti-TNFα does not induce reactivation of latent Salmonella enterica serovar Typhimurium infection in C3H/HeN mice. Scand. J. Immunol. 65, 407–411. https://doi.org/10.1111/j.1365-3083.2007.01920.x

van Sorge, N.M., Zialcita, P.A., Browne, S.H., Quach, D., Guiney, D.G., Doran, K.S., 2011. Penetration and Activation of Brain Endothelium by Salmonella enterica Serovar Typhimurium. J. Infect. Dis. 203, 401–405. https://doi.org/10.1093/infdis/jiq048

Varatharaj, A., Galea, I., 2017. The blood-brain barrier in systemic inflammation. Brain. Behav. Immun. 60, 1–12. https://doi.org/10.1016/j.bbi.2016.03.010

Verma, S., Nakaoke, R., Dohgu, S., Banks, W.A., 2006. Release of cytokines by brain endothelial cells: A polarized response to lipopolysaccharide. Brain. Behav. Immun. 20, 449–455. https://doi.org/10.1016/j.bbi.2005.10.005

Villarán, R.F., Espinosa-Oliva, A.M., Sarmiento, M., De Pablos, R.M., Argüelles, S., Delgado-Cortés, M.J., Sobrino, V., Van Rooijen, N., Venero, J.L., Herrera, A.J., Cano, J., Machado, A., 2010. Ulcerative colitis exacerbates lipopolysaccharide-induced damage to the nigral dopaminergic system: potential risk factor in Parkinson`s disease. J. Neurochem. 114, 1687–1700. https://doi.org/10.1111/j.1471-4159.2010.06879.x

Villaseñor, R., Ozmen, L., Messaddeq, N., Grüninger, F., Loetscher, H., Keller, A., Betsholtz, C., Freskgård, P.-O.O., Collin, L., Villasenõr, R., Ozmen, L., Messaddeq, N., Grüninger, F., Loetscher, H., Keller, A., Betsholtz, C., Freskgård, P.-O.O., Collin, L., 2016. Trafficking of Endogenous Immunoglobulins by Endothelial Cells at the Blood-Brain Barrier. Sci. Rep. 6, 256–258. https://doi.org/10.1038/srep25658

Vos, Q., Lees, A., Wu, Z.Q., Snapper, C.M., Mond, J.J., 2000. B-cell activation by T-cell-independent type 2 antigens as an integral part of the humoral immune response to pathogenic microorganisms. Immunol. Rev. 176, 154–170. https://doi.org/10.1034/j.1600-065X.2000.00607.x

Wajant, H., 2002. The Fas Signaling Pathway: More Than a Paradigm. Science (80-.). 296, 1635–1636. https://doi.org/10.1126/science.1071553

Wajant, H., Pfizenmaier, K., Scheurich, P., 2003. Tumor necrosis factor signaling. Cell Death Differ. 10, 45–65. https://doi.org/10.1038/sj.cdd.4401189

Wajant, H., Scheurich, P., 2011. TNFR1-induced activation of the classical NF-κB pathway. FEBS J. 278, 862–876. https://doi.org/10.1111/j.1742-4658.2011.08015.x

Wan, W., Janz, L., Vriend, C.Y., Sorensen, C.M., Greenberg, A.H., Nance, D.M., 1993. Differential induction of c-Fos immunoreactivity in hypothalamus and brain stem nuclei following central and peripheral administration of endotoxin. Brain Res. Bull. 32, 581–587. https://doi.org/10.1016/0361-9230(93)90158-8

Wang, J., Du, Y., Qian, H., Yu, H., Li, S., Zhang, X., Li, Z., Yuan, H., Zhao, W., 2014. Engineering and characterization of a humanized antibody targeting TNF-α and RANKL. Biochem. Biophys. Res. Commun. 450, 717–722. https://doi.org/10.1016/j.bbrc.2014.06.046

Wang, X.-L., Zeng, J., Feng, J., Tian, Y.-T., Liu, Y.-J., Qiu, M., Yan, X., Yang, Y., Xiong, Y., Zhang, Z.-H., Wang, Q., Wang, J.-Z., Liu, R., 2014. Helicobacter pylori filtrate impairs spatial learning and memory in rats and increases Î²-amyloid by enhancing expression of presenilin-2. Front. Aging Neurosci. 6, 1–10. https://doi.org/10.3389/fnagi.2014.00066

Wang, X., Wang, B.R., Zhang, X.J., Xu, Z., Ding, Y.Q., Ju, G., 2002. Evidences for vagus nerve in maintenance of immune balance and transmission of immune information from gut to brain in STM-infected rats. World J. Gastroenterol. 8, 540–545. https://doi.org/10.3748/wjg.v8.i3.540

Ward, E.S., Ober, R.J., 2018. Targeting FcRn to Generate Antibody-Based Therapeutics. Trends Pharmacol. Sci. 39, 892–904. https://doi.org/10.1016/j.tips.2018.07.007

Ward, R.J., Zucca, F.A., Duyn, J.H., Crichton, R.R., Zecca, L., 2014. The role of iron in brain ageing and neurodegenerative disorders. Lancet Neurol. 13, 1045–1060. https://doi.org/10.1016/S1474-4422(14)70117-6

Watts, C., 1985. Rapid endocytosis of the transferrin receptor in the absence of bound transferrin. J. Cell Biol. 100, 633–637. https://doi.org/10.1083/jcb.100.2.633

Weber, A., Wasiliew, P., Kracht, M., 2010. Interleukin-1 (IL-1) Pathway. Immunology 3, 1–7.

Weber, F., Bohrmann, B., Niewoehner, J., Fischer, J.A.A., Rueger, P., Tiefenthaler, G., Moelleken, J., Bujotzek, A., Brady, K., Singer, T., Ebeling, M., Iglesias, A., Freskgård, P.O., 2018. Brain Shuttle Antibody for Alzheimer's Disease with Attenuated Peripheral Effector Function due to an Inverted Binding Mode. Cell Rep. 22, 149–162. https://doi.org/10.1016/j.celrep.2017.12.019

Webster, C.I., Hatcher, J., Burrell, M., Thom, G., Thornton, P., Gurrell, I., Chessell, I., 2017. Enhanced delivery of IL-1 receptor antagonist to the central nervous system as a novel anti–transferrin receptor-IL-1RA fusion reverses neuropathic mechanical hypersensitivity. Pain 158, 660–668. https://doi.org/10.1097/j.pain.0000000000000810

Bibliography

Weintraub, M.K., Kranjac, D., Eimerbrink, M.J., Pearson, S.J., Vinson, B.T., Patel, J., Summers, W.M., Parnell, T.B., Boehm, G.W., Chumley, M.J., 2014. Peripheral administration of poly I: C leads to increased hippocampal amyloid-beta and cognitive deficits in a non-transgenic mouse. Behav. Brain Res. 266, 183–187. https://doi.org/10.1016/j.bbr.2014.03.009

Weiss, G., 2005. Modification of iron regulation by the inflammatory response. Best Pract. Res. Clin. Haematol. 18, 183–201. https://doi.org/10.1016/j.beha.2004.09.001

Wendeln, A.-C., Degenhardt, K., Kaurani, L., Gertig, M., Ulas, T., Jain, G., Wagner, J., Häsler, L.M., Wild, K., Skodras, A., Blank, T., Staszewski, O., Datta, M., Centeno, T.P., Capece, V., Islam, M.R., Kerimoglu, C., Staufenbiel, M., Schultze, J.L., Beyer, M., Prinz, M., Jucker, M., Fischer, A., Neher, J.J., 2018. Innate immune memory in the brain shapes neurological disease hallmarks. Nature 556, 332–338. https://doi.org/10.1038/s41586-018-0023-4

Wickham, M.E., Brown, N.F., Provias, J., Brett, B.B., Coombes, B.K., 2007. Oral infection of mice with Salmonella enterica serovar Typhimurium causes meningitis and infection of the brain. BMC Infect. Dis. 7, 1–6. https://doi.org/10.1186/1471-2334-7-65

Wieczorek, M., Swiergiel, A.H., Pournajafi-Nazarloo, H., Dunn, A.J., 2005. Physiological and behavioral responses to interleukin-1β and LPS in vagotomized mice. Physiol. Behav. 85, 500–511. https://doi.org/10.1016/j.physbeh.2005.05.012

Wiley, D.T., Webster, P., Gale, A., Davis, M.E., 2013. Transcytosis and brain uptake of transferrin-containing nanoparticles by tuning avidity to transferrin receptor. Proc. Natl. Acad. Sci. 110, 8662–8667. https://doi.org/10.1073/pnas.1307152110

Xiao, W., Koizumi, K., Nishio, M., Endo, T., Osawa, M., Fujimoto, K., Sato, I., Sakai, T., Koike, T., Sawada, K.I., 2002. Tumor necrosis factor-α inhibits generation of glycophorin A+ cells by CD34+ cells. Exp. Hematol. 30, 1238–1247. https://doi.org/10.1016/S0301-472X(02)00930-X

Yadav, D.B., Maloney, J.A., Wildsmith, K.R., Fuji, R.N., Meilandt, W.J., Solanoy, H., Lu, Y., Peng, K., Wilson, B., Chan, P., Gadkar, K., Kosky, A., Goo, M., Daugherty, A., Couch, J.A., Keene, T., Hayes, K., Nikolas, L.J., Lane, D., Switzer, R., Adams, E., Watts, R.J., Scearce-Levie, K., Prabhu, S., Shafer, L., Thakker, D.R., Hildebrand, K., Atwal, J.K., 2017. Widespread brain distribution and activity following i.c.v. infusion of anti-β-secretase (BACE1) in nonhuman primates. Br. J. Pharmacol. 174, 4173–4185. https://doi.org/10.1111/bph.14021

Yang, T., Wang, Z., Wu, F., Tan, J., Shen, Y., Li, E., Dai, J., Shen, R., Li, G., Wu, J., Wang, L., Wang, H., Liu, Y., 2010. A variant of TNFR2-Fc fusion protein exhibits improved efficacy in treating experimental rheumatoid arthritis. PLoS Comput. Biol. 6. https://doi.org/10.1371/journal.pcbi.1000669

Ye, Q., Hu, H., Wang, Z., Lu, T., Hu, Z., Zeng, X., Zhang, S., Liu, J., Lei, P., Wang, C.Y., Ye, Z., Shen, G., 2012. Generation and functional characterization of the anti-transferrin receptor single-chain antibody-GAL4 (TfRscFv-GAL4) fusion protein. BMC Biotechnol. 12. https://doi.org/10.1186/1472-6750-12-91

Yli-Karjanmaa, M., Larsen, K.S., Fenger, C.D., Kristensen, L.K., Martin, N.A., Jensen, P.T., Breton, A., Nathanson, L., Nielsen, P.V., Lund, M.C., Carlsen, S.L., Gramsbergen, J.B., Finsen, B., Stubbe, J., Frich, L.H., Stolp, H., Brambilla, R., Anthony, D.C., Meyer, M., Lambertsen, K.L., 2019. TNF deficiency causes alterations in the spatial organization of neurogenic zones and alters the number of microglia and neurons in the cerebral cortex. Brain. Behav. Immun. 82, 279–297. https://doi.org/10.1016/j.bbi.2019.08.195

Yoshiyama, Y., Higuchi, M., Zhang, B., Huang, S.M., Iwata, N., Saido, T.C.C., Maeda, J., Suhara, T., Trojanowski, J.Q., Lee, V.M.Y., 2007. Synapse Loss and Microglial Activation Precede Tangles in a P301S Tauopathy Mouse Model. Neuron 53, 337–351. https://doi.org/10.1016/j.neuron.2007.01.010

Yrlid, U., Wick, M.J., 2002. Antigen Presentation Capacity and Cytokine Production by Murine Splenic Dendritic Cell Subsets upon Salmonella Encounter . J. Immunol. 169, 108–116. https://doi.org/10.4049/jimmunol.169.1.108

Yu, Y.J., Atwal, J.K., Zhang, Y., Tong, R.K., Wildsmith, K.R., Tan, C., Bien-Ly, N., Hersom, M., Maloney, J.A., Meilandt, W.J., Bumbaca, D., Gadkar, K., Hoyte, K., Luk, W., Lu, Y., Ernst, J.A., Scearce-Levie, K., Couch, J.A., Dennis, M.S., Watts, R.J., 2014. Therapeutic bispecific antibodies cross the blood-brain barrier in nonhuman primates. Sci Transl Med 6, 261ra154. https://doi.org/10.1126/scitranslmed.3009835

Yu, Y.J., Watts, R.J., 2013. Developing Therapeutic Antibodies for Neurodegenerative Disease. Neurotherapeutics 10, 459–472. https://doi.org/10.1007/s13311-013-0187-4

Yu, Y.J., Zhang, Y., Kenrick, M., Hoyte, K., Luk, W., Lu, Y., Atwal, J., Elliott, J.M., Prabhu, S., Watts, R.J., Dennis, M.S., 2011. Boosting brain uptake of a therapeutic antibody by reducing its affinity for a transcytosis target. Sci. Transl. Med. 3, 84ra44. https://doi.org/10.1126/scitranslmed.3002230

Yu, Y.R.A., O'Koren, E.G., Hotten, D.F., Kan, M.J., Kopin, D., Nelson, E.R., Que, L., Gunn, M.D., 2016. A protocol for the comprehensive flow cytometric analysis of immune cells in normal and inflamed murine non-lymphoid tissues. PLoS One 11, 1–23. https://doi.org/10.1371/journal.pone.0150606

Zalevsky, J., Secher, T., Ezhevsky, S.A., Janot, L., Steed, P.M., O'Brien, C., Eivazi, A., Kung, J., Nguyen, D.-H.T., Doberstein, S.K., Erard, F., Ryffel, B., Szymkowski, D.E., 2007. Dominant-Negative Inhibitors of Soluble TNF Attenuate Experimental Arthritis without Suppressing Innate Immunity to Infection. J. Immunol. 179, 1872–1883. https://doi.org/10.4049/jimmunol.179.3.1872

Zhang, Y., Chen, K., Sloan, S.A., Bennett, M.L., Scholze, A.R., O'Keeffe, S., Phatnani, H.P., Guarnieri, P., Caneda, C., Ruderisch, N., Deng, S., Liddelow, S.A., Zhang, C., Daneman, R., Maniatis, T., Barres, B.A., Wu, J.Q., 2014. An RNA-sequencing transcriptome and splicing database of glia, neurons, and vascular cells of the cerebral cortex. J. Neurosci. 34, 11929–11947. https://doi.org/10.1523/JNEUROSCI.1860-14.2014

Zhang, Y., Pardridge, W.M., 2001a. Mediated efflux of IgG molecules from brain to blood across the blood-brain barrier. J. Neuroimmunol. 114, 168–172. https://doi.org/10.1016/S0165-5728(01)00242-9

Bibliography

Zhang, Y., Pardridge, W.M., 2001b. Rapid transferrin efflux from brain to blood across the blood-brain barrier. J. Neurochem. 76, 1597–1600. https://doi.org/10.1046/j.1471-4159.2001.00222.x

Zhao, A., Li, Y., Deng, Y., 2020. TNF receptors are associated with tau pathology and conversion to Alzheimer's dementia in subjects with mild cognitive impairment. Neurosci. Lett. 738, 1–6. https://doi.org/10.1016/j.neulet.2020.135392

Zhao, M., Cribbs, D.H., Anderson, A.J., Cummings, B.J., Su, J.H., Wasserman, A.J., Cotman, C.W., 2003. The induction of the TNFα death domain signaling pathway in Alzheimer's disease brain. Neurochem. Res. 28, 307–318. https://doi.org/10.1023/A:1022337519035

Zhou, M., Xu, R., Kaelber, D.C., Gurney, M.E., 2020. Tumor Necrosis Factor (TNF) blocking agents are associated with lower risk for Alzheimer's disease in patients with rheumatoid arthritis and psoriasis. PLoS One 15, e0229819. https://doi.org/10.1371/journal.pone.0229819

Zhou, Q., Qiu, H., 2019. The Mechanistic Impact of N-Glycosylation on Stability, Pharmacokinetics, and Immunogenicity of Therapeutic Proteins. J. Pharm. Sci. 108, 1366–1377. https://doi.org/10.1016/j.xphs.2018.11.029

Zhou, Qing Hui, Boado, R.J., Hui, E.K.W., Lu, J.Z., Pardridge, W.M., 2011a. Chronic dosing of mice with a transferrin receptor monoclonal antibody-glial-derived neurotrophic factor fusion protein. Drug Metab. Dispos. 39, 1149–1154. https://doi.org/10.1124/dmd.111.038349

Zhou, Qing-hui Hui, Fu, A., Boado, R.J., Hui, E.K.W., Lu, J.Z., Pardridge, W.M., 2011. Receptor-Mediated Abeta Amyloid Antibody Targeting to Alzheimer ' s Disease Mouse Brain. Mol. Pharm. 82, 280–285. https://doi.org/10.1021/mp1003515

Zhou, Qing Hui, Sumbria, R., Hui, E.K.-W., Lu, J.Z., Boado, R.J., Pardridge, W.M., 2011b. Neuroprotection with a brain-penetrating biologic tumor necrosis factor inhibitor. J. Pharmacol. Exp. Ther. 339, 618–23. https://doi.org/10.1124/jpet.111.185876

Zlokovic, B. V., 2008. The Blood-Brain Barrier in Health and Chronic Neurodegenerative Disorders. Neuron 57, 178–201. https://doi.org/10.1016/j.neuron.2008.01.003

Zlotnik, I., Rennie, J.C., 1963. Further observations on the experimental transmission of scrapie from sheep and goats to laboratory mice. J. Comp. Pathol. Ther. 73, 150–163. https://doi.org/10.1016/S0368-1742(63)80018-1